Schriftenreihe Geotechnik
Universität Kassel

Experimental, Analytical and Numerical Investigations of Excavations in Normally Consolidated Soft Soils

Berhane Gebreselassie

Heft 14

September 2003

Diese Arbeit entstand am Fachgebiet Geotechnik als eine vom Fachbereich Bauingenieurwesen der Universität Kassel genehmigte Dissertation.

Preface

Geotechnical design and execution of excavations in very soft cohesive soils are usually associated with substantial difficulties. In particular, in urban areas deformations due to excavations may often lead to a substantial damage to the nearby structures. Mr. Berhane Gebreselassie deals in his work comprehensively with the computational methods of such excavations. The work begins with a review of the state of the art of the design and construction principles of excavations and the material behaviour of soft soils in a special, careful and detailed way.

An important question in the computation of excavations in soft soils is whether the drained or undrained conditions govern the situation. Mr. Berhane Gebreselassie has tried to find out a reason on the basis of theoretical soil mechanics and extensive experimental results from the literature that preferentially the drained condition may govern the performance of an excavations in soft soils. This is verified among other with the stress paths at different points in the excavation in combination with consolidation theory and it is made transparent using an extensive comparative computations and parameter studies.

The numerous laboratory tests conducted and the documented results in this work, namely drained and undrained, standard and stress path dependant triaxial tests under isotropic and anisotropic consolidation conditions, and one-dimensional, isotropic and anisotropic compression tests on normally consolidated lacustrine soft soil, essentially fill the gab of information, which are seldom available for the design and execution of excavations in very difficulty soil types in such a compressed and an abundance form. From the test results, the soil parameters are derived for the numeric computations and they are validated numerically based on the laboratory test results. With the help of an evaluation matrix, it was possible to sort out the degree of the effect of each material parameter and the extent in which these influences may be considered in an excavation computations. The investigations are supplemented by extensive parameter studies of different excavation situations in soft soils and variation of the relevant influence parameters.

On the basis of systematic and detailed back calculations of two practical projects from the Constance (Bodensee) area in southern Germany with the finite element method, it was possible to drive recommendations for future computations of excavations with similar situation. The extensive investigations also show that computations of excavations with numerical methods still have their own limitations. Since such computations are demanded and implemented increasingly in the practice, the back calculations and the analytical analysis based on soil mechanics theories accomplished by Mr. Berhane Gebreselassie is of importance particularly for the selection and

coordination of an appropriate computation. Furthermore, they are suitable to improve the entire computation and prediction methods of the behaviour of excavations in soft soils.

In the last section of the work, a comparative numerical and analytical computation results are documented, which Mr. Berhane Gebreselassie has carried out in the last years for the working group "Excavations" of the German Society of Geotechnical Engineers (DGGT). The extensive investigations constitute an important basis for the in the meantime available draft recommendation "Excavations in Soft Soils" of the working group "Excavation" (EAB), which gains a positive resonance in the professional world.

Hans George Kempfert

Vorwort des Herausgebers

Baugruben in sehr weichen bindigen Böden beinhalten für die geotechnische Planung und Ausführung erhebliche Schwierigkeiten. Insbesondere im innerstädtischen Bereich sind damit oftmals Randbedingungen verbunden, die aufgrund von Verformungen aus der Baugrubensituation zu erheblichen Schäden an der Nachbarbebauung führen können. Herr Dr.-Ing. Berhane Gebreselassie hat sich in der vorliegenden Arbeit umfassend mit der Berechnung dieser Baugruben beschäftigt. Dabei wurde zunächst der Kenntnisstand aus der Literatur zusammengefasst und in einer besonders sorgfältigen und ausführlichen Art und Weise das Stoffverhalten und die Bodenkenngrößen von weichen bindigen Böden zusammengestellt.

Eine wesentliche Fragestellung zur Thematik der Berechnung von Baugruben in weichen Böden ist die Einschätzung, ob es sich hier für die weichen Böden um drainierte oder undrainierte Bedingungen handelt. Herr Berhane Gebreselassie hat auf der Grundlage von weitergehenden bodenmechanischen Theorien unter Verwendung umfangreicher Literaturergebnisse sowie Messergebnissen von Baugrubenherstellungen eine in sich schlüssige theoretische Begründung dafür gefunden, dass bei Baugruben in weichen Böden bevorzugt mit drainierten Bedingungen zu rechnen ist. Dies wurde u. a. über die wirkenden Spannungspfade bei verschiedenen Baugrubenpunkten in Verbindung mit konsolidationstheoretischen Ansätzen belegt und durch umfangreiche Vergleichsberechnungen und Parameterstudien transparent gemacht.

Die in der Arbeit durchgeführten und dokumentierten zahlreichen Ergebnisse von Laborversuchen im wesentlichen aus drainierten und undrainierten Triaxialversuchen an Seetonproben stellen eine Fülle von Informationen dar, wie sie für die Herstellung von Baugruben in den sehr schwierig zu beherrschenden Bodenarten nur selten in derart komprimierter Form zur Verfügung stehen. Aus den Versuchsergebnissen wurden die stoffspezifischen Parameter für die numerischen Berechnungen abgeleitet und anhand der Laborversuchsergebnisse validiert. In einer Bewertungsmatrix konnte herausgearbeitet werden, welche stofflichen Eigenschaften bestimmte Effekte bodenmechanisch abbilden können und mit welcher Wertigkeit die Einflüsse in die Baugrubenberechnung eingehen. Die Untersuchungen wurden durch umfangreiche Parameterstudien an unterschiedlichen Baugrubensituationen in weichen Böden bei Variation der maßgeblichen Einflussparameter ergänzt.

Auf der Grundlage von systematischen und sehr detaillierten Rückrechnungen mit der Methode der Finiten Elemente für zwei praktische Projekte aus dem Raum Konstanz (Bodensee) konnten Empfehlungen für zukünftige vergleichbare Berechnungen abgeleitet werden. Die umfangreichen

Untersuchungen haben aber auch gezeigt, dass Baugrubenberechnungen mit numerischen Methoden in vielen Punkten auch heute noch an ihre Grenzen stoßen. Da solche Berechnungen zunehmend im praktischen Baugeschehen gefordert und ausgeführt werden, sind die von Herrn Berhane Gebreselassie durchgeführten Rückrechnungen und bodenmechanischen Analysen besonders für die Einordnung und Wertigkeit entsprechender Berechnungen von Bedeutung. Des Weiteren sind sie geeignet, die gesamte Berechnungs- und Prognosetechnik von Baugruben in weichen Böden zu verbessern.

In dem vorletzten Abschnitt der Arbeit sind vergleichende numerische und analytische Berechnungsergebnisse dokumentiert, die Herr Berhane Gebreselassie in den letzten Jahren für den Arbeitskreis Baugruben der Deutschen Gesellschaft für Geotechnik durchgeführt hat. Die umfangreichen Untersuchungen bilden mit eine maßgebliche Grundlage für die zwischenzeitlich vorliegenden Entwürfe der Empfehlungen „Baugruben in weichen Böden" des Arbeitskreises „Baugruben" (EAB), die in der Fachwelt auf positive Resonanz gestoßen sind.

Hans-Georg Kempfert

Acknowledgements

Firstly, my heartfelt and special thanks go to Prof. Dr.-Ing. H.-G. Kempfert, my supervisor, for affording me the opportunity to take part in this research project. I am most grateful to him not only for his consistent scientific support but also for his encouragement, patience, kindness and financial support throughout my research work. His varied assistance made my work and life in Germany much easier.

I gratefully acknowledge the valuable and helpful discussions and comments on various sections of the manuscript from Ao. Univ.-Prof. Dipl.-Ing. Dr.-techn. H. F. Schweiger. I am also thankful to him for proof reading and reviewing the dissertation work. Thanks are also due to Prof. Dr.-Ing. W. Seim and Priv.-Doz. Dr.-Ing. habil Y. Hu for participating in the oral examination.

Many thanks are given to the staff of the department of the geotechnical engineering, who gave me full support and encouragement and created a pleasant and collegial working atmosphere. My special thanks also go to my former colleagues Dr.-Ing. A. Jaup and Dr.-Ing. E. Ott for their continuous support to get used life to the new atmosphere specially during my first years in Germany.

I am grateful to the financial support provided by the German Academic Exchange Service (DAAD) which helped me to complete the major part of this work.

Finally, I would like to express my appreciation and my sincere thanks to my wife Emebet for her love, moral support and for patiently putting up with me during the years I have been working on this work. She generously accommodated the additional time demands which such project inevitably makes.

<div align="right">Berhane Gebreselassie</div>

Table of contents

1   Introduction

1.1   Statement of the problem

The increasing demand for construction of major buildings and transport facilities in urban areas is making excavations very common. The design of such temporary supported excavations requires a knowledge of the expected movements caused by excavations in the surrounding street and building areas. It is difficult or otherwise impossible to prevent totally the ground movements caused by excavation, however, the designer should be in a position to predict the extent and distribution of these movements in order to asses the damage potential and to evaluate the need for any preventive measures or changes in design necessary to minimise the movements.

The problem of movements in an excavation is more serious in normally consolidated soft soils under ground water condition than in other types of soils. Soft soils may be defined as clay or silty clay soils which are geologically young, and come to equilibrium under their own weight but have not undergone significant secondary or delayed consolidation since their formation. They are characterised by the fact that they are just capable of carrying the overburden weight of the soil, and any additional load will result in relatively large deformation. There are also soft soils which are not fully consolidated under their own weight, and results in developing stagnant pore water pressure in the soil layer. In Federal Republic of Germany, soft soils are distributed mainly in two major regions (*Weißenbach/Kempfert (1994)*). Sea silts are found along the coastal area, and along the marshy area of the rivers Ems, Weser and Elbe and lacustrine clay deposits around Lake Constance (Bodensee) and South Bavarian Lakes. The latter was formed by glacial deposit during the latest ice age. The thickness of the soft soil deposit in Constance is estimated to be over 20 m (*Kempfert + Partner (1992/1996)*, *Gudehus et al. (1987)*). Walking along the street of Constance, one can easily observe that a number of buildings are suffering from excessive settlement. One can also see cracks and distortion on parts of old buildings near recently erected buildings. These types of soft soil deposits are also found in many great urban centres of the world, where the need for deep excavation is the greatest (*Mana (1976)*). Such a problem may lead us to an understanding that establishment of a numerical method to predict the movements in an excavation is highly essential.

With the advent of advanced computer technology in the past few decades, numerical modelling of excavations using Finite Element Method (FEM) of analysis has become increasingly popular and powerful analytical tool. Nowadays some FEM codes specially written for geotechnical problems are available on market. Major progress has also been shown in understanding the strength and deformation behaviour of soft soils. Various constitutive models, from simple elastic models to mathematically complex non-linear elasto-plastic models have been developed. However, there is still problem in prediction of movements in and around an excavation with the numerical method. Even for a given real excavation problem with known soil and structural soil

parameters, a large discrepancy of the finite element calculation results submitted by different individuals was reported by *Schweiger (2000)*, let alone the discrepancies in the measured and computed results. *Kempfert/Gebreselasssie (2000)* also reported a large discrepancy among the numerical and analytical comparative results carried out by different groups.

The results of numerical analysis may be influenced significantly by the constitutive relationship chosen to model the behaviour of the soil. Therefore, the choice of one or a group of soil models for one particular problem that addresses the constitutive relations of stress and strain of soil under excavation is very important. Even for a particular soil model, the selection of soil strength and deformation parameters may affect the results. Besides many other factors, the deformation of soils under excavation is found to be stress path dependent. It is therefore necessary to consider whether the state of a stress at a point involves primary loading, unloading, reloading or any other possible stress path.

Most of the previous works to predict or to back analyse the performance of excavations in soft soil by means of the FEM (for example, *Clough/Mana (1976); Clough/Tsui (1974); Mana (1976); Palmer/Kenny (1972); Brooks/Spence (1993); Burland/Hancock (1977); Burland/Simpson (1979); Wong/Broms (1994)*) were based on the undrained strength of the soil. They assumed that the excavation should be constructed quickly enough so that undrained soil behaviour governs. However, in an excavation problem, both drained and undrained strength of soil may be equally important depending on the duration of the excavation, the rate of pore water dissipation and the stress path it follows at different location of the excavation. Unlike other geotechnical problems such as embankment or foundation design, undrained analysis in an excavation problem may not always lead to the unfavourable condition. The choice of the effective stress method of analysis or the total stress in the analytical design and analysis of an excavation needs also to be addressed.

Most excavation problems are analysed as two-dimensional plane strain problems. While this may be accurate enough for relatively long walls, many field cases and excavation procedures are truly three-dimensional and may need to be analysed as such, or at least the 3D-effect should be considered as a factor in the 2D-finite element calculations.

"The Working Group on Excavations" (EAB) of the German Society of Geotechnical Engineers" is working out additional recommendations for excavation in soft soils to complement the already existing recommendations *EAB (1994)*. This is because it becomes very clear that the standard recommendation *EAB (1994)* is not enough for the design and analysis of excavations in soft soils and it was believed that a special treatment is required to avoid possible damages to the surrounding infrastructures. In this work, therefore, some technical questions and others, that raised in the draft work of the recommendation, will be studied and verified through comparative numerical and analytical analysis.

The term "excavation" is used to represent "supported excavation" throughout this work.

1.2 Thesis objective, scope and methodology

The primary objective of the thesis is directed towards studying the behaviour of excavation in normally consolidated soft soil using numerical and analytical methods. The numerical analysis is supported by field data and laboratory test results. With in the framework of the general objective, the following specific points will be assessed:

- Review of the "State of the Art" of the construction and design principles of excavations on one hand, the material behaviour of soft soils on the other hand.

- Discussion of the effective stress and total stress analysis methods and formulation of equations that relate the effective stress and total stress parameters based on the principle of soil mechanics.

- Simulation of the field stress strain condition in laboratory with standard and stress path dependent triaxial tests and compression tests, so that appropriate soil parameters for different soil models in numerical analysis can be obtained, and the study of the effect of stress path on deformation characteristics of excavations in soft soils, and critically examine the existing soil models in connection with the excavation in soft soil.

- Calibration of the soil parameters to the material models by means of FE-simulation of the tests and the study of the sensibility of the model parameters on the stress - strain, volume change and pore pressure characteristics of the specimens.

- Sensibility analysis of an ideal excavation problem in order to study the effect of system geometry, element size, and type of analysis (drained and undrained).

- A series of parameter studies in order to evaluate the effect of variations of soil strength and stiffness parameters, the effect of berms, the effect of bottom slab support.

- Study of the mobilisation of earth pressure in soft soil deposit and develop analytical equations for approximation of the mobilised passive resistance and the total safety factor for passive resistance dependent on the stiffness of the soil and the wall movement.

- Calibration of model parameters based on numerical analysis of practical projects using the FEM.

- Comparison of the numerical and analytical analysis of excavations in soft soils based on the draft recommendation of the EAB.

Two practical projects are chosen as basis for numerical analysis. Both projects are located in Constance city, southern Germany and are founded in thick layer of soft soil deposit.

The numerical calculations were carried out using the Finite Element Code PLAXIS (1998/2002), because this program is specially developed to solve geotechnical problems. The most important elements in numerical calculation of an excavation problem, such as wall element, anchor system, interaction between soil and wall, the construction steps followed in the field during excavation, etc., can be successfully modelled with this code. Furthermore, the program offers a variety of constitutive soil models that are capable of simulating the linear and non linear behaviour, elastic and elasto-plastic behaviour, shear hardening and compression hardening, time dependent behaviour (creep effect), and stress dependent stiffness of soils (*Vermeer/Brinkgreve (1998/2002)*). Different options of analysis methods are also available in the program. These are plastic calculations (drained and undrained), consolidation analysis and update mesh analysis.

In the following chapter a review of the state of the art of design and construction principles are presented and discussed followed by the presentation of the "the state of art" of the material properties of soft soils in chapter 3.

In chapter 4 the total and effective stress analyses of excavations in soft soil deposits have been discussed and analytical approaches of estimating the effective stress parameters from the undrained shear strength have been derived.

The historical development of constitutive soil models are briefly presented in chapter 5. The merits and de-merits as well as the limitations of the various soil models are discussed in relation to excavation problem in soft soils.

A series of triaxial tests; both isotropic and anisotropic consolidation, standard and stress path dependent tests, and one-dimensional, isotropic and anistropic (K_0) compression tests were carried out in order to determine the various soil parameters relevant to numerical modelling of excavations in soft soils. A data bank of the different soil parameters would be found in chapter 6. Tests to study the contact behaviour of wall and soils were also carried out and the results and analyses are included in this chapter.

The soil parameters obtained in chapter 6 are calibrated by means of a FE-simulation of the respective tests in chapter 7. Based on the sensibility study, the influence of the model parameters on the stress-strain, volume change and excess pore pressure behaviour had been studied. The primary focus of this study is to predict numerically the performance of excavations in soft soils. Therefore, the influence of the model parameters on performance of an excavation in soft soil had been examined based on parameter study of fictitious excavation problem. The results of the pa-

rameter studies are given in the second part of chapter 7 followed by analysis of practical projects in chapter 8.

Finally, a review of the comparative analytical and numerical case studies of the draft recommendation for excavation in soft soils of the working group "Excavation" (EAB) of the German society of Geotechnical Engineers is presented in Chapter 9 followed by summery in chapter 10.

2 Review of construction and design principles of excavation in soft soils - "state of the art"

2.1 General

The state of the knowledge regarding the excavation behaviour in soft clays has expanded substantially over the last few decades. Several excellent state of the art reports on this subject have been published (*Peck (1969); Lambe (1970); Bijerrum et al. (1972); Clough/Schmidt (1977); Clough/O'Rourke (1990)*). Moreover excellent handbooks and textbooks, that explain the construction and design principles of excavation in more detail, such as *Smoltczyk (1996); Clayton et al. (1993); Weissenbach (1985); Fang (1996); etc.* are also available. The aim of this chapter is therefore not to repeat the previous works, rather to review and point out some problems yet to be solved.

Peck (1969) summarised the experiences with performance of deep excavation support system, and the factors that are most important in controlling the performance. These factors include the type and strength of the soil around and beneath the excavation, the excavation and supporting procedure, and workmanship. Beside the above factors, the ground water condition, the flexibility or rigidity of the components used for construction, the time taken for construction are also important factors that influence the performance of excavations. *Mana (1978)* classified the factors into: parameters under designer control, parameters partially under designer control, and fixed parameters not subject to designer control (Table 2.1).

Table 2.1: Factors affecting the performance of supported excavations (after *Mana (1978)*)

Parameters under designer control	Parameters partially under designer control	Fixed parameters not subject to designer control
1. Type of support system	1. Method of support system construction	1. Subsoil conditions and properties
2. Stiffness of support system	2. Construction period	2. Surrounding structures
3. Degree of wall embedment	3. Method of construction of structures within excavation	3. Excavation shape and depth
4. Degree of pre-loading (pre-stressing)	4. Size of surcharge loads	
	5. Weather	

The magnitude and extent of ground movement around an excavation depends as much on the method of construction as on any of the above factor. Although the designer may specify a particular form or method of construction, the precise details of support, their sequence and timing can not be controlled accurately since they depend on a large factor which vary from day to day

on a construction site. These make the exact simulation of the construction process in numerical analysis complex and difficult. This may be one of the reasons for the discrepancy in the FE-computational results and the field measured data.

The topic of excavation and its support system is very broad. Thus, this study limits itself only to the temporary or permanently supported excavations in urban areas and its influence on nearby structures. The term excavation is used throughout of the text to represent the supported excavation.

2.2   Type of wall

The components making up a retaining structure can be broadly classified into: facings and supports. The common type of facings include: Kingposts and planking (braced excavation), bored piles, diaphragms, and steel sheeting. Kingpost and planking include: steel H-sections (solider piles) with timber sheeting and bored piles with gunnite and mesh facings, and the contiguous, secant and tangent piles belong to the bored piles group. The main differences between the different types of walls are: the construction technology, the material in which they are made of, and the flexibility and rigidity of the wall. The feasibility of any construction method depends to a great extent upon the ground and groundwater conditions at the site, and upon locally available skill, equipment and experience. For excavations in normally consolidated soft clays, stiffer walls such as diaphragms and bored pile walls are usually recommended. However, even with stiffer walls, it is practically impossible to completely eliminate the ground movements in and around an excavation in soft soils (*Palmer/Kenny (1972); Burland et al. (1979); Fujita (1994)*).

After statistically analysing the data from literature about construction and performance of deep excavation support systems since 1962, *Duncan/Bentler (1998)* reported that the percentage of excavations supported by sheet piles have decrease over time, while the percentage of excavations supported by diaphragm walls and other walls (mainly secant, tangent and contiguous pile walls) has increased steadily. They also found that settlements and horizontal movements due to excavation are tending to decrease with time. This improvement in performance is likely related to more frequent use of stiffer walls, such as concrete diaphragm walls and greater care in construction. The introduction of bentonite technology to a new area of the world, the rapid change in boring and excavation techniques and the fact that they can deal satisfactorily with difficult soil conditions, greatly contribute to the frequent use of the diaphragm and bored pile walls.

2.3   Type of wall support

Tie back anchors, ground anchors, struts, props or rakers, berms, basement floors (in top down construction), and soilcrete-slab (jet grouting) are the most common types of support systems. These support systems are schematised in Figure 2.1. The relative rigidity of these components and the facings, and their interconnection and packing, is important in determining the amount of ground movement, and thus the reduction in ground pressure, and the forces and stresses applied to a wall.

a) Cantiliver wall   b) Berm and Slab   c) Single proped wall   d) Multi-proped wall   e) Soilcrete-slab

f) Tie-back wall   g) Ground anchors   h) Top-down construction   i) Braced   excavation
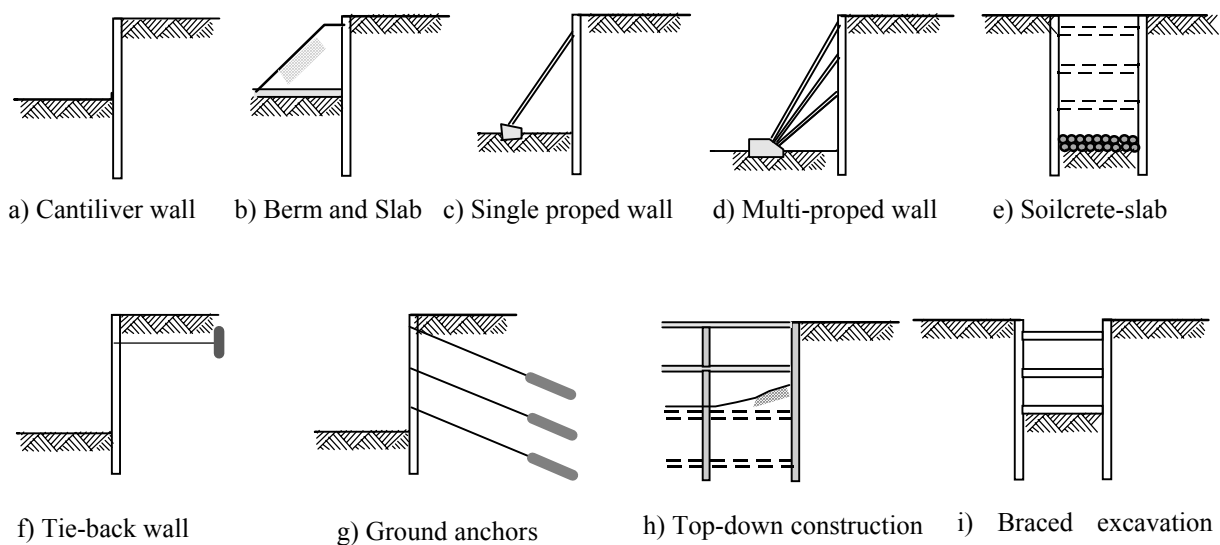
Figure 2.1:   Common types of support schemes

Duncan/Bentler (1998) indicated that there is a tendency to use struts more frequently than tie back anchors. This is mainly due to the problem associated with the installation of the tie back anchors, i.e., the installation of anchors might lead to settlement or heaving of the ground in built up area. Some times it may also be difficult to install tied back anchors in built up areas due to land ownership problem. The use of the top-down construction method has also increased, but still represents a small number. Though the top-down method of construction is widely known in preventing the ground movements effectively, the construction method is relative complicated and there is very limited experience available in practice.

2.4   Behaviour of excavations

2.4.1   General

In soil mechanics the two common limits occur due to:

i)   shear failure of the soil, leading to excessive distortion of a structure or a disruption of highways and services;

ii)   excessive displacement of the soil, inducing unacceptably high stresses in a structure as a result of differential movement.

For retaining structures, failure is a performance problem, related to either strength or deformation. A retaining structure can fail to perform in a satisfactory way for a number of reasons, associated with the failure of the structure itself, failure of the soil or because of unacceptable deformation.

Some possible failure situations in retaining structures are shown in Figure 2.2. In general, the design of a retaining structure should considered the following points: moment equilibrium of the system (overturn), horizontal force equilibrium (sliding), vertical equilibrium (bearing capacity), overstress of any part of the structure (bending or shear), and the general stability of the soil around the structure (slope failure, overall stability, basal stability). The stability of the structure should be satisfactory both in short term and in the long term. Because many retaining structures are associated with decreased level of total stress, it is normal to carry out long-term analysis in terms of effective stresses and effective strength parameters. This will normally give the worst conditions (*Clayton et al. (1993)*).

On the other hand, a retaining structure may perform unsatisfactorily because of the excessive displacement it undergoes. It is seldom possible to predict such movements of the retained ground with any degree of confidence analytically. To limit the excessive displacement, it is common to apply a large factor of safety against failure to the critical area. For example a factor of safety of 1.5 to 2.0 (*EAB (1994)*) is applied on the passive resistance to reduce tilt and lateral displacement of the wall in sands and stiff clays.

The design of a retaining wall include the selection of the type of the retaining wall, determination of the depth of penetration of the wall, determination of the section size of the wall, determination of the strut or anchor load, prediction of the deflection of the wall and ground movements, and checking the stability of the excavation. In the following subsequent sections, the most important components of retaining structures design, namely a) earth pressure, strut and anchor load, and bending moment of the wall, b) ground movements in and around an excavation, c) stability of retaining structures, in particular basal stability, and d) safety factor in the design of retaining structures are presented.

a) Overturning   b) Sliding   c) Overstress of foundations

d) Overstress of the wall   e) General stability   i) Berm and simple slope failure

g) Bottom heave   h) Bulcked struts
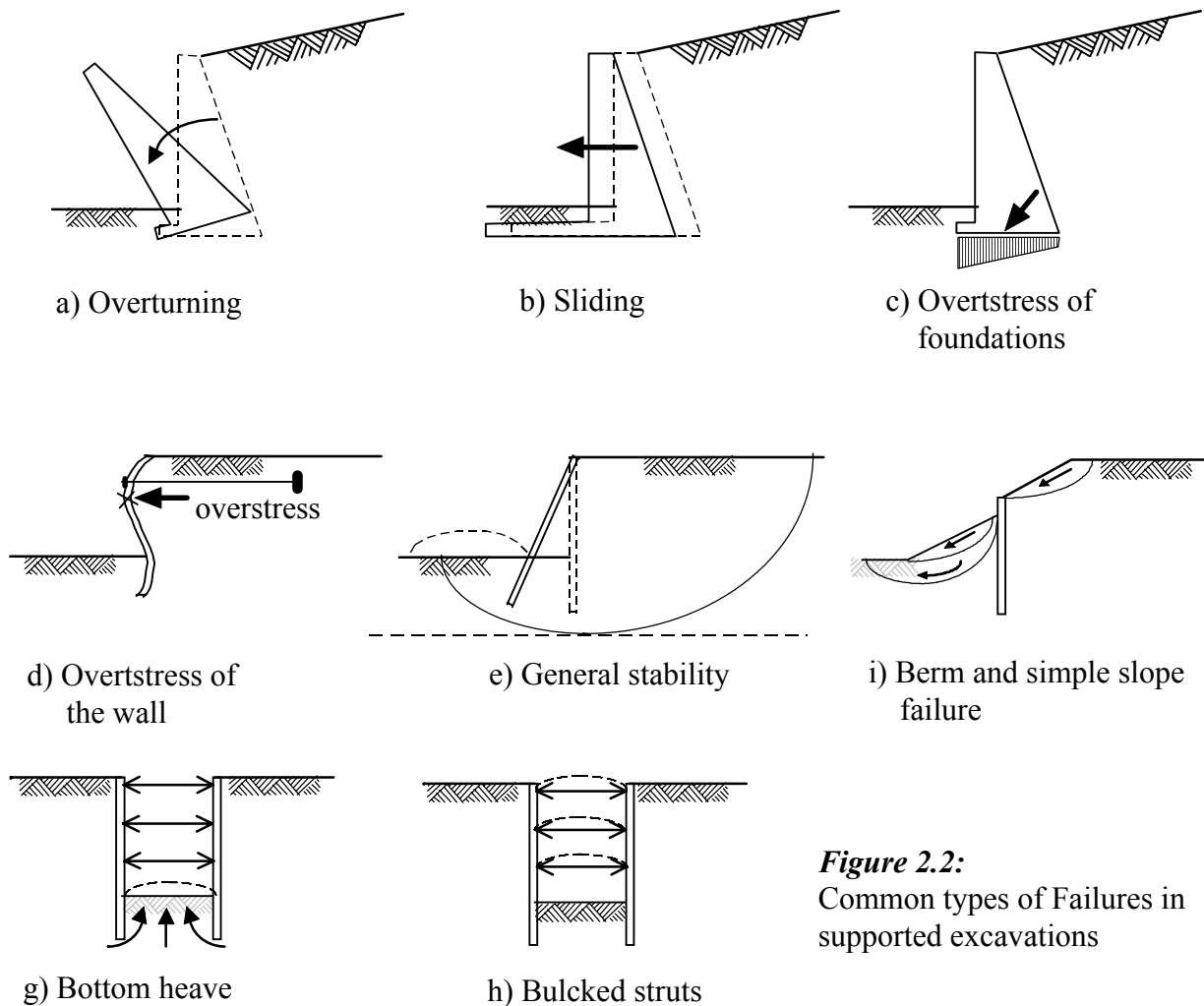
Figure 2.2:
Common types of Failures in supported excavations

2.4.2 Earth pressure, reaction and section forces

2.4.2.1 Earth pressure

Pradel (1994) grouped earth pressure computations into three categories:

a) Methods based on the theory of plasticity determine stresses assuming that plastic failure is fulfilled either in the whole mass or along specific lines or surfaces. They can be divided into slip line (*Brinch Hansen (1953); Sokolovski (1960)*), lower bound (*Rankine (1857); Arai and Junk (1990)*) and upper bound methods (*James/Brandsby (1971); Chen (1975)*).

b) Methods based on extreme conditions select a slip surface and then determine the forces acting on the boundaries of the earth mass. The definite slip surface is the one that gives the maximum or minimum earth pressure (*Coulomb (1773); Janbu (1957); Bang (1985)*).

c) Methods based on constitutive soil models can be used to characterised the stress-strain be-
   haviour of a soil. Using the numerical techniques such as FEM the values of stresses and de-
   formations can be found throughout the soil mass. This methods require extensive testing to
   obtain the constants of the constitutive models and access to a sophisticated computer pro-
   gram.

Whatever the method used, the lateral earth pressure on a retaining structure depends on several
common factors. These include: the physical properties of the soil, the time dependent nature of
the soil, the imposed loading, the interaction between the soil and retaining structure at the inter-
face, and the general characteristics of the deformation in the soil-structure composite.

Traditionally, the Rankine´s method is typically used to compute the earth pressure distribution in
normally consolidated cohesive soils. Table 2.2 shows the different formulas (Equations 2.1 to
2.5) used to calculate earth pressure at different state condition and type of analysis, where K_0 is
the coefficient of earth pressure at rest (see section 3.3.2.1), K_a and K_p are the coefficients of ac-
tive and passive earth pressure respectively and depend on the effective friction $\varphi´$, the wall fric-
tion δ and the geometry of the wall and the retained soil, $c´$ is the effective cohesion, $\gamma´$ is the ef-
fective unit weight of the soil, z_a is the depth to the point of interest from surface,
$z_c = 2 \cdot c / \gamma \cdot \sqrt{K_a}$ is the depth to the tension crack from the surface z_p is the depth from bottom of
excavation downward, $\sigma_z´(z)$ is the vertical effective stress at depth z_a, and c_u is the undrained
shear strength of the soil.

Table 2.2:   Formulas for lateral earth pressure calculations

Type of analysis	State	Equation	Equation No.
Effective	Rest	$e_{0h} = K_0 \gamma' z_a$	(2.1)
Effective	Active	$e_{ah} = K_a \gamma'(z_a - z_c)$	(2.2)
Effective	Passive	$e_{ph} = K_p \gamma' z_p + 2c' \sqrt{k_p}$	(2.3)
Total	Active/Passive	$e_h(z) = \sigma_z'(z) \mp 2c_u$ *	(2.4)
Total	Active/Passive	$e_h(z) = \sigma_z'(z) \mp 2\lambda_u \sigma_{vc}'$ *	(2.5)

* (-) Active, (+) Passive

The undrained shear strength c_u is usually normalised by the effective consolidation pressure σ_{vc}'
to give a dimensionless constant λ_{cu}. *Kempfert/Stadel (1997)* rewrote Equation 2.4 by replacing
$c_u = \lambda_{cu} \cdot \sigma_{vc}'$ and the new equation is given by Equation 2.5. λ_{cu} is found to fall within a range of
values for normally consolidated cohesive soft soils (see section 3.4.3.5). The shear strength pa-
rameters required to calculate the earth pressures should be obtained from the corresponding

laboratory or field tests. If the undrained shear strength is obtained from field vane test, the value should be corrected by a factor to account for the effect of the strain rate and anisotropy on the strength of the soil (see section 3.4.3). The choice which type of analysis to use for a particular type of excavation depends on factors such as the construction time, the drainage conditions, the stress path and soil type (see section 3.4.2).

In order to reduce or increase the earth pressure from "at-rest" condition to an active or passive earth pressure state respectively, a certain amount of wall movement is required. The amount of the movement required to activate the active or the passive earth pressure depends on the type of the wall movement pattern. There are four types of wall movements patterns recognised in the literature. These are: rotation of the wall about the toe, rotation of the wall about the top, deflection of the wall, and lateral translation of the wall. Most often, a combination of the above movement pattern may also takes place. The movement required to reach extreme pressures depends on the type and density of the soil. The movement required to reach the passive state is of the order of ten times as large as the movement required to reach the active state (*Clough/Duncan (1991)*). Much experimental work has not been done on the effect of wall movement on earth pressure in clays in general let alone in soft clay. On the other hand, a lot of experimental works have been conducted on sand. *Bijerrum et al. (1972)* stated that the movement of the wall required to reduce the lateral pressure in soft to medium clays to its active value is of the same order of magnitude as those observed in sand and amounts to 0.1 - 2% of the depth of excavation. After revising different model studies on sand, *Weissenbach (1985)* agreed that a minimum average value of wall movement of 0.1% of the depth of excavation is required to reduce the pressure from rest condition to active state. He further asserted that for soft cohesive soils the normal wall movements are sufficient enough to reduce the lateral earth pressure to its active state. *Das (1987)* indicated that the amount of wall movement required to reach the passive state in the case of rotation of the wall about the bottom of the wall in soft clay is about 5% of the depth of penetration.

The type of wall movement pattern will also have an influence on active and passive pressure distributions. Figure 2.3 shows the distribution of active earth pressure for different wall movements in an excavation supported by sheet pile wall. Except for the case of the fixed end cantilever wall (Figure 2.3a), the earth pressure distributions deviate from that of Rankine. These differences are mainly caused by the arching effect as a result of non-uniform deformation of the soil mass. In a braced excavations the amount of arching is controlled by the magnitude of deformations in the soil beneath the excavation relative to those of the struts (*Bijerrum et al. (1972)*). For tied back flexible sheet pile walls, the amount of arching is controlled by the deflected shape of the wall and anchor yield. It increases with increasing deflection of the wall and decreases with an increase in anchor yield. A typical active earth pressure distribution in a tie-back wall is shown in Figure 2.4. As it can be seen from Figures 2.3 and 2.4, the total resultant active pressure

is approximately equal to the resultant of the Rankine active earth pressure calculated over the entire depth of the wall, provided that the wall movements are large enough to induce active earth pressure state (*Bijerrum et al. (1972); Mana (1978)*).
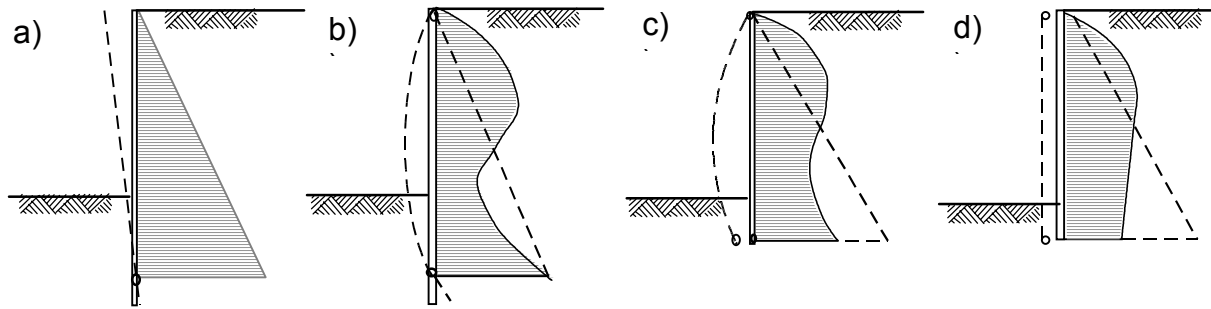
Figure 2.3:   Effect of wall movement on active earth pressure distribution behind a sheet pile wall: a) fixed end cantilever wall, b) fixed end and supported at the top of the wall, c) free end and supported at the top, and d) free end and supported at several positions (after *Weissenbach (1985)*)

Collective works of different Authors on the effect of wall movement on passive earth pressure distribution in sand can be found in *Weissenbach (1985)*. Most of the works indicate that the passive earth pressure distribution is more or less parabolic; concave downward when the wall rotates about the bottom of the wall (Figure 2.5a) and concave upward when the wall rotates about the top of the wall (Figure 2.5b). For the lateral transition of the wall, the passive distribution remains more or less linear (Figure 2.5c).
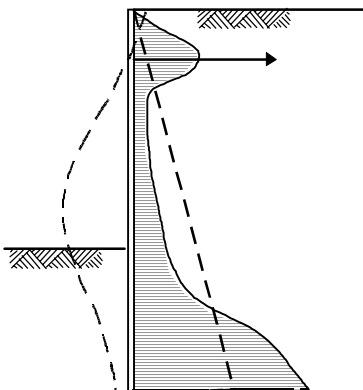
Figure 2.4:
Typical active pressure distribution behind a flexible wall
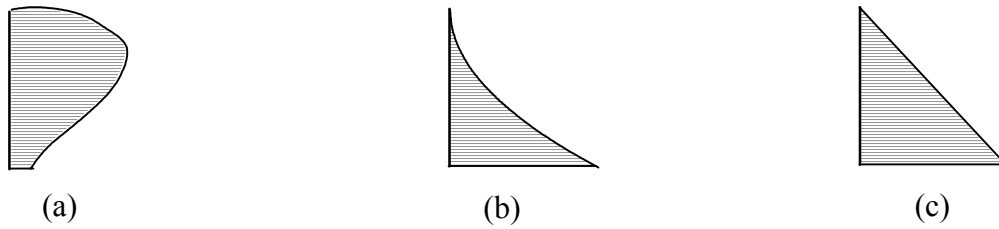
Figure 2.5: Art of the passive earth pressure distributions dependent on the wall movement patterns, (a) rotation about the bottom, (b) rotation about the top, and (c) lateral translation of the wall

2.4.2.2 Reaction forces

The pressure exerted against bracing is different from that usually assumed for retaining walls for the reasons explained in section 2.4.2.1. Most design of braced excavation is made based on empirical methods developed from field tests data. The most widely used load diagram for struts and anchors in soft to medium clay (undrained condition) is that recommended by *Terzaghi/Peck (1967)* and modified by *Peck (1969)* (Figure 2.6). Although several load diagrams have been developed, all versions are based upon the Terzaghi and Peck distributions and are somewhat similar (*Mana (1978)*). The load diagram for rakers, however, follow the classical earth pressure distribution (*Fang (1991)*).

As the excavation depth increases, the stability number of the layer also increases. According to *Terzaghi/Peck (1967)*, a plastic zone begins to form in the clay near the lower corner of the excavation at about N values on the order of 3 to 4, and as N increases the plastic zone enlarges. As a result the wedge behind the cut merges with the plastic zone bounded by a surface of sliding that extends much farther from the edge of the cut and much deeper into the subsoil than normally assumed sliding surface that extends from the ground surface to the lower bottom of the cut. Correspondingly the earth pressure increases. For this reason, Terzaghi and Peck introduced a reduction factor m (Figure 2.6). As far as N does not exceed 4, m can be taken as unity. However, if N exceeds 4 and the plastic zone could form freely below the bottom of excavation, m can be assumed as less than unity. A value of m as small as 0.4 is possible. *Peck (1969)* had modified the above as follows: m = 1 for N < 6 to 8, and m = 0.4 for N > 6 to 8 provided that the soft clay extends to a great depth below the cut. Omitting the reduction factor m and introducing a new stability number N_b for the soil below the cut, *Peck et. al. (1974)* recommended that as far as N_b < 7 the strut loads can be determined from the conventional diagram in Figure 2.6 even for values of N as great as 10 to 12, however, the width of the diagram should not be less than $0.4 \cdot \gamma \cdot h$, regardless of the value of N. When N_b exceeds 7 and base failure is imminent, no recom-

mendation was given except that the strut loads could be much larger than those determined from the conventional diagram. After studying the case of the load diagram using the finite element method, *Mana (1978)* believed that the recommendation by *Peck et. al. (1974)* is reasonable.
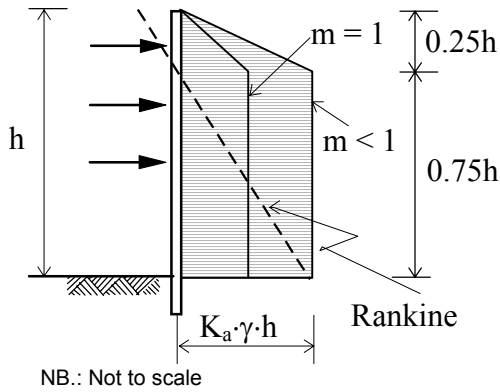
$$K_a = 1 - m \cdot \left(\frac{4 \cdot c_u}{\gamma \cdot h} \right) = 1 - m \cdot \frac{4}{N}$$

m = 1 if N ≤ 4
m < 1 if N > 4
where N is the stability number

Figure 2.6:
Apparent pressure diagram for calculating strut loads in soft to medium clays
(after *Terzaghi/Peck (1967)*)
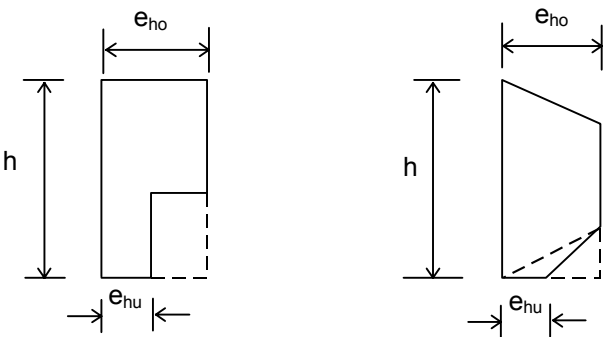
The apparent pressure diagram by Terzaghi and Peck was developed for flexible structures and does not include the effect of the position of the struts or anchors and number of the struts. On the other hand, the German working group "Excavation" (EAB) recommends apparent pressure diagrams that incorporates the influence of the above factors. The shape of the diagram varies from simple rectangular to trapezoidal distribution according to the position of the struts, the number of the struts, and type of the structure. Table 2.3 summarises the (EAB) recommendations for non cohesive and stiff clays. The superposition is based on the assumption that the resultant pressure on the struts is equal to that computed from classical theories. The Working Group is currently drafting a new recommendation for the design and construction of excavations in normally consolidated soft soils.

2.4.2.3   Section forces

According to *Simpson (1992)*, there are two methods of determining the bending moment in the wall. These are: i) The bending moment is calculated by taking the full strength of the soil, i.e., safety factor equal to unity, and multiplying the maximum bending moment by a factor 1.4 or 1.5 for ultimate design of the wall section; or ii) The depth of penetration is determined using the stability requirement, i.e., applying the appropriate factor of safety (see Section 2.4.5) and use the derived bending moment directly for ultimate limit state design. This often gives a higher bending moment than method (i). In Federal Republic of Germany, the second method is usually adopted with safety factor η_p between 1.2 and 1.5 on passive pressure for retaining wall in sands and stiff clays (*EAB (1994)*).

Table 2.3: Apparent pressure diagrams for supported excavations in sand and stiff clays according to the recommendation of *EAB (1994)*

Support condition	Location of the support from the top of the wall	Shape of the apparent pressure diagram	Location of the change in the apparent pressure diagram	e_{ho}/e_{hu}	
				Soldier piles	Sheet piles and cast in-situ walls
a) single support 1	$\leq 0.1 \cdot h$	Rectangle	uniform	1.0	1.0
2	between $0.1 \cdot h$ and $0.2 \cdot h$	Two rectangles	$0.5 \cdot h$	>1.5	>1.2
3	between $0.2 \cdot h$ and $0.3 \cdot h \cdot$	Two rectangles	$0.5 \cdot h$	>2.0	>1.5
b) double support 1	when the first support is near the top of the wall and the second support is within the top half of the excavation dept	Two rectangles	at the second support positions	2.0	1.5
2	when the first support is near the top of the wall and the second support is about half of the excavation depth	Trapezoid	at the first and the second support positions	∞	2.0
3	when both struts are located at lower position	Rectangle or trapezoid	uniform for soldier piles; at the second support position for sheet pile walls and cast in-situ walls	1.0	1.0
c) three or more supports	equally spaced supports	trapezoid	at the second and the third support positions for walls with three supports; at the second and the forth support positions for walls with more than three supports	∞	2.0

NB: 1) The hidden lines show the possible shapes of the apparent pressure diagram for different loading and/or wall types.

2) The ordinates e_{ho} and e_{hu} are determined in such a way that the resultant force from theoretical pressure distribution will be equal to the resultant force from the apparent pressure diagram.

Due to the fact that the earth pressures on flexible sheet piles are different from those predicted by the classical earth pressure theories, the moments in the wall are smaller than the classical theories would indicate. *Rowe (1952/1955)* introduced a reduction factor based on the flexibility of the wall to reduce the maximum bending moment in the wall for excavations in sands, if the bending moment is calculated on the basis of the classical earth pressure distributions. *Skempton (1953)* suggested that no moment reduction is required for walls in clays. *Powrie (1997)* also commented that Rowe's moment reduction factor may be unsuitable for walls in clays where the in-situ earth pressure coefficient is high, because of Rowe's analysis assumes an active state in the retained soil. There is no information, however, how to apply the reduction factors for walls in soft clays or the safety factors to determine the bending moment, and thus requires a further

study. At present, the "Working Group on Excavation" (EAB) of the German Society of the Geotechnical Engineering is drafting a new recommendation for excavations in soft soils

2.4.3   Movements in and around an excavation

2.4.3.1   General

Ground movements in and around excavations are caused by changes in stress field in the surrounding material primarily due to the horizontal and vertical relief of stresses. The horizontal stress relief leads to horizontal movement of the wall and settlement of the ground around an excavation where as the vertical stress relief at the base of an excavation can give rise to both heaving of the soil beneath the base of the excavation and lateral movement of the wall. Moreover, driving, drilling and grouting, lowering of ground water, overexcavation, inadequate support, timing, unpredicted traffic etc. may contribute to the total ground movements.

Ground movements can be categorised as horizontal movement (usually known as the displacement of the wall), vertical ground movement (settlement behind the wall), and heaving of the bottom of the excavation.

2.4.3.2   Horizontal movements

The horizontal movements are very much a function of the mode of deformation of the wall. The mode of deformation of the wall in turn is a function of the support system, the properties of the ground and construction practice. The designer of lateral support can take account of the first two of the above factors in predicting deformations, however, factors related to construction activities tend to be unpredictable as they often arise in response to the conditions encountered on site during the excavation of the work.

The stiffness of the support system may be considered in terms of the lateral (struts, anchors), flexural (wall system) and the vertical (wall system, anchors) stiffness components. Each support system possesses a combination of these components which determines both the magnitude and shape of the deflection. Where a system with a high lateral support stiffness is used, much of the deformation at any level within the retained ground occurs prior to installation of the lateral support and is governed by the flexural stiffness of the wall and the ground property. *Burland/Hancock (1977)* reported that 75 to 85 % of the observed total deformation at any depth of excavation occurred prior to the installation of the prop at that level for diaphragm wall propped by the floors of the permanent structure. Similar phenomenon was reported by *Day (1994)*, in

which significant deformations (more than 50%) were observed prior to support installation particularly over the lower half of the face in an excavation supported by soldier piles with anchor system. The movement of the ground after installation of the lateral support is governed by the horizontal stiffness of supports (*Day (1994)*). This depends not only on the stiffness of the lateral support elements but also on the point at which the load is transferred to the soil.

A significance difference in performance can also be expected between support systems where the wall is installed prior to commencement of excavation and those where the wall is constructed hand-over-hand as excavation progresses. In the case of hand-over-hand excavation, the ground movement prior to the installation of wall and support highly depends on the stiffness of the soil.

The maximum horizontal deflection of the wall can be related to the depth of excavation as shown in Figure 2.7. According to *Clough/O'Rourke (1990)*, on average the maximum horizontal deflection of the wall in stiff clays, residual soils and sands is about 0.2% of the depth of excavation, but there are cases where it becomes 0.5% or more. No significant differences are noted between the different type of walls in Figure 2.7.

2.4.3.3   Ground settlement behind the wall

The prediction of the ground settlement behind the wall is very important as it is directly related to the safety of the nearby structures. The ground settlement behind the wall is generally caused by one of the following:
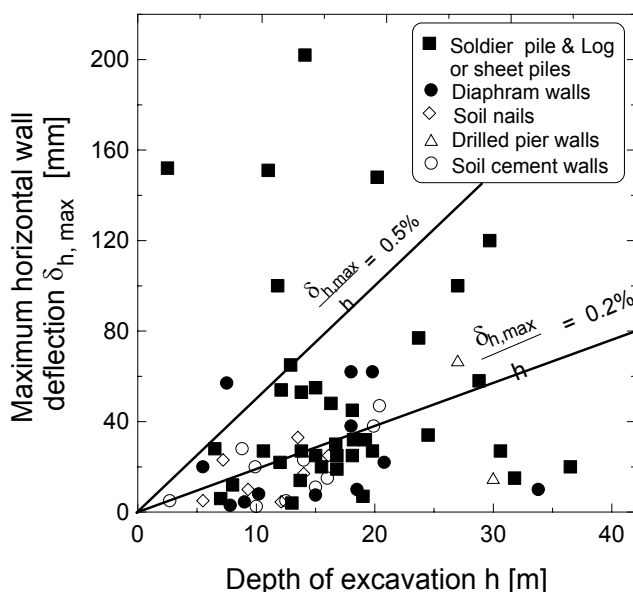
Figure 2.7:

Observed maximum horizontal deflection of wall for various wall types in stiff clays, residual soils and sands (After *Clough/O'Rourke (1990)*)

a) Ground settlement induced by wall deflection during excavation:

During excavation, the relief of horizontal stresses results in inward movement of the ground and the wall. The horizontal movement of wall results in the settlement of the ground behind the wall. The magnitude of the surface settlement in fact depends on the type and stiffness of the support, position of the support, and on the stiffness of the wall. For example, if the wall is permitted to deflect as a cantilever (Figure 2.8a), the horizontal movement can be greater than the settlements (*Burland et al. (1979)*), and the maximum settlement usually takes place directly behind the wall. On the other hand, if the wall is well propped near the surface (Figure 2.8b), inward movements will usually takes place at a deeper depth. In such cases the horizontal surface movements will be significantly less than the settlements, and the maximum settlement may take place further from the wall. In both cases the settlement profiles can be viewed as nearly parabolic curves joined by tangent lines or inflection points that can be divided into two categories: concave downward (hogging) and concave upward (sagging) (*Boone (1996)*).

Clough/O'Rourke (1990) reported that the maximum horizontal wall movement is considered to be about 0.2% (Figure 2.7), while the average maximum settlement is about 0.15% (Figure 2.11) of the depth of excavation. This shows that the maximum settlement is about 75% of the wall maximum horizontal movement in a braced diaphragm or bored pile walls. They also reported that in the case of soldier piles with wood lagging or sheet piles, substantial settlement occurred behind the wall. On the other hand, *Duncan/Bentler (1998)* showed that there is a wide variation in the ratio between the maximum vertical settlement $\delta_{v,max}$ and maximum horizontal settlement $\delta_{h,max}$. The ratio $\delta_{v,max}/\delta_{h,max}$ varies widely from 0.25 to 4.0. This wide variation is an indication of the importance of construction procedure and construction details. Factors that contribute to large settlements do not necessarily produce large horizontal movements, but the reverse is always valid, i.e., factors that contribute to large horizontal movement may produce large settlement.
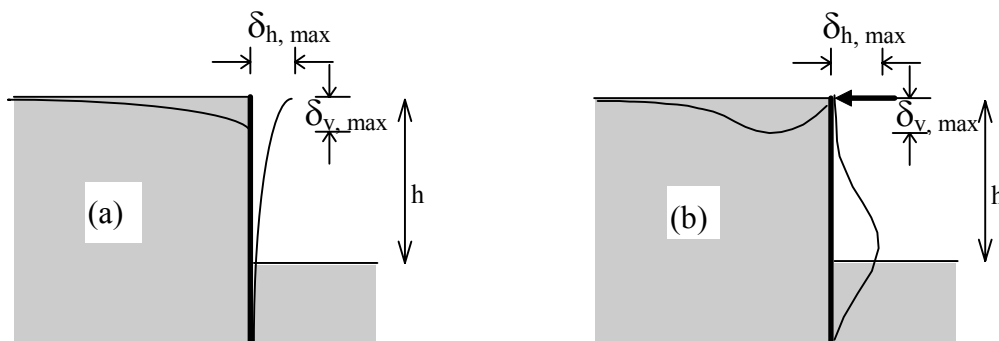
Figure 2.8:   Horizontal deflection and settlement pattern of a retaining wall: a) cantilever wall, and b) propped wall

b) Ground settlements induced by wall installation:

Excavation walls may be of either a displacement or a replacement type. Displacement type walls are typically placed by driving either steel or pre-cast concrete sections into the soil. It is unlikely that the driving of commonly used sheet piles sections will lead to a significance change in in-situ horizontal stress conditions. However, some ground settlements are usually observed during driving or vibrating the sheet piles, and in case of temporary support, during removal of the sheet pile walls after completion of the excavation. *Fujita (1994)* reported that about 50% of the total settlement of the ground 2.5 m behind the wall in a 14.65 m deep braced excavation was caused during driving and extracting of the sheet piles.

On the other hand, the excavation of diaphragm wall panels or bored piles is certain to result in significant total stress relief, because during formation of the wall a hole, unsupported or sup-ported by bentonite slurry, must be excavated in the soil. The total horizontal stresses on the boundary of this hole will reduce from the initial in-situ horizontal total stresses in the undis-turbed soil to either zero if the hole is unsupported, or to a value which approximates to pressure exerted by a fluid with the same bulk density as bentonite (*Gunn/Clayton (1992)*). This reduction in the total horizontal initial stresses may result in a ground movement. Moreover, the vibrations produced during boring and excavating the slurry trench may contribute to the ground move-ments. *Burland/Hancock (1977)* reported that the vertical and horizontal ground movements out-side the excavation due to the installation of the diaphragm walls and piling amounted to ap-proximately 50% of the total movements recorded on the completion of the main design in Lon-don clay. Similarly, *Lehar et al. (1993)* reported that about 60% of the total settlement at the ground surface was due to the installation of the diaphragm wall constructed in Salzburg lacus-trine soft clay. After studying the performance of diaphragm wall at different sites, *Clough/O'Rourke (1990)* also reported that the ground settlements caused by the installation of diaphragm walls, with the exception of few cases where heaving was observed, ranges from about 5 to 15mm. Figure 2.9 shows the settlement envelope caused by the installation of dia-phragm walls. *Poh/Wong (1998)* had observed a maximum settlement of 23.5 mm and a maxi-mum lateral movement of 45 mm during trench excavation in a well instrumented 55.5 m deep field trial test diaphragm wall in predominantly soft soil layer.
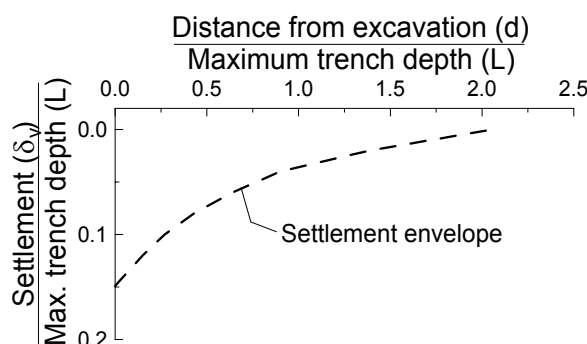
Figure 2.9:

Ground settlement caused by installation of diaphragm walls (after *Clough/O'Rourke (1990)*)

c) Ground movements induced by anchor installation:

Similar to the wall installation, a hole is required to install the anchor tendons. The amount of ground movements depend on the method of drilling and material used for temporal support of the boring process. The effect can be considerable when anchoring is made in soft cohesive soil under ground water conditions. More than 70% of the total settlement was recorded during the installation of the anchor in an excavation in lacustrine soft soil in Constance, Germany (see Section 8.3.4 and *Kempfert/Gebreselassie (1999)*).

d) Ground movements induced by dewatering

The contribution of dewatering to the settlement of the ground is evident. Normally consolidated clays may settle to a far greater extent in response to dewatering than clays heavily consolidated. *Schweiger/Breymann (1994)* reported that about 75% of the settlement of the ground at the surface was occurred during the lowering of the ground water in an excavation supported by diaphragm wall in Salzburg lacustrine soft soil.

Thus, the total ground settlement is the sum of the settlements induced by all of the above factors. The prediction of ground movements may be made using finite element method. With the use of realistic input soil parameters and modelling the detailed construction technique and sequences, a reasonable prediction of the ground movements may be made. Some of the effect of the above factors can be taken into account in the analysis of ground deformations using finite element method. For example, *Gunn et al. (1993), De Moor (1994), Ng et al. (1995), Schweiger et al. (1995), Gourvenec/Powrie (1999)* and *NG/Yan (1999)* showed how to model the effect of wall installation. However, the effect of vibrations, overexcavations, delay and inadequate support, and unpredicted traffic near the excavation is difficult to take into account in the analysis of ground deformations.

Empirical methods can also be employed to estimate ground movements behind an excavation wall from graphical summaries of information from previously instrumented cuts. *Peck (1969)* was the first to present a summarised study of the observations of vertical movements around a number of braced excavations in various soil types in graphical form (Figure 2.10). According to this figure, the size of the settlement behind the wall varies according to the three categories of ground. In other words, for average workmanship, the maximum settlement is less than 1% of the depth of the excavation in sand and soft to hard clay, and is more than 2% in case of very soft to soft clay with a significant depth.
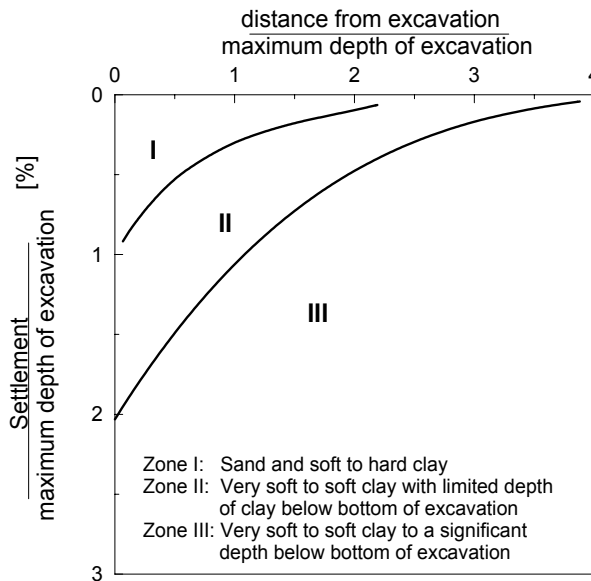
Figure 2.10: Summery of surface settlements adjacent to braced excavation in various soils (after *Peck (1969)*)
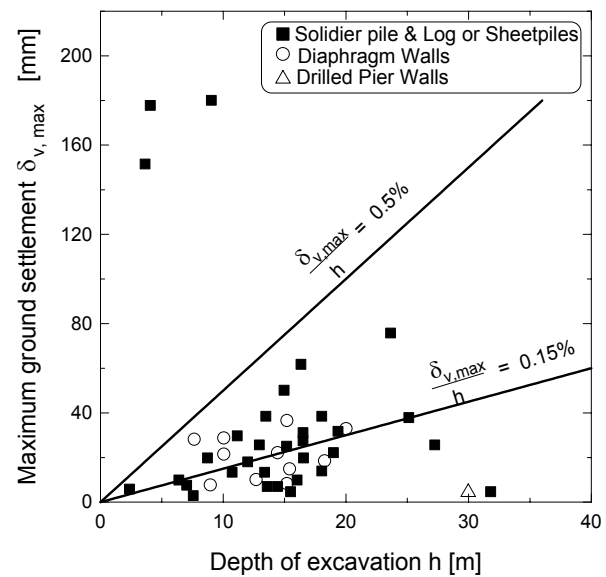
Figure 2.11: Observed maximum settlements adjacent to excavations (after *Clough/O'Bourke (1990)*)
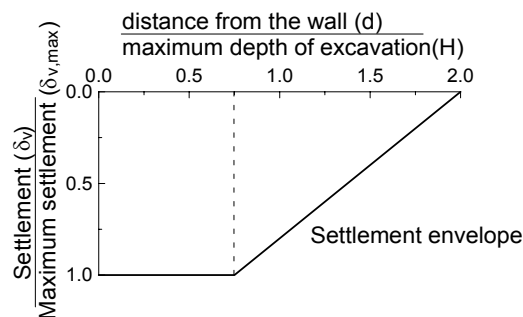
Figure 2.12:

Dimensionless settlement profile recommended for estimating the distribution of settlement adjacent to excavation in soft to medium clays (after *Clough/Bourke (1990)*)

However, with the development of recent design and construction technologies, and frequent usage of more stiffer walls such as diaphragm and bored pile walls, the magnitude of ground movement has generally declined. *Clough/O'Bourke (1990)* showed that on average $\delta_{v,max}/H$ is about 0,15% (Figure 2.11) and $\delta_{h,max}/H$ is about 0.2% (Figure 2.7). They produced a dimensionless ground surface settlement envelope for estimating the distribution of settlement adjacent to an excavation in soft to medium clays as shown in Figure 2.12. According to this figure, the vertical movement may extend from the edge of an excavation to a distance twice the depth of excavation for soft to medium clays. In Peck's diagram (Figure 2.10), however, the influence extends as far as 2 to 4 times the depth of excavation in very soft to soft soils. *Fujita (1994)* also quoted a report from *Uchida et al. (1993)* that a maximum settlement of 0.08% the depth of the excavation had occurred in a 36.6 m deep excavation in soft ground in Tokyo. *Duncan/Bentler (1998)* sum-

marised the performance of excavation in soft to stiff clays since 1960 and showed that the average value of $\delta_{v,max}/H$ was 1.3% for the 1962-1975 time period, where as for the 1990-1998 time period $\delta_{v,max}/H$ was about 0.4%.

2.4.3.4 Excavation heave

Bottom heave in an excavation in normally consolidated soft soils is primarily caused by the elastic swelling of the bottom of excavation due to the relief of vertical stresses during the excavation process, the deflection of the foot of the wall which pushes the soil inwards, and the plastic deformation of the soil below the excavation level due to the change of the principal stresses. The factors that affect the heave at bottom of the excavation include the depth of excavation, the stiffness (primarily) and strength (secondarily) of the ground, and the depth to the firm layer below bottom of excavation.

The elastic part of the heave δ_{vh} can be predicted analytically from the equations shown in Table 2.4. The main difference between the three equations in Table 2.4 is that *Weissenbach (1977)* assumes the un/reloading modulus of elasticity instead of the modulus of elasticity for primary loading. Moreover, equation 2.7 takes into account the contribution of the horizontal displacement of the foot of the wall to the heave of the cut. This approach seems more reasonable because the soil below the cut is under unloading condition during excavation.

Table 2.4:   Prediction of the elastic part of the heave at the center of an excavation

Equation	Equation No.	Reference
$\delta_{vh} = \mu_1 \cdot \mu_2 \cdot \dfrac{N}{\xi}$	(2.6)	*Bijerrum et al. (1972)*
$\delta_{vh} = \dfrac{4 \cdot i_{si} \cdot \gamma \cdot h \cdot \Delta z}{E_{ur}} + \dfrac{3 \cdot s_d \cdot t}{b}$	(2.7)	*Weissenbach (1977)*
$\delta_{vh} = C_r \cdot \Delta_{strip} \cdot \dfrac{\gamma \cdot h^2}{E_u}$	(2.8)	*Fang (1991)*

where δ_{vh} is the elastic vertical heave at the centre of the excavation; μ_1 and μ_2 in equation 2.6, i_{si} in equation 2.7, and Δ_{strip} in equation 2.8 represent the effect of the width of excavation, depth of excavation, and depth to a firm strata, though they are referred to different charts or tables according to the corresponding Authors; $N = \gamma \cdot h/c_u$ or in the case of a surcharge load p (*Clough/Schmidt (1977)*), $N = (\gamma \cdot h + \gamma \cdot p)/c_u$ is the stability number; ξ is a constant that relate the undrained shear strength with the undrained modulus of elasticity ($E_u = \xi \cdot c_u$, and ξ usually lies between 200 and 800 (Table 3.9) for normally consolidated soft clays); Δz is the thickness of the soil below the cut; t is the depth of penetration of the wall; s_d is the horizontal displacement of the foot of the wall, C_r is a shape factor, E_u and E_{ur} are the undrained modulus of elasticity for loading and unloading.

The stress path method (*Lambe (1967); Lambe/Marr (1979)*) may also give reasonable estimate of the heave of the cut provided that a stress path test can be conducted in laboratory that simulate the possible stress path in the field. This method also requires the stress history of the soil deposit. Of course the best means of prediction the heave in an excavation today is the finite element method, where the heave due to stress relief, plastic deformation of the soil and the wall displacement and deflection at the foot of the wall can be evaluated simultaneously by choosing the appropriate soil behaviour model.

2.4.4   Excavation stability in soft soils

The stability failure modes: the failure of berm and slopes surrounding the excavation, deep-seated rotational type failure and basal heave failure are among the possible mode of failure in an excavation in soft clays shown in Figure 2.2. Most often, the stability failure may not show a complete collapse, rather manifests itself in large movements. The stability of berms, slopes surrounding excavations, and deep-seated rotational failure can be checked using the common type of conventional slope stability analysis methods.

However, a special procedure is usually adopted to check the stability of an excavation against basal heave failure. Heave failure is caused by the relief of the vertical stress during excavation. Several basal heave analysis methods have been suggested in literature, however, only four of them will be presented here, because most of them are based on similar principles. *Terzaghi (1943)* was the first to develop a method for bottom heave analysis for shallow or wide excavation (*h/b < 1*) as shown in Figure 2.13. For *r > b*, the factor of safety against basal heave is given by

$$F.S. = \frac{5.7 \cdot c_u}{h \cdot \left(\gamma - \frac{c_u \cdot \sqrt{2}}{b} \right)} \qquad (2.9)$$

and for *r < 0.7b*

$$F.S. = \frac{5.7 \cdot c_u}{h \cdot \left(\gamma - \frac{c_u}{r} \right)} \qquad (2.10)$$

where c_u is the undrained shear strength of the soil, γ is the unit weight of the soil, and *h, b*, and *t* are the depth of the excavation, the width of the excavation and the depth to firm layer respectively as shown in Figure 2.13.

Later, *Bijerum/Eide (1956)* developed a method for bottom heave analysis for deep strutted excavations in soft clays (Figure 2.14a). It is given by

$$F.S. = \frac{N_c \cdot c_u}{h \cdot \gamma + p} \tag{2.11}$$

where N_c is the bearing capacity coefficient (Figure 2.14b) and p is the surcharge load. Both methods above are developed based on the principles of bearing capacity failure of the clay below the excavation level while neglecting the effect of support flexibility above the excavation level and the influence of the stiffness and depth of the wall below the excavation.

Based on similar principle as the above methods but assuming different shape of the failure zone (Figure 2.15), considering the friction force between the moving block above the excavation level and the rest of the retained soil, and taking into account the depth of penetration of the wall, *Weissenbach (1985)* formulated the safety factor against basal heave failure as:

$$F.S. = \frac{P_G + R_v}{G + P} \tag{2.12}$$

$G = b_g \cdot (h + t) \cdot \gamma$, $P = p \cdot b_g$, $R_v = E_{av} + K_v$, $E_{av} = E_{ah} \cdot /tan\varphi /$, $K_v = c \cdot (h + t)$,
$P_G = (\gamma \cdot t \cdot \lambda_t + \gamma \cdot b_g \cdot \lambda_b + c \cdot \lambda_c) \cdot b_g$, E_{ah} is the horizontal earth pressure force on the right side of the sliding block (Figure 2.15), and λ_t, λ_b and λ_c are the bearing capacity coefficients according to *DIN 4017-1*.

Since the determination of the values of G, P and P_G require the value of b_g which is unknown, the factor of safety should be calculated for different value of b_g until a minimum safety factor is obtained. According to *Weissenbach (1985)*, the length of the failure surface $l_g \leq b + 0.5 \cdot b_g$ (Figure 2.15) is the critical situation and $l_g \geq b + 0.5 \cdot b_g$ is impossible.

On the other hand, *Kempfert/Stadel (1997)* proposed a method based on the principal of virtual work done for analysing the basal heave failure in wide excavations ($h/b < 1$) in normally consolidated soft clays. The failure mechanism is shown in Figure 2.16. The safety factor against basal heave is thus given by

$$F.S = \frac{c_{u1} \cdot (3 \cdot t + h) + 6.87 \cdot r \cdot c_{u2}}{r \cdot \sqrt{2} \cdot (h \cdot \gamma_r + p)} \tag{2.15}$$

where c_{u1} and c_{u2} are the undrained shear strength of the soil above and below the excavation level respectively. *Kempfert/Stadel (1997)* recommended that the value of c_{u1} on the passive side should be reduced by half in order to account for the effect of the inherent anisotropy on the strength of the soil. They further suggested that if the wall is made up of bored piles and the firm

strata is at relatively shallow depth below the excavation level, it is recommended to extend some of the piles up to the firm layer in order to reduce the danger of the basal heave failure.
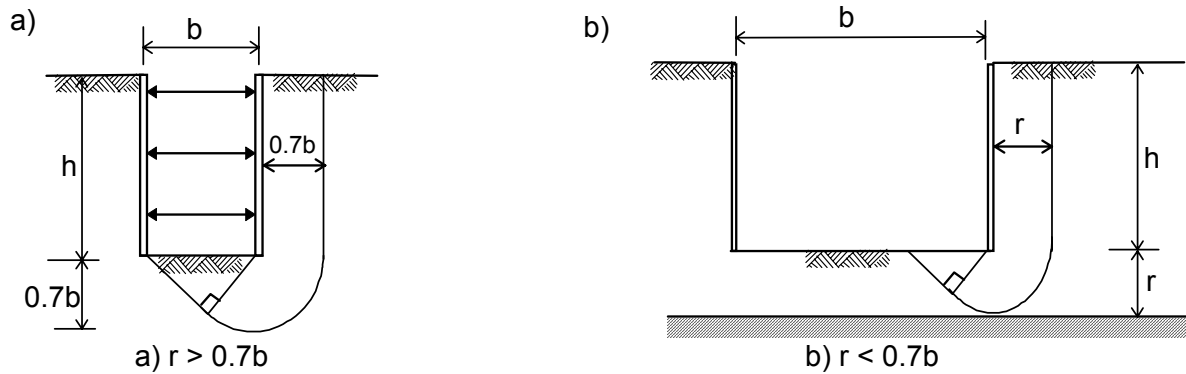
Figure 2.13: Bottom heave analysis for deep excavations (*h/b < 1*) (after *Terzaghi (1943)*)
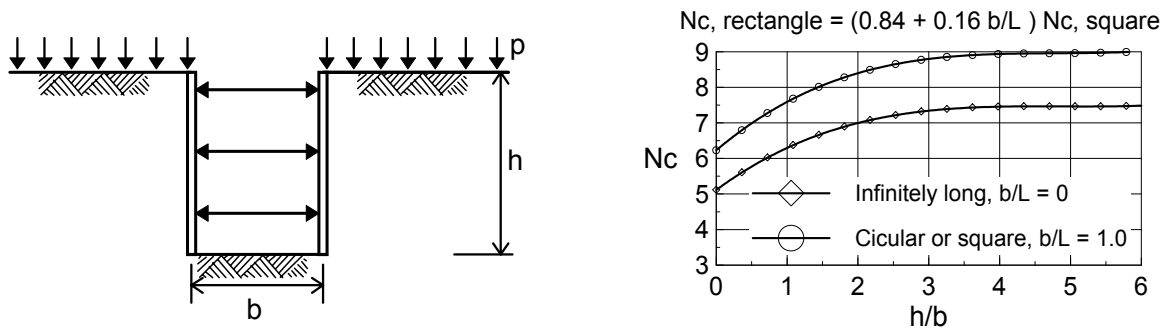
Figure 2.14: Bottom heave analysis for deep excavations (*h/b > 1*) (after *Bijerrum/Eide (1956)*)
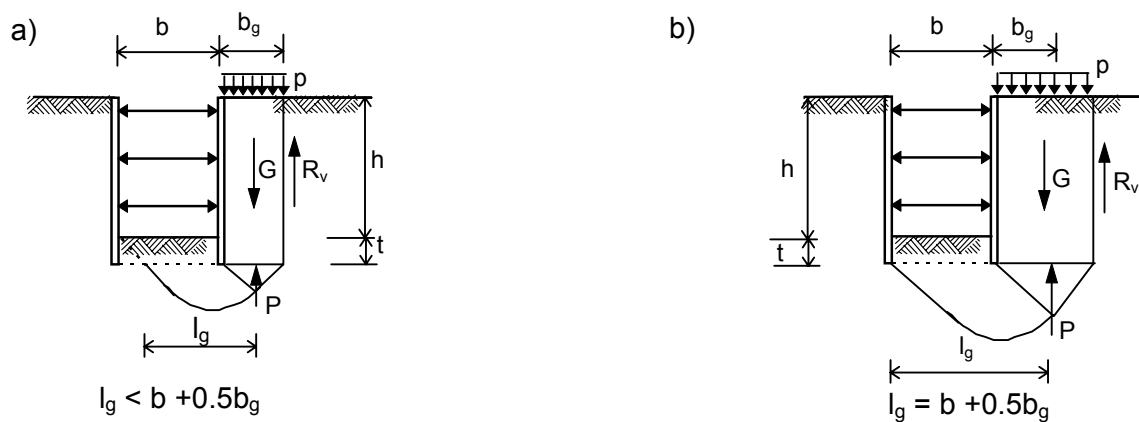
Figure 2.15: Failure mechanism for basal heave analysis (after *Weissenbach (1977)*)
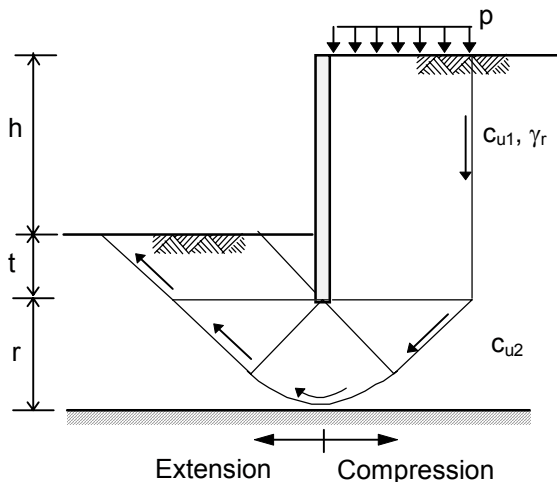
Figure 2.16:
Failure mechanism for basal heave analysis (*Kempfert/Stadel (1997)*)

2.4.5   Safety factor in the design of retaining structures

In the design of retaining structures safety factors are applied on one hand in order to account for the uncertainty in applied load, soil strength parameters, ground water conditions and soil geometry, on the other hand to provide a margin of safety against failure, and to keep deformations with in acceptable limit. Most design of retaining walls are based on either working stress method (total factor of safety) or limit state method (partial factor of safety).

Figure 2.17 illustrates the different methods employed in retaining wall design, where the shaded part of the pressure diagram shows those forces contributing to the resisting and mobilising moments after applying the corresponding factor of safety. These methods are:

1. Factor of safety on passive earth pressure: This method is based on Terzaghi's finding that passive pressure require more movement to mobilise it than did active pressure. Hence, the passive pressure used in design is reduced by a factor η_p (Figure 2.17a). Values of η_p between 1.5 and 2.0 are usually employed (*CP2 (1951); EAB (1994)*).

2. Factor of safety on net total passive pressure: The design condition in this method is such that the moment of the net active forces should not exceed a fraction of $1/\eta_{np}$ of the moment of the net passive force (Figure 2.17b). η_{np} is a load factor and a value of 2 is normally adopted (*Burland et al. (1981)*).

3. Factor of safety on all effective strength parameters: The strength of the soil used in the design is reduced by a factor γ_s (γ_φ, γ_c, γ_{cu}). This has the effect of increasing the active pressure and reducing the passive pressure (Figure 2.17c). Values of γ_φ between 1.25 and 1.5 and γ_c between 1.5 and 2.0 are commonly used (*Burland et al. (1981); Valsangkar/Schiver (1991);*

Clayton et al. (1996)). Eurocode 7 recommends values of γ_φ between 1.2 and 1.25 and γ_c between 1.5 and 1.8.

4. Factor of safety on passive effective strength parameters*:* This is the same as method (3) except that the soil parameters are reduced by a factor of safety γ_{sp} before the passive earth pressure coefficients are calculated (Figure 2.17d) (*CIRIA report No. 54 (1974); GCO (1982)).* Values γ_{sp} between 1.2 to 1.5 are usually used for clays analysed in long terms (*Clayton et al. (1996)).*

5. Increased depth of embedment to provide a margin of safety: One of the simplest methods of ensuring stability of a sheet pile wall is to determine the depth of embedment to achieve limiting equilibrium (i.e. a factor of safety of unity) and multiply it by a factor F_d. Values of F_d usually lies between 1.2 and 2.0 (*Clayton et al. (1996)).* This method was suggested by *Teng (1962)*, and *Tschebotarios (1973).*

6. Revised factor of safety by *Burland et al. (1981)*: This method was developed based on the analogy with a bearing capacity of strip load. The method requires that the moment of activating forces should not exceed a factor $1/\eta_r$ of the moment of the net available passive resistance of the underlying ground (Figure 2.17e). The mobilising moments arise due to earth pressure on the wall above the excavation level and due to the surcharge applied by the soil above the excavation level, where as the resisting moment derives from both the active and passive side of the wall below the excavation level. Values of η_r between 1.5 and 2.0 were recommended by *Burland et al. (1981)*, whereas *Valsangkar/Schriver (1991)* recommended 1.5.

7. Factor of safety on strength parameter and load: This method is proposed by *Meyerhof (1984)* and recommended by *Canadian Geotechnical Society*. It is based on the overload and understrength factors and thus accounts for the uncertainties in applied loads and shear strength parameters. Load modification factors γ_q and γ_{wa} to active force and water pressure in the active side respectively, resistance modification factors γ_r and γ_{wp} to passive force and water pressure in the passive side respectively, and strength factors γ_φ and γ_c for friction and cohesion respectively are employed in the analysis. Common values are: *$f_q = 1.25$, $\gamma_r = 0.8$, $\gamma_{wa} = 1.25$, $\gamma_{wp} = 0.85$, $\gamma_{\varphi'} = 0.8$ ($\varphi'_f = \tan^{-1}[(\tan\varphi')\gamma_\varphi]$ and $\gamma_c = 0.65$ (Meyerhof (1970/82/84); Valsangker/Schriver (1991)).*
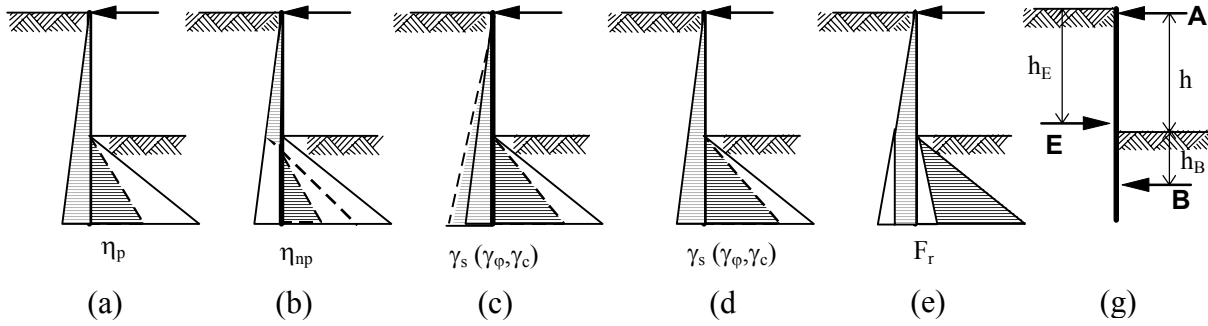
Figure 2.17: Different methods of applying safety factor in the design of earth retaining structures

8. Factor of safety according to *Gudehus/Weissenbach (1996)*: They commented on the partial safety factors on strength and proposed a partial safety factors γ_F to the action forces and η_R on the resisting force. A retaining structure with strut support, for example, can be treated as vertical beam with two supports *A* and *B* (Figure 2.17g). The support forces A and B are assumed to be the nominal action forces and are obtained from the nominal earth pressure E with two equilibrium conditions. The nominal resistance force of the earth support is the passive earth pressure E_p calculated with characteristic soil parameters. Applying the partial safety factor $\gamma_F \approx 1.4$ to B and $\gamma_R = 1.4$ to E_p is the same as the familiar global factor $\eta_p = \gamma_F \cdot \gamma_R = 2.0$. Therefore, according to *Gudehus/Weissenbach (1996)*, the proposed partial factors can be easily related with established global factors with out losing the ample experience suddenly with a new format.

It is clear from the above discussion that there is a considerable difference in applying the safety factors. After carrying a parameter study on the different definitions of the factor of safety in a propped retaining wall, *Burland et al. (1981)* showed that there appears to be no logical or consistent relationship between η_p (method (a)) and the factor of safety on strength γ_s and its use can lead to very conservative values of wall penetration for drained condition with $\varphi' < 25°$ and for undrained conditions. With regard to η_{np} its use with recommended values of about 2 leads to factor of safety on shear strength generally less than 1.1 for both drained and undrained conditions.

Further, *Burland et al. (1981)* showed that method (5) maintains a more or less constant factor of safety for drained conditions in uniform ground, though it is unscientific. However, difficulties and inconsistencies arise when F_d is used in undrained condition or where the strength properties of the ground vary significantly with depth. In undrained analysis, $F_d = 2$ is equivalent to the factor of safety on strength $\gamma_s = 1$ (limiting condition) for all values of undrained strength c_u.

The revised safety factor (method (6)) on the other hand is proved to give results that are logical and consistent with the factor of safety on shear strength for soils ranging from purely frictional to cohesive, for both drained and undrained analysis (*Burland et al. (1981)*).

Valsangkar/Schriver (1991) showed that method (7) will lead to very conservative estimates of the depth of penetration if water pressures are considered on both sides of the wall. However, if net water pressures are used, the estimated depths of penetration will be comparable with those estimated in method (1).

Though the concept of the factor of safety with respect to passive failure of the toe of an embedded retaining wall is widely used in design and has the attraction that the overall stability can be expressed by a single factor, the above discussion shows that the most consistent approach is to apply the factor of safety to the soil strength directly (limit state design method); in particular for normally consolidated soft clays, where the effective angle of friction is usually less than 30° and its undrained strength plays its own role. Recently this method is adopted by standard code of practices (*Eurocode 7-1 DIN V ENV (1997); BSI BS 8002 (1994)*). A further investigation, however, is required to study the relationships and differences between the different method of applying the factor of safety by considering layered soils, interaction between the retained soil mass and the wall, ground water flow, and support conditions.

Moreover, the limit state method implicitly assume that displacements will be a secondary problem, related only to minor serviceability limit states. However, in the case of retaining walls displacements may be larger than normally expected in concrete or steel structures. If the retained soil supports other structures or services, ground movements could be large enough to cause severe distress to them even though the retaining wall itself is quite stable. The distress may be sufficiently severe to constitute an ultimate limit state (*Simpson (1992)*). *Bolten et al. (1990a, b)* developed a method of relating displacements to the degree of mobilisation of the soil strength, or the strength factor γ_φ. Using this method, *Simpson (1992)* indicated that a strength factor in the range 1.2 - 1.3 will not lead to unacceptable displacements in stiff London clay. A more detailed numerical analysis would be worthwhile to examine the relationship between partial safety factor on strength and displacement in normally consolidated soft clays.

Beside the above mentioned method of applying the safety factor, it is common practice to increase 0.5m or 10% of the retained height for the embedded cantilever wall to account for an unplanned excavation in front of the wall (*BSI BS 8002 (1994)*), and to add a uniform surcharge of 10 kPa on the retained surface to account for unseen loads from equipment and others (*BSI BS 8002 (1994), EAB (1994)*).

Recently, the working group on safety in geotechnics of the German National Institute for standards (DIN) issued a standard norm of safety in geotechnical engineering (*DIN 1054 (2003)*)

based on the partial safety factor concept. This is partially based on the concept similar to the method (3) for limit state *GZ 1C* (loss of the overall safety condition) and partially similar to (8) for the limit state *GZ 1B* (failure of structures and structural elements). The limit sate *GZ 1B* governs the design of supported excavation, and it is given my the general limit state condition

$$E_d = E_k \cdot \gamma_F \leq R_k / \gamma_R = R_d \qquad (2.16)$$

where E_d and R_d are the acting and resisting design stresses (forces) respectively, E_k and R_k are the characteristic acting and resisting stresses (forces) respectively, and γ_F and γ_R are the partial safety factors for acting and resisting forces. The partial safety factors γ_F and γ_R may take different values according to the load cases and type of loads (for example, it differentiates among a live load and a dead load). For the overall stability of the excavation, however, a proof of the safety of the excavation should be carried out based on the limit state *GZ 1C*, where the characteristic shear parameters are reduced according to,

$$tan\,\varphi_d = tan\,\varphi_k / \gamma_\varphi \; and \; c_d = c_k / \gamma_c \qquad (2.17)$$

to give the design shear parameters, where γ_φ and γ_c are the partial safety factors on strength parameters. For proof of the safety factor against overturning, uplift and hydraulic failure, the *GZ 1A* governs the situation. The general limit state looks,

$$F_d = F_k \cdot \gamma_{dst} \leq G_k / \gamma_{stb} = G_d \qquad (2.18)$$

where F_d and G_d are the destabilising and stabilising design forces respectively, F_k and G_k are the corresponding characteristic forces, and γ_{dst} and γ_{stb} are the corresponding partial safety factors.

2.5   Some reviews of finite element analysis on excavations

2.5.1   General

The finite element method is one of the powerful numerical methods available to date to predict the ground movement pattern in and around an excavation. In the last 3 to 4 decades several authors used the finite element method to predict or to back analyse the performance of an excavation. *Mana (1978)* had listed the different works in connection with finite element analysis of excavations. Since then there is a lot of progress in understanding the material behaviour of soils, and the application of the finite element method to geotechnical problems. *Freiseder (1998)* also discussed in his thesis the progress of the finite element analysis of excavations and the corresponding constitutive material models. In the seventies and eighties, the analysis of excavations using the finite element method was mostly made using undrained, linear or non-linear, elastic or

elasto-plastic soil behaviours, but nowadays sophisticated programs are available for both drained and undrained analysis. Several finite element programs that are written specifically for geotechnical purposes are also commercially available.

However, the need to obtain realistic input parameters for a complex soil model, and the need to model detailed construction technique and sequences remain the major challenge in using the finite element method. There is also no fast and hard rule on how to specify the extent of the boundary, the type and number of elements. For these and other unknown reasons there is a large discrepancy in the out put of the finite element analysis of the same problem but calculated by different individuals. A good example is the prediction presented by 18 individuals to the test excavation on sand conducted at the University of Karlsruhe (*Andreas 1997*). According to *Andreas 1997*, there was large discrepancies between the predictions, let alone with the actual field test result. Even those predictions that are calculated using the same finite element program did differ to each other. Another similar example is the comparative finite element analysis of excavation in sand and clay recently made by 7 individuals in request of the German working group "Excavation" (EAB) in which the Author was a participant (*Kempfert/Gebreselassie (2000)*). In these comparative analyses more than 150% deviation from the average value was recorded. The comparative analysis of a 16.8 m deep excavation (*Schweiger (2000)*) made by 14 individuals shows also similar discrepancy among the results. According to *Schweiger (2000),* the main reasons for the discrepancy of the results were the identification of parameters in particular the stiffness of the soil in working state, the application of the laboratory results to the in-situ condition, and modelling in general. These leads to the conclusion for an immediate need for standardising the finite element analysis of excavations. At present there is an effort to standardise the calculations methods by the Working Groups on "Excavation" (EAB) and "Numerics in Geotechnics" (AK 1.6) of the German Society of Geotechnical Engineers. These efforts should be supported with further investigation, especially for excavations in normally consolidated soft clay.

Most excavation are analysed assuming plane strain condition. While plane strain analysis can give reasonable results for excavations with relatively long walls in out of plane direction, its result, however, is questionable for short walls. *Varzi/Troughton (1992)* suggested a wall length in excess of 60 m could be considered to be effectively a plane strain condition. Most often, the size of excavations in built up area for high rise buildings is not greater than 60 m. Moreover, the struts at internal corners, the overlap of anchors at external corners, the arrangements of berm construction, and the excavation and placement of bottom slab in slices demand for a three dimensional analysis in excavations for high rise buildings or underground parks. According to *Moormann et al. (2000)* the plane strain analysis overestimates the earth pressure and the wall displacements around the middle of the excavation.

In the following section the factors that affect the performance of an excavation in view of parametric study using the finite element method in the literature are presented.

2.5.2 Factors affecting the performance of excavations in soft clays in view of finite element parametric study

1. Effect of wall stiffness:

In general, a change of the stiffness of the wall within practical limits for a given soil has negligible effect on the ground movements. (*Palmer/Kenny (1972); Burland et al. (1979); Mana (1978); Zeng et al. (1986); Freiseder (1998)*). *Clough/Tsui (1974)* showed that an increase in wall stiffness by a factor of 32 had resulted in the corresponding reduction of the movements by a factor of 2 only. *Clough/Tsui (1974), Mana (1978), Zeng et al. (1986),* and *Freiseder (1998)* reported increase in the rigidity of the wall results in an increase in the bending moment and support loads. *Potts/Fourie (1985)* and *Potts/Bond (1994),* however, commented that the effect of wall stiffness is rather a function of the initial stress condition. It is higher for soils with $K_0 = 2$ than for soils with $K_0 = 0.5$. For smaller values of K_0, for instance $K_0 = 0.5$, the effect is very small on bending moment and almost negligible on support load.

2. Effect of the lateral support stiffness:

A very stiff lateral support system reduces the deflection of the wall at the support levels and increases strut loads and bending moment accordingly (*Palmer/Kenny (1972); Clough/Tsui (1974); Burland et al. (1979); Mana (1978); Zeng et al. (1986); Freiseder (1998)*). However, surface settlement is inevitable, primary because of the amount of deformation which occurred below the excavation are not affected much by the rigidity of the support.

3. Effect of horizontal support spacing:

The effect of horizontal spacing of support is usually included in the stiffness of the support and separate study is not important.

4. Effect of the vertical distance between the support and bottom of the excavation:

Since most horizontal movement occurs at the embedded portion of the walls between the completion of excavation and the installation of the supports at each level, the magnitude of the load acting on that portion and the type of soil and its properties are closely related to the magnitude of the horizontal movement. In order to reduce the magnitude of the load, it is necessary to reduce the distance between the supports to be installed and bottom of excavation for each level. This should be kept as short as possible whilst allowing the work to proceed (*Fujita (1994)*). On the other hand, *Palmer/Kenny (1972)* reported that vertical spacing of supports is only of moderate importance.

5. Effect of pre-stressing supports:

While pre-stressing of the struts and anchors is desirable to reduce the ground movements, the pre-stress loads should be limited by the yield properties of the soft clay soil (*McRostii, et al. (1972)*). It is suggested that a small amount of pre-stress could be beneficial in ensuring early effectiveness of the supporting system but a large amount of pre-stress may not provide additional benefits (*Palmer/Kenny, 1972; Clough/Tsui, 1974; Mana, 1978*). This is, according to *Palmer/Kenny (1972)*, a consequence of the fact that a great deal of the pile deflection occurs well below the excavation level and pre-stressing primarily affects the active soil mass which in itself does not greatly influence the overall performance of the excavation.

6. Effect of depth of excavation:

It is evident that the surface settlement, wall deflection and bending moment increase with the depth of excavation. All back analysis results and parametric studies confirm this fact.

7. Effect of depth of penetration of the wall

If the depth of penetration is determined on the basis of the stability of the excavation, further increase of the penetration depth will have a minimum influence on the performance of the excavation (*Zeng et al. (1986)*). *Mana (1978)* compared the free end and fixed end wall condition for sheet pile wall and showed that the difference in the ground movement pattern is very slight but the fixed end wall has a slightly larger zone of yielding. He further showed that increasing the depth of embedment slightly increases the bending moment in the embedded portion of the wall where as the earth pressure distribution acting on the expose part of the wall are essentially the same for both free end and fixed end walls.

8. Effect of berms as temporary support

Peck (1969) suggested that the berm size should be as large as possible in order to limit wall and soil movements. *Potts et al. (1993)* had made a parameter study on the berm size and confirm Peck's statement that the greater the volume of the berm, the smaller will be the wall deflections and the movements of the retained ground surface behind the wall. An efficiency up to 65% can be achieved with berm volume equal to 30% of the total excavation volume. Figure 2.18 shows the relationship between the efficiency of the berm in reducing the deformation and its total volume.

On the other hand, *Clough/Denby (1977)* showed that the effect of a berm is not a unique function of the berm size rather it is also influenced by wall stiffness, excavation depth, wall end conditions, and soil shear strength. They reported that at low stability numbers, increase in berm size produce minimal movement reduction, where as at high stability number, increasing the berm size leads to a large reduction in settlements. However, at high stability number, even with large berms, large movements may occur because deep seated movements may take place beneath the berm. As a result the effectiveness of the berm is diminished.
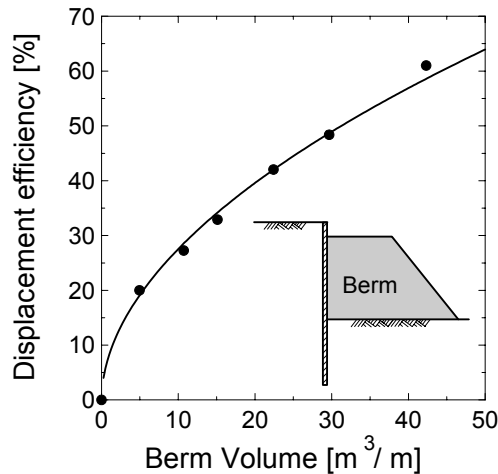
Figure 2.18:

Variation of displacement efficiency with berm volume (after *Potts et al. (1992)*)

9. Effect of soil strength and stiffness:

All back analysis results and parametric study reported in the literature show that primarily the stiffness of the soil and then the shear strength of the soil have the greatest influence on the performance of an excavation. *Palmer/Kenny (1972)*, however, reported that the shear strength do not have significant influence on the behaviour of excavation that was studied. They admitted however, that in the case of excavation with flexible wall, or with stiffer soils, or partially penetrating wall, the soil strength might have greater influence.

10. Effect of in-situ stress (K_0):

There are contradicting views on the effect of the initial stress on the performance of excavation. *Palmer/Kenny (1972)* concluded that K_0 has little influence on the excavation behaviour. On the other hand, by taking a wide range of K_0 (0.5-2.0) in the parametric study and in combination with limit state method, *Potts/Fourie (1985)* and *Potts/Bond (1994)* showed that wall deflection, bending moment of the wall and support load increase as the value of K_0 increases. Recently, *Freiseder (1998)* also indicated that the horizontal wall deflection at the top of a diaphragm wall increases linearly with the increase of K_0, where as the deflection of the wall is almost independent of the value of K_0. Further, he showed that the effect of K_0 is more pronounced on bending moment of the wall, support load and earth pressure. These values increase greatly as K_0 increases from 0.3 to 1.0. *Gunn/Clayton (1992)* also showed that the main reason for the effect of the installation of diaphragm or bored pile wall on the ground movement before soil excavation is the change of the in-situ stresses surrounding the trench or the drill hole. Therefore, the contradicting conclusion of *Palmer/Kenny (1972)* might come from the fact that they had considered a narrow range of K_0 values (0.5 - 0.7), where the effect is very small.

11. Effect of soil-structure interaction:

Freiseder (1998) showed that the variation of the interface reduction factor has insignificant influence on earth pressure and horizontal wall deflection at the wall toe, whereas it has slight influence on the bending moment of the wall and considerable effect on the horizontal wall deflection and vertical displacement of the top of the wall.

12. Effect of width of excavation:

Mana (1978) investigated the effect of width of excavation and showed that the wider the excavation, the larger are the magnitude of ground movements and the size of the yield zones as expected. He also indicated that the predicted zone of yielding are larger than those assumed by *Terzaghi (1943)* (Figure 2.13b), especially on the active side of the wall.

13. Effect of depth to firm layer:

The influence of depth to firm layer is seen to be very important in terms of magnitude and distribution of strut loads (*Mana (1978)*). This is in agreement based on the postulate of *Bijerrum et al. (1972)* (see also section 2.4.2.1), where they said that the increase in earth pressures behind the exposed part of the wall and the resulting large strut load are mostly a function of the soil deformations taking place below the bottom of excavation.

3 Material properties of soft soils - "state of the art"

3.1 General

Since there is such a wide variety of soil types, it is necessary to describe and classify soils in terms which convey their characteristics clearly and concisely, and which are generally accepted and understood by geotechnical engineers and researchers. *Bjerrum (1973)* classify soft clays based on their engineering geological history and emphasising the change in properties which have occurred since their deposition as normally consolidated young clays, normally consolidated aged clays, overconsolidated clays, weathered clays in upper crust, quick clay deposits and cemented clays. In this study, however, the term "soft soil" is defined as clay or silty clay soil which is geologically young, and come to an equilibrium under its own weight but has not undergone significant secondary or delayed consolidation since its formation. It is characterised by the fact that it is just capable of carrying the overburden weight of the soil, and any additional load will result in relatively large deformation. Soils which have not completed the consolidation under their own weight are also included in this group.

The study of soil behaviour may be approached in four main characteristic groups; index properties, compression properties, strength properties and deformation properties under deviatoric loading condition. In the following sections these four main characteristic groups will be discussed.

3.2 Basic index properties of soft soils

The index parameters are a measure of the physical properties and behaviour of a soil. They are generally governed to a large extent by its geological history, mineralogical composition, the amount of clay fraction, the structure and distribution of the grains, texture of the grains. Index parameters are mainly used for the purpose of identification, description and classification of soils. Moreover, since their determination in laboratory is relatively simple, and they share the same factors that influence the strength (Table 3.1) and compression properties, they are usually employed in empirical correlation to predict compression, strength and other parameters. For example, the compression index can be estimated from liquid limit (Table 3.4), the undrained shear strength of clay from liquidity index or plasticity index (Table 3.7). The characteristic groups of the index properties and the corresponding index parameters are listed in Table 3.1.

The principal minerals in a clay deposit tend to influence its engineering behaviour. For example, the plasticity of a clay soil is influenced by the amount of its clay fraction and the type of clay minerals present, since clay minerals greatly influence the amount of attracted water held in a

soil. The undrained shear strength is related to the amount and type of clay minerals present in a clay deposit together with the presence of cementing agents. In particular, strength reduces with increasing content of mixed-layer clay and montmorillonite in the clay fraction (Figure 3.1). The increasing presence of cementing agents, especially calcit enhances the strength of the clay. The principal clay minerals are: kaolinite, halloysite, illite, montmorillonite and chlorite. According to *Scherzinger (1991)*, the lacustrine soft clays in southern Germany are mainly composed of non clay minerals such as carbonate (5-25%), quartz (20-30%), and clay minerals such as chlorite (5-20%), illite (5-10%) and montmorillonite (10-20%).

Table 3.1:   Characteristics and factors hypothesised to have relation with soil strength

Characteristics	Factors considered to have a relation with soil strength
Grain size	Grain size distribution, maximum grain size, mean grain size, coefficient of uniformity, shape of particles, content of fine fraction.
Density	Void ratio, relative density, dry density, specific gravity.
Plasticity	Liquid limit, plastic limit, shrinkage limit, plasticity index, consistency index, liquidity index..
Moisture	Natural moisture content and degree of saturation.
Texture	Type, proportion and structure of minerals and organic matter
Stress history	Age of deposition, number and magnitude of stress change experience, weathering, and physico-chemical effects
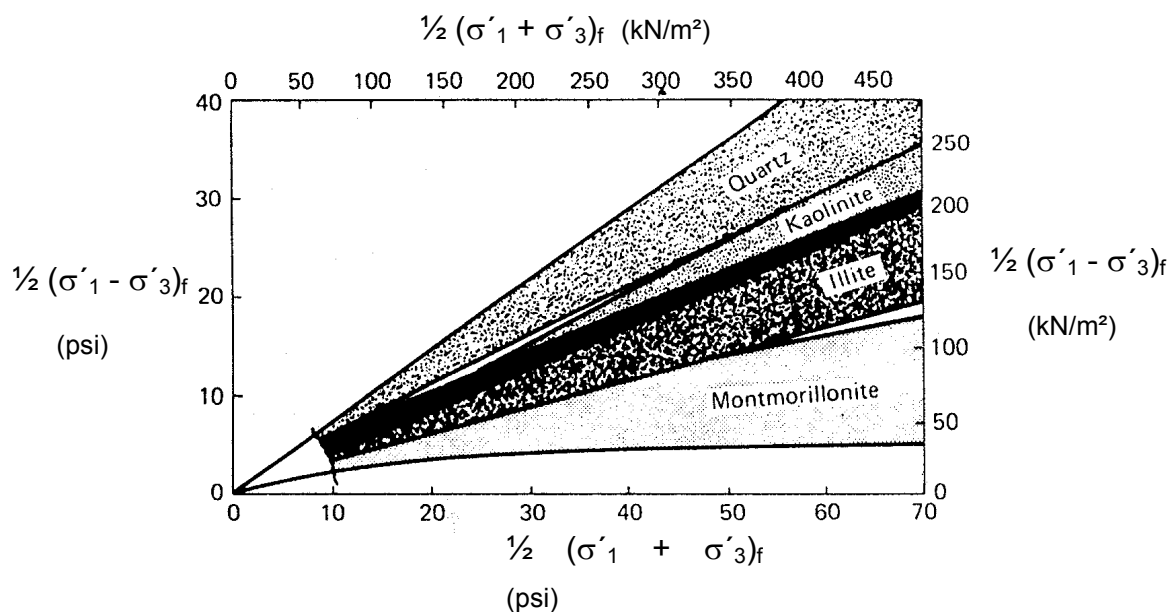
Figure 3.1:   Ranges in effective stress failure envelopes for pure clay minerals and quartz (originally from *Olson (1974)*, reprinted from *Mitchell (1993)*)

Geological age has also an influence on the engineering behaviour of a clay deposit. The porosity, water content and plasticity normally decrease in value with increasing depth, whereas the strength and elastic modulus increase.

The engineering performance of clay deposits is also affected by the total moisture content and by the energy with which this moisture is held. For instance, the moisture content influences their consistency and strength, and the energy with which moisture is held influences their volume change characteristics. The Atterberg limits reflect both the type and amount of clay in a soil. Both liquid and plastic limits are easily determined quantities, and their correlation with soil composition and physical properties have been quite established. The liquid limit and the plastic limit are in effect indicators of the strength of clay at two different water contents of clay. The strength of clay at plastic limit is about 70 - 100 times that at liquid limit. It is generally believed that soils will have almost the same undrained shear strength (1.7-2.5 kPa) at the liquid limit, and different but again constant shear strength at the plastic limit (*Wroth/Wood (1978); Atkinson/Bransby (1978); Mitchell (1993); Powrie (1997)*).
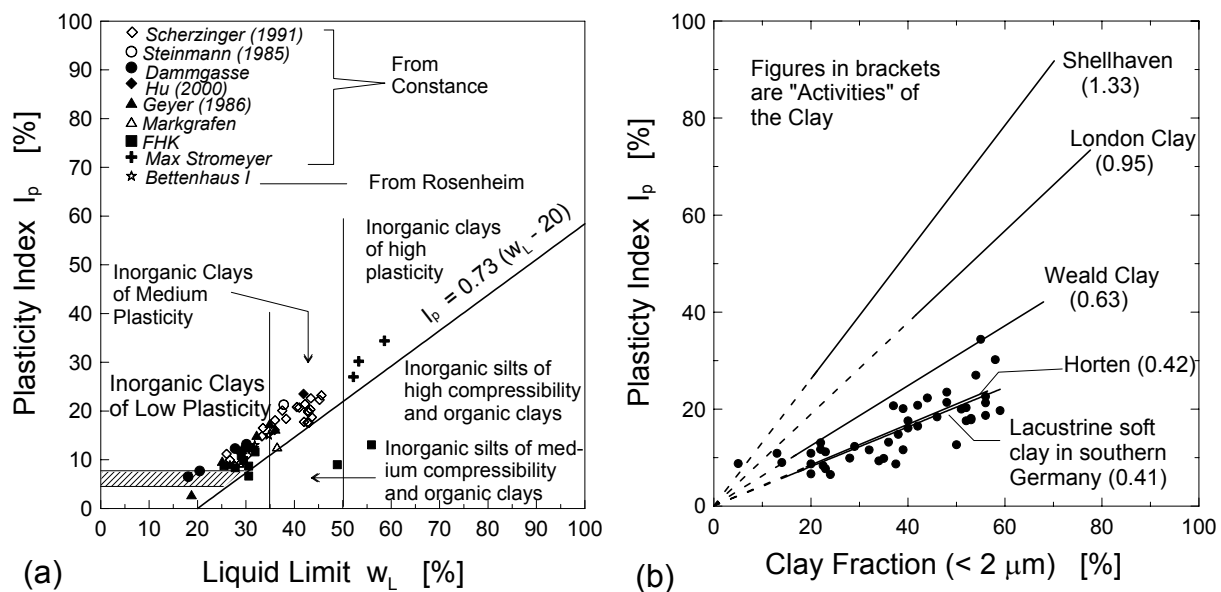
Figure 3.2: a) Plasticity chart (*DIN 18 196 (1998)*), and b) Activity chart (after *Mitchell (1993)*)

A plot of the plasticity index as a function of liquid limit, known as plasticity chart (Figure 3.2a), divides the soils into different groups, and it is an essential part of soil classification system. The data for lacustrine soft soils in south Germany shown in Figure 3.2a, obtained from *Scherzinger (1991)*, Author's own investigation and other sources show that the lacustrine soil lie in the zone of inorganic clay of low to high plasticity except the samples from one location (FHK), where

they lie in the zone of inorganic silts of medium to high compressibility and organic clays and silts (*DIN 18 196 (1998)*). The activity of this soil is also shown in Figure 3.2b. The activity chart is an indication of the influence of the amount of the clay fraction in the behaviour of the soil. The best fit line (Figure 3.2b) for lacustrine soft soils in southern Germany gives an activity value of 0.41, which indicates that the soil is less active. Its consistency varies from very soft (Consistency I_c = -1.46 or liquidity index I_L = 2.46) to stiff (I_c = 1.73 or I_L = -0.73).

3.3   Compression properties of Soft Soil

3.3.1   General

Volume changes in clays may occur:

1) Due to swelling or shrinkage independent of loading. Differences in the period and magnitude of precipitation and evapotransportation are the major factors influencing the swell-shrinkage response of a clay. Generally, kaolinite has the smallest swelling capacity of the clay minerals. Illite may swell by up to 15% but intermixed illite and montmorillonite may swell 60 - 100%. Swelling in Ca montmorillonite is very much less than in the Na variety; it ranges from about 50 to 100%. Swelling in Na montmorillonite occasionally can amount to 2000% of the original volume. One of the most widely used soil properties to predict swell potential is the activity of clay. Figure 3.3 shows the range of the degree of expansiveness of a clay based on the activity. The lacustrine soft clays in southern Germany fall in the area of low expansion zone.
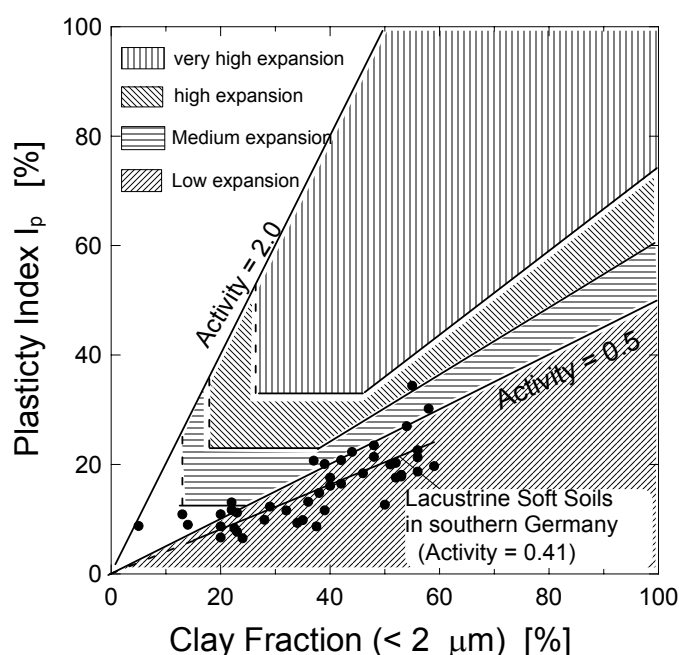
Figure 3.3:
Estimation of the degree of expansiveness of clay soil (after *Bell (1993)*)

Retaining structures built in an unsaturated expansive soil that undergoes substantial changes in volume with changes in water content, require additional attention in the calculation of the earth pressures. The calculation must take into account the additional pressure or suction due to swelling or shrinkage of the soil.

2) As a result of loading and unloading which bring about consolidation and heave respectively. When a load is applied to a clay soil its volume will be reduced, this being principally due to a reduction in the void ratio. If the soil is saturated, the load is initially carried by the pore water which causes an excess pore pressure to develop. The excess pore pressure dissipates at a rate which depends on the permeability of the soil mass and the length of the maximum drainage path, and then the load is eventually transferred to the soil structure (Figure 3.4). The primary consolidation is brought about by reduction in the void ratio due to slippage of the soil particles as the soil skeleton rearranges itself to accommodate higher load. The component of such deformation is described as irrecoverable or plastic.
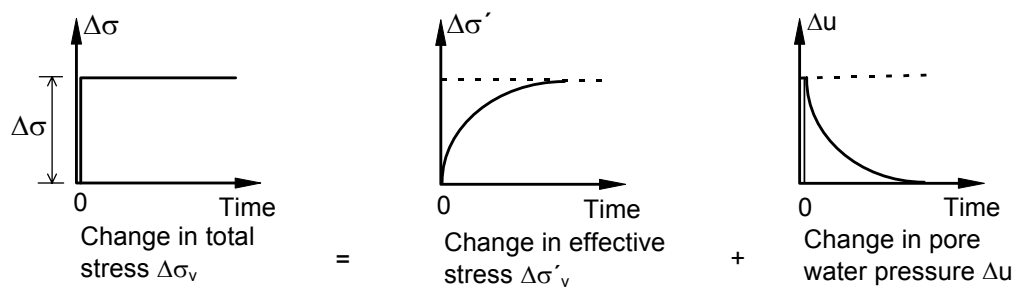
Figure 3.4:   The rate of increase of the vertical effective stress and decrease in pore water pressure during one dimensional consolidation at constant vertical total stress

The heave potential arising from stress release depends upon the nature of the diagenetic bonds within the soil. For example, when an excavation is made in a clay with weak diagenetic bonds, elastic rebound causes immediate dissipation of some stored strain energy in the soil, thus being manifested in certain amount of heave. The component of deformation due to heave (unloading) and reloading is considered as recoverable or elastic, because changes in stress can be accommodated without the need for the rearrangement of the soil skeleton.

Further consolidation may occur due to rearrangement of soil particles or in another word due to the soil creep. Such process is often known as secondary compression. Though in many cases creep deformations are small compared to those due to changes of effective stress, it is necessary to recognise that small time-dependent deformations that are not exclusively due to changes of effective stress. The creep deformation is estimated as large as 5% *(Mitchel, (1993))* of the deformation due to changes of effective stress for normally consolidated soft soils.

3.3.2   One-dimensional compression

3.3.2.1   Primary compression

Soils are compressed by the weight of successive layers of sediments during deposition. During deposition as well as subsequent compression, it is believed that no horizontal strain develop in any element because of symmetry. Therefore, in its natural state, the state of stress of a soil correspond to the state of one-dimensional compression. One-dimensional compression can be simulated in laboratory using odometer, in which the boundary conditions are shown in Figure 3.5.
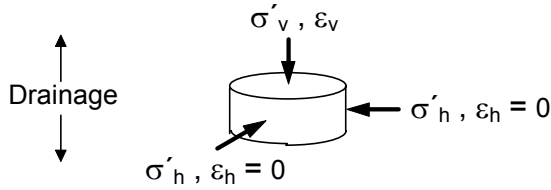
Figure 3.5:
Boundary conditions for one dimensional compression

The ratio of the horizontal effective stress to the vertical effective stress known as the coefficient of earth pressure at rest K_0, is given by:

$$K_0 = \frac{\sigma'_h}{\sigma'_v} \tag{3.1}$$

$$\sigma'_v = \sigma_v - u \tag{3.2a}$$

$$\sigma'_h = \sigma_h - u \tag{3.2b}$$

where σ'_h and σ'_v are the effective horizontal and vertical stresses respectively, σ_h and σ_v are the total horizontal and vertical stresses respectively, the corresponding strains ε_v in vertical direction and $\varepsilon_h = 0$ in horizontal direction, and u is the pore water pressure. K_0 can be obtained either from laboratory test carried out on undisturbed sample or field tests. It may also be estimated readily from the well known *Jaky (1944)* empirical equation:

$$K_0 = 1 - \sin\varphi' \tag{3.3}$$

where φ' is the effective angle of internal friction. K_0 may also reasonably correlate with plasticity index and liquid limit. Some correlation for normally consolidated soft soils are given in *Kempfert/Stadel (1997)* and are re-produced in Table 3.2.

There is no enough available data to correlate the K_0 with plasticity index or liquid limit or others for the lacustrine soft clays in southern Germany. However, in order to identify an empirical

equation that best approximates the K_0 for these soils, the few data from *Scherzinger (1991)* together with the empirical equations in Table 3.2 have been plotted in Figure 3.6. From these figures, it can be seen that *Jaky (1944)* (Figure 3.6c) and *Alpan (1967)* (Figure 3.6a) equations do not fit the data. It is disappointing that the Jaky´s equation, which is the most popular and widely used empirical equation among engineers and researchers, underestimate the K_0 value for this type of soil. On the other hand, the *Lee/Jin (1979)* (Figure 3.6a) and *Sherif/Koch (1970)* (Figure 3.6b) empirical equations seem to fit the data reasonably. In particular, the *Sherif/Koch (1970)* empirical equation is recommended to predict the K_0 value for the lacustrine soft clays in southern Germany.

Table 3.2: Empirical equations to estimate the earth pressure coefficient at rest, K_0 (after *Kempfert/Stadel (1997)*)

Equation	Reference	Regions of Applicability
$K_0 = 0.19 + 0.233 \cdot \log I_p$ (%)	*Alpan (1967)*	Soft clays
$K_0 = 0.24 + 0.31 \cdot \log I_p$ (%)	*Lee/Jin (1979)*	Soft clays
$K_0 = 10^{(0.00275 \cdot (w_L - 20\%) - 0.2676)}$	*Sherif/Koch (1970)*	Soft clays
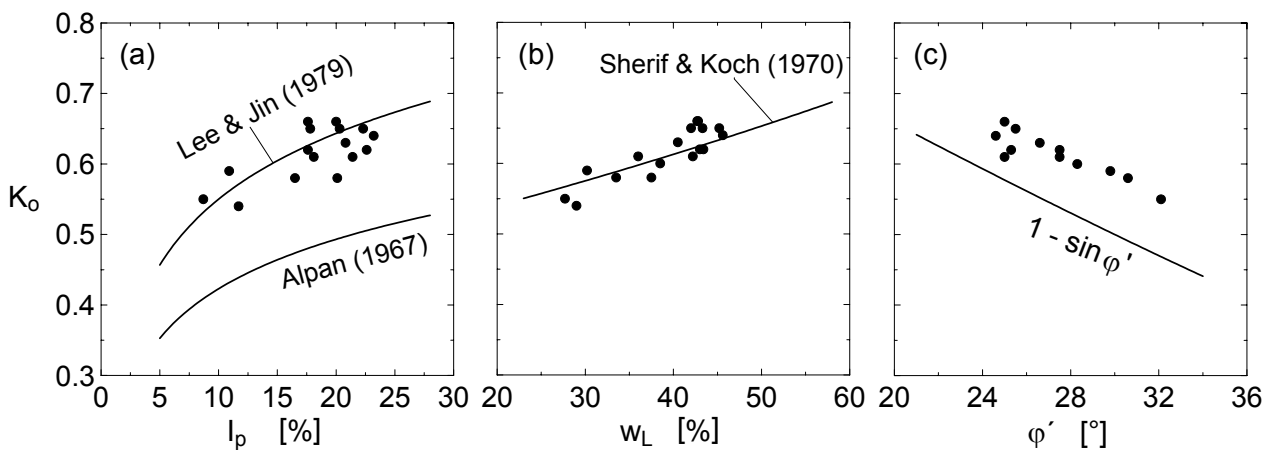
Figure 3.6: Empirical equations to estimate K_0 from a) plasticity index I_p, b) liquidity limit w_L and c) effective angle of friction φ' (data from *Scherzinger (1991)*)

Schmidt (1966) developed an empirical equation to approximate the K_0 value from overconsolidation ratio (OCR) as follows:

$$\frac{K_{0(OC)}}{K_{0(NC)}} = OCR^m \tag{3.4}$$

where $K_{0(OC)}$ and $K_{0(NC)}$ are K_0 values for overconsolidated and normally consolidated cases respectively and *m* is a constant which depend on type of soil. After correlating *m* with plasticity index of several soils, *Ladd et al. (1977)* showed that the value of *m* varies from about 0.42 for low plasticity clays to about 0.32 to high plasticity clays (*Wroth/Houlsby (1985)*). They emphasised that Equation 3.4 should be taken only to estimate the value of K_0 during primary unloading, but K_0 will not be uniquely related to *OCR* for soil deposits that have been subjected to more than one cycle of deposition and erosion. *Schmidt (1966)* and *Schmertmann (1975)* also suggested *m = 0.41*, where as *Meyerhof (1976)* suggested *m = 0.50*. Recently, *Parry (1995)* proposed *m = φ′* (where *φ′* in radian), and *Alpan (1967)* recommended:

$$m = 0.54 \cdot e^{(-I_p/281)} \tag{3.5}$$

where I_p is the plasticity index of the soil. K_0 can also be roughly estimated from cone penetration test results (*Kulhawy/Mayne (1990)*)

$$K_0 = 0.10 \cdot \left(\frac{q_c - \sigma_{v0}}{\sigma'_{v0}} \right) \tag{3.6}$$

where q_c is the cone resistance, σ_{v0}, σ'_{v0} are the total and effective overburden pressures respectively.

Bishop (1958) stated that if the granular structure of the soil behave as an ideal elastic material, it can readily be shown that K_0 would be a function of Poisson's ratio *ν* and would thus be a constant for a given material:

$$K_0 = \frac{\nu}{1 - \nu} \tag{3.7}$$

Although the stress-strain characteristics of soil depart from those of an ideal elastic material even at small strains, it is found experimentally (*Bishop (1958)*) that, K_0 on first loading, is sensibly constant over a wide range of stress. On unloading and reloading, however, hysteresis is evident (Figure 3.7).
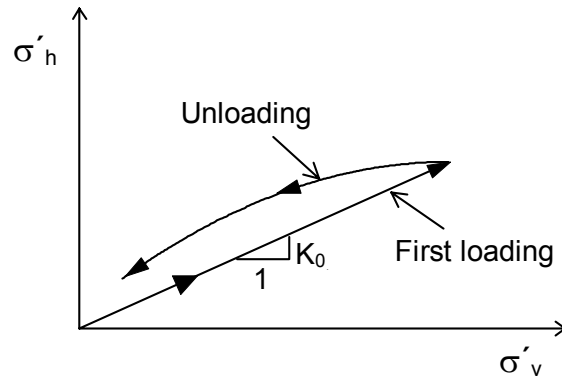
Figure 3.7:
Variation of horizontal effective stress with vertical effective stress for loading and unloading

A typical odometer test result on normally consolidated soil is shown in Figure 3.8. Generally, the result of one-dimensional compression is represented in terms of the effective stress and the corresponding void ratio. The vertical effective stress is plotted either to the natural scale (Figure 3.8a) or to logarithmic scale (Figure 3.8b). The sample is loaded one dimensionally along A-B, unloaded to D, reloaded to B then to C, and finally unloaded to F. The line A-B-C is known as normal consolidation line, where as line B-D and C-E are called the swelling lines. A soil which is on the normal compression line has never before been subjected to a vertical effective stress higher than the current value, and it is described as normally consolidated. However, a soil which is on the swelling line has previously been subjected to higher vertical effective stress than that which currently acts, and it is called overconsolidated. The overconsolidation ratio is defined as:

$$OCR = \frac{\sigma'_{vm}}{\sigma'_{vc}} \qquad (3.8)$$

Where σ'_{vm} is the maximum vertical effective stress in which the soil is subjected and σ'_{vc} is the current vertical effective stress. The various equations necessary to define the settlement-stress curve of one dimensional compression are listed in Table 3.3.
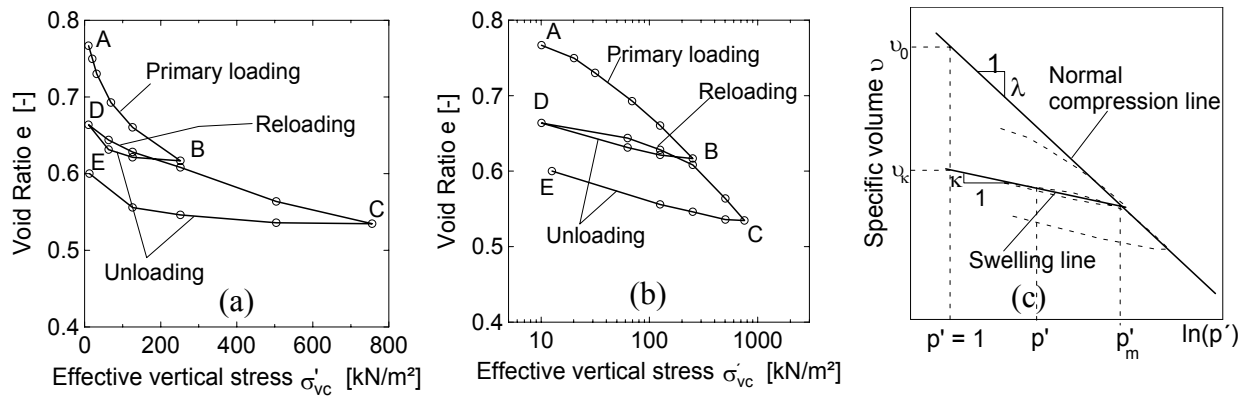
Figure 3.8: One-dimensional compression for normally consolidated lacustrine soft soil; a) natural scale, b) semi-logarithmic scale, and c) idealisation of one-dimensional compression

If the values of σ'_v, σ'_h and the specific volume υ are known throughout a one dimensional compression test, the result may also be plotted on υ versus *ln(p′)* as shown in Figure 3.8c. In this diagram, the one-dimensional compression behaviour of normally consolidated soft soil is idealised by straight lines, in which the slopes and the positions of the lines depend on the particular type of soil. The equations of the normal compression line and the swelling line are given by Equations 3.16 and 3.17 respectively. However, it should be noted that the position of the swel-

ling line is not uniquely defined, but it depends on the maximum previous stress, p'_m. Since $d(\log_{10} \sigma'_v) = 0.434 \cdot d(\ln \sigma'_v)$, $de = d\upsilon$ and K_0 is assumed constant in normal compression line $(d\sigma'_v/\sigma'_v = dp'/p')$, λ can be related to C_c as shown in Equation 3.18. In one dimensional swelling, K_0 is not constant (Figure 3.7), and hence there is no simple relationship between C_s and κ. However, if K_0 is approximately assumed constant, κ may also be approximated from Equation 3.19.

Table 3.3:   List of equations defining the one-dimensional compression behaviour of soils.

Equation	Equation no.	Remark
$-C_c = \dfrac{de}{d \log_{10} \sigma'_v}$	(3.9)	Slope of the primary load line (compression index) (Figure 3.8b)
$-C_s = \dfrac{de}{d \log_{10} \sigma'_v}$	(3.10)	Slope of the reloading/unloading line (swelling index) (Figure 3.8b)
$p' = \dfrac{\sigma'_v + 2 \cdot \sigma'_h}{3}$	(3.11)	Mean principal stress (the intermediate principal stress is equal to the minor principal stress)
$\upsilon = 1 + e$	(3.12)	Specific volume
$\upsilon = 1 + w \cdot G_s$	(3.13)	Specific volume for fully saturated soils
$-\lambda = \dfrac{d\upsilon}{d(\ln p')}$	(3.14)	Slope of normal compression line (Figure 3.8c)
$-\kappa = \dfrac{d\upsilon}{d(\ln p')}$	(3.15)	Slope of swelling line (Figure 3.8c)
$\upsilon = \upsilon_0 - \lambda \cdot \ln p'$	(3.16)	Equation of the normal compression line (Figure 3.8c)
$\upsilon = \upsilon_\kappa - \kappa \cdot \ln p'$	(3.17)	Equation of the swelling line (Figure 3.8c)
$\lambda = 0.434 \cdot C_c$	(3.18)	Relationship between the compression index and the slope of idealised normal compression line
$\kappa \approx 0.434 \cdot C_s$	(3.19)	Relationship between the swelling index and the slope of idealised swelling line
$-C_\alpha = \dfrac{de}{d(\log_{10} t)}$	(3.20)	Coefficient of secondary compression (Figure 3.11)

where e = void ratio, σ'_v, σ'_h = the effective vertical and horizontal stresses respectively, w = moisture content, G_s = specific gravity, υ_0, υ_κ = the specific volumes of corresponding to $p' = 1$ kN/m² for normal compression line and swelling line respectively, t = time

3.3.2.2 Empirical equations to predict compression parameters

In the absence of enough data, the compression parameters can be estimated from simple index parameters using empirical equations. Some empirical equations used to estimate the values of

C_c, C_s, λ, and κ are listed in Table 3.4. It is produced from *Bowles (1984), Nagaraj (1983)* and other sources as indicated in the list. Figure 3.9 also shows the relationship between the plasticity index versus the compression index and swelling index. The C_c and C_s values of the soft soils in southern Germany, are also correlated with natural moisture content and liquid limit as shown in Figure 3.10. It was found that C_c and C_s correlate fairly well with these parameters. The correlation are given by:

$$C_c = 0.00454 \cdot (w - 10), \qquad r^2 = 0.84 \qquad\qquad (3.21)$$

$$C_c = 2.88 \times 10^{-4} \cdot w_L^{1.6352}, \qquad r^2 = 0.74 \qquad\qquad (3.22)$$

$$C_s = 16.433 \times 10^{-6} \cdot w^{2.015}, \qquad r^2 = 0.79 \qquad\qquad (3.23)$$

$$C_s = 6.89 \times 10^{-6} \cdot w_L^{2.215}, \qquad r^2 = 0.70 \qquad\qquad (3.24)$$

where w is the moisture content and w_L is the liquid limit and r^2 is the coefficient of correlation. In terms of r^2, C_c and C_s seems to correlate better with moisture content. The ratio of C_c/C_s is a constant value and varies between 2.5 and 5. For the lacustrine soft clays in southern Germany, *Scherzinger (1991)* found that the ratio C_c/C_s is on average 5.
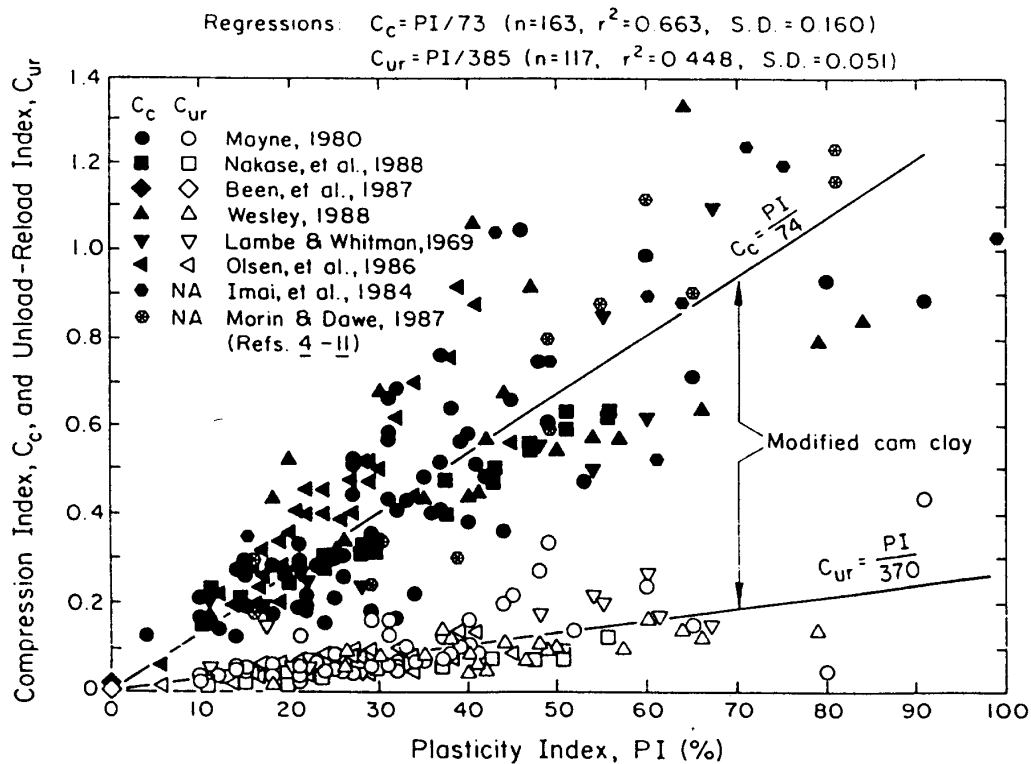
Figure 3.9:   Compression and unload - reload indices as a function of plasticity index (originally from *Kulhawy/Mayne (1990),* adopted from *Mitchell (1993)*)
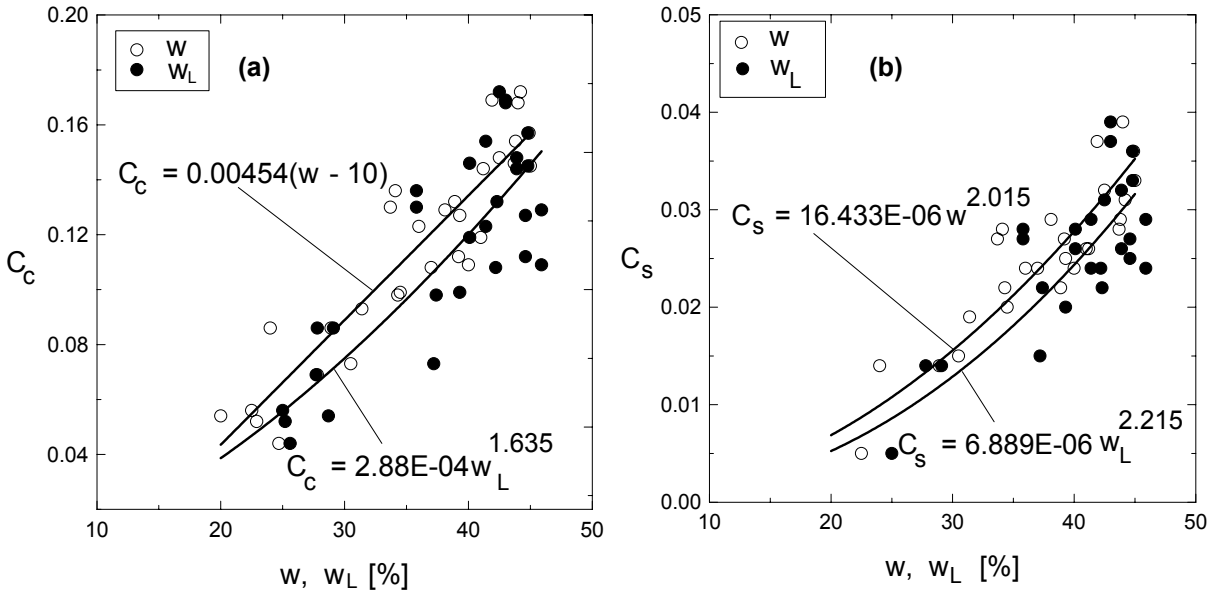
Figure 3.10: Correlation of (a) compression index C_c and (b) the swelling Index C_s, with the natural moisture content w and liquid limit w_L for lacustrine soft clay soils in southern Germany (data are partially obtained from *Scherzinger (1991)*)

3.3.2.3   Secondary compression

The relationship between void ratio and logarithm of time during secondary compression is usually linear (Figure 3.11) for most soils over the time ranges of interest after the completion of primary consolidation. Thus, the coefficient of secondary compression may be defined by Equation 3.20. in Table 3.3. The value of C_α is usually rather uniquely related to the compression index C_c as shown in Table 3.5. *Tsukada/Yasuhara (1995)* had also correlated C_α with initial void ratio for soft soils as

$$C_\alpha = 0.0145 \cdot e_0^{1.555} \tag{3.25}$$
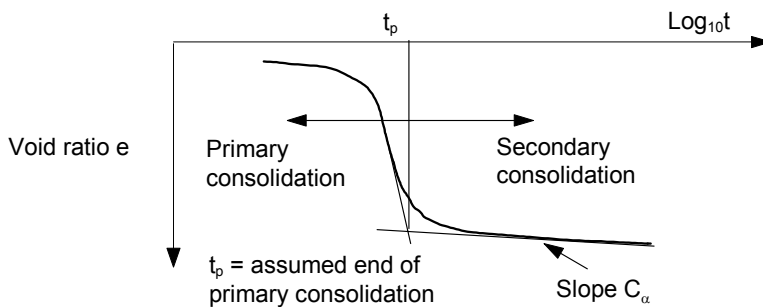
Figure 3.11:
Secondary one-dimensional consolidation

Table 3.4: Empirical equations to predict, C_c, C_s, λ and κ

Equation	Reference	Regions of Applicability
$C_c = 0.007 \cdot (w_L - 10)$	*Skempton (1944)*	Remoulded clays
$C_c = 0.009 \cdot (w_L - 10)$	*Terzaghi/peck (1967)*	Normally consolidated , moderately sensitive
$C_c = 0.007 \cdot (w_L - 7)$	*Bowles (1984)*	Remoulded clays
$C_c = 0.01 \cdot w$	*Koppula (1981), Bowles (1984)*	Chicago clays and Alberta Province in Canada
$C_c = 0.0115 \cdot w$	*Bowles (1984)*	organic silts and clays
$C_c = 0.75 \cdot (e - 0.50)$	*Bowles (1984)*	Soils with low Plasticity
$C_c = 0.0046 \cdot (w_L - 9)$	*Bowles (1984)*	Brazilian clays
$C_c = 1.21 + 1.055 \cdot (e_0 - 1.87)$	*Bowles (1984)*	Motley clays from Sao Paulo city
$\lambda = 0.208 \cdot (e_0 + 0.0083)$	*Bowles (1984)*	Chicago clays
$\lambda = 0.156 \cdot e_0 + 0.0107)$	*Bowles (1984)*	All clays
$C_c = 1.15 \cdot (e - e_0)$	*Nishida (1956)*	All clays
$C_c = 1.15 \cdot (e - 0.35)$	*Nishida (1956)*	
$C_c = 0.54 \cdot (e - 0.35)$	*Nishida (1956)*	Natural soils
$C_c = 0.30 \cdot (e_0 - 0.27)$	*Hough (1957)*	Inorganic silty sand -silty clay
$C_c = 0.256 \cdot e_L - 0.04$	*Burland (1990)*	Remoulded clays, $25 \leq w_L \leq 60$ (soils above the A-line) or $0.6 \leq e_L \leq 4.5$
$C_c = 0.543 \cdot e_L \cdot 10^{(-0.168 \cdot \log_{10} p)}$	*Nagaraj (1983)*	Natural soils in their normally consolidated uncemented state, for pressure range between 25 to 800kPa.
$C_c = 0.141 \cdot G_s^{1.2} \cdot [(1+e_0)/G_s]^{2.38}$	*Herrero (1983)*	All clays
$C_c = 0.5 \cdot (\gamma_w/\gamma_d)^{2.4}$	*Oswald (1980)*	Soil system of all complexities and all types
$C_c = 0.5 \cdot I_p.G_s$	*Wroth/Wood (1978), Wood (1983)*	All remolded normally consolidated clays
$C_c = I_p/74$	*Kulhawy/Mayne (1990)*	Data from different soils
$C_s = I_p/370$	*Kulhawy/Mayne (1990)*	Data from different soils
$\lambda = 0.217 \cdot G_s \cdot I_p$	*Yudhbir/Wood (1989), Atkinson/Bransby (1978)*	Based on critical soil mechanics
$\kappa = 0.048 \cdot G_s \cdot I_p$	*Yudhbir/Wood (1989)*	Based on critical soil mechanics
$\lambda = 0.235 \cdot G_s \cdot I_p$	*Powrie (1997)*	Based on critical soil mechanics
$C_c = 0.24 \cdot e_0 + 0.03$	*Ruppert (1980)*	Lauenberger Ton

w = moisture content (%), w_L = liquid limit (%), e = void ratio, e_0 = initial void ratio, e_L = void ratio at liquid limit, I_p = plasticity index (%), G_s = specific gravity, γ_w = unit weight of water, γ_d = dry unit weight of the soil.

3.3.3   Two and three-dimensional compression

Ladd et al. (1977) reported that the two and three-dimensional loading of a saturated clay results in several important differences from the simple one-dimensional loading condition, because:

1)   An initial settlement, due to undrained shear deformations, occurs upon application of the load and some regions of the foundation clay may undergo local yielding (contained plastic flow).

2)   The initial excess pore pressure beneath the loaded area does not equal the vertical stress increment and strain during consolidation are no longer one dimensional.

3)   Lateral drainage increases the rate of consolidation compared to the one-dimensional case, particularly with soils having high anisotropic permeability ratio.

4)   Creep movements may become more significant both as a result of "undrained" deformations occurring during the consolidation process and due to drained creep after dissipation of excess pore pressure.

Table 3.5:   Values of the ratio of C_α/C_c for natural soils (after Mitchell (1993))

C_α/C_c	Reference	Regions of Applicability
0.03 - 0.04	*Mesri/Godlewski (1977)*	Whangamarino clay
0.025 - 0.06	*Mesri/Godlewski (1977)*	Leda clay
0.026	*Mesri/Godlewski (1977)*	Soft blue clay
0.025 - 0.055	*Mesri/Godlewski (1977)*	Portland sensitive clay
0.04 - 0.06	*Mesri/Godlewski (1977)*	San Francisco bay mud
0.03 - 0.06	*Mesri/Godlewski (1977)*	New Liskeard varved clay
0.032	*Mesri/Godlewski (1977)*	Silty clay
0.055 - 0.075	*Mesri/Godlewski (1977)*	Nearshore clays and silts
0.03 - 0.035	*Mesri/Godlewski (1977)*	Mexico city clay
0.05 - 0.07	*Mesri/Godlewski (1977)*	Post glacial organic clay
0.04 - 0.06	*Mesri/Godlewski (1977)*	Organic clays and silts
0.04 - 0.075	*Mesri/Godlewski (1977)*	New Haven organic clay silt
0.03	*Mesri et al. (1995)*	Batiscan and St Hiaire soft clays
0.02 - 0.04	*Scherzinger (1991)*	Lacustrine soft clays in Constance
0.025 - 0.032	*Klobe (1992)*	Lacustrine soft clays in Constance

The above comments should only be understood in connection with the general stress strain behaviour and rate of consolidation conditions, otherwise, as far as the simple compression parameters C_c, C_s, C_α, λ and κ are concerned, the effect of the two and three-dimensional loading is very minimum. *Atkinson/Bransby (1978)* pointed out that both normal consolidation lines for one-dimensional and isotropic compression are almost parallel with slopes $-\lambda$, and similarly the swelling lines with slopes $-\kappa$ (Figure 3.13). *Mesri et al. (1995)* indicated that the ratio C_c/C_α has the same magnitude for both one-dimensional and three-dimensional compression.

Critical soil mechanics assumes that the soil undergo isotropic compression, before the application of the deviatoric stress. The boundary condition for isotropic compression in a triaxial test is given in Figure 3.12, where an all round cell pressure σ'_c is applied to the specimen, i.e., $\sigma'_c = \sigma'_v = \sigma'_h$. The horizontal strain, however, is different from zero unlike to the one-dimensional case.

$\sigma'_v = \sigma'_c$, ε_v

Drainage

$\sigma'_h = \sigma'_c$, ε_h

$\sigma'_h = \sigma'_c$, ε_h
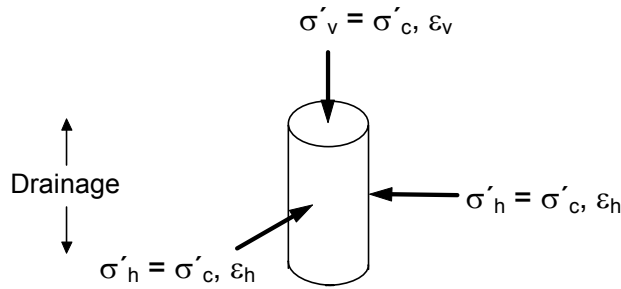
Figure 3.12:
Boundary conditions for isotropic compression

Similar to one-dimensional compression, the isotropic compression may also be idealised by straight lines as shown in Figure 3.13. Equation of the normal compression line for isotropic compression is given by,

$$\upsilon_i = \upsilon_{0i} - \lambda \cdot ln\, p' \qquad (3.26)$$

and for swelling line,

$$\upsilon_i = \upsilon_{\kappa i} - \kappa \cdot ln\, p' \qquad (3.27)$$

where υ_{0i}, $\upsilon_{\kappa i}$ are the specific volumes corresponding to $p' = 1$ kN/m² for normal compression line and an overconsolidated soil respectively.

The location of the normal compression line and swelling line for isotropic compression to the right of the corresponding one-dimensional case as shown in Figure 3.13, implies that for a given value of the specific volume υ, the effective vertical stress carried by the soil under isotropic compression is higher than that of soil under one-dimensional compression.
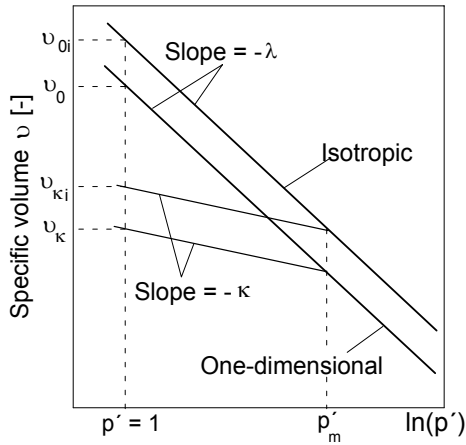
Figure 3.13:
Isotropic and one dimensional compression of normally consolidated soil

3.4   Strength properties of soft clay soils

3.4.1   General

The shearing resistance of a soil depends on many factors, and a complete equation might be of the form (*Mitchel (1993)*):

$$Shearing\ resistance = F(e,\ \varphi,\ C,\ \sigma',\ c,\ H,\ T,\ \varepsilon,\ \dot{\varepsilon},\ S) \qquad (3.28)$$

where e is the void ratio, φ is the angle of internal friction, C is the composition, σ is the effective normal stress, c is the cohesion, H is the stress history, T is the temperature, ε is the strain, $\dot{\varepsilon}$ is the strain rate, and S is the structure. All these parameters may not be independent to each other, however, a functional forms all the factors are not yet known. The Mohr-Coulomb equation, which is a simplified form of Equation 3.28, is by far the most widely used equation for shearing resistance. It states that

$$\tau = c + \sigma \cdot tan\varphi \qquad (3.29)$$

where τ is the shearing resistance of the soil. Equation 3.29 may also be rewritten in terms effective soil parameters as:

$$\tau' = c' + \sigma' \cdot tan\varphi' \qquad (3.30)$$

For practical purposes, the validity of Equation 3.29 and 3.30 are widely accepted, but parameters c' and φ' may take many different values, depending on stress path, stress level and drainage condition. Values of c' and φ' are determined using specified test type such as; direct shear, simple shear, triaxial compression/tension, or other plane strain tests, with due consideration to the

drainage conditions, rate of loading, range of confining pressure, and stress history. In many cases it may be possible to take account of the factors in Equation 3.28 by properly selecting soil specimens and testing conditions which simulate the corresponding field situation.

The general state of a stress in a true triaxial test may be expressed in terms of three principal stresses σ_1, σ_2, and σ_3, where σ_1 is the major principal stress, σ_2 is the intermediate principal stress and σ_3 is the minor principal stress, and $\sigma_1 > \sigma_2 > \sigma_3$. The principal stresses can also be written in the form of the mean principal stress:

$$p = \frac{(\sigma_1 + \sigma_2 + \sigma_3)}{3} \qquad \text{or} \qquad p' = \frac{(\sigma'_1 + \sigma'_2 + \sigma'_3)}{3} \qquad (3.31)$$

and the deviatoric stress may be written as

$$q = q' = \frac{1}{\sqrt{2}} [(\sigma_1 - \sigma_2)^2 + (\sigma_2 - \sigma_3)^2 + (\sigma_3 - \sigma_1)^2]^{\frac{1}{2}} \qquad (3.32)$$

where $\sigma' = \sigma - u$, σ' is the effective stress, σ is the total stress and u is the pore water pressure. In a standard triaxial test, the intermediate principal stress is assumed equal to the minor principal stress, i.e., $\sigma_2 = \sigma_3$, and hence the Equations 3.31 and 3.32 reduces to

$$p = \frac{(\sigma_1 + 2\sigma_3)}{3} \qquad \text{or} \qquad p' = \frac{(\sigma'_1 + 2\sigma'_3)}{3} \qquad (3.33)$$

$$q = q' = (\sigma_1 - \sigma_3) \qquad (3.34)$$

While p or p' and q, usually known as Cambridge composite parameters, are important parameters in critical soil mechanics, the intermediate principal stress is usually ignored in presentation of the triaxial test result and determination of shear strength parameters. Thus, p, p' and q' may be rewritten as

$$p = \frac{(\sigma_1 + \sigma_3)}{2} \qquad \text{or} \qquad p' = \frac{(\sigma'_1 + \sigma'_3)}{2} \qquad (3.35)$$

$$q = q' = \frac{(\sigma_1 - \sigma_3)}{2} \qquad (3.36)$$

At failure the Mohr-Coulomb effective stress envelope is tangential to the effective stress circle, with slope φ' and intercept c' as shown in Figure 3.14. A failure line can also be drawn through the maximum shear stress at A in Figure 3.14 which represents the stress envelope for p - q stress paths. This line is called the K_f - line and has a slope of α' and intercept b'. It is easy to show that $tan\alpha' = sin\varphi'$ and $b' = c' \cdot cos\varphi'$.

Figure 3.14:
Mohr-Coulomb envelope and
K_f - line
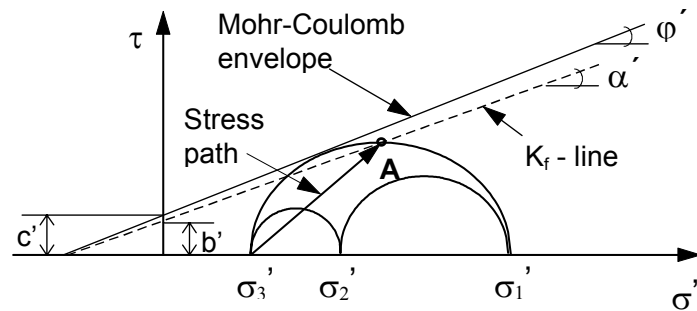
It is possible to take the specimen in a triaxial cell to failure either in axial compression or axial extension. The specimen can be compressed axially either by increasing the axial compressive stress (path OA in Figure 3.15) or decreasing the lateral stress (path OB) or varying the stresses in both direction (path OC). Similarly, axial extension can be achieved either by decreasing the vertical stress (path OD) or increasing the lateral stress (path OE) or varying the stresses in both direction (path OF). Path OA is typical to the state of stress under the axis of an embankment or foundation footing, path OD is typical to the state of stress under the centre of excavation, path OB is typical to the state of stress behind a retaining structure, and path OE is typical to the state of stress in front of the retaining structure and below the excavation level (passive case), where the change of vertical stress due to vertical stress relief is assumed very small. The relief of vertical stress due to excavation and increase of horizontal stress due to the movement of the wall on the passive side may be represented by the path OF, provided that the stress increments in both directions remains the same. Similarly, the increase of vertical stress due to external load at the surface and decrease of the horizontal stress due to wall movement in active side may be represented by path OC.

Rotation of the principal stresses usually occurs around the bottom of the wall and anchor fixing points in an excavation. Although the reversal of the principal stresses on horizontal and vertical principal planes as discussed on the above paragraph may be tested using a modified triaxial apparatus, it is impossible to simulate the rotation of the principal stress on inclined principal planes in a standard triaxial apparatus, unless and otherwise sample are extracted at a specified angel. The rotation of principal stresses, however, can be simulated in a direct simple shear. A true triaxial apparatus where the three principal stresses can vary independent from each other is also available nowadays to simulate the 3-dimensional state of stresses of a soil specimen. Biaxial or plane strain apparatus, where the three principal stresses vary again independently, but the strain in one of the principal stresses direction remains zero, is also widely used for research purpose to simulate a plane strain condition.
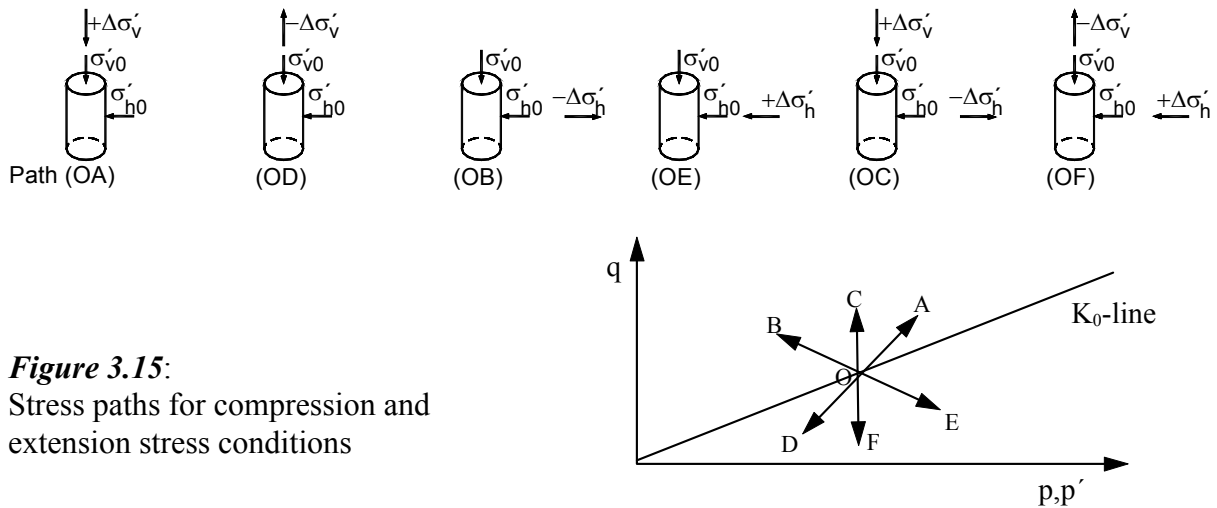
Figure 3.15:
Stress paths for compression and
extension stress conditions

Stroh (1974) produced a diagram showing the zones of different stress paths in an excavation in frankfurter overconsolidated clay supported by multiple ground anchors as shown in Figure 3.16.

Zone-1: The vertical stress remains constant whereas the horizontal stress decreases during excavation.
Zone-2: The vertical stress remains almost constant whereas the horizontal stress increases due to anchor force.
Zone-3: The vertical stress decreases due to excavation and at the same time the horizontal stress increases due to wall displacement.
Zone-4: The vertical stress decreases due to excavation and the horizontal stress remain constant.

Figure 3.16: a) Stress paths in an anchored excavation, b)stress - strain relationships,
c) criteria for different stress paths (after *Stroh (1974)*)

Figure 3.17:
Sub zones of the stress path
(after *Zhu/Liu (1994)*)
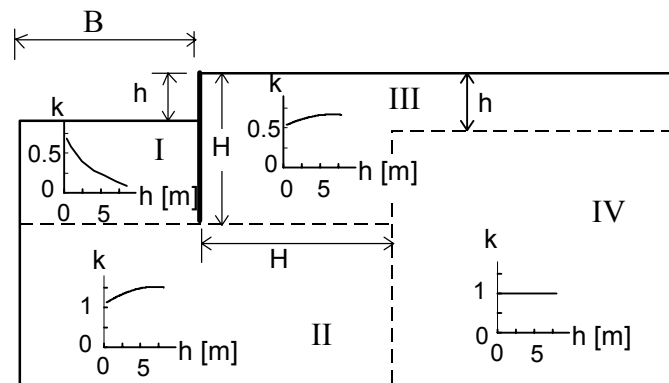
Zhu/Liu (1994) divided the excavation in soft soil in four zones of stress path as shown in Figure 3.17. They used the principal stress ratio k = σ_1/σ_3 to show the variation of the stress paths in the four zones. However, they did not indicate how the σ_1 and σ_3 varies in a particular stress path, which is more important than the stress ratio k.

It would be unwise to generalise the stress path zones as it might differ according to the type of wall system, type of support system, the surcharge load, and ground water conditions. A finite element parameter study might help to identify the different zones particularly in normally consolidated soft clay soils. A typical stress paths at different locations in an excavation is presented in Section 7.3.4.

3.4.2   Total and effective stress analysis

The choice of total or effective stress analysis is of importance in the design and analysis of excavations in soft deposits. This subject will be discussed in Chapter 4 in detail.

3.4.3   Undrained strength

Undrained strength plays an important role in geotechnical engineering, both as an essential input to calculate the short term stability and bearing capacity, and also as an indicator of soil behaviour to correlation with other engineering properties, such as index parameters. The undrained shear strength of a soil is usually determined in laboratory from unconfined compression test or unconsolidated undrained (UU) triaxial test or consolidated undrained (CU) or laboratory shear

vane. In the field it can be readily obtained from field shear vane test, pressuremeter, cone pene-trometer, etc. The major factors that influence the undrained strength of normally consolidated soils are the water content (void ratio), the stress history (anisotropy) and time.

3.4.3.1   Effect of water Content on undrained strength

The undrained strength of clay at plastic limit is about 70 times (*Powrie (1997)*) or 100 times (*Wroth/Wood (1978)*) that at liquid limit. It is generally believed that soils will have almost the same undrained shear strength (0.7 - 2.5 kPa) (*Casagrande (1932), Russel/Mickle (1970), Wroth/Wood (1978), Whyte (1982), Skempton/Northey (1953), Norman (1958), Skopek/Ter-Stepanian (1975), Youssef et al. (1965)*) at the liquid limit, and different but again constant shear strength at the plastic limit *(Atkinson (1978))*.

3.4.3.2   Effect of anisotropy on undrained strength

Anisotropy is one of the most important property of soils which affects their behaviour. Two types of anisotropy are recognised in soil mechanics. These are the inherent anisotropy and the stress induced anisotropy. Anisotropy as a result of preferred particle orientation during one dimensional compression is called inherent anisotropy. Macroscopic variations in fabric can also produce inherent anisotropy. Examples are stiff fissured clays and varved glacial lake deposits containing alternating layers of 'silt' and 'clay' (*Ladd et al. (1977)*). Inherent anisotropy will lead to anisotropy of mechanical properties governing elastic, plastic and failure behaviour. By comparing strengths of the specimens at various angles, a measured of inherent anisotropy can be obtained. This method has been used by a number of researchers such as *Duncan/Seed (1966), Lo/Milligan (1967), DeLory/Lai (1971), Lo/Morin (1972), Eden/Law (1980)*.

Table 3.6 shows the effect of anisotropy on undrained shear strength of normally consolidated soft soils. The undrained strength in the vertical and horizontal direction may differ by as much as 40% (*Mitchell (1993)*) as a result of fabric anisotropy. However, the information in Table 3.6 shows that the difference can be as high as 65%. These differences in undrained strength result from differences in pore water pressures developed during shear (*Duncan/Seed (1966), Bishop (1966)*).

Soil can also exhibit a stress induced anisotropy whenever K_0 is not equal to unity. This results from the fact that different increments of shear stress are required to produce failure as the major principal stress at failure varies between the vertical an horizontal direction (*Ladd et al. (1977)*).

The anisotropy possessed by a soil element existing in-situ under a set of applied stresses, after being subjected to a particular stress history, is a combination of both the inherent and induced anisotropy and is called the initial anisotropy (*Zdravkovic/Potts (1999)*)

Table 3.6:   Effect of anisotropy on undrained shear strength

Equation	Reference	Regions of Applicability
$c_{uc}/c_{ut} \approx 3.0$	*Larsson (1980)*	Inorganic low plastic clays
$c_{uc}/c_{ut} \approx 1.0$	*Larsson (1980)*	Inorganic high plastic clays
$c_{uc}/c_{ut} = 2.5$	*Bjerrum et al. (1972)*	Normally consolidated soil
$c_{uc}/c_{ut} = 1.75$	*Eden/Law (1980)*	Canada South Gloucester soft soil
$\tau_{uv}/\tau_{uh} = 1.25 - 1.54$	*Eden/Law (1980)*	Canada South Gloucester soft soil
$c_{uc}/c_{ut} = 2.0$	*Scherzinger (1991)*	Constance lacustrine soft clays
$c_{uv}/c_{uh} = 1.3$	*Lo (1965)*	Welland clay
$c_{uv}/c_{uh} = 1.43$	*De Lory/lai (1971)*	Welland Clay
$c_{uv}/c_{uh} = 1.28 - 1.56$	*Wesley (1975)*	Mucking Flata clay
$c_{uv}/c_{uh} = 1.25$	*Duncan /Seed (1966)*	San Francisco Bay mud
$c_{uv}/c_{uh} = 1.20$	*Parry/Nadarajah (1974b)*	Fulford clay
$c_{uc}/c_{ut} = 1.60$	*Vaid/Campanella (1974)*	Undisturbed Haney sensitive clay
$c_{uc}/c_{ut} = 2.13$	*Ladd et al. (1971)*	Resedimented Boston blue clay
$c_{uc}/c_{ut} = 1.75$	*Bjerrum (1973)*	Bangkok clay
$c_{uc}/c_{ut} = 1.36$	*Bjerrum (1973)*	Matagami clay, Canada
$c_{uc}/c_{ut} = 2.67$	*Bjerrum (1973)*	Drammen plastic clay
$c_{uc}/c_{ut} = 3.56$	*Bjerrum (1973)*	Vater land clay
$c_{uc}/c_{ut} = 3.78$	*Bjerrum (1973)*	Drammen lean clay
$c_{uc}/c_{ut} = 2.67 - 3.75$	*Aas (1976)(see Janbu(1977)*	Norwegian clay, $10 < I_p < 20$
$c_{uc}/c_{ut} = 2.0 - 2.33$	*Aas (1976)(see Janbu(1977)*	Norwegian clay, $I_p = 40$
$c_{uc}/c_{ut} = 1.63$	*Aas (1976)(see Janbu(1977)*	Norwegian clay, $40 < I_p < 100$
$c_{uc}/c_{ut} = 1.72$	*Jamiolkowski (1985)*	Lean sensitive normally consolidated clay ($K_0 = 0.5$)
$c_{uc}/c_{ut} = 1.12$	*Jamiolkowski, (1985)*	Plastic insensitive normally consolidated clay ($K_0 = 0.75$)

c_{uv} = undrained shear strength in vertical direction, c_{uh} = undrained shear strength in horizontal direction, c_{uc} = undrained shear strength in compression, c_{ut} = undrained shear strength in extension. τ_{uv}, = shear vane strength in vertical direction, τ_{uh} = shear vane strength in horizontal direction

The behaviour of the undrained strength in compression and extension may be determined using the critical soil mechanics concept. The slope of the critical state line (Figure 3.18) in compression is given by:

$$M = \frac{6 \cdot sin\,\varphi_c^{'}}{3 - sin\,\varphi_c^{'}} \qquad\qquad (3.38)$$

and for extension,

$$M = \frac{6 \cdot sin\,\varphi_t^{'}}{3 + sin\,\varphi_t^{'}} \qquad\qquad (3.39)$$

where $\varphi_c^{'}$, and $\varphi_t^{'}$ are the effective internal friction in compression and extension respectively. At critical state the undrained strength is given by

$$c_u = \frac{q}{2} = \frac{M \cdot p'}{2} \qquad\qquad (3.40)$$

Substituting the value of *M* form Equations 3.38 and 3.39 into Equation 3.40, the ratio of undrained strength in compression and extension becomes

$$\frac{c_{uc}}{c_{ut}} = \frac{3 + sin\,\varphi_t^{'}}{3 - sin\,\varphi_c^{'}} \qquad\qquad (3.41)$$

Taking the average values of $\varphi_c^{'}$ = *29°* and $\varphi_t^{'}$ = *26°* for the lacustrine soft soil in Constance (*Scherzinger (1991)*), the ratio c_{uc} /c_{ut} = *1.38* may be obtained. For normally consolidated clays, *Ladd et al. (1977)* compared the undrained strength from triaxial and plane strain tests as follows

$$\frac{c_{u(triaxial)}}{c_{u\,(plain\,strain)}} \begin{cases} = \textit{0.92 + 0.05} \Rightarrow \textit{Compression} \\ \\ = \textit{0.82 + 0.02} \Rightarrow \textit{Extension} \end{cases} \qquad (3.42)$$
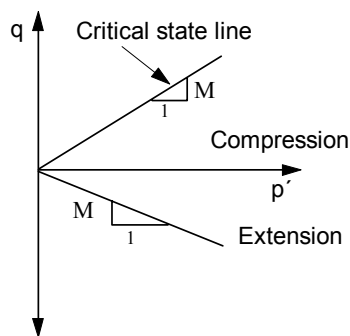
Figure 3.18:
Comparison of triaxial compression and extension at critical state strengths

For practical purposes, however, the combined effect of both components of anisotropy can be considered collectively using K_0 - consolidated undrained test corresponding to the stress system and sample orientation that will exist in-situ (*Ladd (1974)*). This will be in particular very im-

portant in an excavation, where the stress system and orientation behind the wall, in front of the wall and around the bottom of the wall are different.

Bjerrum et al. (1972) introduced a correction factor μ_A to account for the effect of anisotropy in undrained strength of normally consolidated soils obtained form field vane shear test as follows:

$$c_u = \mu_A \cdot \tau_f \qquad\qquad (3.43)$$

For normally consolidated soft soils with plasticity index $I_p < 50(\%)$, *Kempfert/Stadel (1997)* suggested that $\mu_A = 1.5$ for triaxial compression and $\mu_A = 0.5$ for triaxial extension. However, this values must be justified by more data before applying to lacustrine soft soil in southern Germany.

3.4.3.3   Influence of time on undrained strength

Time is a factor of such an importance that it should be considered and taken into account in any stability analysis in which soft clays are involved. It is a factor associated with the cohesive component of the shear strength and that the frictional component of the shear strength is to a greater extent independent of time (*Bjerrum (1973)*). The effect of time can be seen in four different ways: thixotropy, ageing, rate of strain, and creep. It is beyond the scope of the thesis to discuss these four factors. An extensive coverage of this topic can be found in the "state of the art" reports by *Bjerrum (1973), Ladd et al. (1977), Jamiolkowski (1985)* and other text books such as *Mitchell (1993)*.

The effect of the rate of strain on undrained shear strength can be considered in laboratory tests by proper selecting the time to failure and strain at the time of failure. On the other hand it may not be easy to control the strain rate in the field vane shear apparatus, though a rate of 1°/sec (*Ladd et al. (1977)*) is usually recommended. Even then the vane shear strength overestimates the undrained strength of normally consolidated soils. After analysing embankment failures on clay foundations and unsupported excavations, *Bjerrum (1972)* introduced a correction factor μ_R which depends on plasticity index of the soil. Thus

$$c_u = \mu_R \cdot \tau_f \qquad\qquad (3.44)$$

where c_u is the undrained strength of the soil and τ_f is the field shear vane strength of the soil. *Ladd et al. (1977)*, supported by different data, had studied the Bjerrum's curve and confirmed that the relationship between the correction factor μ_R and the plasticity index of the soil is quite sound (Figure 3.19).
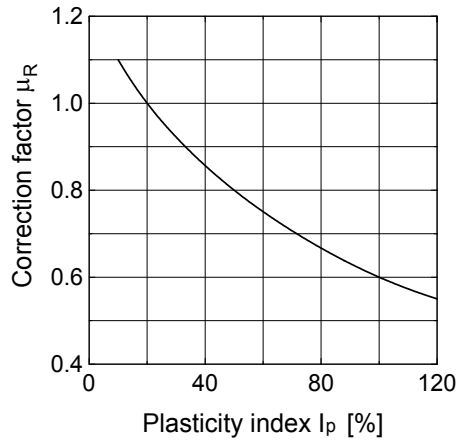
Figure 3.19:
Field vane correction factor versus plasticity index derived from embankment failures (after *Ladd et al. (1977)*)

3.4.3.4 Estimation of undrained shear strength from cone penetration result

The undrained shear strength c_u can also be estimated from the cone penetration field test using the equation:

$$c_u = \frac{(q_c - \sigma_{vo})}{N_k}$$

(3.45)

where q_c is the measured cone resistance, σ_{vo} is the total in-situ vertical stress, and N_k is the empirical cone factor. The value of N_k should be selected according to the experience in a particular soil type. Various attempts to determine the N_k values or to correlate it with plasticity index can be found in *Lunne et al. (1997)*. In general, the value of N_k varies between 10 and 20. *Jorß (1998)* recommends $N_k = 20$ for marine clay and $N_k = 15$ for boulder clays in northern Germany. For the lacustrine soft clays in southern Germany, however, no information on the value of N_k can be found in the literature so far. However, it is the opinion of the author that the value of N_k for lacustrine clays will not deviate much from that of the lacustrine clay in north Germany, since they have more or less similar properties.

Though a standard rate of penetration of the cone 20 mm/s is usually recommended, there are evidences which show that q_c increases with the increasing rate of penetration, and there is a minimum value of cone resistance at a rate of penetration 1 - 2.5 mm/s for slightly overconsolidated soft clays (see *Lunne et al. (1997)*.

3.4.3.5 Estimation of the undrained shear strength from empirical equations

There have been continuous attempts, right from the early stages of the development of soil mechanics, to develop simple methods to predict the undrained strength of soils from simple soil index parameters, such as consistency limits. Although the literature in this respect is very rich, only few of them have been selected and listed in Table 3.7. These simple correlations are used to

estimate the undrained strength for numerical analysis in the absence of data or to check some laboratory investigations. However, attention should be given to the conditions in which the correlation had been made and the statistical accuracy of the equations, before choosing a single empirical equation for a particular type of soil.

Some of the empirical equations and data from Constance lacustrine soft soil (*Scherzinger (1991)*) are plotted in Figure 3.20. It can clearly be observed that neither of the equations would satisfy the Constance soft soil for the given range of data, rather most of the data points lie between $c_u/\sigma'_{vc} = 0.22$ (*Mesri (1975)*) and $c_u/\sigma'_{vc} = 0.33$ (*Larsson (1980)*) lines. After analysing a large number of data from Eastern Canada and Scanadivean soils, *Windisch/Yong (1990)*, also showed that non of the empirical equations would apply to eastern Canadian clays. Instead, they recommend a mean value of $c_u/\sigma'_{vc} = 0.27$. *Burland (1990)* also showed that for remoulded clays the normalised undrained strength remains constant, $c_u/\sigma'_{vc} = 0.30$. *Scherzinger (1991)* also recommended $c_u/\sigma'_{vc} = 0.26$ for the lacustrine soft clay in Constance. Therefore, the normalised undrained shear strength of normally consolidated clay can be fairly assumed to be constant for a particular soil, provided that the ground water is located at relatively shallow depth. *Kempfert/Stadel (1997)* introduced a constant λ, where

$$\frac{c_u}{\sigma'_{vc}} = \lambda_{cu} = cons \tan t \qquad\qquad (3.48)$$

and they used λ_{cu} to calculate the earth pressure at the end of construction stage (initial condition). The value of λ_{cu} varies from soil to soil. For the lacustrine soft clays in Constance, *Scherzinger (1991)* approximated $\lambda_{cu} = 0.26$. For similar lacustrine soils in this region, *Heil et al. (1997)* reported that $\lambda_{cu} = 0.30$ for triaxial test and $\lambda_{cu} = 0.20$ for vane tests.
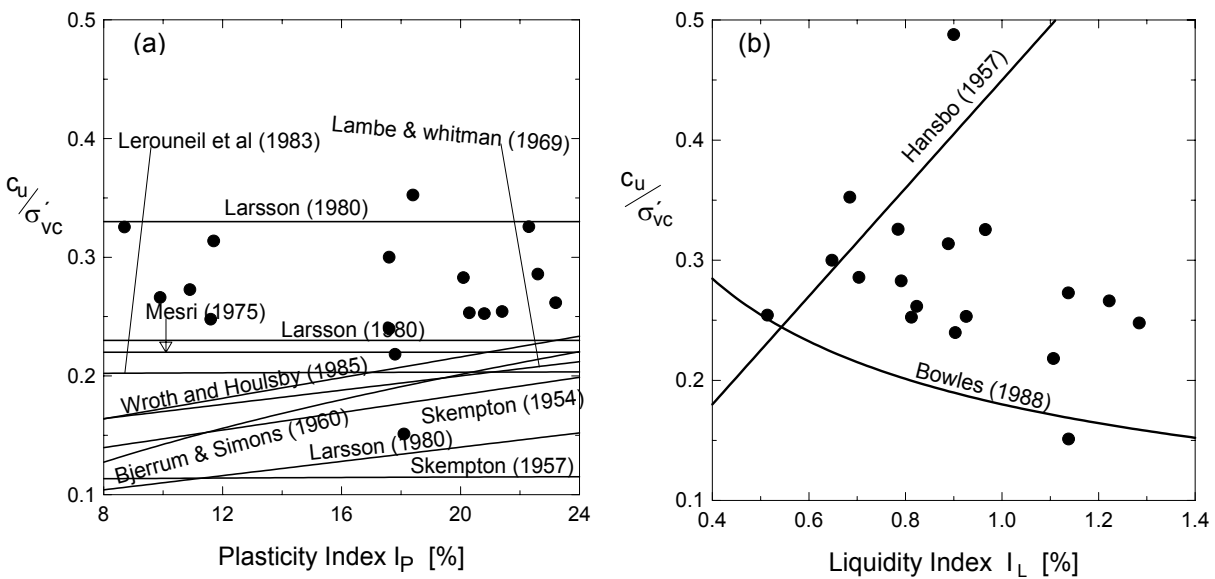

Figure 3.20:   Relations between normalised undrained strength and a) plasticity index,
                 b) liquidity index (Data are obtained from *Scherzinger (1991)*)

***Table 3.7:*** Empirical equations to estimate undrained shear strength

Equation	Reference	Regions of Applicability
$c_u = 170 \cdot \exp(-4.6 \cdot I_L)$ [kPa]	*Wroth/Wood (1978)*	Remoulded clays
$c_u = 1/(I_L - 0.21)^2$ [kPa]	*Mitchell (1993)*	From several clays (remoulded strength)
$c_u/\sigma'_{vc} = 0.11 + 0.0037 \cdot I_p$	*Skempton (1954), Bowles (1984)*	Normally consolidated soils, $I_p > 10\%$
$c_u/\sigma'_{vc} = 0.11 + 0.0037 \cdot \log I_p$	*Skempton (1957)(see Kempfert/stadel (1997)*	Normally consolidated soil, $I_p < 60\%$
$\tau_f/\sigma'_{vc} = 0.2 + 0.0024 \cdot I_p$	*Lerouneil et al. (1983)*	Clays from eastern Canada, $I_p < 60\%$
$\tau_f/\sigma'_{vc} = 0.22$	*Mesri (1975)*	Soft clays
$c_u/\sigma'_{vc} = 0.08 + 0.55 \cdot I_p$	*Larsson (1977)*	Scandinavian clays
$c_u/\sigma'_{vc} = 0.23 \pm 0.04$	*Larson (1980)*	Soft sedimentary clays, $I_p < 60\%$
$c_u/\sigma'_{vc} = 0.33$	*Larsson (1980)*	Inorganic clays
$c_u/\sigma'_{vc} = (0.23 \pm 0.04) \cdot (OCR)^{0.8}$	*Jamiolkowski et al. (1985)*	All clays
$c_u/\sigma'_{vc} \approx 0.26$	*Scherzinger (1991)*	Constance lacustrine soft clays
$c_u/\sigma'_{vc} = 0.45 \cdot w_L$	*Hansbo (1957)*	Scandinavian clays
$c_u/\sigma'_{vc} \approx 0.30$	*Burland (1990)*	Natural sensitive clays
$c_u/\sigma'_{vc} = 0.14 + 0.003 \cdot I_p$	*Lambe/Whitman (1969)*	All clays
$c_u/\sigma'_{vc} = 0.45 \cdot (I_p/100)^{1/2}$	*Bjerrum/Simons (1960)*	Normally consolidated clays
$c_u/\sigma'_{vc} = 0.18 \cdot (I_L)^{-1/2}$	*Bjerrum/Simons (1960)*	Normally consolidated clays
$c_u/\sigma'_{vc} = 0.45 \cdot w_L$	*Bowles (1984)*	Normally consolidated soils, $w_L > 40\%$
$c_u = 11.4 + 0.169 \cdot \sigma'_{vc}$ [kPa]	*Windisch/Yong (1990)*	Barlow-Ojibway Lacustrine clays
$c_u = 2.32 + 0.260 \cdot \sigma'_{vc}$ [kPa]	*Windisch/Yong (1990)*	East Canadian marine clays
$c_u = 3.05 + 0.260 \cdot \sigma'_{vc}$ [kPa]	*Windisch/Yong (1990)*	Champlane sea clays
$c_u = 7.69 + 0.117 \cdot \sigma'_{vc}$ [kPa]	*Windisch/Yong (1990)*	Scandinavian clays
$c_u/\sigma'_{vc} = -0.09 + 0.0092 \cdot I_p$ [kPa]	*Windisch/Yong (1990)*	Scandinavian clays
$c_u/\sigma'_{vc} = -0.18 + 0.0072 \cdot w_L$ kPa]	*Windisch/Yong (1990)*	Scandinavian clays
$c_u/\sigma'_{vc} = -0.18 + 0.0072 \cdot w_L$ [kPa]	*Windisch/Yong (1990)*	Scandinavian clays
$c_u/\sigma'_{vc} = -0.18 + 0.0072 \cdot w_L$ [kPa]	*Windisch/Yong (1990)*	Scandinavian clays
$c_u/\sigma'_{vc} = 0.129 + 0.00435 \cdot I_p$	*Wroth/Houlsby (1985)*	Normally consolidated clays
$\dfrac{c_u}{\sigma'_{vc}} = 0.5743 \cdot \dfrac{3 \cdot \sin\varphi'}{(3 - \sin\varphi')}$	*Wroth/Houlsby, (1985)*	Normally consolidated soils

c_u = undrained shear strength, τ_f = undrained vane shear strength, σ'_{vc} = effective consolidation pressure, w_L = liquid limit, I_p = plasticity index (%), I_L = Liquidity index, OCR = over consolidation ratio, φ' = angle of internal friction

The effect of stress system induced anisotropy can also be seen from correlation of the normalised undrained strength with plasticity index of the soil as shown in Figure 3.21. It would appear from Figure 3.21 that less plastic and often more sensitive clays tend to have higher anisotropy than more plastic clays.

Figure 3.21:
Undrained strength anisotropy from CK$_0$U tests performed on normally consolidated clays (from *Jamiolkowski et al. (1985)*)
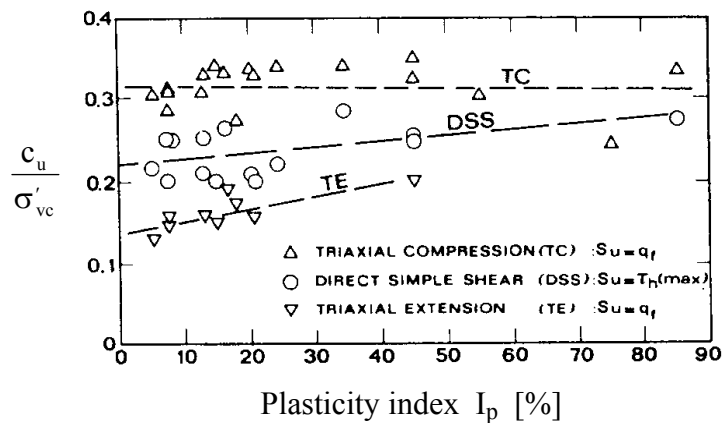
3.4.4   Drained strength

The drained strength of a soil is represented by the parameters c′ and φ′ and used for long-term analysis. Values of c′ and φ′ can be obtained from drained tests or undrained tests with measurements of pore water pressure during shear. The drained strength of a normally consolidated soils is also influenced by the same factors as those that affect the undrained strength, except the magnitude of the influence may be less in drained strength.

Duncan/Seed (1966), Morgenstern/Tchlenko (1967b) stated that the drained strength is independent of the stress orientation relative to fabric orientation. *Mitchell (1993)* also added that the effective stress strength parameters are independent of sample orientation. He showed that the effective parameters for two samples of the same soil but tested in different direction; one in vertical and the other in horizontal direction, are the same though the stress paths followed different direction.

There is a conflicting evidence on the influence of initial stress and structure anisotropy on φ′ at failure, but the bulk of presently available evidence suggests that inherent anisotropy has very little influence on φ′ measured in triaxial compression tests. Compression and extension tests on soft Fulford clay at different sample orientation carried out by *Parry/Nadarajah (1975b)* show that the influence of initial anisotropy to be much less than the influence of stress direction in producing failure (Table 3.8). The difference in c′ values may not be significant, as this parameter is very sensitive to slight changes in test data.

Like in undrained strength the combined effect of both components of anisotropy can be considered collectively using K_0-consolidated undrained test or drained test (triaxial compression or triaxial extension or plane strain test) corresponding to the stress system and sample orientation that exist in situ. This will be in particular very important for excavations, where stress system and orientation behind the wall, in front of the wall and around the bottom of the wall are different.

The effective angle of internal friction seems to depend on the plasticity of the soil and mineralogical composition of the normally consolidated soils as shown in Figure 3.22. Soils with higher percentage of montmorillonite will have lower φ' than those soils with illite and kaolinite respectively.

Table 3.8: Influence of anisotropy on effective stress parameter φ'

Soil type	φ'(comp)/φ'(ext)		Reference
	Vertical	Horizontal	
Soft Fulford clay	0.76	0.83	*Parry/Nadarajah (1974b)*
Koalin (Isotropic)	1.095		*Parry/Nadarajah (1974a)*
Koalin (K_0)	0.75		*Parry/Nadarajah (1974a)*
Speswhite kaolin (1-dimensional, then K_0 consolidated)	0.75		*Atkinson, et al. (1987)*
Speswhite kaolin (Isotropic, then K_0 consolidated)	0.89		*Atkinson, et al. (1987)*
Undisturbed Haney sensitive clay	0.73		*Vaid/Campanella (1974)*
Constance soft soil	1.12		*Scherzinger (1991)*
Undisturbed San Francisco Bay mud	1.08		*Duncan/Seed (1966b)*
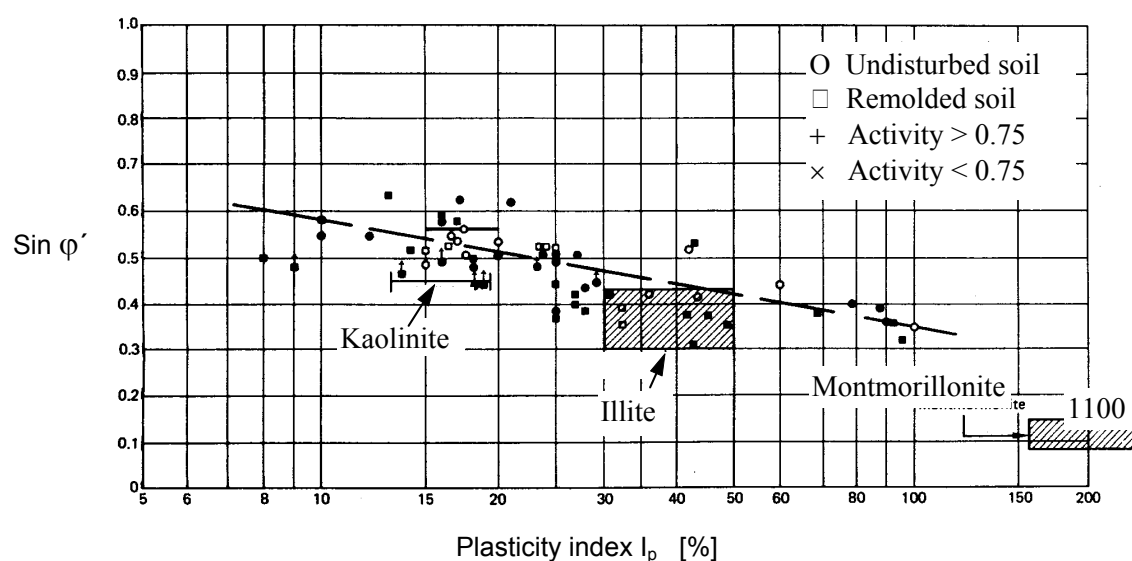
Figure 3.22: Relationship between sin φ' and plasticity index for normally consolidated soils **(**from *Mitchell (1993)***)**

3.5   Deformation properties of soft soils under deviatoric stress

3.5.1   General

Deformation of a soil is one of the most important physical aspect in geotechnical problems. Many investigators have revealed that the soil deformation modulus was found to have the greatest influence on deformation behaviour of excavations in soft soils. The material properties required for deformation analysis are conventionally those four constants used in the theory of elasticity, namely, the Young's modulus E, the Poisson's ratio v, the shear modulus G and the bulk modulus K. In reality, however, the shear modulus G and bulk modulus K can be written in terms of the Young's modulus E and Poisson's ratio v as

$$G = \frac{E}{2(1+v)} \tag{3.49}$$

$$K = \frac{E}{3(1-2v)} \tag{3.50}$$

There are two alternative definitions of the modulus of elasticity, namely, the secant modulus E_{sec}, and tangent modulus E_t (Figure 3.23).

In most stress-strain curves obtained from triaxial test on normally consolidated soil samples, the slope of the curve at a lower strains is not uniquely defined, and the correct estimation of the initial tangent modulus of elasticity is not simple. Moreover, in an elastic calculations the strain depends on both the stress and modulus. If the soil depends on strain, an iterative procedure must be adopted, in which the calculations is repeated until the strain is consistent. For this purpose, it is easier to use the secant, rather than the tangent modulus (*Powrie (1997)*). The PLAXIS FE-program uses the secant modulus at 50% of the maximum deviatoric stress $(\sigma_1' - \sigma_3')_f$ denoted as E_{50} as initial modulus (Figure 3.23).
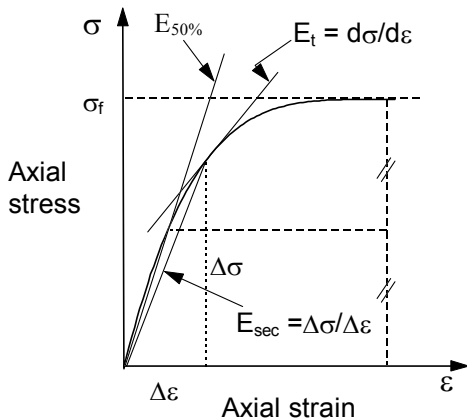
Figure 3.23:
Schematic diagram of stress strain behaviour of soils

3.5.2 Drained and undrained behaviour

Like strength behaviour, it is essential to distinguish between undrained and drained behaviour of the deformation of soils. The relevant elastic properties are either E_u, ν_u or E, ν for undrained and drained conditions respectively.

For perfectly elastic soil, the value of the shear modulus is unaffected by the drainage condition, since the water with in the soil skeleton has zero shear stiffness. Hence

$$\frac{E_u}{2 \cdot (1+\nu_u)} = G_u = G = \frac{E}{2 \cdot (1+\nu)} \tag{3.51}$$

Since the bulk undrained modulus is defined as

$$K_u = \frac{\Delta\sigma}{\Delta\varepsilon_{vol}} = \frac{E_u}{3 \cdot (1-2\cdot\nu_u)} \tag{3.52}$$

and for undrained condition, the volumetric strain $\Delta\varepsilon_{vol} = 0$, K_u becomes infinite. This requires that the undrained Poisson's ratio $\nu_u = 0.5$. Hence

$$\frac{E_u}{E} = \frac{3}{2 \cdot (1+\nu)} \tag{3.53}$$

For most soils, the effective Poisson's ratio ranges between 0.12 and *0.35 (Wroth/Houlsby, 1985)*. Therefore,

$$\frac{E_u}{E} \approx 1.11 \; to \; 1.34 \tag{3.54}$$

3.5.3 Effect of depth on modulus of elasticity

It is necessary to take account of the fact that soil stiffness is likely to increase with increasing effective stress. This effect is often modelled by assuming that the soil stiffness is proportional to the depth. According to *Ohde (1939),*

$$E_t = k \cdot p_{ref} \cdot \left(\frac{\sigma'_{vc}}{p_{ref}}\right)^m \tag{3.55}$$

where k is a dimensionless modulus number, *m* is an exponent, and p_{ref} is reference pressure usually taken as atmospheric pressure. The values of *k* and *m* can be determined from a plot of the effective consolidation stress against the tangent modulus for a series of test data. In practice,

however, it is common to assume the undrained modulus of elasticity to vary linearly with undrained shear strength (Table 3.9), because the undrained shear strength is also assumed to vary proportional with depth.

Table 3.9:   Variations of undrained modulus of elasticity with undrained strength

Equation	Reference	Regions of Applicability
$E_{u,i} = 200 \cdot c_u$	*Clough/Mana (1976)*	San Francisco clay
$E_{u,i} = (600 \text{ to } 1200) \cdot c_u$	*Clough/Mana (1976)*	San Francisco clay (obtained from back analysis of excavation)
$E_{u,i} = 280 \cdot c_u$ *	*Ladd/Edgers (1972)*	Atchafalya CH Clay
$E_{u,i} = 420 \cdot c_u$ *	*Dames/Moore (1975)*	AGS CH Clay
$E_{u,i} = 600 \cdot c_u$ *	*Ladd/Edgers (1972)*	Maine organic CH-OH clay
$E_{u,i} = 670 \cdot c_u$ *	*Ladd/Edgers (1972)*	Bangkok CH clay
$E_{u,i} = 820 \cdot c_u$ *	*Ladd/Edgers (1972)*	Boston CL clay
$E_{u,i} = 280 \cdot c_u$	*Ladd (1964)*	Not known
$E_{u,i} = (250 \text{ to } 500) \cdot c_u$	*Bjerrum(1964)*	Normally consolidated Norwegian clays
$E_{u,i} = 275 \cdot \sigma$ *	*Charles(1964)*	Laqunillas normally consolidated clay
$E_{u,i} = 175 \cdot \sigma$ *	*Charles(1964)*	Kawasaki normally consolidated clay

[*] Values are for stress level $(c_u/c_{u(max)}) = 1/3$, $E_{u,i}$ = initial tangent undrained modulus

3.5.4   Effect of anisotropy on modulus of elasticity

Soils in the field are consolidated under anisotropic stress conditions giving them different stiffness in the vertical and horizontal directions. Normally consolidated soft soils will usually be stiffer in the vertical direction than in the horizontal direction (*Parry (1995)*). For soft recently deposited clays, *Parry/Wroth (1981)* showed that the ratio n between the vertical E_v and horizontal E_h modulus of elasticity is of the order,

$$\frac{E_h}{E_v} = n \cong 0.5 \qquad\qquad\qquad\qquad (3.56)$$

However, they also indicated that the value of *n* varies with different stress paths and sample orientation as shown in Figure 3.24. The combined effect of the stiffness in vertical and horizontal direction may be taken as the average of the two (*Parry (1995)*).

Likewise, the Poisson's ratio in vertical direction differs from that in horizontal direction. If v_v and v_h are assumed the Poisson's ratio in vertical and horizontal directions respectively, the combined effect may be estimated from *(Henke (1971))*

$$v = \frac{1}{2} \cdot v_v \cdot (1+n) \tag{3.57}$$
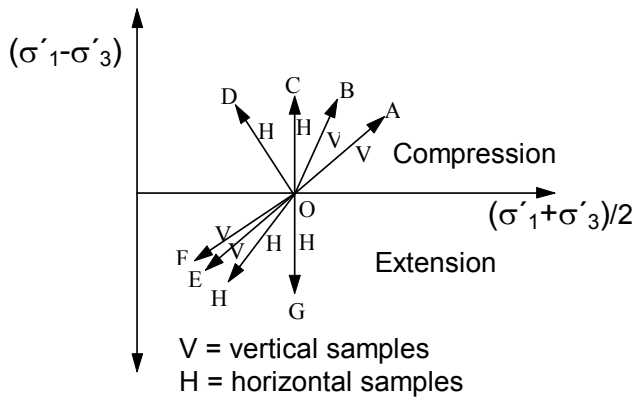
Orientation	n	Stress path	Gradient
Compression			
Vertical	0.5	OA	1.4
Vertical	1.0	OB	3.0
Horizontal	1.5	OC	∞
Horizontal	3.0	OD	-2.4
Extension			
Vertical	0.5	OE	1.4
Vertical	0.25	OF	1.1
Horizontal	1.5	OG	∞
Horizontal	0.75	OH	-2.0

Figure 3.24: Influence of sample orientation on modulus of elasticity (after *Parry, (1995)*)

3.5.5 Constrained Modulus from one-dimensional compression

The constrained modulus from one-dimensional compression odometer E_{oed} can be related with the modulus of elasticity using the elasticity theory as:

$$E = E_{oed} \cdot \frac{(1+v) \cdot (1-2 \cdot v)}{(1-v)} \tag{3.58}$$

For most soils, v' ranges between 0.12 to 0.35. Hence,

$$\frac{E}{E_{oed}} \cong 0.623 \text{ to } 0.967 \tag{3.59}$$

However, since soils are known as elasto-plastic material, the above relationship might not always holds true. *Vermeer/Meier (1998)* asserted that $E_{50} < E_{oed}$ for stiff overconsolidated clay, $E_{50} > E_{oed}$ for soft soils, and $E_{50} \approx E_{oed}$ for sands, specifically for analysis with the FE-code PLAXIS.

3.5.6   Unloading/Reloading modulus of elasticity.

The behaviour of soils during unloading/reloading is assumed elastic, because changes in stress can be accommodated with out the need for a rearrangement of the soil skeleton, i.e., deformation is primarily due to distortion of the soil particle which is recoverable. Hence, soils are stiffer in unloading/reloading than in the first loading, even over the same stress range. The unloading/reloading stress-strain curves are fairly approximated by straight lines, where the modulus of elasticity in unloading and reloading are assumed to be same, and they are denoted by a single symbol E_{ur}. Due to the fact that soil behaves elastically during unloading/reloading, E_{ur} is a true elasticity modulus unlike E_{50}, which determines the magnitude of both the elastic and plastic strains. Hence, using Equation 3.58, E_{ur} can be related with the constrained unloading/reloading modulus $E_{u,\,oed}$:

$$E_{ur} = E_{ur,oed} \cdot \frac{(1+\nu_{ur}) \cdot (1-2\cdot\nu_{ur})}{(1-\nu_{ur})} \qquad\qquad (3.60)$$

where ν_{ur} is the Poisson's ratio for unloading/reloading. The un/reloading modulus is also to some extent dependent on the previous stress level before the unloading has taken place.

4 Total and effective stress analysis of excavations in soft soils

4.1 Definition

The shear strength of a soil in terms of the effective shear parameter is given by Equation 3.30 in Section 3.4.1 and it can be rewritten,

$$\tau = c' + \sigma' \cdot tan \varphi'$$

where $\sigma' = \sigma - u$, $u = u_0 + \Delta u$, u_0 = steady pore pressure, Δu = excess pore pressure, and in terms of the total stress it is given by

$$\tau = c_u \tag{4.1}$$

In Germany, it is a common practice to include the effect of cohesion in the angle of internal friction for soft soils, and hence Equation 3.30 may be redefined as

$$\tau = \sigma'_e \cdot tan \varphi'_s \tag{4.2}$$

where φ'_s is defined as the angle of the overall shear strength and σ'_e is the Hvorslev's equivalent stress (see *DIN 18 137 (1990)* or *Scherzinger (1991)*). In this chapter the term φ'_s will be used instead of φ' through out the text.

For a vertical and smooth wall with horizontal ground surface, the effective active and passive earth pressure are usually determined using the classical Rankine equation from,

$$e_a = \gamma' \cdot z \cdot K_a \tag{4.3}$$

$$e_p = \gamma' \cdot z \cdot K_p \tag{4.4}$$

and the undrained active and passive pressures are also given by

$$e_a = \gamma' \cdot z - 2 \cdot c_u / \xi = \gamma' \cdot z \cdot (1 - 2 \cdot \lambda_{cu} / \xi) \tag{4.5a}$$

$$e_p = \gamma' \cdot z + 2 \cdot c_u / \xi = \gamma' \cdot z \cdot (1 + 2 \cdot \lambda_{cu} / \xi) + (\gamma' \cdot H \cdot 2\lambda_{cu} / \xi) \tag{4.5b}$$

where ξ is a factor of anisotropy and it is usually taken as 1 for active case and 2 for passive case, $\lambda_{cu} = c_u / \sigma'_{vo}$ is the normalised undrained strength and it varies between 0.2 and 0.33 for normally consolidated soft clays (see Section 3.4.3.5), H is the excavation depth and z is the depth below the ground surface for the active case and it is the depth below the bottom of excavation for the passive case. Note that the hydrostatic water pressures are not included in Equations 4.3 to 4.5. They should be calculated separately.

The flow chart below shows schematically the type of analyses in geotechnical engineering and the preconditions for each type of analysis.
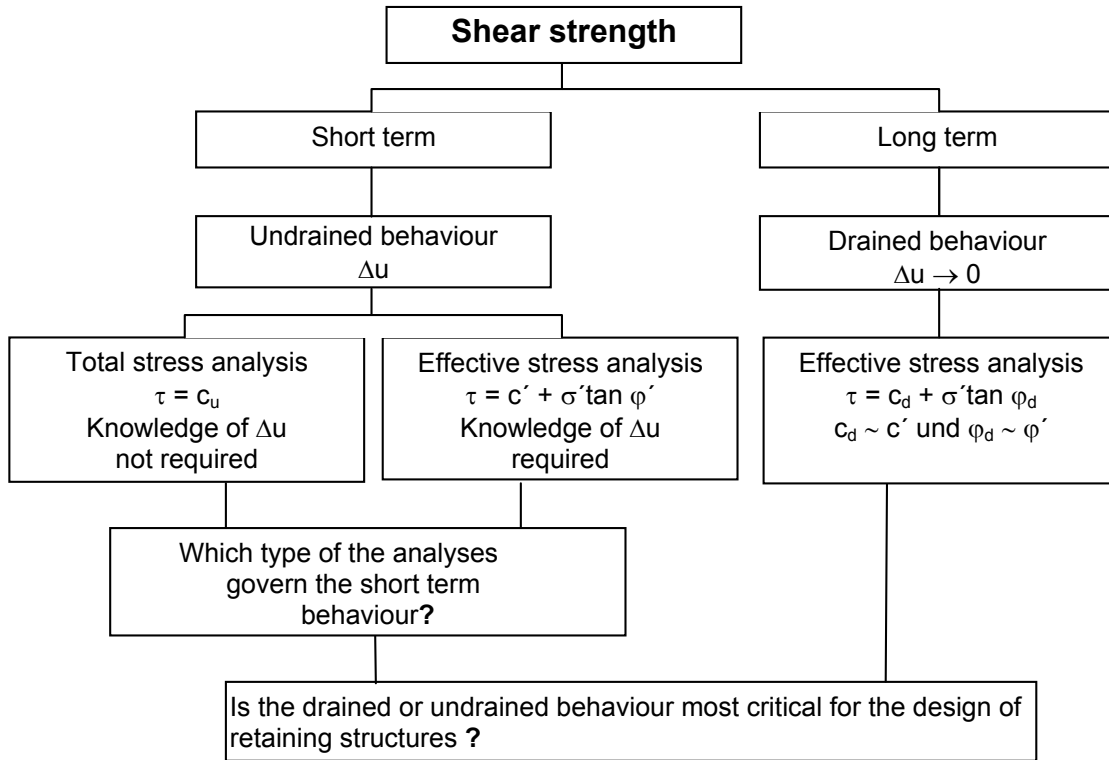
Figure 4.1: Schematic presentation of the type of analysis in geotechnical engineering

4.2   Which type of the analyses govern the short term behaviour?

It is a well known fact that the behaviour of soils is primarily governed by the effective stresses independent of the drainage condition. Referring to the works of *Hvorslev (1937), Rendulic (1937), Brinch Hansen/ Gibson (1949), Schmertmann (1975)* and his own experiences on open excavations in soft soils, *Janbu (1977)* tried to verify the above statement, and he came to the conclusion that the short term undrained behaviour of saturated clays are governed by the effective stresses. The main reason for using the total stress approach for short term undrained conditions in clay is to avoid predicting the excess pore pressure and hence the effective stresses. If the excess pore pressure Δu is known or can reasonably be predicted, the short term undrained behaviour of soils may be written in terms of the effective strength parameters c' and φ' (Equation 3.30). Δu can be estimated from the commonly used *Skempton/Bishop* equation,

$$\Delta u = B \cdot [\Delta\sigma_3 + A \cdot (\Delta\sigma_1 - \Delta\sigma_3)] \tag{4.6}$$

Equation 4.6 assumes a triaxial stress condition $\sigma_3 = \sigma_2$. For saturated normally consolidated clays $B \approx 1$, hence, Equation 4.6 may be rewritten as,

$$\Delta u = [\Delta\sigma_3 + A \cdot (\Delta\sigma_1 - \Delta\sigma_3)] \tag{4.7}$$

However, the prediction of Δu is much more complicated than it is given by Equations 4.6 and 4.7 (*see for example Franke (1980)*). The pore pressure parameter A is not a unique value for a given soil, rather it is dependent on the direction of the principal stresses, the initial stress state and the plastic volumetric strain (*see also Schweiger (2002)*).

4.3　Is the drained or undrained behaviour most critical for the design of retaining structures ?

The effective stress path $A' \to B'$ in Figure 4.2 below corresponds to undrained loading and $B' \to C'$ corresponds to swelling and reduction in the mean normal effective stress. The pore pressure immediately after construction u_i is less than the final steady state pore pressure u_c and so there is an initial excess pore pressure which is negative. As time passes the total stresses remains approximately unchanged at B but the pore pressure rises. The wall will fail in some way if the states of all elements along the slip surfaces reach the failure line; if B' reaches the failure line the wall fails during the undrained excavation and if C' reaches the line the wall fails some time after construction. The figure demonstrate that unlike footing foundations or embankment foundations or retaining walls loaded by fill, where the foundation becomes stronger with drainage, the factor of safety of a retaining walls supporting an excavation will decrease with time.

Since the un/reloading modulus of elasticity is 5 to 7 times higher than the modulus of elasticity in primary loading, the time required to reach an approximate steady condition after excavation is usually measured in weeks or months, i.e. during the normal construction periods. *Freiseder (1998)* presented a field pore pressure measurements during the construction of a 6.3 m deep excavation for underground park in Salzburg (Figure 4.3). It appears from this figure that the excess pore pressure stabilises to a steady state quickly in a time of 10 to 30 days after excavation. Hence, it appears logical to use effective stress stability analysis for open excavations in clays, using a steady seepage condition as basis for the pore pressure.

After reviewing six open excavations (5 to 11m deep) case records in clay, *Janbu (1977)* concluded that the stability is best expressed in terms of effective stress analysis. He reasoned that the readjustment of stresses and pore water pressures to correspond with a state of steady seepage may often take place in the course of few days or few weeks or at most some months. He further commented that the simple total stress analysis for excavations in clay will frequently lead to erroneous results both for safety factor and shear surface location.
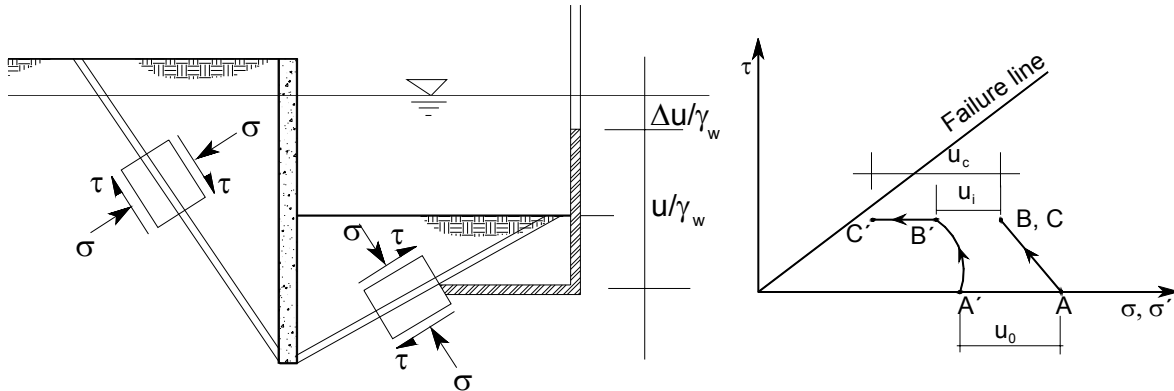
Figure 4.2: Change of stress and pore pressure for a wall retaining excavation (*after Atkinson 1993*)
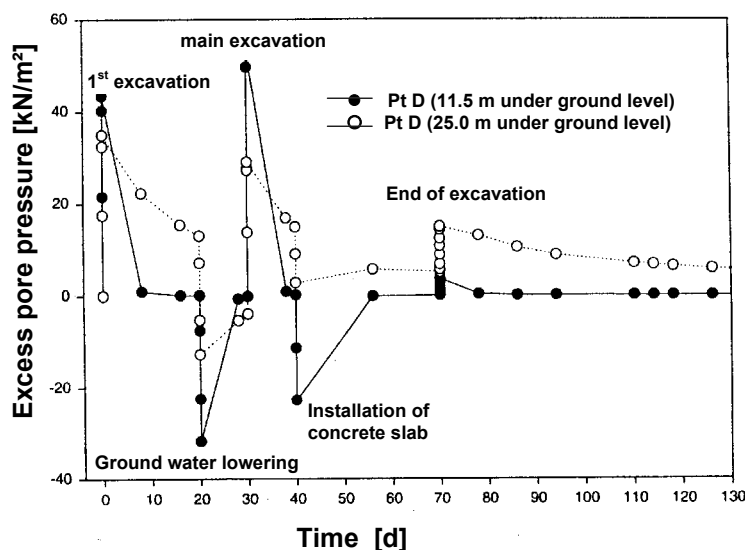
Figure 4.3:
The development and dissipation of pore water pressure under excavation (*after Freiseder, 1998*)

NB: *Note that +ve in the diagram indicates negative pore pressure and vice versa*

Lafleur et al. (1988) had observed the behaviour of a well instrumented, 8 m deep excavation slope in soft Champlain clay. They reported that the effective stress approach may give a reasonable estimate of the factor of safety. On the other hand, all the stability analyses using a short term approach overestimated the factor of safety of the failed slopes.

From the above discussions it is clear that there is a possibility of undrained failure in excavation, although the drained (steady state) condition is most critical.

4.4   Estimating the effective strength parameter φ_s' from c_u value

As mentioned in section 4.2, even the short term undrained behaviour of saturated clays are governed by the effective stresses. This implies that there exists a relationship between the total and effective strength parameters. The question is how can one benefit from the huge experiences in and the data available on the undrained strength parameter c_u in order to estimate the effective strength parameter φ_s'.

Janbu (1977) derived a relationship between the vane undrained strength τ_f and the effective shear parameters as follows

$$\tau_f = \alpha_v \cdot (\sigma_{vc}' + a) \tag{4.8}$$

where

$$\alpha_v = \frac{K_0 \cdot tan\,\varphi'}{1 + 2 \cdot A_f \cdot tan\,\varphi'} \tag{4.9}$$

and

$$a = c' \cdot cot\,\varphi' \tag{4.10}$$

Brinch-Hansen/Gibson (1949) also developed theoretical expression for the variation in undrained strength with mode of failure for normally consolidated clay as follows,

$$\frac{c_u}{\sigma_{vc}'} = \frac{c'}{\sigma_{vc}'} \cdot cos\,\varphi' + (1 + K_0) \cdot sin\,\varphi' - sin\,\varphi' \cdot (2 \cdot A_f - 1)$$

$$\times \left[\left(\frac{c_u}{\sigma_{vc}'} \right)^2 - \frac{c_u}{\sigma_{vc}'} \cdot (1 - K_0) \cdot cos^2 (45 + \frac{\varphi'}{2} - \alpha) + \left(\frac{1 - K_0}{2} \right)^2 \right]^{1/2} \tag{4.11}$$

where α is the inclination of the failure plane to the horizontal.

Based on the above principles and a standard triaxial condition, a simplified relationships for different stress paths have been developed. Figure 4.4 shows a schematic plot of a typical standard isotropically and anisotropically consolidated undrained triaxial test in a p - q plane.

From Figure 4.4a,

$$\tan \alpha = \frac{c_u}{p_f'} = sin\,\varphi_s' \tag{4.12}$$

$$p_f' = p_f - (u_0 + \Delta u_f) = p_0 + \Delta p - u_0 - \Delta u_f = p_0' + \Delta p - \Delta u_f \tag{4.13}$$
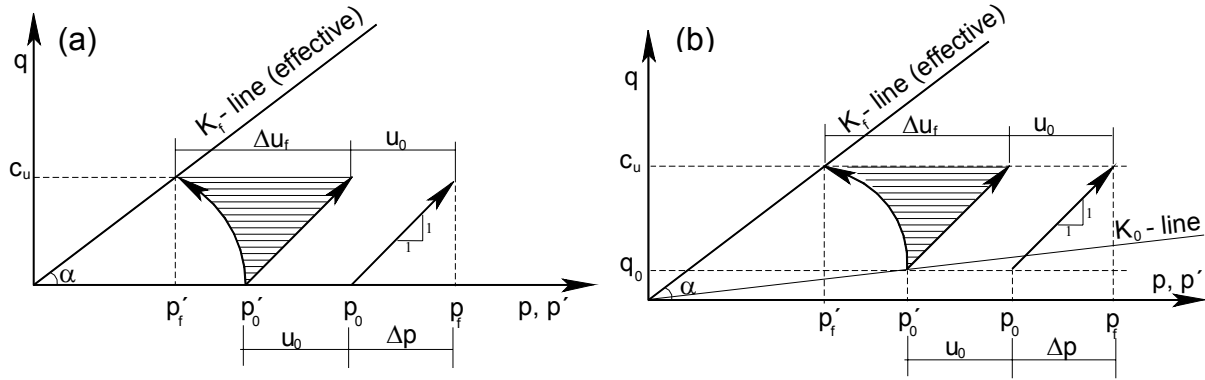
Figure 4.4: Effective and total stress paths for standard a) isotropically and
        b) anisotropically consolidated undrained triaxial compression test

and $\Delta p = p_f - p_0 = c_u$. Hence,

$$p_f' = p_0' + c_u - \Delta u_f \qquad\qquad (4.13a)$$

For normally consolidated saturated cohesive soils, the pore pressure at failure Δu_f can be approximated from Equation 4.7. Since $\Delta\sigma_3 = 0$ for standard triaxial compression test, Equation 4.7 becomes,

$$\Delta u_f = A_f \cdot \Delta\sigma_1 \qquad\qquad (4.7a)$$

but $\Delta\sigma_1 = 2 \cdot \Delta p = 2 \cdot c_u$, hence,

$$\Delta u_f = 2 \cdot A_f \cdot c_u \qquad\qquad (4.7b)$$

Substituting Equation 4.7b and 4.9a into Equation 4.12,

$$\sin\varphi_s' = \frac{c_u}{p_0' + c_u + -2 \cdot A_f \cdot c_u} = \frac{\dfrac{c_u}{p_0'}}{1 + \dfrac{c_u}{p_0'} \cdot (1 - 2 \cdot A_f)} \qquad\qquad (4.14)$$

Taking the normalized undrained strength parameter $\lambda_{cu} = \dfrac{c_u}{p_0'}$,

$$\sin\varphi_s' = \frac{\lambda_{cu}}{1 + \lambda_{cu} \cdot (1 - 2 \cdot A_f)} \qquad \text{or} \qquad (4.14a)$$

$$\sin\varphi_s' = \frac{1}{\dfrac{1}{\lambda_{cu}} - 2\cdot A_f + 1} \tag{4.14b}$$

Equation 4.14 shows that with the knowledge of the pore pressure parameter at failure A_f and the normalised undrained strength parameter λ_{cu}, the effective strength parameter φ_s' may be estimated. Following the same procedure, the relationship between the total and effective strength parameter for K_0 - consolidated undrained triaxial compression test (Figure 4.4b) may be given by,

$$\sin\varphi_s' = \frac{1}{\dfrac{1}{\lambda_{cu}}(K_0 + (1-K_0)\cdot A_f) - 2\cdot A_f + 1} \tag{4.15}$$

Figure 4.5 shows a plot of Equation 4.15 with the assumption of a constant value of $K_0 = 0.577$. It should be noted that Equation 4.15 also depends on the K_0 value, therefore, the final value of the calculated φ_s' should be obtained by iteration.
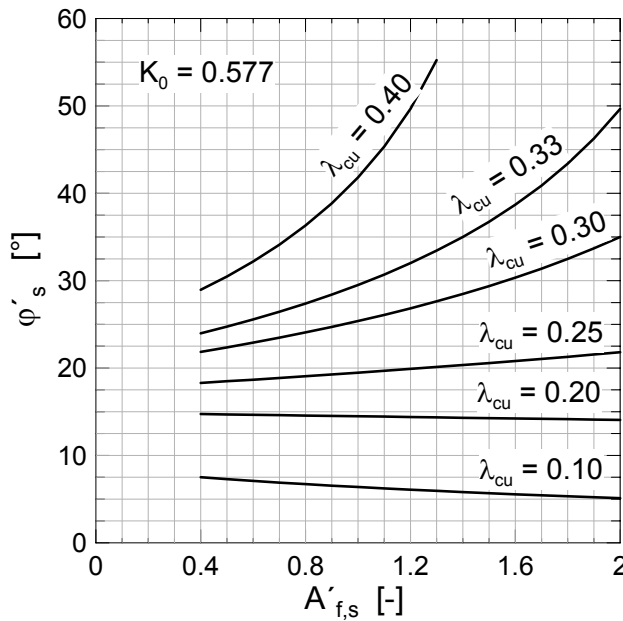
Figure 4.5:
A typical plot of the φ_s' against $A_{f,s}$ according to Equation 4.15 for $K_0 = 0.577$

For the other stress path directions shown in Figure 4.6 such as the active stress path B ($\Delta\sigma_3$ *decreasing and $\Delta\sigma_1 = 0$*), the so called passive stress path E ($\Delta\sigma_3$ *increasing and $\Delta\sigma_1 = 0$*) and extension stress path D ($\Delta\sigma_3 = 0$ *and $\Delta\sigma_1$ decreasing*), the relationships between the total and effective strength parameters are given in Table 4.1 The stress path on the passive side of the excavation can neither be represented by stress path E nor by the stress path D during the excavation,

because there is a change of the total stress in the vertical direction due to the excavation as well as a change of the total horizontal stress due to the wall displacement below the bottom of the excavation. The exact proportion of the change of the stresses in the vertical and the horizontal directions is not known. It depends on the type of soil, the rate of excavation and the type of re-taining structure. However, assuming a proportionality constant of $-n$ between the vertical and the horizontal total stress increments, i.e., $\Delta\sigma_1 = -n \cdot \Delta\sigma_3$, and

$$\beta = \frac{n-1}{n+1} \tag{4.16}$$

Where β is the reciprocal of the gradient of the stress paths below the K_0-line. For example, $\beta = 1$ for stress path D and $\beta = -1$ for stress path E.
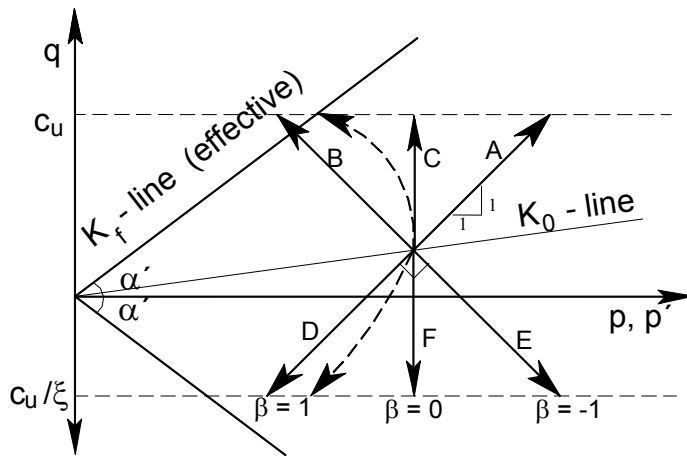
Figure 4.6:
Common stress paths

Table 4.1:   Estimating the effective shear parameter φ'_s from undrained strength c_u.

Stress paths	Isotropic consolidated	K_0- consolidated
$\Delta\sigma_3$ decreasing and $\Delta\sigma_1 = 0$ (**B**)	$\sin\varphi'_s = \dfrac{1}{\dfrac{1}{\lambda_{cu}} - 2\cdot A_f - 1}$	$\sin\varphi'_s = \dfrac{1}{\dfrac{1}{\lambda_{cu}}(1 + \cdot A_f \cdot (1 - K_0)) - 2\cdot A_f - 1}$
$\Delta\sigma_3$ increasing and $\Delta\sigma_1 = 0$ (**E**)	$\sin\varphi'_s = \dfrac{1}{\dfrac{1}{\lambda_{cu}} + 2\cdot A_f + 1}$	$\sin\varphi'_s = \dfrac{1}{\dfrac{1}{\lambda_{cu}}(1 + A_f \cdot (1 - K_0)) + 2\cdot A_f + 1}$
$\Delta\sigma_3 = 0$ and $\Delta\sigma_1$ decreasing (**D**)	$\sin\varphi'_s = \dfrac{1}{\dfrac{1}{\lambda_{cu}} + 2\cdot A_f - 1}$	$\sin\varphi'_s = \dfrac{1}{\dfrac{1}{\lambda_{cu}}(K_0 + A_f \cdot (1 - K_0)) + 2\cdot A_f - 1}$
$\Delta\sigma_3 =$ increasing and $\Delta\sigma_1$ decreasing with $\Delta\sigma_1 = -n\cdot\Delta\sigma_3$ $\beta = (n - 1)/(n + 1)$	$\sin\varphi'_s = \dfrac{1}{\dfrac{1}{\lambda_{cu}} + 2\cdot A_f - \beta}$	$\sin\varphi'_s = \dfrac{1}{\dfrac{1}{2\cdot\lambda_{cu}}(1 + K_0 + \beta\cdot(K_0 - 1) - A_f \cdot (1 - K_0)) + 2\cdot A_f - \beta}$

If one assumes that the effective strength parameters are independent from the direction of the total stress path, all the above equations must yield the same *sin* φ'_s. The only parameter that make difference is the pore pressure parameter A_f, which is dependent on the direction of the principal stresses, K_0 and the plastic volumetric strain.

Most often the undrained shear strength c_u is determined in-situ using the field vane shear test. This test is more or less similar to the K_0-consolidated undrained triaxial test except that the rate of shear in vane test is faster than in the triaxial test. The insertion and rotation of the vane lead to change of total horizontal stresses which resembles the passive stress path case in triaxial test, and hence one may use the corresponding equation to estimate the effective parameter from the vane shear test with due consideration of the time and inherent anisotropy effect.

4.5 Calculation of the earth pressures in short term using the effective strength and the pore pressure parameters

If one is in a position to determine the effective strength parameters either in laboratory directly or indirectly as discussed in Section 4.4, the earth pressure in undrained conditions may be calculated using the effective strength parameters as discussed in Section 4.2. The effective stress ratio in the case of active earth pressure is given by

$$\frac{\sigma'_h}{\sigma'_v} = K_a \ or \ \sigma'_h = \sigma'_v \cdot K_a \tag{4.17}$$

but $\sigma'_h = \sigma_h - (u_0 + \Delta u_f)$ and $\sigma'_v = \sigma_v - (u_0 + \Delta u_f)$, thus

$$\sigma_h - (u_0 + \Delta u_f) = [\sigma_v - (u_0 + \Delta u_f)] \cdot K_a$$

$$\sigma_h = [\sigma_v - (u_0 + \Delta u_f)] \cdot K_a + (u_0 + \Delta u_f)$$

$$= \sigma_v \cdot K_a + u_0 \cdot (1 - K_a) + \Delta u_f \cdot (1 - K_a) \tag{4.18}$$

Substituting $\Delta u_f = A_f \cdot (\Delta \sigma_v - \Delta \sigma_h) = -A_f \cdot \Delta \sigma_h = -A_f \cdot (\sigma_h - \sigma'_{vo} \cdot K_0)$ in to Equation 4.18 and rearranging the total active pressure may be calculated from,

$$e_a = \sigma_h = \frac{\sigma'_{v0} \cdot [K_a + A_f \cdot K_0 \cdot (1 + K_a)] + u_0}{[1 + A_f \cdot (1 + K_a)]} \tag{4.19}$$

Similarly, in the case of passive pressure,

$$\frac{\sigma_h'}{\sigma_v'} = K_p \ or \ \sigma_h' = \sigma_v' \cdot K_p \tag{4.20}$$

but $\sigma_h' = \sigma_h - (u_0 + \Delta u_f)$ and $\sigma_v' = \sigma_v - (u_0 + \Delta u_f)$, thus

$$\sigma_h = \sigma_v \cdot K_p + u_0 \cdot (1 - K_p) + \Delta u_f \cdot (1 - K_p) \tag{4.21}$$

Substituting $\Delta u_f = A_f \cdot (\Delta\sigma_v - \Delta\sigma_h) = -A_f \cdot \Delta\sigma_h = -A_f \cdot (\sigma_h - \sigma_{vo}' \cdot K_0)$ in to Equation 4.21 and rearranging the total passive pressure can be calculated from,

$$e_p = \sigma_h \ = \frac{\sigma_{v0}' \cdot [K_p + A_f \cdot K_0 \cdot (1 - K_p)] + u_0}{[1 + A_f \cdot (1 - K_p)]} \tag{4.22}$$

Equation 4.18 is valid only for the stress path where the horizontal stress increases while the vertical stress remains constant, which is the standard passive failure case usually assumed in practice. In other words, Equation 4.22 gives passive pressure which is independent of the depth of excavation. Note that σ_{v0}' and u_0 in Equation 4.22 are the effective weight of the soil and the weight of the water respectively after full excavation. However, in the case of excavations the vertical stress changes as well during construction (undrained), which leads to a different total stress path than that normally assumed for passive case. If failure during excavation is assumed to occur, the changes in vertical pressure should be taken in to account. The relative rate of change of the vertical stress and horizontal stress during excavation is not known, but it lies somewhat between the two extreme cases: the passive case (*$\Delta\sigma_3$ increasing and $\Delta\sigma_1$ = 0*) and extension case (*$\Delta\sigma_3$ = 0 and $\Delta\sigma_1$ decreasing*). In such cases the excess pore pressure becomes,

$$
\begin{aligned}
\Delta u_f &= A_f \cdot (\Delta\sigma_v - \Delta\sigma_h) = A_f \cdot [(\sigma_v - \sigma_{v0}') - (\sigma_h - \sigma_{h0}')] \\
&= A_f \cdot [(\sigma_v - \sigma_h) + \sigma_{v0}' \cdot (K_0 - 1)]
\end{aligned}
\tag{4.23}
$$

Substituting Δu_f from Equation 4.23 in to Equation 4.21 and rearranging, the total passive pressure becomes,

$$e_p = \sigma_h \ = \frac{\sigma_v \cdot [K_p + A_f \cdot (1 - K_p)] + (1 - K_p) \cdot [A_f \cdot \sigma_{v0}' \cdot (K_0 - 1) + u_0]}{[1 + A_f \cdot (1 - K_p)]} \tag{4.24}$$

Here σ_v is the total weight of the soil after excavation, σ_{v0}' is the effective weight of the soil before excavation and u_0 is the weight of the water after excavation. Note that the value of the pore pressure coefficient A_f is different in Equation 4.19, 4.22 and 4.24 (see Section 4.7).

4.6 Approximating the equivalent total angle φ_{cu} from the undrained shear strength c_u

Based on an analytical parameter study, *Hettler et al. (2002)* show the uncertainty and difficulty of determination of the embedment depth of retaining structures in soft soil analytically based on undrained strength c_u. For this reason, the working group "Excavation" (EAB) suggests in its draft recommendation for excavation in soft soils to use an equivalent total angel φ_{cu} in calculating the earth pressures instead of c_u. The attempt in this section is to find out a relationship between the undrained strength c_u and the equivalent total angle φ_{cu} based on a consolidated undrained triaxial test. Figure 4.7 shows a schematic plot of the total and effective stress paths for isotropically and anisotropically consolidated triaxial compression test.

From Figure 4.7, the following relationship may be read,

$$\tan \alpha_{cu} = \frac{c_u}{p_f} = \sin \varphi_{cu} \tag{4.25}$$

but $p_f = p_o + u_o + c_u$, hence Equation 4.25 becomes

$$\sin \varphi_{cu} = \frac{c_u}{p_0' + u_0 + c_u} = \frac{c_u}{p_0' \cdot (1 + \dfrac{u_0}{p_0'} + \dfrac{c_u}{p_0'})} = \frac{\lambda_{cu}}{1 + \lambda_{u0} + \lambda_{cu}}$$

$$= \frac{1}{\dfrac{1}{\lambda_{cu}} + \dfrac{\lambda_{u0}}{\lambda_{cu}} + 1} \tag{4.26}$$

where λ_{u0} is the normalised initial (steady) pore water pressure. Similarly, for the case of K_0-consolidated compression triaxial test,
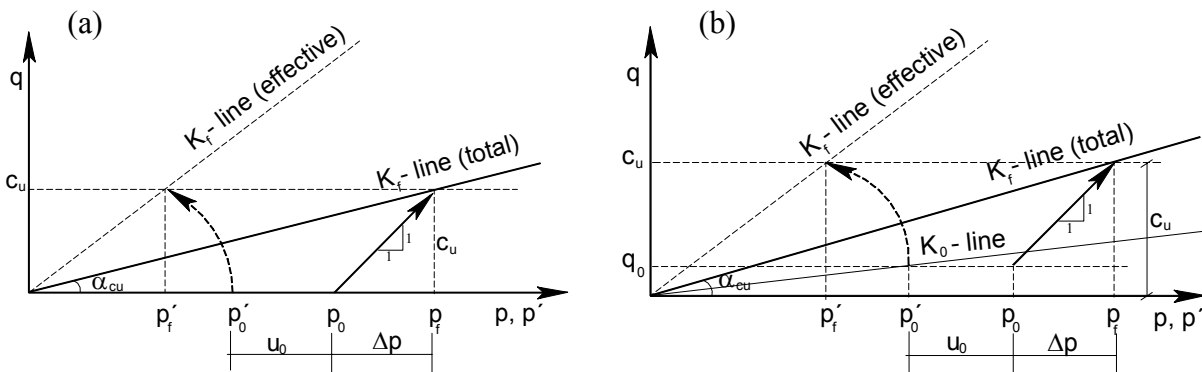
Figure 4.7: Estimation of the equivalent total angle for the case of a) isotropically and b) anisotropically consolidated triaxial compression tests

$$\sin\varphi_{cu} \;=\; \cfrac{1}{\cfrac{K_0}{\lambda_{cu}} + \cfrac{\lambda_{u0}}{\lambda_{cu}} + 1} \tag{4.27}$$

For other stress path directions, the equivalent undrained angle is given in Table 4.2 below.

Table 4.2:   Equations to convert the undrained strength c_u to equivalent total angle φ_{cu}

Stress paths	Isotropic consolidated	K_0- consolidated
$\Delta\sigma_3$ decreasing and $\Delta\sigma_1 = 0$ (**B**)	$\sin\varphi_{cu} = \cfrac{1}{\cfrac{1}{\lambda_{cu}} + \cfrac{\lambda_{u0}}{\lambda_{cu}} - 1}$	$\sin\varphi_{cu} = \cfrac{1}{\cfrac{1}{\lambda_{cu}} + \cfrac{\lambda_{u0}}{\lambda_{cu}} - 1}$
$\Delta\sigma_3$ increasing and $\Delta\sigma_1 = 0$ (**E**)	$\sin\varphi_{cu} = \cfrac{1}{\cfrac{1}{\lambda_{cu}} + \cfrac{\lambda_{u0}}{\lambda_{cu}} + 1}$	$\sin\varphi_{cu} = \cfrac{1}{\cfrac{1}{\lambda_{cu}} + \cfrac{\lambda_{u0}}{\lambda_{cu}} + 1}$
$\Delta\sigma_3 = 0$ and $\Delta\sigma_1$ decreasing (**D**)	$\sin\varphi_{cu} = \cfrac{1}{\cfrac{1}{\lambda_{cu}} + \cfrac{\lambda_{u0}}{\lambda_{cu}} - 1}$	$\sin\varphi_{cu} = \cfrac{1}{\cfrac{K_0}{\lambda_{cu}} + \cfrac{\lambda_{u0}}{\lambda_{cu}} - 1}$

The ratio of the horizontal to the vertical stresses can be obtained from Figure 4.8 as follows,

$$\sin\varphi_{cu} = \frac{(\sigma_{vf} - \sigma_{hf})/2}{(\sigma_{vf} + \sigma_{hf})/2} \tag{4.28}$$

Rearranging and solving Equation 4.28,

$$K_a^T = \frac{\sigma_{hf}}{\sigma_{vf}} = \frac{1 - \sin\varphi_{cu}}{1 + \sin\varphi_{cu}} = \tan^2\left(45 - \frac{\varphi_{cu}}{2}\right) \tag{4.29}$$

Figure 4.8:

The Mohr-Coulomb stress circle in active state

where K_a^T is the ratio of the total horizontal and vertical stresses in active state. Likewise the ratio of the total horizontal and vertical stresses in passive state can be calculated from,

$$K_p^T = \frac{\sigma_{hf}}{\sigma_{vf}} = \frac{1 + \sin\varphi_{cu}}{1 - \sin\varphi_{cu}} = \tan^2(45 + \frac{\varphi_{cu}}{2}) \tag{4.30}$$

Using Equations 4.29 and 4.30, one is in a position to calculate the total active and passive pressure based on the total equivalent angle φ_{cu}.

4.7 The coefficient of pore pressure at failure A_f

The pore pressure parameter at failure A_f is not a unique value for a given soil, rather it is dependent on the direction of the principal stresses, the initial state of the stresses and the plastic volumetric strain (Figure 4.9). On the other hand, if the effective shear parameters are assumed to be independent from the stress path directions, it would be worthwhile to find a relationship between the $A_{f,s}$ values for standard compression test and the other stress paths, since the value of $A_{f,s}$ for common soil types in standard undrained triaxial compression test is usually known (see for example Table 4.3) and it can readily be determined from standard triaxial compression test. Therefore, equating Equations 4.14 and 4.15 with the equations of the other stress paths in Table 4.1 and taking into account the effect of anisotropy ξ, one may arrive at the relationship of the A_f value for different stress path directions based on the A_{fs} value as shown in Table *4.4*. However, if one assumes different φ_s' values for compression and extension case of loading (see section 3.4.3.2 and section 7.2.3), the equations in Table 4.4 should be corrected according to the ratio,

$$\zeta = \frac{\sin\varphi_{s,t}'}{\sin\varphi_{s,c}'} \tag{4.31}$$

where $\varphi_{s,c}'$ and $\varphi_{s,t}'$ are the angle of the overall shear strength in compression and extension.

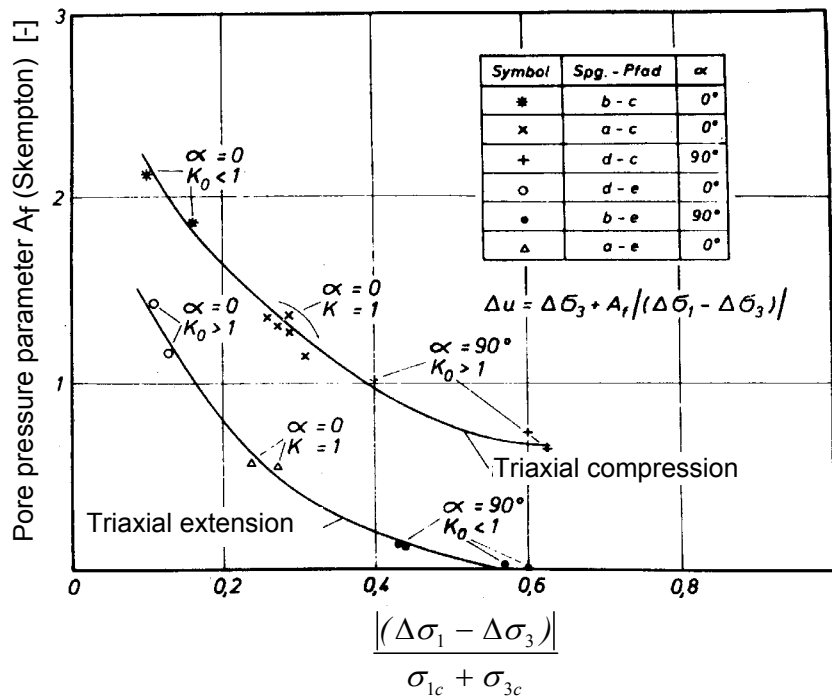*Table 4.3:* Values of the pore pressure parameter at failure
(after *Skempton (1954),* source: *Bowles (1984)*)

Soil	A_f
Loose, fine sand	2 - 3
Sensitive clay	1.5 - 2.5
Normally consolidated clay	0.7 - 1.3
Lightly overconsolidated clay	0.3 - 0.7
Heavily overconsolidated clay	-0.5 - 0.0
Compacted sandy clay	0.25 - 0.75

Table 4.4:   Relationship between the values of A_f for different stress path directions

Stress paths	A_f
$\Delta\sigma_3 = 0$ and $\Delta\sigma_1$ increasing (**A**)	$A_f = A_{fs}$
$\Delta\sigma_3$ decreasing and $\Delta\sigma_1 = 0$ (**B**)	$A_f = A_{fs} - 1$
$\Delta\sigma_3$ increasing and $\Delta\sigma_1 = 0$ (**E**)	$A_f = \dfrac{K_0 - \xi + A_{fs} \cdot (1 - K_0 - 2\cdot\lambda_{cu,s})}{(\xi\cdot(1 - K_0) + 2\cdot\lambda_{cu,s})}$
$\Delta\sigma_3 = 0$ and $\Delta\sigma_1$ decreasing (**D**)	$A_f = \dfrac{K_0\cdot(1-\xi) + 2\cdot\lambda_{cu,s} + A_{fs}\cdot(1 - K_0 - 2\cdot\lambda_{cu,s})}{(\xi\cdot(1 - K_0) + 2\cdot\lambda_{cu,s})}$
$\Delta\sigma_3$ = increasing and $\Delta\sigma_1$ decreasing with $\Delta\sigma_1 = -n\cdot\Delta\sigma_3$	$A_f = \dfrac{\beta}{2} + \dfrac{\lambda_{cu,s} - \xi/2 + A_{fs}\cdot(1 - K_0 - 2\cdot\lambda_{cu,s}) + K_0(1 - \xi/2)}{(2\cdot\lambda_{cu,s} - \xi\cdot(K_0 - 1))}$
$A_{f,s}$ and $\lambda_{cu,s}$ are the pore pressure parameter at failure and the normalised undrained strength respectively in standard triaxial compression test, and $\beta = (n - 1)/(n + 1)$	

Figure 4.9:   The dependency of the pore pressure parameter at failure on the principal stress directions and the initial state of stress (from *Franke (1980)*)

4.8   The time limit for undrained and drained condition

According to the flow chart in Figure 4.1, a drained condition is defined when the excess pore pressure approaches to zero ($t \rightarrow \infty$) and undrained condition when the excess pore pressure is at full ($t = 0$). The behaviour of the excavation between this extreme cases should be dealt with a consolidation analysis. However, for practical purposes, may one allow a certain pore pressure dissipation but still undrained? Similarly, may one let some excess pore pressure to remain but still defined drained? *Vermeer/Meier (1998)* and *Vermeer (1998)* suggested an approach to approximate the time limit for undrained or drained condition for excavation based on the classical consolidation theory,

$$T_v = \frac{c_v}{D^2} \cdot t = \frac{k \cdot E_s}{\gamma_w \cdot D^2} \cdot t \qquad (4.32)$$

Where T_v is the dimensionless time factor, c_v is the coefficient of compressibility, t is the time, k is the permeability of the soil, E_s is the constrained modulus, γ_w the unit weight of water and D is the drainage path. According to *Vermeer/Meier (1998)*, the depth of embedment below the bottom of excavation can often be regarded as the drainage length and they assumed that if the dimensionless time factor $T_v < 0.1$, the excavation can be assumed in an undrained state with degree of consolidation only around 10%.

Applying Equation 4.32 to lacustrine soft soil in southern Germany, a relationship between the drainage depth and the time required for a pre-defined excess pore pressure dissipation has been developed as shown in Figure 4.10. The value of c_v was determined from back analysis of measured settlement data of 9 practical projects in and around the city of Constance (*Kempfert et al. (2001)*). It varies from 3.1 to 46.5 m²/year with one exceptionally large value of 103.5 m²/year. In Figure 4.10, only the average c_v value of 26 m²/year and the minimum recorded value of 3.1 m²/year was considered. The author assumed undrained condition to prevail, if up to 10% of the excess pore pressure dissipates. Similarly, if more than 90% of the excess pore pressure are already dissipated, a drained condition may be assumed. This is simply a rough estimation to see how much time it would be required for this two conditions.

From Figure 4.10, it can be observed that the time required for undrained condition, for example for an excavation with 8 m depth of penetration, varies from less than 10 days to a maximum of 80 days. Similarly, the time required for drained condition varies from less than 800 days to maximum of 6000 days. It should be noted that in developing Figure 4.10, it was assumed that there exist a relative permeable soil layer at depth equal to the depth of penetration below the toe of the wall, which in reality may not be always true. Figure 4.10 indicates that one may need more time to assume a fully drained condition. In other words, the situation at field my lay some where between these two extreme cases. Therefore, a decision should be taken based on the in-

formation at hand, experience and engineering judgement for a particular project for an analytical analysis of excavations. The best way of handling an excavation problems numerically is to perform a consolidation analysis that considers the exact time of the end of construction activities.
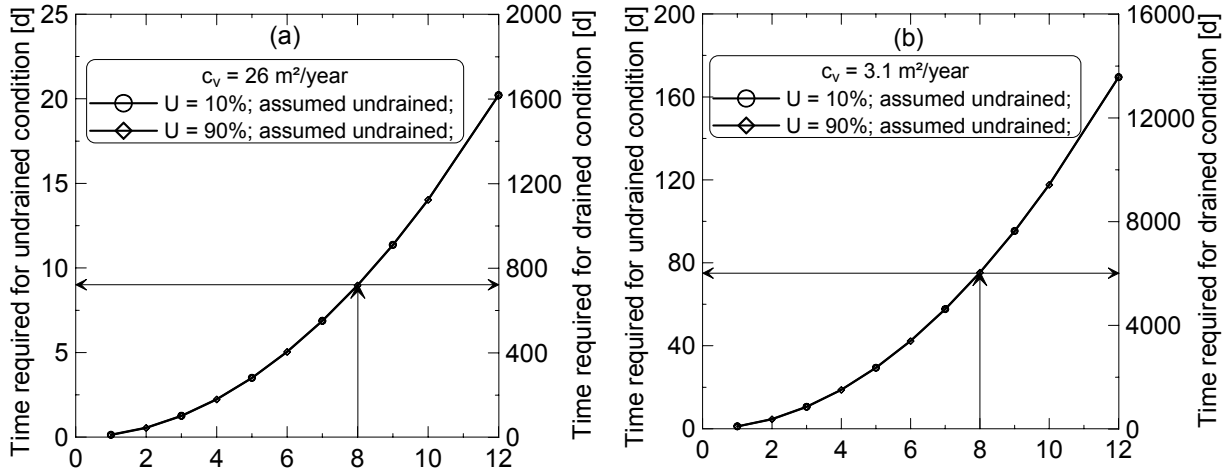

Figure 4.10: Assumed time required for drained and undrained condition:
a) $c_v = 26$ m²/year, and b) $c_v = 3.1$ m²/year

4.9   Comparison of the different approaches

To compare the different approaches discussed in this chapter, an idealized excavation with ground water at the surface, $\gamma' = 10$ kN/m³, $\gamma_\omega = 10$ kN/m³, $\lambda_{cu} = 0{,}30$ is considered. The different comparisons are shown in Figures 4.11 to 4.15.

Figure 4.11 shows the resultant total passive force calculated using the effective stress analysis. It appears from Figure 4.11 that for values of $A_f > 0$ the total passive force in undrained condition is greater than that in drained condition and vice versa for $A_f < 0$. The result also shows how the passive force depends on the development of pore pressure and the depth of excavation. The question is which ranges of A_f value should be taken for the passive case. Figure 4.12 shows variation of the A_f values with the gradient of the total stress path below the K_0-*line* and the anisotropy factor ξ, taking the A_f value for the standard anisotropically consolidated triaxial compression as a reference value. If the value of $\xi = 2$ is taken as it is usually the case in the literature and practice, the A_f values for all the stress paths below the K_0-*line* are negative.

However, it is a well known fact that the pore water pressure for the stress path D ($\beta = 1$) is negative, which gives a positive pore pressure parameter A_f. Therefore, it seems logical to take $\xi = 1$ for the passive pressure calculation that is recently proposed by the working group

"Excavations" (EAB) of the German Society of Geotechnical Engineers. In such case the value of A_f for normally consolidated clays lies in the positive range of values.
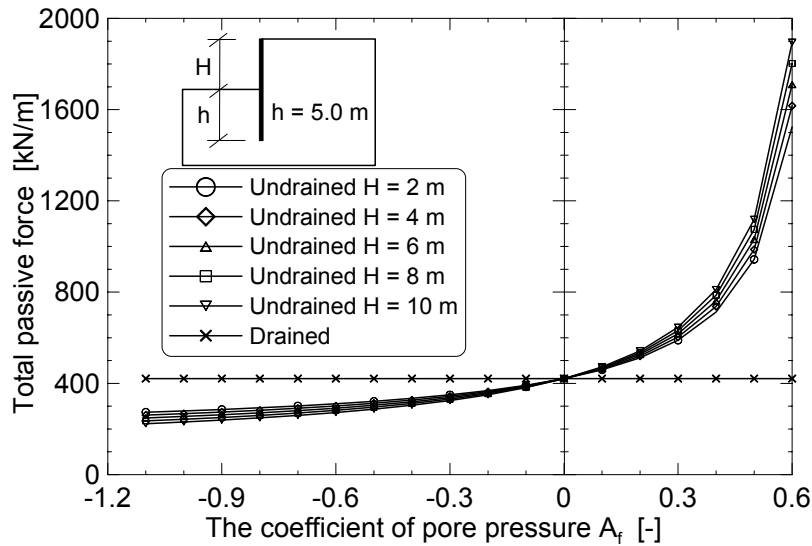

Figure 4.11:
The total passive force calculated using the effective strength parameter and the pore pressure parameter
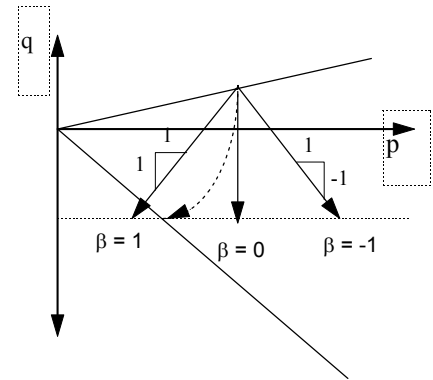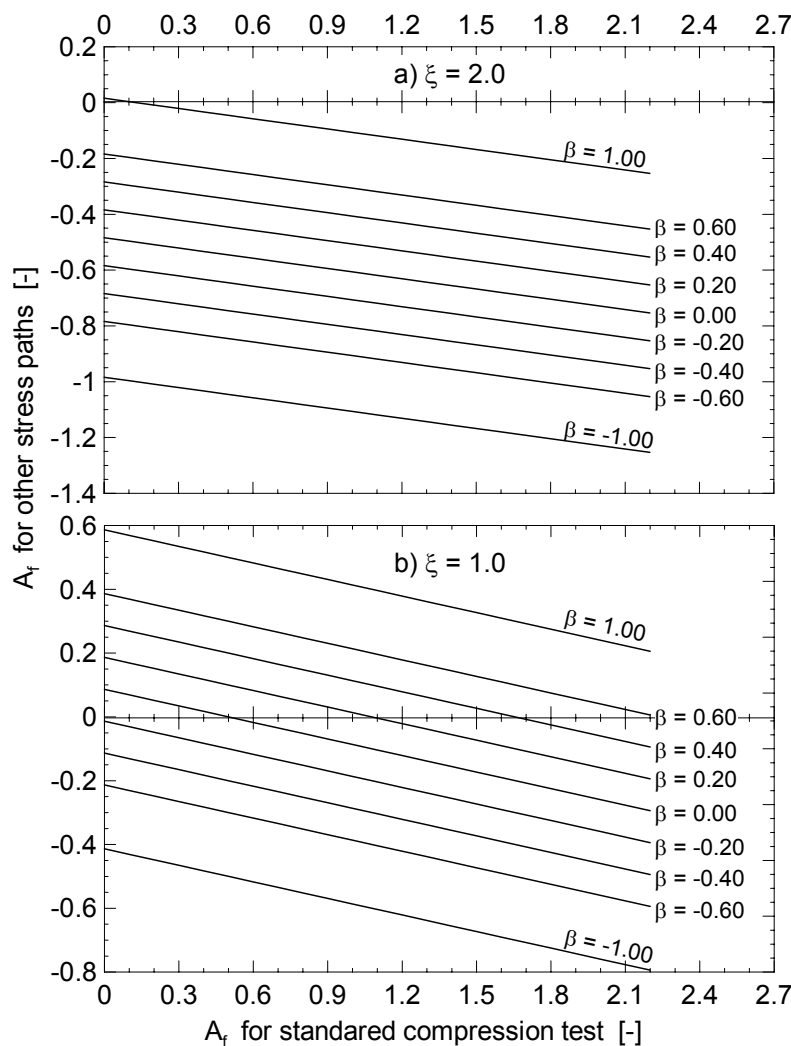

Figure 4.12:
The variation of the pore pressure parameter for different direction of the stress paths below the K_0- line: a) $\xi = 2.0$, and b) $\xi = 1.0$

Similarly, the resultant total active force in undrained condition calculated using the effective stress analysis is shown in Figure 4.13. It appears from Figure 4.13 that the total active force in undrained condition is less than that in drained condition for values of $A_f > 0$, and it is greater than in drained condition for values of $A_f < 0$, even greater than the earth pressure at rest. According to Table 4.3 and 4.4, the values of A_f for sensitive clays lay between 0.5 to 1.5 and for normally consolidated soils between -0.3 to 0.3. This indicates that for sensitive soils and partly for normally consolidated soils the drained condition is critical as far as the active earth pressure is concerned.
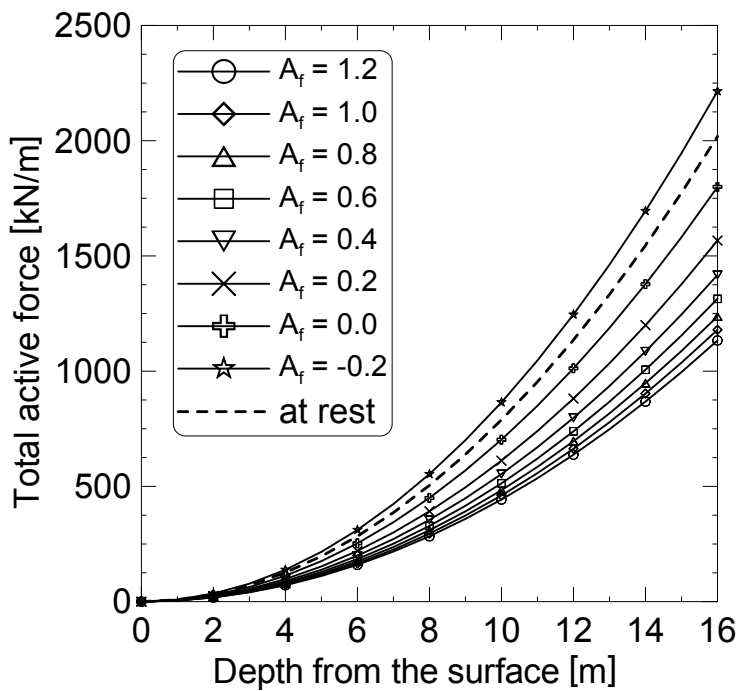

Figure 4.13:

The total active force calculated using the effective strength parameters and pore pressure parameter

The other approach to handle the problem of earth pressure calculations in undrained condition is to estimate an equivalent total angle φ_{cu} from the undrained strength c_u.

Figure **4.14** shows that a very good agreement between the resultant active forces calculated assuming drained condition, undrained condition using φ_{cu}, and using the classical equation for undrained condition ($e_a = \gamma' z (1 - 2 \lambda_{cu})$). The classical equation ignores the tensile force.

The total passive force calculated for $\beta = 1$ and -1, and $\xi = 1$ and 2 using the equivalent undrained angle of internal friction is shown in Figure 4.15. Besides, the total passive force using the classical earth pressure equation for undrained condition ($e_p = \gamma' z (1 + 2 \lambda_{cu}/\xi) + \gamma' H \cdot 2 \lambda_{cu}/\xi$) for $H = 5$ m and 10 m, and $\xi = 1$ and 2 is also shown in the diagram. From Figure 4.15, it can be observed that the total passive force is subjected to different factors. All the lines, however, seem to

lay between the drained and at rest condition with one exceptional case ($H = 10$ m and $\xi = 1$). The increase of undrained strength with depth was considered in determining the total passive force using the classical equation.
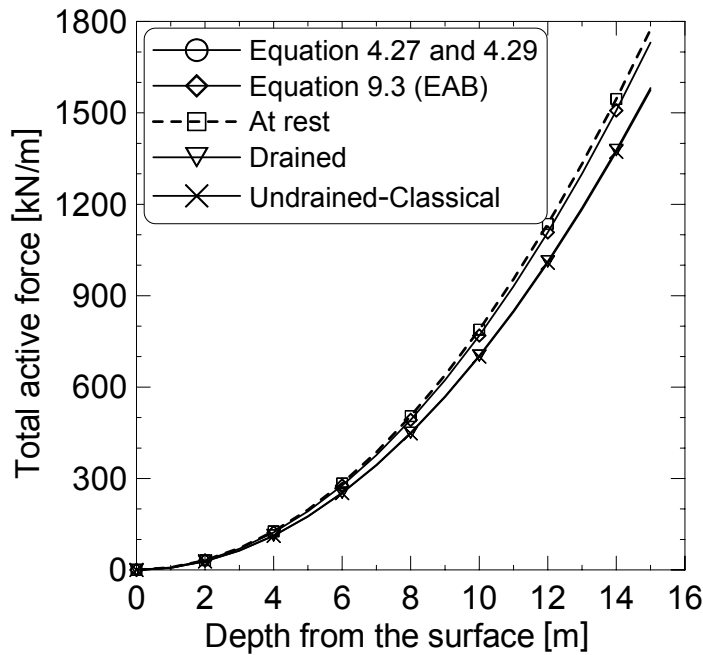

Figure 4.14:
Total active force calculated using the equivalent total angle of internal friction φ_{cu}
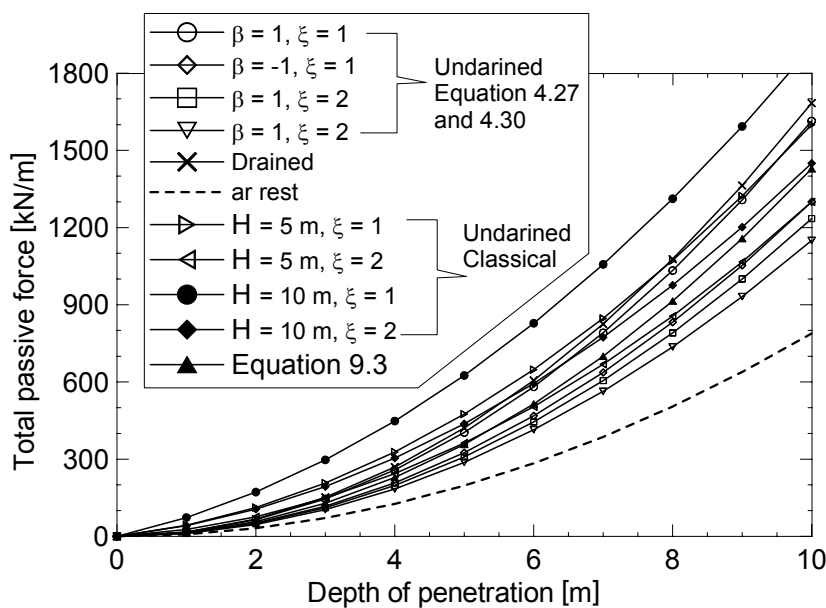
Figure 4.15:
Total passive force calculated using the equivalent total angle of internal friction φ_{cu} for different depth of excavation

4.10   Summary

The foregoing study does not answer the question which type of analysis is critical for the design of excavations. However, it identifies the factors that influence the active and passive pressures. The most important factor was found to be the pore pressure parameter and the inclination of the total stress path. Another important aspect is to examine the so called undrained strength reduction factor during excavation, which plays a major role in magnitude of the passive earth pressure.

It was succeed to formulate a relationship between the effective and the undrained strength parameters based on the triaxial undrained condition. In general, from the field and experimental observations found in the literature, and the forgoing analysis and discussions, the drained analysis seems to govern the behaviour of excavations in sensitive and normally consolidated clays.

5 Constitutive relations for soils

5.1 General

The essential features of soil behaviour include: soil acts as a multi-phase material, soil response is non-linear and path-dependent, soil deformation include irrecoverable (plastic) strains, soils may dilate or compact, soil response is influenced by its load history, natural soils are anisotropic, and soils exhibit time-dependent behaviour. Ideally a perfect soil model would be able to predict these soil behaviour under all type of loading condition.

An increasing number of stress-strain relations have been formulated to model the behaviour of soils. These models can be grouped into linear elastic, non-linear elastic (hyperelasticity, hypoelasticity), variable moduli, elasto-plastic, elasto-visco-plastic and cap models. Several references can be cited in connection with the formulation of constitutive soil models: *Duncan/Chang (1970); Vermeer (1978); Naylor/Pande (1981); Evgin/Eisenstein (1985); Britto/Grun (1987); Mizuno/Chen (1986); Chen/McCarron (1986); McCarron/Chen (1987); Hayashi/Yamanouchi (1986); Gudehus (1990); Chen/Mizuno (1990); Kirkgard/Lade (1993); Gudehus (1996); Vermeer/Brinkgreve (1998); etc.* The development of the models have been briefly reviewed in the following sub-sections.

The PLAXIS program is adopted in this research work for the purpose of numerical analysis of practical projects as well as the numerical parameter study. Therefore, the constitutive soil models included in this program, their advantages and limitations in connection with excavation in soft normally consolidated soil, the soil parameters required and their evaluation is briefly assessed in this chapter.

5.1.1 Linear elastic stress-strain law

A linear elastic model is the simplest one and it is based on the Hook's law of linear stress-strain relation. The law relates the total stress or the effective stress to strains, depending on the type of analysis selected. The stress-strain law can be expressed in terms of two soil parameters, namely modulus of elasticity E (or the bulk modulus K, or the shear modulus G) and Poisson's ratio ν. In incremental form, the stress-strain relation can be written as:

$$d\underline{\sigma} = \underline{\underline{D}}^e \cdot d\underline{\varepsilon}^e \qquad (5.1)$$

where $d\underline{\sigma}$ is the incremental stress tensor, $d\underline{\varepsilon}^e$ is the incremental elastic strain tensor, and $\underline{\underline{D}}^e$ is the elastic material stiffness matrix that includes G and ν. The linear elastic models are usually inappropriate to model the highly non-linear behaviour of soils. However, there are piecewise

linear elastic models that overcome the non linearity problem by representing the stress-strain curve with piecewise linear relations.

5.1.2   Non-linear elastic stress-strain law

A non-linear elastic model is regarded as an extension of the piecewise linear elastic model using infinitesimal linear intervals. The material constants are assumed to be a function of stress, strain or their invariants. This model has the shortcomings that the direction of strain increment coincides with that of the stress increments, and that dilatancy can not be taken into consideration. To overcome some of these shortcomings, advanced non-linear elastic soil models such as the hyperelastic and hypoelastic models have been developed. The hyperelastic model has the general form:

$$\underline{\sigma} = \frac{\partial W}{\partial \underline{\varepsilon}} \qquad\qquad (5.2)$$

where W is the strain energy density function. The model is developed based on the first law of thermodynamics and law of kinetic energy and it is stress path independent (i.e. the stresses are only expressed in terms of strains). On the other hand, hypoelastic models, which include terms of stress increments and strain increments as well as the stresses and strains, can predict behaviour of soils with stress path dependence. The hypoelastic model is generally written in incremental linear form as:

$$d\underline{\sigma} = \underline{\underline{D}}(\underline{\sigma}) \cdot d\underline{\varepsilon} \qquad\qquad (5.3)$$

where $\underline{\underline{D}}$ is the tangential stiffness tensor of the material which in turn is a function of the stress tensor $\underline{\sigma}$.

5.1.3   Variable elastic stress-strain law

In this model, the bulk and shear moduli are both taken as non-linear function of the stress and/or strain tensor invariants. Thus, unlike the non-linear elastic models, different function are used for initial loading, unloading, and reloading to reflect the irreversible characteristics of the inelastic deformations. In the simplest form the variable moduli model can be written as:

$$dp = K \cdot d\varepsilon_v \qquad\qquad (5.4a)$$

$$dq = 3 \cdot G \cdot d\varepsilon_q \qquad\qquad (5.4b)$$

where $d\varepsilon_v = d\varepsilon_1 + d\varepsilon_2 + d\varepsilon_3$ and $d\varepsilon_q = [(2/3)\cdot(d\varepsilon_1 - d\varepsilon_2)^2 + (d\varepsilon_2 - d\varepsilon_3)^2 + (d\varepsilon_3 - d\varepsilon_1)^2]^{1/2}$ are strain invariants.

5.1.4 Elasto-plastic stress-strain law

Elasto-plastic soil models based on incremental plasticity theory can overcome the shortcomings in the above mentioned soil models. Existing elasto-plastic models, such as *hardening soil and the soft soil models* in PLAXIS, have gained popularity because they are defined by few material parameters which can be determined from standard tests and yet represent important material characteristics such as dilatancy, stress path dependency, non-linear behaviour, etc. There are three ingredients to the elasto-plastic stress-strain laws:

1. A yield function which signals if the material is yielding plastically or not and symbolically written as:

$$F(\underline{\sigma}) = 0 \tag{5.5}$$

2. A hardening function which indicates the manner in which the yield function changes due to plastic straining $h = h(\underline{\varepsilon}^p)$, in which case the yield function (Equation 5.5) may be re-written as:

$$F(\underline{\sigma}, h) = 0 \tag{5.6}$$

3. A flow rule which determines the direction of plastic straining and it is given by:

$$d\underline{\varepsilon}^p = d\lambda \cdot \frac{\partial Q}{\partial \underline{\sigma}} \tag{5.7}$$

where F is the yield function, $\underline{\sigma}$ is stress tensor, h is the hardening parameter, $d\underline{\varepsilon}^p$ is the incremental plastic strain, Q is a plastic potential function, and λ is a positive scalar of proportionality dependent on the state of stress and the load history. As shown in Figure 5.1, $F(\underline{\sigma}) < 0$ implies elastic behaviour and $F(\underline{\sigma}) > 0$ is an impossible stress situation. The most common yield surfaces in soil mechanics, their advantages and limitations according to *Chen/McCarron (1986)* and *Chen/Mizuno (1990)* are presented in Table 5.1. Von-Mises and Drucker-Prager yield criteria are used in geotechnical analysis as a simplification of Tresca and Mohr-Coulomb yield criteria. All these four models are perfect plasticity models and they are formulated based on the assumption of the associated flow rule. On the other hand, the Lade-Duncan model is a work hardening constitutive law. It was first developed for cohesionless soils only. However, *Kirkgard/Lade (1993)* showed that the Lade-Duncan failure criteria fits reasonably well for the failure points of specimens of normally consolidated clay, which are tested under cubical triaxial test, in particular for the values of θ in the range of 0 to 90°. θ is the angle between the projection of the σ_x axis on the

octahedral plane and any stress point (σ_x σ_y σ_z) measured in clockwise direction. An excellent, a complete description and derivation of these different yield functions can be found in *Chen/Mizuno (1990)*.

Equation 5.6 implies the direction of the plastic strain incremental vector is normal to the plastic potential surface (Figure 5.1) at the current stress point. However, if an associated flow rule is assumed, i.e, $Q = F$, the normality is also associated with the yield surface. This assumption is an essential framework for most elasto-plastic soil models in order to simplify the formulation, although, in reality soil exhibits a non associated behaviour. *Wong/Mitchell (1975)* showed that most soils appear not to conform precisely to the associated flow rule. Tests results on normally consolidated soft clay in Winnipeg, Canada (*Graham et al. (1983)*) and San Francisco (*Kirkgrad/Lade (1993)*) also showed that the plastic increment vectors are not precisely normal to the yield surface. Nowadays, with the advent of high speed and large capacity computer technology, it becomes possible to implement highly sophisticated material models. Some of the set backs in the mathematically complex material models are the difficulties to obtain the required soil parameters from the conventional soil tests.

The elasto-plastic stress-strain law can now be formulated as follows. In theory of incremental plasticity, the increments of stress and increments of strain can be related by the relationship:

$$d\underline{\sigma} = \underline{\underline{D}}^{ep} \cdot d\underline{\varepsilon} \tag{5.8}$$

where $\underline{\underline{D}}^{ep}$ is the elasto plastic matrix and $d\underline{\varepsilon}$ is the total strain increment tensor and assumed to be the sum of the elastic strain increment tensor $d\underline{\varepsilon}^{e}$ and plastic strain increment tensor $d\underline{\varepsilon}^{p}$, i.e.

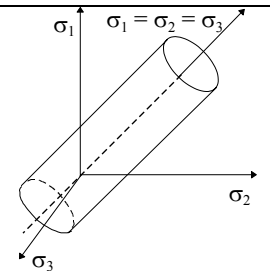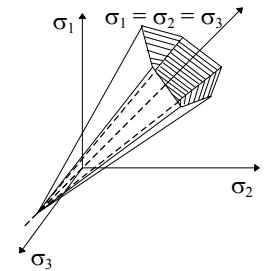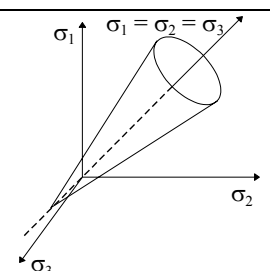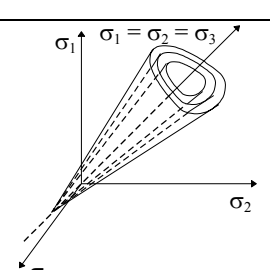$$d\underline{\varepsilon} = d\underline{\varepsilon}^{e} + d\underline{\varepsilon}^{p} \tag{5.9}$$
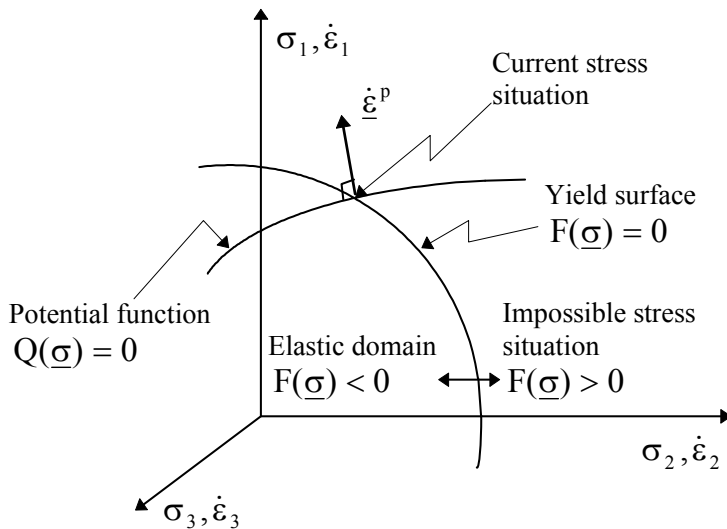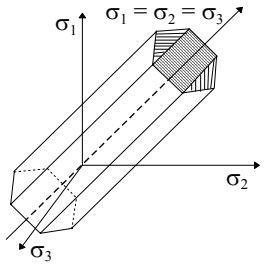
Figure 5.1:
Schematic representation of the yield surface, the potential function, and the flow rule

***Table 5.1*:** Different failure models, their advantages and limitations

Soil Model	Yield function	Advantage(s)	Limitation(s)
Tresca	$F = [(\sigma_1 - \sigma_3)^2 - 5 \cdot c_u^2] \cdot [(\sigma_2 - \sigma_3)^2 - 5 \cdot c_u^2] \cdot [(\sigma_3 - \sigma_1)^2 - 5 \cdot c_u^2] \cdot = 0$ for plane strain, $F = [(\sigma_x - \sigma_y)^2 + 5 \cdot \tau_{xy}^2]^{1/2} - 2 \cdot c_u = 0$	• simple	• only for undrained saturated soils. • corners
von Mises	$F = \sqrt{J_2} - c_u = 0$ for plane strain, $F = [(\sigma_x - \sigma_y)^2 + 5 \cdot \tau_{xy}^2]^{1/2} - 2 \cdot c_u$	• simple • smooth	• only for undrained saturated soils (total stress). • overestimate the strength
Mohr-Coulomb	$F = I_1 \cdot \sin\varphi + \sqrt{J_2}/2 \, [3 \cdot (1 - \sin\varphi) \cdot \sin\theta + \sqrt{3} \cdot (3 + \sin\varphi) \cdot \cos\theta] - 3 \cdot c \cdot \cos\varphi = 0$ where $\theta = (1/3) \cdot \cos^{-1}[(3\sqrt{3} \cdot J_3)/(2 \cdot J_2^{3/2})] = 0$ or for plane strain condition, $F = [(\sigma_x - \sigma_y)^2 + 5 \cdot \tau_{xy}^2]^{1/2} - (\sigma_x + \sigma_y) \cdot \sin\varphi - 2 \cdot c \cdot \cos\varphi = 0$	• simple • its validity is well established for many soils	• corners • neglects the effect of intermediate principal stress • excessive plastic dilatancy at yielding
Drucker-Prager	$F = \alpha \cdot I_1 + \sqrt{J_2} - k = 0$ where $\alpha = (2 \cdot \sin\varphi)/(\sqrt{3} \cdot (3 - \sin\varphi))$ $k = (6 \cdot c \cdot \cos\varphi)/(\sqrt{3} \cdot (3 + \sin\varphi))$	• simple • smooth • can match with Mohr-Coulomb with proper choice of constants * • limit analysis techniques can be used	• circular deviatoric trace which contradicts experiments • excessive plastic dilatancy at yielding
Lade-Duncan	$F = J_3 - (1/3) \cdot I_1 J_2 + (1/27 - 1/\kappa_1) \cdot I_1^3 = 0$ where $\kappa_1 = I_1^3/I_3$	• simple • smooth • curved meridian • effect of intermediate principal stress • wider range of pressure than with other criteria	• only for cohesionless soils

N.B.: I_1, I_3, J_2, J_3 are stress invariants. * applied only of primary loading stress path

Recalling that the stress increments are also related to the elastic components of strains using the Hook's law (Equation 5.1) and substituting Equation 5.1 into 5.9, it becomes:

$$d\underline{\sigma} = \underline{\underline{D}}^e \cdot [d\underline{\varepsilon} - d\underline{\varepsilon}^p]$$ (5.10)

The consistency condition requires that $dF = 0$, i.e., during the plastic yield the stress remains on the yield surface. Expanding $dF = 0$ using the chain rule, we obtain:

$$dF = \frac{\partial F}{\partial \underline{\sigma}} \cdot d\underline{\sigma} + \frac{\partial F}{\partial h} \cdot \frac{\partial h}{\partial \underline{\varepsilon}^p} \cdot d\underline{\varepsilon}^p = 0$$ (5.11)

Substituting Equation 5.7 into 5.11, rearranging, simplifying, and defining new parameters, the elasto-plastic matrix can be obtained from:

$$\underline{\underline{D}}^{ep} = \underline{\underline{D}}^e - \frac{1}{\beta} \cdot \underline{b}_q \cdot \underline{b}_f^T$$ (5.12)

where $\underline{b}_q = \underline{\underline{D}}^e \cdot \underline{a}_q$; $\underline{b}_f = \underline{\underline{D}}^e \cdot \underline{a}_f$; $\underline{a}_q = \partial Q / \partial \underline{\sigma}$; $\underline{a}_f = \partial F / \partial \underline{\sigma}$; $\beta = H + \underline{a}_f^T \cdot \underline{\underline{D}}^e \cdot d\underline{\varepsilon}$, and finally $H = -\frac{\partial F}{\partial h} \cdot \left(\frac{\partial h}{\partial \underline{\varepsilon}^p} \right)^T \cdot \underline{a}_q$. For ideal plasticity, such as Mohr-Coulomb model, the yield function is independent of hardening parameter, i.e., $\partial F / \partial h = 0$, hence, $H = 0$ and $\beta = \underline{a}_f^T \cdot \underline{b}_q$.

The choice of the hardening rule depends on the type of the material and on the ease with which it can be applied. Three types of hardening rules are commonly used to describe the behaviour of soils. These are isotropic, kinematic, and mixed hardening. Isotropic hardening represents a uniform expansion of the yield surface in all direction, where as the kinematic hardening represents a simple means of accounting plastic anisotropy, i.e., during plastic flow, the yield surface is assumed to translate as a rigid body, maintaining its size, shape and orientation. Mixed hardening represents a combination of the isotropic and kinematic hardening. As far as this work is concerned, however, it is limited to an isotropic hardening only, because the soil models in the available finite element code (PLAXIS) for this study is based on this type of hardening.

Equation 5.12 is an important part of the element stiffness matrix $\underline{\underline{K}}^{ep}$ for elasto-plastic material in the finite element formulation, i.e.,

$$\underline{\underline{K}}^{ep} = \int_v \underline{B}^T \cdot \underline{\underline{D}}^{ep} \cdot \underline{B} \cdot dv$$ (5.13)

where $\underline{B}$ is a matrix that relates the strains inside the element with the nodal displacements and usually referred as the B-matrix or strain matrix. $\underline{\underline{K}}^{ep}$ is a non-symmetric matrix because $\underline{\underline{D}}^{ep}$ is a non-symmetric matrix due to the terms $\underline{b}_q \cdot \underline{b}_f^T$ in Equation 5.12. However, if an associated flow rule ($Q \equiv F$) is assumed, the elasto-plastic matrix becomes symmetric.

5.1.5   Elasto-visco-plasticity

In contrast to the elasto-plasticity, the elasto-visco-plasticity theory assumes that all plastic strains in the material are time dependent and further postulated that the stress trajectories can cross the yield surface so that stress situation outside the yield surface are admissible, i.e., *F > 0*. Otherwise, the concept of yield function, flow law and hardening law developed in the contest of elasto-plasticity are also applied to elasto-visco-plasticity. In incremental form the total strain may be written as:

$$d\underline{\varepsilon} = d\underline{\varepsilon}^e + d\underline{\varepsilon}^{vp} \tag{5.14}$$

where $d\underline{\varepsilon}^{vp}$ represents the visco-plastic strain. The flow equation is given by the rate of visco-plastic strains as:

$$\dot{\underline{\varepsilon}}^{vp} = \mu \cdot \langle F \rangle \cdot \frac{\partial Q}{\partial \underline{\sigma}} \tag{5.15}$$

where μ is the fluidity parameter. The brackets $\langle \rangle$ denotes that the quantity in this brackets = 0 if $F \leq 0$, i.e. $\dot{\underline{\varepsilon}}^{vp} = 0$, but if *F > 0*, the flow Equation 5.15 applies as it is. The plastic strain increment is given by:

$$d\underline{\varepsilon}^p = \dot{\underline{\varepsilon}}^{vp} \cdot dt \tag{5.16}$$

where *dt* represents an infinitesimal time step. Using Equations 5.14, 5.15 and 5.16 and keeping in mind that stresses can be related to elastic strains, one can arrive at the following relationship:

$$d\underline{\sigma} = \underline{\underline{D}}^e \cdot \left(d\underline{\varepsilon} - \mu \cdot \langle F \rangle \cdot \frac{\partial Q}{\partial \underline{\sigma}} \cdot dt \right) \tag{5.17}$$

5.1.6   Cap models

Historically, *Drucker et al. (1957)* were the first to introduce the concept of work hardening plasticity cap models. They introduced a spherical end cap to the *Drucker-Prager* model in order to control the plastic volumetric change of soil. The Cambridge group also developed a family of models for normally consolidated or lightly overconsolidated clay known as Cam-Clay models based on critical state concept (*Schofield/Wroth (1968); Rosco/Burland (1968)*). Since then several attempts have been made to use various version of these models in the numerical solution of boundary value problems and prediction of soil behaviour in the field. A more general cap models for the application of a wide range of soils are in use nowadays. The loading surface for cap model consists of two parts: a failure surface for perfectly plastic material response *F* (Drucker-

Prager or Mohr-Coulomb or other curved surface failure criteria) as discussed in section 5.1.4 above and an elliptical work-hardening cap F_c of the form (*Chen/Mizuno (1990)*):

$$F_c = (I_1 - l)^2 + R^2 \cdot J_2 - (x - l)^2 \qquad (5.18)$$

where l is the position of the centre of the ellipse and R is the aspect ratio of the cap. The movement of the cap is controlled by the increase or decrease of the plastic volumetric strain through the hardening parameter x, which is given by:

$$x = x(\underline{\varepsilon}_v^p) \qquad (5.19)$$
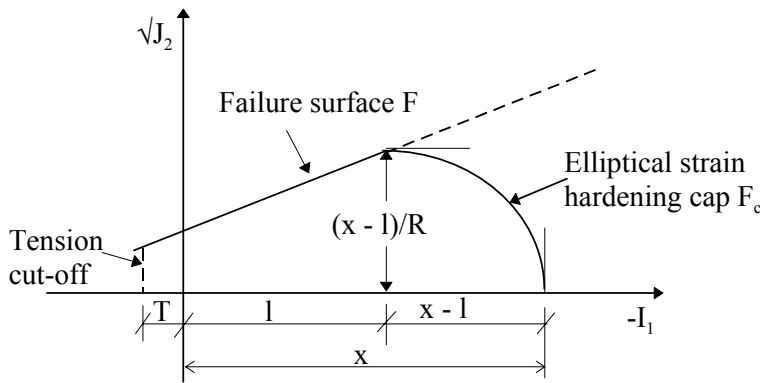
Figure 5.2:
Cap model with elliptic hardening surface

5.2   Soil models used in the parametric study and numerical analysis of practical projects (PLAXIS FE - program)

5.2.1   General

As mentioned in the introductory part of this chapter, the finite element code PLAXIS professional version was selected for the purpose of analysing the practical projects and the parametric studies. The PLAXIS program contains from simple linear elasticity to advanced elasto-plastic cap soil models. The details of each soil model can be found in PLAXIS users manual (*Vermeer/Brinkgreve (1995), Brinkgreve/Vermeer (1998), Brinkgreve (2002)*). A summary of the basic features, the failure criteria, the required soil parameters, range of application, etc. of the three main soil models available in PLAXIS is presented in Table 5.2. In the earlier version of PLAXIS, up to version 6.0, the *hard soil model* (HSM) and the *soft soil model* (SSM) are primarily used for hard soils such as gravels, sands and heavily overconsolidated cohesive soils, and for normally consolidated and lightly overconsolidated clays respectively. This is mainly because the HSM was developed on the assumption that plastic straining is dominated by shearing and asso-

ciated volumetric strains are relatively small and cause dilation rather than compaction which is a property of non-cohesive and heavily consolidated cohesive soils. On the other hand the SSM was developed based on the assumption of compression hardening, which is mainly a property of soft clays. In contrast to this basic formulation of the models, *(Freiseder (1998))* believed that the HSM give more realistic results on deformation of the wall and settlement of ground behind the wall in an excavation in normally consolidated clay than the other models.

In the PLAXIS version 7 and 8, the SSM was superseded by the HSM, and the HSM comes out as advanced double hardening model applied for all types of soils, i.e., it is now based on shear as well as compression hardening, a property of both hard soils and soft soils. In these versions, the name *hard soil model* is replaced by the *hardening soil model*. The HSM assumes a uniform expansion of the yield surface in all direction, i.e., it is based on isotropic hardening. The soft soil model is also modified to include time dependent behaviour of soft soils and it is called the *soft soil creep model* (SSCM). The Mohr - Coulomb model (MCM), which is an elastic- perfect plastic model, can be applied for all types of soils.

Further comments on the three models are given in section 5.3, where the requirement for constitutive relations in connection with excavations in normally consolidated clay is evaluated.

5.3   Requirement for constitutive soil models for normally consolidated soft soils in an excavation problem

Ideally a soil model would be able to predict the stress-strain and time dependent behaviour under all types of loading. However, such models are mathematically complex and difficult to use. Therefore, a solution to practical problems requires that some simplifying idealisation are made regarding the behaviour of soils. The elasto-plastic cap models have the advantage that they address the important behaviour of soils, such as non-linearity, stress-path dependency, plasticity, dilatancy and compaction, etc. However, there is still a need at least to partially evaluate the response of each constitutive model to some typical stress-strain paths associated with laboratory or field conditions. For example, *Gudehus (1985)* suggests that any constitutive law for an excavation analysis in saturated overconsolidated clay should respond to the stress and strain path shown in Figure 5.3 with an adequate accuracy. Figure 5.3 represents the behaviour of undrained earth pressure problem. It consists of soil sedimentation (path 0-1), erosion (path 1-2), and active or passive loading/unloading/reloading (2-3-4-5). Figure 4.3 shows only one case where the wall rotates about its foot. Other arts of wall rotation may lead to different stress and strain paths. The stress and strain paths at different positions with in the excavation are also different.

Table 5.2:   Summary of the main soil models in PLAXIS FE-program.

	Hardening Soil Model (HSM)	Soft Soil Creep Model (SSCM)	Mohr-Coulomb Model (MCM)
Type of model	• elasto-plastic strain hardening cap model	• elasto-plastic work hardening cap model	• elastic perfect plastic
Basic features	• stress dependent stiffness according to power law • plastic straining due to primary deviatoric loading • Plastic straining due to primary compression • Elastic unloading/ reloading • Hyperbolic stress-strain relation • soil dilatancy	• stress-dependent stiffness (logarithmic compression behaviour) • distinction between primary loading and unloading/reloading • Secondary (time-dependant) compression • memory of preconsolidation stress	• offers a special option for the input of a stiffness increasing with depth • soil dilatancy
Failure criterion	• Mohr-coulomb	• Mohr-coulomb	• Mohr-Coulomb
Cap yield surface	$F_c = \dfrac{\tilde{q}^2}{\alpha^2} + p^2 - p_p^2$ • α is a model parameter that relates to K_0 • p_p is isotropic pre-consolidation stress • p is the effective mean stress • $\tilde{q} = \sigma_1 + (\delta - 1)\cdot\sigma_2 - \delta\cdot\sigma_3$ • $\delta = \dfrac{3 + sin\varphi}{3 - sin\varphi}$	$F_c = \dfrac{q^2}{M^2\cdot(p + c\cdot cot\varphi)} + p - p_p$ • M is a model parameter that relates to K_0 • p_p is isotropic pre-consolidation stress • p is the effective mean stress • q is shear stress	• none
Flow rule	• non-associated in shear hardening • associated in compression hardening (cap)	• associated	• non-associated
State of stress	• Isotropic	• Isotropic	• Isotropic
Hardening	• Isotropic; shear and compaction	• Isotropic; compression	• none
required soil parameters	• c', $\varphi`$, angle of dilatancy ψ, secant stiffness in standard drained triaxial test E_{50}^{ref}, unloading/reloading stiffness E_{ur}^{ref}, tangent stiffness for primary oedometer loading E_{oed}^{ref}, power m, Poisson's ratio for unloading/ reloading ν_{ur}, and K_0.	• c', $\varphi`$, ψ, modified compression index λ^*, modified swelling index κ^*, modified creep index μ^*, ν_{ur}, M is a parameter which is a function of K_0,	• c', $\varphi`$, ψ, Young's modulus E, ν
Range of applications	• All types of soils	• Normally consolidated or lightly overconsoildated clay or clayey soils	• All types of soil
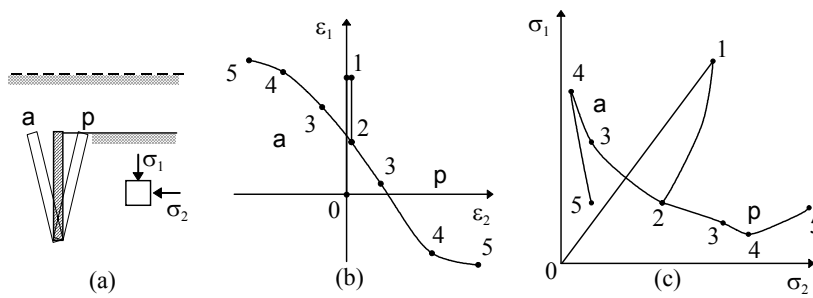
Figure 5.3:
Strain (b) and stress (c) paths in active and passive earth pressure in saturated clay (a) (*after Gudehus, 1985*)

Chen/McCarron (1986); Chen/Mizuno (1990) proved that the cap models are capable of responding to the stress-strain paths and the history dependent behaviour. *Freiseder (1998)* had compared the three soil models (HSM, SSM and MCM) available in the PLAXIS version 6.1 using an idealised excavation in normally consolidated lacustrine clay which is supported by diaphragm wall. He concluded that the HSM provides a realistic result as far as the horizontal deflection of the wall and settlement of the surface behind the wall are concerned, though it was first developed to model the behaviour of non-cohesive soils and overconsolidated clays. He further commented that the response of the HSM to stress path at some points with in the excavation is more realistic than the other models. It should be noted that the HSM in this version was without a cap. Therefore, there should be no doubt that the introduction of the cap in to the HSM in PLAXIS version 7 and 8 will increase its performance and its range of application.

The response of the latest version of the HSM to different stress-strain paths and history in field and laboratory has been evaluated in chapter 7.

5.4   Constitutive relations for interface elements

Clough/Duncan (1971) studied the interaction between the wall and the back fill material with the help of shear box test and showed that the stress-displacement behaviour of the interface is similar to the stress-strain behaviour of soils. In order to implement the interface behaviour in the finite element analysis of retaining walls, *Clough/Duncan (1971)* developed a non-linear, stress dependent stiffness, hyperbolic stress-strain constitutive relation to represent interface behaviour similar to those developed by *Duncan/Chang (1970)* to model the stress-strain behaviour of soils.

Like the behaviour of soils, interface behaviour may also be represented by complex advanced models. However, *Gens et al. (1989)* underlined the use of less complex models. They used an elastic-perfectly plastic model with out dilatancy effect in their finite element study of the soil-reinforcement interaction. In PLAXIS the MCM is used to represent the interface behaviour, whatever model is applied to represent the soil behaviour.

6 The measurements of soil parameters relevant to excavation in normally consolidated soft soils

6.1 General

In the planning, design and construction of excavations in normally consolidated soft clays in urban areas, careful consideration of the magnitude and distribution of the ground movement is required. The prediction of the complete ground movement pattern involves three processes: the choice of an appropriate analytical or numerical model, the choice of the appropriate analysis method, and the selection of appropriate soil parameters.

In order to determine the strength and deformation parameters relevant to an excavation in normally consolidated soft clays, a comprehensive test program has been carried out on specimens trimmed from 104 mm diameter and 300 mm high samples and on some reconstituted samples. The samples were collected from three different locations, namely Dammgasse, Max-Stomey and FHK projects in the city of Constance, southern Germany. These three locations will be referred as site1, site2, and site3 respectively throughout the text. The project at site1 is one of the case studies presented later in this work for numerical analysis. The area is known of thick post-glacial deposit of normally consolidated lacustrine clay, locally known as "seeton/beckenton". The laboratory program includes conventional isotropically consolidated and anisotropically consolidated drained and undrained triaxial tests, controlled stress path tests, one dimensional compression tests, isotropic (triaxial) compression test, anisotropic (triaxial) compression test, direct shear tests, and basic index property tests. The results of these tests are presented and compared, and the choice of the elastic and plastic parameters appropriate for excavation problems are discussed. The general soil properties in and around the city of Constance from conventional soil tests are summarised in Table 6.1.

6.2 Testing program and techniques

6.2.1 The apparatus

The triaxial apparatus used in the series of triaxial compression, and stress path tests are shown in Appendix A.1. The apparatus for conventional compression test consists of two major parts: the cell with all its accessories (cell body, connections to drainage, cell pressure, pore pressure and back pressure, top cap, load piston, etc.) and the motorised load cylinder with built in DMS-load cell to measure the axial load on the sample. The axial load can be regulated at a constant strain rate between 0.0002 to 2 mm/min. The axial deformation of the sample is measured by a displacement transducer directly at the top of the cap. The lateral deformation of the sample was

measured at its mid height using a flexible waterproof band. All pressure systems are maintained through a motorised compressed air system. The cell pressure and the back pressure are regulated whereas the pore pressure, vertical deformation and applied axial load are recorded and saved through a data logger by a personal computer. It was possible to carry out three tests parallel with different cell pressure at one time.

Table 6.1: Summary of the general soil property

Soil property	Damm-gasse	Marke-grafen	Zurich	Max-Stomey	FHK	Fisch-markt [*]	Klaer-werk [*]
Clay content (%)	25 - 40	33 - 50	24 - 40	53 - 57	20 - 40	12-42	48 - 68
Natural water content, w_n (%)	15.1 - 36.5	11 - 34	28.2 - 33.5	30.9 - 31.5	17.0 -94.9	21.1-36.3	32 - 45.6
Liquid limit, w_L (%)	28 - 38	28 - 37	29.9 - 34.7	53 - 59	25.6 - 55.9	21.9-36.5	32.8 - 45.9
Plasticity index, I_p (%)	7.7 - 16.6	9.3 - 13	12.1 - 15	27 - 34	6.7 - 13.1	4.9-21.5	14.8 - 26.3
Consistency index, I_c	0.03 - 0.48	-0.1 - 0.49			0.54 - 1.76		
Liquidity index, I_L			0.73 - 1.3				
Specific gravity, G_s	2.7 - 2.73			2.72	2.65	2.67-2.70	2.67 - 2.70
Unit weight (g/cm²)	1.9 - 2.0	1.9 - 2.0		1.95	1.90 - 2.0		
K_0						0.54 - 0.64	0.61 - 0.66
C_c (x 10^{-3})	150 - 200	170 - 270		195 - 221	75 - 462	44 - 136	109 - 172
C_s (x 10^{-3})	35.6 - 56.8			30.6 - 55	22.5 -36.1	14 - 28	22 - 39
Constrained modulus of elasticity for stress level of 100 kPa (MN/m²)	2.6 - 3.6	3 - 5	4.4 - 6.1	3.5		1.4 - 4.7	1.4 - 4.7
Undrained strength (kPa)	20 - 25	25 - 30	58 - 67	19.0 - 40.0	11.6 - 28.0	14 - 80	14 - 81
c´(kPa)	3.7 - 24.9	5 - 10		10.1 - 27.4	3.0 - 55.9		
φ' (°)	24.3 - 31.8	20 - 25	22	20.5 - 28.6	20.2 - 29.3	25 - 36 [**]	25.5 [**]

[*]   data obtained from *Scherzinger (1991)*
[**]   the effective angle of overall shear strength (inclusive the effect of cohesion c´)

For the K_0-consolidation and controlled stress path tests, a special pneumatic cylinder was coupled with the conventional triaxial cell (Appendix A.1) in order to bring and control additional vertical pressure on the sample independent from the axial load system and cell pressure. In the case of anisotropic consolidation, the sample was subjected to all round cell pressure similar to conventional test, and at the same time an additional vertical pressure was applied through the pneumatic cylinder. After the consolidation process was completed, the axial load was applied through the motorised load cylinder which was fixed at the top of the pneumatic cylinder. With this type of arrangements, it was possible to conduct stress path tests by controlling the vertical and horizontal stresses separately.

The conventional oedometer and the shear box apparatus were used to conduct one-dimensional compression tests. The specimens were loaded in steps using a load increment or decrement of 2 times the previous load.

6.2.2   Specimen preparation

Undisturbed samples from depth of 1.5 - 5 m were recovered by 104 mm diameter thin tube sampler from three locations: site1, site2 and site3. 50 mm high and 50 mm diameter (1:1) specimens were trimmed from 104 mm diameter samples for compression and stress path triaxial tests. Specimens reconstituted at the same water content and density as in-situ were also used. A smooth Plexiglas of diameter 50 mm with a central porous disc of diameter 10 mm and covered with lubricated plastic film was used to reduce the end effect. The glass was free to move so that no constraint would be allowed between the sample and the rigid cap. In addition to the drainage at the top, side drains of filter paper were fitted around the specimen in order to accelerate the rate of drainage. The relatively small height of the specimen coupled with lubricated end result in a greater uniformity of stress distribution and deformation, enabling the sample to maintain its cylindrical shape even at large strains.

The specimens for conventional oedometer tests were 14 mm high and 71 mm in diameter (site1 and site2) and 14 mm high and 20 mm in diameter (site3). Both disturbed and undisturbed samples were tested. The specimens for isotropic and anisotropic compression were prepared in similar fashion as for the standard triaxial test described above.

6.3   Compression parameter and preconsolidation pressure

6.3.1   One-dimensional consolidation

The stress strain relationships of normally consolidated soft clays in one-dimensional consolidation were investigated using the conventional oedometer test with daily increment of vertical load to a submerged specimen contained in a rigid ring. Drainage was permitted through porous stone at the top and bottom. The ratio of the load increment to existing load was 1, i.e. the load is doubled each day assuming that the time required for primary consolidation is 24 h. A classic behaviour of normally consolidated clay in one dimensional consolidation at the three sites are represented in Figure 6.1 (see also Appendix A.2) in which the results have been plotted as axial strain ε_l or void ratio e against the effective consolidation stress σ'_{vc}. The ε_l or e are plotted on the vertical axis on an arithmetic scale and σ'_{vc} on a logarithmic scale. The solid lines in Figure

6.1 are the average of 2 to 3 tests, which are indicated as dashed lines in the diagrams. The plots of void ratio e versus $log\ (\sigma'_{vc})$ were idealised by straight line and give rise to the conventional definition of the compression index C_c and the swelling index C_s. The slope of the normal consolidation line and the swelling lines when the void ratio e is plotted against pressure in natural logarithmic scale is given by the symbol λ and κ respectively. Similarly, when the strain is plotted against pressure in natural logarithmic scale, they are denoted by λ^* and κ^* respectively. The relationship between conventional C_c, λ and λ^* is given by:

$$\lambda^* = \frac{\lambda}{1+e_0} = \frac{C_c}{2.3 \cdot (1+e_0)} \qquad\qquad (6.1)$$

The relationship between C_s, κ and κ^* is given by *Brinkgreve (2002)* as:

$$\kappa^* = \frac{\kappa}{1+e} \approx \frac{2}{2.3}\cdot\frac{C_s}{1+e} \qquad\qquad (6.2)$$

Equation 6.2 was derived based on the assumption that the vertical and horizontal stresses during one dimensional unloading are equal. According to (*Brinkgreve (2002)*) one can use the average void ratio that occurred during the test or just the initial void ration e_0 for e. If the un/re-loading is approximated by a straight line $C_s \approx 2.3\cdot\kappa$, (*Wroth/Houlsby (1985); Atkinson/Bransby (1978)*).

Table 6.2 shows the results of one-dimensional compression tests in primary loading and Table 6.3 shows that of the un/reloading condition for all three sites. From Table 6.3, it may be seen that the swelling index is not a unique value for a particular test, rather it depends on the maximum previous stress σ'_{vm} at which the sample were subjected before it starts to swell. The void ration e in Table 6.3 is the value just before the unloading starts. The values of κ in Table 6.3 were read directly from a plot of e against $ln(\sigma'_{vc})$ assuming that the swelling lines can be fairly approximated by straight lines. These values of κ match very well with those values estimated from the relationship $C_s \approx 2.3\cdot\kappa$. Obviously, the values of κ calculated from Equation 6.2 are twice higher than that approximated or read directly from the plot.

Another very important characteristics of clays is the preconsolidation pressure σ'_p. It is the vertical effective stress beyond which large strains occur and controls the overall behaviour of clays, particularly the sensitive clays. Previously, it was believed that the preconsolidation pressure estimated with *Casagrande* method was primarily due to previous loading, usually of geologic nature. However, it has become evident in recent years that the profile of the preconsolidation stress observed in some deposits is greater than the maximum past pressure that could have existed during its geologic history. This discrepancy was attributed to a number of factors, including desiccation, long-term secondary compression, thixotropy, weathering and cementation (*Fang (1991); Jamiolkowski et al. (1985); Leroueil et al. (1983); Scherzinger (1991)*). Since the exact origin of the σ'_p is difficult to establish, the term has been extended to define the break of

the e - log σ'_p curve (*Leroueil et al. (1983); Scherzinger (1991)*). From practical point of view engineers are interested in this threshold point beyond which important plastic deformation take place, particularly in sensitive clays where the normally consolidated branch of the compression curve is very steep. The preconsolidation pressure serves as basis for normalising the strength and stiffness characteristics of cohesive deposits. For young normally consolidated soft clays, the effective preconsolidation pressure σ'_p is equal to the effective overburden pressure σ'_{v0}, where the soil deposit is not subjected to previous external load such as building loads.
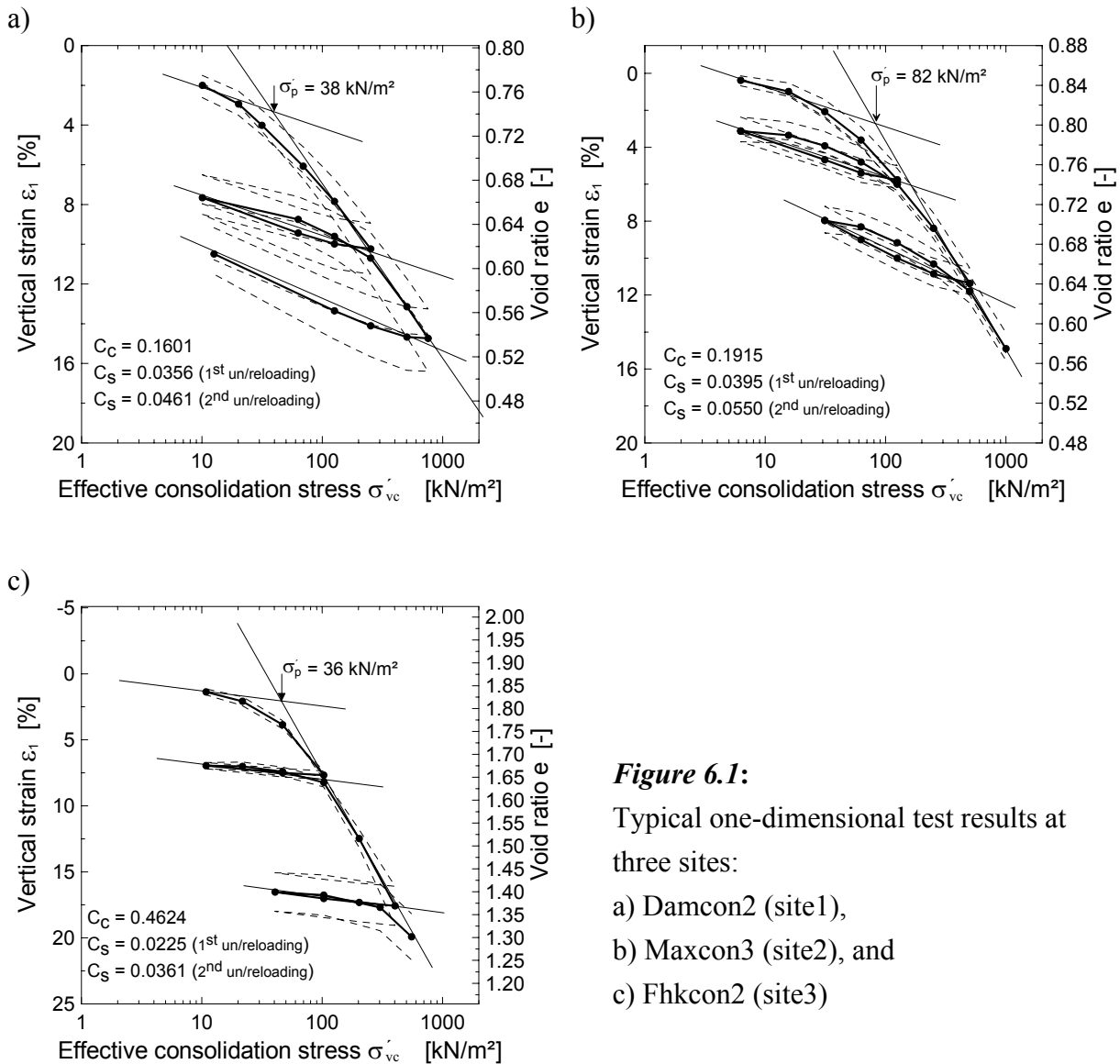

Figure 6.1:

Typical one-dimensional test results at three sites:

a) Damcon2 (site1),

b) Maxcon3 (site2), and

c) Fhkcon2 (site3)

Table 6.2:   Result of one-dimensional compression test (Primary loading)

Location	Test description	w	e_0	C_c	λ	λ^*
		[%]	[-]	[-]	[-]	[-]
site1	Damcon1(D)	28.4	0.661	0.1498	0.0651	0.0392
	Damcon2(U)	31.8	0.803	0.1601	0.0696	0.0386
	Damcon3(U)	33.6	0.881	0.2001	0.0870	0.0462
site2	Maxcon1(U)	30.9	0.815	0.2210	0.0961	0.0529
	Maxcon2(D)	25.4	0.719	0.1592	0.0692	0.0403
	Maxcon3(U)	31.1	0.849	0.1915	0.0833	0.0450
site3	Fhkcon2(U)	70.9	1.881	0.4624	0.2010	0.0697

D and U stands for disturbed and undisturbed samples respectively

Table 6.3:   Result of one-dimensional compression test (unloading/reloading)

Location	Test description	w	e	σ'_{vm}	C_s	κ (read)	$\kappa = C_s/2.3$	$\kappa^* = \kappa/(1+e)$
		[%]	[-]	[kN/m²]	[-]	[-]	[-]	[-]
site1	Damcon1(D)	28.4	0.520	252	0.0524	0.0233	0.0228	0.0153
	Damcon2(U)	31.8	0.618	252	0.0356	0.0150	0.0154	0.0093
			0.537	756	0.0461	0.0200	0.0200	0.0130
	Damcon3(U)	33.6	0.649	202	0.0406	0.0171	0.0177	0.0104
			0.526	806	0.0568	0.0244	0.0247	0.0160
site2	Maxcon1(U)	30.9	0.657	278	0.0406	0.0187	0.0177	0.0113
	Maxcon2(D)	25.4	0.608	157	0.0306	0.0133	0.0133	0.0083
			0.480	916	0.0579	0.0248	0.0252	0.0167
	Maxcon3(U)	31.1	0.743	125	0.0395	0.0169	0.0172	0.0097
			0.639	500	0.0550	0.0233	0.0239	0.0142
site3	Fhkcon2(U)	70.9	1.660	103	0.0225	0.0109	0.0098	0.0041
			1.374	403	0.0361	0.0143	0.0157	0.0060

D and U stands for disturbed and undisturbed samples respectively

Several methods have been proposed in literature for determining σ'_p. The *Casagrande* method is one of the most popular method so far. Another common method is to simply draw tangents to the virgin compression curve and the recompression curve; the intersection is called the preconsolidation stress. *Scherzinger (1991)* compared the two methods for normally consolidated clays in southern Germany using conventional oedometer test result and found out an average ratio of 1.21 between the preconsolidation pressures determined by *Casagrande* method $\sigma'_{p(cas)}$ and by the secant method $\sigma'_{p(sec)}$. *Leroueil et al. (1983)* showed that the in-situ preconsolidation pressure $\sigma'_{p(in-situ)} = \alpha \cdot \sigma'_{p(labor)}$, where $\alpha = 1.1$ for normally consolidated clays (*OCR* < 1.2), $\alpha = 1.0$ for slightly overconsolidated clays (1.2 < *OCR* < 2.5), and $\alpha = 0.9$ for overconsolidated clays (2.5 <

OCR < 4.5). A rough estimation of the preconsolidation pressure found out in this study for the three locations are given in Table 6.4. The values were estimated by the tangent method and corrected to the Casagrande method and in-situ condition. The soil at site3 appear to be unconsolidated.

Table 6.4: Preconsolidation pressure

Test description	σ'_{v0}	$\sigma'_{p(tan)}$	$\sigma'_{p(corrected)}$	OCR
	[kN/m²]	[kN/m²]	[kN/m²]	[-]
Damcon2	34.4	38	46.0	1.34
Damcon3	22.4	25	30.3	1.40
Maxcon1	39	91	99.1	2.54
Maxcon3	39	82	98.4	2.52
Fhkcon2	50.7	36	47.9	0.95

6.3.2   Isotropic compression

The isotropic compression tests were performed in a triaxial cell on two specimens 50 mm high and 50 mm in diameter. The sample specimens were extruded from the same site and depth as that of the specimens for Maxcon3 (site2) oedometer test. An average water content of 33% and an average void ratio of 0.901 were measured before the test. The drainage was permitted at both ends and radial through vertical filter paper strips on the side of the sample. The stresses were applied in equal increments, each having a duration of 12 h and a stress ratio of 1, i.e. $\sigma'_1 = \sigma'_3$. Volume changes were measured by calibrated burette. The result of an isotropic consolidation is usually presented as specific volume υ ($\upsilon = 1 + e$) against the effective mean stress p′ in natural logarithmic scale. The slope of the normal compression line is denoted by λ and the slope of the swelling line by κ. Similar to one-dimensional compression, if instead of the specific volume, the volumetric strain ε_v is plotted against $ln(p')$, the slopes for normal compression and swelling lines become λ^* and κ^* respectively. The λ^* and κ^* are important parameters in some FEM programs. The relationships between these parameters are given in Equation 6.1 and 6.2. Figure 6.2 shows the result of the isotropic compression. The solid lines in Figure 6.2 are the average of 2 tests, which are indicated as dashed lines in the diagram. It can be shown from Figure 6.2 that the reproducibility of the tests were fairly good. The values of $\lambda = 0.100$, $\lambda^* = 0.0526$, $\kappa = 0.0200$ and $\kappa^* = 0.01099$ obtained from isotropic compression are higher than the corresponding values in one-dimensional compression. Values of κ and κ^* are at maximum mean previous stress p'_m = 100 kN/m². The mean preconsolidation stress p'_p = 102 kN/m² is read from the plot using the tangent method and it is higher than the corresponding value in one-dimensional compression.
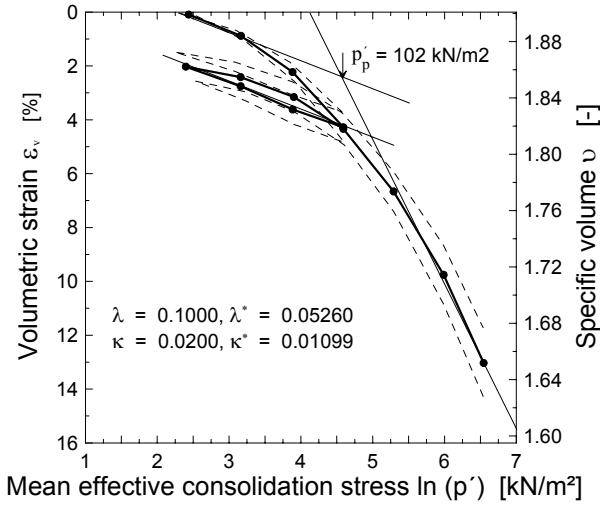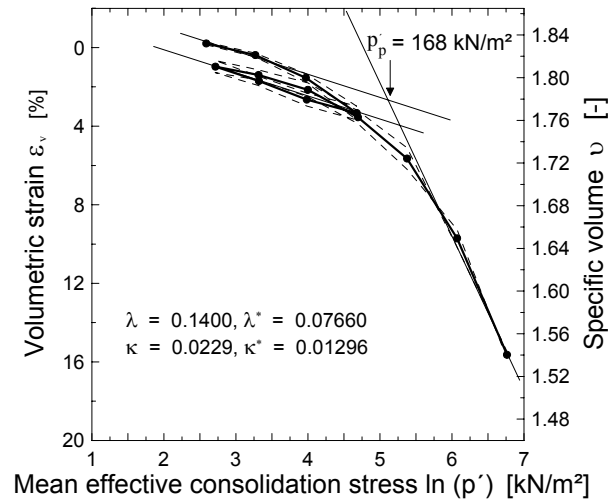
Figure 6.2: Isotropic compression ($K_0 = 1$)   **Figure 6.3:** Anisotropic compression ($K_0 = 0.8$)

6.3.3   Anisotropic (K_0) compression

The source of the specimen, the specimen size and preparation, drainage condition, etc. in the anisotropic compression test are the same as the isotropic compression test, except that the stresses are applied in equal increments, each having a duration of 12 h and a stress ratio of $\sigma_3' / \sigma_1' = 0.80 = K_0$. Figure 6.3. shows a plot of ε_v / υ against $ln(p')$. The solid lines in Figure 6.1 are the average of 2 tests, which are indicated as dashed lines in the diagrams. The reproducibility of the tests were quite good. $\lambda = 0.1400$, $\lambda^* = 0.0766$, $\kappa = 0.0229$, $\kappa^* = 0.01296$, and $p_p' = 168$ kN/m² were estimated from the plot. These value are higher than the corresponding values in one-dimensional and isotropic compression.

6.3.4   Comparison of one-dimensional, isotropic and anisotropic compression

The mean curves from one-dimensional, isotropic and anisotropic compression are re-plotted in Figure 6.4 assuming all the tests to start from the same average void ratio of 0.86. The curves are running parallel to each other up to a stress of approximately 250 kN/m², after which the slope of the isotropic and anisotropic compression curves start to increase and intersect the one-dimensional curve. It appears from Table 6.5 that $\lambda_{(oedo)} < \lambda_{(iso)} < \lambda_{(anis)}$. The reason for the increase of the slope of the isotropic and anisotropic compression curves may be explained in that the specimens start to yield laterally at higher stresses giving rise to higher volumetric strain. The un/reloading lines seems to be parallel to each other with a small differences in κ values where $\kappa_{(oed)} < \kappa_{(iso)} < \kappa_{(anis)}$ (Table 6.5). The preconsolidation pressure obtained from the three tests are

also different: $p'_{p(anis)} = 2.05 \cdot \sigma'_{p(oed)}$, $p'_{p(iso)} = 1.24 \cdot \sigma'_{p(oed)}$ and $p'_{p(anis)} = 1.65 \cdot p'_{p(oed)}$. *Leroueil et al. (1983)* correlated the preconsolidation pressures from conventional oedometer test and anisotropic test as $p'_{p(anis)} = 1.1 \cdot \sigma'_{p(oed)}$, but admitted that there was data scattering. One may observe from *Leroueil et al. (1983)* correlation graph that a factor as much as 1.7 and as low as 0.95 exist. From tabular data given in *Scherzinger (1991)* one may also derive $p'_{p(iso)} = 1.1 \cdot \sigma'_{p(oed)}$.
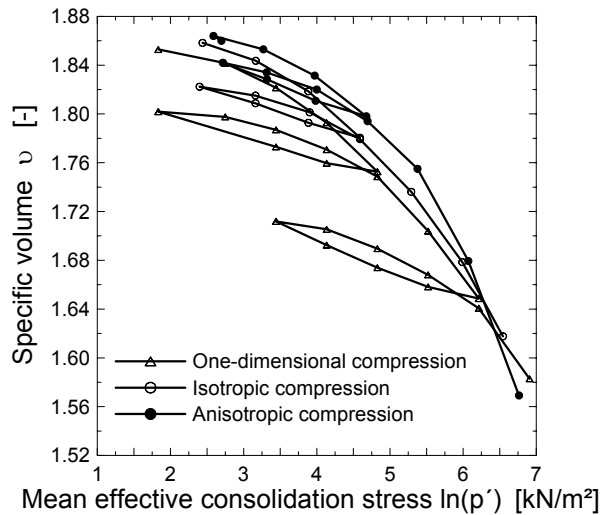

Figure 6.4:

Plot of one-dimensional isotropic and anisotropic compression

Table 6.5:   Comparative values of compression parameters

Test description	Test type	w	e_0	λ	λ^*	e	κ	κ^*
		[%]	[-]	[-]	[-]	[-]	[-]	[-]
Maxcon3(U)	One-dimensional	31.1	0.743	0.1915	0.0833	0.7430	0.0169	0.00970
						0.6390	0.0233	0.01422
	Isotropic($K_0 = 1.0$)		0.901	0.1000	0.0526	0.8196	0.0200	0.01099
	Anisotropic ($K_0 = 0.8$)		0.828	0.1400	0.0766	0.7665	0.0229	0.01296

6.4   Strength parameter

6.4.1   General

To determine the strength and deformation parameters for the FE-analysis, a series of standard triaxial test; drained/undrained and isotropic/anisotropic, and controlled stress path tests had been conducted on undisturbed and reconstituted samples from the three locations in the city of Constance, southern Germany. The result of the tests are presented and discussed in the following sections.

6.4.1.1 The rate of strain

The rate of strain is one of the important factors that influence the strength and deformation properties of soils. The maximum rate of strain to be applied in a strain control triaxial tests can be approximated from,

$$\dot{\varepsilon} = \frac{\varepsilon_f \cdot h}{100 \cdot t_f} \qquad\qquad (6.3)$$

where $\dot{\varepsilon}$ is the rate of strain of the load application in mm/min, ε_f is the strain at failure in percentage (%), h is the height of the specimen in mm, and t_f is the time required to failure in min. For undrained test with side drains and height to diameter ratio of 1:1, the time to failure given by *Head (1986)* is $t_f = 0.201 \cdot t_{100}$ and $t_f = 1.418 \cdot t_{100}$ for drained test with similar conditions. The graph of volume change against square - root time is used to derive the time intercept t_{100}. A typical volume change - time graph for the three sites are shown in Figure 6.5. $t_{100} = 100.7$, 50, and 3.54 min had been determined from this diagrams for the three sites respectively, and the corresponding times to failure for the three sites become 21.5, 13.5 and 0.7 min respectively for the undrained condition and 151.7, 95.4 and 5.0 min respectively for drained conditions. *Head (1986)*, however, recommends that the minimum time to failure should not be less than 120 min. With the assumption that the strain at failure will be 20%, 50 mm specimen height and 120 min time to failure, the maximum rate of strain for undrained test was calculated from Equation 6.3 as 0.083 mm/min for all the three sites. Similarly, for drained tests the maximum rate of strains were 0.066 mm/min for the site1, 0.083 mm/min for the other two sites. However *DIN 18137 (1990)* recommends a maximum rate of strain equal to 0.01 mm/min for drained test and 10 times higher strain rate for the undrained tests. Hence, the undrained tests were performed at conservative values of strain rates of 0.03, 0.05 and 0.08 mm/min for the three sites respectively and the drained tests at strain rates of 0.003, 0.005 and 0,01 mm/min.
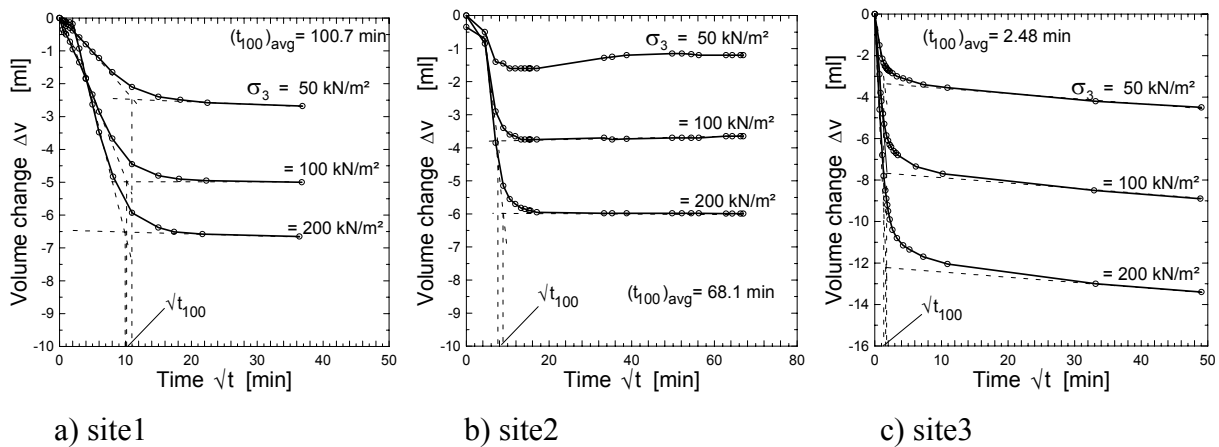

    a) site1   b) site2   c) site3

Figure 6.5:   Typical volume change - root time graph for the three sites

6.4.1.2   Failure criteria

There are different failure criteria for determining the shear strength of a specimen. These are peak deviator stress, maximum principal stress ratio, limiting strain, critical state, and residual state. Most often, the stress-strain diagram for normally consolidated cohesive soils does not show a distinct peak value, rather the stress increases gradually as deformation of the soil sample increases. Here the maximum principal stress ratio and the maximum deviator stress at predefined strain were taken as failure criteria for undrained tests. Since the effective stress changes in drained tests are equal to the total stress changes, the principal stress ratio curve has the same shape as the deviator stress plot. Hence the limiting strain failure criteria was used for drained tests. According to *Head (1986)*, the strain at failure for normally consolidated cohesive soils may be assumed between 15 and 20% for both drained and undrained tests. *DIN 18137/1990* recommends 20% strain at failure where there is no distinct peak point in the deviator stress - strain plot. 20% strain was therefore adopted as limiting strain through out the test in this study whenever it applies.

6.4.1.3   Membrane correction

There is a general argument that the triaxial tests are not reliable type of tests for determining the shear parameters of a normally consolidated soft soils, because such soils are sensitive to sample disturbance and the restraining effect of the rubber membrane enclosing a triaxial specimen, which contributes to resistance offered against compression. *Head (1986)* suggested a membrane correction for samples undergoing a barrelling type of distortion as shown in Figure 6.6. The barrelling mode of distortion is typical in specimens of normally consolidated soft soils. The correction was developed based on the axial strain in the sample, the compression modulus of the membrane and the initial diameter of the specimen. The solid line in Figure 6.6 is the original curve from *Head (1986)*, and is based on 38 mm diameter samples fitted with a membrane 0.20 mm thick. For specimens of any other diameter (D in mm) with any other membrane thickness (t in mm), the correction is multiplied by [($38/D$)·($t/0.2$)]. The dashed line in Figure 6.6 is the corrected membrane correction for specimens of 50 mm diameter, which is the case for all specimens investigated in the triaxial test in this study.

6.4.2   Isotropically consolidated undrained (*CIU*) compression test

A total of 29 (9 series) isotropically consolidated undrained (*CIU*) strain controlled triaxial compression tests were performed on cylindrical specimen 50 mm high and 50 mm in diameter; 15

from site1, 11 from site 2, and 3 from site 3. All samples were vertically oriented except 3 samples from site2 (Maxciu02) which were horizontally oriented. To ensure full saturation of the samples, to avoid air remnants in the drainage system and to prompt the response of the pore water pressure, back pressures of 300 to 400 kPa were applied. *DIN 18137 (1990)* recommends a minimum back pressure of 300 kPa for samples with degree of saturation greater than 95%. All samples were 94 to 100% saturated. The minimum effective consolidation pressure applied was 50 kPa and the maximum was 500 kPa.
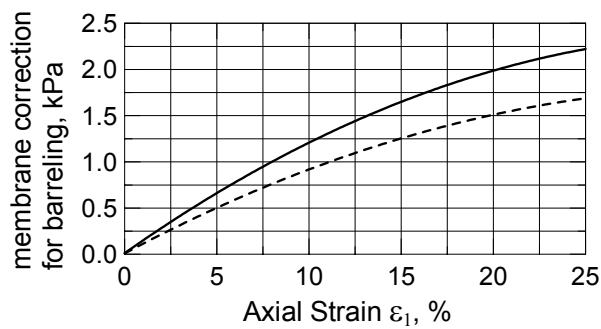

Figure 6.6:
Membrane correction curves for barrelling type of distortion for 38 mm diameter samples (solid line) and for 50 mm diameter samples (dashed line), and membrane thickness $t = 0.2$ mm (after *Head, 1986*)

Typical undrained stress - strain response, the excess pore water pressure during loading un/reloading, and the stress path it followed during shearing for a specimen from site1 are shown in Figure 6.7 (see also Appendix A.5). The stress - strain curves (Figure 6.7a) are non - linear even at low stresses and show no peak values, rather they continue to deform at large strain, but they appear to level off and eventually approach a constant value at a larger axial strain. The effective principal stress ratio diagrams (Figure 6.7c) also show no peak values except for local peaks that had been resulted from the response of the pore water pressure during un/reloading. This is why the strength parameters shown in Figure 6.7d derived using both failure criterion ($(\sigma_1' / \sigma_3')_{max}$ and $(\sigma_1' - \sigma_3')_{at\,20\%}$) were almost the same. As shown in Figure 6.7b, the pore water pressure drops down very quickly to certain minimum value during unloading and starts to build up slowly even before the reloading process was started. During reloading the pore water pressure build up quickly beyond the initial point and it starts to stabilise slowly to its normal position. The effective stress paths during normal loading shown in Figure 6.7d are typical for undisturbed normally consolidated clays and the hysteresis during un/reloading cycles are typical for overconsolidated clays.

Figure 6.8 shows a typical undrained response of the normally consolidated soft soils at site 2 (see also Appendix A.6). The stress - strain curves (Figure 6.8a) show no peak values whereas the effective principal stress ratio curves (Figure 6.8c) show clear peak points. This is mainly

because the pore water pressure (Figure 6.8b) decreases slowly after it had reached a peak point. Such behaviour of the pore water pressure and the shape of the stress path shown in Figure 6.8d are characteristics of compacted samples or lightly overconsolidated clay soils *(Head, 1986)*. This seems to confirm the result of the consolidation test (Section 6.3.1), where an OCR of around 2.5 is found for site2. The strength parameters calculated using the two failure criteria show a clear difference (Figure 6.8d). It seems, however that the increase in cohesion will compensates the decrease in friction angle and vice versa.
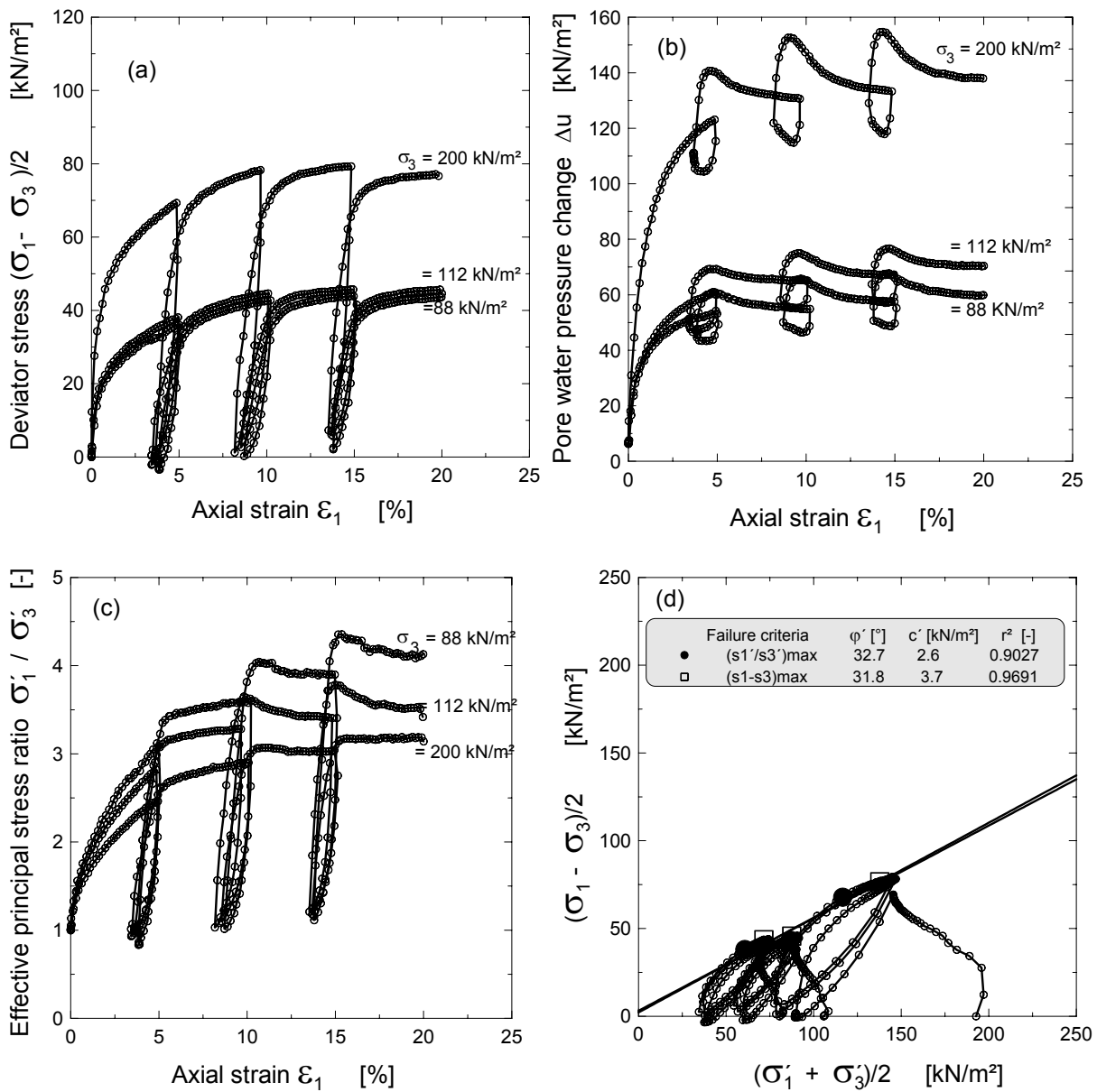

Figure 6.7: a) Stress - strain relationship, b) excess pore water pressure, c) effective principal stress ratio, and d) plot of the stress path from *CIU* test on vertically oriented samples (site1, Damciu14)
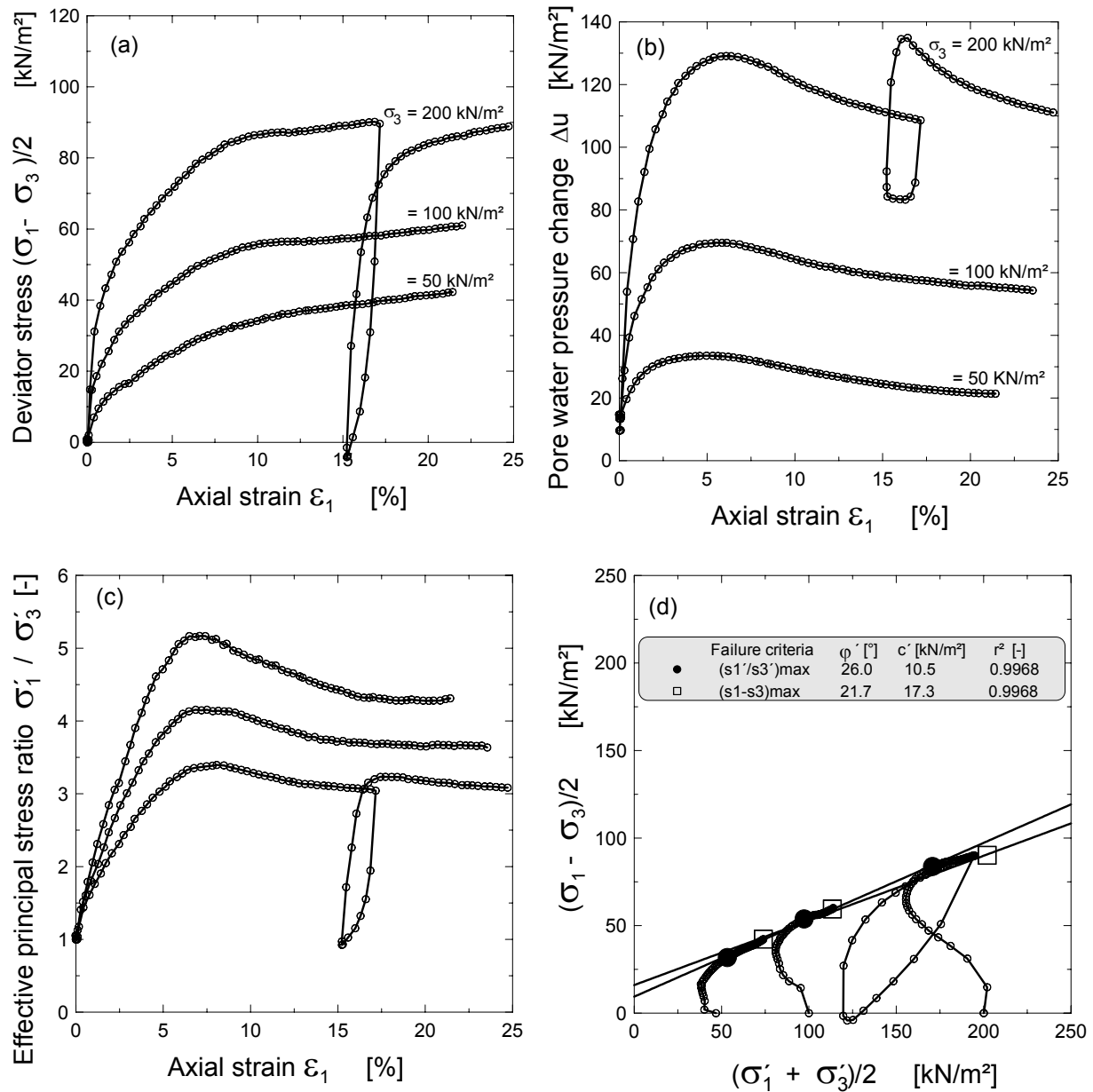
Figure 6.8: a) Stress - strain relationship, b) excess pore water pressure, c) effective principal stress ratio, and d) plot of the stress path from *CIU* test on vertically oriented samples (site2, Maxciu2)

The undrained response of normally consolidated soft soil at site3 is shown in Figure 6.9. The soil at this location is very soft and sensitive, contains organic substances such as grass roots and mussels, and has a water content above 70% and an initial void ratio of 2. The stress - strain curves (Figure 6.9a) are fairly linear at low stresses with high initial stiffness. This may be explained in that the specimens became highly compacted and cemented after the end of consolidation. If one see the volume change time plot of Figure 6.4c, one can observe that the time required for primary consolidation is very short (t_{100} = 2.48 min), and the volume change is rela-

tively large during this short time comparing to the other two in Figure 6.4a and b. Both the stress - strain curves and the effective principal stress ratio show no peak value, that is why the strength parameters (Figure 6.9d) obtained using both failure criterion were the same. The un/reloading curves are fairly non - linear. Unlike to the response of pore water pressure during unloading at site 1, the pore water pressure (Figure 6.9b) tries to maintain its value before the unloading started or in some case even increases slightly, but increases quickly to some maximum value beyond its initial value during reloading and stabilises to its normal position slowly. The stress paths shown in Figure 6.9d are typical for normally consolidated soft soils.
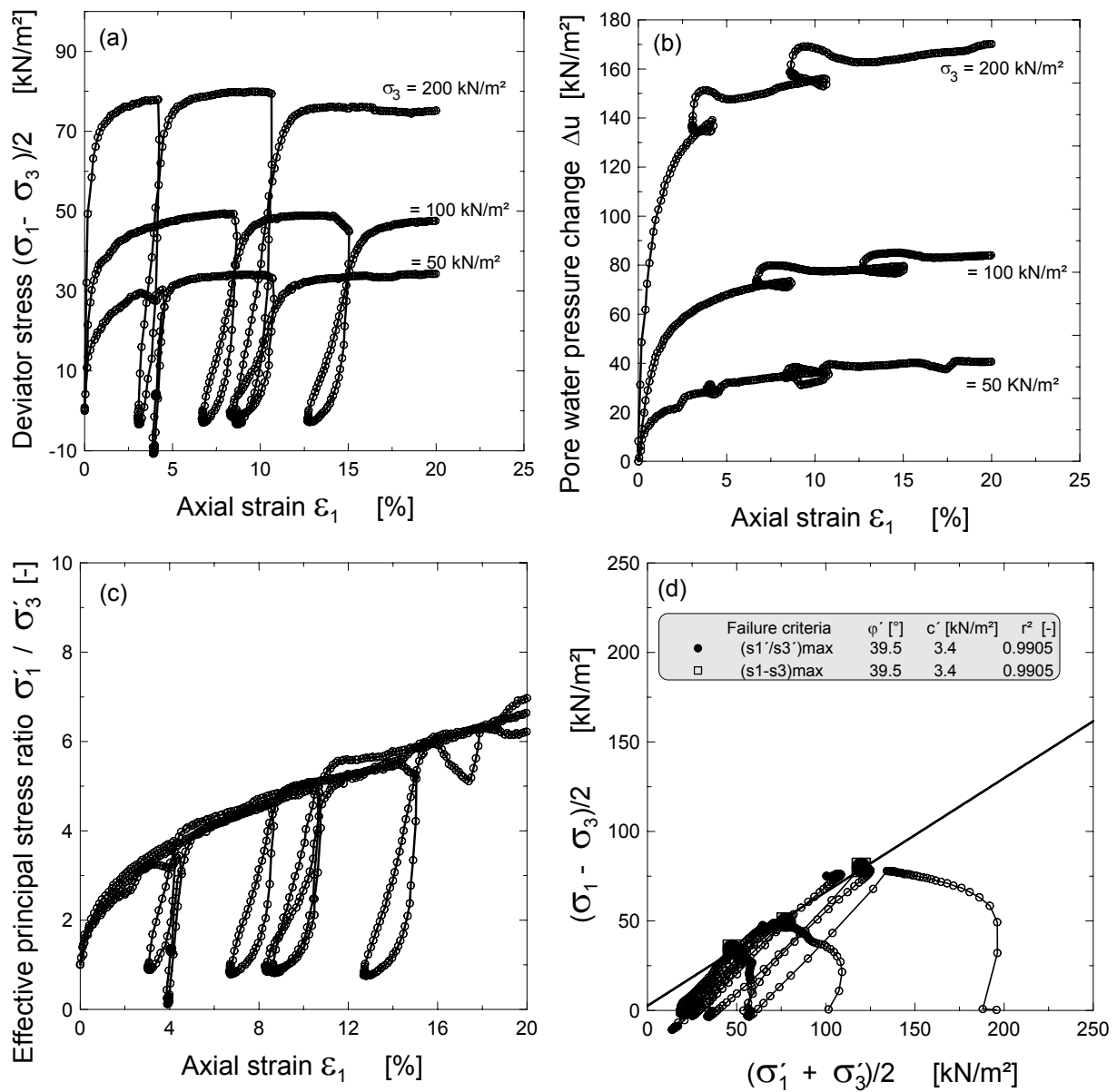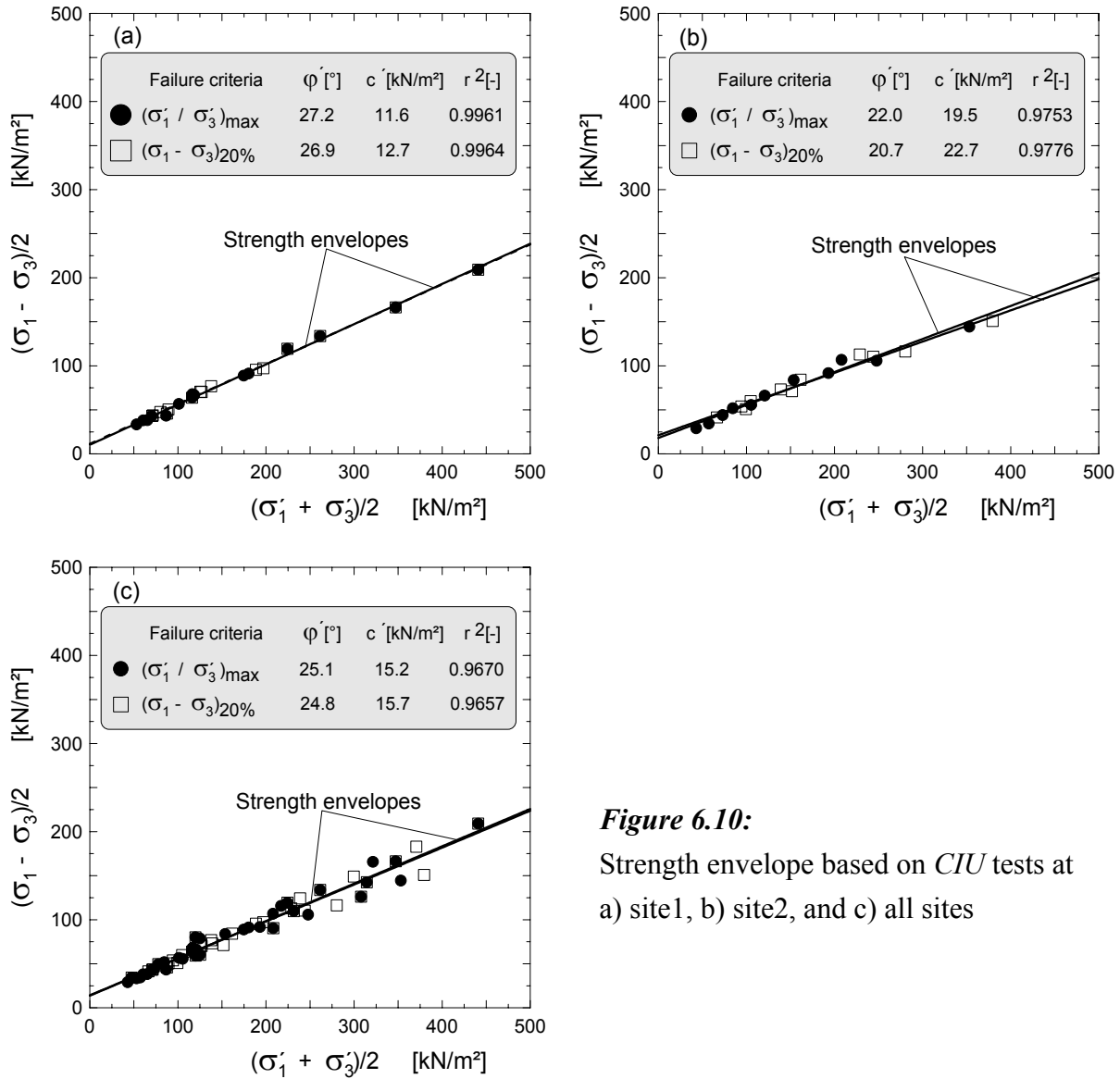

Figure 6.9: a) Stress - strain relationship, b) Excess pore water pressure, c) effective principal stress ratio, and d) plot of the stress path; from *CIU* test on vertically oriented samples (site3, Fhkciu35)

Figure 6.10:

Strength envelope based on *CIU* tests at
a) site1, b) site2, and c) all sites

The shear parameters from the undrained tests using both failure criterion at the three sites and extra three series of tests at another locations (they are obtained from geotechnical reports in the area of Constance) are summarised in Table 6.6. It would appear from Table 6.6 (maxciu3) that the sample orientation would have a negligible influence on the effective strength parameters of this type of soil. The stress conditions at failure from all tests at site1 performed using both $(\sigma_1'/\sigma_3')_{max}$ and $(\sigma_1'-\sigma_3')_{at\,20\%}$ failure criterion are plotted in p - q diagram as shown in Figure 6.10a (site1). All points lie approximately on the strength envelope with coefficient of regression $r \approx 1$. From the strength envelope in Figure 6.10a, a mean value of $\varphi' = 27.2°$ and 26.9°, and c′ = 11.6 and 12.7kN/m² may be estimated using the failure criterion $(\sigma_1'/\sigma_3')_{max}$ and $(\sigma_1'-\sigma_3')_{at\,20\%}$ respectively . In a similar way a mean value of the effective strength parameters $\varphi'= 22.0°$ and 20.7°, and $c' = 19.5$ and 22.7 kN/m² may be estimated from Figure 6.10b (site2). All stress condi-

tions at failure from all sites including the three series of tests from other locations are once more plotted in a p - q diagram as shown in Figure 6.10c. Surprisingly all points lie closed each other around the best fit strength envelope ($r \approx 0.985$), irrespective of their origin. The mean effective strength parameters estimated from the strength envelope of Figure 6.10c are $\varphi' = 25.1°$ and 24.8°, and $c' = 15.2$ and 15.7 kN/m² using the failure criterion $(\sigma_1' / \sigma_3')_{max}$ and $(\sigma_1' - \sigma_3')_{at\,20\%}$ respectively.

Table 6.6:   Strength parameters from *CIU* tests.

Test	Cell pressure	w	γ/γ_d	e_0	τ_f ♣	c' *	φ' *
	[kPa]	[%]	[kN/m³]	[-]	[kN/m²]	[kN/m²]	[°]
site1							
damciu4/30	50, 100, 200, 300, 400, 500	30.3	19.5/15.0	0.80	350	14.1/14.1	26.5/26.5
damciu6	50,100,200	28.3	19.8/15.4	0.74	50	11.1/15.4	27.0/25.0
damciu10	50,100,200	26.5	19.4/15.4	0.75		6.10/5.80	30.6/30.6
damciu14	88,112,200	33.2	19.1/14.3	0.87	17.8	2.60/3.70	32.7/31.8
site2							
maxciu2	50,100,200	30.6	19.5/15.0	0.82	40	10.5/17.3	26.0/21.7
maxciu ♠	50,100,200,300,400	25.6	19.7/15.7	0.73		17.1/18.4	21.6/21
maxciu3 ♦	50,100,200	30.4	19.3/14.8	0.84	19	11.3/13.5	27.7/26.1
site3							
fhkciu35	50,100,200	75.8	15.7/9.02	2.09	13	3.40/3.40	39.5/39.5
Others							
Jaegerkaserne	100,200,300	20.4	20.6/17.1	0.58		9.1/ -	25.5/ -
Schwandorf	100,200,300	16.0	21.3/18.4	0.47		24.4/18.8	26.3/26.4
Fhk	100,200,300	72,8	15.8/9		12	3.0	27.3
Stromeyersdorf	100,200,300	24.0	20.3/16.4	0.65		16.3/ -	21.1/ -

* = According to the two failure criterion $(\sigma_1'/\sigma_3')_{max}$ / $(\sigma_1 - \sigma_3')_{max\ or\ 20\%}$, ♣ = Field shear vane strength (uncorrected), ♦ = Horizontal sample, ♠ = reconstituted samples

6.4.3   Isotropically consolidated drained (*CID*) compression test

A total of 37 (11 series) isotropically consolidated drained (*CID*) strain controlled triaxial compression tests was performed at constant effective consolidation pressure (25 to 500 kN/m²) on cylindrical specimen of 50 mm high and 50 mm in diameter; 9 from site1, 18 from site 2, and 9 from site 3. All samples were vertically oriented except 3 samples from site2 (Maxcid13) and 3 samples from site3 (Fhkcid389) (Table 6.7) which were horizontally oriented. Similar to the undrained tests, back pressure of 300 to 400 kPa were used. The specimens were 94 to 100 %

saturated. The tests were conducted under a constant rate of strain of 0.003, 0.005 and 0.01 mm/min for specimens from site1, site2 and site3 respectively.

Typical stress - strain relationships, volume change characteristics and the stress paths followed in *CID* tests at site1 are shown in Figure 6.11 (see also Appendix A.7). The stress - strain curves (Figure 6.11a) are non linear from the beginning and they show no extreme value, rather they deform continuously to large strains, but they appear to level off and eventually approach a constant value at axial strain greater than 20%. The stresses at 20% strain were taken as failure stresses. The un/re-loading curves show approximately a linear behaviour. The volumetric strains (contraction) in these tests (Figure 6.11b) vary almost linearly up to an axial strain of approximately 10% and they appear to increase further linearly with the axial strain. In Figure 6.11c the lateral strains calculated from band measurement at the mid height around the circumference of the sample and from the measurement of the water drained out of the sample are plotted against axial strain. From Figure 6.11c, it appears that the band measuring method fails to record the lateral deformation of the sample at a lower strain and are not consistent. The Poisson's ratios during the drained test are also plotted against the axial strain in Figure 6.11c. Theoretically, the Poisson's ratio is purely an elastic constant, which is defined as the ratio of the lateral elastic strain to the axial elastic strain. The deformations in a triaxial tests, however, contains both elastic and plastic strains. Hence, the term Poisson's ratio in the analysis and presentation of the triaxial test in this chapter should be understood simply as a ratio of the lateral and axial strains without distinguishing the elastic and plastic part of the strains. It seems that the Poisson's ratio is not a unique value for one type of soil, rather it increases almost linearly with the axial strain. Figure 6.11c shows that the Poisson's ratio varies from an average value of 0.35 at low strain to about 0.45 at 20% strain, with a mean value of 0.395. The average Poisson's ratio from the three test series at site1 vary from 0.374 to 0.460. Finally, the stress paths followed during drained test are shown in Figure 6.11d. Whether it is a normal loading or unloading or reloading, the drained stress path in compression test (σ_3 = *constant*) followed a straight line at 45° degree from the horizontal in anticlockwise direction.

A similar typical stress - strain curves, volumetric strain, and Poisson's ratio in isotropically consolidated drained tests at site2 are shown in Figure 6.12 (see also Appendix A.8). The stress - strain curves are non - linear from the beginning. The volumetric strain during un/reloading are omitted from the plot in Figure 6.12b. The Poisson's ratio varies on average from 0.25 at low strain to 0.50 at 20% strain (Figure 6.12c), with a mean value of 0.413. It can also be seen from Figure 6.12c that the Poisson's ratio varies with the confining pressure, i.e, decreases with increasing confining pressure. The average Poisson's ratio from six test series at site2 vary from 0.374 to 0.470. These values are higher than that usually assumed value of Poisson's ratio between 0.30 to 0.40 for normally consolidated soils based on the assumption of a pure elastic behaviour.
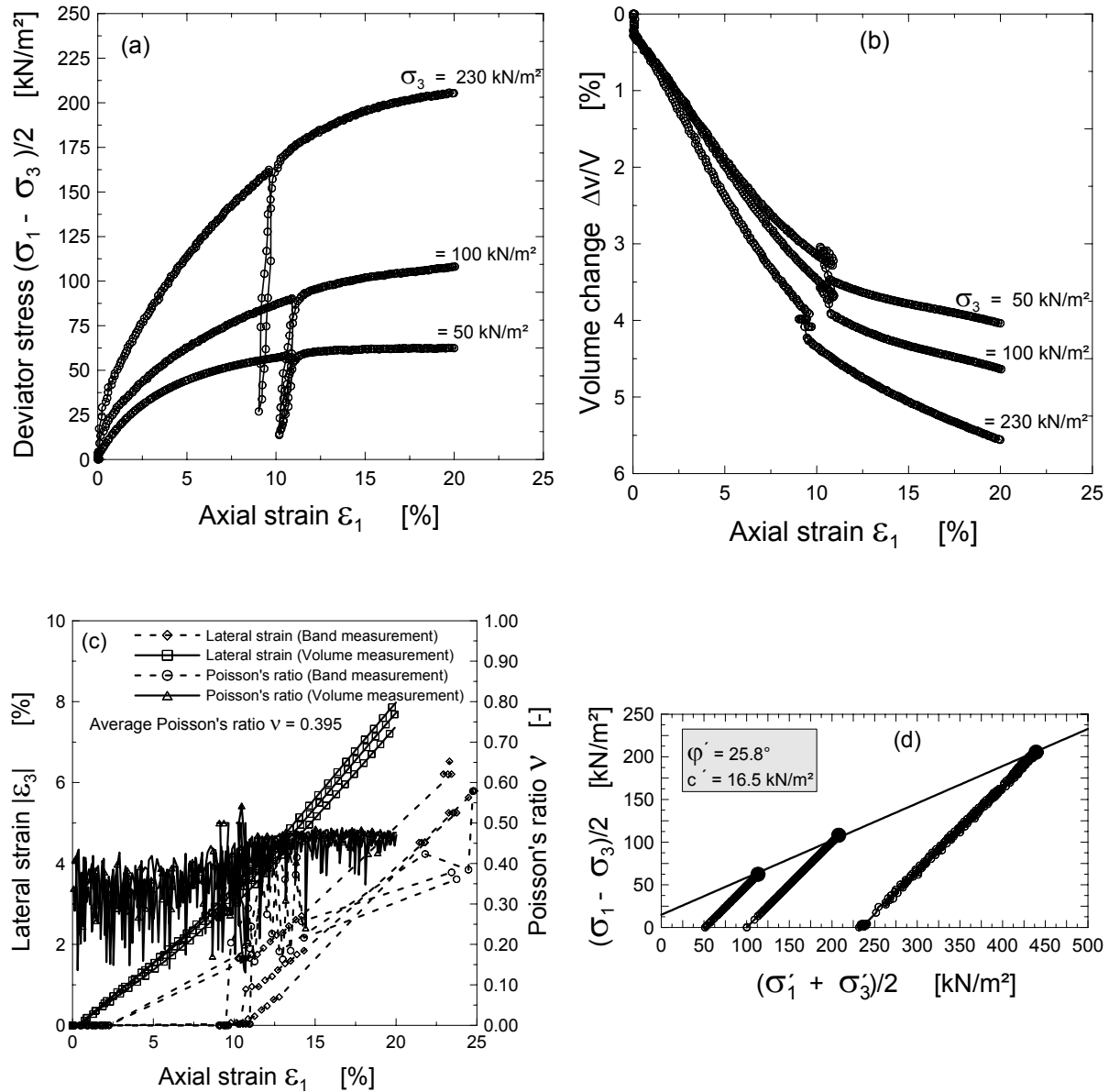
Figure 6.11: a) Stress - strain relationship, b) volume change - strain relationship, c) lateral strain and Poisson's ratio vs axial strain plot, and d) plot of the stress path from *CID* tests on vertically oriented samples (site1, Damcid15)

The stress - strain curves at site3 (Figure 6.13a and Appendix A.9) show a different behaviour. They are approximately linear initially and yielding occurs beyond 1 - 2.5% axial strain, where the stresses increase linearly with the deformation. Even at large deformation (> 30%), they appear not to level off. The failure stresses were assumed at 20% axial strain. The volumetric strains (Figure 6.13b) vary linearly with axial strain. Similar to stress - strain curves, no end to the change of volume of the specimens was observed even at large axial strains (> 30%). The Poisson's ratios for the upper (σ_3 = 26 kN/m²) in Figure 6.13c varies from 0.25 at small strain to 0.35 at 20% axial strain, while the lower curve (σ_3 = 48 kN/m²) remains approximately constant

at 0.26. The Poisson's ratio at the other two curves (σ_3 = 100 and 200 kN/m²) vary on average from 0.10 at low strain to 0.30 at 20% axial strain. These too low value of Poisson's ratio are once again confirmed by the same drained test on similar sample, where on average a variation of the Poisson's ratio between 0.07 to 0.20 had been observed (see Appendix A.9.1). The average value of the Poisson's ratio from the two test series on vertical specimens at site3 vary from 0.154 to 0.206, where as the average value from one test series on horizontal samples was 0.294.

Figure 6.12: a) Stress - strain relationship, b) volume change - strain relationship, c) lateral strain and Poisson's ratio vs axial strain plot, and d) plot of the stress path from *CID* tests on vertically oriented samples (site2, Maxcid15/Maxcid16)
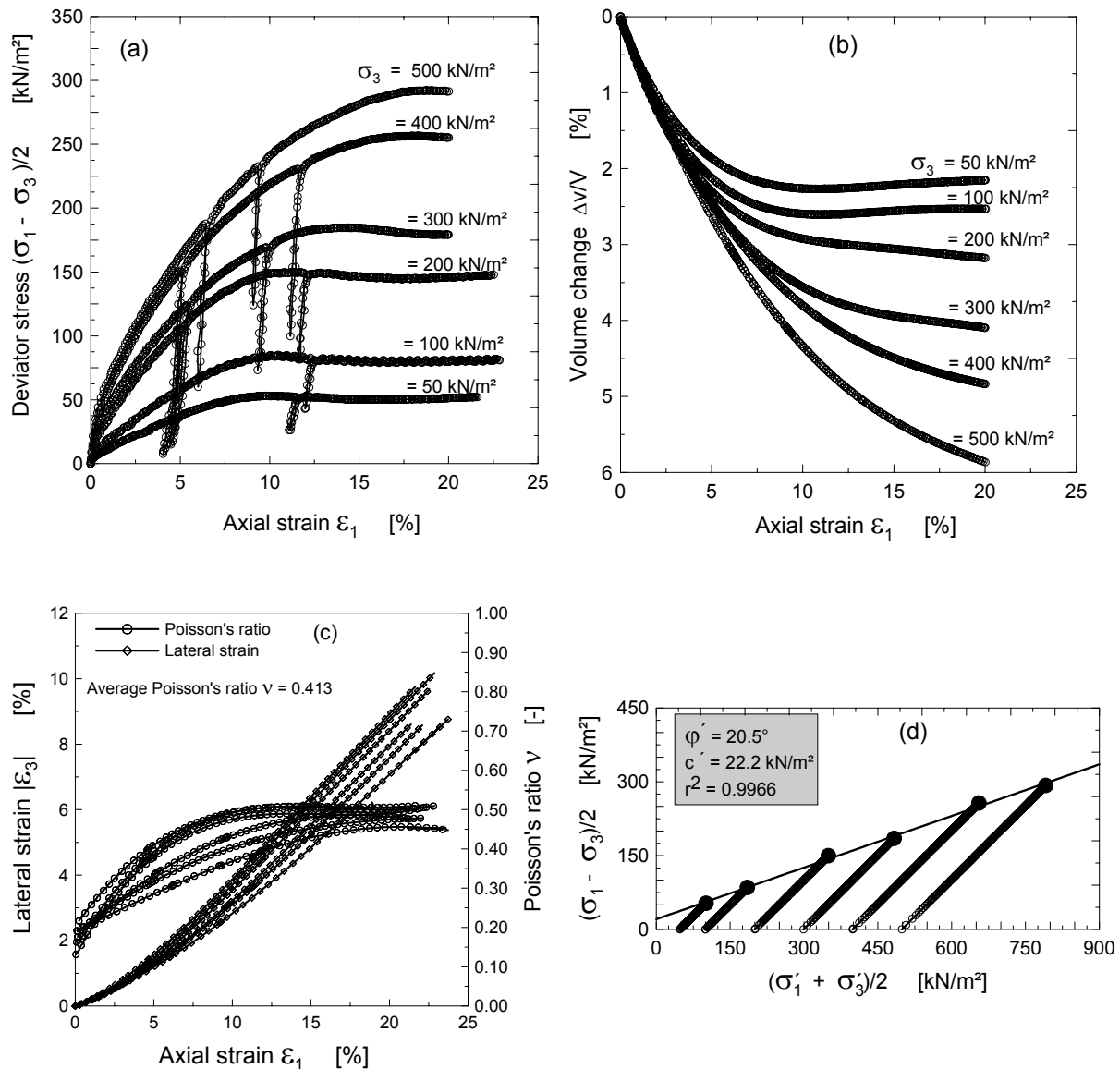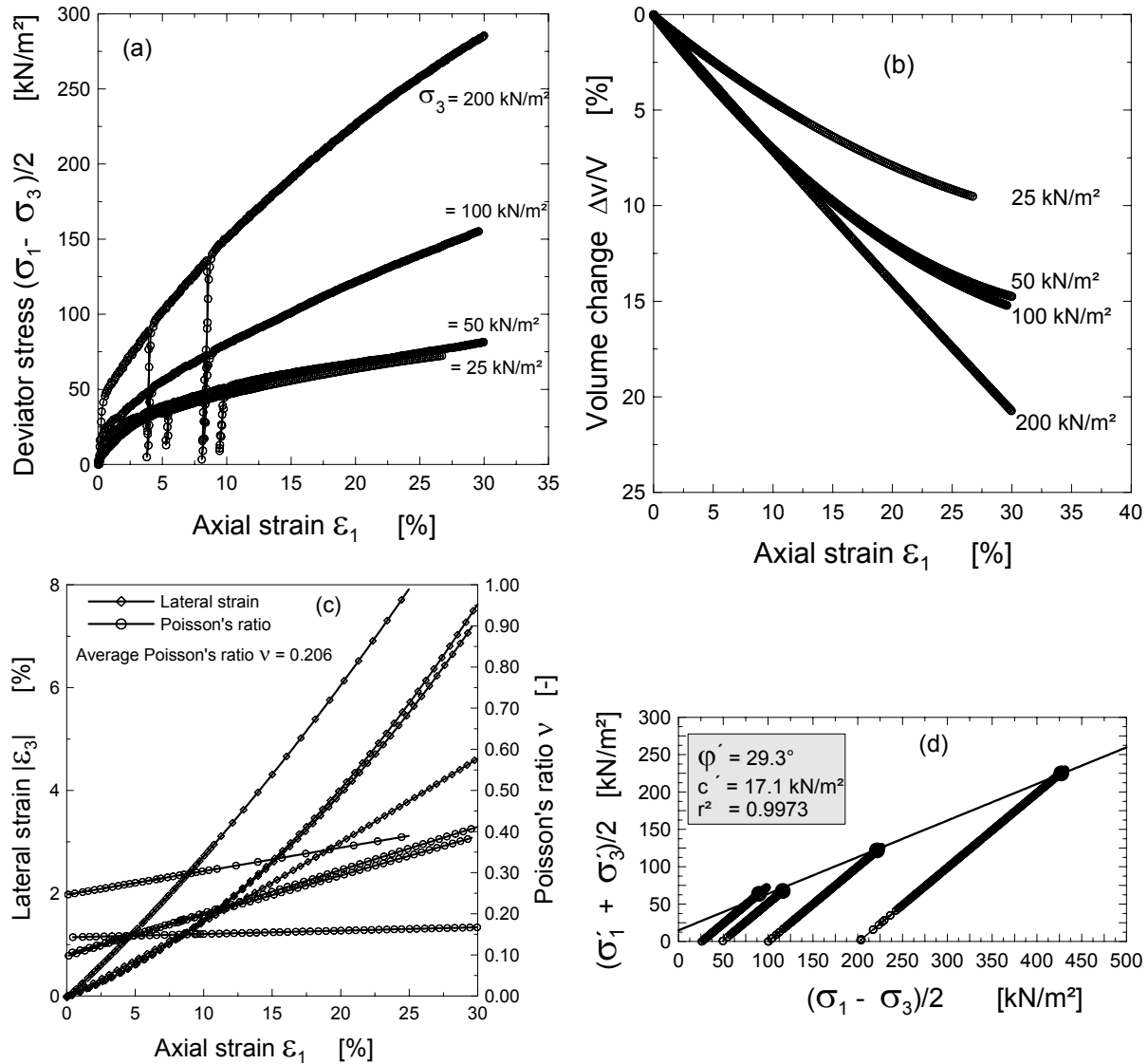
Figure 6.13: a) Stress - strain relationship, b) volume change - strain relationship, c) lateral
strain and Poisson's ratio vs axial strain plot, and d) plot of the stress path
from *CID* tests on vertically oriented samples (site3, Fhkcid36)

The *CID* test results at all sites are summarised in Table 6.7. From this table, it appears that the
strength parameters obtained from *CID* tests on horizontally oriented specimens (maxcid13 and
fhkcid389) are higher than that of vertically oriented similar specimens. The stress conditions at
failure for all *CID* tests at site1 are plotted in one p - q diagram as shown in Figure 6.14a. The
points lie approximately on and near the best fit line (r ≈1), which may be taken as the strength
envelope. The average strength parameters at site1 approximated from the strength envelope are
$\varphi' = 25.3°$ and $c' = 13.2$ kN/m². Similary, the average strength parameters $\varphi' = 20.6°$, $c' = 30.6$
kN/m² and $\varphi' = 30.2°$ and $c' = 16.4$ kN/m was measured from the p - q plots for all tests at site2
(Figure 6.14b) and at site3 (Figure 6.14c) respectively. Figure 6.14d summarises all test data
from the three sites and produces a single strength envelope based on the best fit line (*r* = 0.96).

The average representative shear parameters for all site are estimated to be $\varphi' = 22.5°$ and $c' = 28.8$ kN/m².

Table 6.7: Strength parameters from *CID* tests

| Test	Cell pressure	w	γ/γ_d	e_0	c'	φ'	ν
	[kN/m²]	[%]	[kN/m³]	[-]	[kN/m²]	[°]	[-]
site1							
damcid05	50, 100, 200	30.7	19.5/15.0	0.79	17.7	24.4	0.420
damcid07	50,100,200	28.3	19.7/15.4	0.74	10.7	24.3	0.460
damcid15	50,100,230	34.2	18.7/14.1	0.90	16.5	25.8	0.374
site2							
maxcid01	50,100,200	31.0	19.5/14.9	0.82	20.3	24.8	0.470
maxcid05	50,100,200	34.9	19.1/14.1	0.93	17.7	24.4	0.374
maxcid15/16	50,100,200,300, 400,500	32.8	19.1/14.2	0.89	22.2	20.5	0.413
maxcid ♠	50,100,200	27.5	19.5/15.3	0.78	11.1	22.5	0.395
maxcid13 *	50,100,200	25.6	20.2/16.1	0.69	25.6	28.6	0.466
site3							
fhkcid34	50,100,200	75.1	15.3/8.71	2.16	17.4	25.9	0.154
fhkcid36	25,50,100,200	74.5	15.3/8.77	2.13	17.1	29.3	0.206
fhkcid389 *	50,100,200	74.0	15.2/8.76	2.14	17.3	31.4	0.294

● = horizontal samples, ♠ = remoulded sample
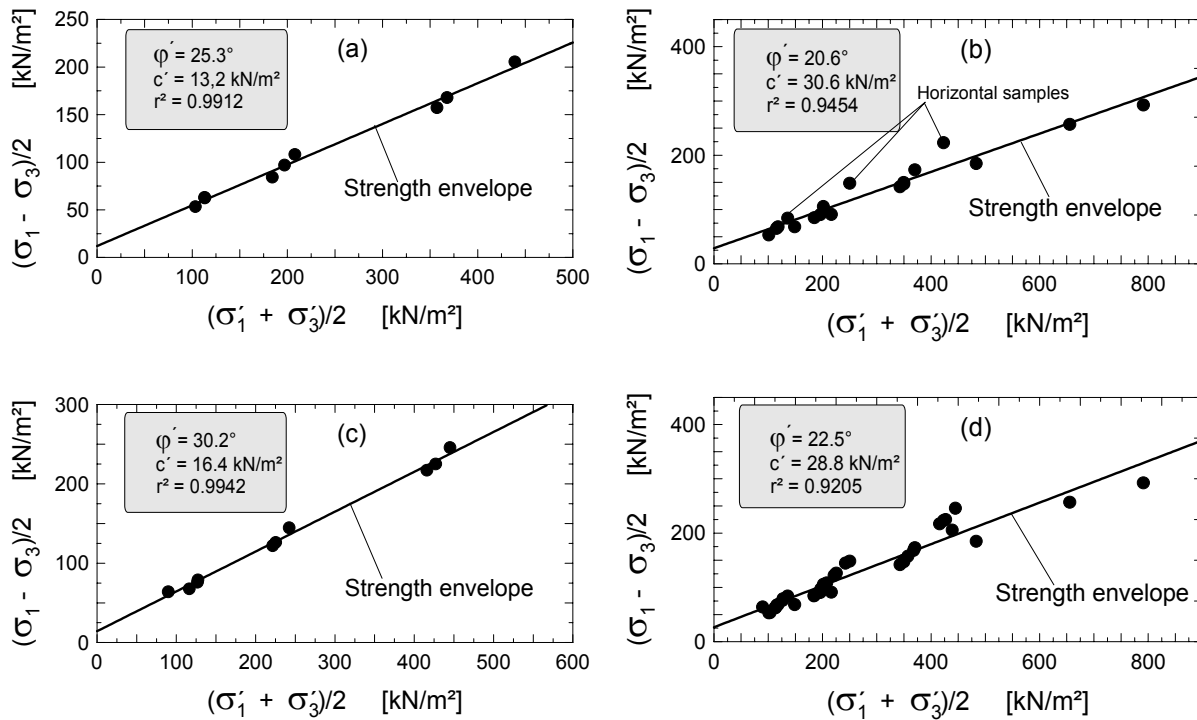
Figure 6.14: Strength envelope based on *CID* tests at a) site1, b) site2, c) site3, and d) all sites

6.4.4   Anisotropically consolidated triaxial compression test

These tests were performed in a triaxial cell with special arrangements for the application of additional vertical stress independent of the axial load and cell pressure during the K_0 consolidation. The special arrangement includes a pneumatic cylinder positioned at the top of the triaxial cell and below the motorised load cylinder (see Appendix A). The specimens were first subjected to all round cell pressure and the vertical stress was simultaneously increased through the pneumatic cylinder to maintain the K_0 condition. After the specimen was fully consolidated, axial load was applied by the motorised load cylinder. The first trial test was performed using $K_0 = 0.58$, which was approximated from *Jaky* empirical equation ($1 - sin\ \varphi'$), and showed that the specimen underwent excessive lateral deformation. This indicates that the $K_0 = 0.58$ was not the appropriate value for the soil at hand or the stress was too large. This may also be verified from Figure 3.6, where it shows that the 1 - sin φ′ line lies quite below the measured K_0 values. A second trial with $K_0 = 0.65$ had also produced a lateral deformation, but to a lesser extent. Finally, $K_0 = 0.80$ was fixed for further tests. A total of four anisotropically consolidated triaxial test on 12 specimens) was performed, among which one test series was undrained (*CAU*), one drained (*CAD*), and two controlled stress path tests under undrained condition. The undrained and drained tests are presented and discussed below while the stress path tests will be presented in the next section (Section 6.4.5).

The undrained tests were performed at a strain rate of 0.05 mm/min while the drained tests were performed at a strain rate of 0.005. The stress - strain relationship, excess pore water pressure, the effective principal stress ratio and the stress path from the *CAU* tests are shown in Figure 6.15. The stress - strain curves from the *CAU* test (Figure 6.15a) seems to have higher initial stiffness, and larger stresses at failure than the stress - strain curves from *CIU* tests (Figure 6.8a) on similar samples. The excess pore water pressure in the *CAU* test (Figure 6.15b) reaches its peak value at relatively lower axial strain (about 3 to 4%) than that in the *CIU* test (5 to 6.5%) (Figure 6.8a). The rate of drop of the pore water pressure after it reaches the peak value is higher in *CAU* tests than in *CIU* tests. The strength parameters from *CAU* test (Figure 6.15c) are higher in cohesion and lower in friction than the corresponding *CIU* test.

The stress - strain relationship, volumetric strain, and the stress paths in the *CAD* tests are shown in Figure 6.16. The course of the stress - strain curves (Figure 6.16a) are similar to that from *CID* tests. However, the stress - strain curves show a higher initial stiffens than from *CID* tests, and the stresses at failure in the *CAD* tests are almost 2 to 3 times higher than the failure stresses in the *CID* tests. It can also be observed that the stress - strain curves appear to level off and approach a constant value at lower strain than in the *CID* tests. The volume change curves in Figure 6.16b show a decrease in volume up to a strain of 5% and an increase in volume afterwards unlike that observed in *CID* tests. The stress path diagram (Figure 6.16c) also shows exceptionally

high value of the strength parameter. These are unexpected for normally consolidated soil and it requires a further investigation to see whether the anisotropy consolidation ($K_0 = 0.80$) are the main reason for such phenomena.
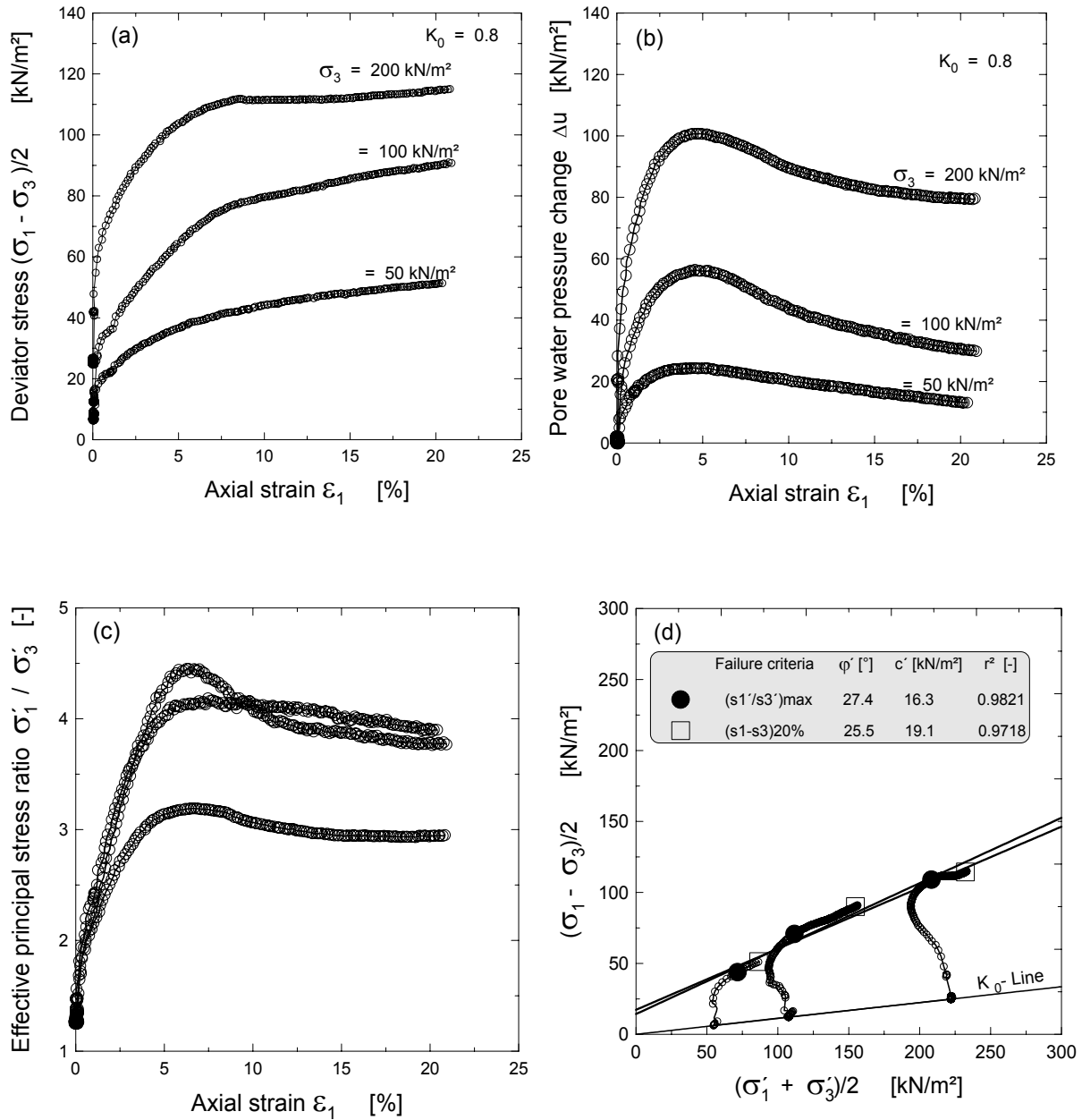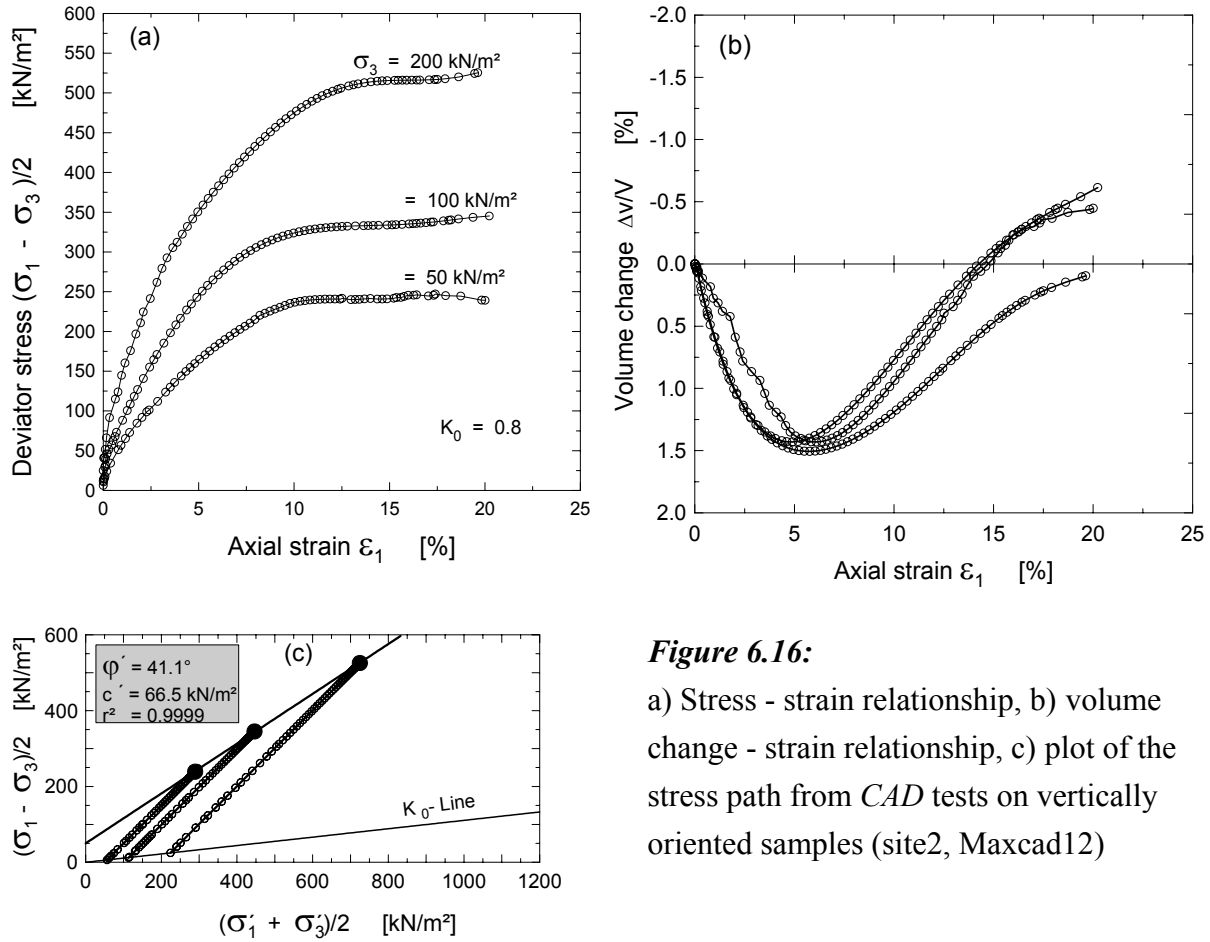

Figure 6.15:   a) Stress - strain relationship, b) excess pore water pressure, c) effective principal stress ratio, and d) plot of the stress path from *CAU* test for vertically oriented samples (site2, Maxcau4)

Figure 6.16:

a) Stress - strain relationship, b) volume change - strain relationship, c) plot of the stress path from *CAD* tests on vertically oriented samples (site2, Maxcad12)

6.4.5 Controlled stress path triaxial tests

The different stress paths in an excavation have been discussed in Section 3.4.1. It is generally believed that the strength and deformation behaviour of a soil at a particular point in the field depends on the stress path it follows. The stress paths assuming an initial anisotropic state of stress at point O are shown in Figure 6.17. Here the stress paths A, B and C were investigated for isotropic and anisotropic initial stress state condition. The path A is the total stress path followed during standard triaxial test ($\Delta\sigma = 0$, $\Delta\sigma < 0$), and it had been presented in Section 6.4.2 and 6.4.4.
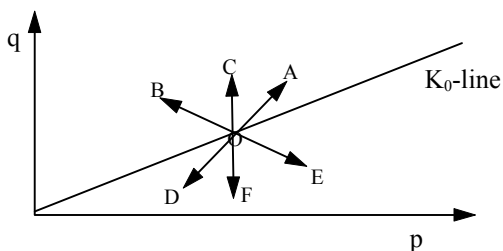
Figure 6.17:

Plot of the total stress paths in p - q diagram

A controlled stress path tests were performed on 6 undisturbed samples and 9 reconstituted samples from site2. The undisturbed specimens were initially anisotropically (K_0 = 0.80) consolidated, while the reconstituted samples were initially isotropically consolidated. The same triaxial apparatus was used as the anisotropically consolidated standard triaxial tests. The controlled stress path tests were effected by varying the stresses incrementally according to the postulated stress paths. Both the increment and decrement of the vertical and horizontal stresses were controlled by computer program. It was possible to apply the pressures in up to 15 pressure increments. In each step, the stress increments or decrements were applied at a stress state of 0.4 - 0.5 kN/m². First the all round cell pressure was adjusted followed by adjustments of the vertical stress through the pneumatic cylinder every minute. The stress rate was approximated from the time required to failure and the stress at failure from previous strain controlled *CIU* tests in order to compare the results with the strain controlled tests. All the stress paths were performed under undrained condition.

The postulated total stress path B at 1:1 slope was effected by decreasing the horizontal stress and maintaining the vertical stress constant. The horizontal stress was decreased by decreasing the cell pressure incrementally. The decrease of the cell pressure would decrease the vertical stress too. Therefore, to maintain the vertical stress constant, a vertical pressure increment which is equal to the cell pressure decrement was applied through the pneumatic cylinder. Similarly, the postulated total stress path C at a slope of infinity was effected by increasing the vertical stress and decreasing the horizontal stress. The decrease of the horizontal stress was effected by decreasing the cell pressure, while the increase of the vertical stress was effected by additional vertical pressure, which was twice higher than the cell pressure.

Figure 6.18 shows the results of controlled stress *CAU* triaxial tests on undisturbed samples at 100, 200, and 300 kPa cell pressure for the postulated stress path B and C. The course of the stress - strain curves in Figure 6.18a and b is similar, even so they are similar to the other standard stress paths, except that they show a gradual small decrease in the deviator stress after they reach 10 - 15% axial strain. The development of the excess pore water pressures are shown in Figure 6.19. The excess water pressure in stress path B (Figure 6.19a) is negative for the cell pressure of 100 and 200 kPa, and it is positive for cell pressure of 300, but very small (< 25 kPa). The excess water pressure in stress path C (Figure 6.19b), with cell pressure 100 and 200 kPa reached their maximum value at an axial strain of 2.5% before they dropped gradually to minimum value at large axial strain, while the pore water pressure with 300 kPa cell pressure reaches its maximum value at 7.5 % axial strain and remains almost constant through out the test. Actually this curve would have to follow the same course as the other two curves.
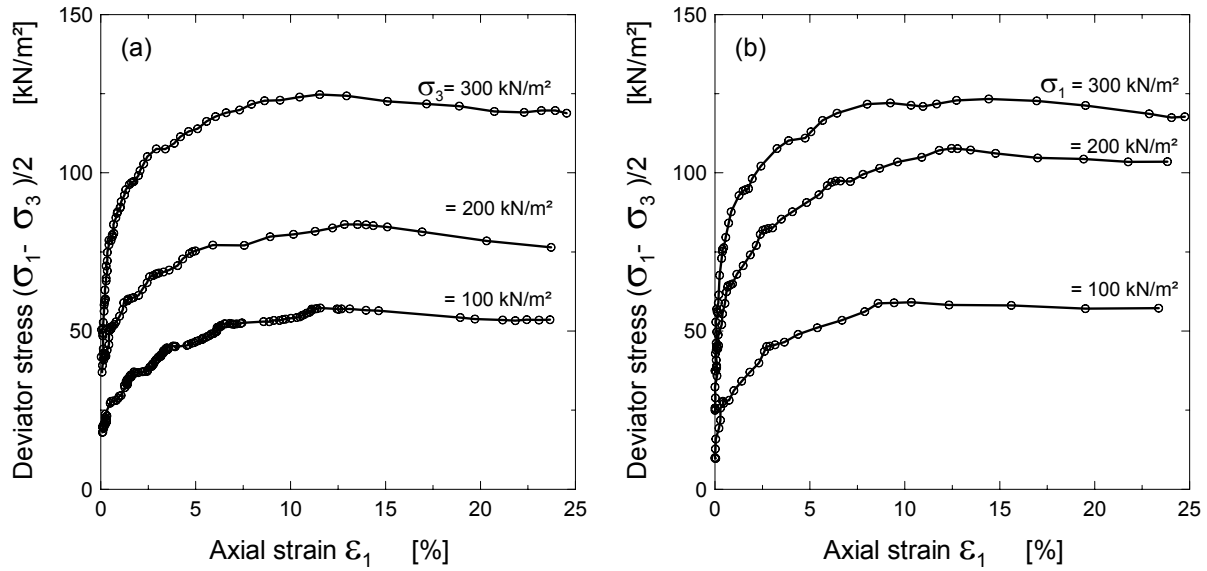
Figure 6.18: stress - strain relationships from stress controlled *CAU* triaxial tests on undisturbed samples for the postulated stress path B (a) and stress path C (b) at site2
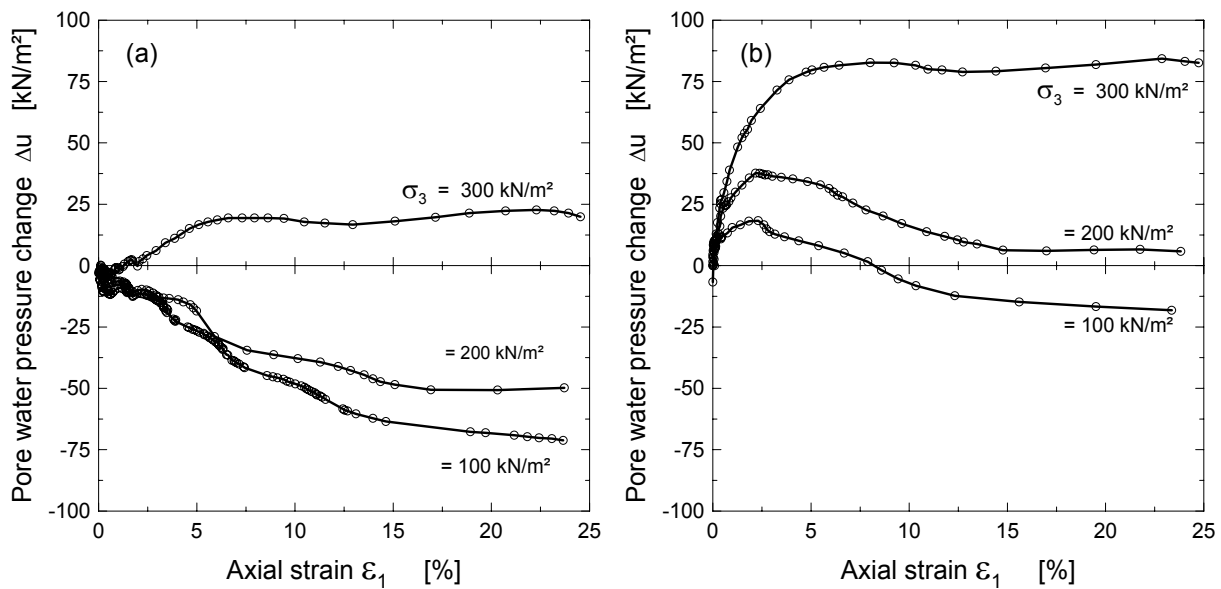

Figure 6.19: Excess pore water pressure in stress controlled *CAU* triaxial tests on undisturbed samples for the postulated stress path B (a) and stress path C (b) at site2

The stress paths in controlled stress path - *CAU* triaxial tests on undisturbed samples for the postulated stress path B and C are shown in Figure 6.20a and b respectively. The test paths in all the specimens are very similar to the postulated stress paths until they approximately reach $(\sigma_1 - \sigma_3)_{max}$ reached, after which the paths begins to deviate from the postulated paths. Since the horizontal stresses and vertical stresses had been changed in a stepwise fashion, the actual stress path reproduced in the laboratory have a zig - zag pattern. However, the general trend of the stress condition were faithfully reproduced. The effective strength parameters $\varphi' = 33.4°$ and $c' = 0$ obtained from the stress path B and $\varphi' = 32.7°$ and $c' = 0$ from the stress path C are comparable to each other, but they are higher than the corresponding value from *CAU* tests. The effective stress path in both stress path B and C appear to be almost the same, independent from the direction of the total stress paths.

Figure 6.20: Stress paths in stress controlled *CAU* triaxial tests on undisturbed samples for the postulated stress path B (a) and stress path C (b) at site2

For the sole purpose of comparison, a controlled stress path - *CAU* triaxial tests were performed on 9 reconstituted samples for the three postulated stress paths; A, B and C. The test results are shown in Figure 6.21. It may be seen from Figure 6.21 that the effective stress path in all the diagrams remain the same. Hence, it may be ascertained that the effective stress paths are independent from the direction of the total stress paths. The effective angle of friction $\varphi' = 24.9°$, $24.6°$ and $24.8°$ from stress path A, B and C respectively are comparable to each other. The variation in the effective cohesion $c' = 16.9$, 18.6 and 20.4 kN/m² is not also extreme (less than 10% deviation), knowing that c' is very sensitive parameter in triaxial tests. These results suggest that the effective strength parameters are fairly the same for all types of controlled stress path tests conducted in this study.
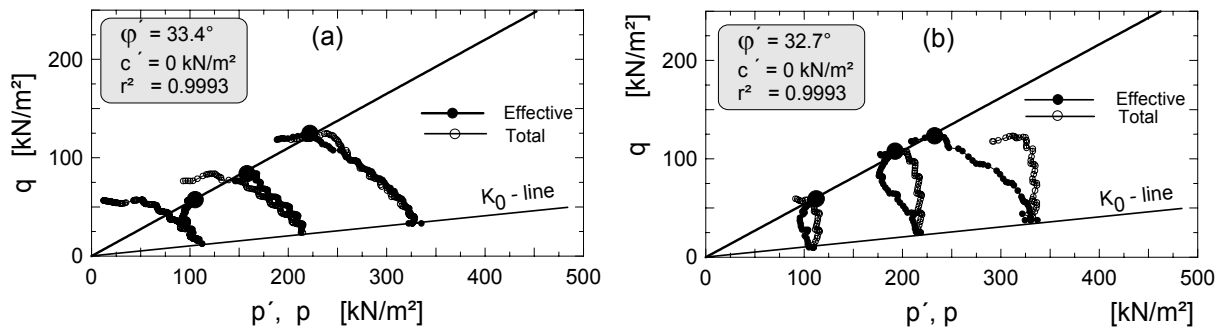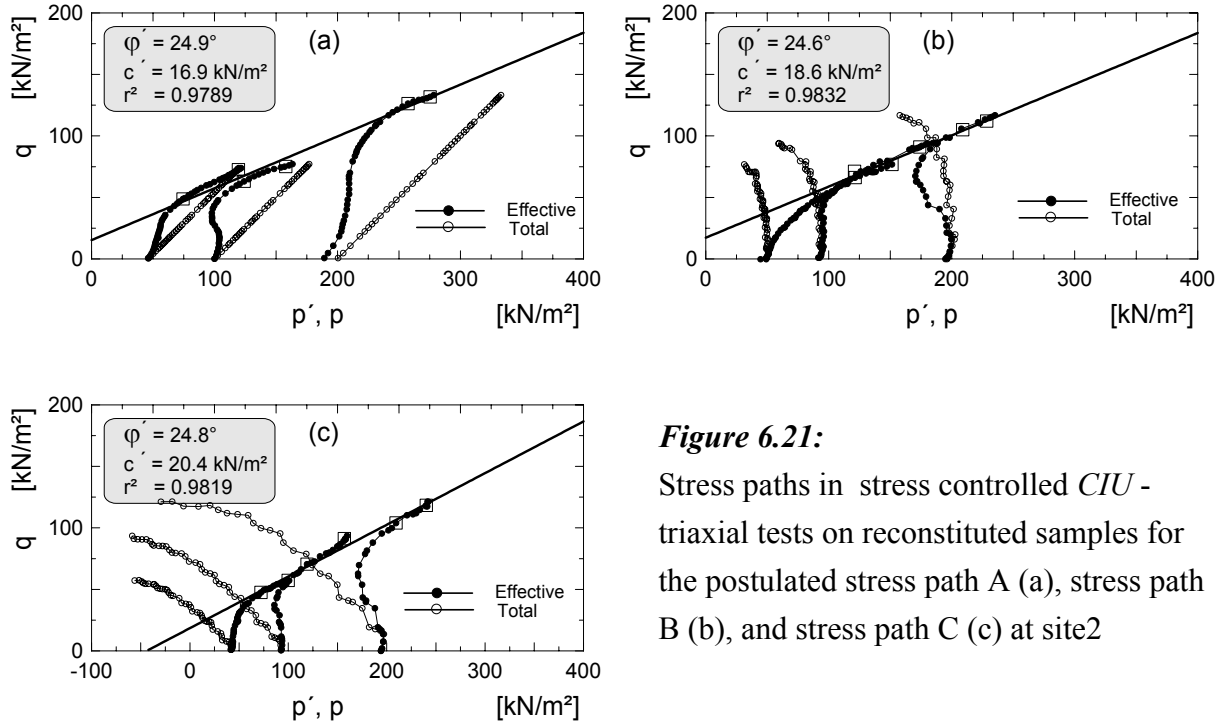
Figure 6.21:
Stress paths in stress controlled *CIU* - triaxial tests on reconstituted samples for the postulated stress path A (a), stress path B (b), and stress path C (c) at site2

6.4.6 Comparison of strength parameters

The strength parameters obtained from various type of tests and from more than three locations in and around the city of Constance have been presented and discussed in the preceding sections. A comparison of the test results, for example the two failure criteria in undrained test, drained/undrained tests, vertically/horizontally oriented specimens, isotropically/ anisotropically consolidated tests, different controlled stress path tests, and standard/stress path tests, will follow in this section.

From Figure 6.10 and Table 6.6, it would appear that the effective strength parameters obtained using the failure criterion $(\sigma_1'/\sigma_3')_{max}$ and $(\sigma_1'-\sigma_3')_{at\,20\%}$ differ not so much, even some times the strength envelopes overlaps one over the other. One may observe, however, that there is a general trend of increasing the effective friction and decreasing effective cohesion using $(\sigma_1'/\sigma_3')_{max}$ failure criteria and vice versa by the $(\sigma_1'-\sigma_3')_{at\,20\%}$ failure criteria. If one is interested in the effective angle of overall shear strength φ_s', one may arrive at the same value from both failure criterion. According to *DIN 18 137, 1990,*

$$tan\,\varphi_s' = tan\,\varphi' + \lambda_c \qquad (6.4)$$

where λ_c is a normalised cohesion and it is given by $\lambda_c = (c'/max\,\sigma_e')$, σ_e' is the equivalence pressure. If one assumes $\sigma_e' \approx \sigma_p' \approx 100\,kN/m^2$, and taking the mean value of $\varphi' = 22°/20.7°$ and $c' = 19.5/22.7$ kN/m² from site2, one may arrive at an average $\varphi_s' \approx 31°$ for both definition of the

failure stress. If one is rather interested in the effective shear parameters φ´ and c´, the author suggests to pass a best fit line through all failure points from both failure criterion and evaluate the mean effective parameters. Theoretically, the effective cohesion in a drained analysis is assumed to be zero, however, the drained and undrained test show a cohesion values ranging from 10 - 20 kN/m².

Regarding the drained and undrained isotropically consolidated tests, the average effective friction in undrained tests at site1 appear to be higher and the effective cohesion lower than the corresponding parameters in drained tests. It seems again that there is a compensation effect between effective friction and effective cohesion. At site2, however, the average friction angles are more or less comparable, but the average effective cohesion values are higher in drained test than in undrained test. Figure 6.22 shows the mean strength envelope from both drained and undrained tests at all sites. From Figure 6.22, it would appear that the failure stress from drained and undrained tests lie on and closed to the mean strength envelope, particularly for $p´ \leq 400$ kN/m². The mean effective strength parameters would be $φ´ = 23.5°$ and $c´ = 22$ kN/m².
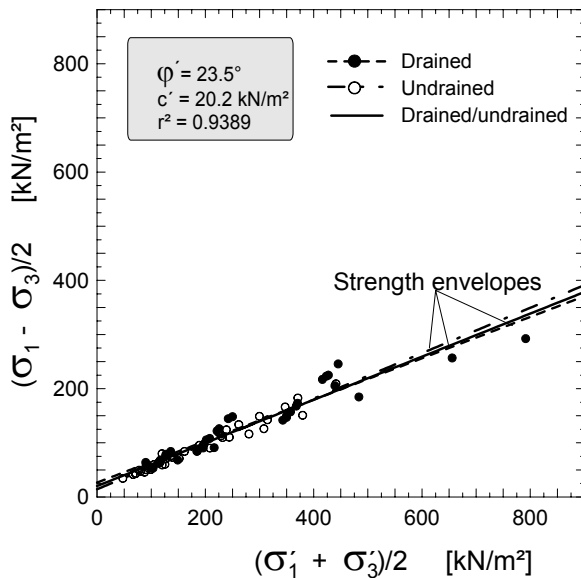
Figure 6.22:
Comparison of drained and undrained stresses at failure

The effective strength parameters from undrained tests on horizontally oriented specimens at site2 arecomparable with those obtained from vertically oriented specimens. On the other hand, the drained tests on horizontally oriented specimens at site2 and site3 seem to produce relatively higher effective friction than those on vertically oriented specimens, but the effective cohesion is comparable. Taking into account the variation of the effective strength parameters that would exist even with in the same group of vertically oriented samples, the small difference between the

effective parameters of vertically and horizontally oriented specimens may be neglected. This assumption lead us to a generalised conclusion that the effective strength parameters for practical purposes remain fairly the same irrespective of the sample orientation.

The strength parameters from *CAU* test are higher in cohesion and lower in friction than the corresponding *CIU* test. On the other hand, it is difficult to compare the effective strength parameters from *CID* with *CAD* tests, because the strength parameters from *CAD* test are exceptionally high.

As far as the effective strength parameters of a soil element are concerned, they appear to be independent of the stress path, to which the soil was subjected during the triaxial test. Both the controlled stress path - *CAU* tests (postulated paths B and C, Figure 6.20) on undisturbed samples and the controlled stress path - *CIU* tests (Postulated Path A, B and C, Figure 6.21) on reconstituted specimens show that the strength parameters are stress path independent. *NG/Lo (1985)* had also arrived at the same conclusion that the strength envelope is insensitive to test type and stress path, and the absolute magnitude of the effective stress parameter c′ and φ′ are the same for compression and extension. Comparing the effective strength parameters from controlled stress path - *CAU* tests with standard strain controlled *CAU* tests, however, it may be shown that the effective friction from the stress path test is higher, and the effective cohesion is lower than that obtained from strain controlled *CAU* tests. Similarly, the effective friction is higher in controlled stress path - *CIU* tests than that from strain controlled *CIU* tests. The effective cohesion, however, remains more or less the same in both tests.

6.5   Deformation parameters

6.5.1   General

The stress - strain relationship for the investigated soils at the three sites from compression and triaxial tests have been discussed in section 6.3 and 6.4. From these strain stress curves, the basic deformation parameters constrained modulus E_{oed}, the modulus of elasticity E, the secant modulus at 50% failure stress E_{50}, the un/reloading modulus of elasticity E_{ur}, and the exponent m (Equation 3.55) were derived. The results are presented and discussed in the following sections.

6.5.2   Constrained modulus E_{oed}

The stress - strain relationships in compression is generally non - linear. As the stress increases, the strain increases but at a decreasing rate. The slope of the load deformation curve at any point is called constrained modulus E_{oed} and by definition, it is

$$E_{oed} = \Delta\sigma'_{vc} / \Delta\varepsilon \qquad\qquad (6.5)$$

However, since the field virgin compression curve is usually approximated by straight lines with a slope of C_c in a logarithmic plot, the stiffness modulus E_{oed} can also be approximated from (*Scherzinger (1991); Gudehus (1981)*),

$$E_{oed} = \frac{1+e_0}{C_c} \cdot \sigma^* \qquad\qquad (6.6)$$

where $\sigma^* = (\sigma' - \sigma'_0)/Ln(\sigma'/\sigma'_0)$ (Figure 6.23). Similarly the un/re-loading soil stiffness $E_{ur,oed}$ may be approximated from,

$$E_{ur,oed} \approx \frac{1+e_{vm}}{C_s} \cdot \sigma^* \qquad\qquad (6.7)$$

where $\Delta\sigma = (\sigma' - \sigma'_{vm})/Ln(\sigma'/\sigma'_{vm})$ (Figure 6.23). It should be noted that the $E_{ur,oed}$ is not a unique value for a given soil, even at the same consolidation pressure. It is dependent on the maximum pressure (σ'_{vm}) that the soil was subjected before it swells. For the same situation, the E_{oed}^{ref} at a reference pressure of p^{ref} may be given by (*Brinkgreve/Vermeer (1998)* or *Brinkgreve(2002)*),
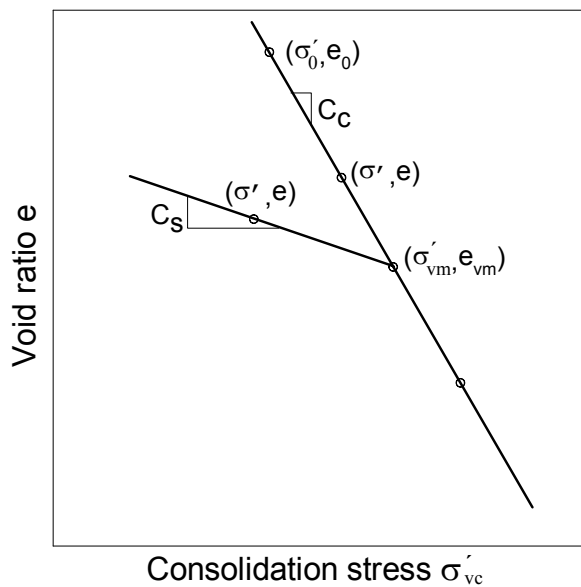
$$E_{oed}^{ref} = \frac{p^{ref}}{\lambda^*} \qquad\qquad (6.8)$$

Figure 6.23:
Idealised plot of one - dimensional compression

and

$$E_{ur,oed}^{ref} = \frac{3 \cdot p^{ref}(1-2\cdot\nu_{ur})}{\kappa^{*}}$$ (6.9)

assuming a plastic soil with the stress exponent $m = 1$ in *Ohde (1939)* expression for the stress dependency of the constrained modulus (Equation 3.55). A modified *Ohde* equation is available in PLAXIS manual *(Brinkgreve/Vermeer (1998)* or *Brinkgreve(2002))*, which includes a term to account the stiffness of the soils at the ground surface. The modified power low is given by,

$$E_{oed} = E_{oed}^{ref} \cdot \left(\frac{c'\cdot cot\,\varphi' - \sigma_{vc}' \cdot sin\,\varphi'}{c'\cdot cot\,\varphi' + p^{ref} \cdot sin\,\varphi'} \right)^{m}$$ (6.10)

where E_{oed}^{ref} is the constrained modulus at a reference pressure of p^{ref}, $E_{oed}^{ref} = k \cdot p^{ref}$, and k is the dimensionless modulus number (Equation 3.55). Equation 3.55 and 6.10 are also valid for the un/re - loading constrained modulus $E_{ur,oed}^{ref}$.

A typical plot of the variation of the constrained modulus with consolidation pressure is shown in Figure 6.24 (see also Appendix A.4). From these figures and Table 6.8, it would appear that the stress exponent m for the investigated soil is not exactly 1. It varies rather from 0.70 to 0.85 with a mean value of 0.81 for the loading condition. For the un/reloading condition, m varies between 0.58 and 0.87 with a mean value of 0.71 during the 1st un/reloading and 0.82 and 1.42 with a mean value of 1.04 during the 2nd un/reloading. Those values above the maximum value of $m = 1$, should be corrected to 1 for practical applications. From Figure 6.24, it may be observed that the data from primary loading fairly lie on the best fit line, where as there is scatter of data in the case of the un/reloading. An average reference constrained modulus $E_{oed}^{ref} = 3162$, 3054, and 1763 kPa were found out at site1, site2 and site3 respectively. The un/reloading modulus is not unique, it depends on the maximum previous pressure at which the soil was subjected before it starts to swell. From Table 6.8, it would appear that there is no trend of the dependency of the un/reloading stiffness of the soil on the maximum previous pressure; sometimes it is lower at higher maximum previous pressure (for example, damcon2, damcon3, maxcon2) and sometimes it is higher at higher maximum previous pressure (for example, maxcon3, fhkcon2). Despite of the data scattering and ignoring the dependency of the un/reloading stiffness on the maximum previous pressure, an average value of $E_{ur,oed}^{ref} = 7932$, 8974, and 17041 kPa may roughly be estimated at site1, site2, and site 3 respectively.

The reference constrained modulus as estimated from Equations 6.8 and 6.9 (assuming $m = 1$ and $\nu_{ur} = 0.2$) are also given in Table 6.8. It appears that the reference stiffness of the soil during the primary loading is underestimated by 19 to 28%, if one assumes $m = 1$ and applies Equation 6.8. On the other hand, the un/reloading reference stiffness from Equation 6.9 are higher than that estimated from Figure 6.24 and Appendix A.4. This is mainly due to the selection of the value of

κ^*. It was mentioned in section 6.3.1 that the value of κ^* derived from Equation 6.2 is 2 times higher than that estimated from the assumption $C_s \approx 2.3 \cdot \kappa$ or directly read from the plot assuming a linear relation (Appendix A.3). It seems that there is an external factor of 2 in Equation 6.2. Hence, if Equation 6.9 is going to be used to estimate the reference un/reloading stiffness, κ should be calculated from Equation 6.2. The average un/reloading stiffness values in Table 6.8 are an arithmetic mean of the values for a given site without consideration of the stress levels.
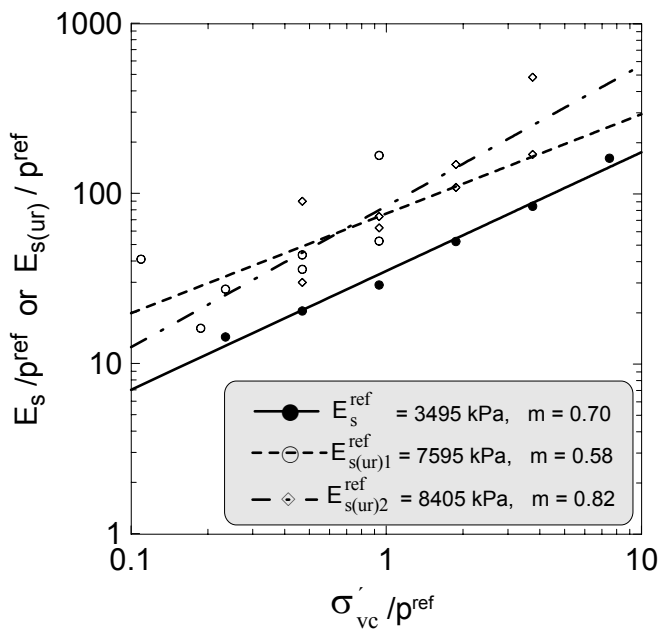

Figure 6.24:
The variation of the constrained modulus with consolidation pressure in one - dimensional compression (site2, Maxcon3)

Table 6.8:   Reference constrained modulus at a reference pressure p^{ref} =100 kPa

Test	E_{oed}^{ref}	m	1st un/reload		2nd un/reload		E_{oed}^{ref} (m=1)	$E_{ur,oed}^{ref}$ (Eq. 6.9, m=1, v_{ur} = 0.2)	
			$E_{ur,oed}^{ref}$	m	$E_{ur,oed}^{ref}$	m	(Eq. 6.8)	1st un/reload	2nd un/reload
	[kPa]	[-]	[kPa]	[-]	[kPa]	[-]	[kPa]	[kPa]	[kPa]
Damcon1	3590	0.82	6223	0.87			2551	11765	
Damcon2	3263	0.85	8411	0.73	6700	1.42	2591	19355	13846
Damcon3	2633	0.82	10092	0.76	8541	1.20	2165	17308	11250
Average	3162	0.83	8242	0.79	7621	1.31	2436	16143	12548
Maxcon1	2512	0.84	14146	0.69			1890	15929	
Maxcon2	3156	0.83	11585	0.79	5271	0.93	2481	21687	10778
Maxcon3	3495	0.70	7595	0.58	8405	0.82	2222	18556	12676
Average	3054	0.79	11109	0.68	6838	0.88	2198	18724	11727
Fhkcon2	1763	0.78	11729	0.58	22353	0.82	1435	43902	30000

NB.: For the stress level at which the unloading starts, refer to Table 6.3.

6.5.3 Deformation property under deviatoric loading

The relationship between axial strain ε and deviator stress $2 \cdot q = (\sigma_1 - \sigma_3)$ in a conventional triaxial compression test of a soil may be expressed by the hyperbola (*Kondner (1963)*),

$$q = \frac{1}{2} \cdot \frac{\varepsilon}{a + b \cdot \varepsilon} \qquad (6.11)$$

where a and b are constants. If the stress-strain data (Figure 6.25a) are plotted on the transformed axes (Figure 6.25b), the value of the constants a and b may be determined readily, where Equation 6.11 is rewritten on the following form,

$$\frac{\varepsilon}{2 \cdot q} = a + b \cdot \varepsilon \qquad (6.12)$$

It may be noted that a and b are the intersect and the slope of the resulting straight line (Figure 6.25b). It may also be readily seen that $1/a = E_i$, the initial tangent modulus, and $1/b = q_{ult}$, the ultimate asymptotic value of the deviatoric stress. *Duncan/Chang (1970)* introduced a failure stress ratio $R_f = q_f / q_{ult}$, because usually the q_{ult} exceeds q_f, where $q_f = (\sigma_1 - \sigma_3)_f / 2$. Equation 6.11 can now be rewritten as

$$q = \frac{\varepsilon}{\dfrac{2}{E_i} + \dfrac{R_f \cdot \varepsilon}{q_f}} \qquad (6.13)$$
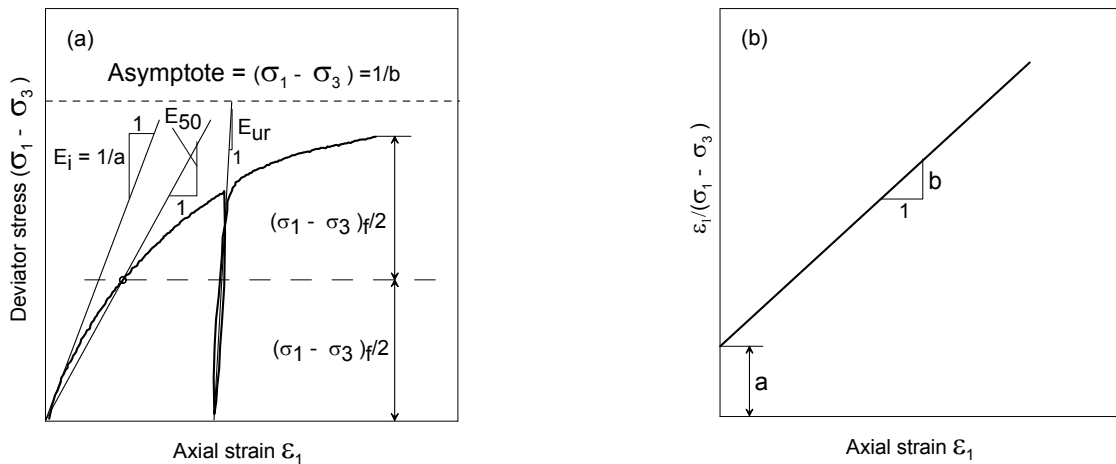
Figure 6.25: a) Hyperbolic stress - strain curve, b) transformed hyperbolic stress strain curve

For an anisotropically consolidated clay, a state of zero strain is associated with a non zero end of consolidation deviator stress $q_0 = \sigma_3 \cdot (1 - K)/K$, where $K = \sigma_3 / \sigma_1$ is the consolidation stress ratio. As in the case of conventional isotropically consolidated clay, a state of zero stress associated with a state of zero strain is required in hyperbolic stress - strain relations. This requires an intro-

duction of a new definition of deviatoric stress after consolidation q_m, where $q_m = q - q_0$, and it is zero at the end of the consolidation. Equation 6.13 could be rewritten by analogy as

$$q_m = q - q_0 = \frac{\varepsilon}{\dfrac{2}{E_i} + \dfrac{R_f \cdot \varepsilon}{q_{mf}}} \qquad (6.14)$$

In undrained tests the drained initial tangent modulus E_i in Equations 6.13 and 6.14 should be replaced by the undrained initial modulus E_{ui}.

Except in the case of unconsolidated - undrained tests on saturated soils, the tangent modulus and compressive strength of soils have been found to vary with the confining pressure employed in the tests (*Duncan/Chang (1970)*) according to Equation 3.55. A modified *Ohde* equation is available in PLAXIS manual *(Brinkgreve/Vermeer (1998)* or *Brinkgreve(2002))*, which includes a term to account the effect of the cohesion on the stiffness of the soils. The modified power low is given by,

$$E_i = E_i^{ref} \cdot \left(\frac{c' \cdot \cot\varphi' - \sigma_3' \cdot \sin\varphi'}{c' \cdot \cot\varphi' + p^{ref} \cdot \sin\varphi'} \right)^m \qquad (6.15)$$

where σ_3' is the effective confining pressure in triaxial test, E_i^{ref} is the reference initial tangent modulus at a reference pressure of p^{ref}, and m is the exponent. $E_i^{ref} = k \cdot p^{ref}$, where k is the dimensionless modulus number in Equation 3.55.

The secant modulus at 50% of the failure stress E_{50} is used in PLAXIS as main input stiffness property, because the exact determination of the initial tangent modulus for soft and sensible soils is difficult. Another important form of the modulus of elasticity is the modulus of elasticity during unloading and reloading, denoted by E_{ur}. It is believed that E_{ur} is much higher than E_i or E_{50}. Like the E_i, E_{50} and E_{ur} also vary with the confining pressure according to Equation 3.55 and 6.15, the only thing to do is to substitute E_{50} or E_{ur} instead of E_i, and E_{50}^{ref} and E_{ur}^{ref} instead of E_i^{ref}.

6.5.3.1   Drained modulus of elasticity

1) *Isotropically consolidated drained tests:*
The stress-strain curves in drained tests at the three sites are already discussed in Section 0. The initial tangent modulus E_i and the failure factor R_f from the CID tests have been approximated using the hyperbola relationship in Equation 6.13 for all range of confining pressure, while E_{50} and E_{ur} were read directly from the stress - strain curves by drawing a tangent through the corre-

sponding points (*Figure 6.25*a). It may be noted that the transformed test data from damcd15 (site1) in Figure 6.26a fairly approximates a linear relationship, indicating that the stress - strain curve for this test is fairly hyperbolic in shape, in spite of the small divergent from the linear relationships at very low strains. On the other hand, the data from Maxcd15/16 (site2) and Fhkcid36 (site3) in Figure 6.26b and c respectively diverge from a linear relationship, indicating that the stress - strain curve for this test is not exactly hyperbolic in shape. The transformed data seem to follow a non - linear wave like curve in (Figure 6.26b) and a non-linear hyperbolic curve in (Figure 6.26c), particularly at lower confining pressure, instead of a straight line as it would be expected. However, the transformed data are approximated by the best fit lines. The deviation of the transformed data from the straight line at a very low strains are reported in the literature. More transformed stress strain curves are given in Appendix A.7 to A.9. In almost all the tests, it may be observed that the data in the transformed-stress-strain curves is non-linear at low strains (sometimes up to 5% axial strain). If the test data are approximated by a best fit line or by a line passing through the points where 70% and 95% of the strength are mobilised according to *Duncan/Chang (1970)*, it will underestimate the initial stiffness of the soil particularly at lower strains. *Amann et al. (1975)* suggested a two line piecewise approach, where one line approximate the test data at low strain and the other line the rest of the data. With this approach, they attained a better hyperbolic approximation of the stress - strain curves of the test data on sands. This suggestion have, however, its practical limitations due to the fact that it is difficult to apply it in the already available computers codes.

Another observation from the transformed stress - strain curves include the divergence of the data from a linear relation is more prominent in specimens with low confining pressure, for instance $\sigma_3' = 50\,kN/m^2$.
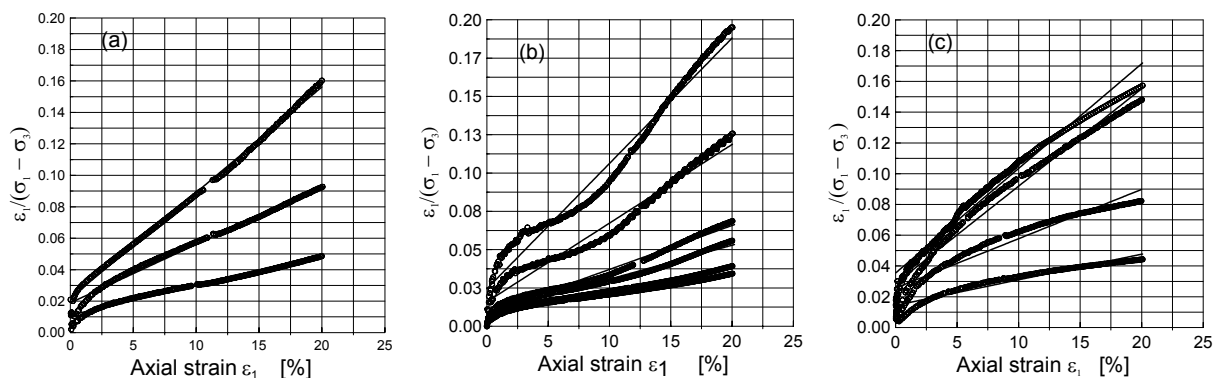

Figure 6.26: A typical transformed hyperbolic stress - strain curves for the three sites, a) site1 (Damicd15), b) site2 (Maxcid15/16), and c) site3 (Fhkcid36)
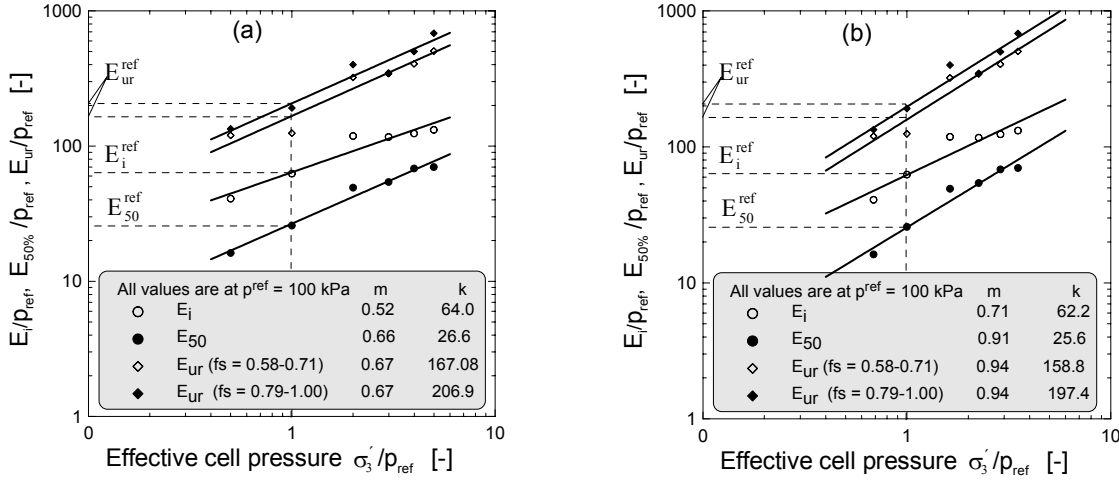
Figure 6.27:   The variation of the modulus of elasticity with confining pressure under CID at site2, a) Equation 3.55, and b) Equation 6.9

The values of E_i^{ref}, E_{50}^{ref}, E_{ur}^{ref} and the corresponding m values are determined at a reference pressure p^{ref} =100 kPa using Equation 3.55. For a typical stress - strain curve at site1 (Figure 6.12), the reference modulus determined from Equation 3.55 are compared with those values determined using Equation 6.15 (Figure 6.27) (Equation 6.15 in PLAXIS v7 was without the *sin φ* component, hence this comparison is made based on the old equation in v7). It may be seen from Figure 6.27 that the introduction of cohesion component into Equation 3.55 has very negligible influence on the values of E^{ref}, where as it has a remarkable effect on the values of m. The values of m obtained using Equation 6.15 are 1.37 - 1.4 higher than those obtained using Equation 3.55.

All values of E_i, E_{50}, E_{ur} and R_f, for all *CID* tests at each confining pressure, and the corresponding values of *m* and *k* for each test are listed in Appendix A.11. All values at a reference pressure p^{ref} = 100 kPa are also summarised in Table 6.9. From Table 6.9, it would appear that $m_{tangent}$ < m_{secant} < $m_{un/reloading}$ with an average value of 0.53, 0.57, and 0.78 respectively. The ratio E_i^{ref}/E_{50}^{ref} varies between 1.9 to 2.2 with an average value of 2.1, the ratio E_{ur}^{ref}/E_i^{ref} varies between 2.9 to 6.53 with an average value of 4.2, the ratio $E_{ur}^{ref}/E_{50}^{ref}$ varies between 5.9 to 12.7 with an average value of 8.6, and R_f varies between 0.73 to 0.88 with a mean value of 0.82. Due to the limited number of tests performed on horizontal oriented samples (only two), it is not correct to draw a general trend, however, they appear to be 1.1 to 2.2 stiffer than the vertical oriented samples, which opposes to what usually would expected. A plot of all the data from all CID tests shown in Figure 6.28 seems to verify the arithmetic mean values obtained from Table 6.9. In spite of the scattering of the data, it would appear from Figure 6.28 that E_{ur}^{ref} remains unaffected from the relative stress level at which the unloading started. The relative stress level denoted as f_s, is defined as the ratio between the stress at which the unloading starts and the stress at failure.

Table 6.9: Deformation parameters from *CID* tests at a reference pressure p^{ref} = 100 kPa

Test	P^{ref}	Tangent modulus		Secant modulus		Un/re-loading modulus		R_f
		m	E_i^{ref}	m	E_{50}^{ref}	m	E_{ur}^{ref}	
	[kN/m²]	[-]	[kN/m²]	[-]	[kN/m²]	[-]	[kN/m²]	[-]
site1								
damcid05	100	0.30	5300	0.39	2700			0.81
damcid07	100	0.31	8430	0.51	3830			0.88
damcid15	100	0.42	5990	0.45	3230	0.74	19170	0.80
Average	100	0.34	6573	0.45	3253	0.74	19170	0.83
site2								
maxcid01	100	0.72	5600	0.66	2550			0.82
maxcid05	100	0.70	4400	0.71	2360	0.61	11860	0.80
maxcid16/15	100	0.52	6400	0.66	2660	0.67	16710	0.83
maxcid	100	0.79	3600	0.84	1910			0.73
maxcid13 *	100	0.60	11480	0.65	5040	0.94	30000	0.86
Average	100	0.67	6296	0.70	2904	0.74	19523	0.81
site3								
fhkcid34	100	0.56	4870	0.51	2430	0.89	22400	0.84
fhkcid36	100	0.42	4680	0.38	2480	0.79	36500	0.82
fhkcid389 *	100	0.54	5400	0.54	2780	0.85	38470	0.79
Average	100	0.51	4983	0.48	2563	0.84	32457	0.82

* = horizontal samples
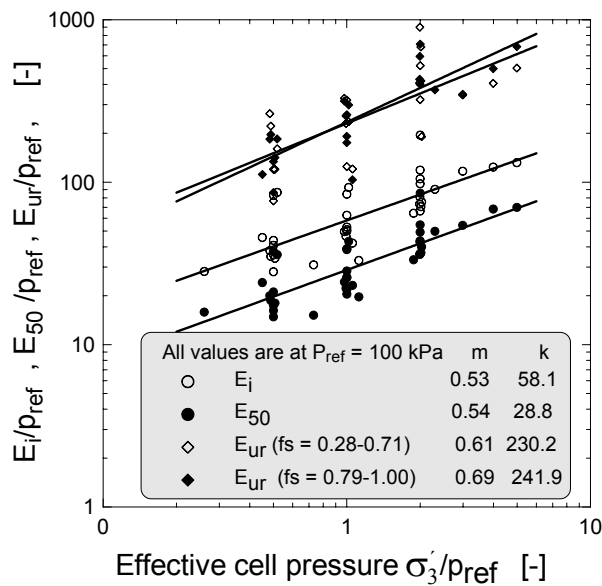
Figure 6.28:

The variation of the modulus of elasticity with confining pressure under *CID* test at all sites

2) *Anisotropically consolidated drained test:*

The stress - strain curves for the anisotropically consolidated drained tests at site2 (Maxcad12) are given in Figure 6.16a, and they appear to be initially stiffer than those from *CID* tests. The transformed stress - strain relations and the variation of the modulus of elasticity are shown in Figure 6.29. Similar to what was observed in the *CID* tests on similar specimen, it may be noted that the data (Figure 6.29a) also diverge from a linear relationship, indicating again that the stress - strain curve for this particular test is not precisely hyperbolic in shape. However, the data are approximated by best fit lines. From Figure 6.29b, the reference modulus E_i^{ref} = 22840 kPa and E_{50}^{ref} =11110 kPa, and the corresponding m values of 0.55 and 0.61 respectively are determined.
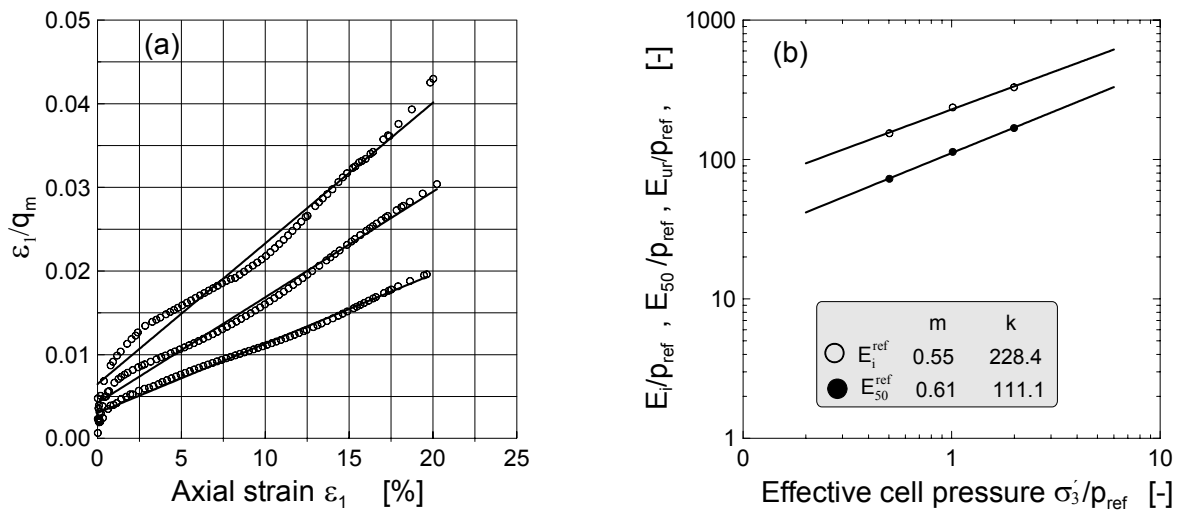
Figure 6.29: a) Transformed stress - strain relationship, and b) the variation of the modulus of elasticity with confining pressure under *CAD* tests at site2

6.5.3.2   Undrained modulus of elasticity

1) *Isotropically consolidated undrained test:*

Typical stress - strain curves at the three sites are already shown in Figure 6.7a, Figure 6.9a and Figure 6.9a, and others are also documented in Appendix A.5 and A.6. Similar to the drained tests, the undrained deformation parameters are determined from these strain stress diagrams, assuming that the curves may be represented by hyperbolic relationship. Typical transformed hyperbolic stress - strain curves corresponding to stress - strain relations in Figure 6.7a, Figure 6.8a and Figure 6.9a are given in Figure 6.30. The transformed stress - strain curves are fairly linear, except that the curves in Figure 6.30a and b show non - linear relationship at low axial

strains (< 2.5%). In other words, the stress - strain relationship of these curves are fairly hyperbolic. The undrained deformation parameters E_{ui}, $E_{50(u)}$, the stress exponent *m*, the undrained modulus number *k*, and the failure ratio R_f for each test at each confining pressure are given in tabular form in Appendix A.12. A plot of the variation of the modulus of elasticity with the confining pressure from all *CIU* tests is also shown in Figure 6.31.
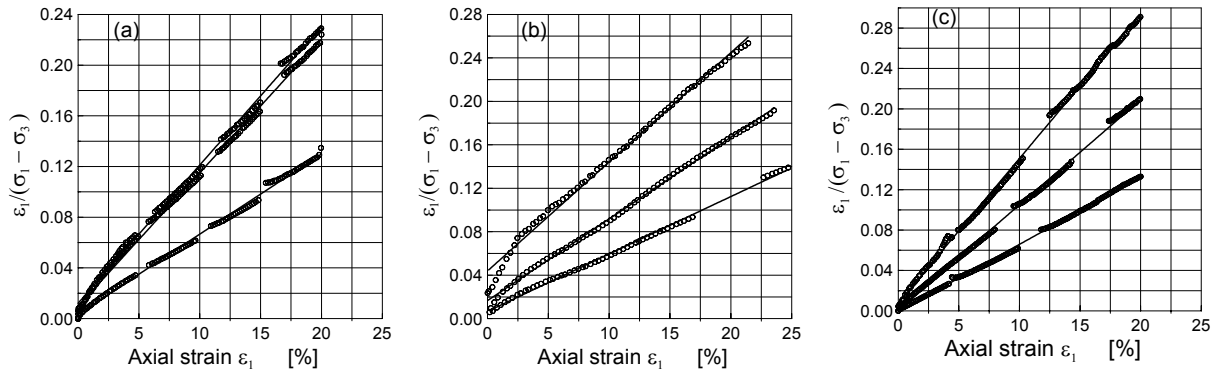

Figure 6.30: A typical transformed hyperbolic stress - strain curves under undrained condition for the three sites, a) site1 (Damciu14), b) site2 (Maxciu2), and c) site3 (Fhkciu35)

As far as the strength of normally consolidated soils is concerned, we have seen in Section 6.4 that the strength parameters obtained by applying both failure criterion are almost the same. However, this is not the case when it comes to deformation parameters. From the table in Appendix A.12 and Figure 6.31, it would appear that the choice of the failure criteria has a considerable influence on the value of the secant modulus $E_{50(u)}$ and the corresponding *k, m* and R_f values. In general, $E_{50(u)}$and k obtained by applying the $(\sigma_1' / \sigma_3')_{max}$ failure criteria are 1 to 2 and 1 to 1.5 times higher than those obtained by using the $(\sigma_1 - \sigma_3)_{20\%}$ failure criteria respectively. Therefore, in order to get a consistent deformation parameters, one has to decide which of the limiting state to use. Though it not easy to answer the question, which of the limiting state governs the failure mechanism of normally consolidated soils, the Author suggests to use the maximum (or 20%) deviator stress failure criteria, because 1) there is hypothesis that the normally consolidated soils require larger deformation to reach their limiting state, and 2) the constitutive soil model (the Hardening Soil Model) selected for numerical analysis later in this study is based on the deviator stress failure mechanism.

The effective confining stress σ_3' in undrained triaxial test is not constant throughout the test due to the development of excess pore water pressure. The effective confining pressure σ_3' is assumed constant in the analysis of the stress dependency behaviour of the E-modul under undrained condition.
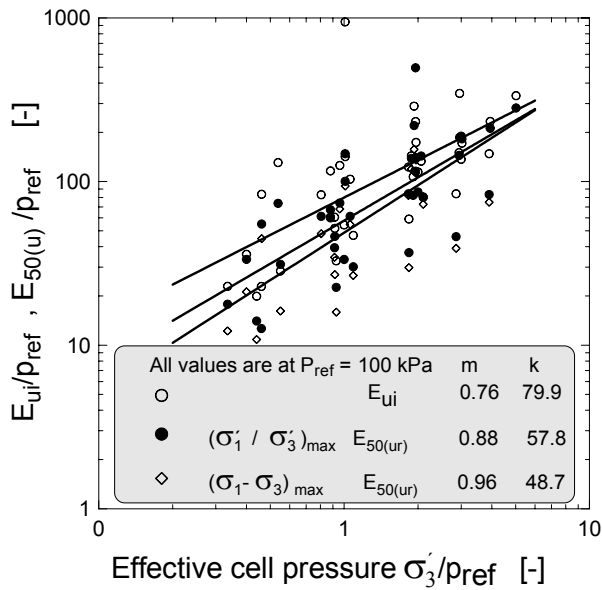
Figure 6.31:
The variation of the modulus of elasticity with the confining pressure from the *CIU* tests

Table 6.10: Deformation parameters from *CIU* triaxial tests at p^{ref} = 100 kPa.

Test	p^{ref}	m	E_{ui}^{ref}	m	$E_{50(u)}^{ref}$	R_f
	[kN/m²]	[-]	[kN/m²]	[-]	[kN/m²]	[kN/m²]
site1						
damciu04	100	0.83	4360	1.14	2850	0.88
damciu06	100	0.90	9550	1.12	6450	0.91
damciu10	100	1.06	5470	1.32	3360	0.90
damciu14	100	1.48	10600	1.43	5880	0.96
damciu30	100	1.50	2990	1.25	3780	0.94
Average		1.15	6594	1.25	4464	0.92
site2						
maxciu02	100	0.99	6710	1.11	4040	0.86
maxciu	100	0.88	3720	0.84	1907	0.83
maxciu03 *	100	0.71	13930	0.64	7230	0.96
Average		0.86	8120	0.86	4392	0.88
site3						
fhkciu35	100	1.73	51560	1.48	17050	0.99
Others						
Jaegerk.	100	0.86	6860	0.92	6890	0.70
Schwand	100	0.78	12930	0.62	9220	0.93
Stromey.	100	0.87	5610	0.98	3570	0.77
Average		0.84	8467	0.84	6560	0.80

* = horizontal sample

The deformation parameters corresponding to the maximum deviator stress failure criteria for a reference pressure p^{ref} = 100 kPa are given in Table 6.10. From this table, it can be seen that E_{ui}^{ref} varies between 2990 to 51560 kPa. The higher stiffness was recorded at site 3. The soil at this location is very soft and sensitive, contains organic substances such as grass roots and mussels, and has a water content above 70% and an initial void ratio of 2 (see Section 6.4.3). The values of m corresponding to E_{ui}^{ref} ranges from 0.72 to 1.73. The $E_{50(u)}^{ref}$ varies between 1907 to 17050 kPa, and the corresponding value of m varies between 0.64 to 1.48 with, and R_f varies between 0.70 to 0.96. The exponent m is believed to vary between 0 and 1 for a drained condition. To the knowledge of the Author, there are no comparable data available in the literature regarding the exponent m in undrained condition. Hence, until further studies, the value of the exponent greater than 1 should be set to one for practical applications. The ratios E_{ui}^{ref} / $E_{50(u)}^{ref}$ varies between 1.29 to 3.02 with an average value of 1.9. Only one *CIU* test on 3 horizontally oriented specimens was conducted, however, it appears that these specimens are stiffer than those similar vertically oriented specimens. From Table 6.9, it can be seen that E_{ui}^{ref} and $E_{50(u)}^{ref}$ from horizontally oriented specimens are 2.1 and 1.8 times higher than those similar vertically oriented specimens respectively.

2) *Anisotropically consolidated undrained tests:*

The stress - strain curves of the anisotropically consolidated undrained tests at site2 (Maxcau4) are already given in Figure 6.15a, and they appear to be initially stiffer than those from *CIU* tests. The transformed stress - strain relations and the variation of the modulus of elasticity are shown in Figure 6.32. Similar to what was observed in the *CIU* tests on similar specimens, the data (Figure 6.32a) are fairly linear except at low axial strain (< 2.5%), indicating again that the stress - strain curves for this particular test are fairly hyperbolic in shape. From Figure 6.29b, the reference modulus E_{ui}^{ref} = 8420 kPa and $E_{50(u)}^{ref}$ = 6530 kPa are determined.

3) *Controlled stress path - consolidated undrained tests:*

The stress - strain curves under controlled stress path anisotropically consolidated undrained tests on undisturbed specimens at site2 for the postulated stress paths B and C are already given in Figure 6.18. The transformed stress strain relationships and the variation of the modulus of elasticity for the postulated paths B and C are shown in Figure 6.33 and Figure 6.34 respectively. It can be seen from Figure 6.33a and Figure 6.34a that the transformed data may fairly be approximated by a straight lines, though non - linearity to some degree exists, in particular in those curves with confining pressure of 100 kPa. The values of the deformation parameters at a reference pressure of 100 kPa are given in Table 6.11. The result of three more stress path - *CIU* tests on reconstituted specimens for the postulated stress paths A, B and C are also given in Table 6.11. It appears from this table that no general conclusion can be made regarding the dependency of the stiffness of the soil sample on the direction of the total stress paths. For example, the stress path C appear to be stiffer than stress path B in the CAU test on undisturbed samples, whereas

the opposite can be observed from the CIU test on reconstituted samples. This shows a need for further investigation on a number of samples in order to have a general picture of the relationship between the stiffness of the soil and the stress paths.
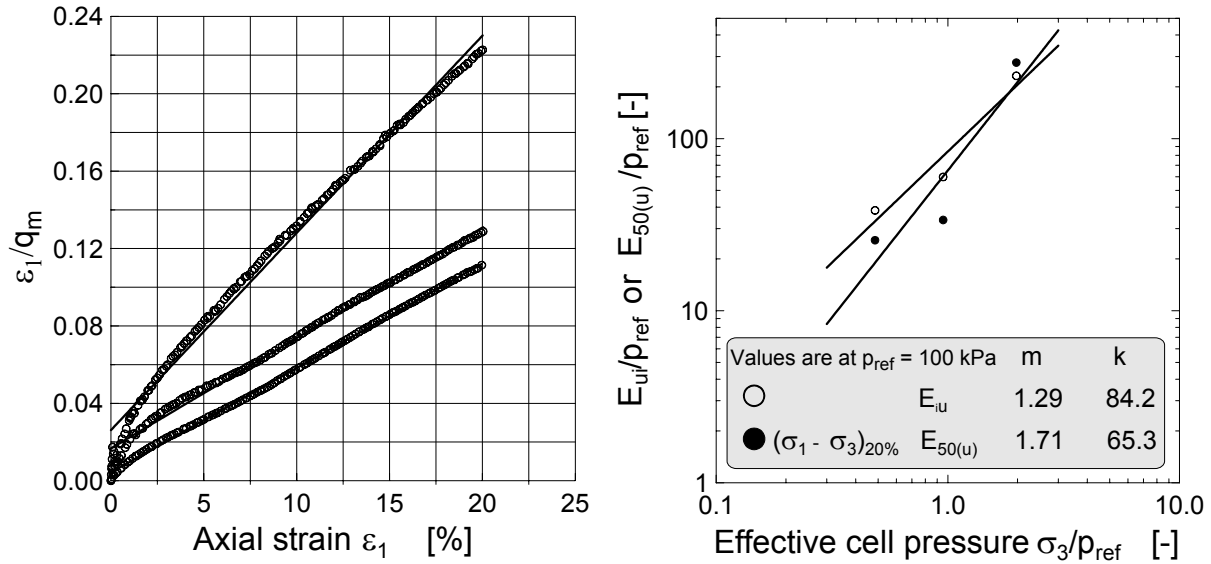

Figure 6.32: a) Transformed stress - strain relationship, and b) the variation of the modulus of
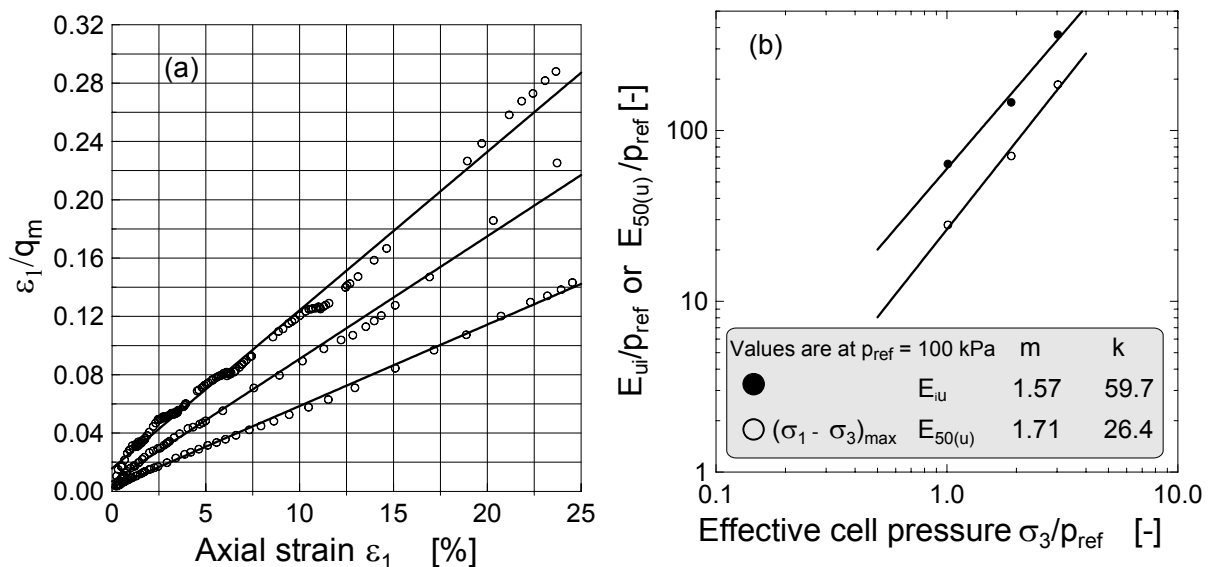elasticity with confining pressure under *CAU* tests at site2 (Maxcau4)

Figure 6.33: a) transformed stress strain relationships, b) variation of the modulus of elasticity
with confining pressure, under controlled stress path B - *CAU* test at site2
(MaxspcauB)
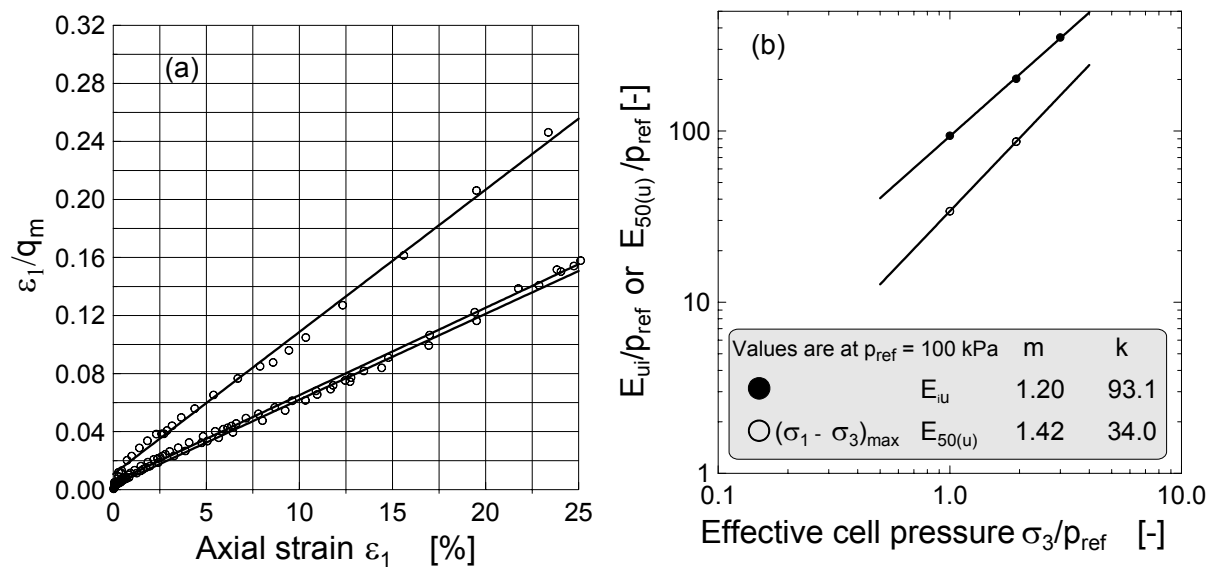
Figure 6.34: a) transformed stress strain relationships, and b) variation of the modulus of elasticity with confining pressure, under controlled stress path C - *CAU* test at site2 (MaxspcauC)

Table 6.11: Deformation parameters from controlled stress path at p^{ref} = 100 kPa.

Stress path	p^{ref}	Tangent modulus		Secant Modulus		
		E_{ui}^{ref}	m	$E_{50(u)}^{ref}$	m	R_f
	[kPa]	[kPa]	[-]	[kPa]	[-]	[-]
Controlled stress path - CAU tests on undisturbed samples						
B	100	5970	1.57	2640	1.71	1.00
C	100	9310	1.2	3400	1.4	1.00
Controlled stress path - *CIU* tests on reconstituted samples						
A	100	6340	0.75	4000	0.69	0.843
B	100	6094	0.64	3890	0.59	0.805
C	100	5560	0.58	3210	0.87	0.842

6.5.4   Comparison of deformation parameters

In the foregoing sections, the deformation parameters obtained from different type of tests have been presented and discussed. In this section, the different deformation parameters are compared to each other. The comparisons are between the deformation parameters from oedometer and

triaxial test, from the drained and undrained tests, from isotropic and anisotropic consolidation tests, from the standard and stress path tests, from different stress paths, from vertically and horizontally oriented specimens, from first loading and unloading (reloading), etc.

The average ratio of $E_i^{ref} / E_{oed}^{ref}$ is found to be 2.08, 1.63 and 2.82 at site1, site2 and site3 respectively. Comparing the reference constrained modulus with the reference secant modulus in drained test, the ratio $E_{50}^{ref} / E_{oed}^{ref}$ is found to be 1.03, 0.77 and 1.45 at site1, site2 and site3 respectively. The range of the ratio $E_{ur}^{ref} / E_{ur,oed}^{ref}$ is 2.33 to 2.52, 1.29 to 2.09 and 1.32 to 2.51 at the three sites respectively.

The relationships between drained and undrained modulus of elasticity is given by Equation 3.53. The ratio E_u/E approximately varies between 1.11 to 1.34 for range of Poisson's ratio between 0.12 to 0.35 (Equation 3.54). The average ratio E_{ui}^{ref} / E_i^{ref} is found to be 1.08, 1.29 and 10.3 at the three sites respectively. Taking into account the high value of the Poisson's ratio found in the drained test, the ratio of the undrained to drained modulus at site1 & 2 seems to fall in the range of Equation 3.53, where as site3 is exceptionally high and unacceptable. In general, the stress exponent m is found to be higher in undrained tests than in drained tests.

The modulus of elasticity from *CAD* tests is found to be 3.6 to 5.2 (on average 4.4) times higher than that from *CID* tests. The m values are lower in *CAD* test than those in *CID* tests. The undrained modulus of elasticity in *CAU* tests are 1.3 to 1.6 higher than the corresponding values from *CIU* tests. The m values are higher in *CAU* test than those in *CIU* tests.

The stiffness of the soil in the horizontal direction appears to be 1.8 to 2.0 and 1.1 times higher than the stiffness of the soil in vertical direction at site2 and site3 respectively. This seems to contradict with that given in Section 3.5.4, where it is stated that normally consolidated soils are stiffer in vertical direction than in horizontal direction and hence it requires further investigation.

No general conclusion can be made regarding the dependency of the stiffness of the soil sample on the direction of the total stress paths. For example, the stress path C appear to be stiffer than stress path B in the *CAU* test on undisturbed samples, whereas the opposite can be observed from the *CIU* test on reconstituted samples. The general understanding is that the soil behaves stiffer as the stress path direction changes from right to left. This shows a need for further investigation on a number of samples in order to have a general picture of the relationship between the stiffness of the soil and stress paths.

The undrained stiffness of the soil specimens under controlled stress path - *CIU* test appears to be higher than the stiffness of the specimen under standard undrained tests. This is not, however, because of the stress paths that the specimens were subjected to follow, but it is most probably because of the type of the application of the load. The postulated stress path A is the same as the

standard total stress path in drained/undrained triaxial compression test *($\Delta\sigma_3 = 0$, $\Delta\sigma_1 > 0$)*, however, it shows higher stiffness in stress controlled tests than in strain controlled tests.

An average failure ratio $R_f = 0.82$, 0.89, 0.90, is found from drained, undrained and controlled stress path tests respectively. The value of *m* is different for tangent modulus, secant modulus and un/reloading modulus. An average vales of 0.53, 0.57 and 0.78 respectively are found out from drained tests. Similarly, average *m* = 1.05 and 1.1 was found out from the undrained tests for tangent modulus and secant modulus respectively.

The range of the ratios between the different forms of the modulus of elasticity are given in Table 6.12.

Table 6.12:   The ratio between different forms of deformation parameters

site	Test condition	E_i^{ref} / E_{50}^{ref}	E_{ur}^{ref} / E_i^{ref}	$E_{ur}^{ref} / E_{50}^{ref}$	$E_{oed,ur}^{ref} / E_{oed}^{ref}$
site1	Drained	2.02	3.20	5.93	2.60
	Undrained	1.48			
site2	Drained	2.17	3.10	6.72	3.63
	Undrained	1.84			
site3	Drained	1.94	6.55	12.66	6.65
	Undrained	3.02			
Average	Drained	2.04	4.28	8.43	4.29
	Undrained	2.11			

6.6   Contact behaviour between wall material and soft soil

6.6.1   General

The contact behaviour between the retaining wall and the soil plays an important role in numerical simulations of retaining structures. Most standards recommend a wall friction value of zero for soft soils, which results in unrealistic deformations of the wall and the soil in numerical analysis. *Terzaghi* was the first to study the influence of wall friction on earth pressures in early 1930's. After him a number of studies had been conducted to study the frictional characteristics of interfaces between soils and structural elements (*see for example Potyondy (1961) and Clough/Duncun (1971)*).

Beside the wall friction, the stiffness of the interface is equally important to simulate the contact behaviour. Some FE-programs, for example PLAXIS, requires an input parameter R_{inter} (an interface factor, which is taken as the ratio of the wall friction to friction of the soil) for the inter-

face elements. The interface elements take the material property from nearby soil cluster after reducing the values of all parameters by a factor R_{inter}, even the shear modulus which is a key parameter as regard to the deformation of the soil should be reduced by factor $(R_{inter})^2$ (*see Freiseder (1998) and Brinkgreve/Vermeer (1998) or Brinkgreve (2000)*). This results in unrealistic deformations. Though the PLAXIS version 7 and 8 allows a separate material input of the interface elements, the exact values of the input parameters (wall friction and stiffness) for soft deposits is still open. The purpose of this study is therefore, to examine the contact behaviour between soft soil deposits and retaining structures qualitatively with the help of interface tests using large and small scale direct shear boxes.

6.6.2   Description of the interface test

To determine the friction and stiffness behaviour of the contact elements, a strain controlled large size (365 x 550 mm) direct shear boxes (*LSB*) was used. Rusted steel and rough concrete plates were used as construction material. The specimens were prepared from disturbed lacustrine soil at an average dry density of 14.72 kN/m³ and corresponding water content of 32%. The soil specimens had an average liquid limit of 56% and plasticity index of 31%. The soil was compacted in the lower part of the shear box, and the concrete or the steel plate was placed on the top of the soil in the upper box. The specimen was first consolidated at normal stress of 50, 75, 100, 150 200, and 300 kN/m² and then sheared at an average constant rate of strain of 0.025 mm/min. At the end of the test a drop in water content (on average $w = 27.9\%$) and an increase in the dry density (on average $\gamma_d = 16.01$ kN/m³) was observed. A total of 18 tests were conducted, among which 10 tests were on concrete soil contact and the rest on steel soil contact.

Moreover, 30 interface tests were conducted at 32% and 40% water content in a medium (100 x 100 mm) and small (63 x 63 mm) scale shear boxes (*SSB*) for the purpose of comparison. The normal stresses applied were 50, 75, 100, 150, 200 and 300 kN/m². The contact between the soil and concrete/steel was subjected to shear stress at a constant strain rate of 0.02 mm/min.

6.6.3   Wall friction

Typical results of the interface tests are shown in Figure 6.35. For comparison purpose a soil to soil shear tests were also performed in a medium size and small size direct shear box (*SSB*) with normal stresses of 25, 50, 75, 100, 150, 200 and 300 kPa at water content of 32% and 40%. Figure 6.35a shows the shear strength diagram of the soil. The results are summarised in Table 6.13.

As shown in Table 6.13, the angle of wall friction δ obtained from small shear box (*SSB*) is in general higher than that determined from large scale shear box (*LSB*) for the same water content. The minimum ratio of δ/φ for soil - concrete plate contact is found to be 0.462 and for that soil - steel contact δ/φ = 0.458. The adhesion c_a seems, however, larger than the cohesion c for both construction materials. This is theoretically unacceptable because the adhesion should not be larger than the minimum of the cohesion of the elements in contact. On the other hand, one may assume a ratio of 1 taking into account the sensibility of the determination of the adhesion or cohesion in shear tests. The influence of the water content on the wall friction is evident from the *SSB* interface tests.
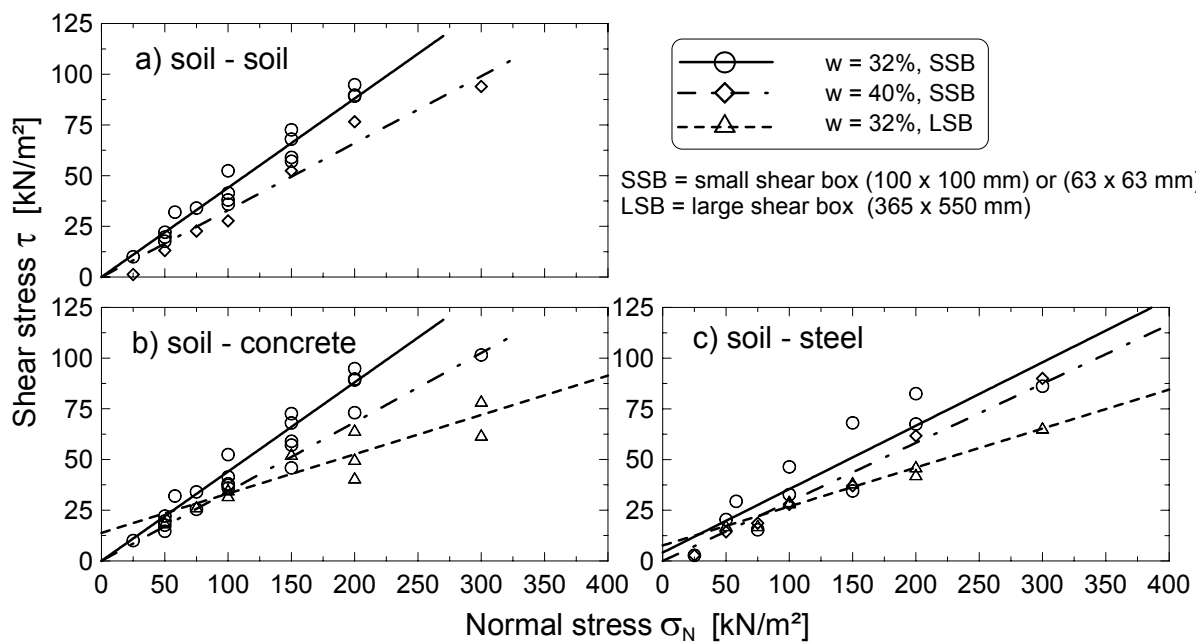
Figure 6.35: Wall friction : a) Soil to soil, b) soil to concrete contact, and c) soil o steel contact

Table 6.13: Relative values of friction and adhesion of the contact surfaces.

		Soil - Soil		Soil - Concrete			Soil - Steel		
		SSB	*SSB*	*SSB*	*SSB*	*LSB*	*SSB*	*SSB*	*LSB*
		w = 32%	*w = 40%*	*w = 32%*	*w = 40%*	*w = 32%*	*w = 32%*	*w = 40%*	*w = 32%*
c or c_a	*[kPa]*	0	0	3.1	0	13.8	4.2	0	7.7
φ or δ	*[°]*	23.8	18.3	20.2	18.9	11	17.4	16.2	10.9
c_a/c	*[-]*	0	0		0				
δ/φ	*[-]*	1.000	0.769	0.849	0.794	0.462	0.731	0.681	0.458
$\tan \delta/\tan \varphi$	*[-]*	1.000	0.750	0.834	0.776	0.441	0.710	0.659	0.437

6.6.4   Stiffness property of the interface

Figure 6.36 show the non-linear stress - displacement relations of the soil and the interfaces. From Figure 6.36, one may observe that the interfaces seem to react initially stiffer than the soil.
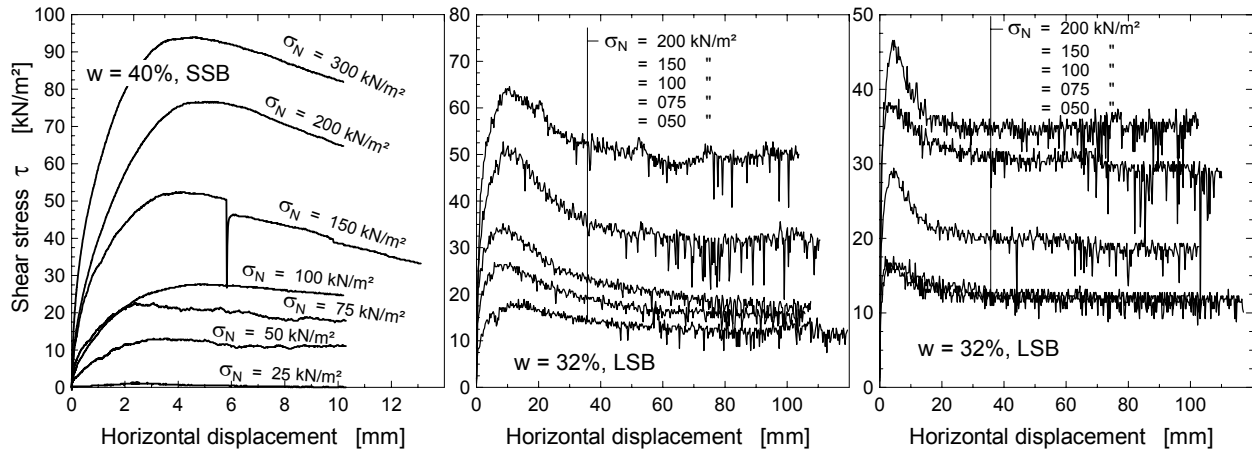

Figure 6.36: Shear stress - displacement behaviour of the soil and interface: a) soil to soil, b) soil to concrete, and c) soil to steel

The stress - displacement behaviour of the interface up to the point of assumed failure shear stress may be conveniently represented by means of equations similar to those developed by *Duncan/Chang (1970)* to model the stress - strain behaviour of soils (see Section 6.5.3). The transformed curves are shown in Figure 6.37. It should be noted that in the transformed data, only those data points up to the assumed failure shear stress were considered. From Figure 6.37, one can easily read the initial shear stiffness, here denoted as G_{si}. The variation of the initial shear stiffness with the normal stress may be expressed analogue to the *Ohde (1939)* equation as,

$$G_{si} = G_{si}^{ref} \cdot \left(\frac{\sigma_N}{p^{ref}} \right)^m \qquad\qquad (6.16)$$

where G_{si}^{ref} is the reference initial shear stiffness at reference stress of p^{ref}, σ_N is the normal stress and m is the stiffness component. The double logarithmic plot of Equation 6.16 is shown in Figure 6.38. For the results shown in Figure 6.38, the initial shear stiffness has the value 96.8, 107.9 and 64.3 kN/m²/mm for soil-soil, soil-concrete and soil-steel contact respectively. This shows that the stiffness of the contact surface is not as low as usually being assumed. Hence, adopting the stiffness of the soil fully to the interface element might help in reducing the excessive and unrealistic deformations of the wall in an excavation in soft deposits.
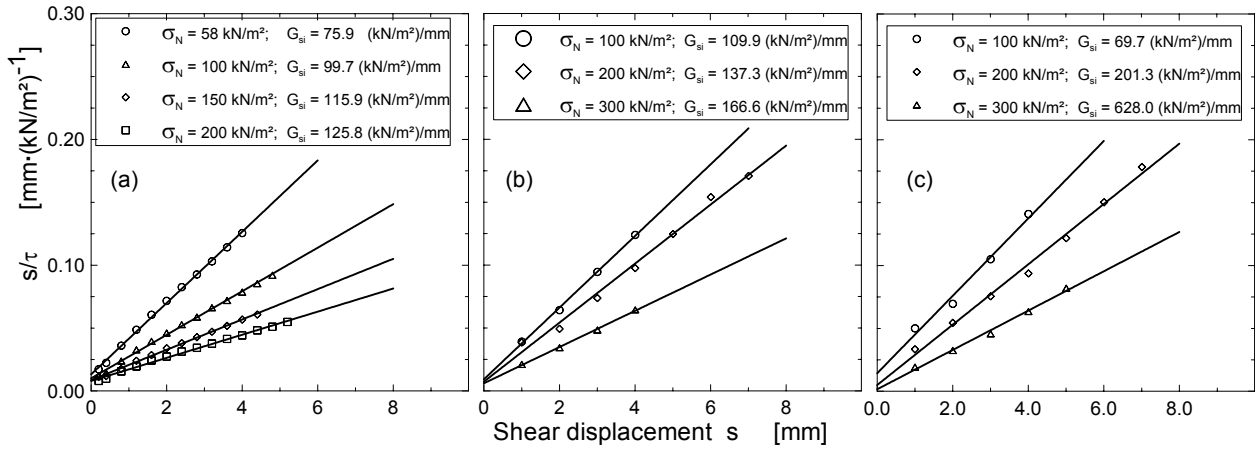
Figure 6.37: Transformed stress - displacement curves for a) soil to soil, b) concrete to soil, and c) steel to soil contacts
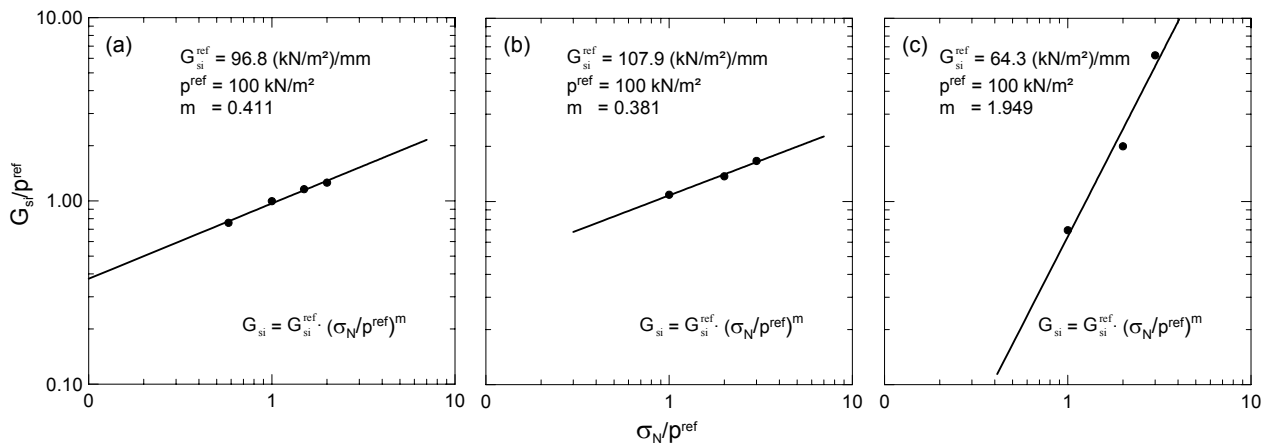
Figure 6.38: The initial reference shear stiffness: a) soil to soil, b) concrete to soil, and c) steel to soil contacts

6.7   Summary

In order to determine and analysis the strength and deformation parameters of the normally consolidated soft clays relevant to open excavations, a total of 87 specimens from three sites; 61 vertically oriented undisturbed specimens, 9 horizontally oriented undisturbed specimens, and 17 reconstituted samples, were investigated in triaxial test under different conditions and at a confining pressure ranging from 25 to 500 kPa. The test program includes standard isotropically con-

solidated drained/undrained tests, anisotropically consolidated drained/ undrained tests and controlled stress path tests. Moreover, a one-dimensional compression test on 15 undisturbed specimens and 6 reconstituted specimens, isotropic/anisotropic compression test on 4 undisturbed specimens were performed. The test results were evaluated and compared with each other. The results are shortly summarised below:

1. There exists a single and unique effective stress path above the isotropic line or the K_0 - *line* independent from the type of the test and type of the stress path and sample orientation. The value of the cohesion measured for vertically oriented samples both in drained and undrained standard test ranges between 2.6 - 22.2 kPa, which is much higher than the expected.

2. The failure criteria according to the maximum effective principal stress lead to a relatively a higher effective angle and a lower effective cohesion than the maximum deviatoric stress failure criteria, which shows that there exist a compensation between the effective angle and the cohesion. In other words the overall effective strength might remain unaffected.

3. As would expected, a higher stiffness is measured in undrained tests than in drained tests with an average factor of 1.08, 1.29 at site1 and site2 respectively and lies with in the range of values according to the theory of elasticity.

4. The average constrained modulus E_{oed} = 3108 kPa at reference pressure of 100 kPa and the corresponding average value of the stress exponent m = 0.81 are found out from one - dimensional compression tests at site 1 &2.

5. The average initial tangent modulus E_i = 6435 kPa and E_{ui} = 7727 kPa, and secant modulus at 50% of the failure stress E_{50} = 3079 and $E_{50(u)}$ = 5139 kPa, and un/reloading modulus E_{ur} = 19347 kPa at a reference pressure of 100 kPa are estimated from drained and undrained stress - strain curve respectively. Values from site1 are not included.

6. The following average ratios between the stiffness parameters are determined: E_i/E_{50} = *2.08*, E_{ur}/E_i = *3.2*, E_{ur}/E_{50} = *6.3*, $E_{oed,ur}/E_{oed}$ = *3.1*. All values are at reference pressure of 100 kN/m² and does not include the values from site1, where a higher values have been observed.

7. It was observed that the value of the exponent m is not constant for a particular soil specimen, rather it is dependent on the type of test (drained / undrained) and the form of the modulus (tangent modulus / secant modulus / un/reloading modulus). The values of m greater than unity in undrained tests should be ignored.

8. The average failure stress ratio R_f was 0.82 in drained tests and 0.90 in undrained tests.

9. Contrary to the expectation, horizontally oriented specimens are found to be stiffer than the vertically oriented specimens, however, further investigation is recommended.

10. The stiffness of the soil in *CAD* and *CAU* tests is higher than the corresponding *CID* and *CIU* tests with an average factor of 4.4 in drained and 1.5 in undrained condition.

11. The undisturbed soil specimen under the postulated stress path B seems stiffer than under stress path C in *CAU* test, whereas no remarkable differences among the stiffness of reconstituted specimens under the stress paths A, B and C in *CIU* test were observed. However, due to the limited number of stress path tests, no complete generalisation can be drawn.

12. Most of test data showe a divergence from a linear relationship in the transformed stress-strain curves at lower axial strains (up to 5%). Some test results show, particularly at low confining pressures a complete divergence from the linear relationship indicating that the stress - strain curves may not be exactly hyperbolic. These should be proofed and calibrated using the Hardening Soil Model (*HSM*) in the finite element program PLAXIS.

13. The wall friction is rather far from smooth as it would usually assumed. A value of $\delta = 0.460 \cdot \varphi$ and a stiffness value as high as the stiffness of the soil for both soil to concrete and soil to steel sheet contact are measured in large shear box. Taking into account the effect of the ground water in field, the new draft recommendation of *EAB (EB95, Weissenbach (2002))* that $\delta = \varphi/3$ seems reasonable.

The various soil parameters obtained in this chapter will be calibrated for finite element application in chapter 7 and will be applied in the numerical analysis of practical projects in chapter 8. The main objective is directed towards deriving soil parameters calibrated on practical cases and to recommend a realistic determination of soil parameter for numerical calculation of excavation in normally consolidated soft soils.

7 Parameter study

7.1 General

A parametric study is a study of the effect on the solution or behaviour of a problem of varying the value of one parameter while keeping all other parameters at a constant or reference value. By doing so, the sensibility of the performance of the problem, in this case excavation and laboratory tests, to each model parameter or geometry or others can be identified. The finite element method (FEM) provides the best condition for parametric studies. In this work, the two dimensional FE - program "PLAXIS" version 7.2 and 8.1 was used to perform the parametric studies. Triangular elements with 15 nodes (*see Brinkgreve/Vermeer (1998) and Brinkgreve (2002)*) were used in all the FEM- computations in this chapter. This element provides a fourth order interpolation for displacements and it involves twelve numerical integration stress points (Gauss points). Basically, the hardening soil model (HSM) was used to simulate the soil behaviour and the Mohr-Coulomb model (MCM) to simulate the interface element. An elastic behaviour was assumed for all structural elements.

The parameter study in this chapter is divided into three main sections. First, the triaxial and oedometer test results will be been calibrated and the sensibility of the tests to various parameters examined. Next follows the study of the sensibility of a fictitious excavation problem to model size and the various HSM parameters. The study of the effect of berm and bottom support, and the comparison of the undrained and drained analysis belong to this group. Finally, a study of the mobilisation of the passive resistance as a function of the stiffness of the soil and the wall displacement is presented.

7.2 Calibration of soil parameters

In this section the soil parameters obtained from triaxial tests and compression tests as presented in chapter 6 have been calibrated for the hardening soil model using the PLAXIS finite element program. The aim of the calibration is to see whether the finite element simulation of the tests shall give the same result as the test result, if not to find out the possible factors that lead to such variations, and to recommend adjusted soil parameters for further parameter study and practical applications.

7.2.1   Drained test behaviour

7.2.1.1 General

The isotropically consolidated drained triaxial tests and one-dimensional compression tests at site 1 were randomly chosen as a reference test for comparison with the FEM-computational results and for further sensitivity study of the soil parameters in this section. The other test results from the other two sites have also been compared with the FEM- results after collecting experiences from site1. The average reference soil parameters for the hardening soil model at site 1 are given in Table 7.1 below. These parameters are obtained from triaxial and one-dimensional compression tests in chapter 6 (see Table 6.5, 6.6 and 6.7).

Table 7.1:   Reference soil parameters from site 1 for hardening soil model

γ	φ'	ψ'	c'	E_{50}^{ref}	E_{oed}^{ref}	E_{ur}^{ref}	p^{ref}	m	R_f	K_0^{nc}	v_{ur}
[kN/m³]	[°]	[°]	[kN/m²]	[kN/m²]	[kN/m²]	[kN/m²]	[kN/m²]	[-]	[-]	[-]	[-]
19.5	25.3	0	13.2	3253	2948	19170	100	0.63	0.83	0.573	0.20

The triaxial test and the oedometer test were simulated by means of an axisymmetric geometry, with the real dimension of the test set-up, that represent half of the soil sample (0.025 x 0.05 m in case of the triaxial test and 0.035 x 0,02 m in case of oedometer test). In the triaxial model, the displacements normal to the boundaries are fixed and the tangential displacements are kept free to allow for smooth movements along the axis of symmetry (the left hand side) and the bottom boundaries. The top and the right side boundaries are fully free to move. The geometry, the mesh and the boundary condition of the triaxial model are shown in Appendix B.1a & B.2a. Similarly, the displacements normal to the boundaries are fixed and the tangential displacements are kept free to allow for smooth movements along the axis of symmetry (the left hand side) and the right hand side boundaries in the oedometer model. Both the normal and tangential displacements along the bottom boundary are fixed, whereas the top boundary is fully free to move.

The triaxial test procedure was modelled by means of applying first an all round confining pressure $\sigma_3' = \sigma_1' = 50, 100,\ and\ 200\ kN/m²$ for three specimens respectively and then by increasing the vertical stress $\Delta\sigma$ up to failure. The choice of the three confining pressure allows the study the influence of the different soil parameters at the reference pressure $p^{ref} = 100\ kN/m²$ and at stress level below and above the reference pressure possible. Similar to the test condition, the following load increments were used in the FEM - simulation of the oedometer test: 10.8, 20.1, 30, 69, 126, 252, 126, 69, 10.8, 69, 126, 252, 504, 756, 504, 126, 12.6 kN/m².

In order to study the effect of the different hardening soil model parameters on the stress-strain, the strength and the volume-change behaviour of the soil specimens, several variations of the soil parameters have been considered during the FEM-computations. These variations are listed in Table 7.2.

Table 7.2: Variations of the soil parameters for the FEM - computations under drained condition

Cases	Parameter
FEM-1	reference parameters (Table 7.1)
FEM-2	same as FEM-1, but E_{50}^{ref} increased by a factor of 1.25
FEM-4	same as FEM-1, but E_{50}^{ref} increased by a factor of 2.0
FEM-6	same as FEM-1, but $m = 0.83$ (m from oedometer test result, see Table 6.6)
FEM-8	same as FEM-1, but $E_{oed}^{ref} = E_{50}^{ref} = 3253 \, kN/m^2$
FEM-9	same as FEM-1, but E_{oed}^{ref} reduced by a factor of 0.75
FEM-10	same as FEM-1, but E_{oed}^{ref} increased by a factor of 1.25
FEM-11	same as FEM-1, but $E_{ur}^{ref} = 3 \cdot E_{50}^{ref} = 9759 \, kN/m^2$
FEM-12	same as FEM-1, but K_0^{nc} increased to 0.71
FEM-13	same as FEM-1, but K_0^{nc} reduced to 0.48
FEM-14	same as FEM-1, but $\nu_{ur} = 0.10$
FEM-15	same as FEM-1, but $\nu_{ur} = 0.30$
FEM-16	same as FEM-1, but $R_f = 0.97$
FEM-17	same as FEM-1, but $R_f = 0.67$
FEM-18	MCM with $E_{oed} = 2948 \, kN/m^2$ for a confining pressure of $\sigma_3' = 100 \, kN/m^2$ and $\nu = 0.35$
FEM-19	MCM with $E_{50} = 3253 \, kN/m^2$ for a confining pressure of $\sigma_3' = 100 \, kN/m^2$ and $\nu = 0.35$
FEM-23	same as FEM-1, but E_{50}^{ref} increased by a factor of 1.1, E_{oed}^{ref} reduced by a factor of 0.90, $m = 0.73$, $K_0^{nc} = 0.59$, and $\nu_{ur} = 0.05$

7.2.1.2 Stress - strain behaviour of a soil specimen in triaxial and one-dimensional compression test

The stress strain relationship of the soil specimen from the FEM computation and test results are presented in Figure 7.1. The test results are indicated with dashed lines and the shaded regions show the range of the variation of the test results. Note that Figure 7.1a shares the same legend as Figure 7.1b. Since the hardening soil model requires soil parameters both from the triaxial test

and one-dimensional compression test, the comparison of the FEM- results are presented parallel, for example, Figure 7.1a for the triaxial loading system and Figure 7.1b for oedometer loading condition.

It would appear from Figure 7.1a that the FEM-results of the triaxial model (FEM-1) underestimate the stiffness of the soil specimen at an axial strain less than 5 - 6 % for all cases of confining pressures. This might be happen due to the fact that the hardening soil model use the secant modulus E_{50} instead of the initial tangent modulus E_i ($E_i \approx 2 \cdot E_{50}$, see Section 6.5.4). The FEM-simulation of the triaxial test, however, lies reasonably within the range of variations of the test results for an axial strain greater than 5 - 6%.

On the contrary to the triaxial simulation, the FEM-simulation of the oedometer (FEM-1) overestimates the stiffness of the specimen up to a vertical strain of 7% , and thereafter it joins the region of the range of the test results (Figure 7.1b).

The FEM simulates very well the un/reloading stiffness of the specimen in the triaxial loading condition, whereas it overestimates it in the oedometer loading condition. Lowering the un/reloading modulus to $E_{ur}^{ref} = 3 \cdot E_{50}^{ref}$ (FEM-11), which is given in PLAXIS as a default value, would result in underestimation of the un/reloading stiffness of the triaxial test, whereas it still overestimates it in the oedometer test for the 1st un/reloading at about a vertical pressure of 200 kN/m², but much closer to the test result than the reference case (FEM-1). For the 2nd un/reloading case at higher stress level in the oedometer test, the FEM simulation underestimates the un/reloading stiffness. If one wants to keep the triaxial un/reloading stiffness unchanged, since it match very well to the test results, and on the other hand to adjust it to the test results in the oedometer simulation, the only possibility available is to vary the value of the Poisson's ratio for un/reloading v_{ur}. This parameter is the only parameter that influence the un/reloading behaviour of the one-dimensional compression without affecting much the un/reloading behaviour in the deviatoric state of stress.

Apart from its influence on the un/reloading behaviour of both test conditions, the E_{ur}^{ref} has no significant influence on the stress-strain behaviour of the specimen during the 1st loading.

The assumption $E_{oed}^{ref} = E_{50}^{ref}$ (FEM-8), which is recommended in PLAXIS as a default value, has no significant influence on the deviatoric stress-strain behaviour, whereas it reacts stiffer in one-dimensional compression (Figure 7.1). This approves that the E_{oed}^{ref} is largely a compression hardening parameter (cap parameter). In both loading systems, the assumption $E_{oed}^{ref} = E_{50}^{ref}$ has no effect on the un/reloading stress -strain behaviour. Of course, the difference between the two is about 10% which is small to make a difference on the result.
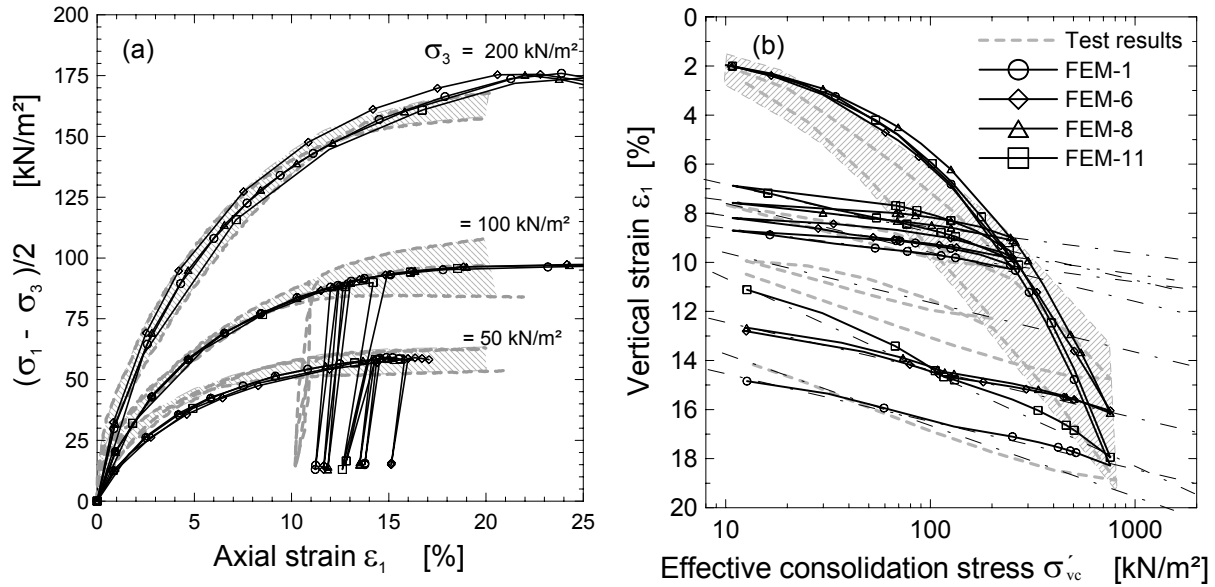
Figure 7.1: Calibration of the HSM parameters based on drained triaxial and oedometer test results at site 1

Taking the value of the exponent $m=0.83$ (FEM-6) from oedometer test result (see Table 6.6) instead of $m=0.63$ from triaxial test increases the stiffness of the soil specimen for a stress level above the reference pressure and decreases the stiffness for a stress level below the reference pressure in both loading conditions (Figure 7.1) as it would expected. The optimal solution seems to lay between these two values.

It would appear from Figure 7.1 that the deviatoric stress at failure remains unaffected by the variations of the parameters m, E_{oed}^{ref} and E_{ur}^{ref}, although the strain at which the failure occur might be different. This is because the failure stress is mainly controlled by the shear parameters c´ and φ´ in drained analysis.

Stress - strain at a lower axial strain:

Figure 7.2a shows a zoomed out stress - strain diagram at lower axial strain ($< 4\%$) for specimen with a confining pressure of 100 kN/m². From the figure, it can be seen that the FEM-computational result (FEM-1) remains below the test result for the reference case. This is probably due to the use of the secant modulus of elasticity E_{50} instead of the initial tangent modulus E_i. Doubling the stiffness of the soil (FEM-4) may narrow the gab between the measured and computed lines at a lower strain, but it exaggerates the stiffness thereafter (Figure 7.2b). Such problem may be overcome by introducing two hyperbola with two different stiffness lines (*Amann et al. (1975)*), and loading the specimen piecewise in two steps each with different material sets (see also Section 6.5.3.1). The first loading step may run up to a known limit stress with

a higher stiffness. Then the second loading step may follows till failure with the corresponding relatively smaller stiffness. The stress level dependent limit stress (the transition stress) can be estimated from the test results using the power law. This kind of load and stiffness arrangement is not implemented in the HSM and it may violate the hyperbolic assumption of the model.
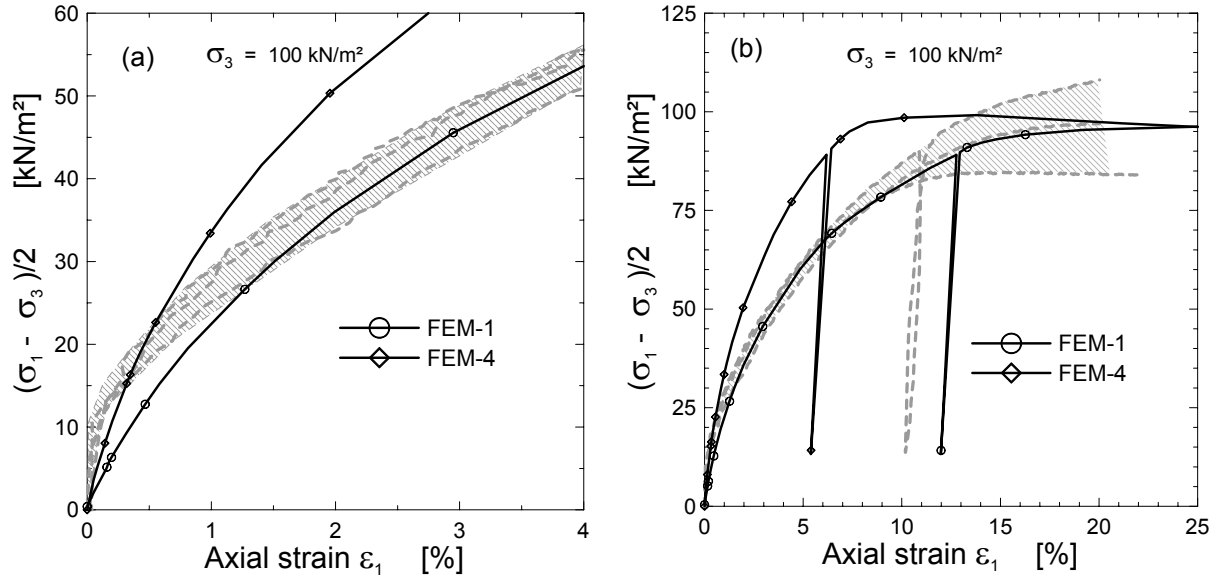

Figure 7.2:   The deviation of the FEM - computational results from the test results at lower axial strain, a) at a lower strain, and b) till failure

Influence of the stiffness parameters E_{50}^{ref}, E_{oed}^{ref} ***and*** E_{ur}^{ref} ***on stress - strain behaviour:***

In order to study the influence of the different hard soil model parameters on the stress - strain behaviour of the soil specimen, various FEM - computations were conducted according to the cases listed in Table 7.2. The first group of variations were the stiffness parameters E_{50}^{ref}, E_{oed}^{ref} and E_{ur}^{ref}. Increasing the value of the E_{50}^{ref} by 25% (FEM-2) shifts the reference curve upwards and partly lies above the range of the measured values, but it joins the reference curve as failure approaches (Figure 7.3a). The E_{50}^{ref} has no effect at all on the one-dimensional compression as shown in Figure 7.3b. On the other hand, changing the value of E_{oed}^{ref} by ±25% (FEM-9 & 10) has no significant influence on the deviatoric stress, whereas it affects the stress -strain charac-teristics of the one-dimensional compression accordingly. This is a clear proof of the fact that the parameter E_{50}^{ref} is purely shear hardening parameter (shear yield surface), whereas the parameter E_{oed}^{ref} is purely a compression hardening parameter (cap yield surface).

Although lowering the value of the parameter E_{ur}^{ref} as much as 50% of the reference value (FEM-11) has no significant influence on the stress - strain curves of both loading systems during the

first loading, it affects both loading systems equally during un/reloading. Hence, E_{ur}^{ref} is a parameter common to both yield surfaces.

For a purpose of comparison, the respond of the Mohr-Coulomb model (MCM) to the triaxial test condition for two different cases are presented in Figure 7.3a. It would appear from the figure that taking the constrained stiffness modulus E_{oed}^{ref} as a reference value (FEM-18) underestimates the stiffness of the specimen considerably. Although the use of the E_{50}^{ref} as a reference parameters (FEM-19) partly underestimates and partly overestimates the stiffness of the soil specimen, however, it is more closer to the test result than the case of the FEM-18.
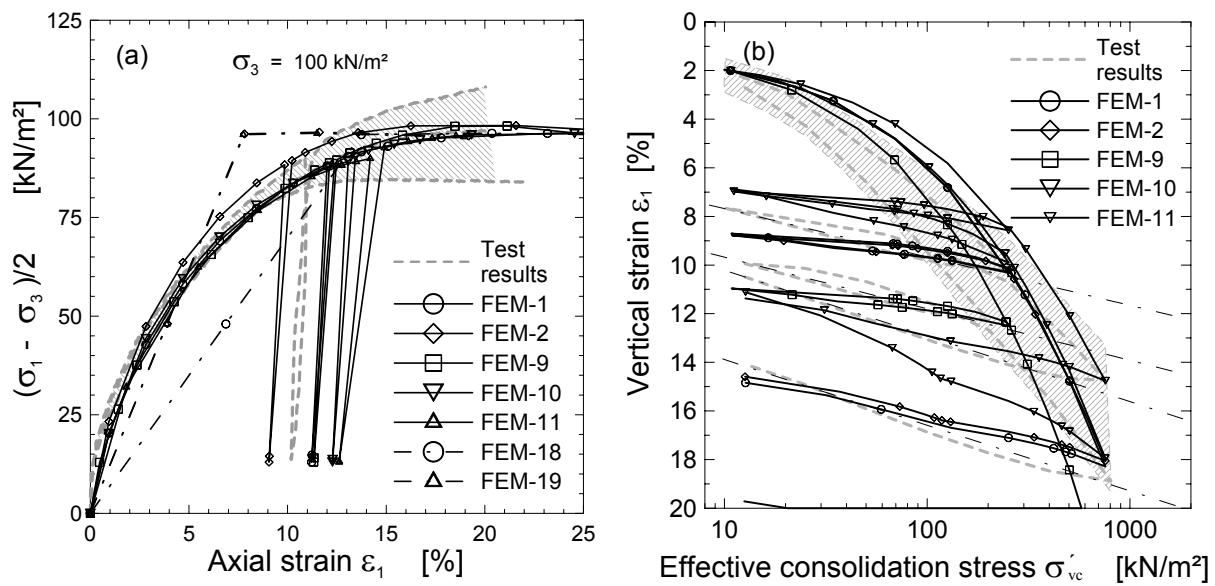

Figure 7.3: The influence of the parameters E_{50}^{ref}, E_{oed}^{ref} and E_{ur}^{ref} on the stress strain characteristics of a soil specimen in a) triaxial loading system at effective confining pressure of 100 kN/m², and b) oedometer loading system

Comparing the MCM with the HSM, one would expect relatively a higher deformation from the MCM up to a stress approximately equal to half of the stress at a failure and vice versa thereafter. Once the soil reaches the failure stress, the deformation in MCM depends mainly on how long the soil can be allowed to plastisfy. Since both soil models are based on the Mohr-Coulomb failure criteria, the deviatoric stress at failure remains the same independent of the variation of the stiffness parameters, except that the strain at which the failure may occur might be different.

Influence of the parameters v_{ur}, K_0^{nc} ***and*** R_f ***on stress - strain behaviour:***

In the second group of variation belong the parameters v_{ur}, K_0^{nc} and R_f. Varying the value of the v_{ur} to 0.1 (FEM-14) and to 0.3 (FEM-15) has no significant influence on the deviatoric pri-

mary loading and un/reloading state of stress (Figure 7.4a), whereas it has a considerable effect on the un/reloading stiffness of one dimensional compression (Figure 7.4b). While lowering the v_{ur} to 0.1 decreases the un/reloading stiffness and fairly approaches the test result, increasing the v_{ur} to 0.3 tends to increase the un/reloading stiffness and diverges further from the test results. The v_{ur} is the single parameter that affects the un/reloading stiffness of the one-dimensional compression without affecting the corresponding un/reloading stiffness of the deviatoric loading system. If a match of the computation and the test results during the un/reloading state is desired, this is the suitable parameter for a variation to deal with.

The HSM distinguishes between the model parameter K_0^{nc} and the K_0 to define the initial state of stresses. Since the initial stresses in the very small triaxial model will have no as such an influence, it was assumed that $K_0^{nc} = K_0$. Increasing the value of K_0^{nc} by 25% (FEM-13) results in a divergence of the stress - strain curve below the reference curve whereas decreasing its value by the same amount (FEM-12) leads to an increase of the stiffness of the soil above the reference value in both triaxial (Figure 7.4a) and oedometer(Figure 7.4b) loading systems. However, the effect of varying the K_0^{nc} seems to be stronger for the triaxial loading system than for the one-dimensional loading system. In both cases, the K_0^{nc} seems to have no significant influence on the un/reloding state of stress.
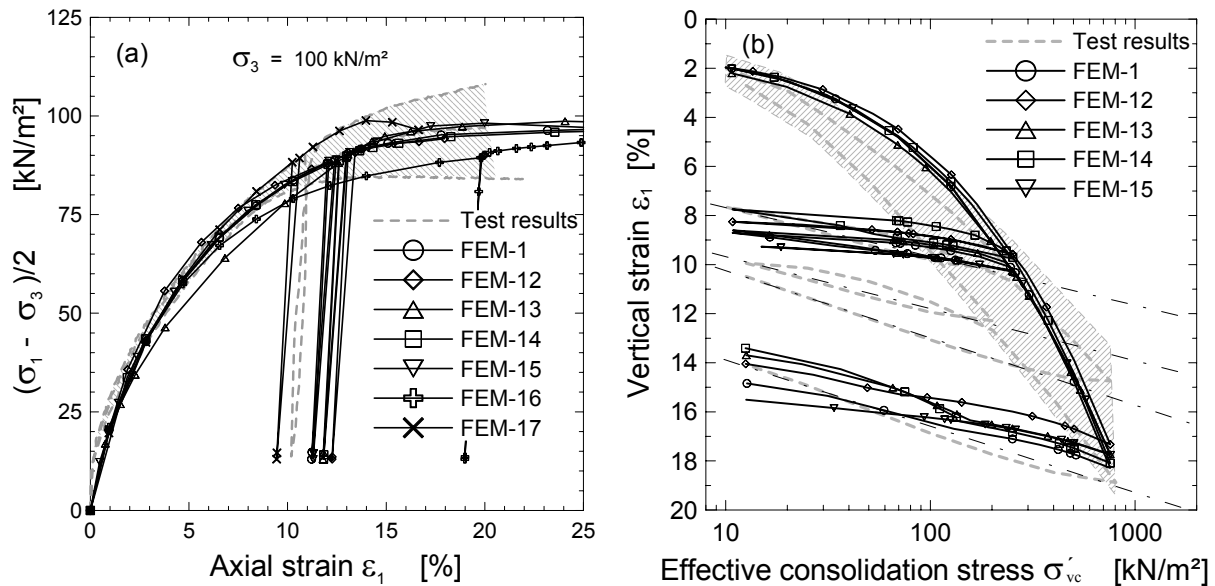
Figure 7.4: The influence of the parameters v_{ur}, K_0^{nc} and R_f on the stress strain characteristics of a soil specimen in a) triaxial loading system at effective confining pressure of 100 kN/m², and b) oedometer loading system

The lines of the FEM simulation of the variation of the influence of the failure factor R_f above (FEM- 16) and below (FEM- 17) the reference value in Figure 7.4a, rans together along the refer-

ence curve up to approximately an axial strain of 5% from which they start to diverge upwards (FEM-17) and downwards (FEM- 16). Their final effect is to retard the failure in the case of increasing R_f value and to accelerate it in the case of lowering the R_f value. The influence of increasing the R_f value above the reference value seems to be larger than the opposite one.

7.2.1.3 The volume change behaviour of a soil specimen in a triaxial test

The volume change behaviour of the specimen under drained triaxial test condition was also studied by means of varying the soil parameters for the hardening soil model. The results of the element study against the test results for a specimen with a confining pressure of 100 kN/m² are shown in Figure 7.5. It can be seen from the figure that the range of the test results is very wide and it is difficult to compare the computational result with the test result directly. However, one can see the general tendency of the volume change behaviour from the test results and the influence of each parameter from the sensitivity study. From Figure 7.5, it would appear that all the parameters in one way or the other way may affect the volume change behaviour of the specimen. The most sensitive parameters with regard to the volume change behaviour are the E_{oed}^{ref} (FEM-8, 9 & 10) and K_0^{nc} (FEM-12 & 13), and the least sensitive parameter is the v_{ur} (FEM-14 & 15). It is interesting to see that increasing the E_{50}^{ref} value above the reference value increases the volumetric strain, when one expects the opposite result.
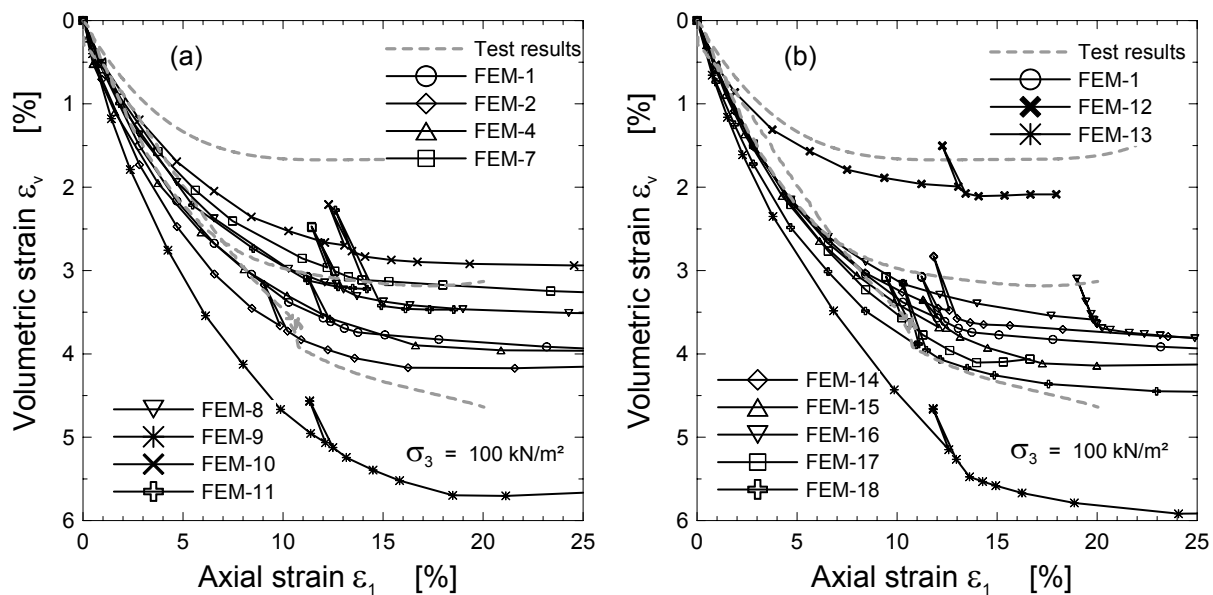

Figure 7.5: The influence of the hardening soil model parameters on the volume change behaviour of a soil specimen from site 1 at a confining pressure of 100 kN/m²:
　　　　　　a) stiffness parameters: E_{50}^{ref}, E_{oed}^{ref}, E_{ur}^{ref}, and m, and
　　　　　　b) other parameters: K_0^{nc}, R_f and v_{ur}

7.2.1.4 The effect of cohesion on the coefficient of the earth pressure at rest

Janbu (1977) indicated that the coefficient of the earth pressure at rest is not only dependent on the friction angle, but also on the attraction of a cohesive material. He formulated the relation as follow:

$$K_0 = \frac{\sigma'_{30} + c' \cdot \cot \varphi'}{\sigma'_{10} + c' \cdot \cot \varphi'} \tag{7.1}$$

To study the effect of the cohesion on the earth pressure coefficient at rest, a one-dimensional compression test was simulated and various FEM - computations were conducted by means of varying the cohesion c' and the effective angle φ'. A general tendency of increasing the value of K_0 with increasing cohesion was observed for all values of the friction angle as shown in Figure 7.6a. The ratio f_{K_0} between the computed K_0^{comp} and the default value $K_0^{nc} = 1 - \sin \varphi'$ may be given by:

$$f_{K_0} = \frac{K_0^{comp}}{K_0^{nc}} = a \cdot c'^{(b)} \tag{7.2}$$

where a and b are curve constants and they are a function of the angle of internal friction φ'. Figure 7.6b shows the relationship between the constants a, b and the angle of internal friction φ'. This relationships are given by a potential equation of the form:
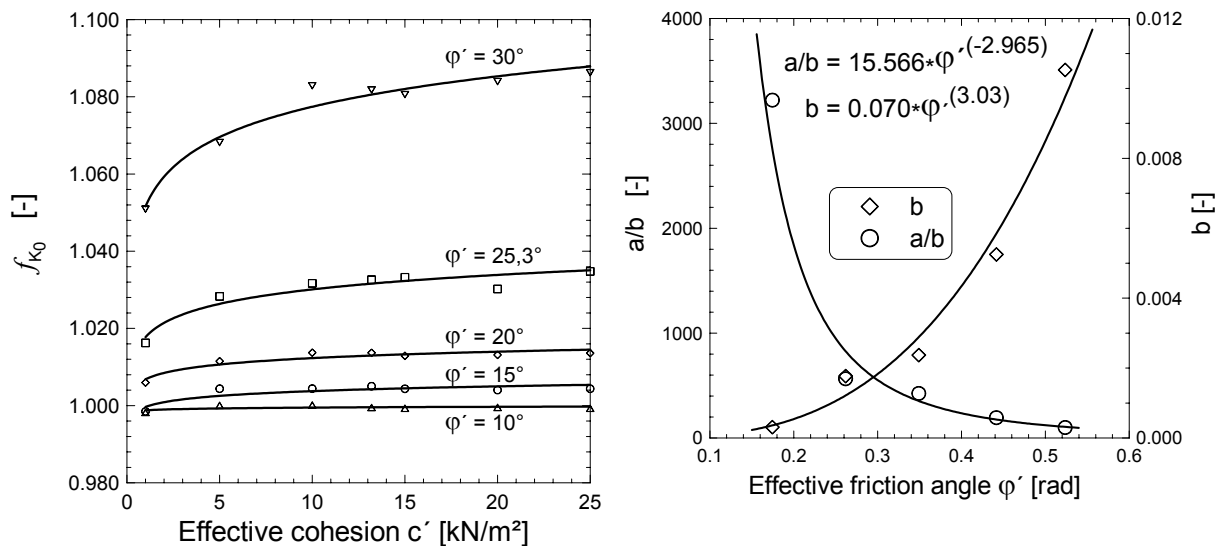

Figure 7.6:   a) The effect of cohesion on the coefficient of the earth pressure at rest as a function of the effective friction angle, b) Correlation of the curve constants a and b with the effective friction angle

$$b = 0.070 \cdot \varphi'^{(3.03)} \qquad\qquad\qquad\qquad\qquad\qquad (7.3)$$

$$\frac{a}{b} = 15.566 \cdot \varphi'^{(-2.965)} \qquad (7.4)$$

where φ' is in radians. It can be observed from Figure 7.6a that the factor f_{K_0} varies , for instance, from about 1.0 for $\varphi'=10°$ to about 1.09 for $\varphi'=30°$, say for an effective cohesion of 25 kN/m².

7.2.1.5 Effect of the angle of the overall shear strength φ_s on the FEM computation results

It is a common practice here in Germany to use the angle of the overall shear strength φ_s instead of the effective shear parameters c' and φ' provided that the equivalent preconsolidation pressure σ'_{eq} is known or can be reasonably estimated. The φ_s may be calculated from:

$$\varphi_s = \arctan(\tan\varphi' + \lambda_c) \qquad\qquad\qquad\qquad (7.5)$$

where $\lambda_c = c'/\sigma'_{eq}$. Taking $\sigma'_{eq} = \sigma'_3$ for the triaxial case and substituting the effective shear parameters for the reference case from Table 7.1 into Equation 7.5, the value of φ_s can be estimated. In general the use of φ_s value instead of the effective shear parameters c' and φ' leads to an overestimation of the stiffness and strength of the soil specimen as shown in Figure 7.7. Beside the case with the reference parameters (FEM-1), four cases are presented in Figure 7.7. The value of $\varphi_s = 31°$ in the first case was determined based on the assumption $\sigma'_{eq} = \sigma'_3 = 100\,kN/m^2 = p^{ref}$ and was assumed constant for all cases of confining pressures. The

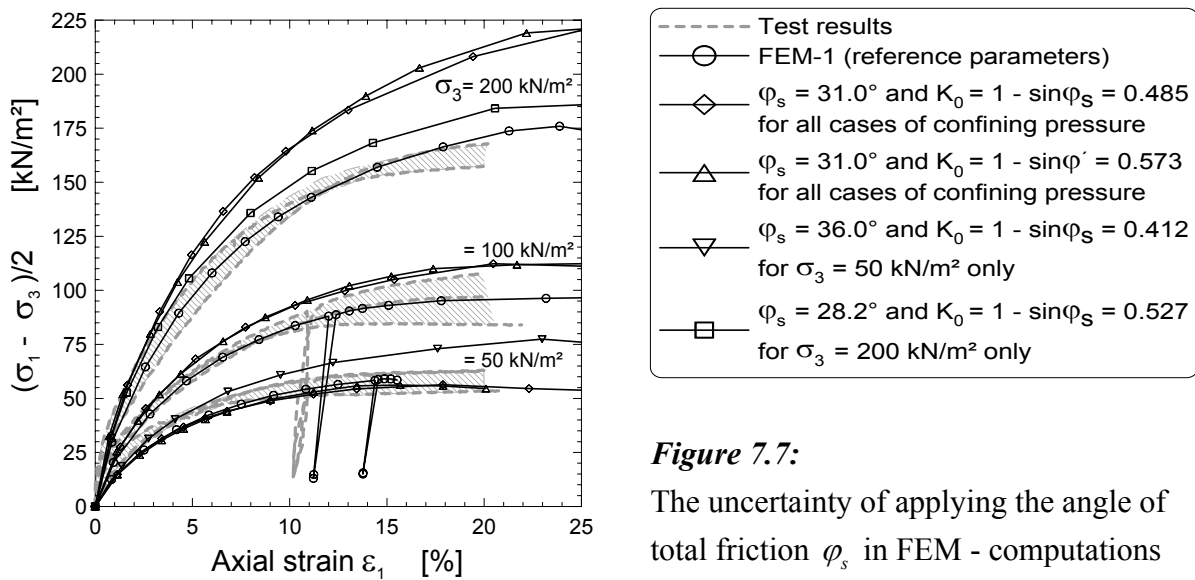*Figure 7.7:*

The uncertainty of applying the angle of total friction φ_s in FEM - computations

second case was same as above, but with $K_0^{nc} = 1 - \sin\varphi'$ instead of $K_0^{nc} = 1 - \sin\varphi_s$. This option shows no significant effect on the result. The values $\varphi_s = 36°$ and $\varphi_s = 28.2°$ were determined based on the assumption $\sigma'_{eq} = \sigma'_3 = 50$ and $200\,kN/m²$ respectively and they were used in the FEM - computation only for those specimen with a confining pressure of 50 and 200 kN/m² respectively.

Unlike the c' and φ' parameters, which are quasi stress independent for given layer of soil and specific range of stresses, the φ_s is solely dependent on the equivalent pressure. Therefore, assuming a constant value of φ_s for a given thick layers of soil may lead to a false result (Figure 7.7).

7.2.1.6   The influence of the membrane in a triaxial test on the strength of the soil specimen

The influence of the rubber membrane used in triaxial test on the strength and stiffness of soil samples has been discussed in section 6.4.1.3. A correction has been applied to all the triaxial tests according to *Head (1986)*. The aim of this section is to show with the help of FEM-simulation of the triaxial test, that whether the membrane corrections for soil samples undergoing barrelling type distortion were really necessary. For that purpose, a triaxial test was simulated with end caps and a geotextile membrane at the free side. The geotextile element was fixed at the top with the cap and at the bottom with the base pedestal. Refer to Appendix B.1 to see the configuration of the geometry for the FEM computation. The rubber membrane used in the tests has a thickness of 0.2 mm and a stiffness of EA = 0.2 kN/m. The results of the FEM-simulation are presented in Figure 7.8 for various conditions. It can be observed from Figure 7.8 that the rubber membrane with the standard stiffness of EA = 0.2 (in the computation double membrane was assumed, i.e. EA = 0.4 kN/m) has no significant effect on strength and stiffness of the soil sample. On the other hand, increasing the stiffness of the membrane by a factor of 10 and 100 respectively affects the test result considerably. In all cases, the initial stiffness of the soil up to approximately 4.5 % axial strain remains unchanged.

The other observation from Figure 7.8 is that the introduction of end cap into the FEM - model will affect the FEM-computation result positively but slightly. The introduction of an interface element (R_{int} = 0.1) between the end caps and the soil sample, in order to simulate the lubricated Plexiglas used in the test to avoid end restraint, seems to have no influence on the FEM-computational result as shown in Figure 7.8.
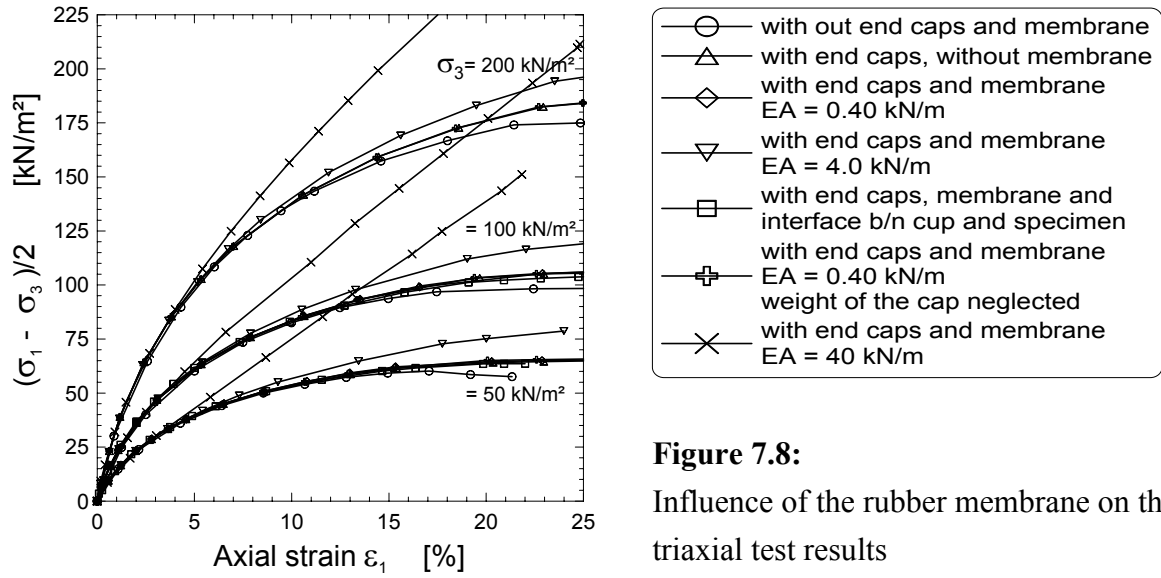
Figure 7.8:

Influence of the rubber membrane on the triaxial test results

7.2.1.7 Adjusted parameters:

The computational result after a slight adjustment of the parameters (FEM-23) according to the foregoing parameter studies are shown in Figure 7.9.
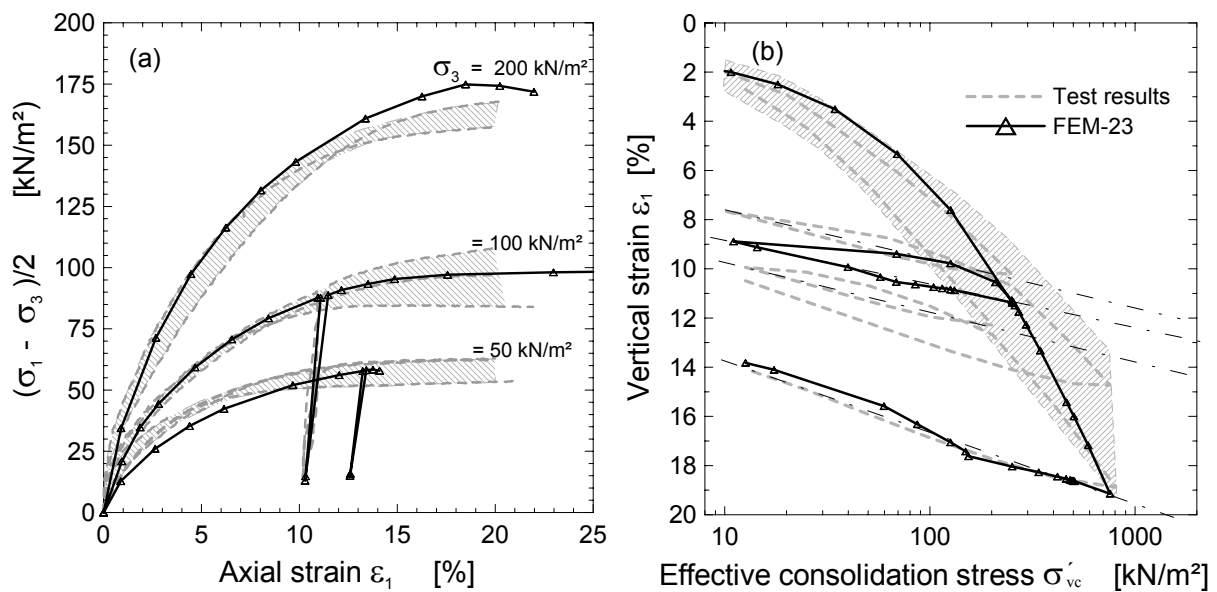
Figure 7.9:   Adjusted soil parameters for the case of drained condition at site 1

7.2.1.8 Comparison of the drained test results at site 2 & 3 with the FEM-computation

The comparison of the drained test results at site 2 & 3 with FEM -computational result and calibration of the hard soil model parameters are given in Appendix B.3 & B4.

7.2.2 Undrained test behaviour

7.2.2.1 General

In PLAXIS FE - program it is possible to perform undrained analysis using the effective shear and stiffness parameters. The program calculates the rate of the excess pore water pressure from the volumetric strain rate according to:

$$\dot{\sigma}_w = \frac{K_w}{n} \cdot \dot{\varepsilon}_v \tag{7.6}$$

where $\dot{\sigma}_w$ is the rate of the excess pore water pressure, K_w is the bulk modulus of water, n is the porosity of the soil, and $\dot{\varepsilon}_v$ is the rate of the volumetric strain. The ratio $K_{w,ref}/n$ in Equation 7.6 is calculated from:

$$\frac{K_{w,ref}}{n} = K_u - K' \tag{7.7}$$

where,

$$K_u = \frac{2 \cdot G(1+v_u)}{3(1-2 \cdot v_u)} \qquad \text{und} \qquad K' = \frac{E'}{3(1-2 \cdot v')} \tag{7.8}$$

K_u, v_u (≤ 0.495) and K', v' are the undrained and drained bulk modulus and Poisson's ratio respectively. G and E' are the shear modulus and the effective modulus of elasticity of the soil. For detail derivations and relations regarding the calculation of the rate of the excess pore water pressure, refer to *Brinkgreve/Vermeer (1998) or Brinkgreve (2002))*.

The program accepts the effective model parameters v', c', φ' and E', and calculates automatically the undrained balk modulus using the Hook's law of elasticity according to the Equation 7.8. Theoretically, the effective shear parameters should be the same from drained and undrained tests. The test results from both test type in Figure 6.22 may serve as a proof of this postulate taking into account the usual scatter of data expected in geotechnical tests. Hence, one has the choice to determine effective shear parameters from either of the two. It is obvious, however, that the modulus of elasticity in undrained test E_u is higher than the drained modulus of elasticity E'. Assuming a linear elastic behaviour, the two parameters can be related using the Equation 3.53.

To be consistent with the previous section, however, the effective parameters in Table 7.1 were adopted as a reference parameters for the FEM-simulation of the undrained triaxial test using the hardening soil model.

Similar to the drained test, various variations of the soil parameters have been made in the FEM-computations in order, first to see whether the FEM-results match with the test results, and second to study the influence of each parameter on the behaviour of the stain - stress and excess pore water pressure of the soil specimen. The various cases considered in the FEM-computations of the triaxial test under undrained loading condition are listed in Table 7.3. The geometry, the mesh and the boundary condition of the FEM-model are similar to the drained test model shown in Appendix B.1a & B.2a.

Table 7.3: Variations of HSM parameters for the FEM-computations of a triaxial test under undrained loading condition.

Cases	Parameter
FEM-UD1	reference parameters (Table 7.1)
FEM-UD2	same as FEM-UD1, but $E_{oed}^{ref} = E_{50}^{ref} = 3253 \; kN/m^2$
FEM-UD3	same as FEM-UD1, but $E_{50}^{ref} = E_{oed}^{ref} = 2948 \; kN/m^2$
FEM-UD4	same as FEM-UD1, but $E_{ur}^{ref} = 3 \cdot E_{50}^{ref} = 9759 \; kN/m^2$
FEM-UD5	same as FEM-UD1, but E_{oed}^{ref} reduced by a factor of 0.75
FEM-UD6	same as FEM-UD1, but E_{oed}^{ref} increased by a factor of 1.25
FEM-UD7	same as FEM-UD1, but $v_{ur} = 0.10$
FEM-UD8	same as FEM-UD1, but $v_{ur} = 0.30$
FEM-UD9	same as FEM-UD1, but K_0^{nc} reduced to 0.44
FEM-UD10	same as FEM-UD1, but K_0^{nc} increased to 0.71
FEM-UD11	same as FEM-UD1, but $R_f = 0.70$
FEM-UD12	same as FEM-UD1, but with an assumed dilatancy $\psi = 5°$
FEM-UD13	same as FEM-UD1, but with un/reloading phases (Table 7.1)
FEM-UD14	same as FEM-UD13, but $v_{ur} = 0.05$
FEM-UD15	same as FEM-UD13, but $E_{ur}^{ref} = 2 \cdot E_{50}^{ref} = 6506 \; kN/m^2$
FEM-UD16	same as FEM-UD1, but E_{50}^{ref} increased by a factor of 1.25

7.2.2.2 Comparison of the undrained computational results with the test results

The comparison of the FEM - computation results of the triaxial test model under undrained loading condition with the test results of the specimens from site 1 for a range of confining pres-

sure from 50 to 500 kN/m² are shown in Figure 7.10. To compare the respond of the FEM - simulation to the deviatoric stress and the development of the excess pore water pressure in the specimen, they are presented side by side in Figure 7.10a & b respectively. The stress paths are also shown in Figure 7.10c.

It would appear from Figure 7.10 that the FEM - results match badly with the test results. If we look at the result of the FEM with the reference parameters (FEM-UD1), they deviate from the test result both at the beginning of the curve and while approaching failure. The deviation of the FEM-result at the beginning of the curve may be corrected mainly by adjusting the stiffness parameters, while the main reason for the deviation of the FEM-results approaching failure is accounted to the gradual falling of the excess pore water pressure in the test after it has reached a maximum value at lower axial strain (around 5%) (Figure 7.10b). This is a typical behaviour of a dilatant material, although the material in question is not known as dilatant material. The volume change behaviour of similar specimens in the drained tests show no dilatant behaviour. However, if one considers the angle of overall shear strength φ_s, i.e. the sum of the effect of effective cohesion c' and effective friction angel φ', one may come to the result $\varphi_s = 36.7°, 32.2°, 29.8°, 28.9°, 28.5°, 28.2°$ for confining pressure of 50, 100, 200, 300, 400, and 500 kN/m² respectively. From this result one can see that the effect of the cohesion on the overall shear strength ceases as the confining pressure increases from 50 to 500 kN/m². This in turn will have an effect on the development of the excess pore water pressure, which can clearly be seen from the test results in Figure 7.10b, where the rate of the drop of excess pore water pressure ceases gradually as the confining pressure increases from 50 to 500 kN/m². The HSM in its current stand cannot simulate the drop of the pore pressure as can be seen in Figure 7.10b.

For the matter of completeness, the effect of the assumptions $E_{oed}^{ref} = E_{50}^{ref}$ (FEM-UD2), $E_{50}^{ref} = E_{oed}^{ref}$ (FEM-UD3), and $E_{ur}^{ref} = 3 \cdot E_{50}^{ref}$ (FEM-UD4) on the FE- simulation are also presented in Figure 7.10. The 1st assumption has no significant influence on the initial stiffness up to approximately 5% axial strain, and deviates slightly from the reference curve while approaching failure. However, it affects the excess pore water pressure right from the beginning. Obviously, the 2nd assumption has a significant influence right from the beginning, but tends to converge to the reference line while approaching failure. The 3rd assumption has considerable influence on the deviatoric stress and excess pore water pressure. In all cases of the assumptions, their influence on the deviatoric stress and excess pore water pressure increases with the confining pressure.

The stress path diagram (Figure 7.10c) shows that the strength parameters of the specimen remain unaffected by the various assumptions, although the deviatoric stress at failure changes. The stress at failure in the p - q diagram changes accordingly, but it remains on the failure line by shifting itself to a new position. Unlike the drained condition the deviatoric stress at failure is not

only dependent on the effective shear parameters, but also on those parameters which affect the excess pore water pressure. These parameters are discussed in the following section.
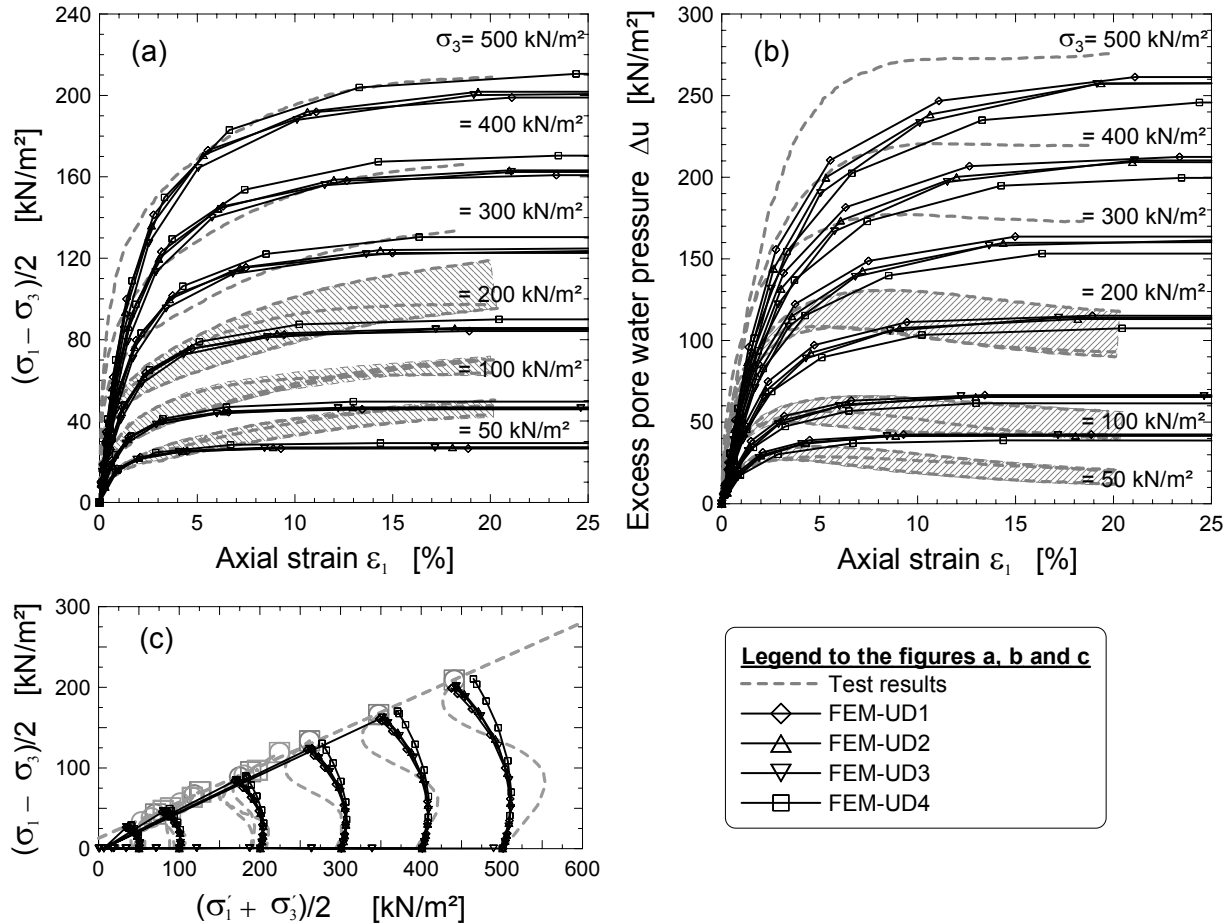

Figure 7.10: The respond of a triaxial FEM- Model to undrained loading condition as compare to the test results from site 1: a) deviatoric stress vs. axial strain, b) excess pore water pressure vs. axial strain, and c) the stress path

7.2.2.3 Sensitivity study of the model parameters under undrained loading conditions

The influence of the hardening soil model parameters under undrained loading condition has been studied by varying the parameters in the FEM- computations according to the Table 7.3 for selected specimen with confining pressure of 100 kN/m². The results of the sensitivity study are shown in Figure 7.11. As it would appear from the figure that all the parameters in question, namely the E_{oed}^{ref} (FEM-UD5 & 6), v_{ur} (FEM-UD7 & 8), K_0^{nc} (FEM-UD9 & 10), E_{50}^{ref} (FEM-UD16), E_{ur}^{ref} (FEM-UD4), and R_f (FEM-UD11) have an effect on the deviatoric stress and excess pore water pressure. The most sensitive parameter, however, is the K_0^{nc}. Varying the K_0^{nc}

from the default value of $K_0^{nc} = 1 - \sin\varphi' = 0.573$ to a lower value of 0.44 (FEM-UD9) and a higher value of 0.71 (FEM-UD10) results in considerable decrease/increase of the deviatoric stress and increase/decreases of the excess pore water pressure respectively, specially while approaching failure stress. The effect of the E_{50}^{ref} is more noticeable on the first part of the curve, say up to 5 to 6% axial strain for this particular test, whereas the effect of the E_{oed}^{ref}, E_{ur}^{ref} and K_0^{nc} is at later stage of the curve while approaching failure. It is obvious that the decrease of the E_{oed}^{ref} results in more compressibility of the soil, which give rise to more excess pore water pressure, in particular while the soil approaches failure as shown in Figure 7.11 (see also *Schweiger (2002)*).
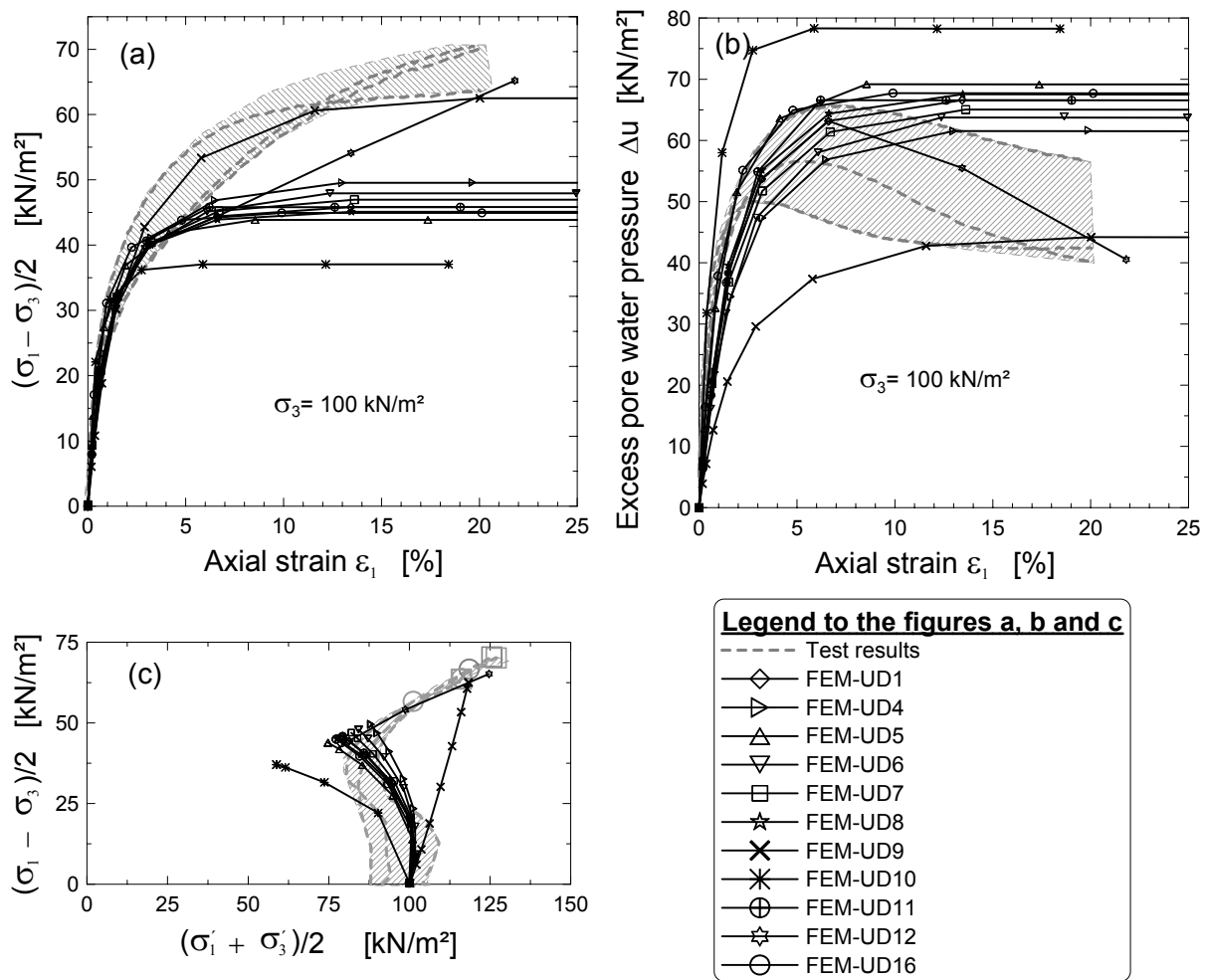
Figure 7.11: Sensitivity study of the influence of the hardening soil parameters on the
a) strain - stress behaviour, b) development of excess pore water pressure, and
c) stress path of a specimen with a confining pressure of 100 kN/m² at site 1

Although the soil in question is not known to posses a dilatancy behaviour, an introduction of the dialatancy angle $\psi = 5°$ (FEM-UD12) into the FEM-computation at least shows the general ten-

dency of the drop of the excess pore water pressure and increase of the deviatoric stress with the axial strain. However, even the introduction of ψ did not help to follow the course of the deviatoric stress curve exactly.

Similar to what discussed above in Section 7.2.2.2, the deviatoric stress at failure remains on the failure line independent of the variation of the parameters (Figure 7.11c). However, it shifts its position to the right or left of the reference point according to the variation of the the various parameters.

7.2.2.4 Simulation of the undrained test (CIU) using the undrained parameters

In the previous sections, the undrained test was simulated using the effective soil parameters from drained test. What about if one has only the CIU or CAU test results available? The effective shear strength parameters are independent from the drainage condition (Section 6.4.6& 7.2.2.1), and hence they can be used as it is in the FEM- computation. The question is how can the effective secant modulus E_{50} be determined. There are two ways to deal with this problem. The first way is to approximate the effective E_{50} from experience and perform a triaxial simulation under undrained condition. If the computed results does not match with the test results, the computation should ran iterative further with adjusted E_{50} each time until a fair match of the computed and the measured result will be attained.

The second method is to roughly estimate the E_{50} from the undrained $E_{50(u)}$ assuming a linear elastic behaviour according to Equation 3.53, although the effective secant modulus E_{50} in the HSM is known to be an elasto - plastic parameter. The value of the E_{50} obtained in this way should only serve as initial value and it should be calibrated by simulating the triaxial test.

7.2.2.5 Response of the FE-Model to un/reloading state of stress under undrained condition

A FEM - simulation of the un/reloading under undrained condition was carrid out using the HSM parameters in Table 7.1. The FEM-simulation with the reference parameters (FEM-UD13) fails to respond correctly to undrained loading condition as shown in Figure 7.12. Firstly, the un/reloading phases occur earlier than it was expected. It was assumed that the 1st, 2nd, and the 3rd un/reloading phase would occur at around an axial strain of 5, 10 and 15% respectively according to the test result. This shows that for a given stress level, the FEM-model reacts stronger than the test, which is not usually the case in drained simulations. Secondly, the un/reloading stiffness is much higher in the FEM - result than the measured value. Since the un/reloading modulus E_{ur} is

an elastic parameter, it can be approximated from the undrained un/reloading modulus $E_{u,ur}$ according to the elasticity theory using the Equation 7.9 (see also Section 3.5.2)

$$E_{u,ur} = \frac{3}{2 \cdot (1 + v_{ur})} \cdot E_{ur} \qquad (7.9)$$

For $E_{ur}^{ref} = 19.2 \, MN/m^2$ from drained test and $v_{ur} = 0.2$, one may obtain $E_{u,ur} = 24.0 \, MN/m^2$, which is much higher than the measured undrained modulus (4.5 MN/m^2). If $E_{u,ur}$ from the test result will be used as a basis for the FEM - computation by converting it to E_{ur} according to Equation 7.9, one obtains $E_{ur} = 3.6 \, MN/m^2$. This value is much lower than the minimum un/reloading modulus allowed in PLAXIS, i.e., $E_{ur}^{ref} \geq 2 \cdot E_{50}^{ref} = 6.51 \, MN/m^2$. Obviously, the use of $E_{ur}^{ref} = 2 \cdot E_{50}^{ref}$ (FEM-UD15) will narrow the difference of the slope of the un/reloading lines between the FEM and test results (Figure 7.12a), but on the other hand it has the effect of lowering the excess pore water pressure and increasing the deviatoric stress (Figure 7.12a & b). The considerable deviation of the FEM - computation result from the test result can also be seen from the stress path diagram (Figure 7.12c).
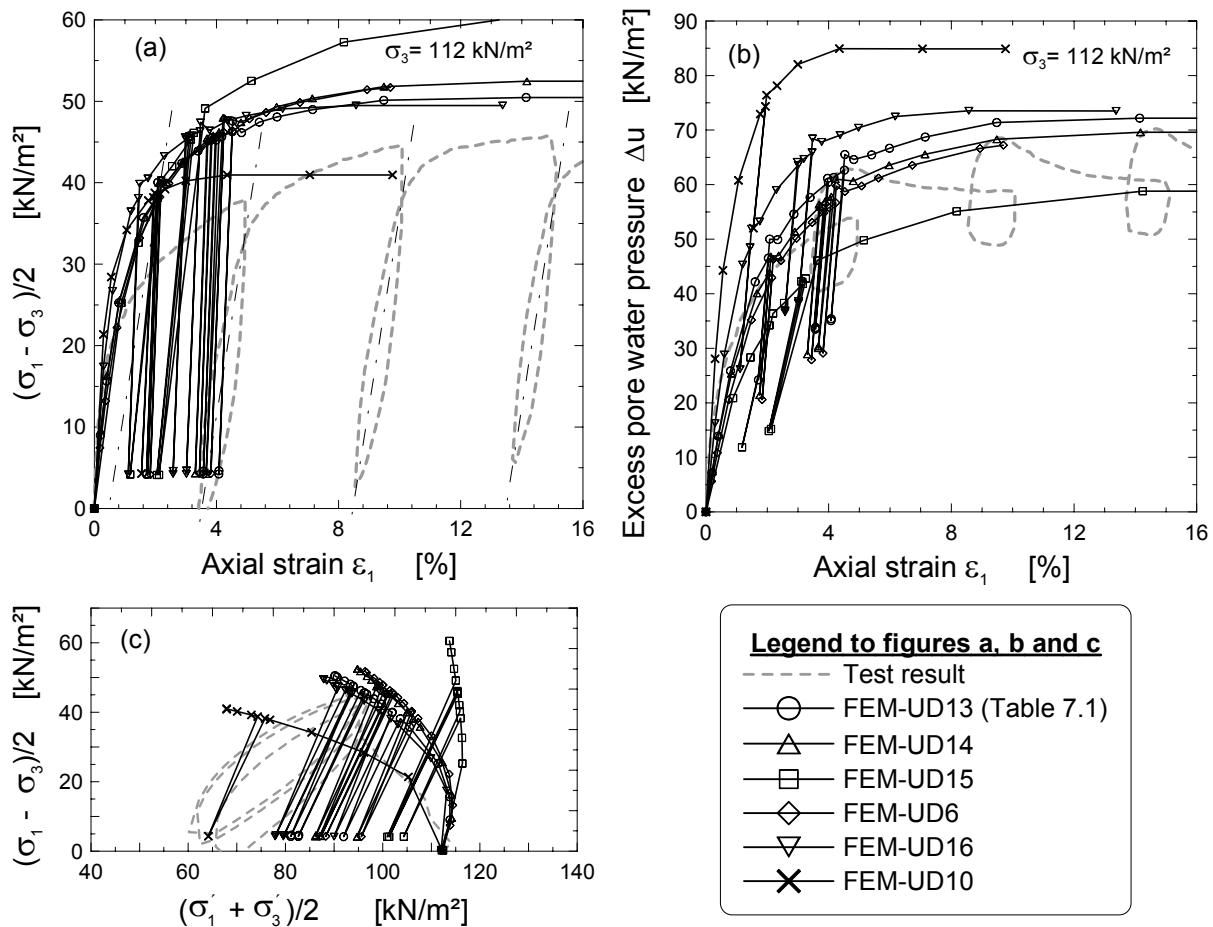

Figure 7.12: Response of the FEM-simulation under undrained un/reloading condition:
a) deviatoric stress, b) excess pore water pressure, and c) stress path

The other parameters such as ν_{ur} (FEM-UD14), E_{oed} (FEM-UD6), E_{50} (FEM-UD16) and K_0^{nc} (FEM-UD10) have shown no effect on the un/reloading behaviour of the soil specimen (Figure 7.12).

The smooth reaction of the excess pore water pressure to the unloading, its stable position at $\Delta\sigma = 0$, its sudden rise on reloading beyond its value before unloading, and gradual drop of the excess pore water pressure observed during the test is not to see from the FEM - computation. In general, on may conclude that the simulation of the undrained test both during the primary loading, unloading or reloading was not as satisfactory as the drained test.

7.2.2.6 Comparison of the undrained tests at site 2 and site 3 with FEM - simulation

The calibration of the hardening soil model parameters under undrained condition using the undrained test results at site 2 and site 3 are shown in Appendix B.5 &B.6. The effective soil parameters from the respective drained tests were adopted in the computation.

7.2.3   Stress paths

7.2.3.1   General

The response of the hardening soil model to different stress paths for the case of isotropic (left) and K_0 - consolidation (right) are shown in Figure 7.13. The model parameters are the same as those given in Table 7.1. In the case of isotropic consolidation, the specimen was first consolidated under a confining pressure of $\sigma_{30} = \sigma_{10} = 100 \ kN / m^2$, before it had undergone to different stress paths. Similarly, the specimen was consolidated first at a confining pressure of $\sigma_{30} = 100 \ kN / m^2$ and $\sigma_{10} = 175 \ kN / m^2$, i.e. $K_0 = 1 - \sin\varphi' = 0.573$ in the case of the K_0 - consolidation.

As shown in the Figure 7.13a &b, the effective stress path for all total stress paths above the isotropic stress line or above the K_0 - line (compression), i.e., the stress paths A, B and C, is unique. That is also true for those total stress paths (D, E and F) below the isotropic stress line or below the K_0 - *line* (extension). This is an approval of the test results in section 6.4.5. The unique effective stress paths in compression as well as in extension also leads to a unique deviatoric stress at failure (Figure 7.13c &d). It is not only the deviatoric stress at failure, but also the courses of the deviatoric stress vs axial strain for the total stress paths A, B, and C in compression, and D, E, and F in extension respectively are exactly the same.

However, The deviatoric stresses at failure in compression and extension are different. This leads to differences in the undrained shear strength c_u and the overall angle of the shear strength φ_s in compression and in extension. The ratios of the respective values are calculated to be:

$$\frac{c_{uc}}{c_{ut}} = \begin{cases} 1.41, & \textit{isotropic consolidation} \\ 1.33, & K_0-\textit{consolidation} \end{cases} \tag{7.10}$$

and

$$\frac{\tan\alpha_{sc}}{\tan\alpha_{st}} = \frac{\sin\varphi_{sc}}{\sin\varphi_{st}} = \begin{cases} 0.87, & \textit{isotropic consolidation} \\ 0.92, & K_0-\textit{consolidation} \end{cases} \tag{7.11}$$

Equation 7.10 is comparable with Equation 3.42, but not to all values listed in Table 3.6. This is because the c_{uc}/c_{ut} is not a constant value, rather it depends on the plasticity of the material (see Figure 3.21). Equation 7.11 is also fairly comparable with most of the values listed in Table 3.8.

Comparing the isotropic consolidation with K_0 - consolidation, the later reacts stronger than the earlier one. The deviatoric stress at failure in the case of K_0 - consolidation is higher by a factor of 1.4 than the case of isotropic consolidation for the given specimen.

Unlike to the effective stress path and the deviatoric stress, the development of the excess pore water pressures for the different stress paths are quite different (Figure 7.13e &f). The excess pore water pressure at failure (or approaching failure) for stress paths A and B is lower and for the stress paths D, E and F higher in the case of K_0 - consolidation than in the case of isotropic consolidation, while the stress path C remains unaffected by the type of consolidation.

From the above discussion it would appear that there is no need to reduce the undrained strength to account for stress induced anisotropy in FEM - computations under undrained condition. However, the inherent anisotropy remains ignored in the FEM - computation.

7.2.3.2   Comparison of the controlled stress path tests with the FE-simulation

The comparison of the controlled stress path C test results (see also section) with the FEM-computation is shown in the Figure 7.14. The reference parameters for the FEM - computation were taken from drained test result in Appendix B3. As shown in the figure, the FEM - result with the reference parameters (FEM-SP-C1) does not match the test result, though the deviation by the deviatoric stress diagram (Figure 7.14a) is relatively moderate as compare to the excess pore water pressure (Figure 7.14b). One reason for such deviation of the results might be the
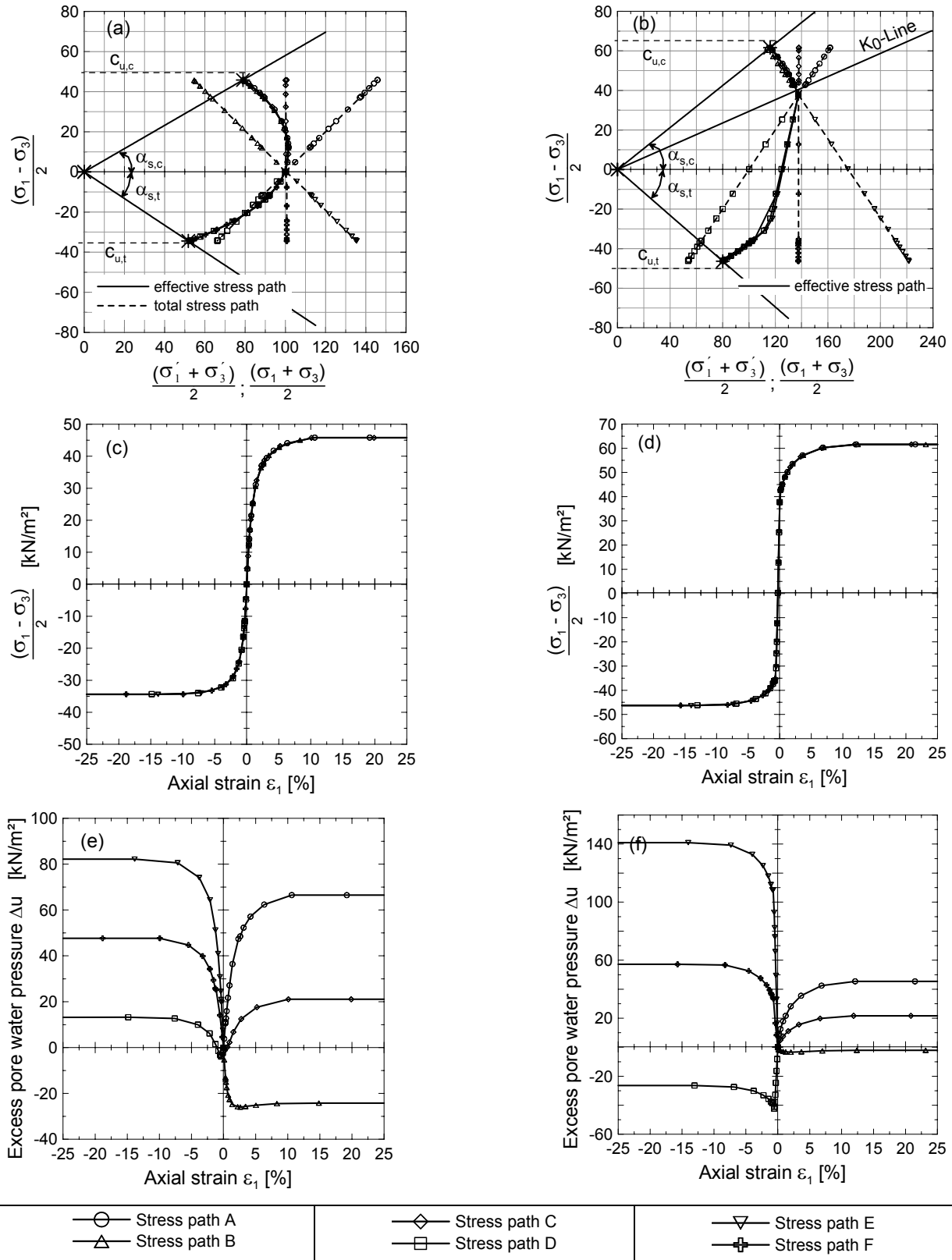
Figure 7.13: Response of the hardening soil model to different stress paths: a) & b) stress paths, c) & d) deviatoric stress, and e) & f) excess pore water pressure, for the case of isotropic consolidation (left) and K_0 - consolidation (right)

choice of the default value of $K_o^{nc} = 0.573$, whereas $K_0 = 0.80$ was used in the test. Adjusting the value of K_o^{nc} to 0.71 (FEM-SP-C2), which is the maximum allowable value for the given soil parameters, led to a higher excess pore pressure and proportionally to a lower deviatoric stress at failure. The p - q diagram in Figure 7.14c shows a better match of the results in the case of FEM-SP-C2, specially for confining pressure of 200 and 300 kN/m². By adjusting the K_o^{nc} value further, one may attain a better match of the results with due consideration of the deviations among the test results. The computational result according to the modified parameters at this site is given by line FEM-SP-C3. The HSM fails again to simulate the drop of the excess pore water pressure and the increase of the deviatoric stress with strain.

It would appear from Figure 7.14 that the FEM may simulate the deviatoric stress fairly taking into account the possible deviations within the test results, whereas the simulation of the excess pore water pressure is not optimal. Similar tendency can also be observed from the comparison of the controlled stress paths B test result and the FEM - simulation (Appendix B.7).
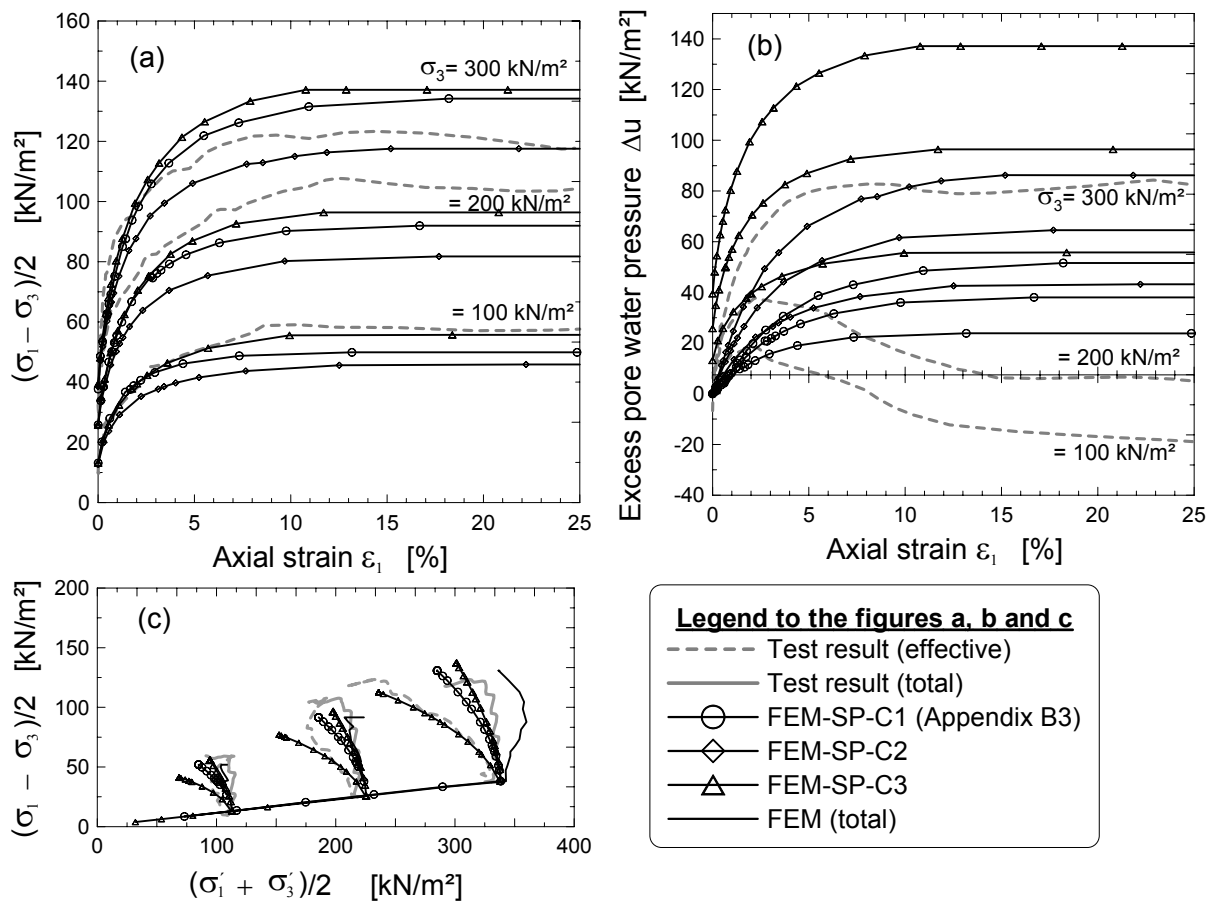

Figure 7.14: Comparison of the stress path C test with the FEM-simulation:
a) deviatoric stress, b) excess pore water pressure, and c) the stress path

7.2.4 Summary

The drained tests can fairly be simulated with the FEM with a slight modification of parameters. As would expected, the E_{50}^{ref} is the main parameter that determines the stress-strain behaviour of a soil specimen in a triaxial primary loading condition, and it has negligible influence on one - dimensional loading condition. Similarly, the E_{oed}^{ref} has insignificant effect on the triaxial loading condition, but plays the main role in one-dimensional loading. The E_{ur}^{ref} is the single parameter that influences the un/reloading condition both in triaxial and one dimensional state of stresses. Contrary to the expectation, the v_{ur} has only an effect on the one-dimensional un/reloading condition. It seems that the K_0^{nc} will have no significant influence on the un/reloading state of stress in both loading systems. In general, it was observed that the FEM simulation underestimates the stiffness of the soil at a lower strain (say up to around 2.5% axial strain).

The E_{oed}^{ref} and K_0^{nc} values appear to play the leading role in determining the volume change characteristic of the specimen in a triaxial compression, although all the other parameters with the exception of the R_f contribute their part. This and the above discussion show the separate function of the E_{oed}^{ref} as a cap parameter that controls the compression hardening and the E_{50}^{ref} as a parameter that controls the shear hardening.

The undrained triaxial stress - strain behaviour in primary loading condition seems to be affected by various parameters. Beside the E_{50}^{ref}, the E_{ur}^{ref} and K_0^{nc} have a significant effect on its behaviour. The other parameters have also their part, but in a small scale. The simulation of the undrained test did not give the expected match of the computed and the measured results. This is partly due to the difficulty of simulation of the drop of the excess pore pressure on one hand and the increase of the deviatoric stress on the other hand. All the parameters appear to affect the development of an excess pore pressure, but the effect of the K_0^{nc} is very remarkable.

The simulation of the stress path tests has further proven that the effective stress path is unique for all total stress paths on the compression and extension zones. The only difference between the various total stress paths is the difference in the development of the excess pore pressure. An attempt has also been done to follow the stress-strain and excess pore pressure development curves from test results numerically, however, the same difficulty as in undrained test condition discussed above was encountered.

The influence of the different hardening soil model parameters on the stress strain, strength and volume change behaviour of a soil specimen keeping the effective shear parameters constant is summarised in Table 7.4.

Table 7.4:   Summary of the influence of the hardening soil parameters

Soil parameter	Stress - Strain behaviour						Volume change	Excess pore water pressure	strength at limit state	
	Triaxial loading condition				One-dimensional compression					
	Drained		Undrained							
	loading	un/reloading	loading	un/reloading	loading	un/reloading			Drained	Undrained
E_{50}^{ref}	✓✓✓	✗	✓✓	✗	✗	✗	✓✓	✓✓	✗	✓
E_{oed}^{ref}	✗	✗	✓✓	✗	✓✓✓	✗	✓✓✓	✓✓	✗	✓✓
E_{ur}^{ref}	✓	✓✓✓	✓✓	✓✓✓	✗	✓✓✓	✓✓	✓✓	✗	✓✓
m	✓✓	✓	✓✓	✓	✓✓	✓	✓✓	✓✓	✗	✓✓
v_{ur}	✗	✗	✓	✗	✗	✓✓✓	✓	✓✓	✗	✓
K_0^{nc}	✓✓	✗	✓✓✓	✗	✓	✗	✓✓✓	✓✓✓	✗	✓✓
R_f	✓✓	✗	✓	✗	✗	✗	✗	✓✓	✗	✗

✓✓✓ = has a considerable effect;   ✓✓ = has an effect;   ✓ = has a slight effect;   ✗ = has no effect

The use of the angle of the overall shear strength in numerical method should be taken with care, since it is dependent on the stress level. A constant value for the whole depth might lead to over-estimation or underestimation of the strength of the soil.

Janbu (1977) asserted that the effective cohesion of soils might affect the value of the K_0. This effect has been studied by varying c´ and $\varphi´$ in the FE - calculation of a one-dimensional test model. A general tendency of increasing K_0 value was observed for all values of $\varphi´$ considered, and an empirical Equation 7.1 was recommended.

7.3   Parameter study on idealized excavation problem

7.3.1   General

The influence of the hardening soil model parameters on the stress - strain, volume change and excess pore pressure behaviour has been discussed in the forgoing sections for a triaxial and one dimensional compression test condition. Once more, the influence of these parameters on the performance of an idealised excavation will be investigated in this section. First, however, the recommendation of the working group "Numerics in Geotechns" (AK 1.6) of the German Society of Geotechnical Engineers (*Meißner (2002)*), regarding the size of the finite element model of an excavation will be examined for excavations on soft soils.

Berms provide support to the retaining structures before the strut or anchor or bottom slab or propped support are installed in place. The efficiency of the berms in reducing the movement of the wall and the soil will also be dealt with in this section.

An installation of a support at the bottom of excavation prior to the end of excavation either by means of a column jet pile or soilcrete or bottom concrete slab placed in slices reduces the wall movement at the toe and at the excavation level to some extent. The efficiency of such support system will also be dealt with in this section.

7.3.2   System geometry

In order to investigate the influence of the size of the FEM - model on the deformation behaviour of an excavation, an idealized excavation shown in Figure 7.15 has been chosen. The ground is assumed to be a deposit of a homogeneous lacustrine soft soil with the ground water table located at 1.5 m below the ground surface. The excavation 6.0 m deep was supported by a sheet pile wall of the type Hoech 134 with a total length of 13.0 m, with an embedment depth of 8.1 m and with two level of struts (IPB 360 St 37). A building load of 50 kN/m² at a distance of 3 m behind the wall and a traffic load of 10 kN/m² was assumed at the ground surface.

The hardening soil model (HSM) was used to simulate the soil behaviour, whereas a Mohr - Coulomb model (MCM) was used for the interface elements. A drained type of analysis has been used, because it was believed that this condition is most unfavourable condition for excavations in soft deposits. The reference soil parameters in Table 7.1 were used for the HSM. The stiffness of the soil were taken as it is for the interface element, whereas the shear parameter were reduced by a factor of 1/3 in the MCM. The wall and the struts were assumed elastic with the following material properties:

$$\text{Wall:} \quad EA = 3.591 \times 10^6 \text{ kN/m}, \ EI = 5.355 \times 10^4 \text{ kN-m}^2/\text{m}, \ \omega = 1.34 \text{ kN-m/m}, \ \nu = 0.30$$
$$\text{Strut:} \quad EA = 3.801 \times 10^6 \text{ kN}, \ L_{spacing} = 2.0 \text{ m}$$

Three excavation width B = 12, 24, and 48 m were considered in the parametric study. For each case of the excavation width, the horizontal distance behind the wall and the vertical depth below the bottom of the excavation up to the right side and bottom boundaries respectively were varied according to the table in Figure 7.17. In order to avoid the influence of the size and number of the elements on the results of the comparison, an inner zone which is 12 m behind the wall and below the excavation bottom was defined. The number of elements in this inner zone were held as much as possible constant for all cases of variations, whereas a slight variation in the size of the elements out side this zone were possible. The program automatically generates the mesh of the model which makes it difficult to control the size of the elements in case of a change of model geometry.
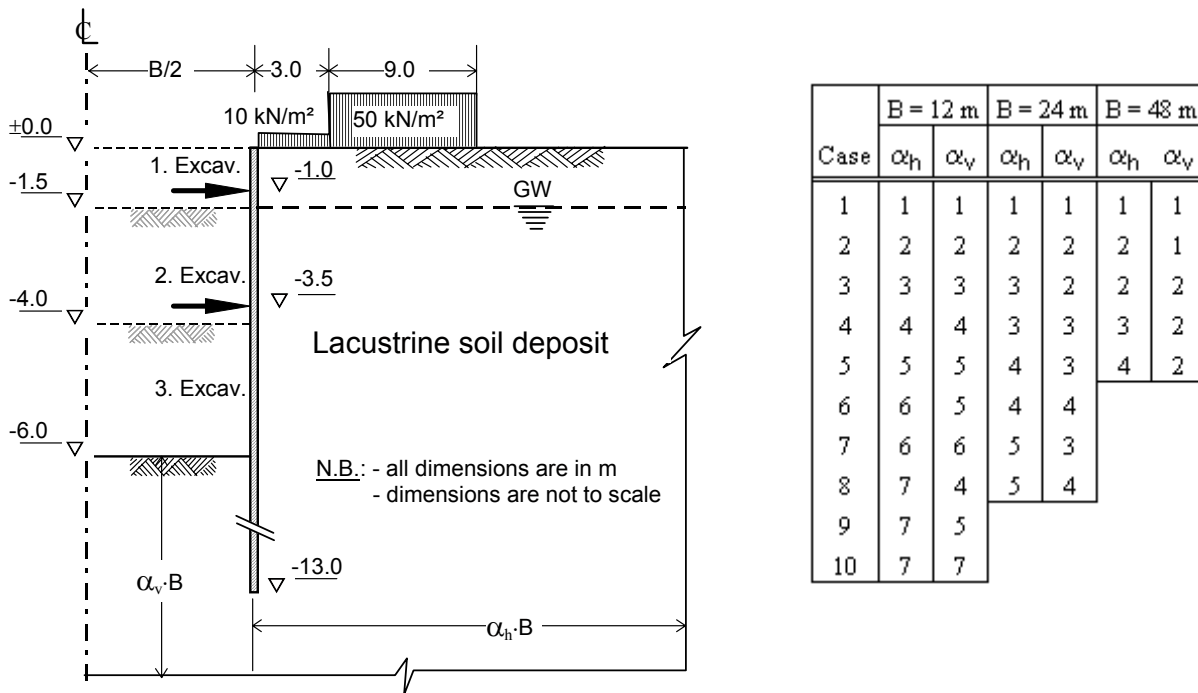
Figure 7.15: Idealized excavation problem and variation of the geometry of the FE - Model

The results of the variation of the geometry of the model are shown in Figure 7.16. It would appear from the Figure 7.16a that the effect of the FEM - model size on the deflection of the wall is very minimum. The maximum difference in the deflection of the wall from the different size of the geometry lies below 4% for a given width of excavation. However, the deflection of the wall seems to increase as the width of the excavation increases (Figure 7.16a).

The effect of the model size may clearly be seen on the heave of the bottom of the excavation (Figure 7.16b). The heave increases with the increase of the geometry, but its rate of increase ceases with the geometry size. For example, an increase of the geometry size from 84 x 78 m to 108 x 102 m for the case of B = 24 m results in a 3.8% increase of the maximum heave. On the other hand, it would appear from Figure 7.16b that the height of the model plays a significant role on the heave property of the excavation than its width. Keeping the height of the model constant and enlarging its width resulted in almost no heave at the bottom of the excavation (Figure 7.16b). This is very important in regard to the selection of the model size, because the depth of the soft soil is somewhat limited (for example the lacustrine soft soil deposit in southern Germany limited to a maximum depth of 60 to 70 m). Underneath the soft soil a bearing layer, for example gravely sand moraine or boulder clay is usually encountered. In other words, if the depth of the model to the lower boundary can be fixed, there is no need to enlarge the model in the horizontal direction more than twice the excavation width.

(a)

(b)

(c)
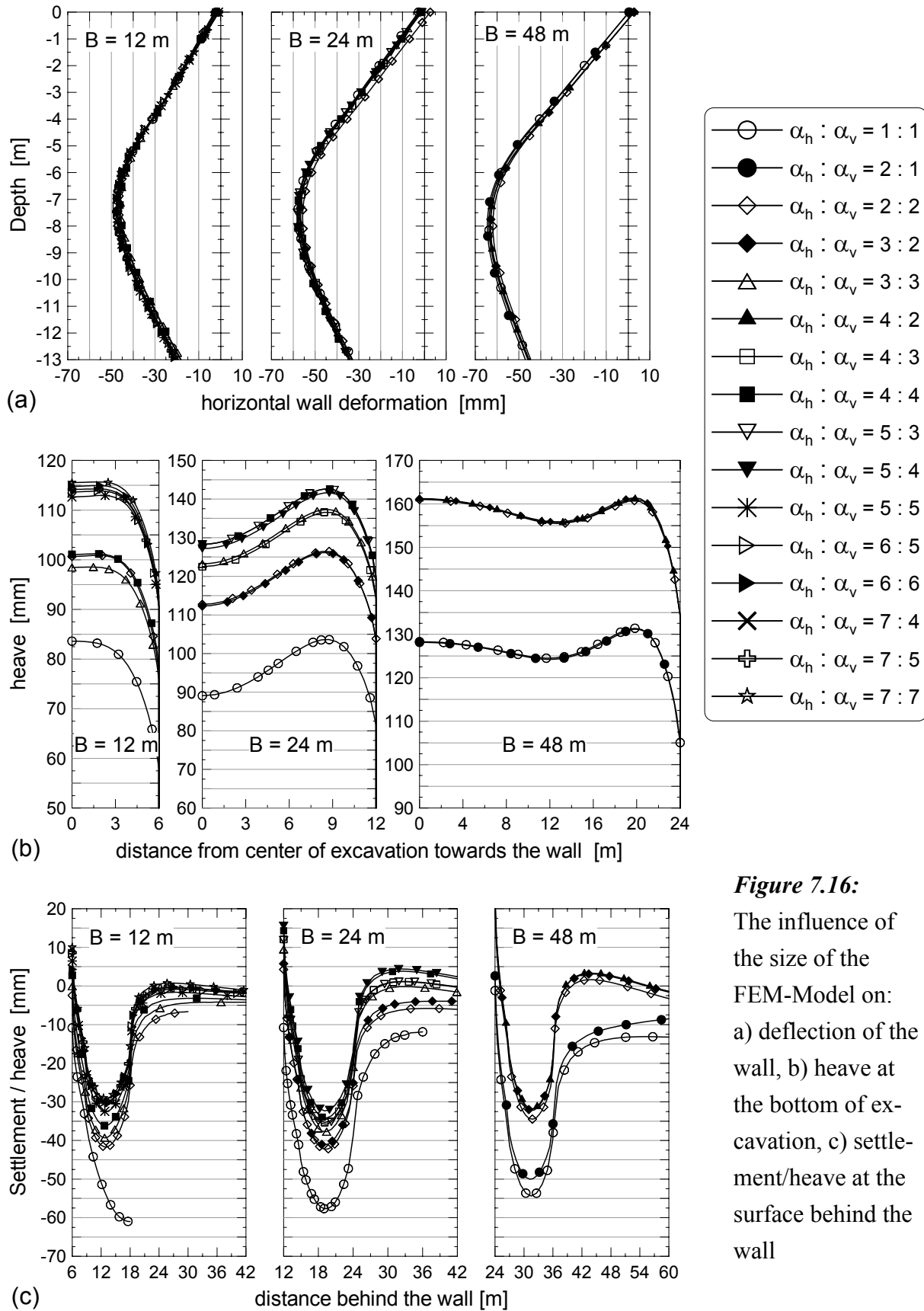
Figure 7.16:
The influence of
the size of the
FEM-Model on:
a) deflection of the
wall, b) heave at
the bottom of ex-
cavation, c) settle-
ment/heave at the
surface behind the
wall

In general the following conclusions can be made from the result of the above parameter study. Horizontal wall deflection and displacements do not be affected by the size of the model, however, the deflection increases with the increase of the width of excavation. The main factor that influence the heave at the bottom of the excavation and settlement at the surface is the height of the model rather than the width of the model. Another general observation is that the deflection of the wall, the heave at excavation bottom increase with increase of the width of excavation, whereas the settlement at the surface tends to decrease with increasing width of excavation.

7.3.3 Sensitivity study of the hardening soil model parameters

The FEM - sensitivity study of the hardening soil parameters has been conducted on triaxial test specimens in Section 7.2. In this section a further study of the influence of each HSM parameters on the performance of an idealised excavation problem has been investigated. The FEM - model chosen was similar to that used for the study of the model geometry in Section 7.3.2, except that the geometry of the FEM-model here was fixed to 48 x 42 m. The idealised excavation problem is shown in Figure 7.17 on the left and on the right is the corresponding section of the FEM - model and its mesh. The ground was assumed to consist a homogeneous lacustrine soft soil deposit and the support system was the same as that described in Section 7.3.2.
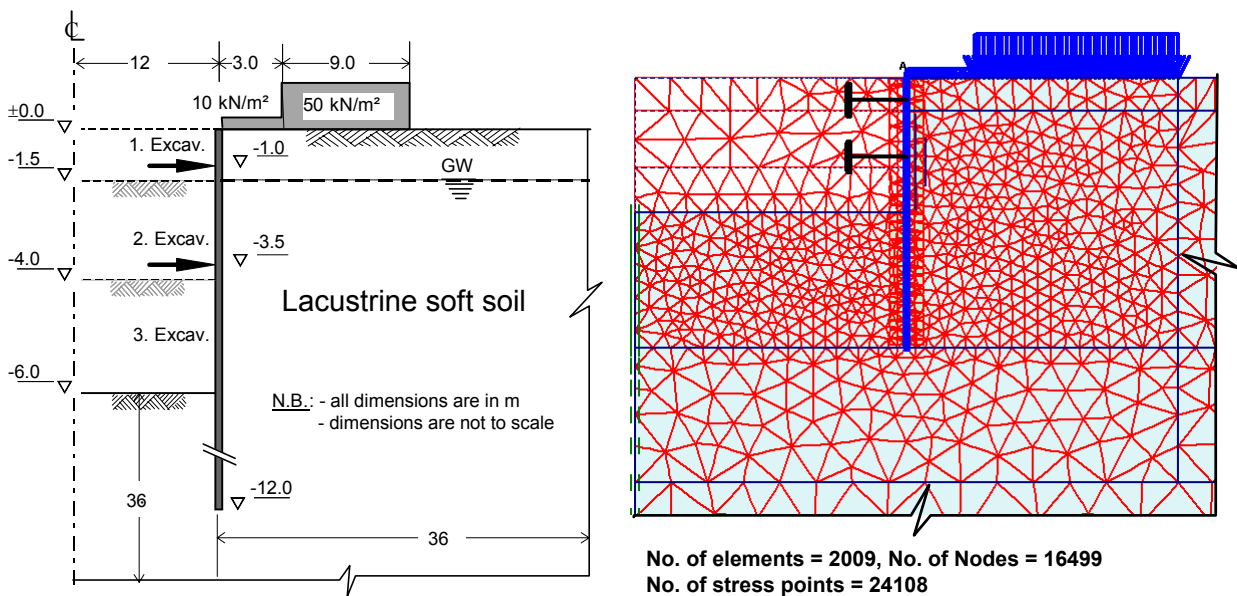

No. of elements = 2009, No. of Nodes = 16499
No. of stress points = 24108

Figure 7.17: Idealized excavation problem and the corresponding FEM-model with mesh

7.3.3.1 Drained condition

For the drained analysis of the idealised excavation problem, the HSM parameters in Table 7.1 was adopted as a reference parameters for the soil body. The shear parameters for the contact surface were adopted from the soil body after reducing the values by a factor of 1/3. The stiffness of the interface elements was assumed to be the same as the soil. The following construction stages were followed in the FEM- calculation:

Stage 0:	*generation of the initial stresses (K_0 - method)*
Stage 1:	*application of the surcharge and traffic loads*
Stage 2:	*installation of the wall*
Stage 3:	*first excavation*
Stage 4:	*installation of the 1st strut and 2nd excavation*
Stage 5:	*installation of the 2nd strut and 3rd excavation*

The results of the sensitivity study for the case of the end of excavation under fully drained condition are shown in Figures 7.18 to 7.22.

The effect of the variation of the Poisson's ratio ν_{ur}:
As it can be seen from Figures 7.18a to 7.22a (left), the parameter ν_{ur} seems to be a pure deformation parameter. In other words, the ν_{ur} may affect the deformation of the wall and soil movements but not the earth pressure and bending moment of the wall. A change of the ν_{ur} from its reference value of 0.2 to a smaller value of 0.05 and a larger value of 0.3 has resulted in a uniform change of the wall deflection by about -7 and 4% respectively. Similarly, a change of the heave by about 15 and -10%, and a change of the surface settlement by about -21 and 15% respectively were observed (Figures 7.18a to 7.22a (left)).

The effect of the variation of the coefficient of the earth pressure at rest K_0^{nc} :
The HSM treats K_0^{nc} and K_0 separately. While K_0^{nc} is a model parameter which is closely related to the stiffness parameters E_{50}, E_{ur}, E_{oed} and ν_{ur}, the K_0 is purely used to define the initial state of the stresses. For normally consolidated soils, however, these values are more or less the same. The value of K_0^{nc} can not be varied indefinitely, for example, for the given reference parameters, the minimum and maximum possible values of K_0^{nc} are 0.437 and 0.71 respectively. In this parameter study the K_0 was assumed to vary with the K_0^{nc}. As it can be seen from Figures 7.18a to 7.22a (middle), the parameter K_0^{nc} would affect the deformation of the wall, the soil movements, the earth pressure and bending moment of the wall, although the magnitude of its influence is moderate as compare to the triaxial case discussed in Section 7.2. Varying the value of K_0^{nc} from the reference value of 0.573 to those extreme values has resulted in a change of the maximum wall deflection by about -21 and 3% respectively. Similarly, a change of the heave by about 2

and -9%, a change of the surface settlement by about -5 and 7% , a change of the earth pressure by about -21 and 8%, and a change of the bending moment by about -18 and 2% respectively were observed (Figures 7.18a to 7.22a (middle)). From the above percentage difference presentation and the Figures 7.18a to 7.22a (middle), it appears that varying the K_0^{nc} value towards the lowest limit is more sensitive than varying its value towards the upper limit, although the difference between the reference value and the extreme values is almost the same.
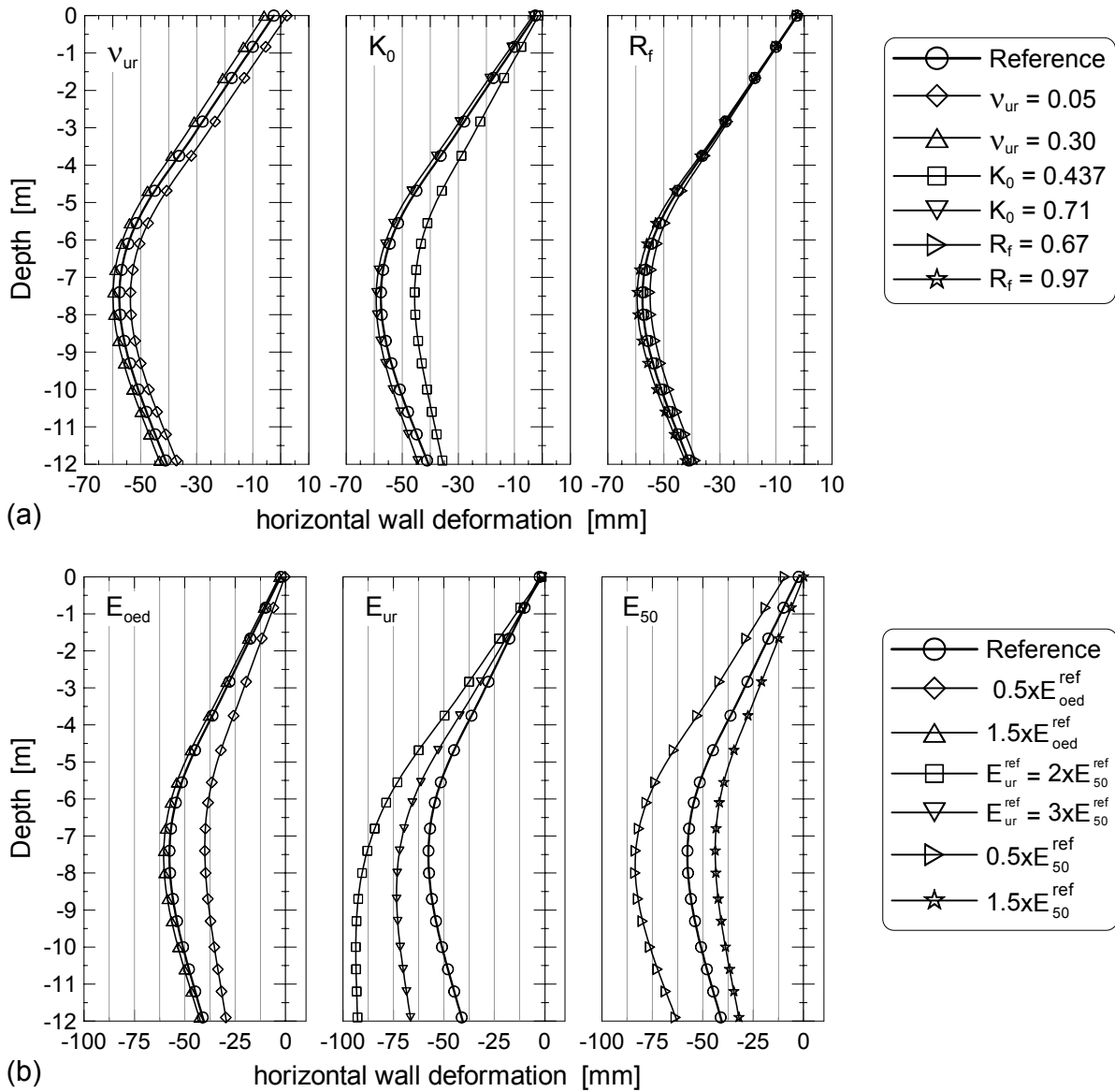

Figure 7.18*:* The influence of a) ν_{ur}, K_0^{nc} and R_f, and b) E_{oed}, E_{ur}, and E_{50} on the deflection of the wall under fully drained condition

The effect of the variation of the failure factor R_f:
In Section 7.2, it has been proved that the failure factor R_f plays an important role in enhancing

or retarding the failure of the soil body. Its influence on the idealised excavation, however, seems to be minimum, with exception of the settlement behind the wall (Figures 7.18a to 7.22a (right)). Varying the value of R_f from the reference value of 0.83 to 0.67 and 0.97 has resulted in a change of the surface settlement by about -8 and 6% respectively. For all the other cases, the difference remains below ±5%.
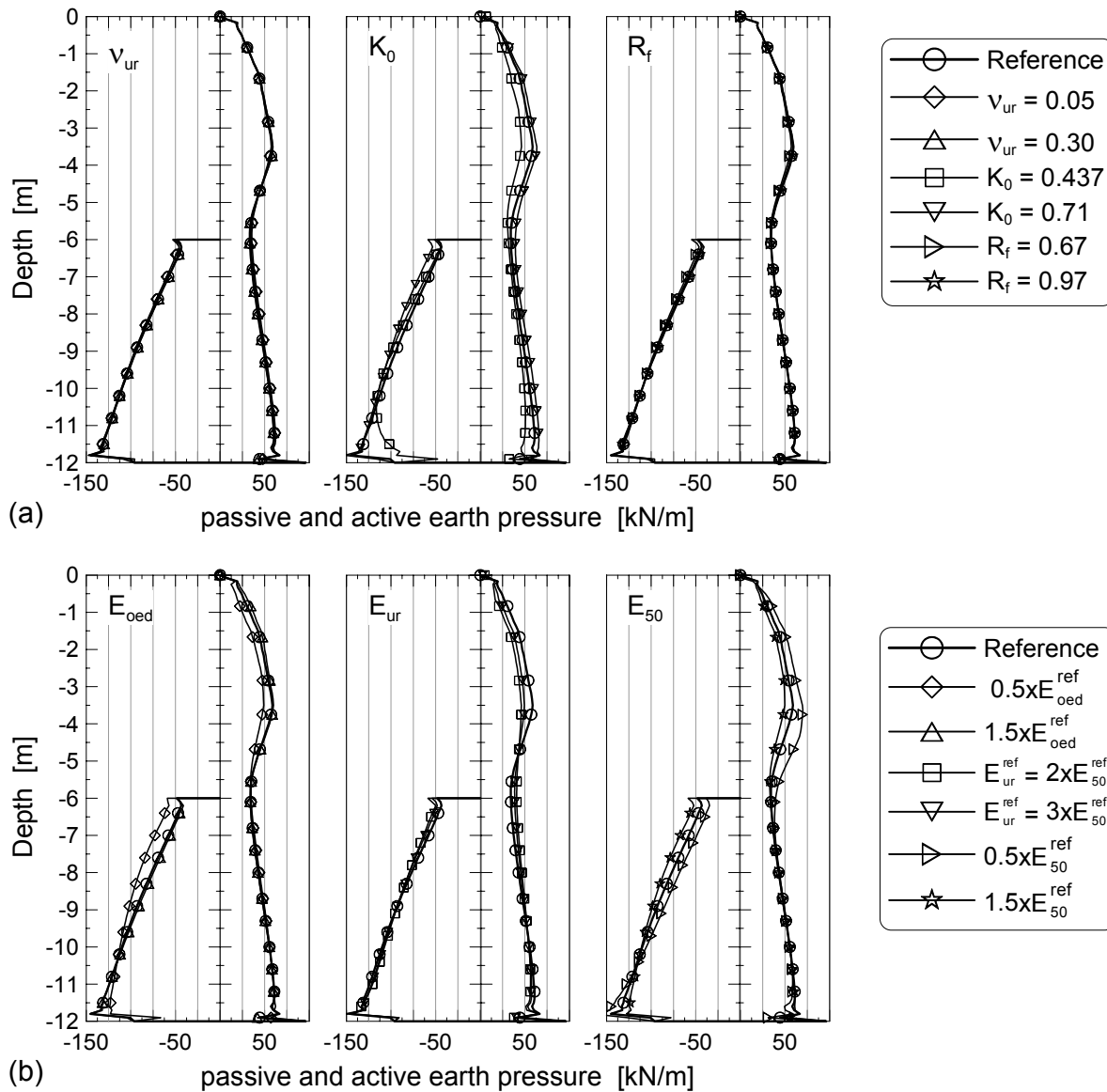

Figure 7.19: The influence of a) ν_{ur}, K_0^{nc} and R_f, and b) E_{oed}, E_{ur}, and E_{50} on the earth pressure distribution under fully drained condition

The effect of the variation of the constrained modulus E_{oed}:

As shown in Figures 7.18b to 7.22b (left), a variation of the constrained modulus E_{oed} by about ∓50% its reference value, has resulted in a change of the maximum wall deflection by about -30

and 5% respectively. Similarly, a change of the heave by about -17 and -4%, a change of the surface settlement by about -24 and 2%, a change of the maximum earth pressure above the bottom of excavation by about -17 and 2%, and a change of the bending moment by about -23 and 3% respectively were observed (Figures 7.18b to 7.22b (left)). Hence, the following conclusion may be drawn with regard to the response of the excavation to the change of E_{oed}.
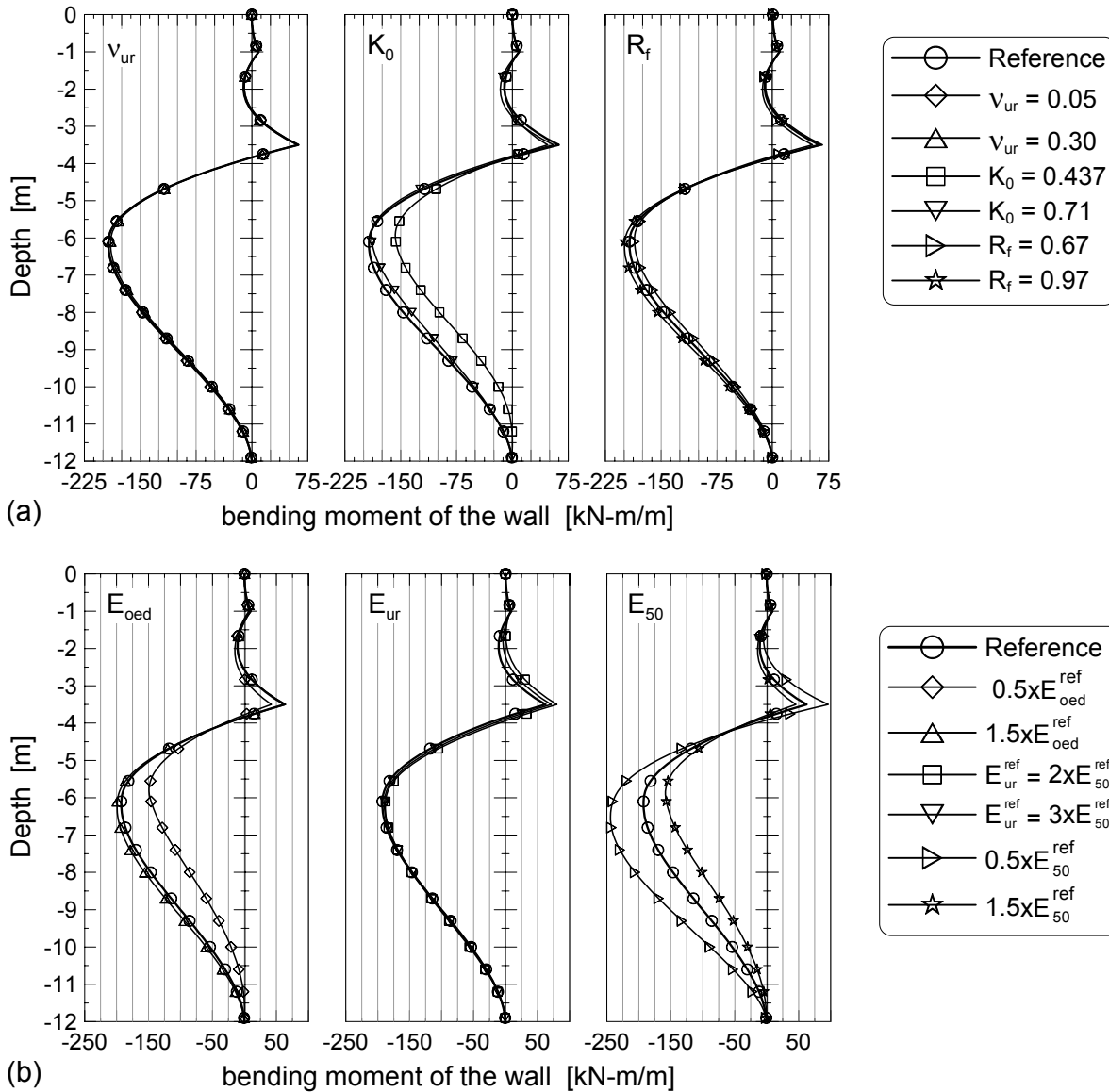

Figure 7.20: The influence of a) ν_{ur}, K_0^{nc} and R_f, and b) E_{oed}, E_{ur}, and E_{50} on the bending moment of the wall under fully drained condition

a) In all cases the E_{oed} is more sensible to a change of value below the reference value than to value greater than the reference. It can be seen from Figures 7.18b to 7.22b (left) that a reduction of the reference value of the E_{oed} by 50% has caused a reduction of the wall and soil

movements, the active earth pressure and the bending moment by about 17 to 30%, whereas increasing the reference value by same amount (50%) show no significant influence (2 to 5%). Maybe the ratio of the E_{50} /E_{oed} is more important than the absolute value of the E_{oed}. For the reference case this ratio becomes 1.1. If the E_{oed} is increased or decreased by 50%, the ratio becomes 0.73 and 2.20 respectively. The ratio in the case of increasing the E_{oed} is more closer to the reference ratio than the other way round. This might be the reason why the change of the E_{oed} is more sensible to a value below the reference than above the reference value.

b) Contrary to expectation, a reduced value of E_{oed} has resulted in a reduced wall and soil moments.

c) Figure 7.19b (left) shows a reduced active pressure and an increased passive pressure for the case of E_{oed} smaller than the reference value. This again contradicts with the reduced wall movement that is discussed in (b). A reduced wall movement would have resulted in an increased active pressure and reduced passive pressure.

d) A reduced active pressure on one side and an increased passive pressure on the other side has resulted in a reduced bending moment, which seems logical in respect to the given loading condition but not in the general sense.

The effect of the variation of the un/reloading modulus of elasticity E_{ur}:
The reference value of E_{ur} was directly taken from triaxial test result (Table 6.7) and it is equal to $5.9 \cdot E_{50}^{ref}$. Lowering the reference value to $3.0 \cdot E_{50}^{ref}$, which is usually recommended in practice with the absence of a test result, and further lowering the reference value to $2.0 \cdot E_{50}^{ref}$ has resulted in an increase of the displacement of the toe of the wall by about 27 and 63% respectively. Similarly, a change of the heave of the bottom of excavation by about 75 and 150%, a change of the surface settlement by about -15 and 30%, a change of the active pressure above the bottom of excavation by about -16 and 22% respectively, and an insignificant change of the maximum bending moment (below 2.5) were observed (Figures 7.18b to 7.22b (middle)). The earth pressure below the excavation level on both active and passive side also shows no significant change relative to the reference value. Contrary to the expectation, the settlement at the surface for the reduced values of the E_{ur} is less than that from the reference value. This is mainly due to the upward displacement of the wall. The whole soil body seems to heave due to lower values of the E_{ur}

The effect of the variation of the secant modulus of elasticity E_{50}:
Figures 7.18b to 7.22b (right) show the effect of the variation of the E_{50} by $\mp 50\%$ from its reference value. These variations of the E_{50} have resulted in a change of the maximum wall deflection by about 45 and -24% respectively. Similar change of the heave by about 21 and 11%, the surface settlement by about 71 and -37%, the maximum earth pressure above the bottom of excavation by about 19 and -15%, and the maximum bending moment by about 27 and 18% respectively were observed (Figures 7.18b to 7.22b (right)).
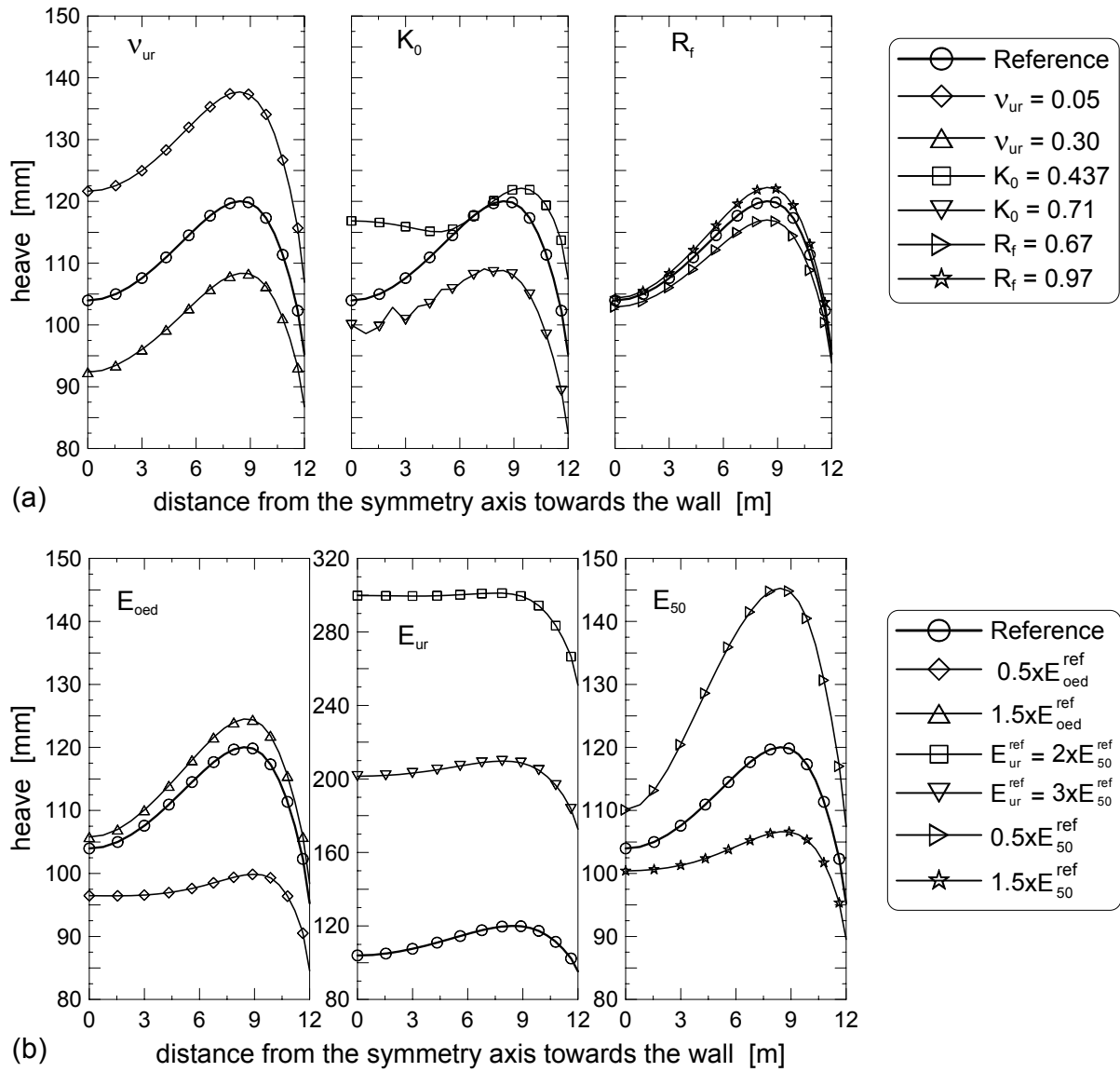
Figure 7.21: The influence of a) ν_{ur}, K_0^{nc} and R_f, and b) E_{oed}, E_{ur}, and E_{50} on the heave at the bottom of excavation under fully drained condition

At first glance, it seems that an increased wall movement should result in higher passive resistance, because the soil is more close to the passive limit state. However, as the numerical study of the mobilisation of the passive resistance in Section 7.4 also shows the passive resistance is lower for lower values of the modulus for a given displacement of the wall and keeping the shear parameter constant. This is exactly what one can observe in Figure 7.19b (right). Lower E_{50} leads to higher wall movement but a lower passive resistance and vice versa.
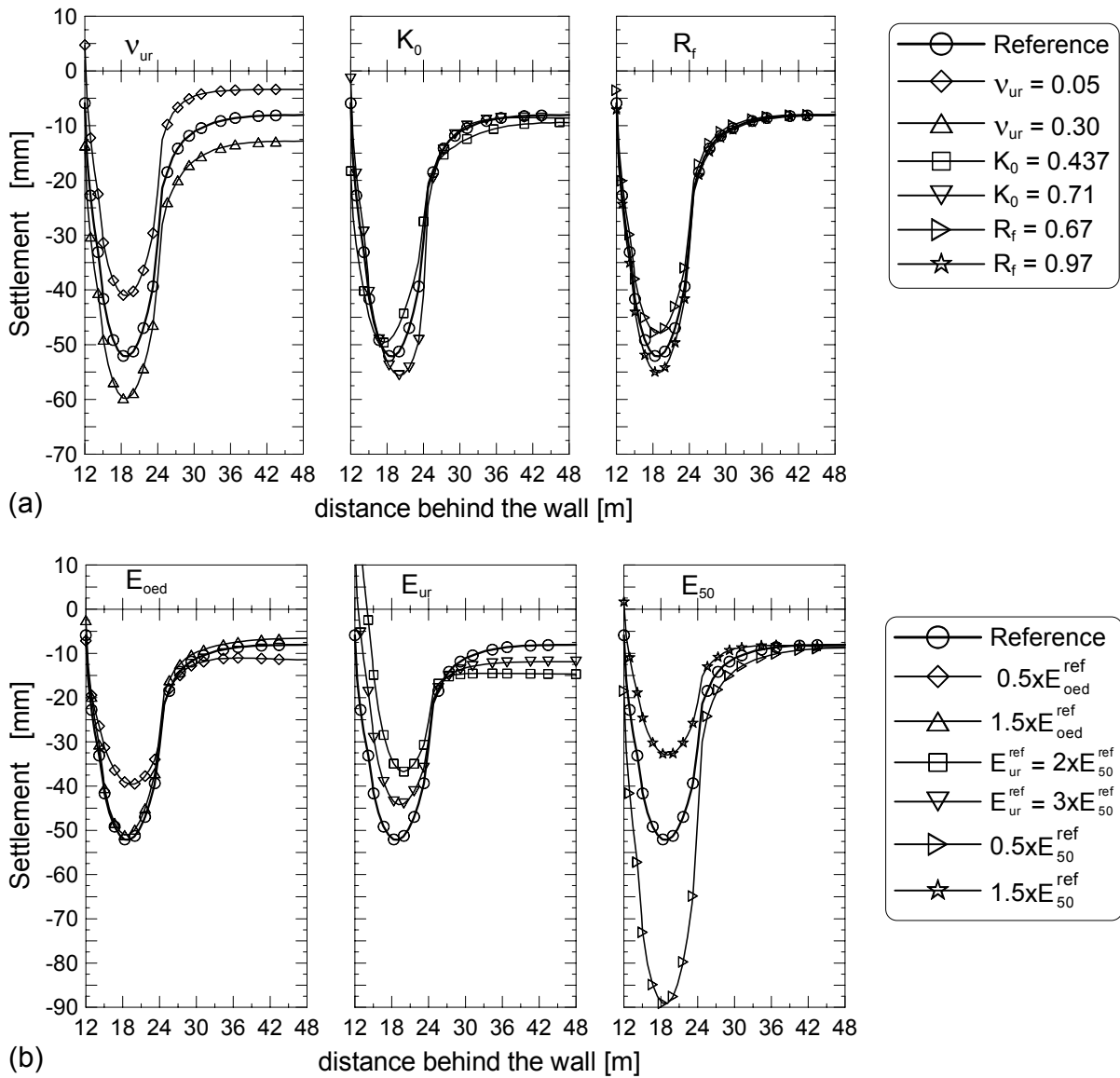
Figure 7.22: The influence of a) ν_{ur}, K_0^{nc} and R_f, and b) E_{oed}, E_{ur}, and E_{50} on settlement at the surface behind the wall under fully drained condition

7.3.3.2 Undrained condition

For a reason of comparison, the HSM parameters in Table 7.1 were adopted as a reference pa-
rameters for the soil body in the undrained analysis of the idealised excavation problem in Figure
7.17 similar to the drained analysis. As it was already mentioned in Section 7.2.2.1, it is possible
to perform undrained analysis with the PLAXIS program using the effective shear and stiffness
parameters. The parameters for the contact element were the same as the drained analysis except
that the analysis was undrained. The construction steps followed in the undrained analysis were

also the same as the drained analysis. However, the undrained behaviour was ignored in the first three calculation phases.

The results of the sensitivity study for the case of end of excavation under undrained condition are shown in Figures 7.23 to 7.28.

The effect of the variation of ν_{ur}, R_f and K_0^{nc} :
Figures 7.23a to 7.28a (left) show a negligible influence of the variation of ν_{ur}. Similarly, the variation of R_f has shown no significant influence on the wall and soil movements, earth pressure and bending moment of the wall (Figures 7.23a to 7.28a (right)).
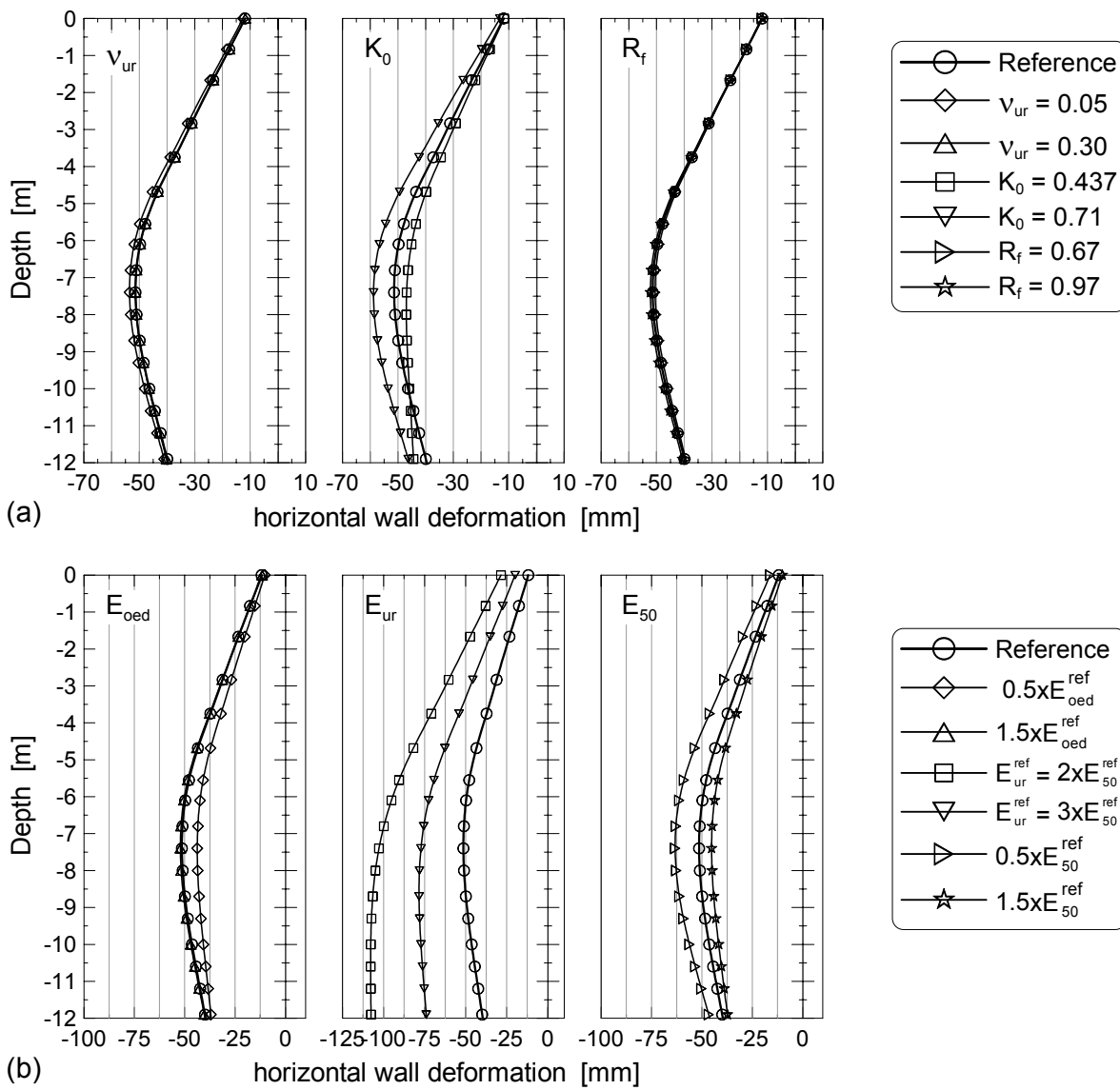

Figure 7.23: The influence of a) ν_{ur}, K_0^{nc} and R_f, and b) E_{oed}, E_{ur}, and E_{50} on the deflection of the wall under undrained condition

On the other hand the variation of the K_0 from the reference value to the lower and upper limit value has resulted in a change of the maximum wall movement by about -9 and 14%, a change of the maximum heave of the bottom of excavation by about 7 and 2%, a change of the maximum settlement at the surface by about -5 and 6%, a change of the active earth pressure by about -10 and 9%, and a change of the maximum bending moment of the wall by about -19 and 10% respectively (see Figures 7.23a to 7.28a (middle)).

In most of the cases shown in Figures 7.23a to 7.28a, the maximum heave has occurred at about 3 m away from the wall, except the case with $K_0^{nc} = 0.437$, where the maximum heave has occurred at the middle of the excavation.
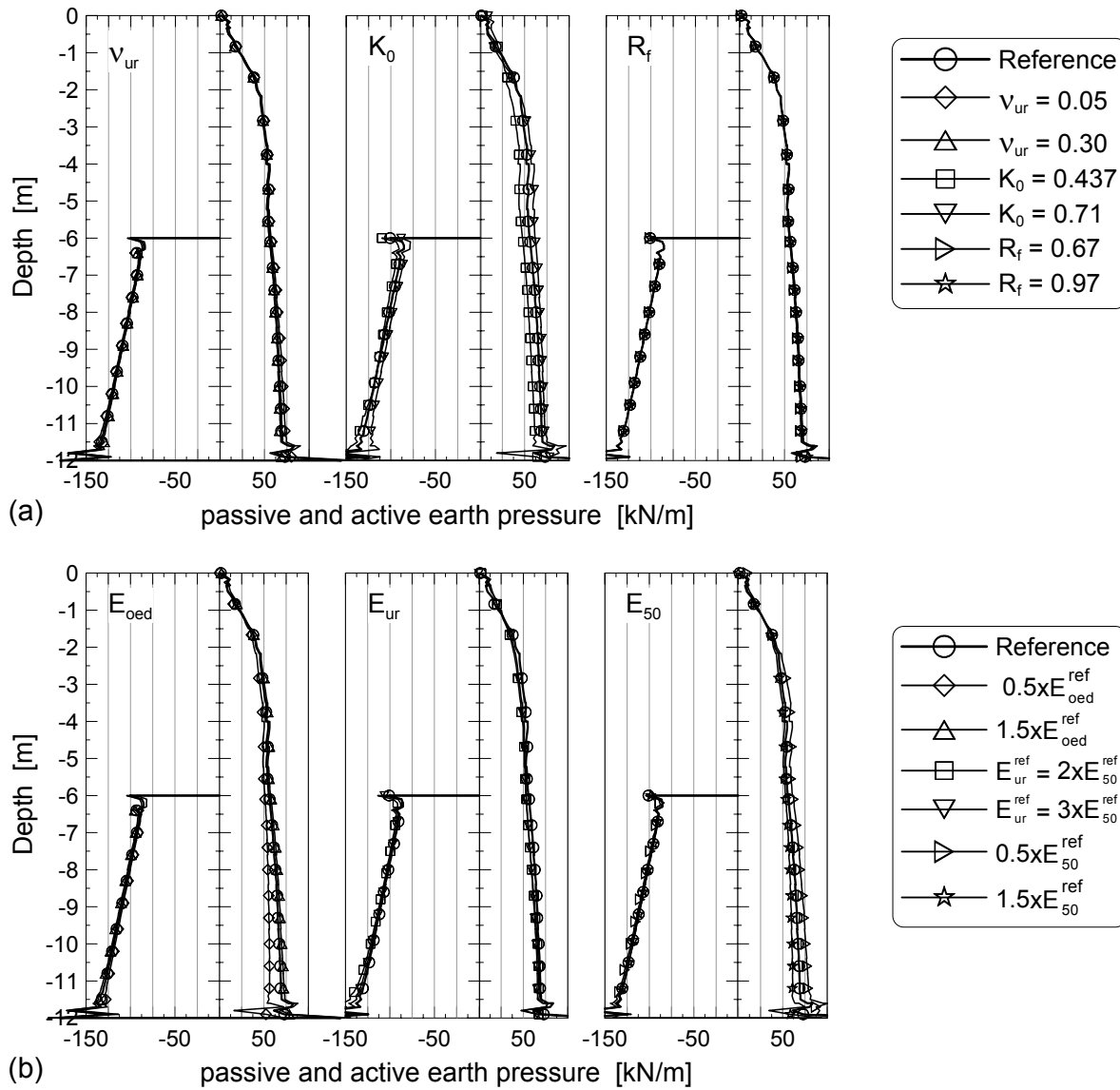

Figure 7.24: The influence of a) ν_{ur}, K_0^{nc} and R_f, and b) E_{oed}, E_{ur}, and E_{50} on the effective earth pressure distribution under undrained condition

The effect of the variation of E_{oed}, E_{ur} and E_{50}:

The effect of the E_{oed} can be seen in Figures 7.23b to 7.28b (left). From these figures, a similar surprise as in case of drained analysis (Section 7.3.3.1) may be observed, i.e., lowering of the E_{oed} by 50% has led to a reduction of the maximum wall movement and the maximum bottom heave by about 15% and the maximum settlement at the surface by about 18%. This is again contrary to the expectation, where a lower value of the deformation parameter E_{oed} would have resulted in a larger deformations of the wall and movements of the soil. On the other hand, increasing the E_{oed} by 50% beyond the reference value seems to have a negligible influence on the wall and soil movements, the earth pressures and the bending moment of the wall. Similar to the drained condition, the ratio of E_{50}/E_{oed} maybe is more important than the absolute value of the E_{oed}.
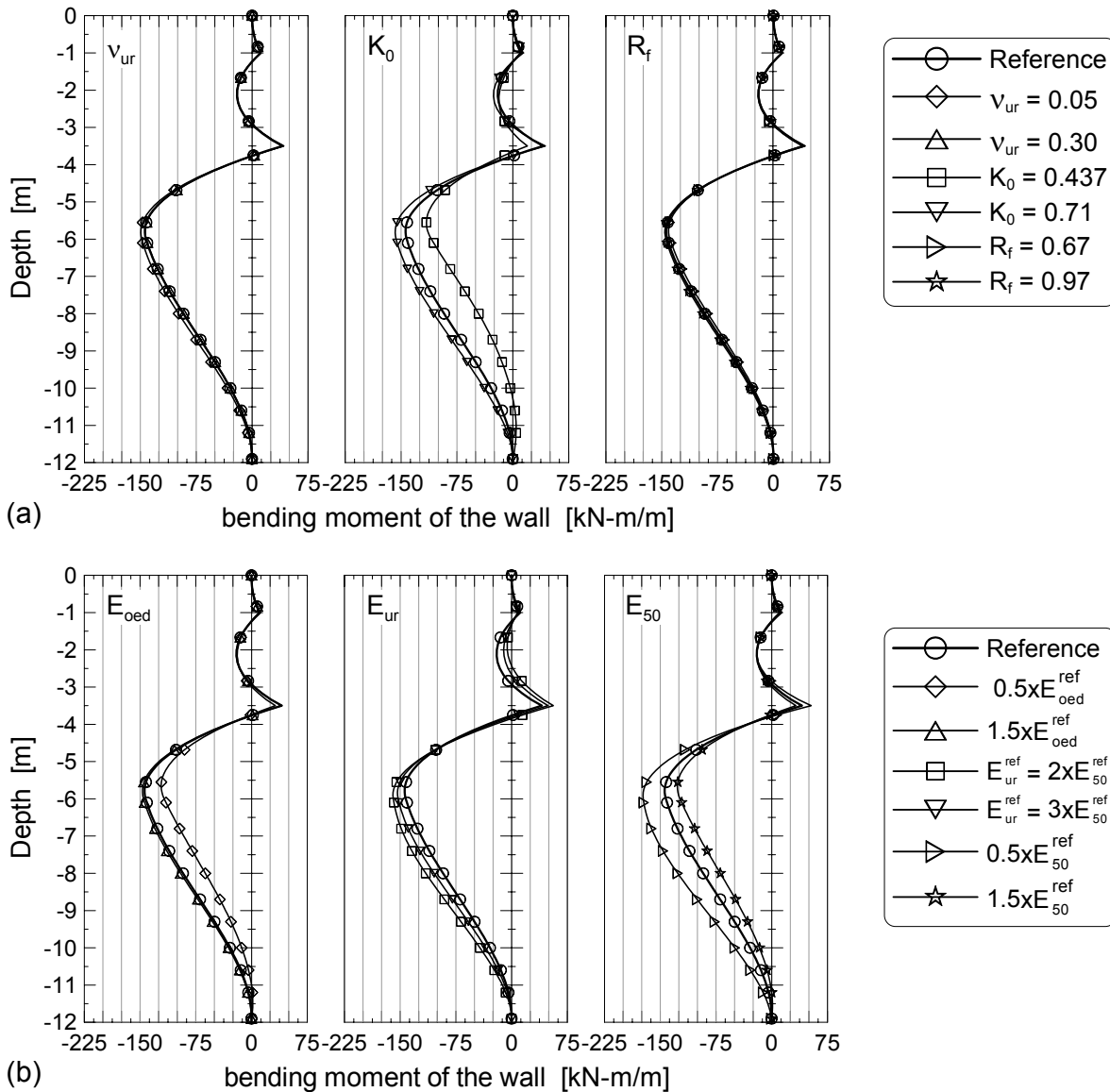

Figure 7.25: The influence of a) ν_{ur}, K_0^{nc} and R_f, and b) E_{oed}, E_{ur}, and E_{50} on the bending moment of the wall under undrained condition

Figures 7.23b to 7.28b (middle) shows the effect of the variation of the E_{ur} from the reference value of $5.9 \cdot E_{50}^{ref}$ to a Lower value of $3.0 \cdot E_{50}^{ref}$ and $2.0 \cdot E_{50}^{ref}$. It appears from the figures that the E_{ur} plays an important role in controlling the wall and soil movements, but it has a small effect on the earth pressure and the bending moment of the wall.
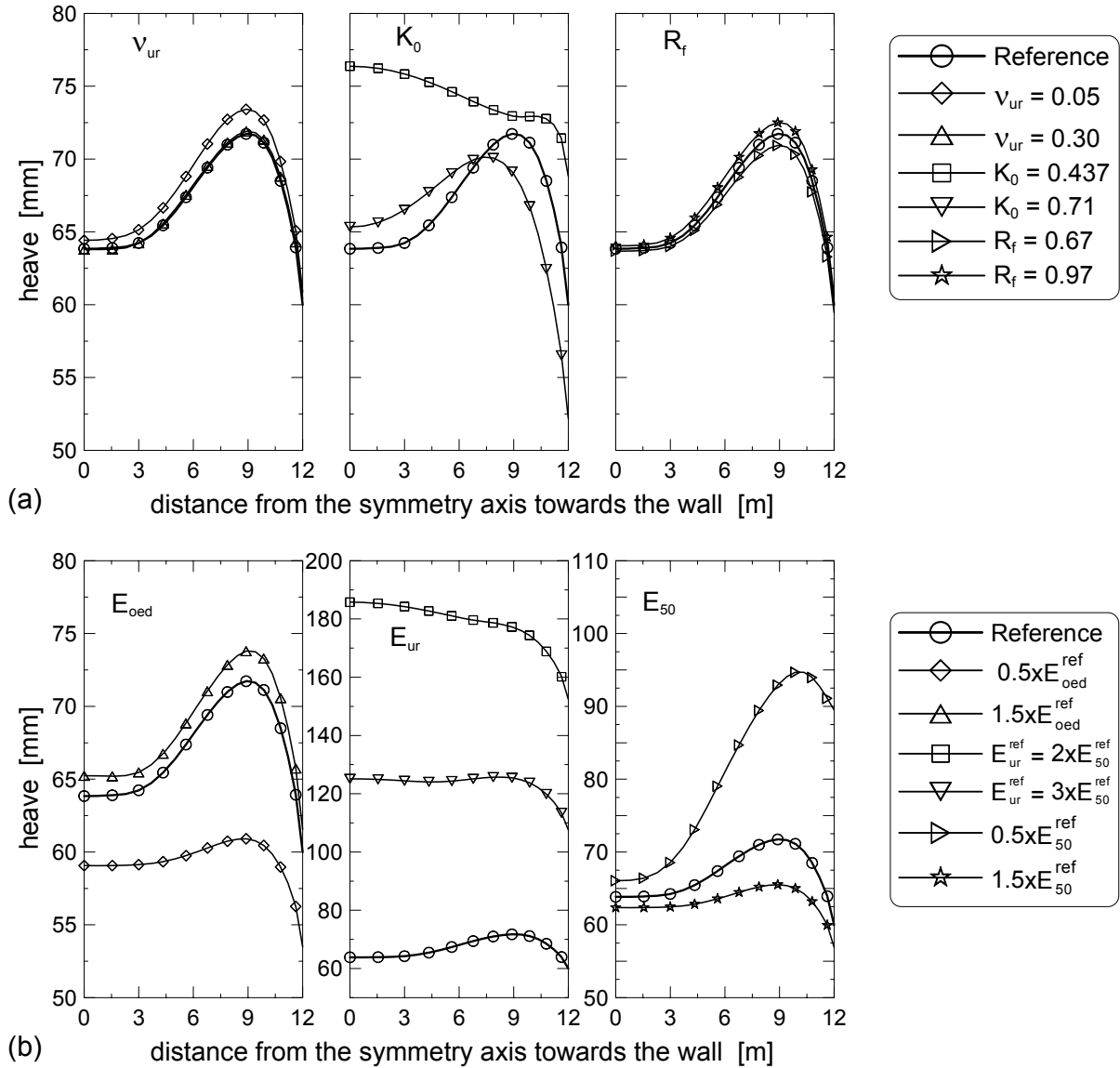

Figure 7.26: The influence of a) ν_{ur}, K_0^{nc} and R_f, and b) E_{oed}, E_{ur}, and E_{50} on the heave at the bottom of excavation under undrained condition

The E_{50} seems to be the only parameter that affect both the wall and soil movements on one hand and the earth pressure and bending moment on the other hand (Figures 7.23b to 7.28b (right)). A variation of the E_{50} by $\mp 50\%$ of the reference value has led to a change of the maximum wall movement by about 23 and -12%, the maximum heave at the bottom by 32 and -9%, the maxi-

mum settlement at the surface by 34 and -18%, the active pressure by about 17 and -12%, and the maximum bending moment by about 20 and -12% respectively. It obvious that the parameter E_{50} is more sensible to a value lower than the reference value than to a higher value because of the non-linearity of the soil model.
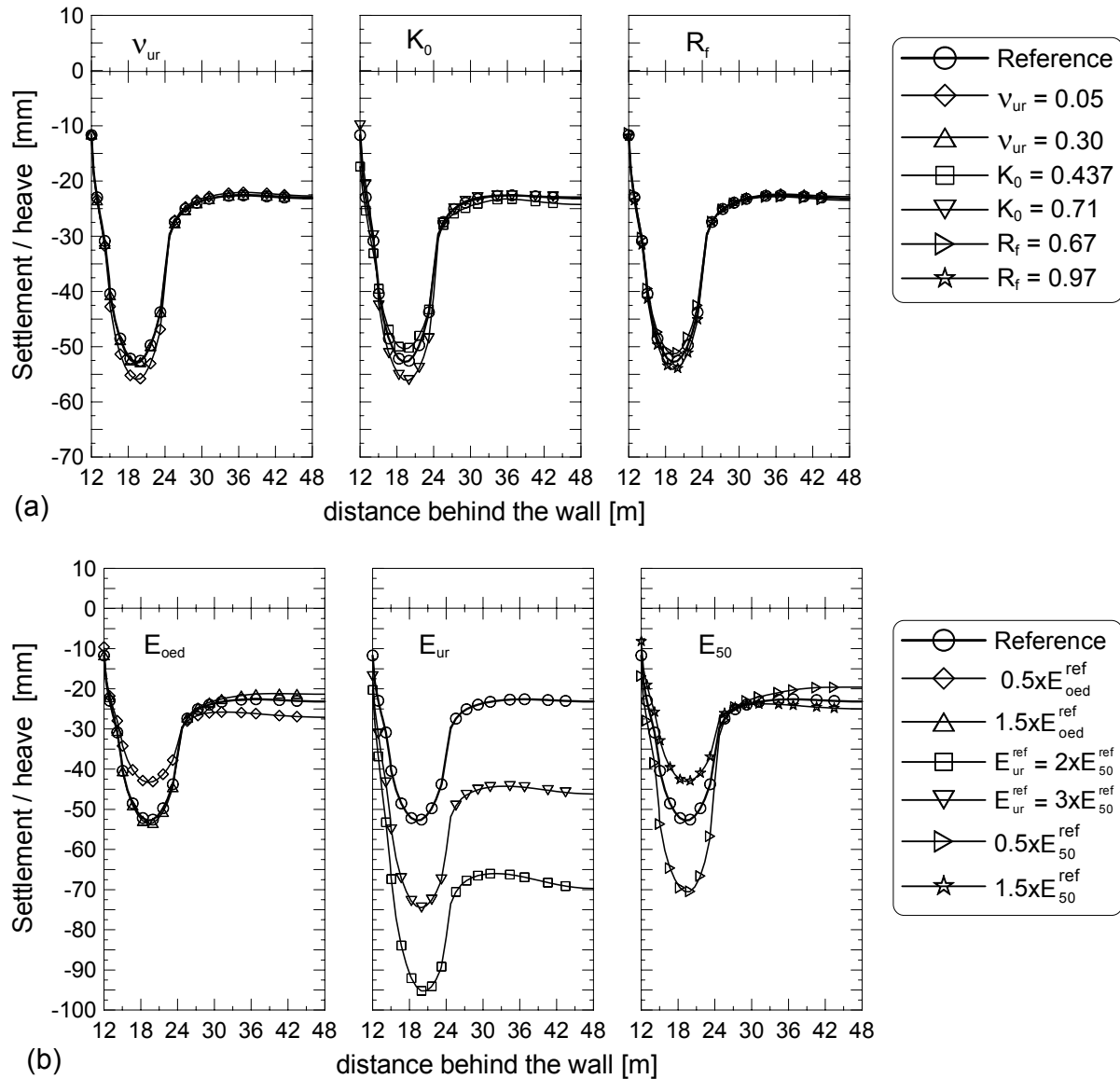

Figure 7.27: The influence of a) ν_{ur}, K_0^{nc} and R_f, and b) E_{oed}, E_{ur}, and E_{50} on the settlement at the surface behind the wall under undrained condition

The effect of the parameters ν_{ur}, R_f, K_0^{nc}, E_{oed}, E_{ur}, and E_{50} on excess pore water pressure: The sensibility of the excess pore water pressure to the variation of the HSM parameters is shown in Figure 7.28. As shown in the figure, three points were selected for the sensibility study: one at the middle of the excavation and just below the bottom of the excavation (Point B), one near the

wall and just below the bottom of excavation(Point C), and the other just below the wall toe (Point E). It can be seen from the Figure 7.28 that the excess pore water pressure is more sensible to the variation of the K_0^{nc} value (Figure 7.28a) and the parameter E_{ur} (Figure 7.28b). The influence of this two parameters on the excess pore water pressure is abundantly clear at Point E. At this point the other parameters v_{ur}, R_f, E_{oed} and E_{50} did also affect the excess pore pressure to some extent. It can be seen from the relative shear shading for the reference case (Figure 7.28c) that the soil around point E is at failure or near failure, whereas the point B is far away from failure. Almost $3/4^{th}$ of the strength of the soil around point C is already mobilised. It was observed in Section 7.2.2.3 that the influence of some parameters starts first while the soil approaches failure. This maybe the reason why the influence of these parameters at point E is abundantly clear.

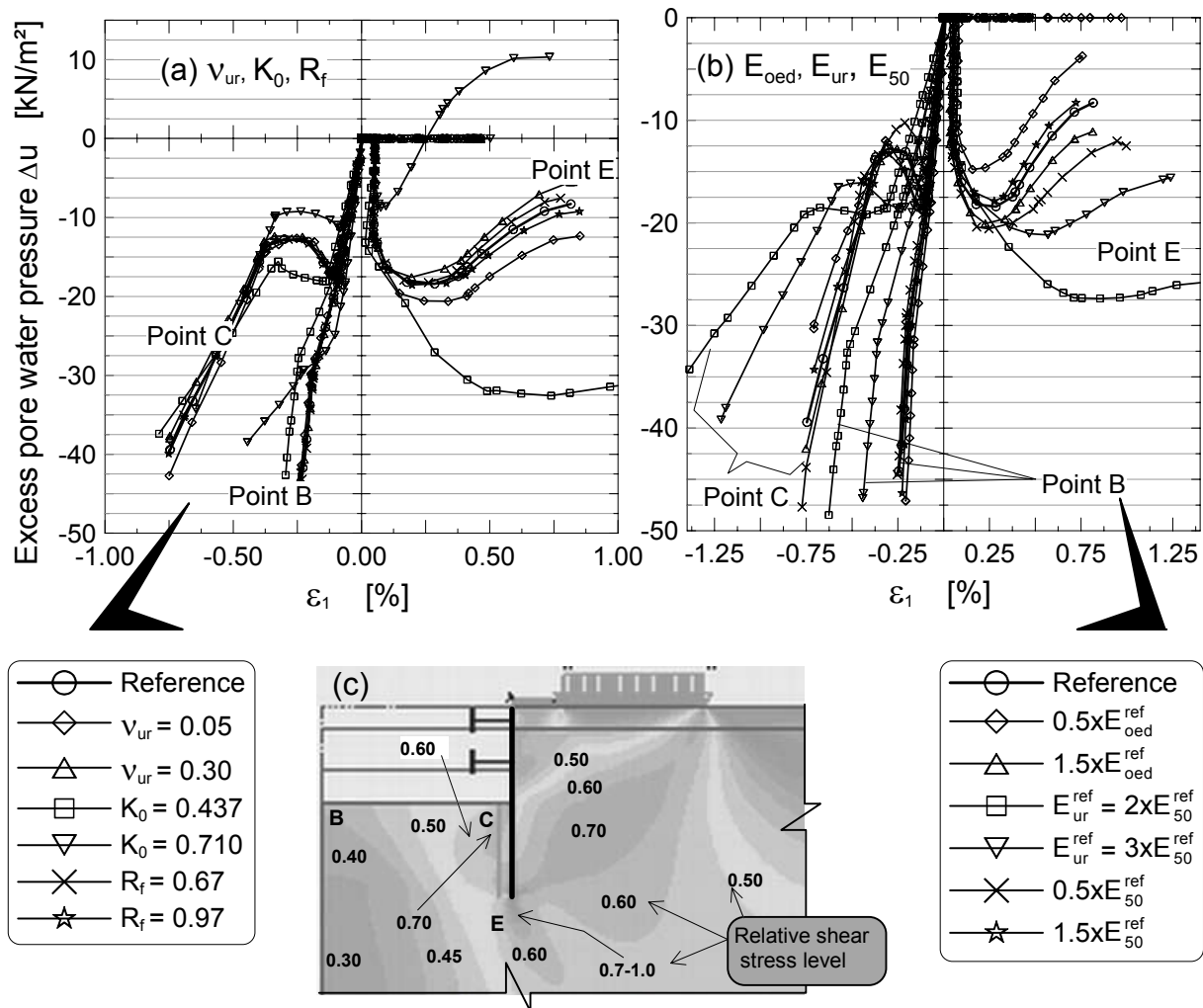

Figure 7.28: The influence of a) v_{ur}, K_0^{nc} and R_f, and b) E_{oed}, E_{ur}, and E_{50} on the development of the excess pore pressure at selective points, and c) the relative shear stresses contour for the reference case

7.3.4   Stress paths in an excavation

Idealised stress paths are shown in Figure 3.15 and Figure 4.4. It is possible to follow some of these stress paths in laboratory in triaxial test apparatus. The question is, however, whether these stress paths represent the actual stress paths in the field, in particular in the case of excavations. To investigate the stress paths at different locations of the supported excavation, representative points as shown in Figure 7.29 were selected. Here a separate FEM -analysis was not conducted, rather the undrained analysis (Section 7.3.4.2) of the idealized excavation problem (Figure 7.17) using the reference parameters from Table 7.1 was adopted to study the stress paths at the given locations. The effective and the total stress paths followed at different locations in the excavation are shown in Figure 7.30. In order to study only the stress paths during the excavation, the stress paths starting from stage 3 (1st excavation) are presented in Figure 7.30.
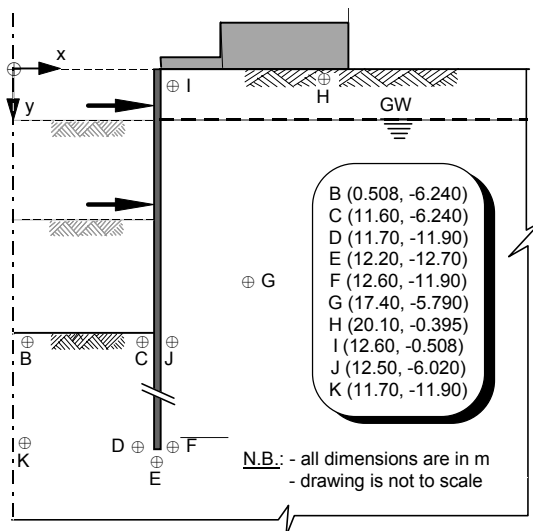

Figure 7.29:

Location of the stress path points

B (0.508, -6.240)
C (11.60, -6.240)
D (11.70, -11.90)
E (12.20, -12.70)
F (12.60, -11.90)
G (17.40, -5.790)
H (20.10, -0.395)
I (12.60, -0.508)
J (12.50, -6.020)
K (11.70, -11.90)

N.B.: - all dimensions are in m
        - drawing is not to scale

Figure 7.30a shows both the effective and total stress paths at points (B, C, D and K) at the passive side of the wall below the bottom of excavation. As expected all the stress paths at these points lie on the extension zone (below the K_0 - *line*). The total stresses at locations B and K follow a path downwards towards left, whereas the effective stresses follow a vertically downward path. The total stress path at these points are fairly comparable with the stress path OD in Figure 3.15 or stress path D in Figure 4.4, i.e the vertical decrement of the stress was more dominant than the horizontal increment of the stress due to the wall movement.

The total stress path at location C first runs parallel to the stress path at B (stage 3), then changes its direction downward with a slight inclination to the right and then to the left (stage 4), and finally it deflects to the left and follows the path parallel to the stress path at point B (stage 5). There is no single stress path among the idealised stress paths in Figure 3.15 that can match with

this stress path at point C. One can, however, match the total stress path at C stagewise as follows:

- *Stress path at point C during the 1ˢᵗ excavation (Stage 3) ⇒ Stress path OD (Figure 3.15),*
- *Stress path at point C during the 2ˢᵗ excavation (Stage 4) ⇒ Stress path OF (Figure 3.15),*
- *Stress path at point C during the 3ʳᵈ excavation (Stage 5) ⇒ Stress path OD (Figure 3.15),*

i.e., both the vertical stress decrement due excavation and the horizontal stress increment due to the wall movement has proportionally played a role during stage 4, whereas the vertical stress decrement due to the excavation has remained dominant during stage 3 and 5.
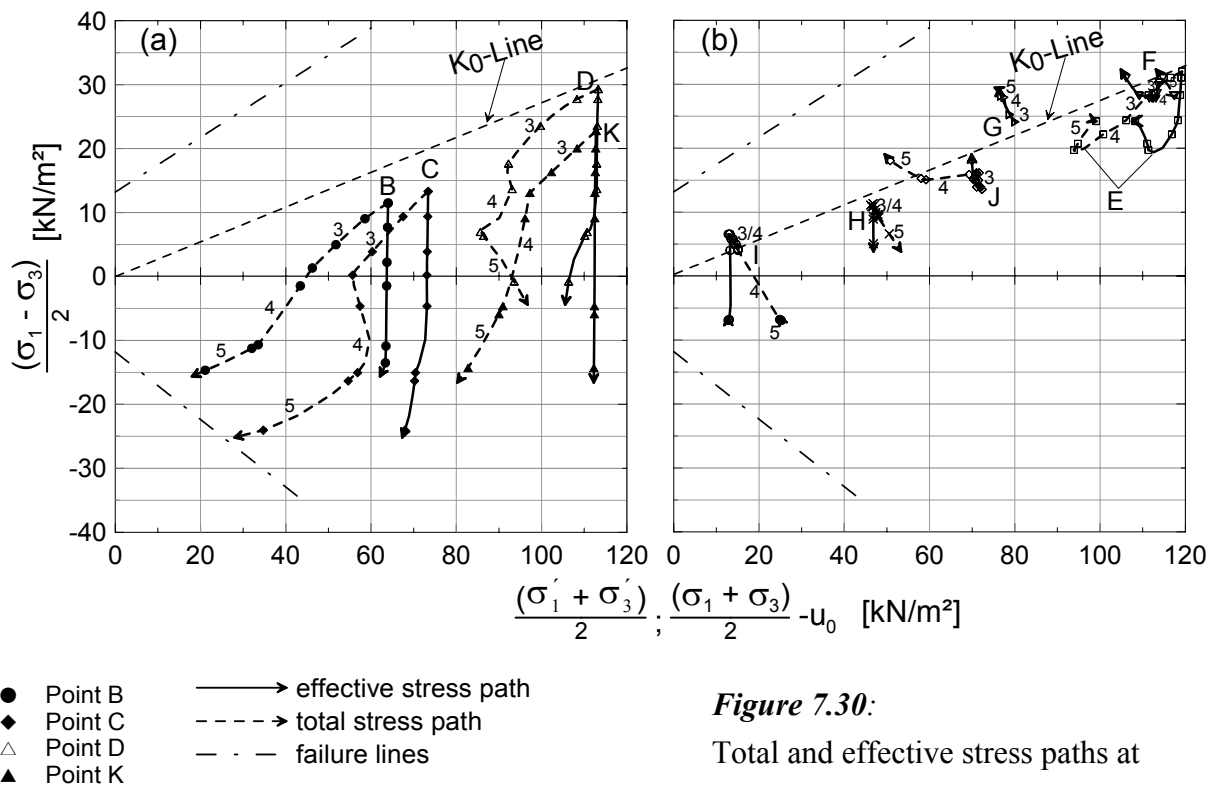

Figure 7.30:

Total and effective stress paths at selective location in an excavation

Similarly, the total stress at point D first follows a parallel path to the stress path at location K (stage 3), then changes its path downwards before it deflects towards left at the end of stage 4, and finally it deflects downward towards the right (stage 5). Again there is no single stress path among the idealised stress paths in Figure 3.15 that can match with this stress path, but it can be fairly matched stagewise as follows:

- *Stress path at point C during the 1ˢᵗ excavation (Stage 3) ⇒ Stress path OD (Figure 3.15),*
- *Stress path at point C during the 2ˢᵗ excavation (Stage 4) ⇒ Stress path OF (Figure 3.15),*
- *Stress path at point C during the 3ʳᵈ excavation (Stage 5) ⇒ Stress path OE (Figure 3.15),*

i.e, the horizontal stress increment due to wall movement was more dominant during stage 5.

Figure 7.30b also shows the effective and total stress paths at points (F, G, H, I and J) at the active side of the wall and at point E just below the toe of the wall. As can be shown from the figure, the stress paths at the active side of the wall may not necessarily all lie with in the compression zone (above the K_0 - *line*). The total stress at point I starts with an upward path towards the left during stage 3 ($\approx$ path OB in Figure 3.15), then it turns its direction by 180° and follows a downward path towards the right during stage 4 ($\approx$ path OE in Figure 3.15), where it completes its path in the extension zone. During stage 5 the total stresses remained constant with a slight change of its direction upwards. There appears to happen a rotation of the principal total stresses at this point.

The total stress at point H follows similar course as the stress path at point I during stage 3 and 4. During the stage 5 it follows its course further downwards towards the right. The total stress at point J follows first a vertical upward path (stage 3), then it turns its direction towards the left with slight inclination downwards (stage 4), before it finally turns its direction upwards towards the left (stage 5) and completes its path in the compression zone.

The point G lies approximately along the active sliding line behind the wall. The total stress path at this location is the only path that starts and ends in the compression zone. It also shows no significant change of direction of its path during the construction stages 3, 4 and 5 and it can be fairly approximated by idealised stress paths OB in Figure 3.15. As can be seen from the Figure 7.30b, the total and effective stress path at point G almost overlap each other, indicating that no significant excess pore water pressure was developed during the excavation phases.

The total stress path at F forms a triangular loop, where it starts its path downwards towards the left (stage 3), then changes its course and runs horizontally towards the right (stage 4), and finally it closes up the loop by changing its course once again upwards towards the left (stage 5). The effective stress path does not close in a rectangular loop showing that there was an excess pore water pressure at this point at the end of the excavation.

The point E is located in a zone where maximum rotation of the principal stresses usually occurs. The total stress path at this point (Figure 7.30b) proves this fact. It starts downward towards the left (stage 3), runs further downward again towards the left but with a moderate slope (stage 4), and finally it changes its course in the upward direction towards the right (stage 5).

The stress paths in Figure 7.30 are only valid for the given excavation case supported by a sheet pile. For other excavation cases and support conditions, a different stress paths maybe possible, but the general trend remains the same.

7.3.5   Effect of berms on deformation of excavations

The FEM-model in Figure 7.17 was adopted to study the efficiency of berms. The geometry, the material properties of the soil, the contact element and the structural elements remain the same as in Section 7.3.3. The construction steps are also the same as in Section 7.3.3, except that the last excavation has been executed stepwise in six additional sub-steps as shown in Figure 7.31. There were two cases investigated. In case 1, the excavation was assumed to proceed from the middle of the excavation towards the wall (Figure 7.31(left)), whereas in case 2 the excavation was assumed to proceed in the opposite direction (Figure 7.31(right)). The soil body in front of the wall is not as such a berm, but since it is there to provide support and hence reduce the soil and wall movements, it is considered as a berm in this parametric study.
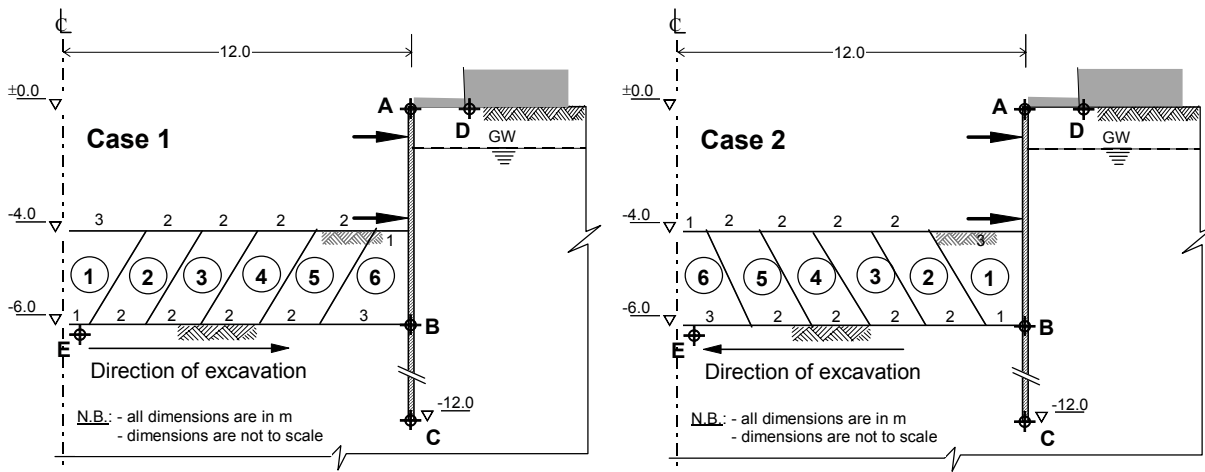

Figure 7.31:   Model for the study of the berm effect

The deformation and displacement of the wall at the locations A, B, and C, the heave of the bottom of excavation at location E, and the settlement at the surface at point D (Figure 7.31) were considered to evaluate the efficiency of the berms. The efficiency was defined as:

$$Efficiency\ [\%] = (1 - \frac{deformation\,/\,heave\,/\,settlement\ at\ the\ end\ of\ each\ stage\ x}{deformation\,/\,heave\,/\,settlement\ without\ berm})\cdot100$$

The results of the parameter study under fully drained condition are shown in Figure 7.32. The efficiency at points A, B, C and D drops rapidly at the beginning (100 - 80%) in both cases and continue to fall linearly or non-linearly in a form a parabolic curve as the volume of the berm decreases. At point E in case 1, however, the efficiency drops slowly at the beginning and joins the other curves later. The reason for the increase of the efficiency at this point beyond 100% in case 2 is that the soil at this point was undergone settlement rather than heave during the first excavation.
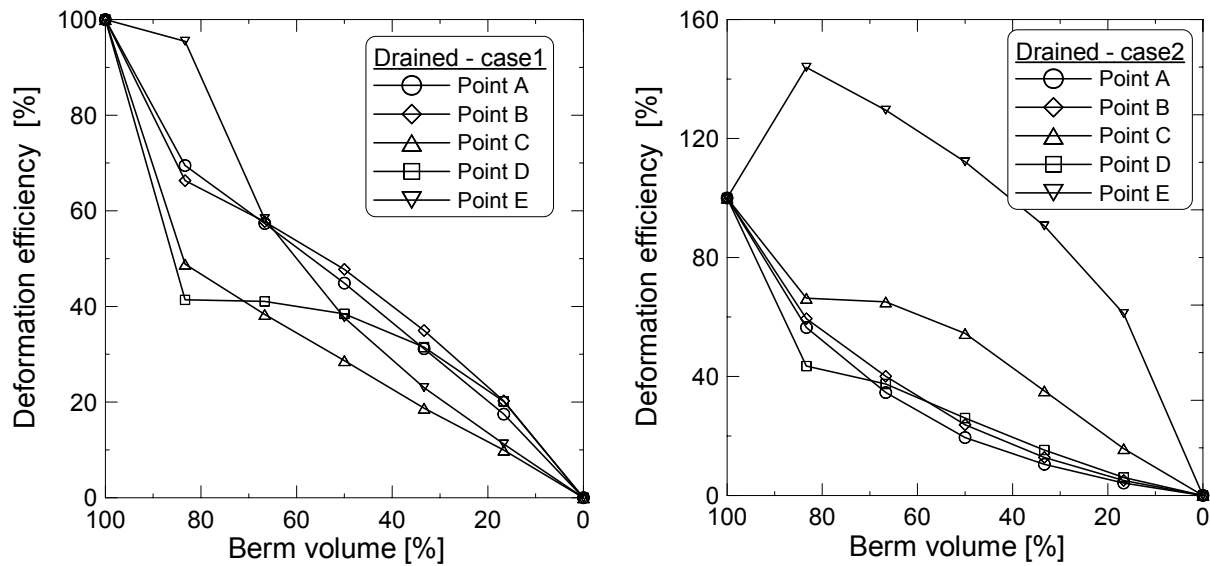
Figure 7.32: Efficiency of berms under fully drained condition

For the case of the undrained condition and case 1, the efficiency lines of all points are almost linear with the exception of point E, which follows an inverted parabolic shape (Figure 7.33(left)). On the contrary, the efficiency lines of all points in case 2 are non-linear with the exception of point C, which follows a linear line (Figure 7.33(right)). It can be seen from Figure 7.33(right) that no support can be expected for a berm volume of $\leq 20\%$.
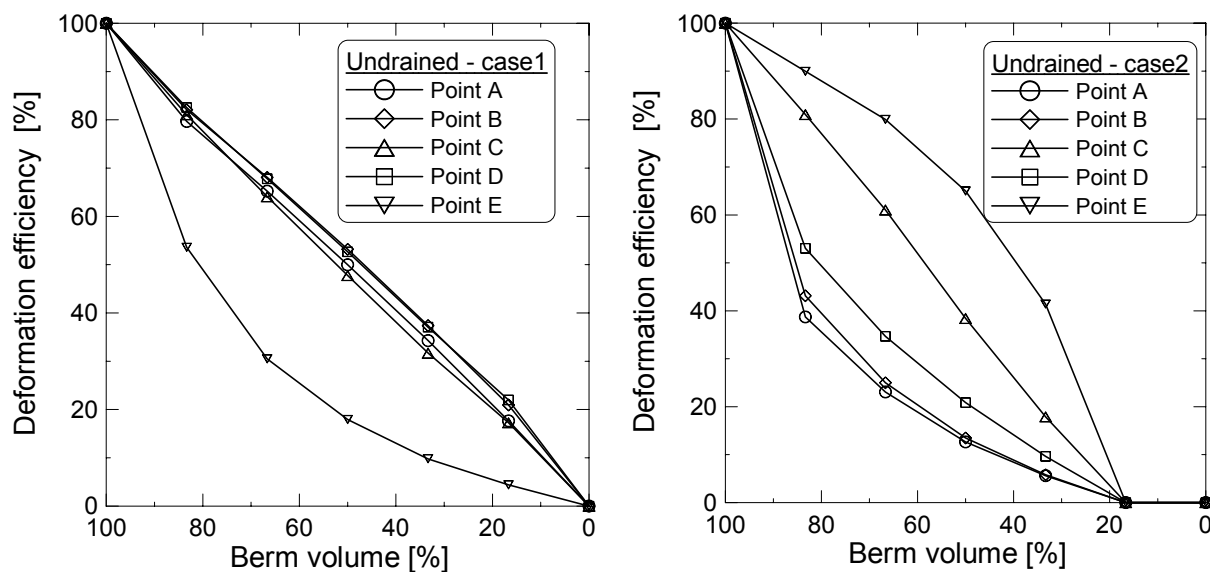

Figure 7.33: Efficiency of berms under undrained condition

It would appear from Figure 7.32 that about 40% berm volume may help to reduce the settlement at the surface (point D) by about 35 and 20% for case 1 and case 2 respectively under drained condition. Similarly, for the case of undrained condition (Figure 7.33) about 43 and 15% reduction of the settlement at the surface (point D) may be achieved with a berm volume of 40% for the case 1 and case 2 respectively. As far as the settlement at the surface and the wall movements are concerned, the second way of handling the excavation (case 2) may not help much to increase the efficiency of the berms.

7.3.6 Effect of the bottom support

Again the FEM-model in Figure 7.17 was used to study the effect of bottom support except that here a bottom support is introduced at different stage of constructions. The geometry, the material properties of the soil, the contact element and the structural elements remain the same as in Section 7.3.3. As a bottom support, a 50 cm thick concrete slab with a stiffness EA = $15 \cdot 10^6$ kN/m was assumed. The cases investigated include:

Case 1:   *Reference situation, i.e., without bottom support*
Case 2:   *Bottom support installed before the 1st excavation*
Case 3:   *Bottom support installed after the 1st excavation but before the 2nd excavation*
Case 4:   *Bottom support installed after the 2nd excavation but before the 3rd excavation*

The locations of the selective points for the evaluation of the deformation efficiency of the bottom support are same as shown in Figure 7.31. These include the deformation of the wall at three locations, namely, at the top (point A) at the bottom of the excavation (point B) and at the toe (point C), the settlement at the surface behind the wall (point D) and the heave at the bottom of excavation (point E). The results of the parametric study are shown in Figure 7.34 and 35. Figure 7.34 shows the effect of the installation of the bottom support at different construction stages on the deformation of the wall at locations A, B and C. The wall at the location A deflects first towards the excavation during the 1st excavation and it deflects back towards the soil during the consequent excavations. As shown in the Figure 7.34 (top-left), the effect of the bottom support on deflection of the wall at the top is mainly limited to prevent the deflection towards the soil. By installing the bottom support before the 1st excavation (case 2), before the 2nd excavation (case 3) and before the final excavation (case 4), an efficiency of about 97, 92, and 36% respectively may be achieved at point B (Figure 7.34 (top-right)). Similarly, an efficiency of about 37, 37, and 24% respectively may be achieved at point C (Figure 7.34 (bottom-left)).

The effect of the installation of the bottom support has a negligible effect on the heave of the bottom of the excavation at point E (Figure 7.35 (right)). At point D, however, an efficiency of about 76, 72 and 29% may achieved for the cases 2, 3 and 4 respectively (Figure 7.35 (right)).

Comparing the efficiency achieved at all points for cases 2 and 3, one can observe that the installation of the bottom support before the 1st excavation would have no significance effect, i.e., a comparable efficiency may be achieved by installing the bottom support before the 2nd excavation.
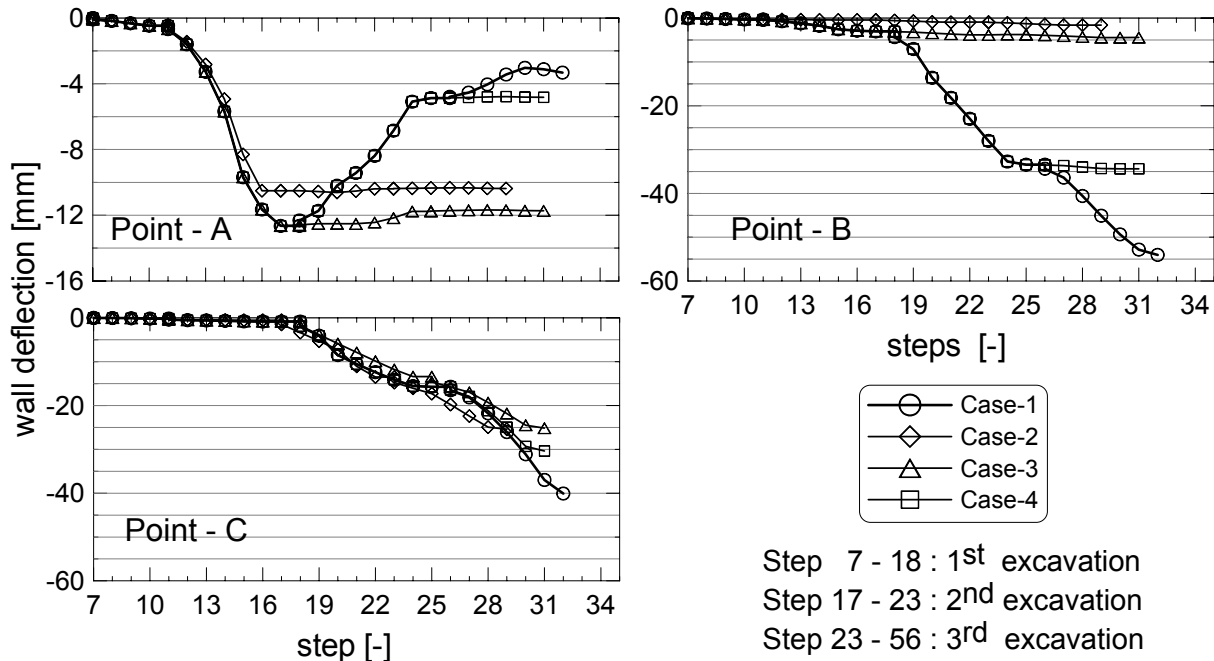

Figure 7.34: The effect of installation of a bottom support at different construction stages on the deformation of the wall at the top (Point A), at the bottom of excavation (Point B) and at the toe (Point C)
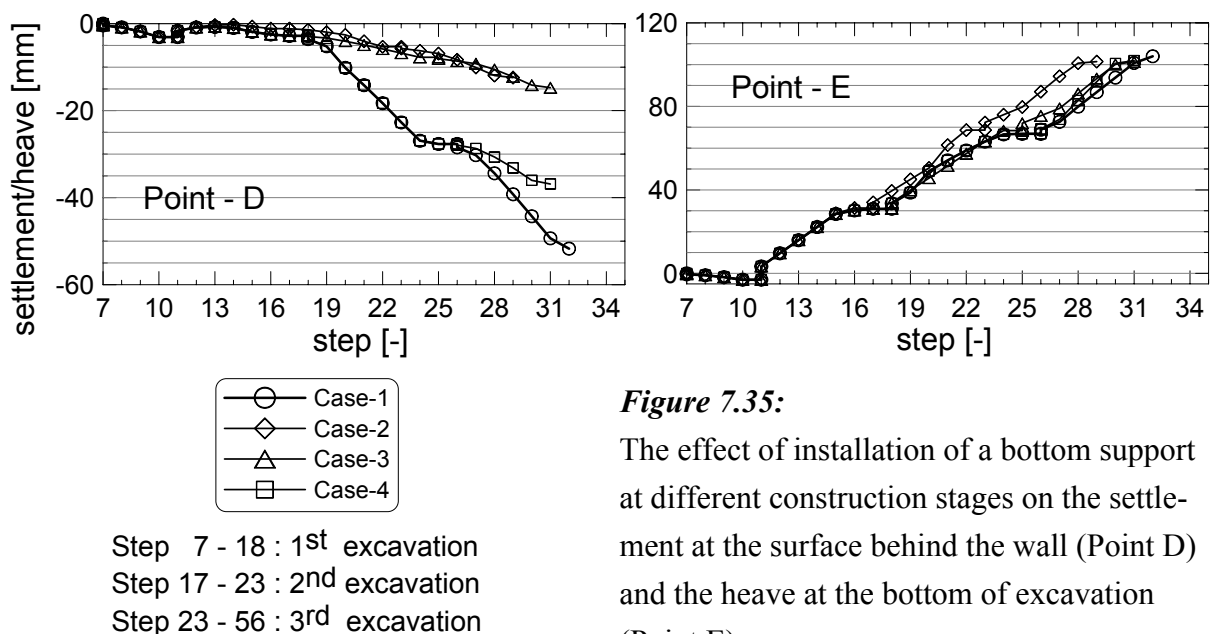

Figure 7.35:

The effect of installation of a bottom support at different construction stages on the settlement at the surface behind the wall (Point D) and the heave at the bottom of excavation (Point E)

7.3.7 Comparison of drained and undrained analysis

One may expect that a drained analysis is nothing other than performing an undrained loading followed by consolidation analysis with an infinite consolidation time (untill the excess pore water pressure approaches to zero). However, because the two types of analysis follow different stress paths, the end result of both analysis may not necessarily be the same. In order to see the difference in the result of the two analysis, a numerical comparison between the drained analysis and undrained analysis followed by consolidation has been conducted. The FEM- model used was the same as that shown in Figure 7.17 except that a 12 m thick sand layer was introduced at the bottom of the model instead of a homogeneous lacustrine soft soil throughout the depth in order to allow drainage downwards. A thick lacustrine soft soil underlain by a moraine (gravely sand) is typical soil profile in the southern Germany town of Constance and the surroundings. The HSM was used to simulate the behaviour of the sand layer and the corresponding parameters are listed in Table 7.5. The following cases have been investigated:

Drained: *drained analysis with reference parameter from Table 7.1*
Undrained: *undrained analysis followed by consolidation analysis after full*
                     excavation (the same parameters as case 1)

For all cases of undrained analysis followed by consolidation, a minimum pore water pressure of 1 kN/m² has been achieved at the end of the consolidation process. The soil was allowed to consolidate first after the full excavation had been reached

Table 7.5:   HSM parameters for the sand layer

γ_{sat}	φ'	ψ'	c'	E_{50}^{ref}	E_{oed}^{ref}	E_{ur}^{ref}	p^{ref}	m	R_f	K_0^{nc}	v_{ur}
[kN/m³]	[°]	[°]	[kN/m²]	[kN/m²]	[kN/m²]	[kN/m²]	[kN/m²]	[-]	[-]	[-]	[-]
21.0	33.0	3.0	1.0	35000	35000	140000	100	0.50	0.90	0.455	0.20

$k_x = k_y = 0.5$ m/day

The result of the numerical study is given in Figure 7.36 and 7.37. The comparison of the deformation of the wall and the soil movements between the two cases listed above have been made at a selective reference points. The location of these reference points are shown in Figure 7.31. The drained and undrained analysis have shown different wall deformations at point A (Figure 7.36 - top-left). At locations B (Figure 7.36 - top-right) and C (Figure 7.36 - bottom - left) the undrained analysis has reached almost the same deformation as the drained analysis before even consolidation started. After the consolidation phase, the deformation at C remains almost unchanged, whereas at B the deformation increased further slowly.
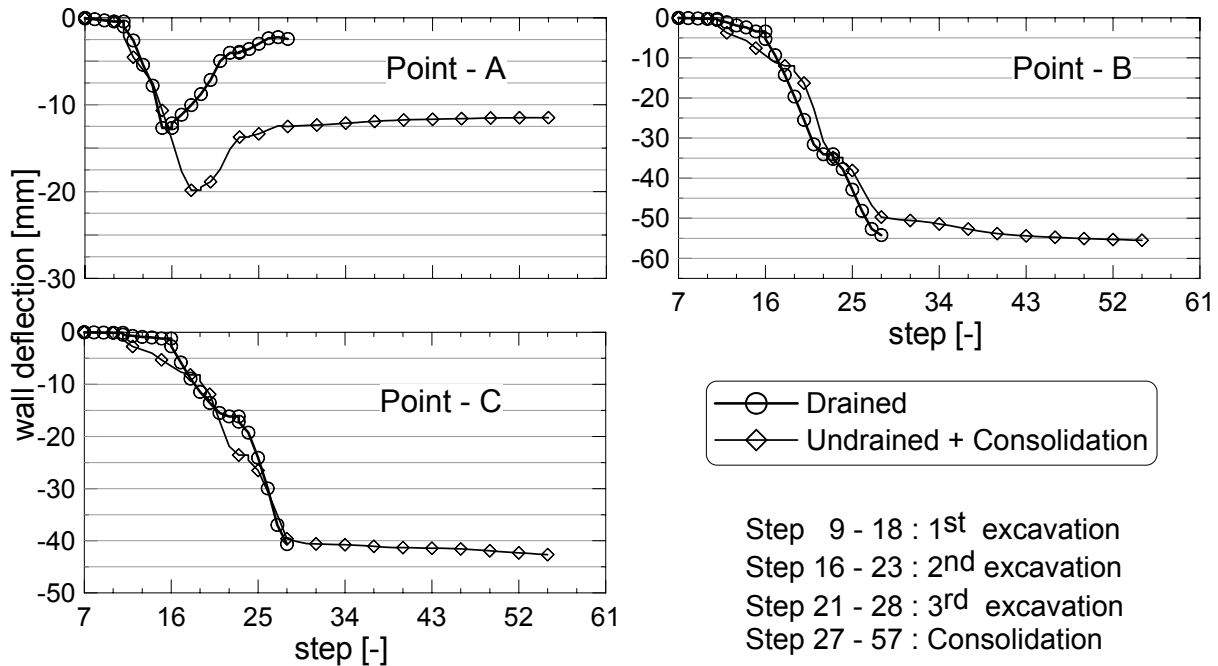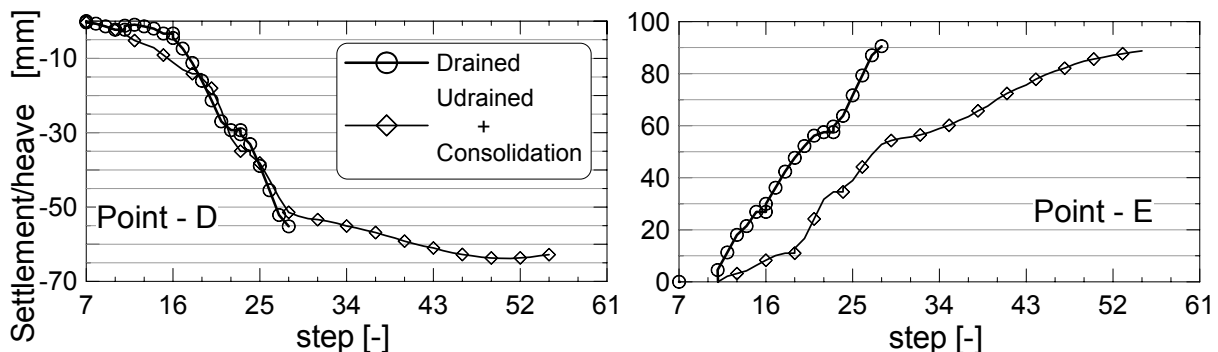
Figure 7.36:   Comparison of the drained and undrained FEM - computation results of the
                deformation of the wall at locations A, B and C

Similar phenomenon may be observed from Figure 7.37 - left, where the undrained analysis has
resulted almost the same settlement at point D even before the consolidation started. On the other
side, the soil at point E (Figure 7.37 -right) has reacted stiffer under undrained condition. The
heave at point E at the end of the undrained analysis followed by the consolidation phase was the
same as that at the end of the drained analysis. As can be seen from the Figure 7.36 and 7.37, no
significant difference in the deformation results of the two undrained analysis cases can be ob-
served except at point A.

Step   9 - 18 : 1st excavation
Step 16 - 23 : 2nd excavation
Step 21 - 28 : 3rd excavation
Step 27 - 57 : Consolidation

Figure 7.37:
Comparison of drained and undrained FEM - compu-
tational results of the settlement at point D and the
heave at point E

To summarise, the wall displacement at the toe and at the level of the bottom of excavation and the surface settlement behind the wall seem to be unaffected by the type of the analysis, whereas more heave at the middle bottom of the excavation was computed from undrained analysis followed by consolidation. This shows that the assumption drained = undrained + consolidation should not necessarily be always true as mentioned previously.

7.4 Stiffness dependent mobilisation of the passive resistance of a cohesive soil

7.4.1 General

In order to mobilise the earth pressure fully, active or passive, a certain wall movement is required. The amount of the movement required depends on the type of the wall movement pattern and soil type. The wall movement required to reach the passive state is of the order of ten times as large as that of the active state. There are four types of wall movements patterns recognised in the literature. These are: rotation of the wall about toe, rotation of the wall about the top, bending of the wall, and lateral translation of the wall. Most often, a combination of the above movement pattern may also takes place. Much experimental work has not been done on the effect of wall movement on earth pressure in clays let alone in soft clay. On the other hand, a lot of experimental works have been conducted on sand. *Besler (1998)* summarised different model tests on sand and one on cohesive soil in his dissertation work. The attempt on all the model tests was to develop a mobilisation function for the passive resistance dependent on the wall displacement. The mobilisation function by different authors have also been discussed in *Besler (1998)*. Based on model tests on sand, *Besler (1998)* had also developed a mobilisation function of the form:

$$K'_{ph}(\xi) = A + \frac{B}{C + \xi} \tag{7.12}$$

where $K'_{ph}(\xi)$ is the mobilised earth resistance; ξ is the ratio between the available wall displacement and the wall displacement at limit state; C is a function of ξ, the earth resistance at limit state K_{ph} and the earth pressure at rest K_0; A and B are a function of C, K_{ph} and K_0. Refer to *Besler (1998)* for a detailed information on the mobilisation function.

In this section an attempt has been made to develop a mobilisation function of the earth resistance dependent on the stiffness of the normally consolidated soft soils with the help of the FE - method. The second objective of this study is to formulate a soil stiffness dependent function of the total safety factor for passive resistance based on the mobilisation function.

7.4.2   Formulation of the problem and model geometry

Three types of the wall movement have been investigated. These are: parallel translation of the wall, rotation of the wall about the top and rotation of the wall about the toe (Figure 7.38). A homogeneous soft soil was assumed, whose behaviour can be simulated using the HSM (Table 7.6). Since the main aim of the study is to develop a soil stiffness dependent mobilisation function of the earth resistance, the stiffness of the soil, namely the $E_{50}^{ref} = E_{oed}^{ref}$ was varied between 0.75 - 10 MN/m² and the ratio $E_{ur}^{ref} / E_{50}^{ref} = 5$ was kept constant. The contact element was simulated using the MCM and its properties are given in Table 7.7. The wall was assumed rigid, elastic and weightless with a stiffness of $EA = 7.5 \times 10^6\ kN/m$ and $EI = 1.0 \times 10^6\ kNm²/m$.
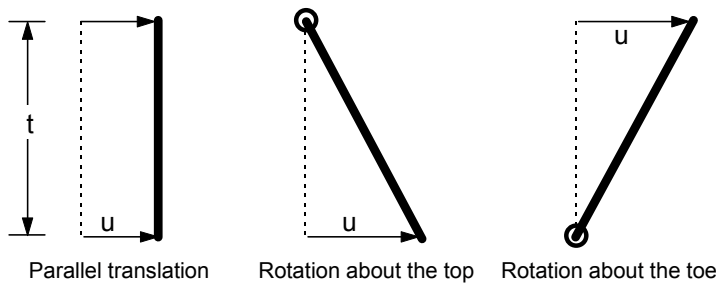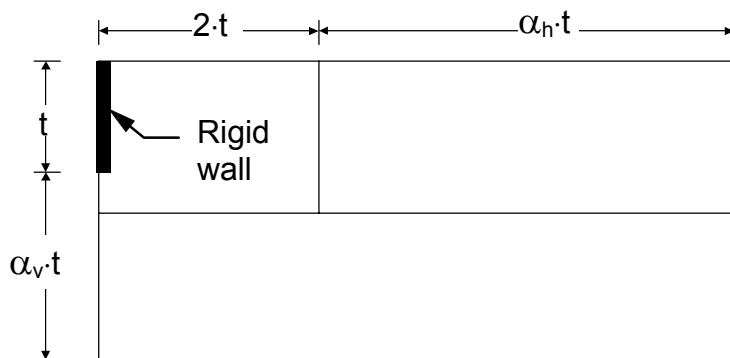

Figure 7.38:
Types of the wall movement

In order to limit the influence of the model geometry on the mobilisation of the passive resistance, a preliminary analysis was performed by varying the width and height of the model as shown in Figure 7.39. The smallest soil stiffness ($E_{50}^{ref} = E_{oed}^{ref} = 0.75 MN/m²$) was assumed in this preliminary study. A uniform prescribed displacement u = 1.2 m in the direction of the soil mass was applied to the 8 m long rigid wall.

Model	α_h	α_v
1	2	1
2	3	1
3	4	1
4	5	1
5	2	2
6	3	2
7	4	2
8	5	2

Figure 7.39:   Selection of model geometry

The result of the preliminary FEM - calculations is presented in Figure 7.40. The figure shows the passive force as a function of the displacement for the various model sizes, but for t = 8 m and $E_{50}^{ref} = E_{oed}^{ref} = 0.75 MN/m²$. As it can be seen from the Figure 7.40, the passive resistance forces obtained from different model sizes lie in a very narrow band showing a negligible influence of the model size. After closed observation of the principal stress orientations and the displacement vectors near the boundaries, and based on Figure 7.40, the model 8 was chosen for a further numerical study of the mobilisation of the earth resistance.

Table 7.6: HSM parameters for the soft soil layer

$\gamma_{sat}^{'}$	$\varphi_s^{'}$	$\psi^{'}$	$c^{'}$	$E_{50}^{ref} = E_{oed}^{ref}$	E_{ur}^{ref}	p^{ref}	m	R_f	K_0^{nc}	v_{ur}
[kN/m³]	[°]	[°]	[kN/m²]	[kN/m²]	[kN/m²]	[kN/m²]	[-]	[-]	[-]	[-]
19.5	25.0	0.0	1.0	750 - 10000	$5 \cdot E_{50}^{ref}$	100	0.90	0.90	0.577	0.20

Table 7.7: MCM parameters for the interface element

γ_{sat}	$\delta = \frac{1}{3} \cdot \varphi_s^{'}$	$\psi^{'}$	$c^{'}$	E_{ref}	$E_{increment}$	y_{ref}	c_{ref}	v
[kN/m³]	[°]	[°]	[kN/m²]	[kN/m²]	[kN/m²]	[kN/m²]	[-]	[-]
19.5	8.33	0.0	0.03	750 - 10000	0.0	0.0	0.0	0.35

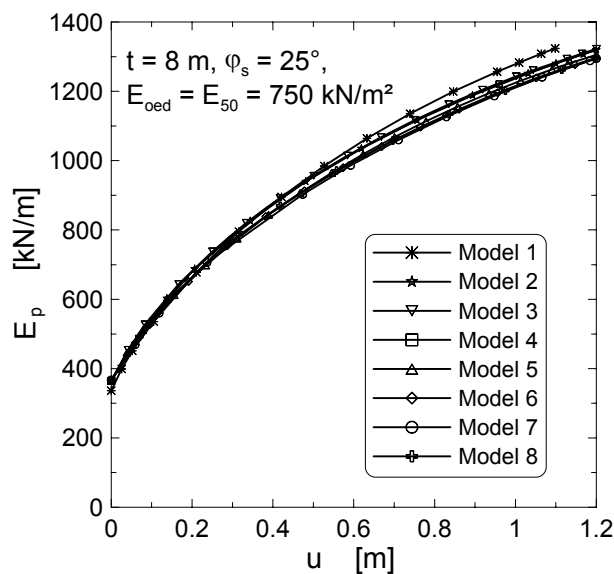***Figure 7.40:***
Mobilised passive force from different model sizes

7.4.3   Mobilisation of the passive earth pressure

Once the model geometry had been fixed and the soil model parameters were identified, the FEM-calculations were started by applying a prescribed displacement u = 1.2 m either uniformly in the case of parallel translation or in a triangular shape with zero at the top and maximum at the bottom in the case of rotation about the toe or again triangular shape but reversed in the case of rotation about the head. Two cases of the height of the wall t = 8 m and t = 4 m, seven variations of the stiffness of the soil $E_{50}^{ref} = E_{oed}^{ref} = 0.75, 1.5, 3.0, 4.5, 6.0, 7.5, 10.0$ MN/m² were investigated. All in all 42 (3 × 2 × 7 = 42) FEM-calculations were performed.

The results of the parametric studies are shown in Figure 7.41. A dimensionless presentation was preferred to avoid the effect of the height of the wall on the results and in order to treat the net resistance instead of the total passive force which includes the earth pressure at rest. The dimensionless mobilised net passive resistant is defined as:

$$K_{p(mob)}^{*} = \frac{(E_{ph} - E_0)}{(\frac{1}{2} \cdot \gamma \cdot t^2)} \tag{7.13}$$

where E_{ph} is the passive force in limit state and E_0 the earth pressure at rest. The dimensionless displacement is also given by u/t. As can be observed from Figure 7.41, the mobilised resistance for t = 8 m and t = 4 m lie on the same line in all cases of the wall movement showing the advantage of using the dimensionless parameters.
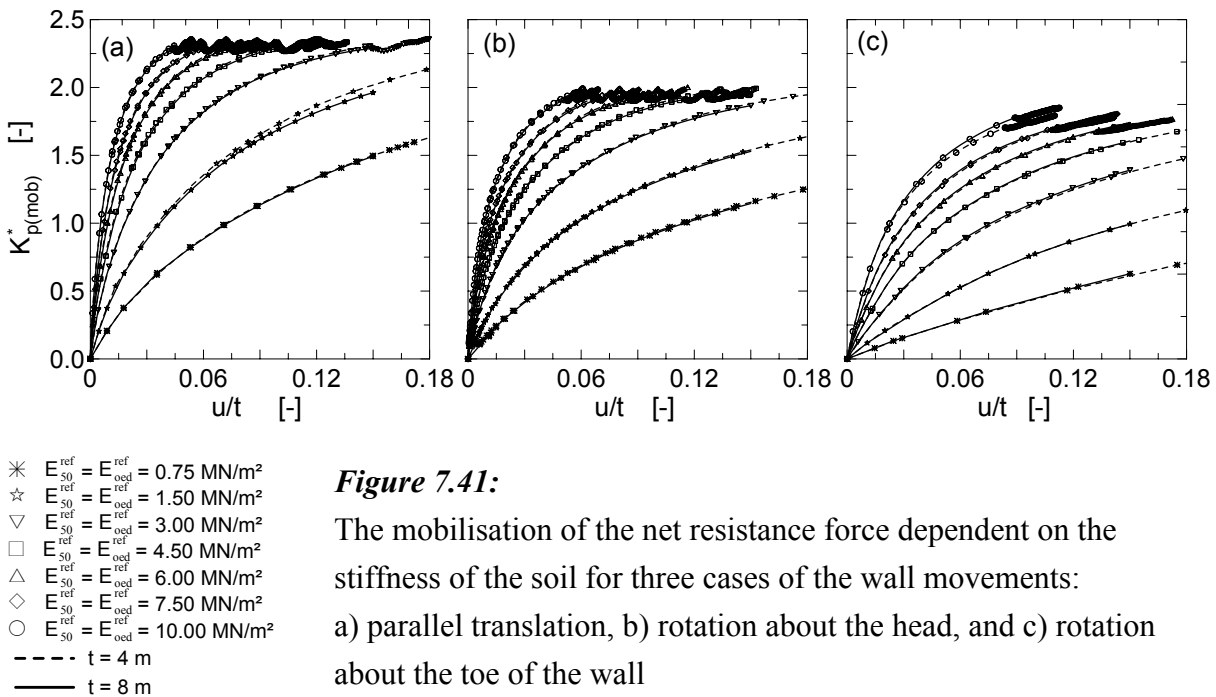

Figure 7.41:
The mobilisation of the net resistance force dependent on the stiffness of the soil for three cases of the wall movements:
a) parallel translation, b) rotation about the head, and c) rotation about the toe of the wall

7.4.4 Derivation of an analytical mobilisation function

The mobilisation curves in Figure 7.41 may be approximated by a hyperbolic function analogue to the *Kondner/Zelasko (1963)* hyperbolic equation as follows:

$$K_{p(mob)}^{*} = \frac{(u/t)}{[a + b \cdot (u/t)]} \tag{7.14}$$

or in a transformed form,

$$\frac{(u/t)}{K_{p(mob)}^{*}} = [a + b \cdot (u/t)] \tag{7.15}$$

where a and b are the intercept and the slope of the transformed straight lines in Figure 7.42. The constants a and b may be obtained from the best fit line of the transformed lines, but the question remains weather there exists a definite relationship between these curve constants and the physical parameters of the soil. Figure 7.43 shows that the curve parameter a may almost be 100% correlated with the normalised stiffness parameter of the soil using a potential function of the form

$$a = \alpha_1 \cdot \left[\frac{E_{oed}}{\gamma \cdot t} \right]^{\alpha_2} \tag{7.16}$$

$\ast$ $E_{50}^{ref} = E_{oed}^{ref} = 0.75$ MN/m²
$\star$ $E_{50}^{ref} = E_{oed}^{ref} = 1.50$ MN/m²
$\triangledown$ $E_{50}^{ref} = E_{oed}^{ref} = 3.00$ MN/m²
$\square$ $E_{50}^{ref} = E_{oed}^{ref} = 4.50$ MN/m²
$\triangle$ $E_{50}^{ref} = E_{oed}^{ref} = 6.00$ MN/m²
$\diamond$ $E_{50}^{ref} = E_{oed}^{ref} = 7.50$ MN/m²
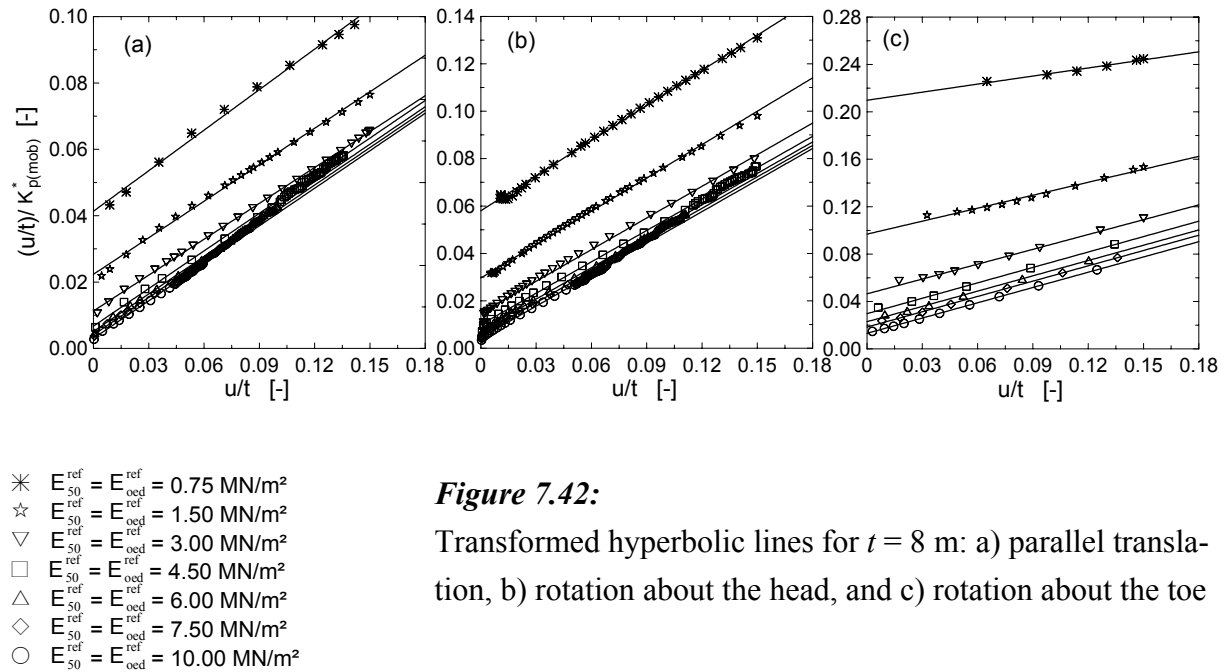$\circ$ $E_{50}^{ref} = E_{oed}^{ref} = 10.00$ MN/m²

Figure 7.42:

Transformed hyperbolic lines for $t = 8$ m: a) parallel translation, b) rotation about the head, and c) rotation about the toe

The values of the constants α_1 and α_2 are given in Figure 7.43 for the three cases of wall movement. The slope *b* is usually related to the deviatoric stress at failure in approximating the stress - strain behaviour of soils with a hyperbolic function according *Duncun/chang (1970)* (see also Section 6.5.3). Analogue to that, *b* may be related to the passive resistance at limit state, namely with the coefficient of the passive earth pressure K_{ph}. That is

$$b = \frac{\beta}{K_{ph}} \tag{7.17}$$

Reading the value of the slope *b* from Figure 7.42 and K_{ph} from standard tables for $\varphi_s' = 25°$, the value of β may be calculated for different stiffness values of the soil (Table 7.8). It appears from Table 7.8 that the values of β are fairly constant for a given range of stiffness of the soil. Therefore, the value of β may be fixed as an average value as shown in Table 7.9 for two ranges of the stiffness values.

Hence, substituting *a* and *b* from Equation 7.16 and 7.17 into Equation 7.14, one may arrive at mobilisation function of the form:

$$K_{p(mob)}^* = \frac{(u/t)}{\left[\alpha_1 \cdot \left(\dfrac{E_{oed}}{\gamma \cdot t} \right)^{\alpha_2} + (u/t) \cdot \dfrac{\beta}{K_{ph}} \right]} \tag{7.18}$$
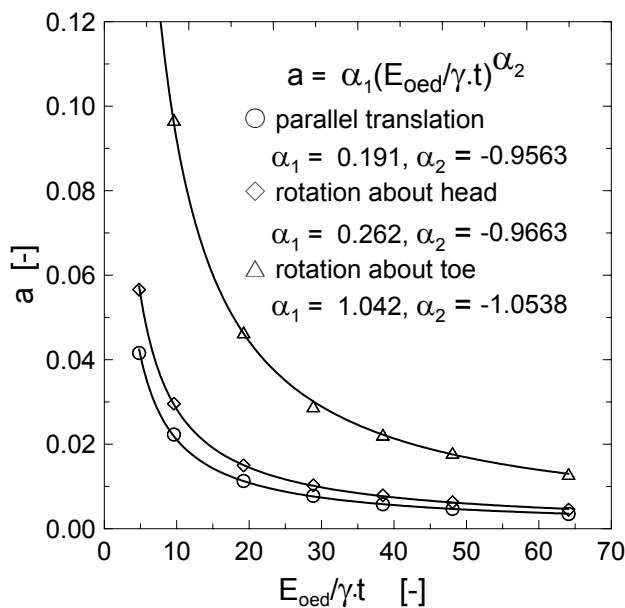

Figure 7.43:

Relationships between the normalised constrained modulus E_{oed} and the curve constant *a* for *t* = 8 m

Table 7.8: Values of the constant β dependent on the stiffness of the soil

$E_{50}^{ref} = E_{oed}^{ref}$	Values of β		
[kN/m²]	Parallel translation	Rotation about head	Rotation about toe
750	1.2428	1.5855	0.7017
1500	1.3331	1.4681	1.1275
3000	1.1136	1.3936	1.2891
4500	1.1068	1.3488	1.3624
6000	1.1053	1.3389	1.3494
7500	1.1031	1.3398	1.3448
10000	1.1019	1.3377	1.3318

Table 7.9: Values of the constant β for a range of stiffness of the soil

$E_{50}^{ref} = E_{oed}^{ref}$	Values of β		
[kN/m²]	Parallel translation	Rotation about head	Rotation about toe
< 3000	1.1880	1.5268	0.9146
≥ 3000	1.1106	1.3518	1.3355

7.4.5   Comparison of the developed equations with the FEM - results

Figure 7.44 shows a comparison of results of the analytical calculation using the mobilisation function (Equation 7.18) and the FEM for two selective stiffness values of the soil ($E_{50}^{ref} = E_{oed}^{ref}$=3.0 and 4.5 MN/m²) and for the case of parallel translation of the wall. The two results match fairly well for the case of $t = 8$ m and $\varphi_s = 25°$ (Figure 7.44a) and for the case of $t = 8$ m and $\varphi_s = 20°$ (Figure 7.44c). However, for values of $t = 4$ m and $\varphi_s = 25°$ (Figure 7.44b), the two results do not match each other. This is mainly due to the fact that the E_{oed} was normalised by $t = 8$ m in finding a correlation with the constant a (Equation 7.16). Hence inserting $t = 4$ m into Equation 7.18 results in a lower value of the intercept a and in turn a higher value of the mobilised resistance. To correct this deviation, a dimensionless factor f was introduced into Equation 7.18, so that the term $(E_{oed}/\gamma \cdot t)$ remains constant for all values of t. The corrected mobilisation function is given by Equation 7.19.

$$K_{p(mob)}^{*} = \frac{(u/t)}{\left[\alpha_1 \cdot \left(\dfrac{E_{oed}}{f \cdot \gamma \cdot t}\right)^{\alpha_2} + (u/t) \cdot \dfrac{\beta}{K_{ph}}\right]} \qquad (7.19)$$

where $f = \dfrac{8}{t}$ and t is the wall height in m.
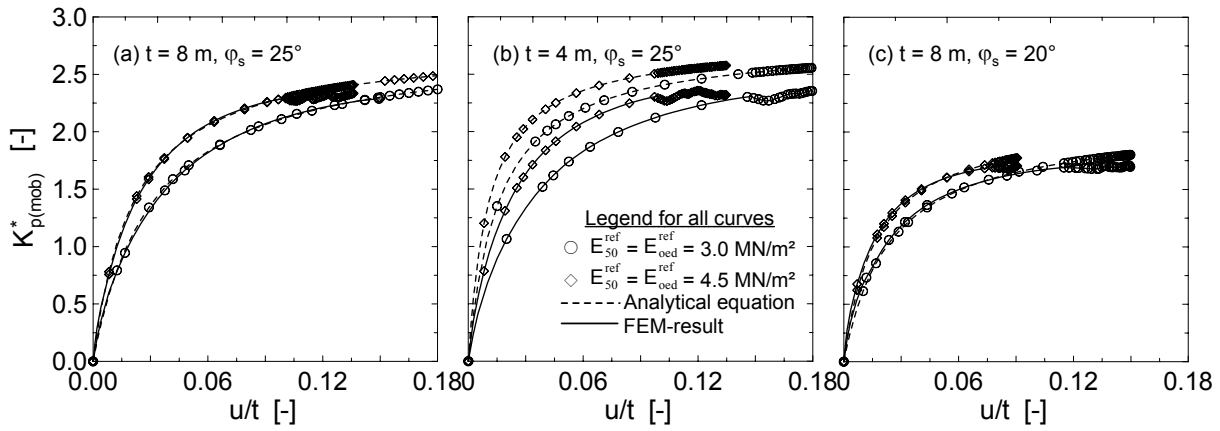
Figure 7.44: Comparison of the analytical Equation 7.18 with FEM result

The comparison of the FEM - results with the analytical results from Equation 7.19 are given in Figure 7.45, 7.46 and 7.47 for the cases of parallel translation of the wall, rotation about the head and rotation about toe respectively. It appears from these figures that the results of the FEM and the analytical agree very well. Therefore, the mobilisation of the passive resistance may fairly be approximated using Equation 7.19.

Figure 7.45: comparison of the analytical (Equation 7.19) and FEM - results for the case of parallel translation of the wall

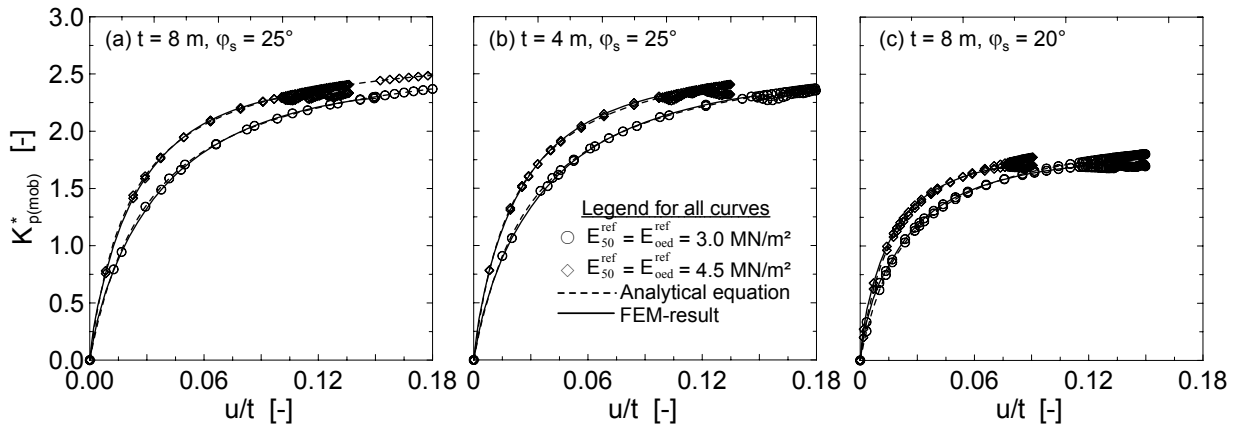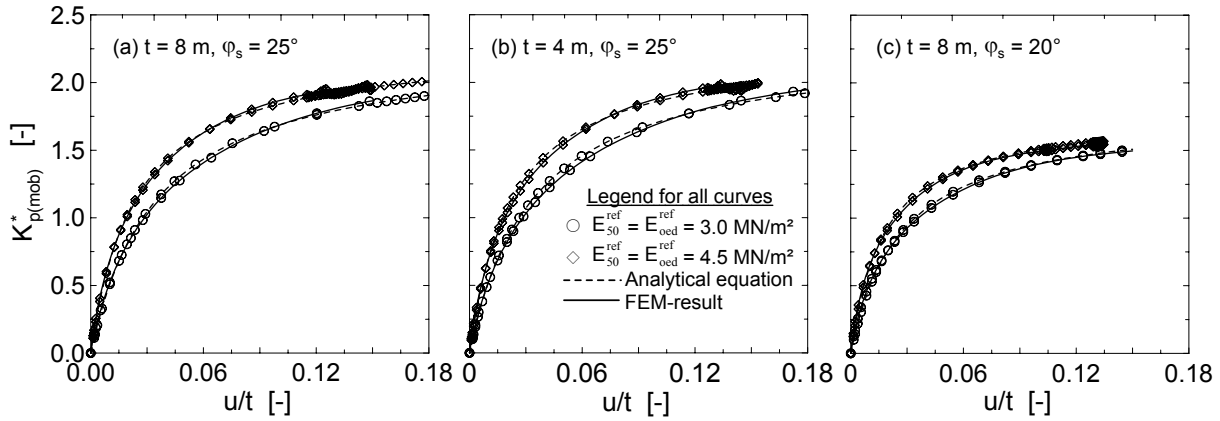**Figure 7.46:** comparison of the analytical (Equation 7.19) and FEM - results for the case of rotation of the wall about head
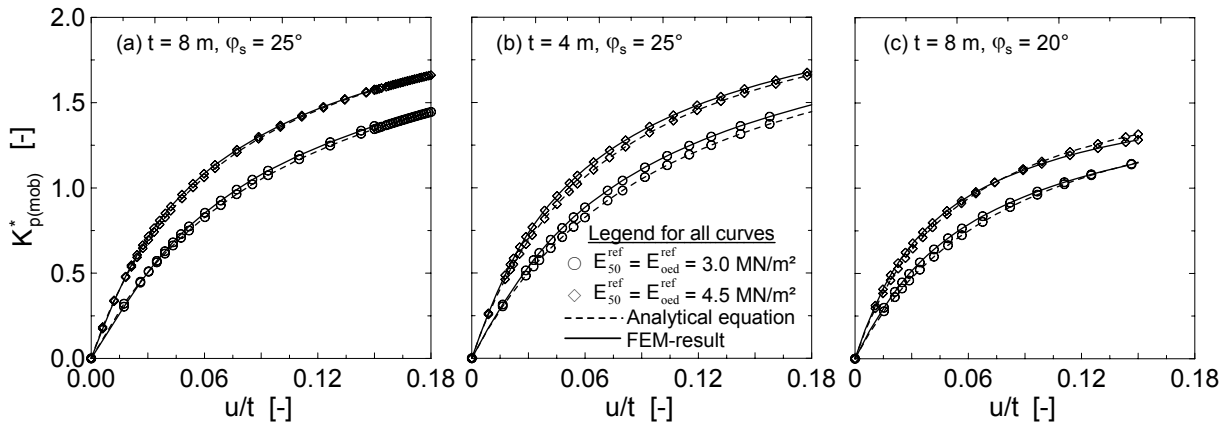
Figure 7.47: comparison of the analytical (Equation 7.19) and FEM - results for the case of rotation of the wall about toe

7.4.6   Stiffness dependent total safety factor for passive resistance

According to the recommendations of the working group "Excavations" (EAB), a safety factor of $\eta_p = 1.1$ to 1.5 (total safety factor concept) should be provided for the determination of the allowable passive earth pressure in the case of dense to medium dense non-cohesive soils and stiff cohesive soils. For normally consolidated soft soils, however, there is no specific recommendations for the safety factor η_p except that a higher value of the safety factor was recommended. The question, how high and under which condition the safety factor should be increased is still not clear and it is examined by the working group "Excavations" EAB at present. The aim of the

following section is to formulate a function of the total safety factor which is dependent on the stiffness of the soil and the wall displacement.

The total safety factor for passive resistance is defined by

$$\eta_p = \frac{maximum\ passive\ resistance\ (E_{ph})}{mobilized\ passive\ resistance\ (E'_{ph})} \quad or \quad = \frac{K_{ph}}{K'_{ph}} \tag{7.20}$$

The mobilised passive resistance can be estimated using Equation 7.19 as already discussed in the previous section. From the mobilised passive resistance diagram, one can determine the passive resistance at the limit state and the corresponding wall displacement. Dividing the values at the limit state with different safety factor, the workable wall displacements may be obtained. Figure 7.48 shows a plot of the normalised displacement of the wall for different safety factors as a function of the normalised stiffness of the soil. The relationship between the displacement of the wall and the stiffness of the soil may fairly be described by a potential function of the form:

$$\frac{u}{t} = \xi_1 \cdot \left(\frac{E_{oed}}{\gamma \cdot t} \right)^{\xi_2} \tag{7.21}$$

where ξ_1 is a variable which depends on the type of the wall movement and safety factor, and ξ_2 is independent of the safety factor but depends on the type of the wall movement. The values of the ξ_1 and ξ_2 are given in Table 7.10.
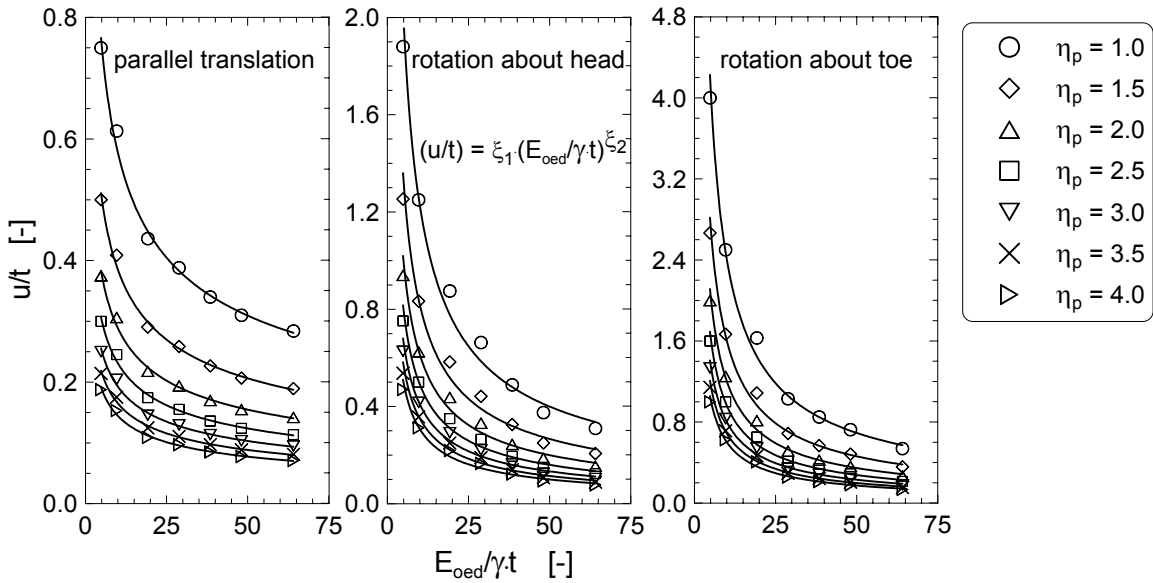

Figure 7.48: The displacement of the wall as a function of the normalised constrained modulus for all types of wall movements

Table 7.10: Values of the variables ξ_1, ξ_2 and ξ_3

Safety factor	Parallel translation			Rotation about the head			Rotation about the toe		
	ξ_1	ξ_2	ξ_3	ξ_1	ξ_2	ξ_3	ξ_1	ξ_2	ξ_3
$\eta_p = 1.0$	1.4082	-0.3874	1.4082	6.0835	-0.6960	6.0835	14.2154	-0.7723	14.2154
$\eta_p = 1.5$	0.9388	---"---	---"---	4.0557	---"---	---"---	9.4770	---"---	---"---
$\eta_p = 2.0$	0.7041	---"---	---"---	3.0418	---"---	---"---	7.1077	---"---	---"---
$\eta_p = 2.5$	0.5633	---"---	---"---	2.4334	---"---	---"---	5.6862	---"---	---"---
$\eta_p = 3.0$	0.4694	---"---	---"---	2.0278	---"---	---"---	4.7385	---"---	---"---
$\eta_p = 3.5$	0.4023	---"---	---"---	1.7381	---"---	---"---	4.0616	---"---	---"---
$\eta_p = 4.0$	0.3521	---"---	---"---	1.5209	---"---	---"---	3.5539	---"---	---"---

Plotting the values of ξ_1 against the safety factor, a potential relationship may be found between the two parameters as shown in Figure 7.49 and it may be written as

$$\eta_p = \frac{\xi_3}{\xi_1} \tag{7.22}$$

where ξ_3 is a variable dependent on the type of the wall movement and its values are given in Table 7.10. Substituting ξ_1 from Equation 7.21 in to Equation.7.22, a general empirical function of the total safety factor against the passive resistance may be obtained as follows:
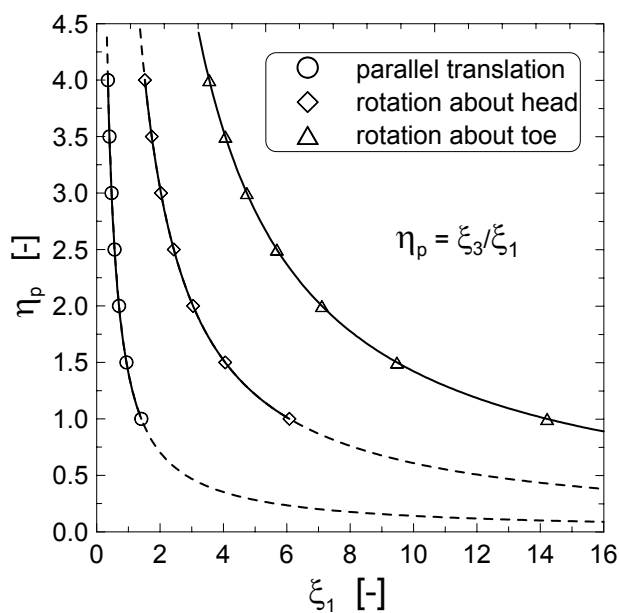
Figure 7.49:
Total safety factor for the passive resistance dependent on the stiffness of the soil

$$\eta_p = \frac{\xi_3 \cdot \left(\dfrac{E_{oed}}{\gamma \cdot t} \right)^{\xi_2}}{\dfrac{u}{t}} \tag{7.23}$$

Hence, using Equation 7.23 one may approximate the total safety factor for passive resistance knowing the constrained modulus, the expected normalised displacement of the wall and the type of wall movement.

7.4.7   Summary

This is a first attempt to formulate a passive mobilisation function for soft soils based on the FEM. Using the developed formula, one can easily estimate the mobilised passive resistance knowing the expected movement of the wall. However, it should be noted that the computations were performed using a particular type of soil model, namely the hardening soil model. Hence, a broad investigation is required to check the validity of the developed equations using other soil models. Even within the HSM parameters, it was shown in the previous sections that the other parameters may also have a significant influence on the deformation behaviour. However, a constant value of all HSM parameters except the stiffness of the soil was assumed in developing the mobilisation functions in this work.

8 Calibration of soil parameters based on practical projects

8.1 General

The area of the lake Constance, locally known as Bodensee, is known to consist a thick layer of post glacial soft lacustrine deposit. Excavation on such thick soft soils in urban areas is usually prone to movements of soils which damages the nearby structures. Now a days the possible movement of soil in excavations in urban areas is predicted by means of the Finite Element Method. However, experiences show that predicted deflection of wall and settlement behind the wall does not usually match with the measured values.

The aim of this chapter is to perform a back analysis of the practical excavation projects on soft soils with the FEM, so that to identify the possible cause of the deviation of the calculated and measured results and to calibrate the soil parameters accordingly. The back analysis was carried out using the two-dimensional FE-program PLAXIS 8.1 professional version. A plane strain analysis was adopted using 15 node triangular elements. The hardening soil model (HSM) was used to simulate the behaviour of the soils in all the layers, whereas the Mohr-Coulomb Model (MCM) was adopted to simulate the contact behaviour. The structural elements were assumed to behave elastically.

Besides the understanding of the soil and the soil-structure-interaction behaviour, and their simulation using an advanced constitutive soil models, the understanding and simulation of each detail of the construction process is also equally important. This problem has been also be discussed under this chapter.

The author would like to emphasise that the field measurements present in this chapter were not accompanied by a scientific expertise, rather they were conducted by geotechnical engineering consulting office in the frame work of supervision of the safety of the nearby structures and the working area.

8.2 Project-I-Damgasse - Constance

8.2.1 General

A multi-storey building for the purpose of apartments and shopping centre which include two floor underground park was built in 1997/98 in the old part of the Constance city, southern Germany. The site was fairly level (397.50 MSL), measured about 40 x 60 m and surrounded by old and relatively new 3 - 5 storey buildings (Figure 8.1). The retaining structure used was a sheet pile wall of the type Hoech 134. There were a double row of sheet pile walls on the north and

south part of the site. Figure 8.2 is a section through the site. The walls were temporarily supported by wooden ($\phi = 26\,cm$) strut, propped wooden plumbs ($\phi = 36\,cm$), propped I-Steel beam (IPB 360) and bottom concrete slab (d = 25 and 30 cm). The positions of the support are shown in Figure 8.3. The soil exploration, monitoring and construction information are documented in *Kempfert + Partner (1994-1998)* and are partly reported by *Berner (1997)*. Hence, this work will give more emphasis to the numerical analysis of the project after brief introduction to the site condition, instrumentation and recorded data.
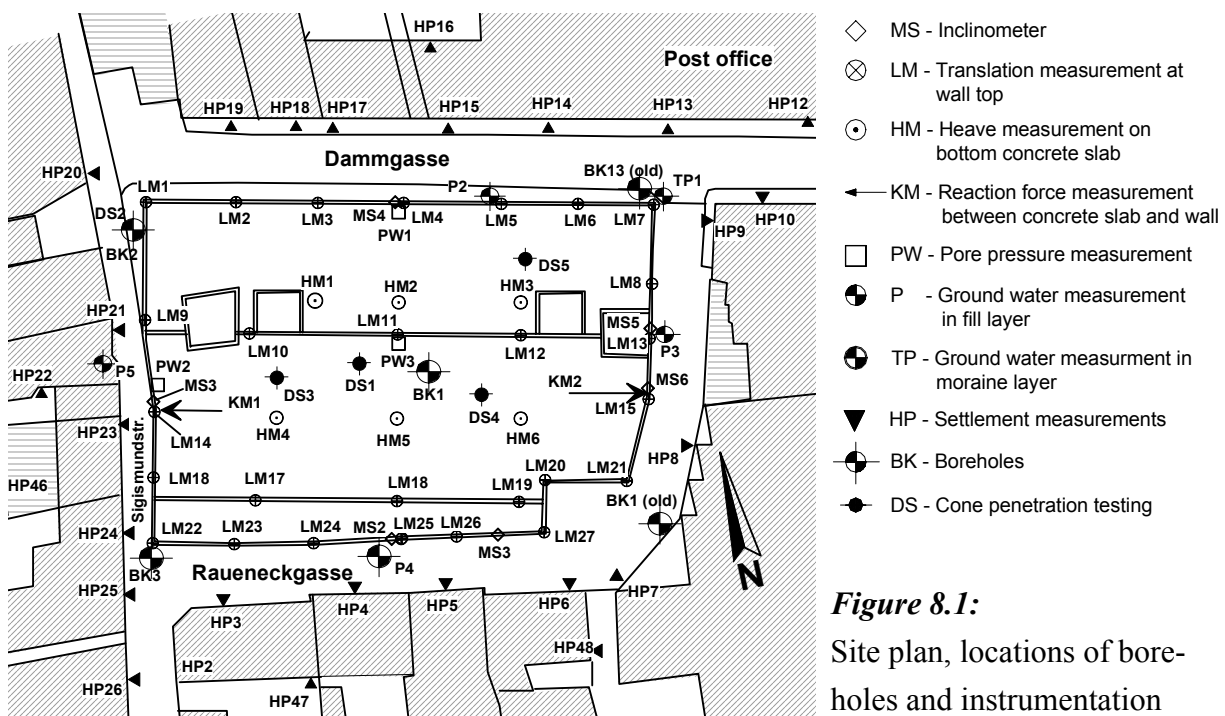
Figure 8.1:

Site plan, locations of bore-holes and instrumentation

8.2.2   Construction stages

The excavation was proceeded in slices in a daily output basis according to the construction phases shown in Figure 8.3. After each slice was excavated, a fast hardening concrete had been placed providing support to the walls (see Figure 8.4), before the next slice excavation had begun. The construction stages consists of:

1) Excavation to a depth of 1.2 m below the surface (11.11.96 - 20.11.96).

2) Cutting a trench for sheet pile wall installation (15.11.96 - 23.11.96).

3) Sheet pile wall installation (04.12.96 - 29.01.97).
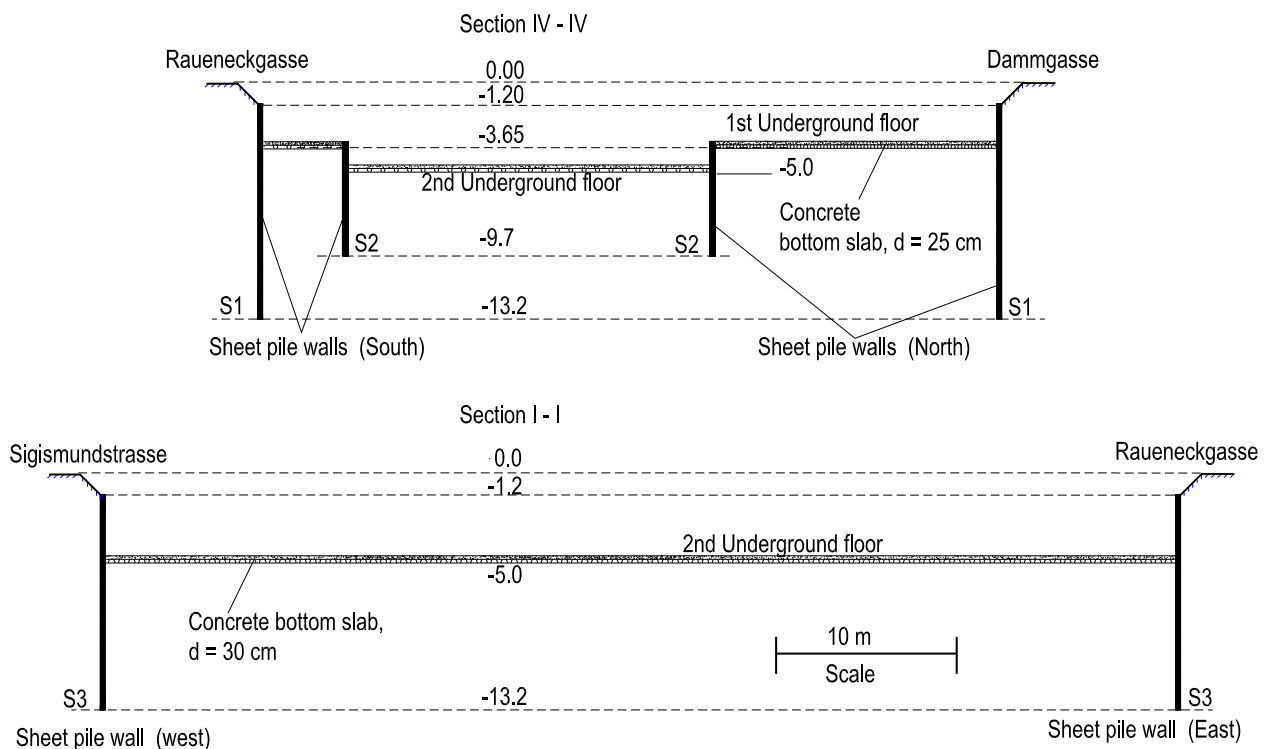
Figure 8.2: Section through site

4) Inserting the wooden struts and excavation phase 1a and simultaneously placement of the bottom fast hardening concrete slab on daily output basis, Slices 1.1 - 1.20, South (03.02.97 - 26.02.97).

5) Excavation phase 1b and simultaneously placement of the bottom fast hardening concrete slab on daily output basis, Slices 1.1 - 1.7, North (21.02.97 - 27.02.97). The wooden struts in phase 1a removed.

6) Excavation phase 2 and simultaneously placement of the bottom fast hardening concrete slab on daily output basis, Slices 2.1 - 2.9, (04.03.97 - 18.03.97).

7) Cut away the inner sheet pile walls S2 up to the 1st underground floor level.

8) Inserting the wooden propped support in trench, excavation phase 3 and simultaneously placement of the bottom fast hardening concrete slab on daily output basis, Slices 3.1 - 3.18, North (03.04.97 - 14.07.97).

9) Inserting the wooden propped support in trench, excavation phase 4a and simultaneously placement of the bottom fast hardening concrete slab on daily output basis, Slices 4.1 - 4.9, West (09.04.97 - 21.04.97).

10) Inserting the wooden propped support in trench, excavation phase 4b and simultaneously placement of the bottom fast hardening concrete slab on daily output basis, Slices 4.1 - 4.9, East (30.06.97 - 17.07.97).

11) Placement of the basement reinforced concrete slab and removal of the propped support.
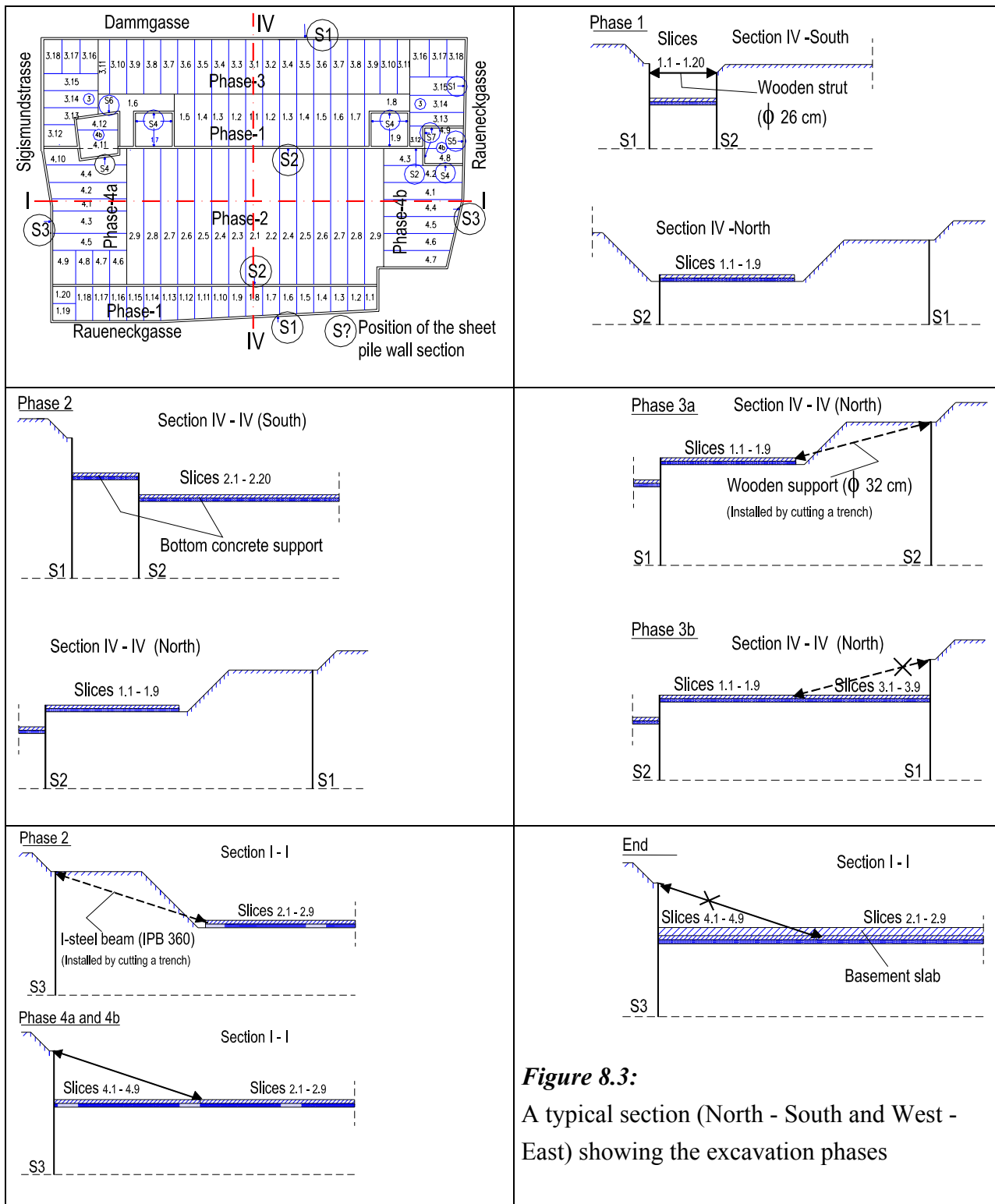

Figure 8.3:
A typical section (North - South and West - East) showing the excavation phases

Figure 8.4: Overview of the excavation project: Dammgasse *[Photo: Kempfert]*

Figure 8.5: Excavation and placement of the bottom slab in slices *[Photo: Kempfert]*

8.2.3   Site condition

Altogether 3 boreholes were drilled, 5 test pits were excavated, 5 cone penetration test were conducted on the site for the purpose of exploring the soil and investigating the ground water condition. Two additional bore logs were also available from old soil exploration on the site. Their locations are shown in Figure 8.1. The site investigation revealed 2.6 to 5.3 m fill material comprising gravel, sand and rubble from old buildings, overlaying soft lacustrine deposit to a depth of 12 to 30 m. Beneath the lacustrine soil, a moraine comprising sandy and silty gravel was encountered to a depth of 20 m up to a depth greater than 30 m. Though it was not bored at this site, a boulder clay is believed to be found beneath the moraine. Figure 8.6 is a typical bore log and cone penetration result along with the distribution of the water content with the depth.
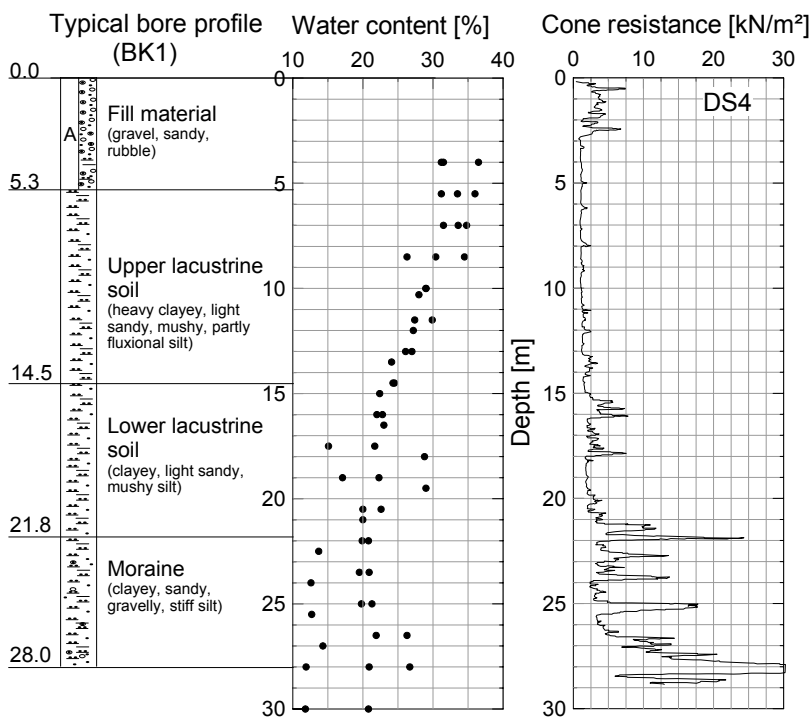
Figure 8.6:
Typical soil profile and properties

Immediately after the boring a water level at 1.6, 1.4, and 1.05 m below the ground in the fill layer at bore holes BK1, BK2 and BK3 (Figure 8.1) respectively was observed. A confined water pressure was encountered at a depth of 22 m at BK2 and at a depth of 21 m at BK3 and raised to a height of 2 m and 12.2 m below the surface respectively. The old bore hole B13 showed three water levels at 2.5 m, 6.0 m and 8.5 m below the surface level. In order to investigate the ground water condition seriously during the excavation and to avoid the ambiguity shown in the other boreholes, additional 4 standpipes deep in the fill layer and one piezometer deep in to the moraine layer (24 m deep) were installed (see Figure 8.1 for locations of the standpipes). The result of the ground water observations are shown in Figure 8.7. The shallow standpipes P2, P3 and P4 showed almost a constant water level at about 2 m below the ground surface on average. The

standpipe P5, which is located on the courtyard (Figure 8.1) showed a higher water level which is at about the surface level. This may not be other than a local reservoir in this area. The deep piezometer showed a confined water that had on average a head of 1 m below the surface. The fluctuation of the water level in TP1 is related to the fluctuation of the water level of the Constance lake. The highest and the middle water level of the Constance lake is located at 396.56 and 395.56 MSL respectively, or in other words, 1 m and 2.15 m below the ground surface in reference to the average surface level at the site (397.50 MSL).
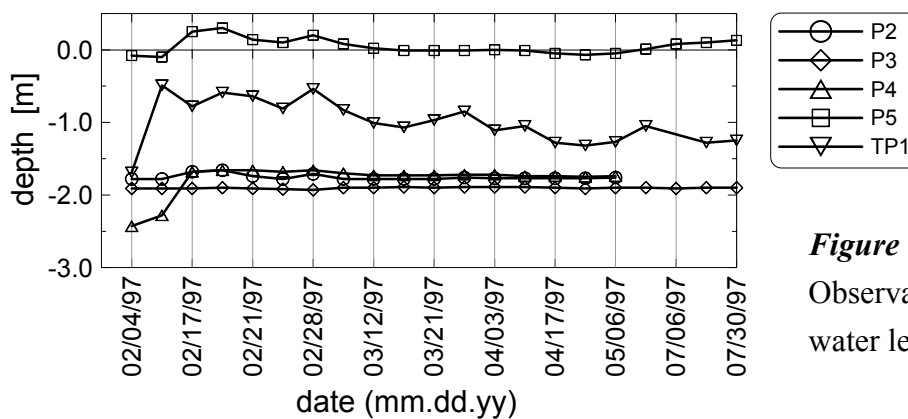
Figure 8.7:
Observations of the ground water level during excavation

8.2.4   Instrumentation

Instrumentation was used to record the wall movement, the settlement of the nearby existing buildings, the heave of the basement slab, the pore water pressure in the lacustrine soil layer and the reaction forces between the wall and the basement slab and the propped support. Wall movement was measured in two ways. The top of the wall was monitored using Geodometer at 27 points. The wall deflection was measured using 6 inclinometers which provides a result to an accuracy of ±1 mm. The settlement at 50 locations near the existing buildings were monitored using surface surveying starting prior to the beginning of the construction activities at the site. The potential heave of the basement slab was measured using surface surveying at 6 points. In addition to the ground water observation mentioned in Section 7.2.2, pore water pressure was measured at the inner side of the sheet pile wall at 3 points.

8.2.5   Results of monitoring

a)   Settlements near existing buildings:
Figure 8.8 shows the measured vertical surface movement from prior to the start of the excava-

tion in Nov. 1996. A maximum surface settlement of 23 mm was recorded at measuring point HP4 in southern part of the Raueneckgasse street, in which about 25% of the settlement has already occurred during the wall installation. At the opposite street, Dammgasse, a maximum settlement of 3 mm was measured, whereas at Sigismundstrasse a maximum settlement of 14 mm was recorded. In eastern part of the Raueneckgasse street a maximum settlement of 4 mm was observed. At points far from the wall (16 - 25 m) no significant surface settlement was measured, even a heave of 3mm was recorded at measuring point HP16.
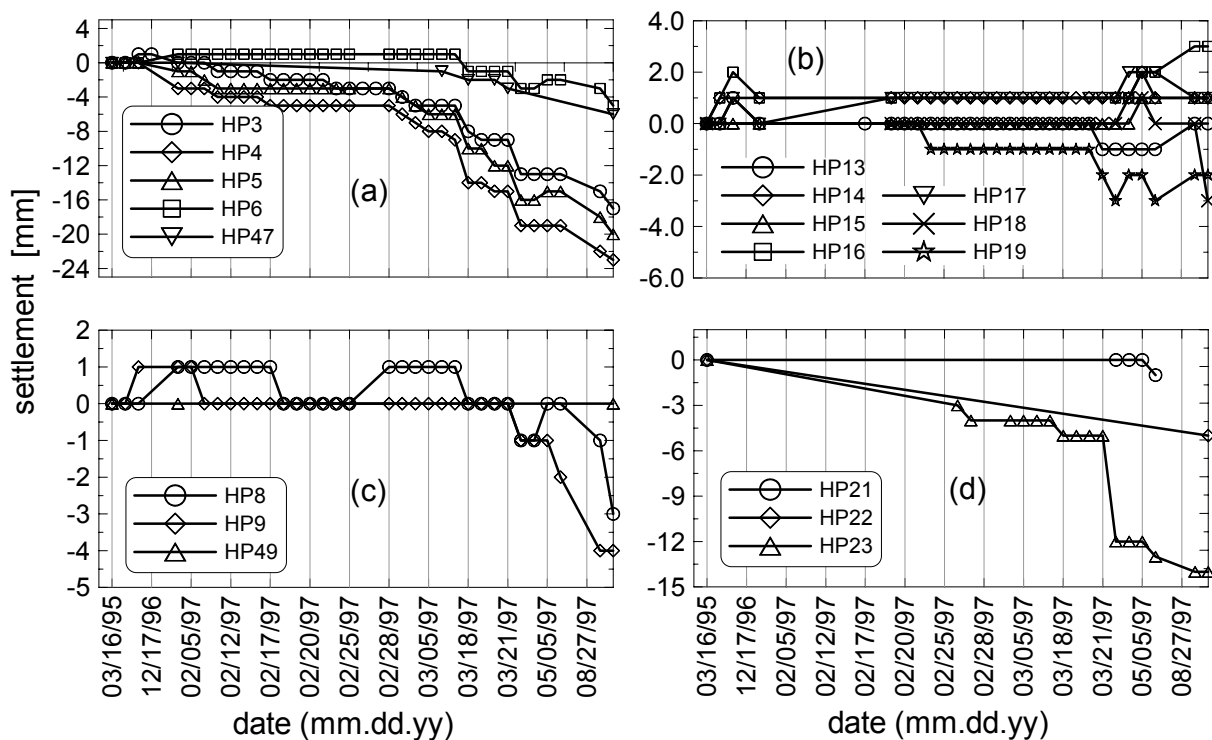
Figure 8.8:   Settlements near the existing buildings: a) Raueneckgasse-south, b) Dammgasse, c) Raueneckgasse-east, and d) Sigismundstrasse

b)   Wall displacement at the top:

The movement of the wall head was measured using Geodometer, which measures the wall head movement in the three directions (x-y-z). The wall head movement at selected points are given in Figure 8.9.

c)   Wall deflection:

The observed horizontal deflection of the sheet pile wall at the various stages of excavation and support at the measuring locations MS2, MS4, MS3 and MS6 (Figure 8.1) are shown in Figure 8.10. It was reported that there were difficulties in the interpretation of the inclinometer reading at the location MS6.
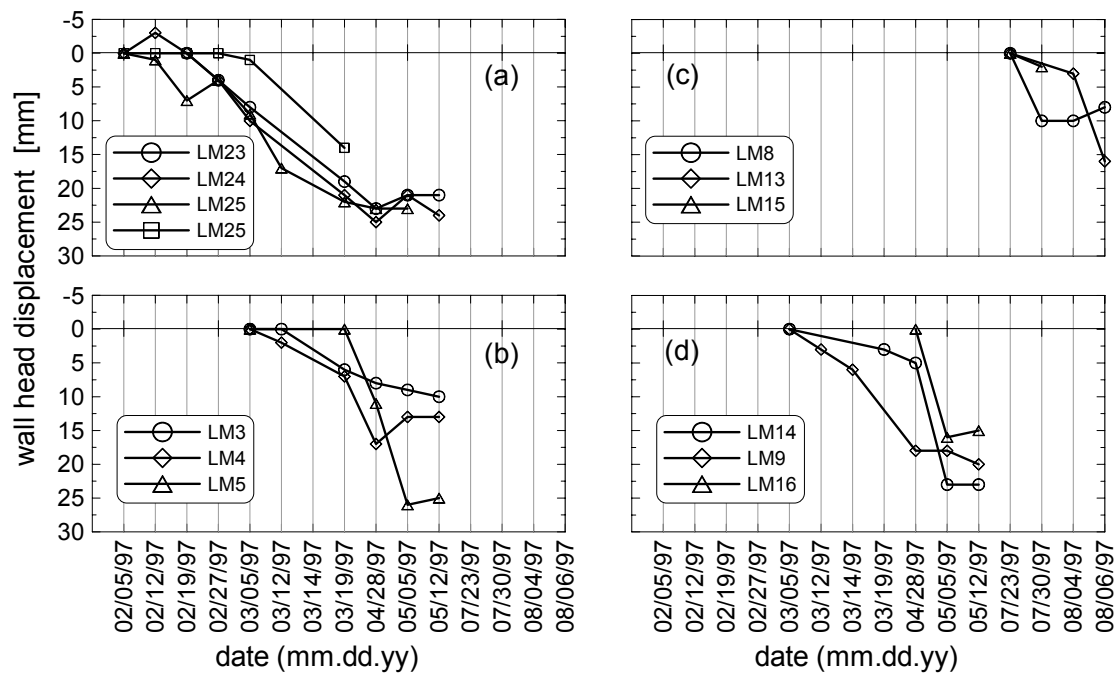
Figure 8.9: Observed movement of wall head towards excavation: a) Raueneckegasse - South, b) Dammgasse, c) Raueneckegasse - east, d) Sigismundstrasse
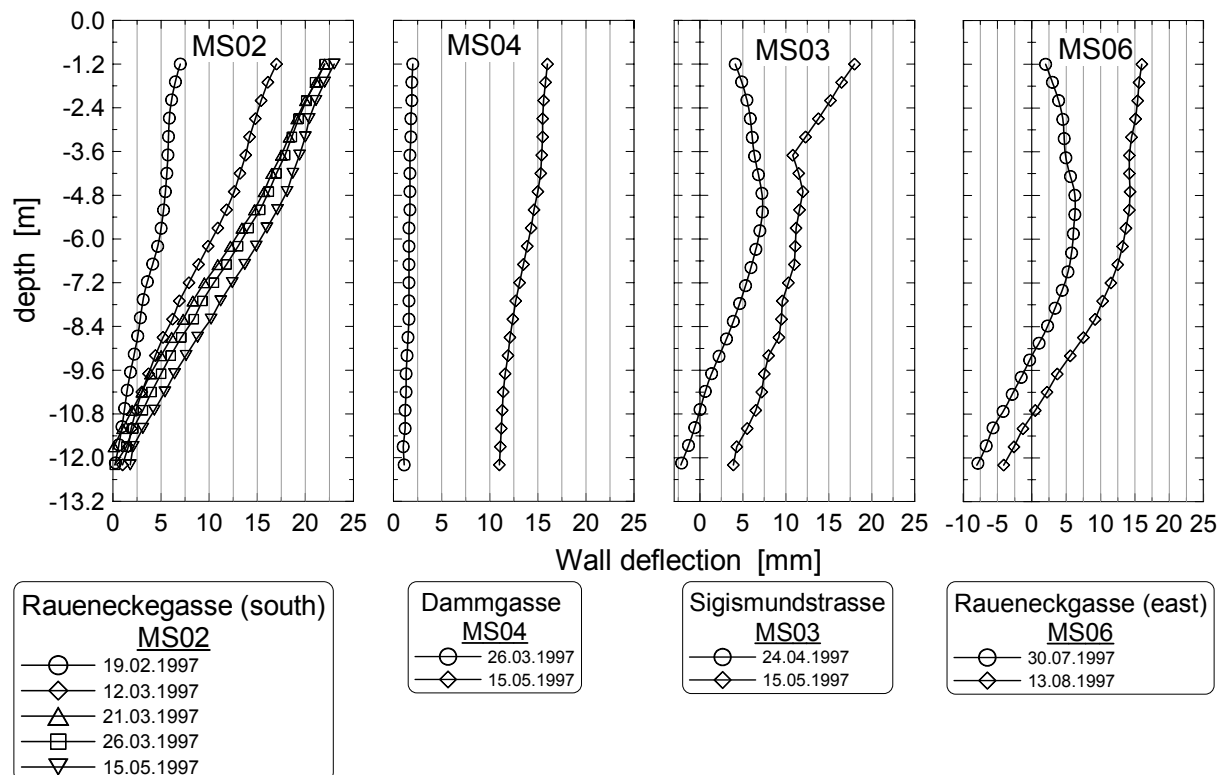
Figure 8.10: Deflection of the sheet pile wall towards excavation at three inclinometer positions (MS02, Ms04 and MS03)

d)   Excess pore pressure

The excess pore pressure was measured using pressure transducers and are shown in Figure *8.11*. It can be shown from the figure that the measurements were started a bit late. The first measurement (25.02.1997) was carried out after almost the excavation of phase 1a and phase 1b had been completed. It was also reported that the initial readings were influenced by the installation process (*Kempfert + Partner (1994-1998)*).
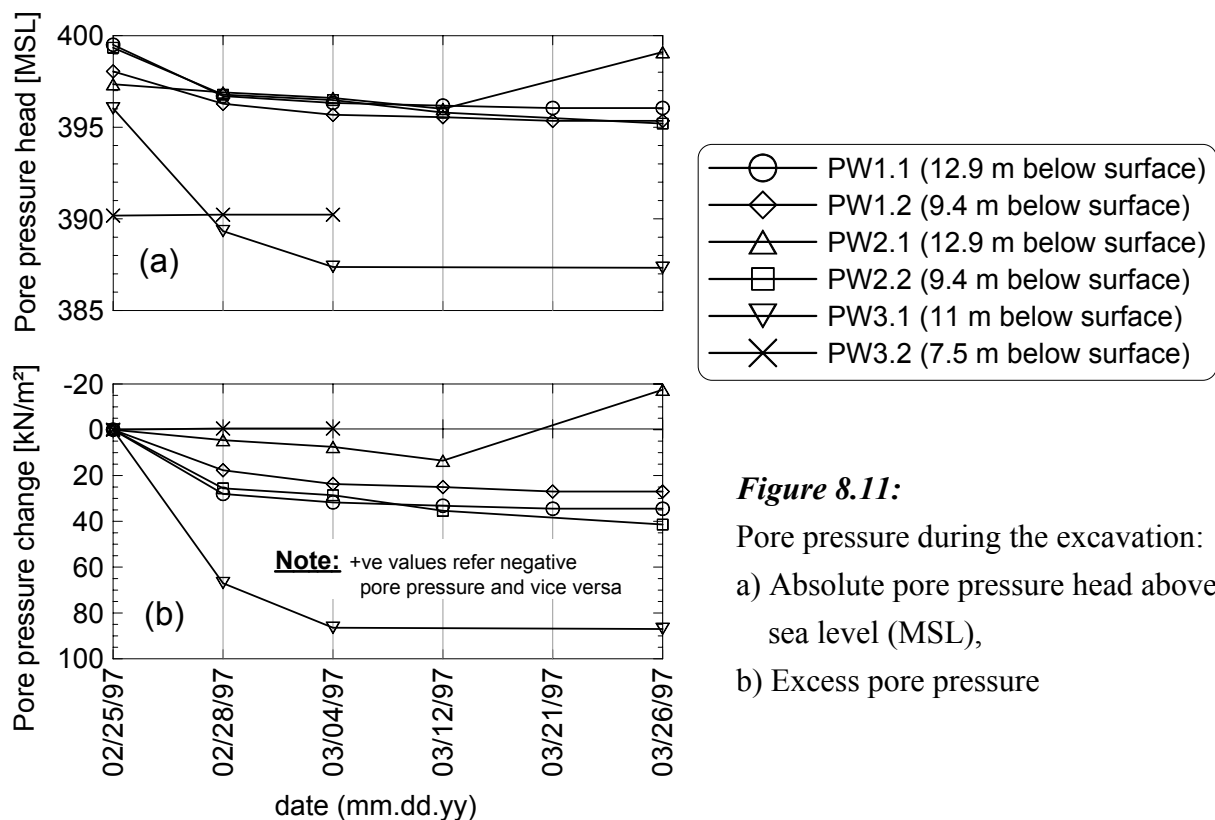
Figure 8.11:

Pore pressure during the excavation:

a) Absolute pore pressure head above sea level (MSL),

b) Excess pore pressure

e)   Reaction forces

A reaction force of 159 and 222 kN/m² was measured between the I-steel propped support and the wall at the location KM1. At the same location a reaction pressure of 23.5 kN/m² was recorded between the bottom slab and the wall at the end of excavation but before the removal of the propped support, and 5.5 kN/m² after placement of 60 cm thick basement concrete slab of the underground floor and the removal of the steel support.

8.2.6   Back analysis of the excavation project using the FEM

8.2.6.1   Model geometry

The first step in any FE-analysis of geotechnical problem is to convert the data from the geotechnical reports to a simplified soil profile, idealise the structural elements and to determine the extent of the model geometry. Figure 8.12 shows the section through site (South - north section) showing the idealised soil profile, arrangement of the structural elements and sequences of the excavation. A similar west - east section is also shown in Figure 8.13. These sections are identified as section IV-IV and I-I on the site plan (Figure 8.1).
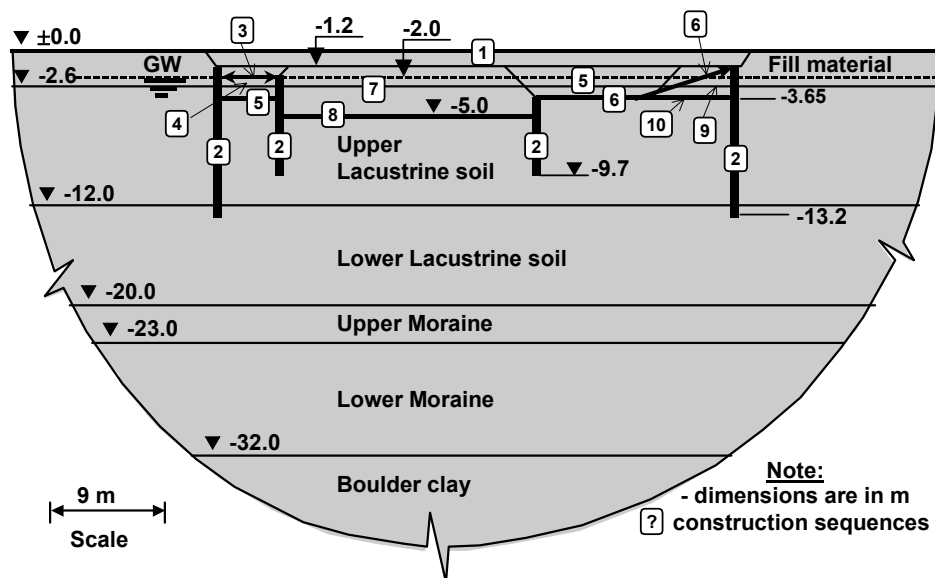
Figure 8.12:   Section through the site (south - north), soil profile and construction sequence

The finite element model and its mesh are shown in Figure 8.14 and 8.13. These figures are zoomed in order to show the main part of the model that consist the structural elements, the loads, the soil layers and the excavated section. The geometry of the excavation, the arrangement of the sheet piles and the sequences of the excavation did not allow the use of the advantage of the symmetrical model. That is why the system as a whole as shown in Figure 8.12 and 8.13 were modelled in the analysis. The size of the models were chosen according to the recommendation of the working group ''Numerics in Geotechnic`` (*Meißner (2002)*) and the parameters study in Section 7.3.2. The finite element mesh at south-north section was extended to a depth of 82 m where a fixed boundary was imposed and a zero horizontal displacement was imposed at a distance of 82 m from the edge of the wall. The size of the model as a whole was 204 m wide and 82 m high (Figure 8.14). Similarly, The finite element mesh at west-east section was extended to a depth of 125 m and to a distance of 120 m from the edge of the wall (all in all 300 × 125 m)

(Figure 8.15). Since the excavation site was surrounded by existing buildings, a surcharge load of 33 kN/m² and 23 kN/m² at the southern and northern side (Figure 8.14) respectively were applied at the level of the underground floor. Similarly, a load of 20 kN/m² and 32 kN/m² at the western and eastern side of the excavation (Figure 8.15) respectively were applied on the model. The weight of the soil above the underground floor was considered in the calculation of the surcharge loads. In both cases a traffic load of 10 kN/m² was applied between the wall and the existing buildings.
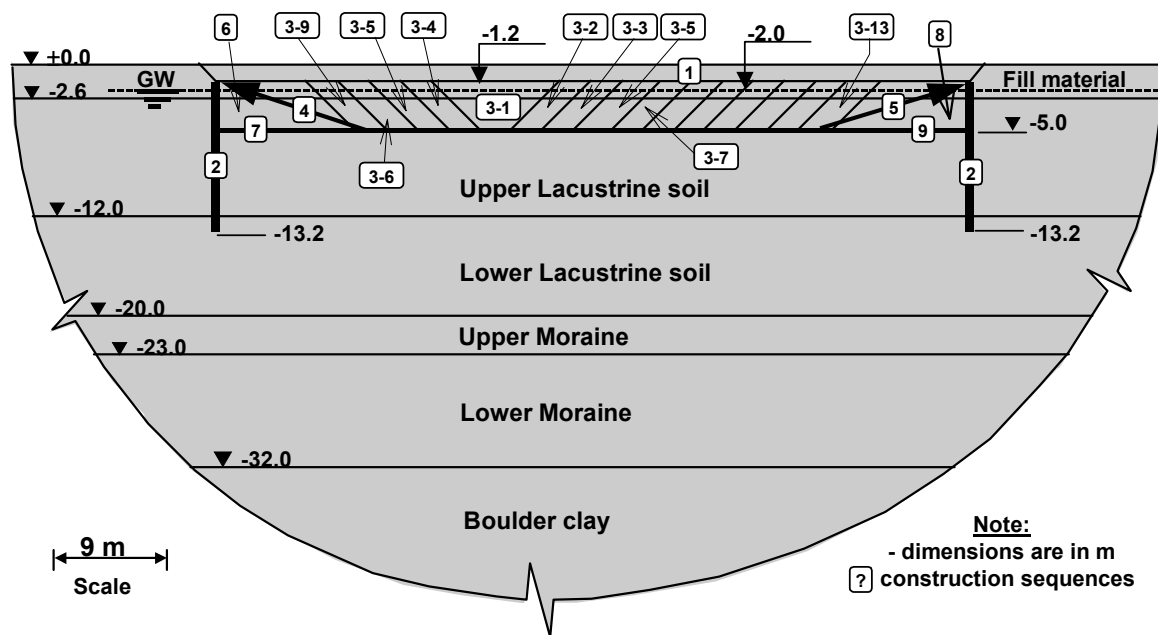

Figure 8.13: Section through the site (west - east), soil profile and construction sequence
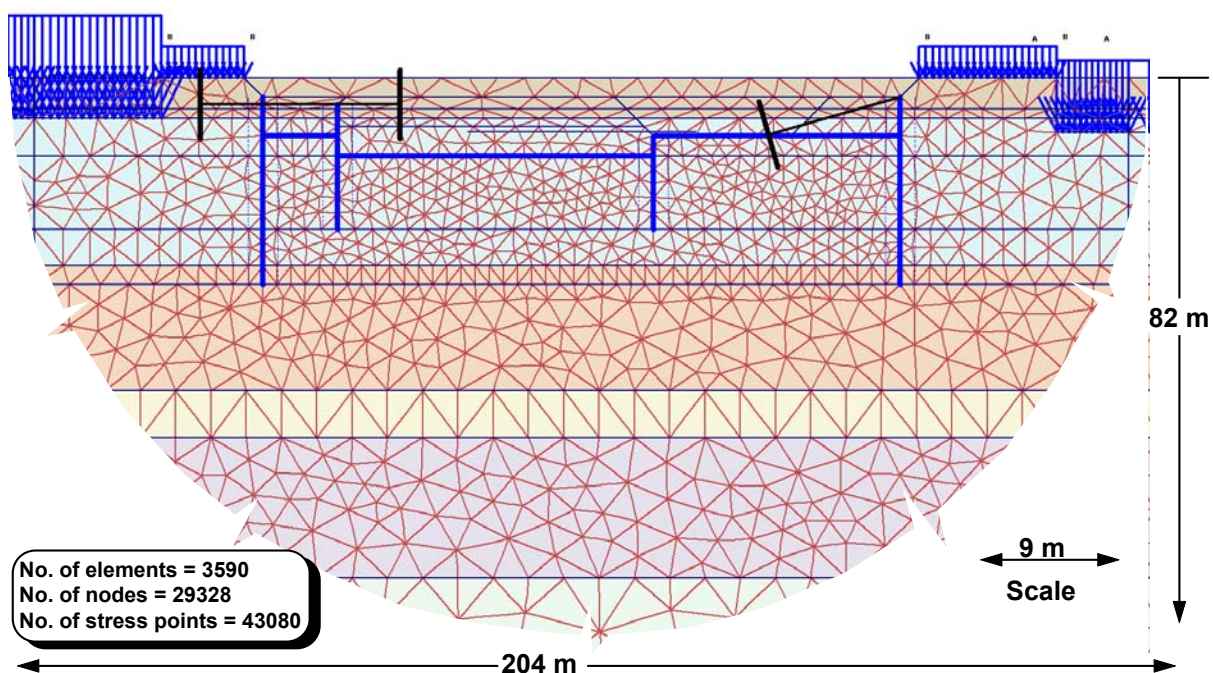
Figure 8.14: Main part of the finite element mesh: south - north section
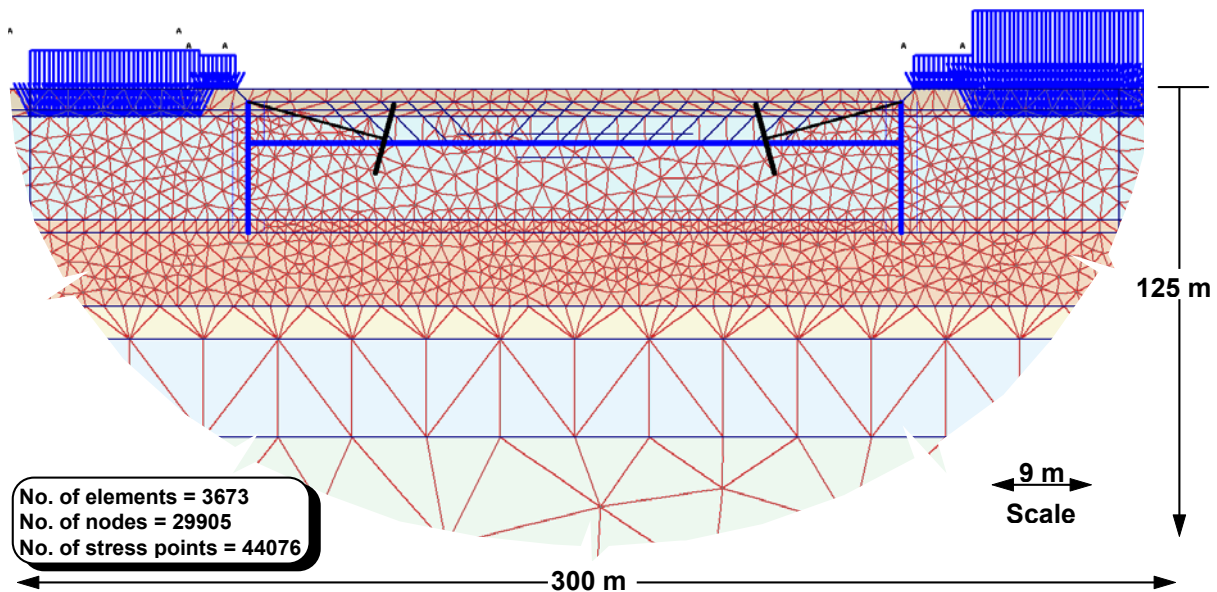
Figure 8.15   Main part of the finite element mesh: west - east section

8.2.6.2   Material properties

As it was already mentioned at the beginning of this chapter, the HSM is the main constitutive model that was used to simulate the behaviour of the soil. The soil parameters required for the FE - computation with the hardening soil model under drained condition are given in Table 1. As it was already mentioned in Section 7.2.2, PLAXIS provides an option of performing an undrained analysis using the effective strength and stiffness parameters. Hence, the parameters in Table 1 may also be used for the consolidation analysis. The program accepts the effective stiffness parameter and calculates the balk modulus according to the Hook's law of elasticity. The excess pore pressures are calculated from the volumetric strain rate, the bulk modulus of water and the porosity of the soil medium. The layers of the lacustrine soils and the fill material only were assumed undrained in the consolidation analysis, whereas the other layers remain drained. Although the boulder clay layer is relatively impermeable, it was assumed drained, taking into account the long calculation time needed and numerical instability during the consolidation analysis. Since the boulder clay is located at deeper depth (> 32 m), where the influence of the stress change becomes minimum, ignoring its undrained behaviour may not significantly affect the overall result.

The soil parameters of the lacustrine soil layers were directly taken from intensive laboratory tests on undisturbed soil samples from the site and are calibrated using a finite element simulation of the laboratory tests in Chapter 7. The soil parameters of the remaining layers were derived

from penetration and sounding field tests documented in the geotechnical reports after converting them to suit for HSM.

A separate material set was defined for the interface elements. The shear parameters of the contact elements were adopted from the corresponding layers of soils after reducing the values by a factor of 1/3, whereas the stiffness of the soil layers were adopted as it is (see Section 6.6). The secant modulus E_{50} of the corresponding soil layer and a Poisson's' ratio $v = 0.35$ were used as stiffness parameters for the MCM of the interface elements.

The material properties of the structural elements are given in Table 8.2. All the structural elements are assumed to behave elastically.

Table 8.1:   Soil parameters for the HSM for drained and consolidation analyses

a) Unit weight, permeability and earth pressure at rest

Soil layer	depth	γ_{sat}	γ_{unsat}	k_x	k_y	K_0^{nc}	
	[m]	[kN/m³]	[kN/m³]	[m/d]	[m/d]	[-]	
Fill material	±00.0 - -02.6	17.0	20.0	8.64E-5	8.64E-5	0.577	
Upper lacustrine soil	-02.6 - -12.0	19.5	19.5	8.64E-5	8.64E-5	0.590	
Lower lacustrine soil	-12.0 - -20.0	19.5	19.5	8.64E-5	8.64E-5	0.546	
Upper moraine	-20.0 - -23.0	20.0	20.0	8.60E-3	8.60E-3	0.463	
Lower moraine	-23.0 - -32.0	21.0	21.0	1.0	1.0	0.405	
Boulder clay	-32.0 - -82.0	22.0	22.0	8.60E-6	8.60E-6	0.500	

b) Stiffness parameters

Soil layer	depth	E_{50}^{ref}	E_{oed}^{ref}	E_{ur}^{ref}	p^{ref}	v_{ur}	m
	[m]	[kN/m²]	[kN/m²]	[kN/m²]	[kN/m²]	[-]	[-]
Fill material	±00.0 - -02.6	6000	6000	30000	100	0.20	0.700
Upper lacustrine soil	-02.6 - -12.0	3578	2653	19170	100	0.20	0.730
Lower lacustrine soil	-12.0 - -20.0	5367	3980	28982	100	0.20	0.730
Upper moraine	-20.0 - -23.0	24000	24000	120000	100	0.20	0.500
Lower moraine	-23.0 - -32.0	28000	28000	140000	100	0.20	0.500
Boulder clay	-32.0 - -82.0	40000	40000	20000	100	0.20	0.800

c) Shear strength parameters

Soil layer	depth	c'	φ'	ψ'	R_f		
	[m]	[kN/m²]	[°]	[°]	[-]		
Fill material	±00.0 - -02.6	10.0	25.0	0.0	0.90		
Upper lacustrine soil	-02.6 - -12.0	13.2	25.3	0.0	0.82		
Lower lacustrine soil	-12.0 - -20.0	14.1	27.0	0.0	0.82		
Upper moraine	-20.0 - -23.0	5.0	32.5	2.5	0.90		
Lower moraine	-23.0 - -32.0	5.0	36.5	6.5	0.90		
Boulder clay	-32.0 - -82.0	10.0	30.0	0.0	0.90		

Table 8.2: Material properties of the structural elements

Structural element	Type	*EA*	*EI*	*w*	*ν*	$L_{spacing}$
		[kN/m°]	[kNm²/m°]	[kN/m²]	[-]	[m]
Sheet pile wall	Hoech 134	3.591E6	53550.0	1.3	0.30	-
Bottom slab	Concrete slab, d = 25 cm	7.500E6	39063.0	6.3	0.20	-
	Concrete slab, d = 30 cm	9.000E6	67500.0	7.5	0.20	-
Strut	Wooden plumb, d = 26 cm	9.557E4	-	-	-	2.5
Propped support	Wooden plumb, d = 32 cm	1.448E5	-	-	-	2.5
	I-Steel beam (IPB 360)	9.503E5	-	-	-	4.0

8.2.6.3 Preliminary analysis and results

A preliminary analysis of the excavation was carried out using the finite element models shown in Figure 8.14 and 15 and the material properties in Table 8.1 and 8.2. In all the computation cases present in this section, a hydrostatic ground water located at 2 m below the surface was assumed. During the excavation, the groundwater table behind the walls was assumed to remain at this depth, whereas it was lowered to the depth of the respective excavation inside the excavation. Both drained and undrained (consolidation) analyses were performed separately.

a) *South-north section (Section IV-IV)*
a1) *Drained analysis*

The general construction stages and the duration of each construction stage are presented in Section 8.2.2. The main construction phases can also be shown in Fig. 4 in plan and in Fig. 6 in section.. The construction stages followed in the FE-computation were the same as those describe above, but they are simplified and optimised as shown in Table 8.3 below. The displacements that occurred during the first four phases (Phase 00 - Phase 03) of the computation were set to zero.

Table 8.3: Construction phases: drained analysis (Section IV-IV)

Phase 00: generate the initial stresses	Phase 08: installation of bottom slab (6) and strut (6), and removal of the strut (3)
Phase 01: activate the surcharge and traffic loads	
Phase 02: 1st excavation to a depth of -1.2 m (1)	Phase 09: 5th excavation (7)
Phase 03: installation of the walls (2)	Phase 10: installation of the bottom slab (8)
Phase 04: 2nd excavation to install the strut (3)	Phase 11: 6th excavation (9)
Phase 05: installation of the strut (3)	Phase 12: installation of the bottom slab (10)
Phase 06: 3rd excavation (4)	Phase 13: removal of the strut (6)
Phase 07: installation of bottom slab (5) and simultaneously 4th excavation (5)	
N.B.: numbers in brackets are construction sequences (Figure 8.10)	

a2)   Consolidation analysis

The new professional version of PLAXIS v8.1 provides an option of performing a consolidation and simultaneous loading in the sense of changing the load combination, stress state, weight, strength or stiffness of elements activated by changing the load and geometry configuration or pore pressure distribution by means of stage construction. This is very important in regard to excavation, because the excavation usually takes some days or weeks or in extreme case also some months, and the pore pressure has the possibility to dissipate already during the excavation. It is possible to calculate the amount of the pore pressure dissipated during the excavation starting at day one and after excavation at day x. This option of consolidation and simultaneous excavation was utilised in the back analysis of the excavation. The calculation phases followed and the consolidation time allotted for each stage are given in Table 8.4 below. The undrained behaviour was ignored in the first 4 construction phases, because no major excavation was undertaken at these stages and it was assumed that the excess pore water pressure due to the building loads had been fully dissipated at the time of the begin of the excavation. Similar to the drained case, the displacements in the first four phases were set to zero.

Table 8.4:   The construction phases: consolidation analysis (Section IV-IV)

Phase 00: generate the initial stresses	Phase 09: installation of bottom slab (6) and strut (6), [5 days]
Phase 01: activate the surcharge and traffic loads	
Phase 02: 1st excavation to a depth of -1.2 m (1)	Phase 10: consolidation time [6.5 days]
Phase 03: wall installation (2)	Phase 11: 5th excavation (7) [11 days]
Phase 04: 2nd excavation (3) [4 days]	Phase 12: bottom slab installation (8) [12 days]
Phase 05: strut installation (3) [4 days]	Phase 13: consolidation time [6 days]
Phase 06: 3rd excavation (4) [7 days]	Phase 14: 6th excavation (9) [17 days]
Phase 07: installation of bottom slab (5) [8 days]	Phase 15: bottom slab installation (10) [17 days]
Phase 08: 4th excavation (5) and removal of strut (3) [4 days]	Phase 16: removal of the strut (6) [12 days]
N.B.: numbers in () are construction sequences (Figure 8.10) and [] are consolidation and execution time	

Figure 8.16 shows the calculated results of the displacement of the wall at the end of the excavation stage. Both the results from drained and consolidation analyses are presented in the diagram. It can be seen from Figure 8.16 that the FEM - computation shows significantly large displacement than it was measured at the field. A maximum displacement of 112.3 mm (drained) and 79.3 mm (consolidation) at the top of the southern outer wall was computed compared to the measured top displacement of 23 mm. Similarly, 30.9 mm (drained) and 28.4 mm (consolidation) was computed at the top of the northern outer wall compared to a measured value of 16 mm. As would expected the consolidation analysis has led to a lesser displacement than the drained analysis.
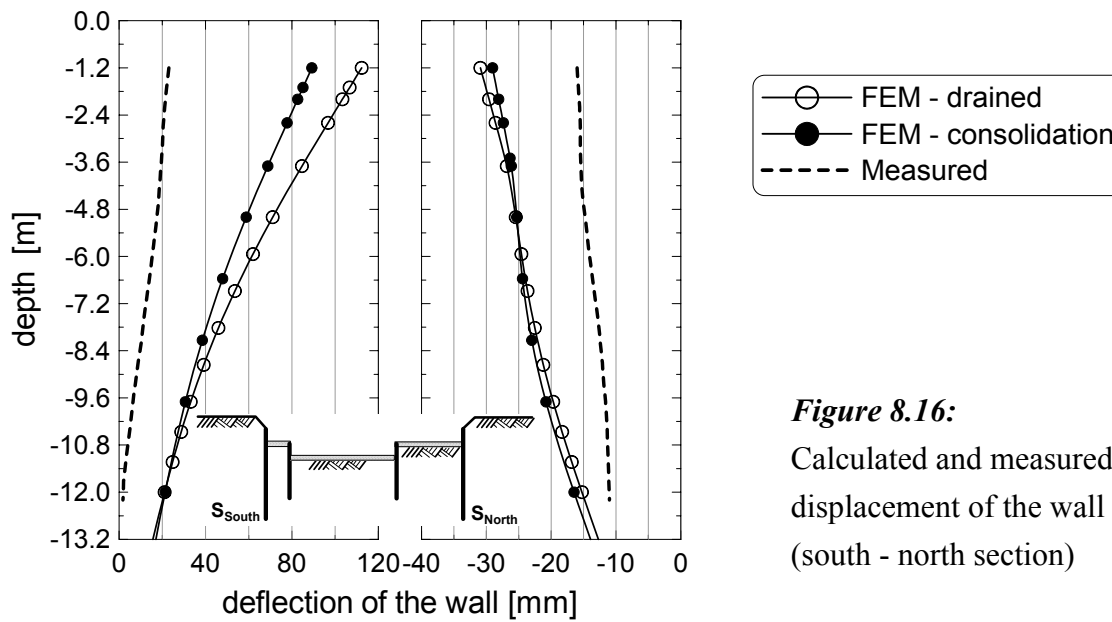
Figure 8.16:
Calculated and measured displacement of the wall (south - north section)

b)   *West-east section (Section I-I)*

The excavation in the west-east section consists of several slices of trenches that were executed on the daily output basis (Figure 8.3). After each slice of trench had been cut, it followed immediately the placement of fast hardening concrete bottom slab securing a bottom support to the walls in the south-north direction. The excavation was started at strip No. 2.5 (Figure 8.3) or sequence No. 3-1 (Figure 8.13) and proceeded to the left and right alternately towards the berms supporting the walls. An attempt has been done to simulate these excavation and construction processes in the FEM-computations, and both drained and consolidation analyses have been carried out. The simulation of the excavation of each trench and placing of the slab immediately may have no much influence on the results of a drained analysis, because it is quite the same whether a mass of soil is excavated at once or in parts. The sum of the excavation at end is more important than the consequence and duration of each trench excavation.

b1)   *drained analysis*

The construction stages followed in the drained analysis are presented in Table 8.5 in a simplified manner. Displacements up to the installation of the wall (inclusive) were set to zero.

Table 8.5:   Construction phases: drained analysis (Section I-I)

Phase 00: generate the initial stresses	Phase 13: installation of propped support (4)
Phase 01: activate surcharge load	Phase 17: installation of propped support (5)
Phase 02: 1st excavation to a depth of -1.2 m (1)	Phase 18: excavation of the slices 4.1 - 4.9 (6)
Phase 03: installation of the walls (2)	Phase 19: placement of the bottom slab (7)
Phase 04: excavation of slice 2.5 (3-1)	Phase 20: excavation of the slices 4.1 - 4.7 (8)
Phase 05 - 16: excavation of the slices in succession and placement of the bottom slab (3-2) to (3-13)	Phase 21: placement of the bottom slab (9)
	Phase 22: removal of the propped supports (4)&(5)
N.B.: numbers in brackets are construction sequence numbers in Figure 8.11	

b1)   consolidation analysis

The calculations phases in Table 8.6 have been followed in the consolidation analysis of the excavation in Section IV-IV. The undrained behaviour in the first 4 construction stages had been ignored. Also here the displacements up to the installation of the wall were set to zero.

Table 8.6:   Construction phases: consolidation analysis (Section I-I)

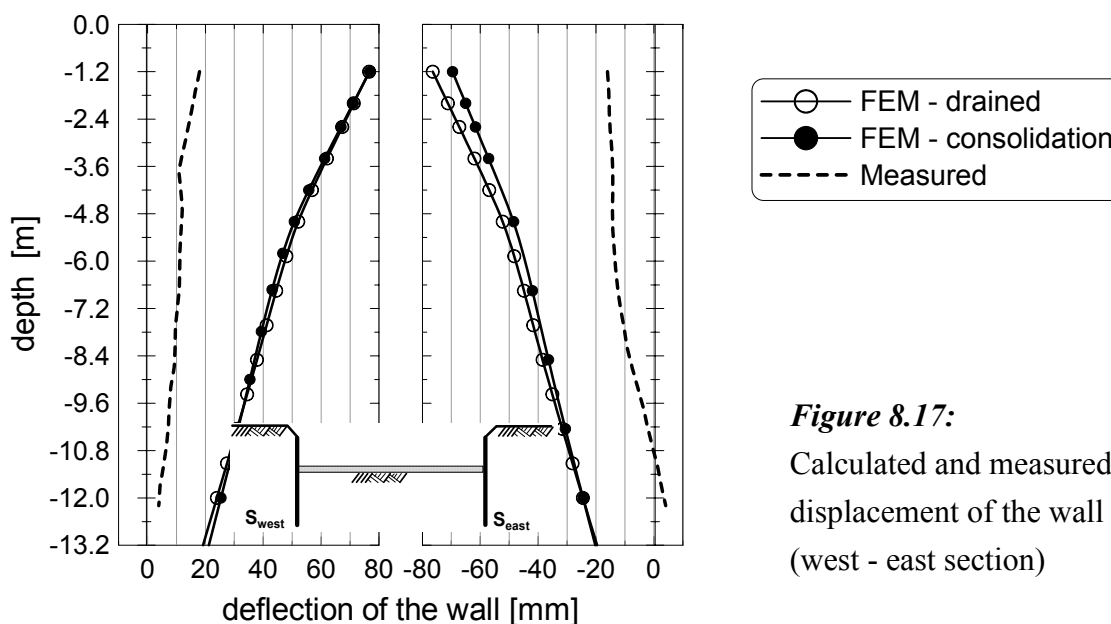|	
Phase 00: generate the initial stresses Phase 01: activate surcharge load Phase 02: 1st excavation to a depth of -1.2 m (1) Phase 03: installation of the walls (2) Phase 04: excavation of the first strip 2.5 (3-1) [1 day] Phase 05: excavation of the next strip 2.4 (3-2) [1 day] Phase 06: consolidation time [1 day] Phase 07: excavation of the next strip 2.3 (3-3) [1 day] Phase 08: consolidation time [2 days] Phase 09 - 13: excavation of the strips 2.6, 2.1+2.7, 2.8, 2.2, 2.4 in succession (3-4) to (3-8) [1 day each] Phase 14: consolidation time [3 days] Phase 15: excavation of the next strip 2.5 + 2.9 (3-9) [1 day each] Phase 16: consolidation time [8 days] Phase 17: excavation of the next strip 2.6 (3-10) and installation of the left support (4)[1 day]	Phase 18: consolidation time [4 days] Phase 19 - 21: excavation of the strips 2.7, 2.8 2.8, in succession (3-11) to (3-13) [1 day each] Phase 22: installation of the right support (5)[1 day] Phase 23: excavation of the strips 4.1-4.9 (6) [10 days] Phase 24: placement of the bottom slab (7) [11 days] Phase 25: consolidation time [10 days] Phase 26: removal of the left support (4)[2 days] Phase 27: consolidation time [3 days] Phase 28: excavation of the strips 4.1-4.9 (8) [7 days] Phase 29: placement of the bottom slab (9) [8 days] Phase 30: consolidation time [22 days] Phase 31: removal of the right support (5)[2 days] Phase 30: consolidation time [4 days]
N.B.: 1) numbers in () are construction sequence (Figure 8.11) and numbers in [] are consolidation and execution time *2) placement of the bottom slab in the previous trench followed during the excavation of the next strip*	

Figure 8.17:
Calculated and measured displacement of the wall (west - east section)

The computed and measured results of the displacement of the walls at the end of the excavation stage for the west-east section are shown in Figure 8.17. Surprisingly, Both the drained and consolidation analyses have led to almost the same wall displacement, but they are far from the measured value. Compared to the measured value of the displacement (18 mm) at the top of the west wall, a maximum displacement of 76.6 mm (drained) and 78.1 mm (consolidation) were obtained from the FEM-computations. Similarly, displacements 76.4 mm (drained) and 71.2 mm (consolidation) were computed at the top of the eastern wall compared to a measured value of 16 mm. It can also be seen from Figure 8.17 that the amount and shape of the displacement of the wall are almost identical, as if the excavation was symmetrical in respect to the loading and geometry.

It would appear from the preliminary analysis and comparison of the measured and computed displacement of the walls that the results did not match to each other. The possible cause of the deviation of the FEM - results from the measured values may be summarised in three points as follows:

1)   Measured values are incorrect,
2)   Soil parameters are not correct or
3)   Construction details are not simulated correctly.

Since the field measurements are not accompanied by scientific expertise, the probability of mistakes during measuring and interpretations may not be fully ignored. However, the probability of making a mistake that lead to more than 300% differences at all measuring points is very unlikely. The deflection of the wall was measured using inclinometer with an accuracy of ±1 mm according the geotechnical report. Moreover, the construction was successfully completed without no remarkable damages on the surrounding structures. Therefore, point 1 may be ruled out as possible source of the deviation of the results. To investigate the two points as the main causes of the problem, a parameter study on a simplified geometry has been carried out and are presented in the section below.

8.2.6.4   Parameter study on simplified model geometry

In order to investigate the possible causes of deviations of the FE-computation results and the measured values, a simplified model geometry (Figure 8.18) was selected for further parametric study. This section was chosen for three reasons: the excavation was started here, there are relatively more measurements data available at this section, and the greatest deviation of the computed and measured deflection of the wall occurred at this section. The parameter study includes the interface properties, the ground water conditions, the stiffness of the soil, and an aspect of

constructional procedures. All the FEM-computations have been performed under drained condition. Hence, the parameters in Table 8.1 and 8.2 (Section 8.2.6.3) were adopted as a reference for the parameter study. The calculation stages are listed in Table 8.7.

Table 8.7: The construction phases for the reference case

Phase 00: generate the initial stresses Phase 01: activate the surcharge load Phase 02: 1st excavation to a depth of -1.2 m (1) Phase 03: installation of the walls (2) Phase 04: strut installation (3) and 2nd excavation (4)	Phase 05: installation of bottom slab (5) and removal of the strut (3) Phase 06: 3rd major excavation (6) Phase 07: placement of the bottom slab (7)
N.B.: numbers in brackets are construction sequences (Figure 8.18)	
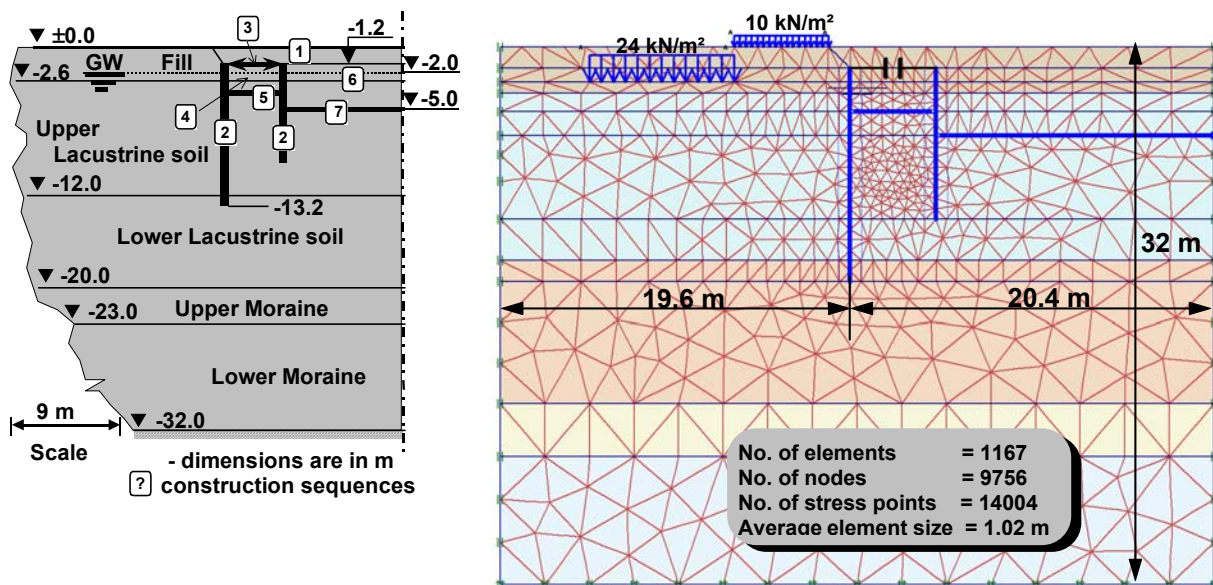
Figure 8.18: Section and FE-mesh for the parametric study of the project

The interface behaviour

The interface behaviour was simulated using the MCM. Instead of relating the interface properties to the soil properties by the so called interface factor R_{inter}, a separate material set was defined for the interface elements independent from the soil clusters. Defining the interface behaviour by the factor R_{inter} may not only reduce the shear parameters by this factor, but also the shear modulus of the contact surface by a factor of $(R_{inter})^2$ (*see Freiseder (2000) and PLAXIS MANUAL (2002)*). This in turn may results in excessive and unrealistic deformations in excavations in soft soil, where a small value of R_{inter} should be used. For this reason and according to the test result of the contact property (Section 6.6) the stiffness of the interface elements was set the same as the surrounding soil elements throughout this study, while the shear parameters were

reduced by a factor of 1/3 for the soft soils. In this section the possible influence of the interface properties has been examined by varying the shear parameter of the interface and the virtual thickness of the interface. The following cases have been investigated:

Case 0:   Reference case (R_{inter} = 0.33 and Virtual thickness factor = 0.10 (default))
Inter-case 1: R_{inter} = 0.50
Inter-case 2: R_{inter} = 0.75
Inter-case 3: R_{inter} = 1.00
Inter-case 4: Virtual thickness factor = 0.05
Inter-case 5: Virtual thickness factor = 0.20
Note that the factor R_{inter} was only applied on the shear parameters.

Figure 8.19 shows the influence of the variation of the interface properties at three selected points, namely, at wall head (A), at wall toe (B) and around 6.5 m behind the wall (C) . It can be noted that varying the value of R_{inter} from the reference value of 0.33 to 1.00 has led to a reduction of wall displacement at A by about 25%, no significant change at point B, up to 40% reduction of the surface settlement at C. These changes are not large enough to bring the computed displacements to the measured values. It is also interesting to note that the higher the value of R_{inter}, the lesser will be the deformation differences and that the interface properties has no remarkable influence on the toe displacement. Compared to the reference values, no significant change was observed for the cases of varying the virtual thickness of the interface from the default value 0.1 to 0.05 and 0.20. Therefore, one may rule out the interface properties as a main source of the differences between the calculated and measured results, though it might contribute partly to the problem.
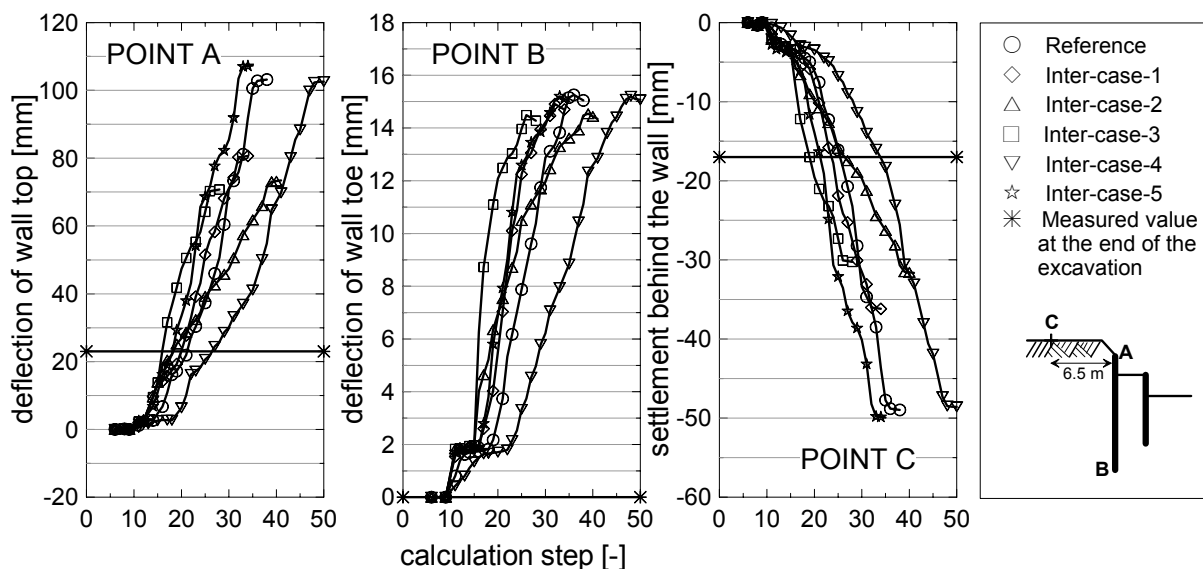

Figure 8.19: The influence of the interface properties

The stiffness of the soil

It is well known that the modulus of deformation of the soil strongly influences the calculated behaviour of the excavation. The differences in the measured and calculated deformations, not only by excavations but also by shallow foundations, are usually related in the literature that the estimation of the deformation modulus in laboratory test underestimates the real stiffness of the soil at the field. On the other hand, we have seen in Section 7.3.3 that increasing the E_{50}^{ref} by 50% above the reference value contributed to about 24% reduction of the maximum wall displacement only, and increasing the E_{oed}^{ref} by the same amount have had no major influence. To examine the effect of the stiffness parameters based on the practical project, the following cases have been investigated:

Case 0:   *Reference case*
SS-case 1:   *Increase the E_{50}^{ref} and E_{oed}^{ref} of the fill, the upper and the lower lacustrine layers*
               by a factor of 1.5 and the E_{ur}^{ref} by a factor of 1.3
SS-case 2:   *Increase the above stiffness parameters by a factor of 4*
SS-case 3:   *Increase the stiffness of the fill layer only by a factor of 4*
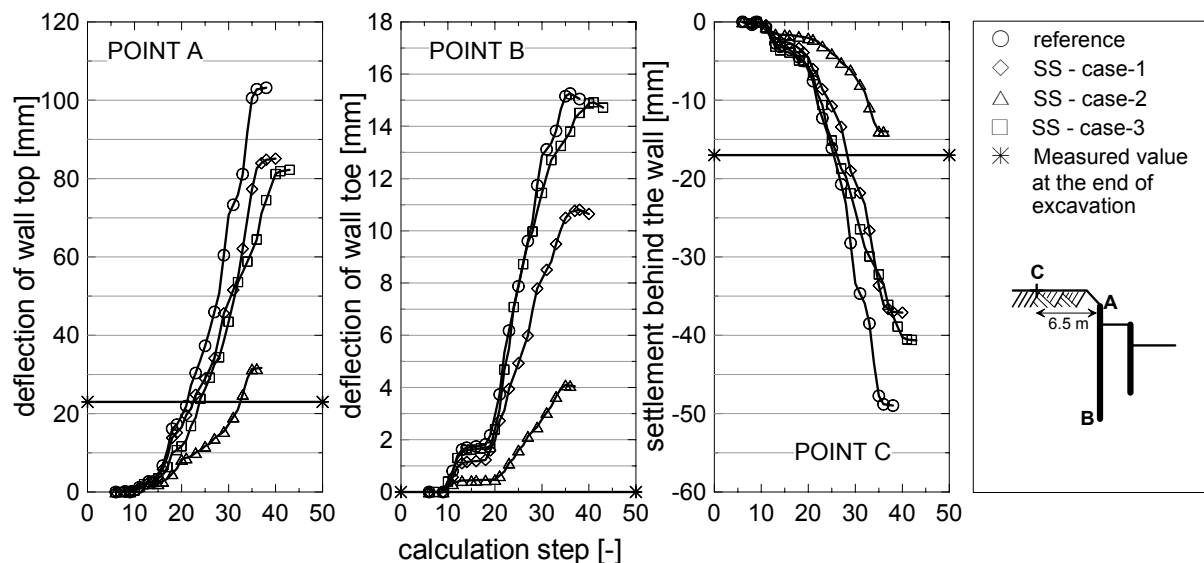
Figure 8.20:   The influence of the stiffness parameters

Figure 8.20 shows that the stiffness values of the upper three layers should increase by a factor as high as 4 in order to arrive at computed deformations that are fairly comparable with the measured values. An efficiency of deformation reduction up to 73% was achieved in the case of increasing the stiffness values by a factor 4 (*SS-case-2*). The assumption that the fill layer can be stiffer than usually would have taken due to the existing buildings and asphalt streets (SS-case3) does not help to reduce the deformations to a level of the measured values. The parameter variations has clearly shown the influence of the stiffness parameters, however, whether this was the

main source of the difference between the computed or the measured values should be cleared later in this section.

The groundwater condition

The reference computation was carried out by assuming a hydrostatic groundwater level at 2 m below the ground surface for all soil layers. In the geotechnical report, however, different ground water levels are indicated for different layers (see Section 8.2.3). A free water in the fill layer at - 2 m depth on average (Figure 8.7) and a confined groundwater in the moraine layer was encountered, but it was not well known which water table governed in the relatively impermeable layer of the lacustrine soft soil. A drainage filter was also constructed just behind the sheet pile wall to a depth of 1.2 m below the wall head (Figure 8.21), in order to relieve the wall from groundwater fluctuations. These variations of the ground water condition together with groundwater flow analysis have been considered in the study and they are categorised as follows:

GW-case 1: *GW flow analysis instead of hydrostatic groundwater table*
GW-case 2: *Consider the drop of the GW due to drainage filter*
GW-case 3: *Assume the GW table at -2 m for the fill layer, at -1 for the moraine layer and for the lacustrine layers interpolate between the two*
GW-case 4: *Assume the GW table at -2 m for the fill layer, at -12 for the moraine layer and for the lacustrine layers interpolate between the two.*
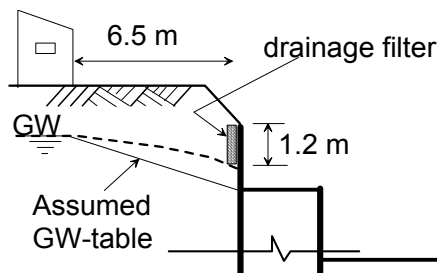
Figure 8.21:

Sketch of the drainage filter behind the wall and assumed groundwater line

Figure 8.22 shows no significant change of the deformations at point A and C due to the groundwater flow analysis but there is up to 45% reduction of the deformation at point B when compared to the reference values. The second case of the GW analysis shows a 22 and 17% reduction of the wall displacement at points A and B and an increase of the settlement at C by about 11%. The GW-case 3 shows no significant influence at points A and C but a reduction of the wall toe displacement by about 31%. The most noticeable effect can be observed from the GW-case 4 analysis results. As it can been seen from Figure 8.22 that there is a 50 - 65% reduction of the deformations at the given points. In general, the above results show that the importance of the detailed information on the groundwater condition and the type of analysis.

Figure 8.22: The influence of the groundwater conditions

Other various factors

To this group belong the effect of the plastic behaviour of the sheet pile wall, the no surcharge effect, the effect of considering the surcharge as a rigid body in stead of distributed load, the effect of replacing the bottom slab with a fixed strut, the effect of shifting the transition between the upper and lower lacustrine layer to -9.7 m from 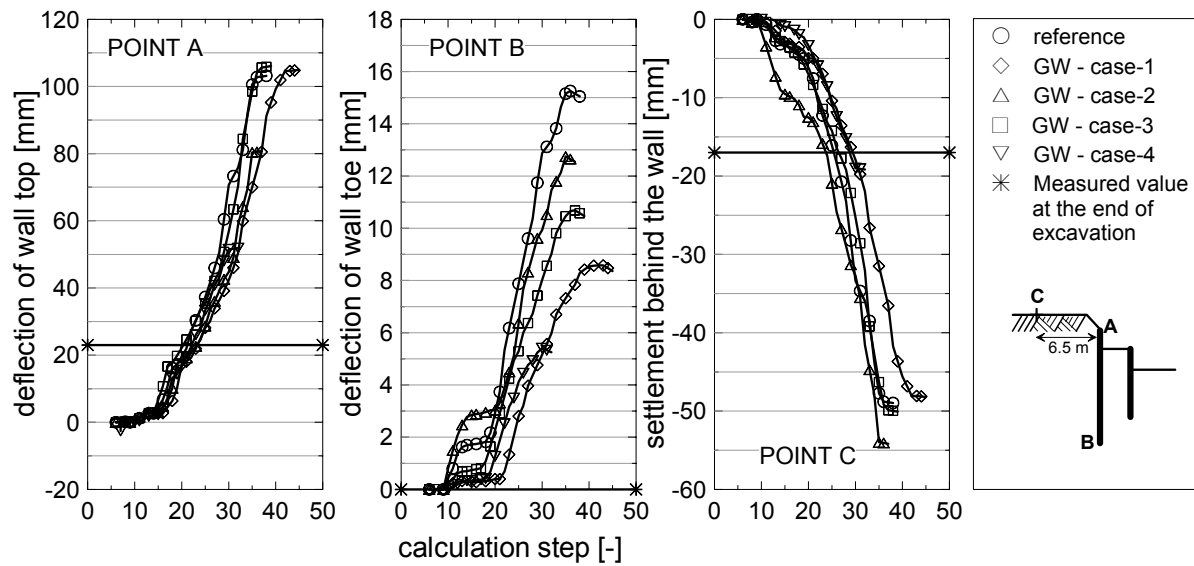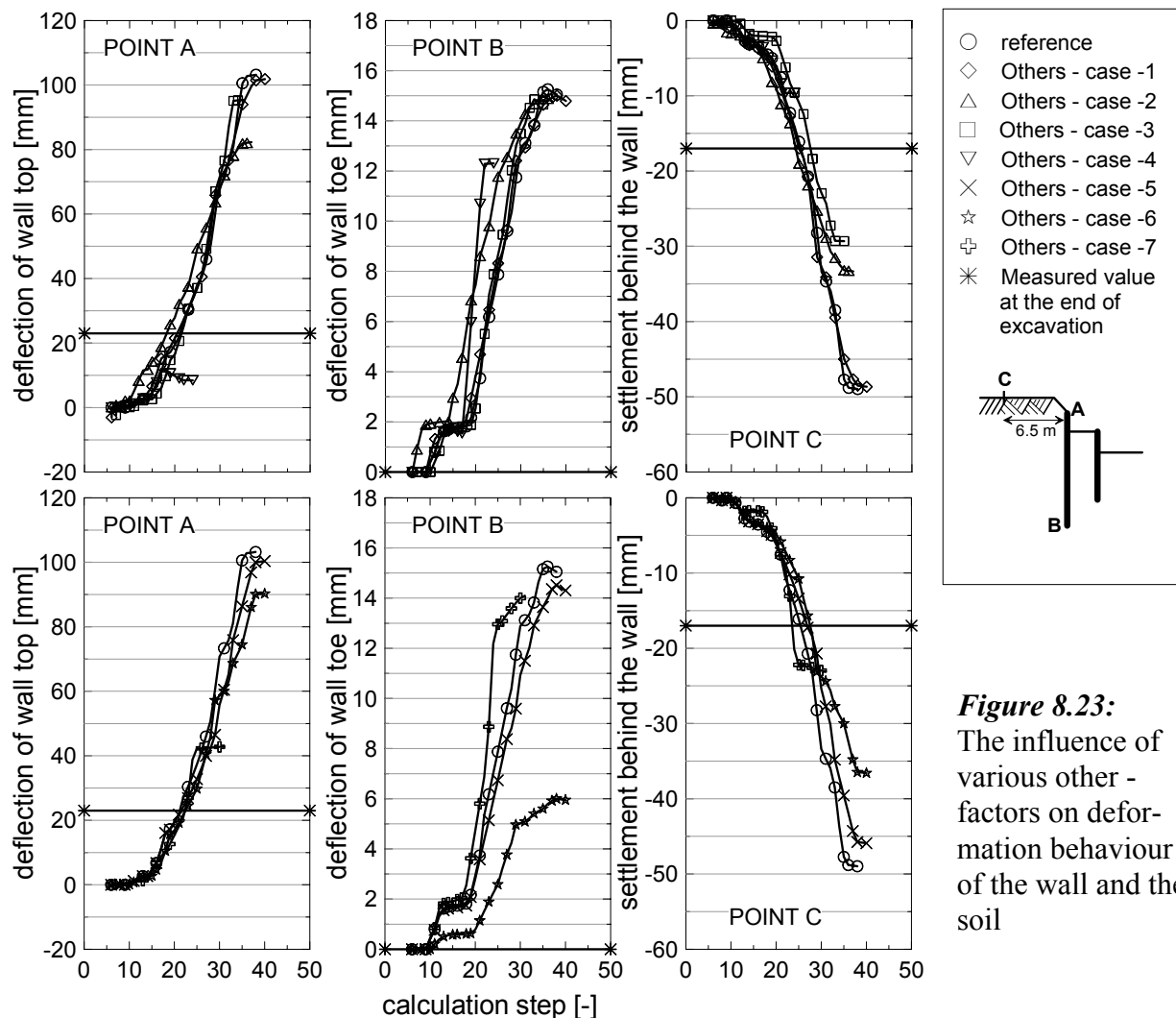the -12.0 m depth below the ground surface and, increasing the stiffness of the lower lacustrine layer by a factor of 3 (after shifting the layer).

Others-case 1: Plastic behaviour of the sheet pile wall: Most often the assumption of the elastic behaviour of the wall might be sufficiently enough for practical purposes. To examine the possible effect of the plasticity, the material behaviour of the wall was defined as elastoplastic by defining an additional parameters: the maximum bending moment of $M_p = 505\ kNm/m$ and the maximum axial force of $N_p = 3612\ kNm/m$ (Profile ARBED AZ18-240). The analysis result (Figure 8.23-top) shows no influence of this variant on the displacement of the wall at the top (A) and at the toe (B) and the settlement of the ground surface at C.

Others-case 2: Without surcharge load: A surcharge load of 24.4 kN/m² and a traffic load of 10 kN/m² was assumed in the computation of the reference case at a depth of -2 m and at the ground surface respectively. To see the possible effect of these loads, they are set to zero. The result of the analysis (Figure 8.23-top) shows about 20% less displacement at A and about 30% less settlement at C, but no effect on the wall displacement at B.

Others-case 3: Simulation of the building load with a rigid porous body: A cluster was defined which is equal to the building width and 2.0 m deep below the ground surface with a porous linear elastic material property ($\gamma = 18\ kN/m^2\ and\ E = 1.0 \times 10^7$). This is equivalent to the total

weight of a 3 storey building ($\approx$ 36 kN/m²). This assumption led to a negligible effect at point A and B, but to about 40% settlement reduction at C (Figure 8.23-top).

Figure 8.23: The influence of various other - factors on deformation behaviour of the wall and the soil

Others-case 4: The bottom slabs assumed as fixed struts instead of plates: The bottom slabs were represented by a plates in the reference case. This may have a negative effect, because the slab plates are automatically connected (either fixed or hinged) to the wall, i.e., the wall may move upward when the slab moves, which does not mirror the situation in the field. The hinge connection was chosen in this study. The advantage of such plates is their flexibility and stability effect because of their weight. An alternative to the simulation of the bottom slab is to introduce a fixed support, but this option does not allow any horizontal movement. The comparative effect of both options are investigated under the *others-case 4*, and the results are shown in (Figure 8.23-top). At first glance, it would appear that this option would be the most effective means of reduction the displacements, as the displacements at A, B and C are reduced by about 92, 18 and 80% respectively compared to the reference value. There is even 50% less displacement of the wall at A.

However, looking at Figure 8.24 one can easily observe the shape of the computed displacement of the wall which is completely opposite to the shape of the measured displacement. The fixed struts at the level of the bottom of excavation (sequence (5), Figure 8.18) provide non-yielding support to both wall, even it holds back the internal wall. The whole system above the excavation level reacts rigid, but this does not show the reality, and therefore should be ruled out from the options.
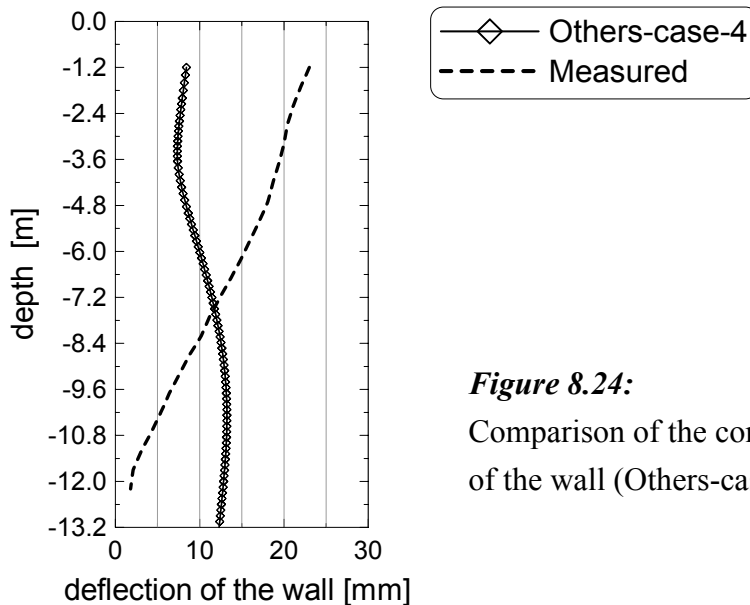

Figure 8.24:

Comparison of the computed and measured displacement of the wall (Others-case-4)

Others-case 5: Shifting the depth of the transition from the upper to the lower lacustrine soil layer to a depth of -9.7 m: It can be seen from the measured values (Figure 8.10) that no displacement was recorded at the toe of the outer sheet pile wall (south), indicating a possible fixed support of the wall around the foot. In order to provide a fixed support at the foot, the layer of the lower lacustrine soil was shifted upward to a depth of -9.7 m below the ground surface. If one closely examine the cone penetration field test results, there is a room for possible variation of the boundaries of the layers. However, this option alone did not help to avoid the computed wall displacement at the toe of the wall (Figure 8.23-bottom). Further, one more variation was investigated by improving the stiffness of the lower lacustrine layer by a factor of 3 under the name *"Others-case 6"* in addition to the shifting of the layer. This option provides a 56% reduction of the wall displacement at B (Figure 8.23-bottom), whereas its effect at points A and B are moderate.

Others-case 7: Allowing the bottom slab support to effect earlier (3D effect): At last but not least, the 3D effect was investigated. As shown in Figure 8.2, the excavation was executed in slices of trenches based on daily output. Immediately after excavation of each trench, a fast hardening concrete was placed which provided a bottom support to the walls in south north directions, be-

fore the next excavation has been proceeded. The measured wall displacements (Figure 8.10) also clearly show the effect of the bottom slab, in which a buckling of the sheet pile wall at the level of the bottom slab can be seen. In other words, the slab was already in effect before the end of the excavation. Such excavation procedure is a 3D problem, and can be best solved using corresponding 3D-finite element programs. However, in this 2D study an earlier effect of the bottom slab was assumed by means of activating it after excavating half of the soil mass but before the end of excavation in each excavation phase. That is, the calculation phases 04 to 07 (Table 8.7) was changed as shown in Table 8.8.

Table 8.8: Modified construction phases for the analysis of *"Others-case 7"*

Phase 00: generate the initial stresses Phase 01: activate surcharge load Phase 02: 1st excavation to a depth of -1.2 m (1) Phase 03: installation of the walls (2) Phase 04: strut installation (3) and 2nd excavation (4) to half of its depth	Phase 05: activate the bottom slab (5), rest excavation (4) and removal of the strut (3) Phase 06: 3rd major excavation (6) to half of its depth Phase 07: activate the bottom slab (7) and rest excavation (6)
N.B.: numbers in brackets are construction sequences (Figure 8.18)	

A comparative presentation of the results of the analysis of this variant with the reference and measured values is also shown in Figure 8.23-bottom. It appears that the computed result nears the measured value at point A and C, whereas it shows a little influence at point B. However, it should be noted that the assumption that the supporting effect of the slab starts after 50% excavation of the soil mass in the corresponding cluster, is purely a rough estimate. Therefore, an additional investigation using FE-3D-programm is required before this factor may be used in the analysis of practical projects and it should only serve for purpose of comparison of the measured and computed data in this study.

8.2.6.5 Presentation and discussion of the final results

Once the possible impact of the different parameters, construction and ground water condition have been studied, the next step is to make use of this parameter study to analyse the actual project. Although all the cases studied above might have impact on the deformation behaviour of the excavation, the last case (*Others-case-7*) in combination with the case *"Others-case-6"* has been identified as the major important factor. The earlier effect of the bottom slab has a major influence on the wall displacement at the top, and improving the stiffness of the soil around the toe will have an effect on the toe displacement. A combination of these two factor might lead to a result comparable with the measured values. Thus, the following cases have been considered for the final analysis of the excavation project in question:

Final-case-1: the same as "Others-case-7" in the parameter study (Section 8.2.6.4)
Final-case-2: the same as "Final-case-1" but with combination with "Others-case-6" in the
*   parameter study (Section 8.2.6.4)*
Final-case-3: the same as " Final-case-2"but with the consideration of the drop of the
*   groundwater table behind the wall due to the drainage filter (Section 8.2.6.4)*

Both drained and consolidation analyses were carried out, and the results are given in the figures below.

a)   Wall displacements

Figure 8.25 shows the computed and measured displacements of the southern and the northern walls for the cases described above. It appears from the figure that the consolidation analysis provides a smaller displacement than the drained analysis as expected. It is also interesting to observe that the first case (*Final-case-1: consolidation)* led to a displacement at the top which is comparable to the measured values, but it shows more displacement at the toe. However, combining this effect with improving the stiffness of the lower lacustrine soil (*Final-case-2: consolidation*) still results more computed displacement at the toe of the southern wall and a lesser displacement at the toe of the northern wall than the measured value. The possible explanation can be the difference in soil profile at this particular points. The third variant (*Final-case-2*) show no significance effect, and it can be neglected.
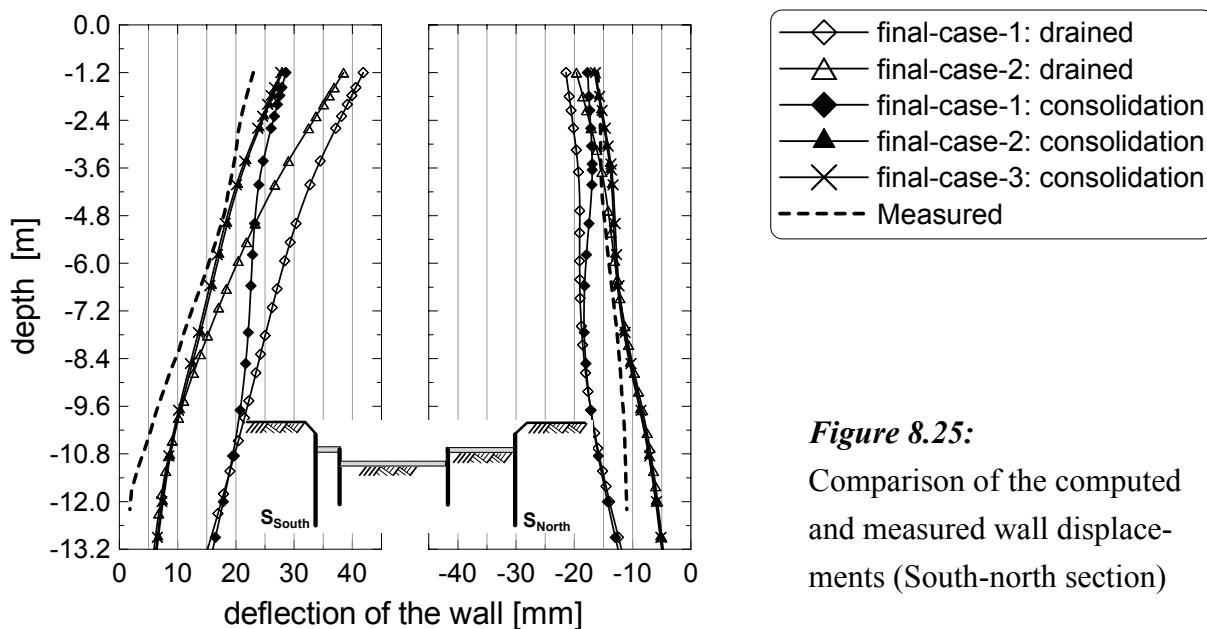

Figure 8.25:
Comparison of the computed and measured wall displacements (South-north section)

The computed displacement of the west-east walls for the variant *"Final-case-2"* only is shown in Figure 8.26. It can be seen from the Figure 8.26 that the computed displacement from the consolidation analysis match fairly well the measured displacement of the wall. The shape of the

measured displacement of the eastern wall does not match with the computed shape. The toe of the wall also shows movement in the direction of the soil mass. A difficulty of interpretation of the inclinometer measurement at this location was reported in the geotechnical report, and hence the comparison with the computed displacement should take this into account.
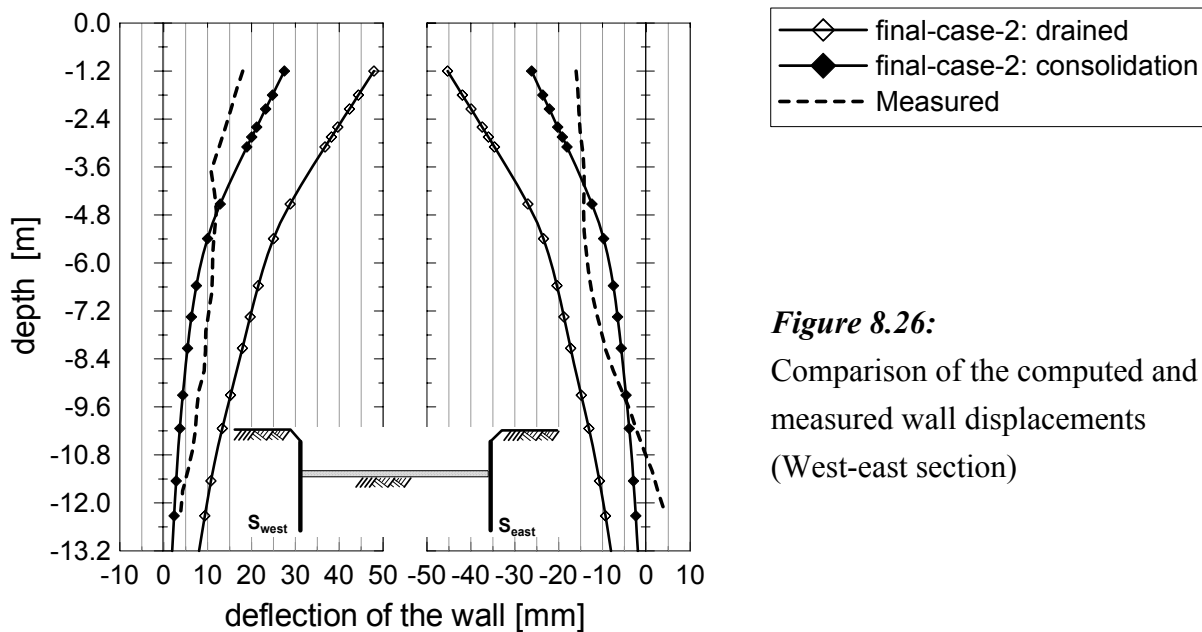
Figure 8.26:
Comparison of the computed and measured wall displacements (West-east section)

b)   Displacements at the wall top

The measured displacements of the wall head at selective points on the southern wall compared to the computed displacements are shown in Figure 8.27. It can be seen from the figure that the consolidation analysis (*Final-case-2: consolidation*) result matchs fairly good with the observed displacements at the locations LM23 to LM26.
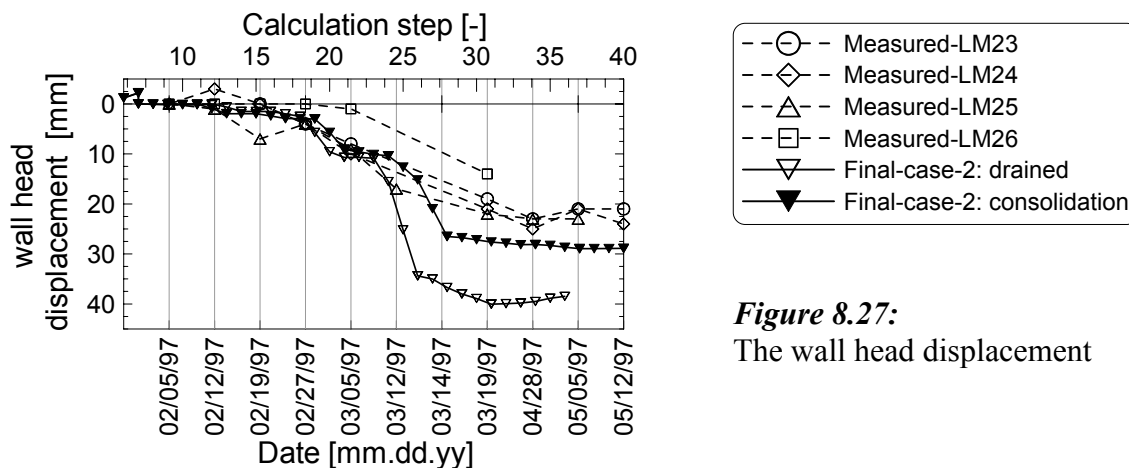
Figure 8.27:
The wall head displacement

c)   *Settlement at the surface behind the wall*

Two representative computed settlements from drained and consolidation analyses are given in Figure 8.28 for the variant *"Final-case-2"*. The Figure 8.28a shows the computed ground surface settlement at the location in front of the existing building which is 6.5 m behind the southern wall (Raueneckegasse) and the measured settlements at the locations HP4 and HP5. The course of the computed and measured settlement curves is more or less similar. It should be noted that the computed settlements are given in terms of the calculation steps, whereas the measured settlements are drawn based on the real construction time. However, one can clearly identify the different construction phases from the course of the curves, and one may easily compare the computed and measured results. Moreover, the computed settlements up to the installation of the walls (inclusive) have been set to zero, whereas the measured settlements are displayed from the beginning of the construction. For example, a total settlement of about 5 mm was measured at HP4 immediately after the installation of the wall, and adding this value to the computed settlement will result even to a better agreement of the computed and measured settlements.

Similarly, Figure 8.28b shows the computed ground surface settlement behind the western wall (Sigismundstrasse) at a distance of 10.5 m compared to the measured settlements at measuring points HP23 and HP21. The consolidation analysis result shows a good agreement with the measured value as far as the course of the settlement curves is concerned.

Figure 8.28:

Computed and measured settlements:

a) behind the southern wall;

b) behind the western wall
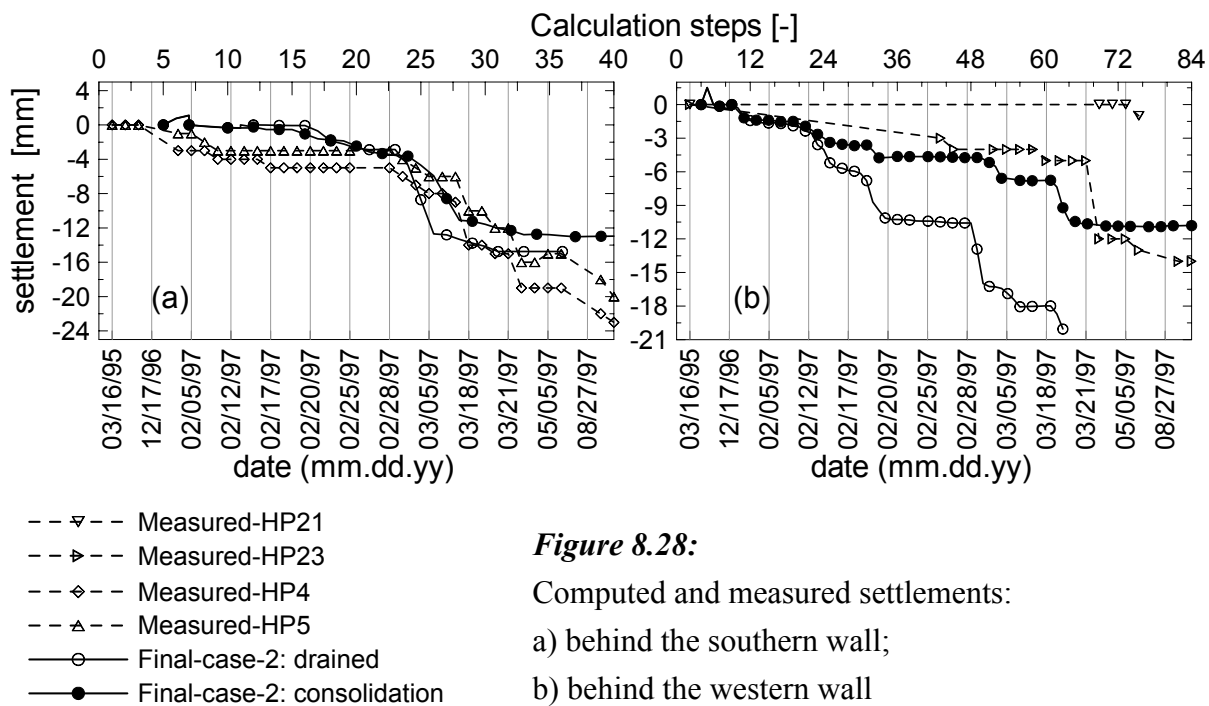
As would expected, the surface settlement from drained analysis is more than that of the consolidation analysis. As can be seen from Figure 8.28, the difference of the settlements is higher in the

west-east section than that of the south-north section, which indicates the effect of the simulation of the excavation of each slice, subsequent placement of the bottom slab and simultaneous consolidation.

d)   Pore pressure

The calculated excess pore pressure at three locations and at two different depths are shown in Figure 8.29. The measured pore pressure in Figure 8.11 shows a negative pore pressure as large as 80 kN/m², which could not be verified by the FE-analysis. It was mentioned (Section 8.2.5) that there was disturbance of the initial readings during the boring and installation of the transducers. Hence, taking the 2nd rows of readings as initial readings, that were recorded in three days difference to the first readings and there was no major excavation in this period, leads to a measured values that are comparable to the computed values (Figure 8.29).
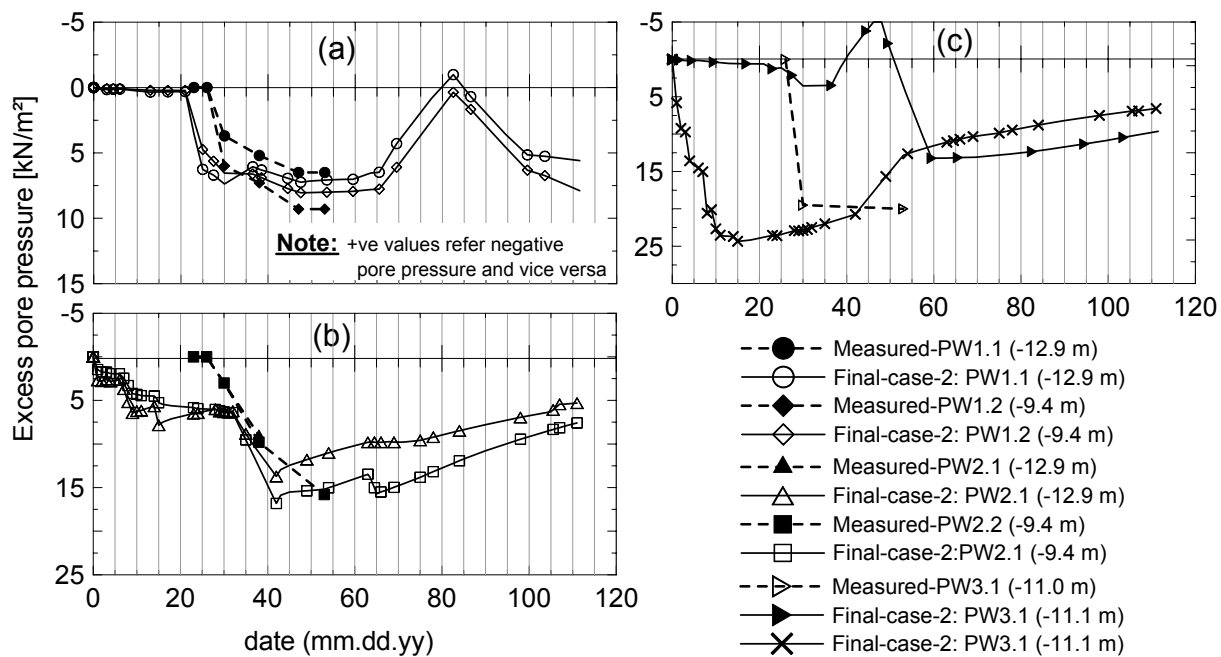
Figure 8.29: Computed and measured excess pore pressure

8.2.6.6   Summary and recommendations

From the preceding parameter studies and analyses of the actual excavation project, it may be concluded that all the variants considered may exercise an influence on the performance of the excavation, but the 3D-effect and the stiffness of the lower lacustrine soil showed the maximum influence. Therefore, for practical applications the following points should be considered:

1) Although the interface behaviour influences the FE- analysis result of an excavation, defining a separate material set with the stiffness properties adopted one to one from the corresponding soil layer and reducing the shear parameters by a factor 1/3 may lead to a reasonable results. This is also in agreement with the recommendation of the working group "Excavation" (EAB) (*Weißenbach (2002)*) for excavations in normally consolidated soils, where a wall friction angle of $\delta = \frac{1}{3} \cdot \varphi'$ was recommended. It was also shown that increasing the factor to higher value than 0.5 would not have much influence on the deformation. One may used a strength reduction factor R_{inter} between 0.33 and 0.5 for numerical computation of excavations in soft soils, keeping in mind the stiffness of the interface should remain the same as that of the soil.

2) Obviously, the groundwater situation will have a remarkable impact on the computation results. Hence a maximum effort and care should be taken in locating the groundwater table. The different water tables for different soil layers should also be considered in the analysis. The next important thing is the investigation of the pore pressure situation in the relatively impermeable lacustrine soil layer. Usually, the water table in the impermeable layer is interpolated between the water table of the layer beneath and above it. The author presumes that the actual water pressure in the impermeable layer might be less than that obtained from interpolation, because no free water was usually observed in such layers during excavation. A further investigation of the water pressure in such layers is highly recommended.

3) Although the effect of the stiffness of the soil on the deformation behaviour of the excavation is obvious, the author believes that the shear and stiffness parameters of the soft soil layer obtained from carefully conducted laboratory tests in combination with the consideration of the 3D-effect (see paragraph 6 below) and construction details may lead to a reasonable prediction of the upper bound of the deformations. Hence, the importance of performing triaxial, oedometer and permeability tests in laboratory for the soft soil layers should be underlined. In the absence of laboratory test results, the soil parameters of the relatively bearing layers may be estimated from the field penetration results after adusting them to fit to the selective soil model.

4) The bottom concrete slab should be modelled by means of plates, but not by a fixed end support, since the later might lead to a rigid system in contrary to the reality.

5) As far as this particular excavation project is concerned, the plasticity property of the sheet pile wall may have a negligible impact on the deformation behaviour of the excavation.

6) It was proved that the displacement of the top of the wall and the surface settlement behind the wall suffers most from the 3D-effect. The 3D-effect is here defined as the effect of the excavation and placement of the bottom concrete slab in slices of 2.5 m width. As shown in Figure 8.5, the bottom concrete slab in the first slice had already provided support to the wall during the next slice excavation. Such effect can only be modelled using a 3D-FE-programm, however, a simplified assumption has to be made to consider this effect in the 2D-FE-

computations. For example, the bottom slab may be assumed to be effective after 50% of the soil mass above it had been removed. This is purely a rough assumption but not unreal, hence an investigation of the 3D-effect using the 3D-FE-program would be worthwhile to verify the assumption and find out the real 3D-effect factor.

7) The constructional stages and procedures will have definitely an influence on the computational result of the excavation. Hence, it is highly recommended that the one who analyse the project with the FE-computer program should have a first hand information of the details of the excavation execution processes in order to reasonably predict the deformation behaviour of the excavation.

8) A consolidation analysis is the best way of evaluating the performance of an excavation at any time t after begin of the construction works. It provides the advantage of considering the yet not fully dissipated negative pore pressure in the excavation. This is also proved by the forgoing computations, where a better match with the measured values has been observed.

8.3   Project-II-Markgrafenstrasse - Constance

8.3.1   General

The excavation site was located in a built up area in southern Germany in the city of Constance. It was intended for the basement of a multi-storey residential apartment and the construction work was completed in 1993. The site plan together with site investigation and instrumentation locations is shown in Figure 8.30. The excavation was 5.4 m to 6.8 m deep, and covered an area of 55 m x 55 m at the longest side. The site was surrounded by 1- to 6-storey (with one basement floor) residential buildings as shown in Figure 8.30. All buildings are rested on mat foundation. At two sides (along MS2 and MS5), the excavation was very close (1.2 to 1.5 m) to the existing buildings. The soil exploration, the monitoring and the construction information are documented in *Kempfert + Partner (1991-1993)* and partly reported by *Kempfert/Stadel (1994)* and *Kempfert (1997)*. The main emphasis will be given to the back analysis of the project using the FEM after brief introduction of the site condition, instrumentation and recorded data.

8.3.2   Site condition

The site investigation revealed a ground comprising upper lacustrine silty clay of thickness 3 to 4 m with low to medium plasticity and soft to stiff consistency, overlying very soft lower lacustrine clay of thickness 6 to 8.5 m. Beneath the lower lacustrine layer was a low plastic lacustrine clay

mixed boulder clay of thickness 2 to 3.5 m overlying moraine gravel. Although no investigation was made to estimate the extent of the moraine layer, it was believed from the experience that it extends at least up to the depth of 32 m below the ground surface. Beneath the moraine layer, a boulder clay layer is usually assumed in Constance area. The groundwater was assumed to be located at 2 m below the ground level.
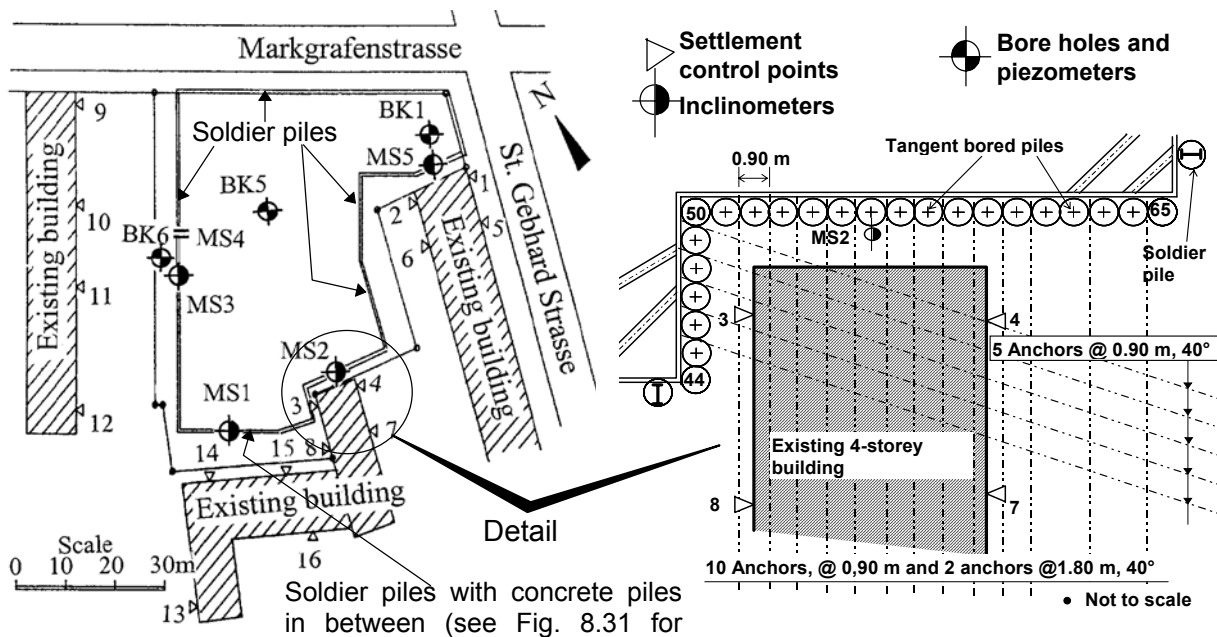
Figure 8.30: Site plan, location of boreholes and instrumentation

8.3.3   Support system

The excavation was supported by three types of wall systems. The larger part of the excavation, i.e., the west-northern side (along MS3 &MS04), the north-eastern side (parallel to markgrafen street) and part of the east-southern side (Figure 8.30) were supported by soldier piles with timber sheeting. The soldier pile was made up of IPB 600 I-steel beam section, and it was placed in a pre-bored 90 cm diameter concrete footing which penetrates 2.5 m deep inside the moraine layer starting just below the excavation bottom. The piles were located at a spacing of 2 and 2.5 m.

In the south-western side (along MS01), the excavation was supported in a similar way as above with soldier piles, but concrete pile sheeting instead of the timber sheeting. One 75 cm diameter reinforced concrete piles and two 62 cm diameter concrete piles (Figure 8.31) were placed between the soldier piles. These concrete piles penetrated 2 m below the excavation depth.

Figure 8.31: Detail of support along the side where MS01 is located **(**Figure 8.30*)*
[Photo: Kempfert]
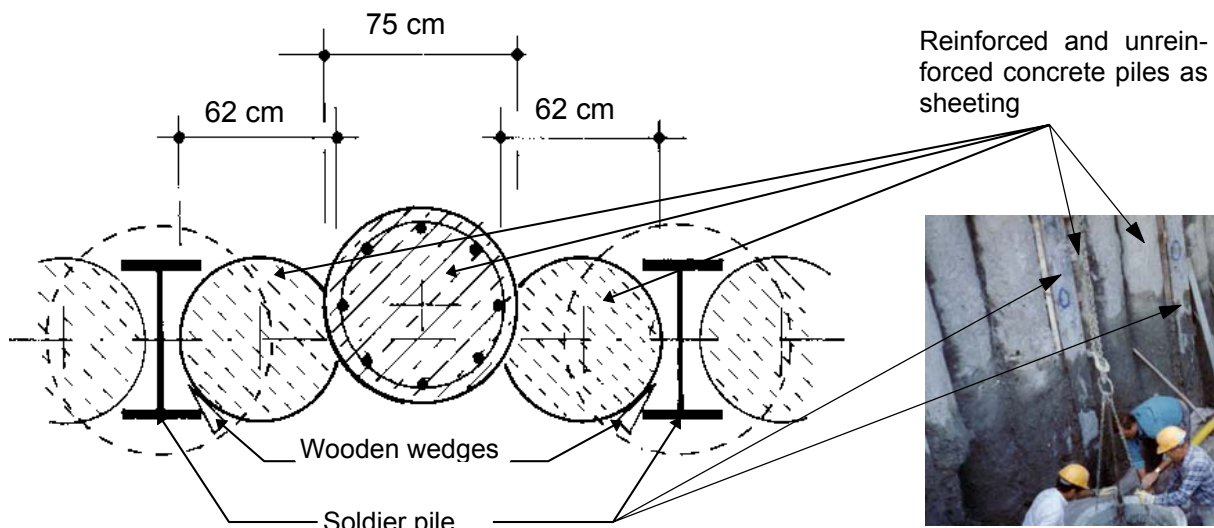
The rest of the excavation (along MS02 and MS05) were supported by 0.90 m diameter tangent bored concrete piles (see detail on the left side of Figure 8.30). The piles penetrated 2 - 3 m into the moraine layer.

All the wall systems were supported by ground anchors of the type "Techno-Anchor, 6ϕ 12 St 1420/1579" inclined at 40° below the horizontal at a spacing of 0.9 m in the case of tangent concrete piles and 2 to 2.5 m in the case of soldier piles. The anchors extended 3.8 to 4.5 m deep into the moraine layer. All anchors were supposed to be pre-stressed to a load of 80-100% of their design load. The walls were supported by struts at all internal corners.

8.3.4   Results of monitoring

a)   Surface settlements

The settlements at 16 locations near the existing buildings were monitored using surface surveying starting prior to the beginning of the construction activities. The locations of the measuring points are shown in Figure 8.1. Figure 8.32 shows the result of settlement monitoring. As shown in Figure 8.32 a, c and d, no significance settlement was recorded at the corresponding measuring points. On the contrary, unlike the expectation a maximum settlement of 12 to 55 mm was observed at measuring points 3, 4, 7 and 8 (Figure 8.32 b), where there was a very stiff wall system on this side of the excavation. As shown in Figure 8.32b about 80% of the settlement occurred during the installation of the anchors. The cause of this problem was reported and discussed by

Kempfert/Stadel (1994) and *Kempfert (1997)*. Also *Kempfert/Gebreselassie (1999)* tried to follow the settlement due to anchor installation of this project using a combination of analytical and numerical methods.

b)   Wall deflection

The deflection of the wall was monitored by means of inclinometers at five locations. The results of the inclinometer measurements at three measuring points (MS01, MS02 and MS03) are given in Figure 8.33. As can be seen from this figure, the walls deflect toward the soil due to the anchor pre-stressing, showing that the soil in the upper layers could not bear the load. The anchors were pre-stressed to a force of 80-100% of the design load, i.e., 400, 630 and 429 KN at MS01, MS02 and MS03 respectively (Figure 8.34). The subsequent measurements also show no significant change of the deflection of the wall even at the end of the excavation.
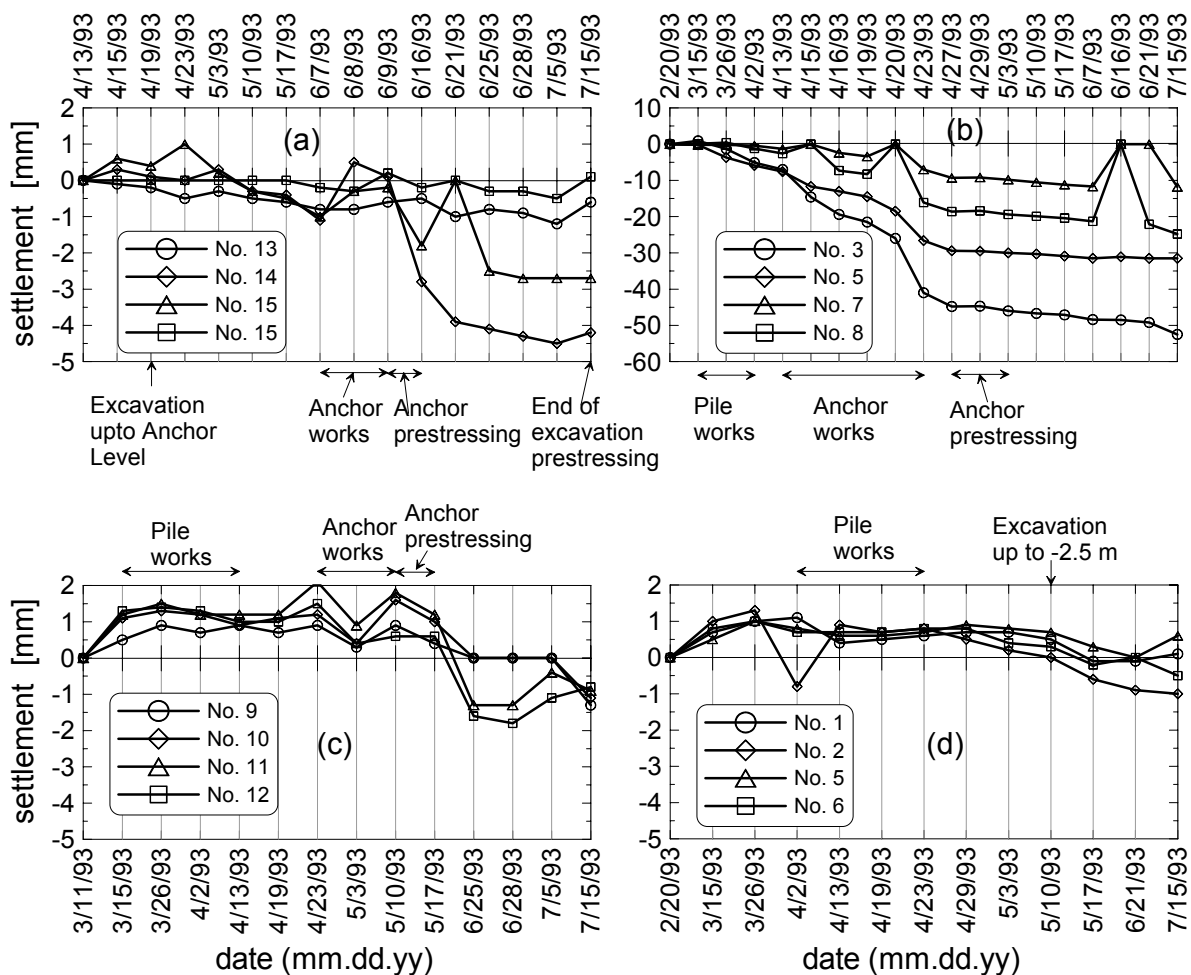
Figure 8.32:   Measured settlements around the existing buildings
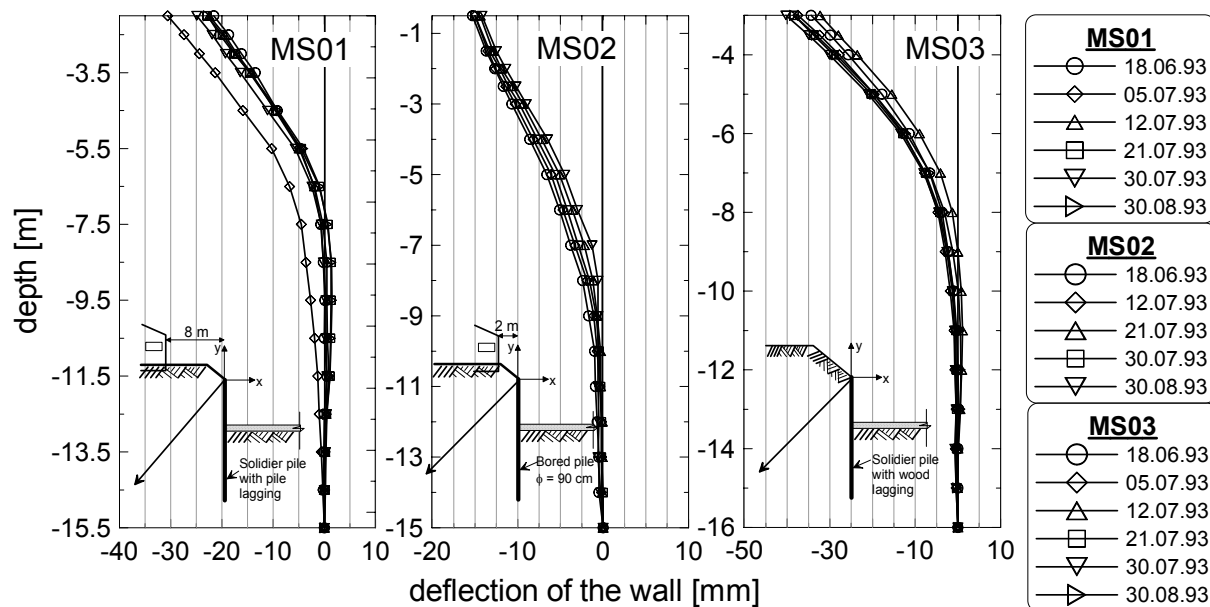
Figure 8.33: Measured deflection of the wall

c) Anchor force

The anchor forces were also measured at different time of the construction stages. As shown in the Figure 8.34, the anchor had yielded slightly during the subsequent excavations showing a drop of 37, 20 and 29 kN at the measuring points MS01, MS02 and MS03 respectively.
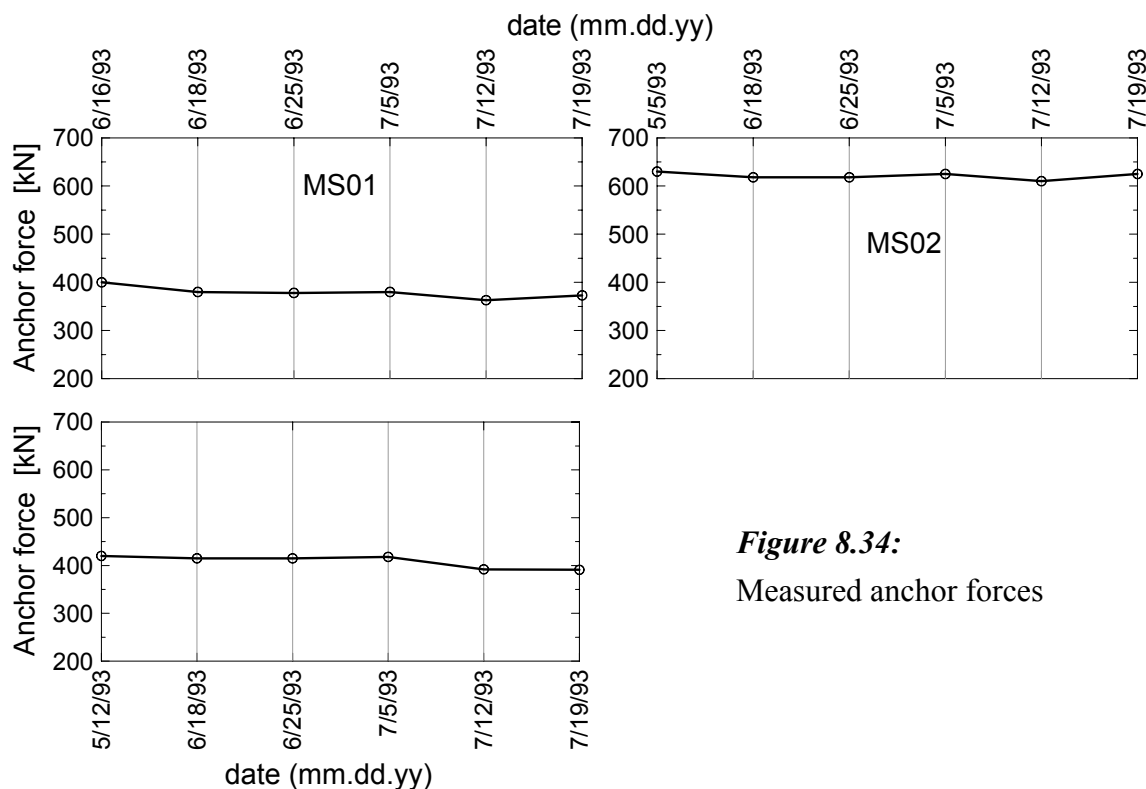
Figure 8.34:
Measured anchor forces

8.3.5   Back analysis of the excavation project-II using the FEM

8.3.5.1   Model geometry and the finite element mesh

Three sections, namely, section through the inclinometer measuring points MS01, MS02 and MS03, were selected for the back analysis of the excavation project using the FEM, because there were three different wall systems (see Section 8.3.3) at these locations and settlement and wall deflection measurements were available. The soil profile at these section were more or less the same. The idealised soil profile, arrangement of the structural elements, sequences of the construction and zoomed finite element mesh at the sections MS01, MS02 and MS03 are drawn in Figure 8.35, Figure 8.36 and Figure 8.37 respectively.
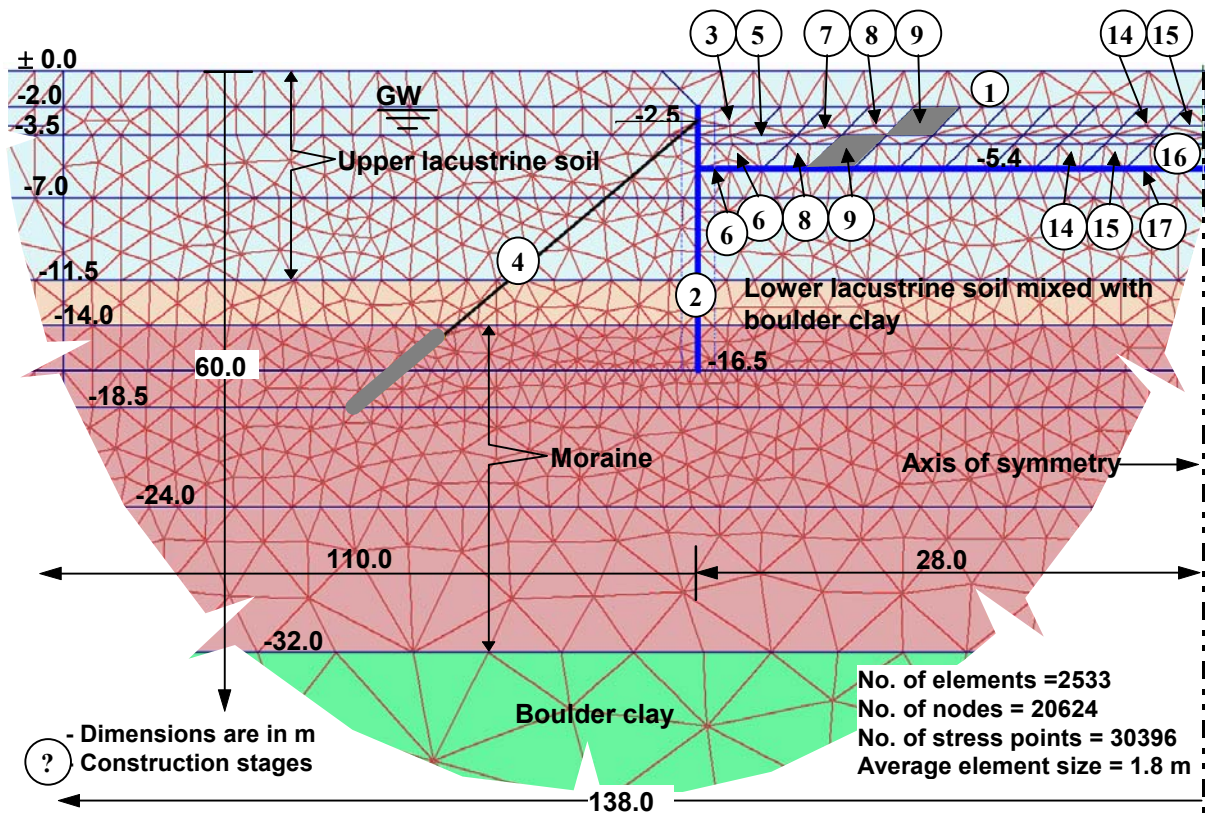
Figure 8.35:   Model geometry, excavation sequences and the finite element mesh for the section through MS01

The size of the models were chosen according to the recommendation of the "Working Group Numeric in Geotechnical Engineering" (*Meißner (2002)*) and the parameter study in Section 7.3.2. The finite element mesh at MS01 and MS02 was extended to a depth of 60 m where a fixed

Figure 8.36: Model geometry, excavation sequences and the finite element mesh for the section through MS02

Figure 8.37: Model geometry, excavation sequences and the finite element mesh for the section hrough MS03

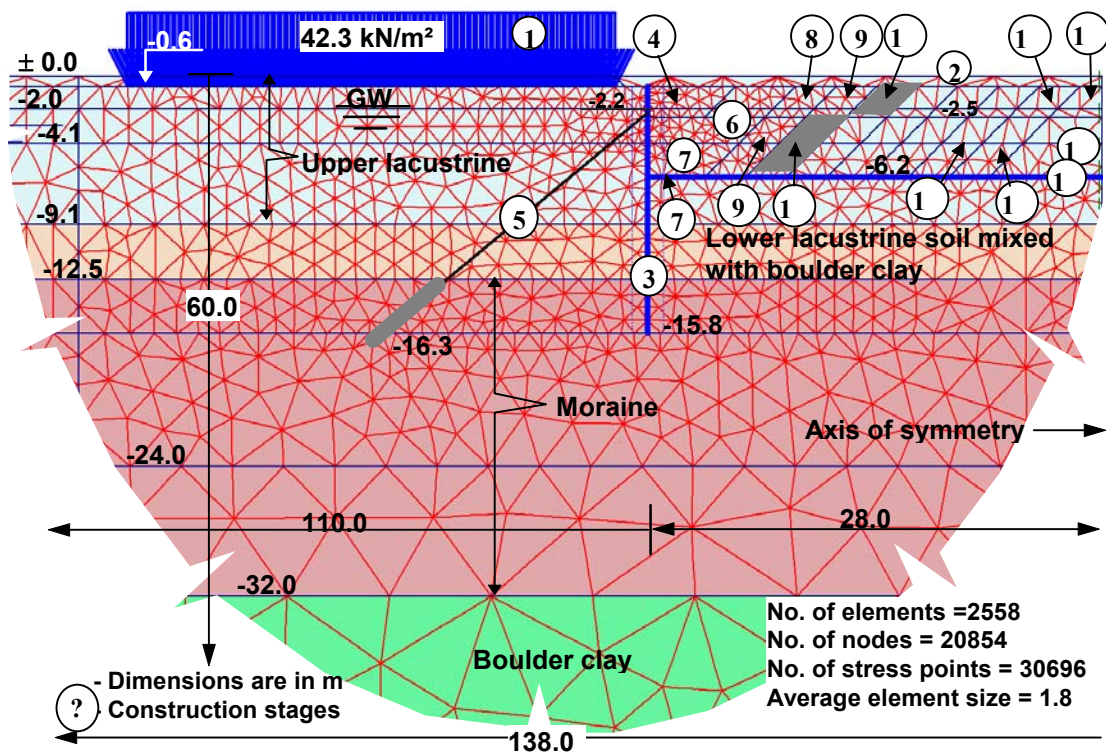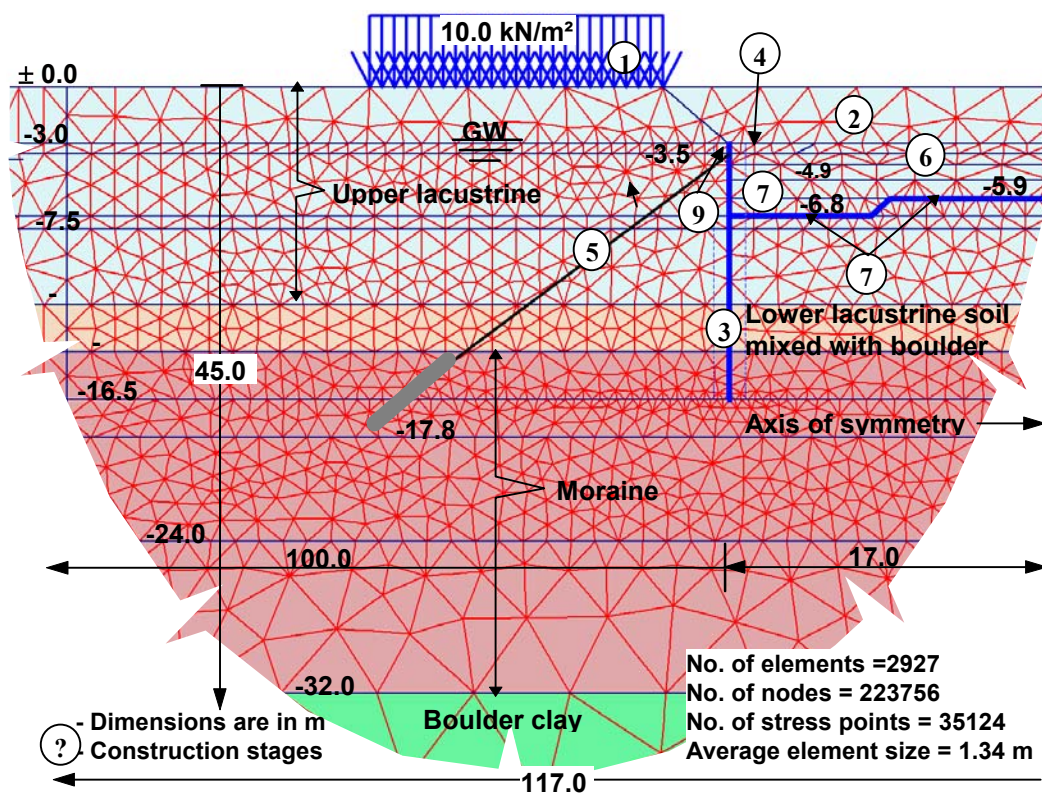boundary was imposed and a zero horizontal displacement was imposed at a distance of 110 m behind the edge of the wall. A symmetrical axis was defined at a distance of 28 m from the wall, where only no horizontal displacement was imposed. The size of the models as a whole was 138 m wide and 60 m high (Figure 8.35 and Figure 8.36). Similarly, The finite element mesh at MS03 was extended to a depth of 45 m and to a distance of 100 m behind the edge of the wall (all in all 117×45 m) (Figure 8.37). A symmetrical axis was defined at a distance of 17 m from the edge of the wall.

At Section through MS01, the load from the one-storey building was ignored with the assumption that the weight of the soil above the basement floor shall play the same purpose. A surcharge load of 42.3 kN/m² was applied at MS02 to simulate the load from the existing 4 - storey building. At section MS03, a traffic load of 10 kNm² was applied to simulate the only traffic load on the road behind the walls. The influence of the existing building at this section was ignored.

8.3.5.2 Material properties

Like project -I, the HSM was used as main constitutive model to simulate the behaviour of the soil. The soil parameters required for the FE - computation with the hardening soil model for drained and consolidation analyses are given in Table 8.9. The modified soil parameter at site 2 (Appendix B3) was taken as a reference parameter for the lacustrine soil layer. In the first reference analysis of the project the upper and lower lacustrine soil layers were taken as one layer. The soil parameters for the other layers were adopted from the geotechnical report (*Kempfert + Partner (1991-1993)*) after adjusting them to suit the material model. In the absence of comparative triaxial and compression tests, the reference value of the constrained modulus E_{oed}^{ref} for the other layers was assumed to be equal to the reference value of the 50% secant modulus E_{50}^{ref}.

The layers of the lacustrine soil and the lacustrine soil mixed with boulder clay were assumed undrained in the consolidation analysis, whereas the other layers remain drained. Hence, the moraine and boulder clay soil layers in the undrained analysis shares the same parameters as in the drained analysis (Table 8.9). Although the boulder clay layer is relatively impermeable, it was assumed drained, for the same reason given in Section 8.2.6.2.

Similar to the project-I, a separate material set was defined for the interface elements. The shear strength reduction factor of 1/3 was assumed for the lacustrine and lacustrine mixed with boulder clay layer, whereas a factor of 2/3 was assumed for the moraine layer. As explained in project -I, the stiffness of the contact surface remained the same as the surrounding soil.

Table 8.9: Soil parameters for the HSM for drained and consolidation analyses

a) Unit weight, permeability and earth pressure at rest							
Soil layer	depth	γ_{sat}	γ_{unsat}	k_x	k_y	K_0^{nc}	
	[m]	[kN/m³]	[kN/m³]	[m/d]	[m/d]	[-]	
Lacustrine soil	±00.0 - -11.5	19.5	19.5	8.64E-5	8.64E-5	0.629	
Lacustrine soil mixed with boulder clay	-09.1 - -14.0	20.0	20.0	8.64E-6	8.64E-6	0.531	
Moraine	-12.5 - -32.0	21.0	21.0	1.0	1.0	0.391	
Boulder clay	-32.0 - -60.0	22.0	22.0	8.60E-6	8.60E-6	0.500	
b) Stiffness parameters							
Soil layer	depth	E_{50}^{ref}	E_{oed}^{ref}	E_{ur}^{ref}	p^{ref}	ν_{ur}	m
	[m]	[kN/m²]	[kN/m²]	[kN/m²]	[kN/m²]	[-]	[-]
Lacustrine soil	±00.0 - -11.5	3785	2901	14285	100	0.20	0.900
Lacustrine soil mixed with boulder clay	-09.1 - -14.0	15000	15000	75000	100	0.20	0.900
Moraine	-12.5 - -32.0	63250	63250	316230	100	0.20	0.500
Boulder clay	-32.0 - -60.0	40000	40000	200000	100	0.20	0.800
c) Shear strength parameters							
Soil layer	depth	c'	φ'	ψ'	R_f		
	[m]	[kN/m²]	[°]	[°]	[-]		
Lacustrine soil	±00.0 - -11.5	20.1	23.2	0.0	0.82		
Lacustrine soil mixed with boulder clay	-09.1 - -14.0	10.0	28.0	0.0	0.82		
Moraine	-12.5 - -32.0	1.0	37.5	7.5	0.90		
Boulder clay	-32.0 - -60.0	10.0	30.0	0.0	0.90		

The equivalent modulus of elasticity of the soldier pile (IPB 600) with timber sheeting (MS03) was estimated according the recommendation of the Working Group *"Numerics in Geotechnics"* *(2001)* of the German Society of the Geotechnical Engineers. from Equation 8.1 as:

$$E_{equivalent} = \sqrt{\frac{E_{st}^2 \cdot A_{st}^3}{12a^2 \cdot I_{st}}} \tag{8.1}$$

and the equivalent thickness of the wall from Equation 8.2 as

$$d_{equivalent} = \frac{E_{st} \cdot A_{st}}{a \cdot E_{equivalent}} \tag{8.2}$$

where E_{st}, A_{st}, and I_{st} are the modulus of elasticity, the cross sectional area and the moment of inertia of the I-steel beam respectively, and a is the spacing between the I-beams. The soldier pile was placed in a 90 cm concrete footing starting just below the excavation bottom up to 2.5 m

deep in the moraine layer. Hence, a separate material property was defined for the lower part of the soldier pile. The combined modulus of elasticity of the steel and the concrete footing was estimated based on the weighted average as follows

$$E_{combined} = \frac{E_{st} \cdot I_{st} + E_{con} \cdot I_{con}}{I_{combined}}$$ (8.3)

The equivalent modulus of elasticity was then estimated from Equation 8.1 by substituting the $E_{combined}$ and $I_{combined}$ in place of the E_{st} and I_{st}.

The soldier with concrete pile sheeting (MS01) was assumed to react together against bending. Hence, the stiffness of the upper part of soldier pile with concrete pile sheeting was taken as the sum of the stiffness of the steel beam and the three concrete piles. The stiffness of the lower part was estimated analogue to the lower part of the soldier pile with concrete footing (MS03).

Table 8.10: Material properties of the walls and the bottom concrete slab

Structural element		Type	EA	EI	w	v
			[kN/m°]	[kNm²/m°]	[kN/m²]	[-]
Soldier pile with timber sheeting:	Upper	IPB 600	2.836E6	1.7969E5	1.753	0.30
	Lower	IPB 600 and Concrete	1.100E7	3.8612E5	8.040	0.25
Soldier pile with concrete sheeting:	Upper	IPB 600 and Concrete	2.136E7	8.0966E5	13.90	0.25
	Lower	IPB 600 and Concrete	1.100E7	3.8612E5	8.040	0.25
Tangent bored piles		Concrete $\phi = 90$ cm	2.120E7	1.0740E6	11.70	0.20
Bottom concrete slab		Concrete d = 30 cm	9.000E7	6.7500E4	7.5	0.20

Table 8.11: Material properties of the support system

Structural element	Type	EA	$L_{spacing}$
		[kN/m°]	[m]
Anchor (MS01)	Techno-anchor $6\phi12$ St 1420/1570	71252.0	2.00
Anchor (MS02)	Techno-anchor $6\phi12$ St 1420/1570	158333.0	0.90
Anchor (MS03)	Techno-anchor $6\phi12$ St 1420/1570	71252.0	2.00
Grout body	Cement grout	100000.o	-

The bottom slab was simulated as a plate and the stiffness parameters were estimated accordingly. The material properties of all the structural elements are given in Table 8.10. All of them are assumed to behave elastically.

8.3.5.3 The FE-calculation phases

A preliminary analysis of the excavation was carried out using the finite element models shown in Figure 8.35 - 37 for the sections through MS01, MS02 and MS03 respectively and using the material properties in Table 8.9 - 8.13. Both drained and consolidation analyses were performed separately. In all the computations, a hydrostatic groundwater was assumed. The idealisation of the construction stages are presented in the following sub-sections.

a)   *Section through MS01, drained analysis*

An attempt was done to indicate the construction stages at the section through MS01 in Figure 8.35. The excavation was started at the corner, extended side wise, and then proceed in slices in a step form toward the middle of the excavation by stabilising the slopes and immediate placement of the bottom concrete slab (see Figure 8.38). The exact day to day activities were not documented or they are not included in the geotechnical report available to the author. However, an attempt has been done to idealise the construction stages in the computation based on in the formation from field measurements and photos as shown in Table 8.12.

Table 8.12:   Construction phases: drained analysis (MS01)

Phase 00: generate the initial stresses Phase 01: 1st pre-excavation to a depth of -2.0 m (1) Phase 02: wall installation (2) Phase 03: 2nd excavation to a depth of -3.0 m and 3.5 m wide (3) Phase 04: Anchor installation and pre-stressing (4) Phase 05: 3rd excavation to a level of -4.0 m and 5 m wide (5) Phase 06: 4th excavation to a level of bottom excavation but only 3.5 m wide(6) and at the same time installation of the bottom slab (6)	Phase 07: the next slice excavation to a depth of -3.5 m (7) Phase 08: the next slice excavation to a full depth of excavation (8) Phase 09 - 16: excavation proceed in slices in a stair case form toward the middle of the excavation (9)-(16). The bottom slabs of the previous slices have been activated during the excavation of the next slice Phase 17: placement of the last bottom slab (17) and end of calculation
N.B.: numbers in () are construction sequence (Figure 8.35)	

b)   *Section through MS01, consolidation analysis*

As already discussed in Section 8.2.6.3, it was possible to perform a construction stage and a consolidation process simultaneously, i.e., the excess pore pressure starts to dissipate immediately after the start of the excavation. The construction stages are similar to that shown in the drained analysis, except some phases are added to consider the consolidation processes between two consecutive construction Stages. These idealised computation phases and the corresponding consolidation and execution times are presented in Table 8.13.

Figure 8.38: View of the construction stages *[Photo: Kempfert]*

Table 8.13: Construction phases: consolidation analysis (MS01)

Phase 00: generate the initial stresses	Phase 12: the next slice excavation to a depth of -3.5 m (7) [1 day]
Phase 01: 1st pre-excavation to a depth of -2.0 m (1)	Phase 13: the next slice excavation to a full depth of excavation (8) on daily output basis [1 day]
Phase 02: wall installation (2)	Phase 14 - 16: excavation proceed in slices in a stair case form toward the middle of the excavation (9)-(11). The bottom slabs of the previous slices have been activated during the excavation of the next slice [each 1 day]
Phase 03: 2nd excavation to a depth of -3.0 m and 3.5 m wide (3) [2 days]	
Phase 04: Consolidation [48 days]	
Phase 05: Anchor installation (4) [2 days]	
Phase 06: Anchor pre-stressing (4) [2 days]	
Phase 07: Consolidation [10 days]	Phase 17: Consolidation [2 days]
Phase 08: 3rd excavation to a level of -4.0 m and 5 m wide (5) [30 days]	Phase 18 - 22: same as phases 14 - 16 but slices (12) - (16) [each 1 day]
Phase 09: Consolidation [4 days]	Phase 23: placement of the last bottom slab (17) [2 days]
Phase 10: 4th excavation to a level of bottom excavation but only 3.5 m wide(6) and at the same time installation of the bottom slab (6) [2 days]	Phase 24: Consolidation [45 days]
Phase 11: Consolidation [2 days]	

N.B.: numbers in () are construction sequence (Figure 8.35) and in [] are consolidation and execution time

c) Section through MS02, drained analysis

Figure 8.36 shows the general construction sequences at the section through MS02. Similar to the section at MS02, the excavation was started near the wall, by first excavating a small working space for the installation of anchors, and then proceeded further till the bottom of the excavation in a width of about 3.5 m. Once this area was secured and a bottom concrete slab (fast hardening cement) was placed in position, the excavation continued in slices in a step form toward the middle of the excavation by stabilising the slopes and immediate placement of the bottom slab. These construction procedures are idealised in the drained analysis of the project at this section as given in Table 8.14.

Table 8.14: Construction phases: drained analysis (MS02)

Phase 00: generate the initial stresses
Phase 01: activate the surcharge load (1)
Phase 02: 1st pre-excavation to a depth of -0.6 m (2)
Phase 03: wall installation (3)
Phase 04: 2nd excavation to a depth of -2.5 m and
        3.5 m wide (4)
Phase 05: Anchor installation and pre-stressing (5)
Phase 06: 3rd excavation to a level of -4.1 m and 5.6 m
        wide (6)
Phase 07: 4th excavation to a level of bottom
        excavation but only 3.5 m wide(7) and at the
        same time installation of the bottom slab (7)
	Phase 08: the next slice excavation to a depth of
	        -2.5 m (8)
	Phase 09: the next slice excavation to a full depth of
	        excavation (9)
	Phase 10 - 16: excavation proceed in slices in a stair
	        case form toward the middle of the
	        excavation (10)-(16). The bottom slabs
	        of the previous slices have been activated
	        during the excavation of the next slice
	Phase 17: placement of the last bottom slab (17) and
	        end of calculation

N.B.: numbers in () are construction sequence (Figure 8.36)	

d) *Section through MS02, consolidation analysis*

The construction stages in the consolidation analysis of this section are more or less the same as the drained analysis, except that some calculation phases are introduced to simulate the consolidation process between two consecutive construction stages. Beside the consolidation processes between the two consecutive stages, the execution and consolidation time of each stage was modelled. Table 8.15 shows the idealised calculation phase inclusive the assumed execution and consolidation times in the consolidation analysis of the section through MS02.

Table 8.15: Construction phases: consolidation analysis (MS02)

Phase 00: generate the initial stresses
Phase 01: activate the surcharge(1)
Phase 02: 1st pre-excavation to a depth of -0.6 m (2)
Phase 03: wall installation (3)
Phase 04: 2nd excavation to a depth of -2.5 m and
        3.5 m wide (4) [2 days]
Phase 05: Consolidation [9 days]
Phase 06: Anchor installation (5) [10 days]
Phase 07: Anchor pre-stressing (5) [7 days]
Phase 08: Consolidation [50 days]
Phase 09: 3rd excavation to a level of -4.1 m and 5.6 m
        wide (6) [4 days]
Phase 10: Consolidation [3 days]
Phase 11: 4th excavation to a level of bottom
        excavation but only 3.5 m wide(7) and at the
        same time installation of the bottom slab (7)
        [2 days]
	Phase 12: Consolidation [2 days]
	Phase 13: the next slice excavation to a depth of
	        -2.5 m (8) [1 day]
	Phase 14: the next slice excavation to a full depth of
	        excavation (9) on daily output basis [1 day]
	Phase 15 - 17: excavation proceed in slices in a stair
	        case form toward the middle of the
	        excavation (10)-(12). The bottom slabs
	        of the previous slices have been activated
	        during the excavation of the next slice
	        [1 day each]
	Phase 18: Consolidation [2 days]
	Phase 19 - 22: same as phases 15 - 17 but slices
	        (13) - (16) [1 day each]
	Phase 23: placement of the last bottom slab (17)
	        [2 days]
	Phase 24: Consolidation [45 days]

N.B.: numbers in () are construction sequence (Figure 8.36) and in [] are consolidation and execution time	

e) *Section through MS03, drained analysis*

At this section only few construction stages were enough (Figure 8.37), because the excavation in slices parallel to the walls along MS01 and MS02 can not be modelled with 2D-FE-programs. This is similar to the section IV-IV in project-I (see Section 8.2.6). One slice excavation parallel

to these walls reached the whole excavation width at section through MS03. In fact, the 3D-effect remain the same as in section IV-IV in project-I, and it was assumed that the bottom slab started to effect after 50% of the soil mass above it had been removed. Table 8.16 shows the idealised calculation stages in drained analysis of the section through MS03.

Table 8.16:   Construction phases: drained analysis (MS03)

Phase 00: generate the initial stresses
Phase 01: activate the surcharge load (1)
Phase 02: 1st pre-excavation to a depth of -3.0 m (2)
Phase 03: wall installation (3)
Phase 04: 2nd excavation to a depth of -3.5 m and
        3.5 m wide (4)
	Phase 05: Anchor installation (5)
	Phase 06: Anchor pre-stressing (5)
	Phase 07: 3rd excavation to a level of -4.9 m (6)
	Phase 08: final excavation to a level of bottom
	        excavation (7) and at the same time
	        installation of the bottom slab (7)

N.B.: numbers in () are construction sequence (Figure 8.37)	

f)   Section through MS01, consolidation analysis

The calculation phases are the same as in the drained analysis, except that few phases are added to consider the consolidation time between two consecutive stages (Table 8.17)

Table 8.17:   Construction phases: consolidation analysis (MS03)

Phase 00: generate the initial stresses
Phase 01: activate the surcharge load (1)
Phase 02: 1st pre-excavation to a depth of -3.0 m (2)
Phase 03: wall installation (3)
Phase 04: 2nd excavation to a depth of -3.5 m and
        3.5 m wide (4) [6 days]
Phase 05: Consolidation [4 days]
Phase 06: Anchor installation (5) [17 days]
Phase 07: Consolidation [2 days]
	Phase 08: Anchor pre-stressing (5) [5 days]
	Phase 09: Consolidation [38 days]
	Phase 10: 3rd excavation to a level of -4.9 m (6)
	        [12 days]
	Phase 11: final excavation to a level of bottom
	        excavation (7) and at the same time
	        installation of the bottom slab (7) [12 days]
	Phase 12: Consolidation [45 days]

N.B.: numbers in () are construction sequence (Figure 8.37) and in [] are consolidation and execution time	

In all the cases the computed displacements till the installation of the wall (inclusive) has been set to zero.

8.3.5.4   Results of the back analysis

The first analysis carried out was on the reference case with the soil profile, finite element model, the material properties and the construction stages discussed and presented in the preceding sections. This reference case is hereafter called as "case-1". In the reference case, a homogeneous layer of the lacustrine soil was assumed to start with the worst condition. However, experience from project-I and also from geotechnical report of this project show that there might exist two layers of the lacustrine soil; the upper and the lower layers. Hence, a second case was defined as

"case-2", which separates the lacustrine soil into the upper and lower lacustrine soils. The separation occurred at a depth of -3.5, -3.0, and -4.5 m below the ground surface at the sections through MS01, MS02 and MS03 respectively. The soil parameters of the upper lacustrine layer remain unchanged, but for the lower lacustrine soil layer the material parameters from similar situation in project-I (Dammgasse) for the reference case were adopted (refer to Table 8.1). The only difference is that the lower lacustrine soil layer at Dammgasse was encountered at deeper depth than here at Markgrafenstrasse. The third and last case, known as "case-3", is same as case-2 but with increased stiffness parameters of the lower lacustrine soil by a factor of 3. The results of the analyses are presented and compared with the measured values in three groups, namely, deflection of the wall, surface settlement and anchor forces.

a) Wall deflection

Figure 8.39 shows a comparable presentation of the calculated and measured deflection of the wall at the end of the excavation at section through MS01. The drained analysis are shown on the left and the consolidation analysis on the right. As can be seen from the figure, the result of the drained analysis of "case-1" shows a deflection of about 5.7 mm more at wall head in the direction of the soil mass and about 7.2 mm more below the bottom of the excavation in the direction of the excavation as compared to the measured deflection. The second drained analysis "case-2" shows a deflection of about 4.1 mm less at the top, whereas the deflection below the bottom of excavation remains almost the same as in "case -1". Increasing the stiffness of the lower lacustrine layer "case-3" did not help much in reducing the bending and displacement of the wall below the bottom of excavation to the minimum level of the measured value, whereas at the top of the wall it led to deflection about 10.1 mm less than the measured value. Hence, this option was neglected in the consolidation analysis of this section and the other two sections.
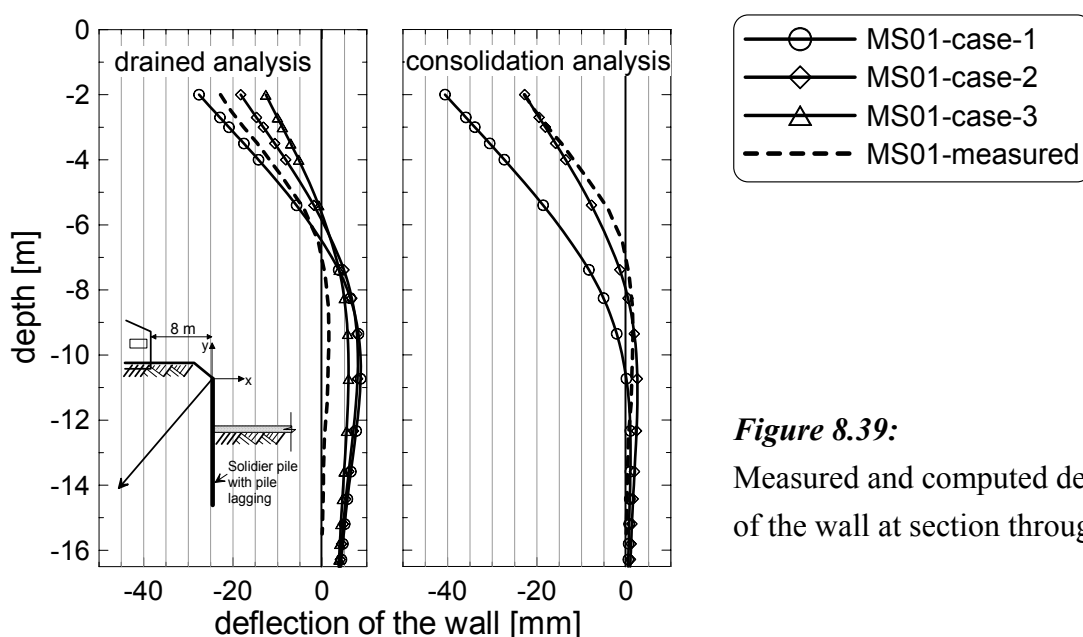

Figure 8.39:

Measured and computed deflection of the wall at section through MS01

In contrary to the drained analysis, the result of the consolidation analysis shows a fixed end support of the wall below the bottom of excavation, even it matches exactly to the measured deflection in the case of the variant "case-2". A possible reason for the difference in the results of the drained and consolidation analyses can be the negative excess pore pressure that still exist below the bottom of the excavation at the end of the construction or at the time of the last measurement.

The result of the drained analysis of the section through MS02 (Figure 8.40-left) shows more than double deflection at the top and wall displacement below the bottom of excavation level in both the variants (case-1 and case-2) as compared to the measured values. Again, the results of the consolidation analysis (Figure 8.40-right) shows a relatively better match, but it is still far from the measured deflection. The existing building at this section is found very near to the wall at a distance of 2 m. The foundation of the building and the walls of the basement floor might contributed to the stiffness of the whole system and reacted rigidly to the anchor pre-stressing, hence smaller measured deflection of the wall at the top. If the possible increase in the stiffness of the soil layer up to the depth of the basement floor would be considered in the FEM-computations, the deflection of the wall will definitely comes close to the measured value.
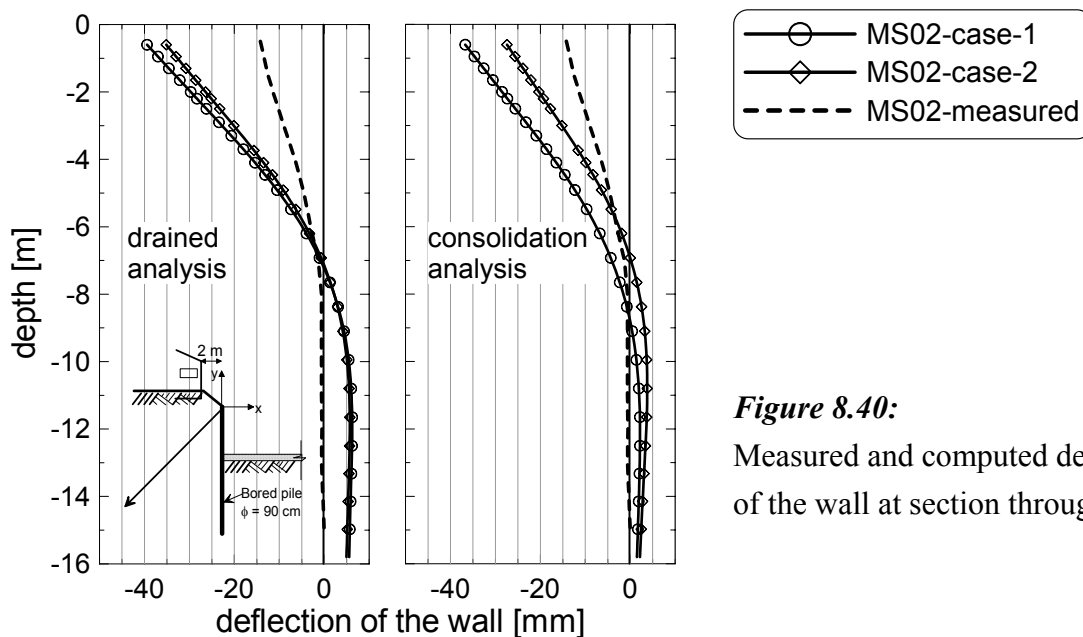

Figure 8.40:

Measured and computed deflection
of the wall at section through MS02

A very surprisingly result is to see in Figure 8.41. This figure shows the result of the drained analysis (left) and the consolidation analysis (right) of the section through MS03. The result of the consolidation analysis "case-2" matches almost 100 % to the measured deflection of the wall.

In general, it would appear that the measured deflection of the wall can fairly be approximated with FE-computations, specially by means of the consolidation analysis and with the application of the soil parameters according to the „case-2".
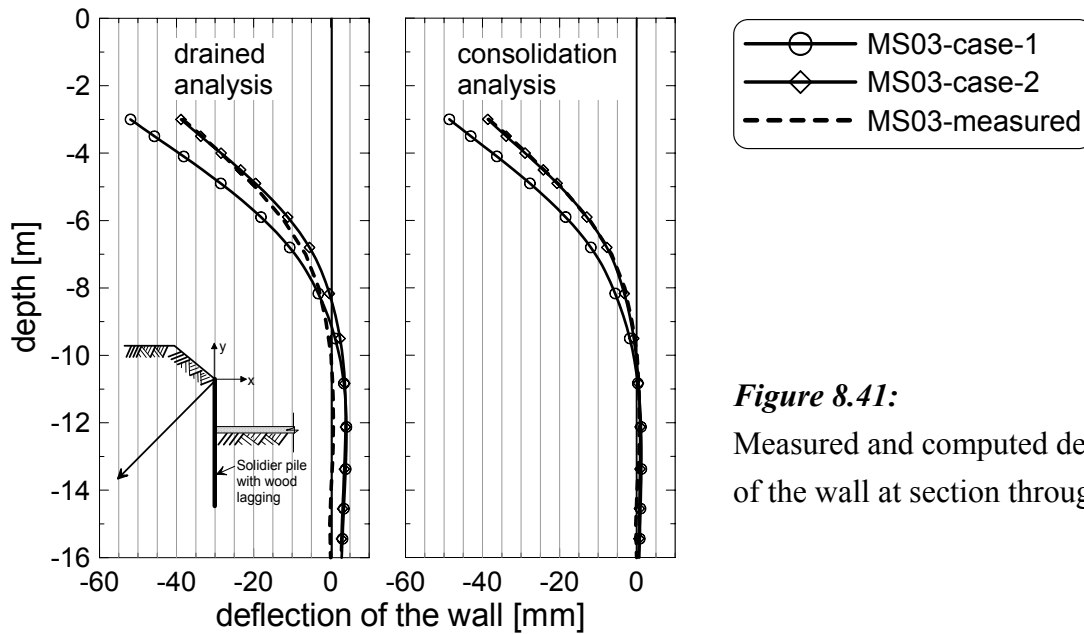
Figure 8.41:

Measured and computed deflection of the wall at section through MS03

b)   *Settlement at the ground surface*

The results of the drained analysis at all sections and for all cases analysed are presented in Figure 8.42 compared to the measured settlements. The computed settlements are plotted as a function of the calculation steps and the measured settlement as a function of the date of measurements. At first glance, it seems difficult to compare the results, but they can be compared based on the course of the settlement curves. The arrows in the diagrams can help to approximately indicate the time point of the start of the anchor installation in the field and in the FE-calculations.

The measured settlements at the sections MS01 and MS03 are as such very minimum (max. 4 mm at MS02). The computed settlements are (case-1 and case-2) relatively more than the measured settlements, but they remain in the minimum ranges (max. 8 mm at ME01). The reason for excessive settlements at the section through MS02 was already explained and corresponding sources in literature are referred in Section 8.3.4. Above 80% of the settlement occurred during the anchor installation. This part of the settlement can not be modelled directly by means of the 2D-FE-computations. An approach to approximate such settlements at re-entry corners based on 2D-FE-anylsis and analytical means are given in *Kempfert/Gebreselassie (1999). Therefore*, there is no wonder to observe the large difference between the measured and computed settlements in Figure 8.42 at a section through MS02. However, if one ignores the part of the settlements during the anchor installation and shift the settlement curves upward, a fair match of the computed and measured settlements may be obtained. Note also that the computed settlements of the first three calculation phases are not included in the diagrams.
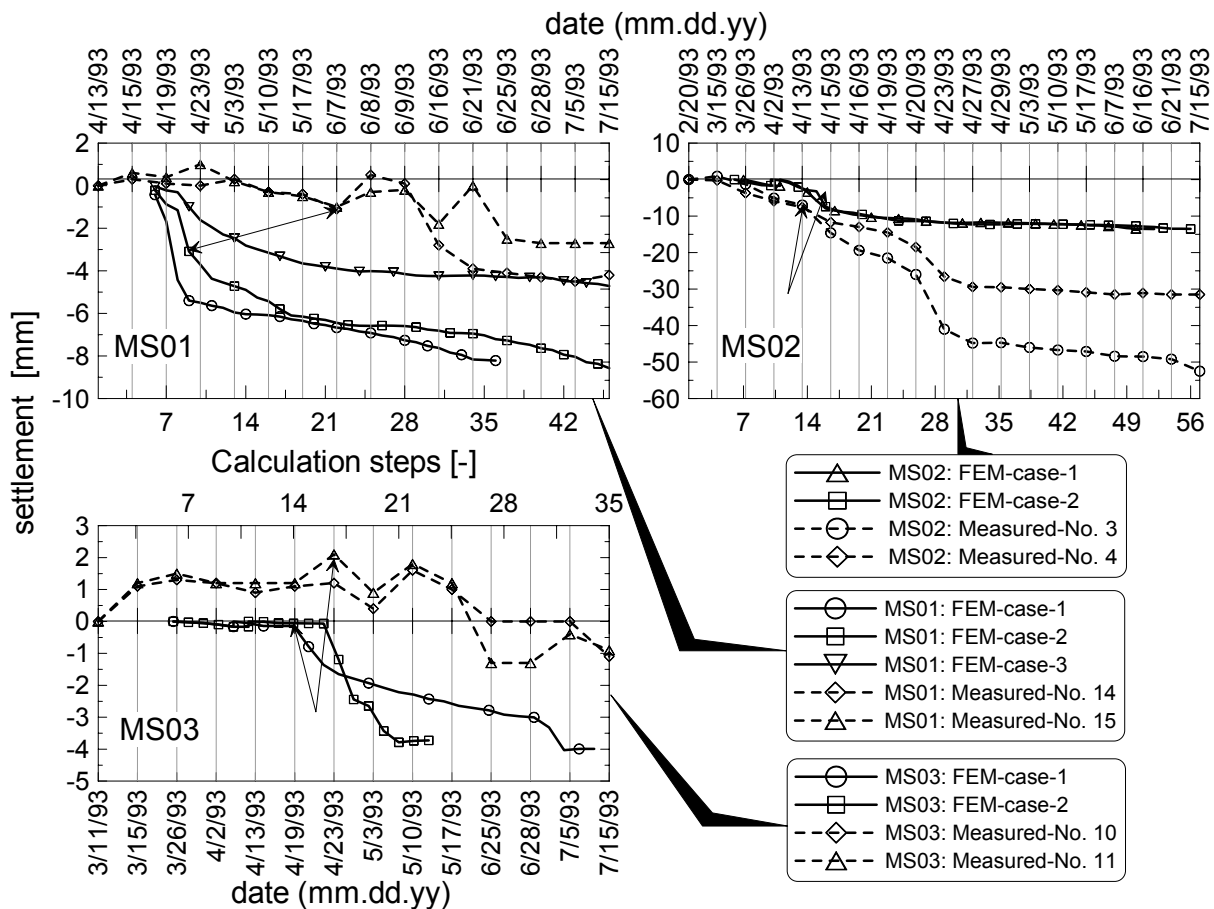
Figure 8.42: Measured and computed settlements based on drained analysis

A further observation from Figure 8.42 is that no significant difference was observed in the computed settlements of case-1 and case-2 at all three sections. This indicates that the upper lacustrine layer mainly contributes to the settlements at the ground surface.

The settlement results of the consolidation analysis compared to the measured results are plotted in Figure 8.43. The computed results at all sections show up to 2 - 6 mm heave during the anchor pre-stressing. Although such heave due to horizontal loading is theoretically possible, no remarkable heave was recorded during the surface surveying. The course of the computed settlement after anchor pre-stressing resembles the measured settlement lines.

c)   *Anchor forces*

The computed anchor forces (*Figure 8.44*) in drained analysis show an icreasing trend during the various construction stages, whereas the anchor forces in the consolidation analysis show a slight drop during the excavation stages immediately after pre-stressing, rises very slowly to the position of the pre stressing force at section through MS01 and MS02, and remains constant at section
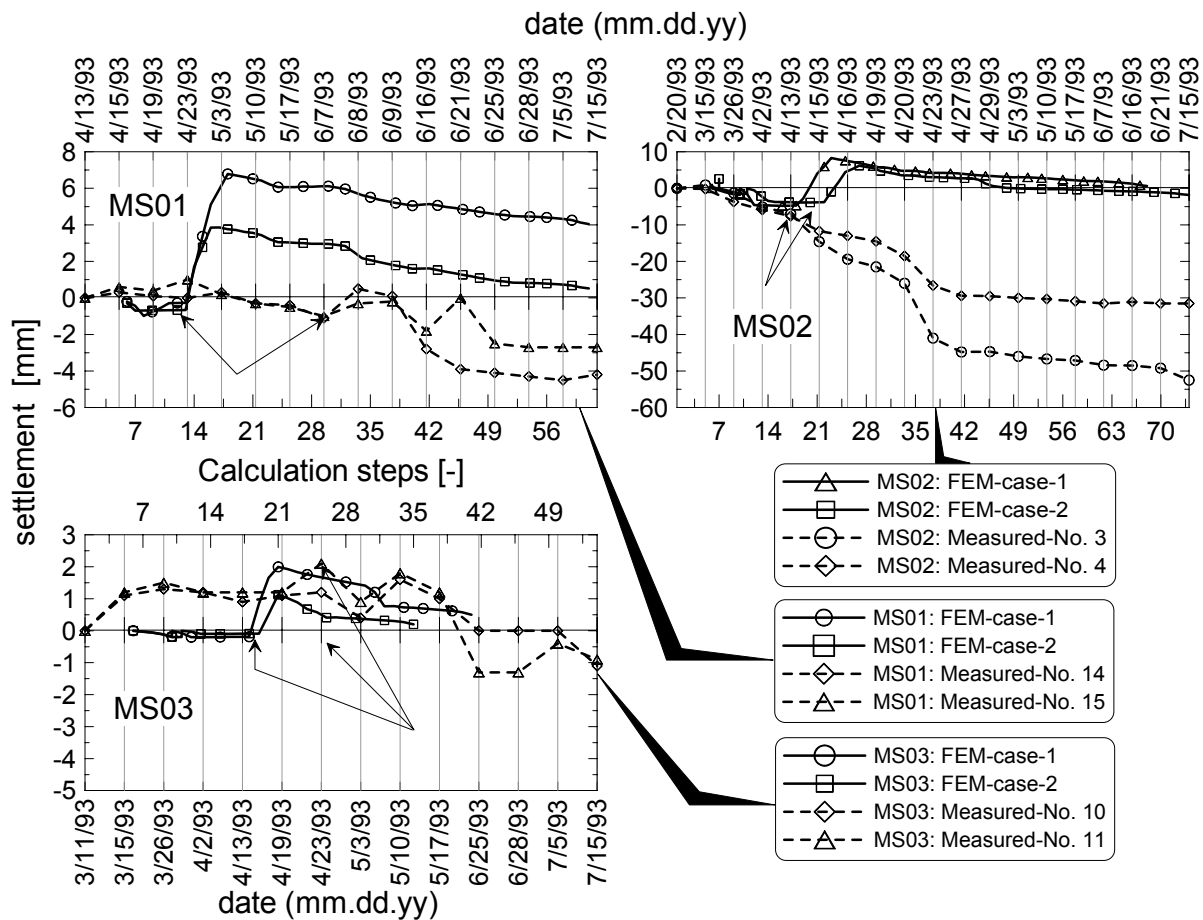
Figure 8.43: Measured and computed settlements based on consolidation analysis

through MS03. In general, one can say the consolidation analysis can fairly estimate the development of the anchor forces during the various construction stages.

8.3.5.5 Summary

It appears from the back analyses of the project-II that the performance of the excavation of the project -II (Markgrafenstrasse) may fairly be estimated by means of the finite element method and using the advanced constitutive soil models such as the Hardening Soil Model (HSM) implemented in the FE-program "PLAXIS" without any major modification of the material properties from laboratory and field penetration and sounding tests. It also show that a better match with measured data may be achieved by performing a consolidation analysis.
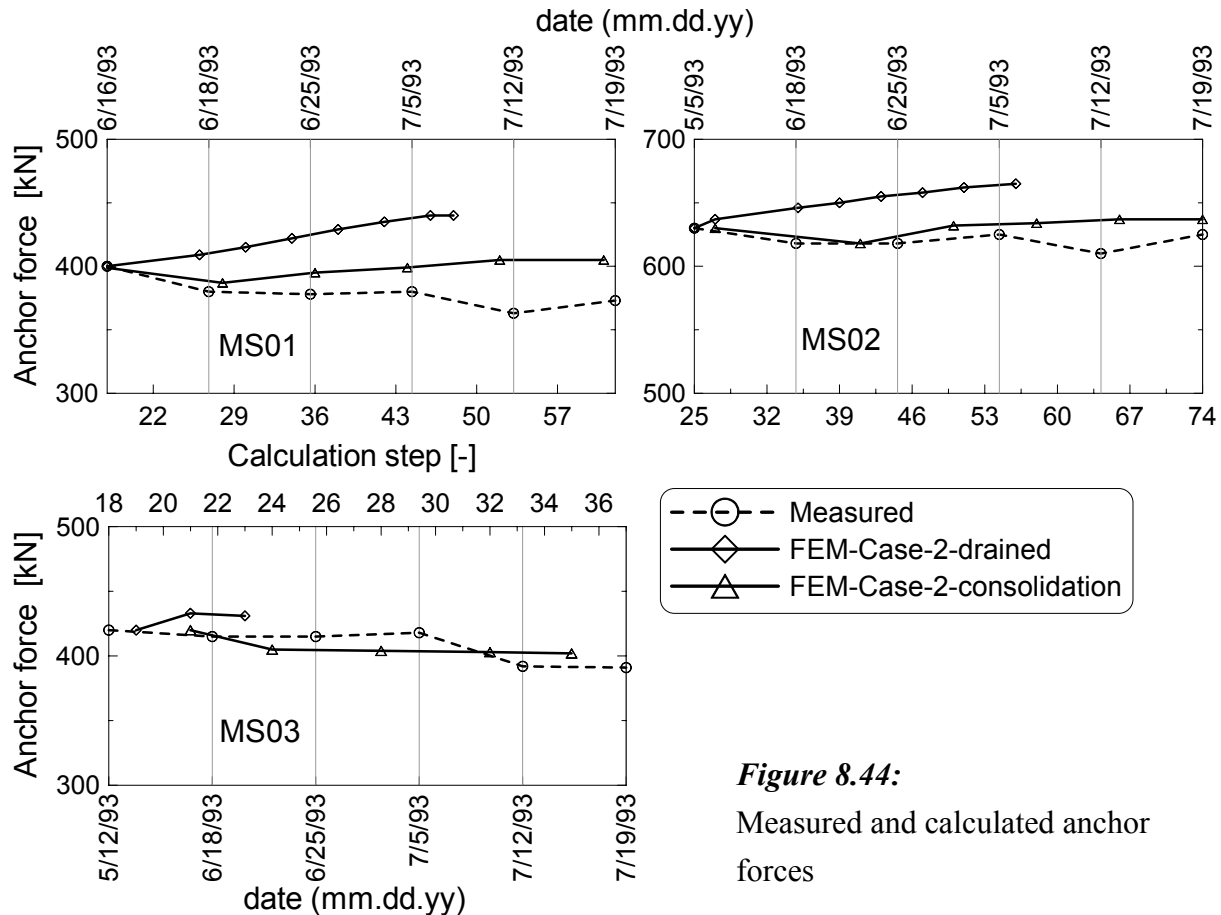
Figure 8.44:
Measured and calculated anchor forces

The deflection of the wall toward the soil mass shows that the soft lacustrine soil can not bear the horizontal loads, which in turn shows that the lacustrine soil can not provide a fixed end support for the wall toe. The pre-stressing of the anchors to 100% its design load had helped the wall from deforming further in the direction of the excavation during the consecutive construction stages, but it would have also damaged the existing structures.

The importance of considering the stiffness of the existing foundation and the walls of the basement floor in the estimation of the stiffness of the upper soil layer up to a depth of the basement floor should be underlined. As alternative the basement floor can also be defined as a rigid cluster, elastic and porous medium. Similarly, the stiffness of the streets due to the asphalt, the highly compacted base, sub-base and subgrade layers should be considered in the estimation of the stiffness of the upper layer.

9 Analytical and numerical examinations of the draft recommendation of "EAB" for excavations in soft soils

9.1 General

The working group "Excavations" (EAB) of the German Society of Geotechnical Engineers (DGGT) have extended the known standard recommendation for excavations (*EAB (1994)*) to include a new recommendation for excavations in soft soils. Parallel to the main theme of the dissertation work, the author accompanied the draft recommendation for excavations in soft soils EB 94 to EB 97 through various analytical and numerical parameter studies regarding the content of the analytical calculation approaches in the new draft with close co-operation with the members of the working group. Selected investigations of the draft work are summarised in the following sections. The objective of the investigation was, first to show where the analytical EAB recommendation can give a realistic solution to this very difficult excavation problem in soft soils, and where possibly the analytical calculation can still supply a considerable uncertainty in its application. The draft work of the recommendation for excavations in soft soil was already published (*Weißenbach (2002)*) for discussion and the final version to come soon.

9.2 The shear strength and the coefficient of earth pressure at rest

The discussion of the drained and undrained analyses in chapter 4 was originally motivated through the working group "Excavations" (EAB). The members of the group had different opinion on the type of analysis to adopt for excavations in soft soils. After the discussion on the drained and undrained analyses in chapter 4 (*Kempfert/Gebreselassie (2002)*) and the analytical parameter study on undrained analysis of excavations in soft soils by *Hettler et al. (2002)*, the group recommends to use the drained analysis as governing method of the calculation of excavation in soft soils, but leaves room for the geotechnical expert to decide based on the situation at the site. To perform the drained analysis, one requires the effective shear parameters. These can only be determined in triaxial or direct shear tests in laboratory. However, the soft soil is very sensible to such kind of test. The disturbance of the structure of the soil specimen during sampling, the rubber membrane used in triaxial test, and the friction resistance in shear box, etc. might lead to failure in estimating the shear parameters, and hence the laboratory tests are conditionally suitable to determine the effective shear parameters according to the draft recommendation of the EAB. On the other hand there are a huge experiences available in the undrained strength of normally consolidated soft soils. Therefore, it is worthwhile to make use of these experiences and data bank to estimate the effective shear parameters. This is what was done in chapter 4 of this work, namely, to estimate the effective shear parameters from the undrained shear strength with the help of the *Skempton's* pore water coefficient at failure A_f. The EAB refer

to this work for estimation of the effective shear parameters φ_s' (the angle of the overall shear strength), for example,

$$sin\,\varphi_s' = \cfrac{1}{\cfrac{1}{\lambda_{cu}} \cdot (K_0 + A_f \cdot (1-K_0) - 2 \cdot A_f + 1}} \qquad (9.1)$$

On the other hand, dependent on the range of application and on local conditions where a positive excess pore water pressure may be expected, the undrained conditions might govern the analysis of the excavation. If this is the case, the EAB recommends to use an equivalent angle of total friction φ_{cu} instead of the undrained strength c_u. Based on the stress paths in a triaxial test, the author suggests Equation 4.23 or the equations listed in Table 4.2 according to the expected stress path to convert the undrained strength c_u into the equivalent angle φ_{cu}. For a comparison purpose, Equation 4.23 is once again displayed below.

$$sin\,\varphi_{cu} = \cfrac{1}{\cfrac{K_0}{\lambda_{cu}} + \cfrac{\lambda_{u0}}{\lambda_{cu}} + 1} \qquad (9.2)$$

Analogue to Equation 8.2, the EAB recommends a simplified form for practical applications as presented below. For soils above the groundwater table and c_u linearly increases with depth (Figure 9.1a),

$$sin\,\varphi_{cu,1} = \frac{c_{cu,1}}{\sigma_{v1}'} = \lambda_{cu,1} \qquad (9.3)$$

Similarly, for soils below the groundwater table and c_u linearly increases with depth (Figure 9.1a),

$$sin\,\varphi_{cu,2} = \frac{\Delta c_{cu,2}}{\sigma_{v2}' - \sigma_{v1}'} = \lambda_{cu,2} \qquad (9.4)$$

For soils with a constant c_u with depth (Figure 9.1b), but above the groundwater table,

$$sin\,\varphi_{cu,1} = \frac{c_{cu,1}}{\sigma_{vm,1}'} = \lambda_{cu,1} \qquad (9.5)$$

Likewise, for soils below the groundwater table and constant c_u (Figure 9.1b),

$$sin\,\varphi_{cu,2} = \frac{c_{cu,2}}{\sigma_{vm,2}'} = \lambda_{cu,2} \qquad (9.6)$$

where σ'_{vm} is the mean effective consolidation stress or the overburden pressure of the layer. A comparison of Equation 9.2 and 9.13 can be found in Figure 4.14.
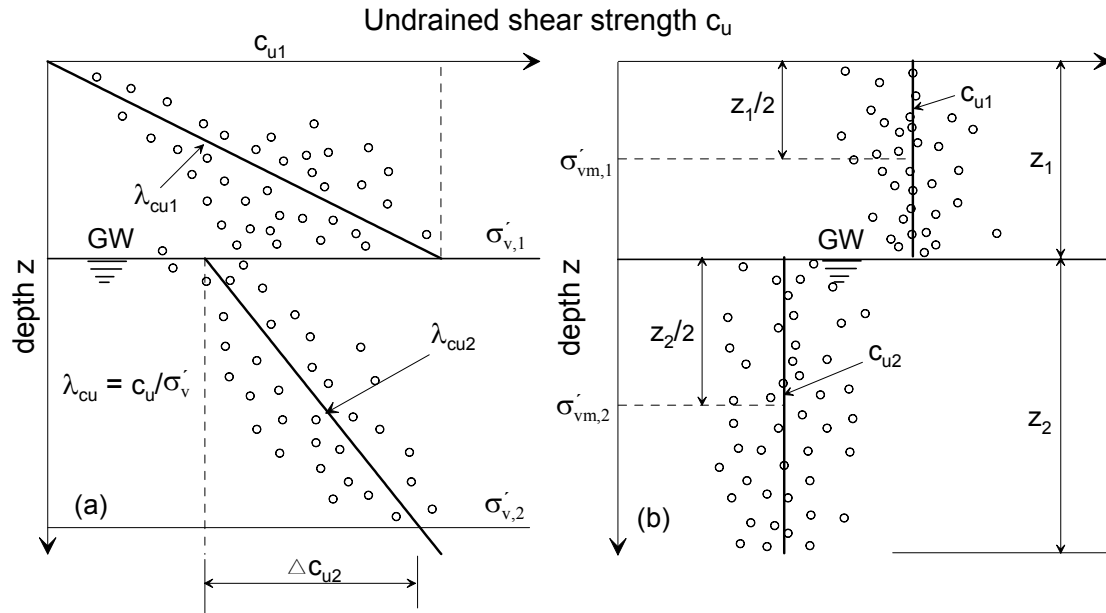

Figure 9.1: Determination of the equivalent angle of total friction φ_{cu}
a) c_u increases linearly with depth, and b) constant c_u with depth

The coefficient of the earth pressure at rest K_0 is usually estimated from the known *Jaki's* formula,

$$K_0 = 1 - sin\,\varphi' \tag{9.7}$$

Table 9.1: The coefficient of the earth pressure at rest K_0 for normally consolidated soft soils

Jaki's equation		Lee/Jin (1979)		Sherif/Koch (1970)	
φ'	K_0	I_p	K_0	w_L	K_0
[°]	[-]	[%]	[-]	[%]	[-]
30	0.500	5	0.456	10	0.505
25	0.577	15	0.605	20	0.540
20	0.658	25	0.673	30	0.575
15	0.741	35	0.719	40	0.613
5	0.826	45	0.752	50	0.653

but there are also empirical equations to estimate the K_0 according to *Alphan (1967)*, *Lee/Jin (1979)* and *Sherif/Koch (1970)* (see Table 3.2 and Figure 3.6) based on the plasticity index and the liquid limit of the soil. After comparing this empirical equations and Equation 9.7 with a

measured K_0 value from *Scherzinger (1991)* (Figure 3.2), the *Alphan (1967)* equation lies far way from the range of the measured values and gives small values of K_0 and hence will not be recommended for soft soils. A tabular values K_0 calculated from the empirical equations and *Jaki's equation* are shown in Table 9.1.

9.3   The development of the earth pressure figures EB 96-1 to EB 96-4 of the draft recommendation of EAB

9.3.1   Preliminary analysis

9.3.1.1   General

In order to safeguard and optimise the draft recommendation of the EAB for excavations in soft soils EB 95 to EB 97, a comparative analytical and numerical analyses were carried out on an idealized excavation problem shown in Figure 9.2. The excavation was 4.5 m deep and contains a homogeneous soft soil deposit with the soil parameters shown in Figure 9.2. The penetration depth of the wall was assigned to be 3 m below the bottom of the excavation. A strut support at 1.5 m below the ground surface and a bottom slab support at the end of excavation level was assumed. The wall has a stiffness EI = 5.36×10^4 kN-m and EA = 3.59×10^6 kN/m. A groundwater table was assumed at 1.0 m below the ground surface.
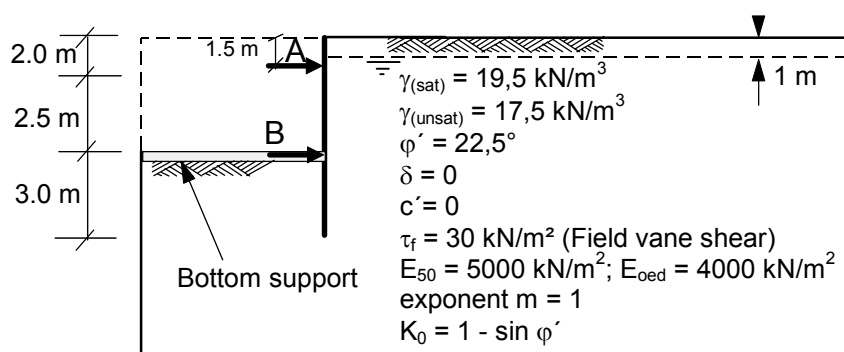

Figure 9.2:
Idealized excavation problem for analytical and numerical comparative analyses

The characteristic undrained shear strength was estimated from $c_u = 0.8 \cdot \tau_f = 24 \, kN/m^2$ according to *Bjerrum (1972)* (Figure 3.19) assuming a plasticity index of 50% .

9.3.1.2   Analytical study

The various cases included in the analytical study are listed in Table 9.2. In general, 20 cases were investigated analytically. In order to compare the analytical and the numerical analyses results, the corresponding cases are shown in the right end column of Table 9.2. The wall was assumed as a beam supported at strut and bottom of excavation levels as shown in Figure 9.3 for the determination of the reaction and section forces. The resultant pressure of the active pressure and the passive resistance was applied on the beam as an external load. The tension reaction forces were neglected, i.e., the support with tension force was set to zero and the reaction force of the next support was increased by the same amount to satisfy the equilibrium condition $\Sigma H = 0$. The excavation was analysed for the case of the end of the excavation only.

Table 9.2:   The overview of the various combinations for analytical parameter study

Case ♠	Ground water	Earth pressure		Earth pressure distribution		Passive resistance		Compare with numeriacal calculation: Variant →
		effektive Shear parameter φ´	totale Shear parameter c_u	classical	transformed	e_{01} *	e_{02} **	
1a	✗	✓	✗	✓	✗	✓	✗	Variant1-4ad
1b	✗	✓	✗	✓	✗	✗	✓	---"---
2a	✗	✓	✗	✗	✓	✓	✗	---"---
2b	✗	✓	✗	✗	✓	✗	✓	---"---
3a-1	✗	✗	✓	✓	✗	✓	✗	Variant1-4au
3a-2	✗	✗	✓	✓ §	✗	✓	✗	---"---
3b-1	✗	✗	✓	✓	✗	✗	✓	---"---
3b-2	✗	✗	✓	✓ §	✗	✗	✓	---"---
4a	✗	✗	✓	✗	✓	✓	✗	---"---
4b	✗	✗	✓	✗	✓	✗	✓	---"---
1-1a	✓	✓	✗	✓	✗	✓	✗	Variant1-4awd
1-1b	✓	✓	✗	✓	✗	✗	✓	---"---
2-1a	✓	✓	✗	✗	✓	✓	✗	---"---
2-1b	✓	✓	✗	✗	✓	✗	✓	---"---
3-1a-1	✓	✗	✓	✓	✗	✓	✗	Variant1-4awu
3-1a-2	✓	✗	✓	✓ §	✗	✓	✗	---"---
3-1b-1	✓	✗	✓	✓	✗	✗	✓	---"---
3-1b-2	✓	✗	✓	✓ §	✗	✗	✓	---"---
4-1a	✓	✗	✓	✗	✓	✓	✗	---"---
4-1b	✓	✗	✓	✗	✓	✗	✓	---"---

✗   excluded
✓   included
* e_{01} is the distribution of the earth pressure at rest that starts from zero at bottom of the excavation.
** e_{02} is the distribution of the earth pressure at rest on the passive side that starts from zero at the ground surface.
§   minimum active earth pressure with the assumption φ´= 40° according to EAB
♠   a represents for no strut pre-stressing and b for strut pre-stressing (pre-stress = 30 kN/m²)

Resultant pressure

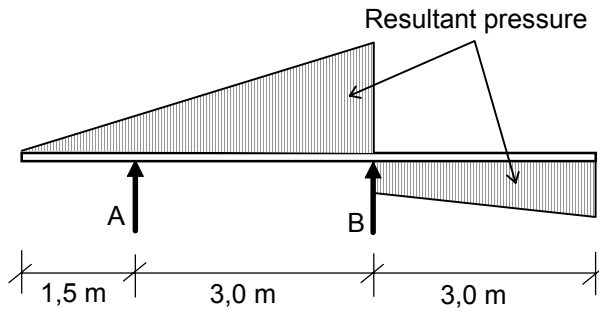
A

B

1,5 m   3,0 m   3,0 m

Figure 9.3:
The wall system as a beam supported at
two locations for determination of the
section forces

A typical results of the analytical effective stress analysis are shown in Figure 9.4 for the case
with ground water and various combinations of the active earth pressure and the passive resis-
tance (case-1-1a to case-2-1b). The rest of the analytical analysis results are documented in Ap-
pendix-C1. There were two combinations of the active earth pressure. These are the classical
earth pressure distribution and the transformed earth pressure, i.e., the classical earth pressure
above the bottom of the excavation was transformed to a rectangular pressure diagram. Since the
response of the soil below the bottom of the excavation (passive side) in the case of a bottom
support was not yet known, two cases of the passive resistance were assumed. The first case was
based on the assumption that the bottom support can provide enough support to the wall and the
passive resistance of the soil may have its minimum value which is equal to the earth pressure at
rest that starts from zero at the bottom of the excavation. This is indicated as e_{01} in Figure 9.4a.
The second case was similar to the first one, but it was assumed that the soil may retain the initial
earth pressure at rest before the excavation starts and it is indicated as e_{02} in Figure 9.4a. The ac-
tual distribution of the passive resistance might lie between the two cases of the earth pressure at
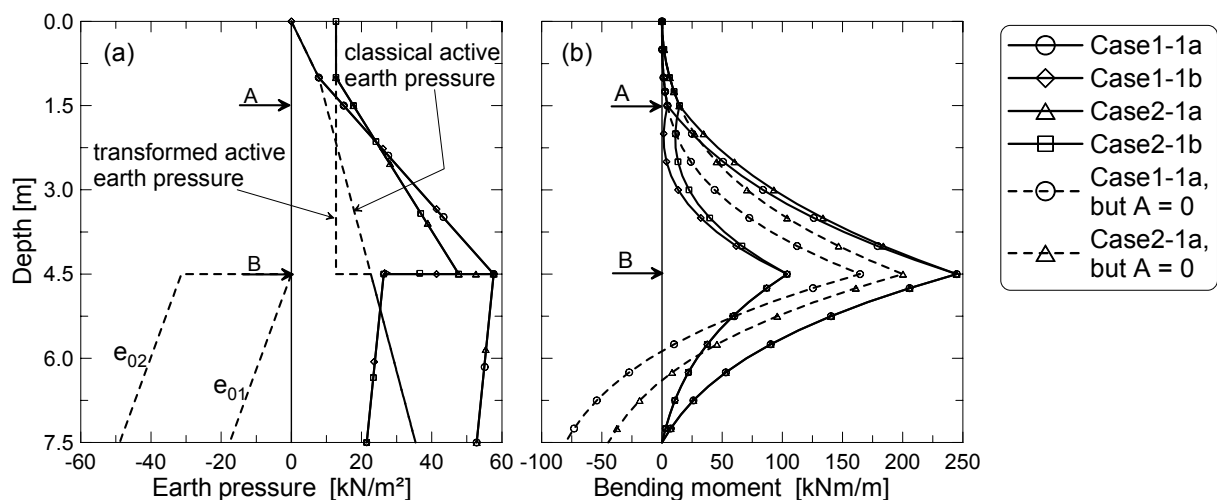rest. A comparative study of the numerical analysis in the next section may serve to clarify the

Figure 9.4:   Typical analytical analysis result for the case with groundwater and various
combinations of the active earth pressure and passive resistance

situation. Figure 9.4b shows the bending moment of the wall subjected to the resultant pressure (inclusive the water pressure). As it can be seen from this figure and the figures in Appendix-C.1, the differences in the magnitude of the bending moment based on the classical and transformed active earth pressure are not as such large. On the other hand the differences in the magnitude of the bending moment based on the assumption of different earth resistance (e_{01} and e_{02}) are very remarkable as would expected. Some of the cases resulted a negative reaction force at A. If these negative reaction forces are set to zero, the bending moment at support B can be decreased as shown by the dashed lines in Figure 9.4b.

9.3.1.3   Numerical comparative analysis

The finite element program PLAXIS v7.1 was used for the numerical study of the idealized excavation (Figure 9.2). The hardening soil model (HSM) was chosen to simulate the soil behaviour. The material parameters required for the HSM are given in Table 9.3 below. Contrary to the analytical calculations, where a wall friction angle of zero was assumed, the strength reduction factor for the interface elements $R_{\mathrm{int}er} = 0.50$ was taken in the FEM-computation, because a lower value of the $R_{\mathrm{int}er}$ would result unrealistic deformations (see section 9.3.2.5).

The are two options to carry out an undrained analysis in the PLAXIS v7.1 program. These are to perform undrained analysis using the effective stress parameters as it was used in the parameters study and back analysis of the practical projects in chapter 7 and 8 or to carry out a drained analysis with the total stress parameter c_{cu}. The second option was chosen in this study in order to compare directly with the analytical analysis results. Unlike the analytical analysis, the full undrained shear strength c_{cu} = 24 kN/m² was considered without introducing the anisotropy reduction factor. It was assumed that the HSM will at least take care of the influence of the stress induced anisotropy due to the rotation of the principal stesses. Though the earth pressure at rest is governed by the effective stresses and has nothing to do with the drained or undrained condition, the program sets the K_0^{nc} value to its default value of 1 (1 - sin 0). Since there was no possibility of changing this value manually in this version of PLAXIS, the default value of the K_0^{nc} = 1 was taken as a model parameter (Table 9.3), but the initial stress was generated assuming a lower values of K_0 = 0.85.

The numerical simulation of the construction stages was made according to the Figure 9.5. There were four variants ready for investigations. The first variant was the classical one, where the installation of the struts follow immediately after the excavation of the soil mass up to the strut level. The second variant considers the introduction of the bottom support (No. 4 in Figure 9.5b) by means of either a column jet pile or soilcrete or bottom concrete slab before the execution of 2nd excavation (Figure 9.6). Third variant was the same as the variant-2, except that the excava-

tion was assumed to proceed in three stages and the bottom support was assumed to be in place before the 3rd excavation (No. 5 in Figure 9.5c). The last variant considers a berm support (No. 5 in Figure 9.5d) before the installation of the bottom slab. Each variant was again investigated for the cases with and without groundwater, with and without pre-stressing the upper strut, and calculation with effective and total shear strength. All in all $4 \times 2 \times 2 \times 2 = 32$ combinations were studied.

Table 9.3: Soil parameters for hardening soil model

Drained condition											
$\gamma_{sat}/\gamma_{unsat}$	φ'/φ_{cu}	c'/c_{cu}	E_{50}^{ref}	E_{oed}^{ref}	E_{ur}^{ref}	p^{ref}	m	R_f	K_0^{nc}	v_{ur}	R_{inter}
[kN/m³]	[°]	[kN/m²]	[kN/m²]	[kN/m²]	[kN/m²]	[kN/m²]	[-]	[-]	[-]	[-]	[-]
19.5/17.5	22.5/0.0	1.0/0.0	5000	3878	15000	100	1.0	0.90	0.617	0.2	0.50
Undrained condition											
19.5/17.5	0.0/0.0	0.0/24.0	6700	6000	15000	100	1.0	0.90	1.00	0.2	0.50
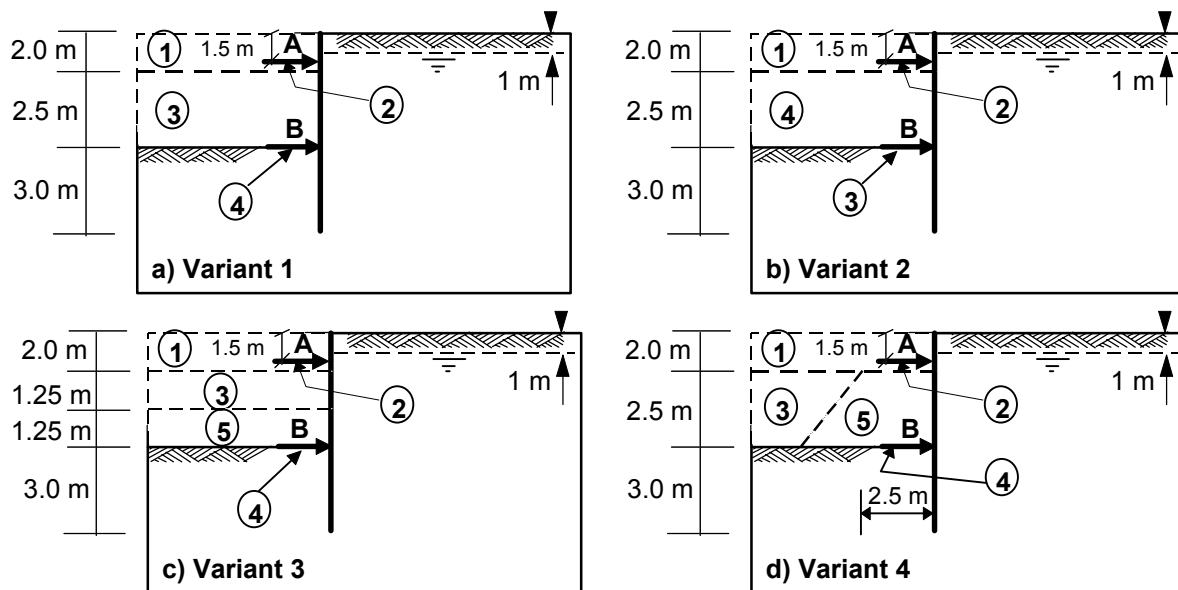
② *construction stages*

Figure 9.5: Four variations of the numerical simulation of the construction stages

A typical FE- model and the mesh for the case of variant-2 is shown in Figure 9.7. A similar FE-models were used for simulation of the other variants. The only difference was the arrangement of the construction stages.
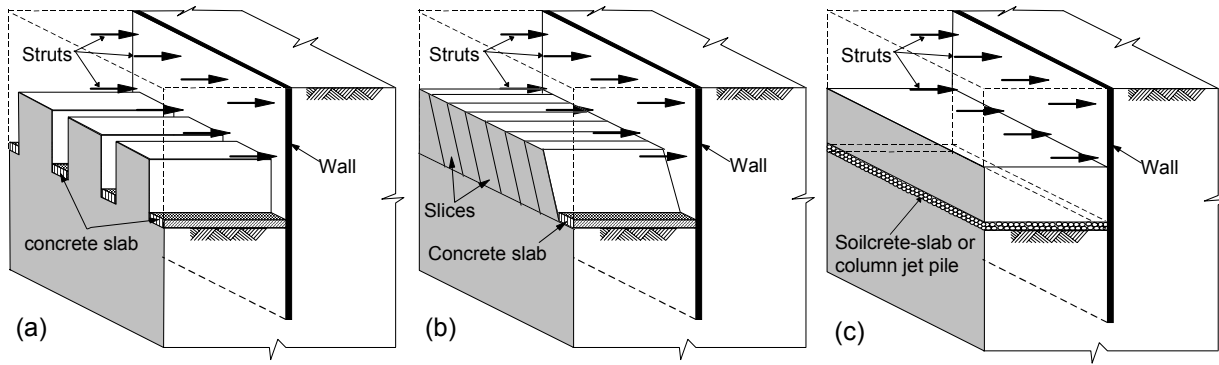
Figure 9.6: Possible means of installation of the bottom support before full excavation
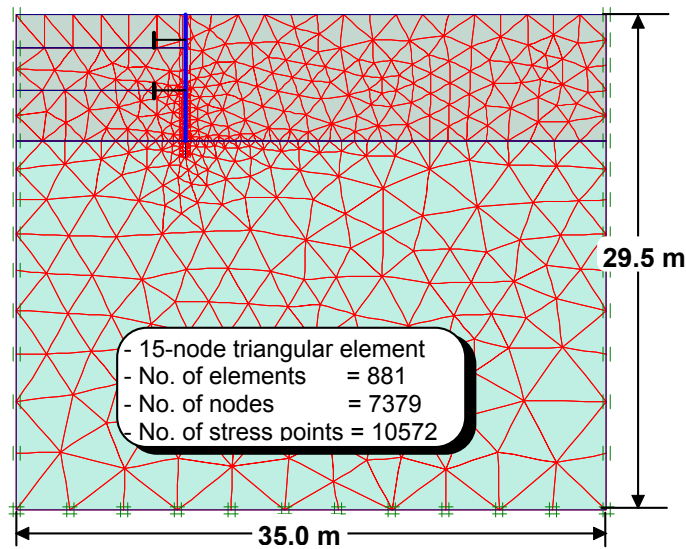
Figure 9.7:

The finite element mesh

Typical results of the FE-computation of the cases of Variant 1 to 4, with groundwater, with pre-stressing of the strut and based on the drained analysis are shown in Figure 9.8. The same computational results but without pre-stressing of the strut are also presented in Figure 9.9. The rest of the results are attached in Appendix-C2. The broken lines in Figure 9.8 and 9.9 shows the analytical earth pressure distributions for a purpose of direct comparison with the numerical results. The symbols in Figure 9.8 and 9.9 should be interpreted as follow:

$$e'_{ph}(\varphi') = e_{ph}(\varphi')/1.5 \tag{9.8}$$

$$e'_{ph}(c_u) = e_{ph}(c_u)/1.5 \tag{9.9}$$

$$e_{ph}(c_u) = \gamma(or\,\gamma')\cdot z + 2\cdot(c_u/2) \tag{9.10}$$

and $e_{ph}(\varphi')$ and $e_{ah}(\varphi')$ are the passive and active earth pressure at limit state for the case of smooth wall $(\delta = 0)$. The name of the different cases "**Variant-1, 2, 3, or 4; a or b; w; d or u**" in Figure 9.8 and 9.9 and the figures in Appendix-C2 have the following meanings:

> 1,2,3,4 = Variant numbers (Figure 9.5)
>
> a, b = without and with pre-stress respectively
>
> w = with groundwater (when w does not appear, it shows no groundwater)
>
> d, u = drained and undrained analyses respectively.

Figure 9.8:   Variant-1 to 4-bwd: with pre-stress of the strut, with ground water and drained analysis at the end of the final excavation stage

Table 9.4:   Reaction forces of the strut and bottom slab (Variant-1 to 4bwd and -1 to 4awd)

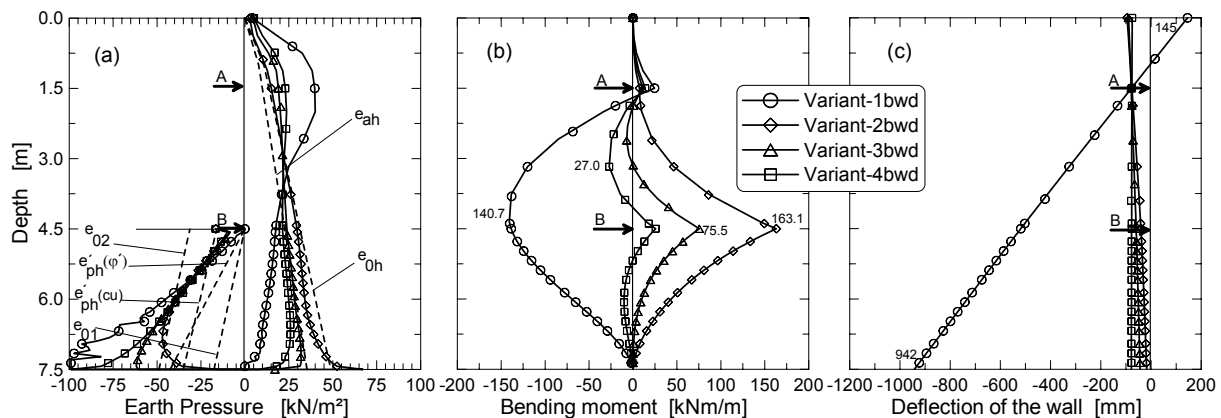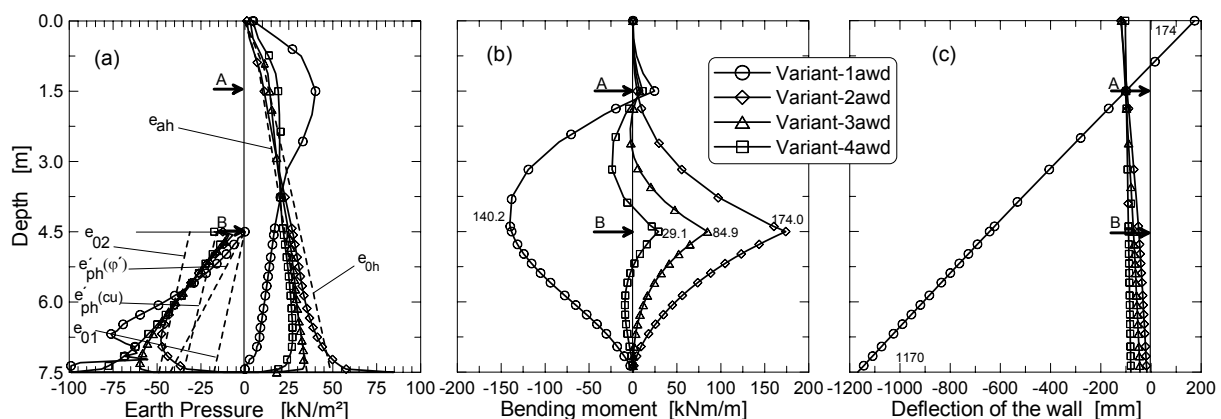| Variant	A [kN/m]	B [kN/m]	Variant	A [kN/m]	B [kN/m]
Variant-1bwd	186.6	0.0	Variant-1awd	165.6	0.0
Variant-2bwd	14.9	242.3	Variant-2awd	0.0	244.2
Variant-3bwd	52.2	167.6	Variant-3awd	36.8	174.9
Variant-4bwd	77.6	127.7	Variant-4awd	66.0	129.2

Figure 9.9:   Variant-1 to 4-awd: without pre-stress of the strut, with ground water and drained analysis at the end of the final excavation stage

9.3.1.4   Analysis and discussion on the preliminary analytical and numerical study

From the preliminary analytical and numerical analyses results, the following observation may be made:

- The differences in the magnitude of the bending moment based on the classical and transformed active earth pressure diagram in the analytical analysis are not as such large. On the other hand the differences in the magnitude of the bending moment based on the assumption of different earth resistance (e_{01} and e_{02}) are very remarkable as would be expected.

- Without the bottom support the excavation would have been collapsed. It shows excessive displacement of the wall at the toe. The passive resistance seems to reach the limit state and the active pressure tends to zero below the bottom of excavation. In fact the penetration depth 3 m is too short for such week soil without a bottom support.

- The effect of the bottom slab support is to reduce the displacement of the wall at the toe and relieve the upper strut by sharing the reaction force. The time point of the installation of the bottom support according to variant-2 to variant-4 (Figure 9.5) respectively has an effect of relieving the bottom support (Table 9.4) and the wall, but the displacement at the toe increases proportionally. It has also an effect of increasing the reaction force of the upper strut, but it is still much lower than the case without the bottom support. Therefore, the decision lies whether to install the bottom support as earlier as possible to minimise the displacement of the wall toe and subject the wall and the bottom support to a higher stresses or to let the wall toe to displace to some extent and relieve the bottom support and the wall. In the first case one should make sure that the bottom support can withstand the high reaction forces.

- The assumption of the earth resistance as e_{01} in the analytical analysis can not be justified by the numerical analysis. The numerical computations show much higher passive resistance than the e_{01}. On the other hand the drained FE-computations show a lower passive resistance just below the bottom of the excavation than the assumed earth resistance e_{02}, but tends to follow the e_{02} line at a lower depth. It seems to follow the passive pressure line at limit state starting form around zero at the bottom of the excavation till it intersects the e_{02} line, and joins the e_{02} line further up to the wall toe. In the case of the undrained analysis without groundwater, the passive resistance appears to follow the e_{02} line, though the e_{02} was determined based on the effective stress ($K_0 = 0.617$).

- The earth pressure distribution lines of the drained numerical analysis on the active side seem to lie between the earth pressure at rest line (e_{0h}) and the active earth pressure line at limit state (e_{ah}), with a slight tendency to diverge toward the e_{0h} line below the bottom of the excavation, and a bit higher pressure at the upper strut level due to the effect of the pre-stress of the strut and slight rotation of the wall in the direction of the retained soil. Without

the ground water and pre-stressing of the strut, the earth pressure line tends to approach the active limit state line (e_{ah}) above the bottom of excavation.

- As would be expected, the drained analysis seems more unfavourable than the undrained analysis as far as the reaction forces, the deformation of the wall and the bending moment of the wall are concerned.

- Though it was not shown in the figures presented, it had been observed that a remarkable amount of deformation had already been occurred before the installation of the upper strut. Hence, it would be advisable to place the strut as much as possible near the ground surface for excavations in soft ground.

9.3.2 The second round of comparative analysis

9.3.2.1 General

The excavation problem in section 9.3.1 was reanalysed in the second round of comparative analysis with certain modifications of the soil parameters, length of the wall, the load and resistance system of the earth pressure. In this round of analysis only two variants of the excavation stages as shown in Figure 9.10 were considered. The first variant was similar to the variant-1 in Figure 9.5a , but without the bottom support, because it was proved that the installation of the bottom support after the final excavation does not have any influence on the performance of the excavation based on drained or undrained (without consolidation) numerical analyses. The second variant was the same as the variant-3 in Figure 9.5c.
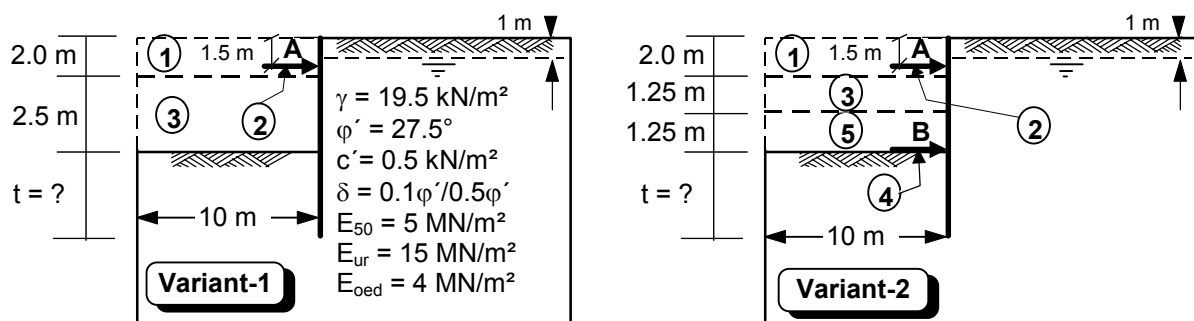

Figure 9.10: Two variations of the idealized excavation problem

9.3.2.2 The penetration depth of the wall

The penetration depth of the wall for the case of the variant-1 (Figure 9.10) was determined according to the classical free earth support method at the end of the excavation. For the case of the variant-2, however, the penetration depth was determined after the 2nd excavation (No. 3 in Figure 9.10) and before the installation of the bottom support. This was done based on the assumption that the bottom support can take care of the equilibrium condition of the system after final excavation. In both cases a wall friction $\delta = \pm 0.10 \cdot \varphi'$ or $\pm 0.10 \cdot \varphi'$ or $\pm 0.50 \cdot \varphi'$ was assumed.

9.3.2.3 The loading and reaction systems for the analytical analysis

In the previous preliminary analysis (Section 9.3.1.4), it was reported that neither the assumed earth resistance e_{01} nor e_{02} matches with the numerical earth pressure distribution on the passive side in the case of excavations with bottom support. Instead the numerical earth pressure starts to follow the passive pressure line at limit state till it intersects the e_{02} line and joins this line thereafter. It was also observed that the numerical earth pressure line on the active side tends to diverge toward the earth pressure at rest e_{0h} line below the bottom of the excavation. These loading and reaction systems were simulated in the analytical analysis of the variant-2 for the case of end of the excavation and are shown as shaded area in Figure 9.14. The point of intersection of the line joining the active pressure line and the earth pressure at rest line was taken the same as the point of intersection of the passive pressure at limit state and the earth pressure at rest with its origin at the top of the wall. For the case of the vaiant-1 and the 2nd excavation phase (No. 3 in Figure 9.10), the loading and the passive resistance system had followed the classical earth pressure distribution. The passive earth pressure at limit state was reduced by a total safety factor of $\eta_p = 2$, before it was used as a reaction to the wall. These loading and passive resistance systems are indicated by the shaded area in Figure 9.13.

9.3.2.4 The soil parameters for HSM and the finite element model

Only drained analysis was carried out in this study, taking into account the comment made in the previous preliminary analysis (Section 9.3.1.4), that the drained analysis leads to unfavourable condition. The soil parameters for the HSM model are given in Table 9.5. The material parameters for the wall and the support system were the same as in the previous preliminary analysis (Section 9.3.1.3). In order to investigate the effect of the interface property, three strength reduction factor $R_{inter} = 0.1$, 0.2 and 0.5 were assumed.

Table 9.5:   The soil parameters for the HSM under drained condition

$\gamma_{sat}/\gamma_{unsat}$	φ'	c'	E_{50}^{ref}	E_{oed}^{ref}	E_{ur}^{ref}	p^{ref}	m	R_f	K_0^{nc}	ν_{ur}	R_{inter}
[kN/m³]	[°]	[kN/m²]	[kN/m²]	[kN/m²]	[kN/m²]	[kN/m²]	[-]	[-]	[-]	[-]	[-]
19.5/19.5	27.5	0.50	5000	4000	15000	100	1.0	0.90	0.538	0.2	0.1/0.2/0.5

Figure 9.11 shows A typical and zoomed finite element model and its mesh for the case of the variant-2 with groundwater condition. The FE-model for the other cases is more or less the same as Figure 9.11, except the different lengths of the wall.
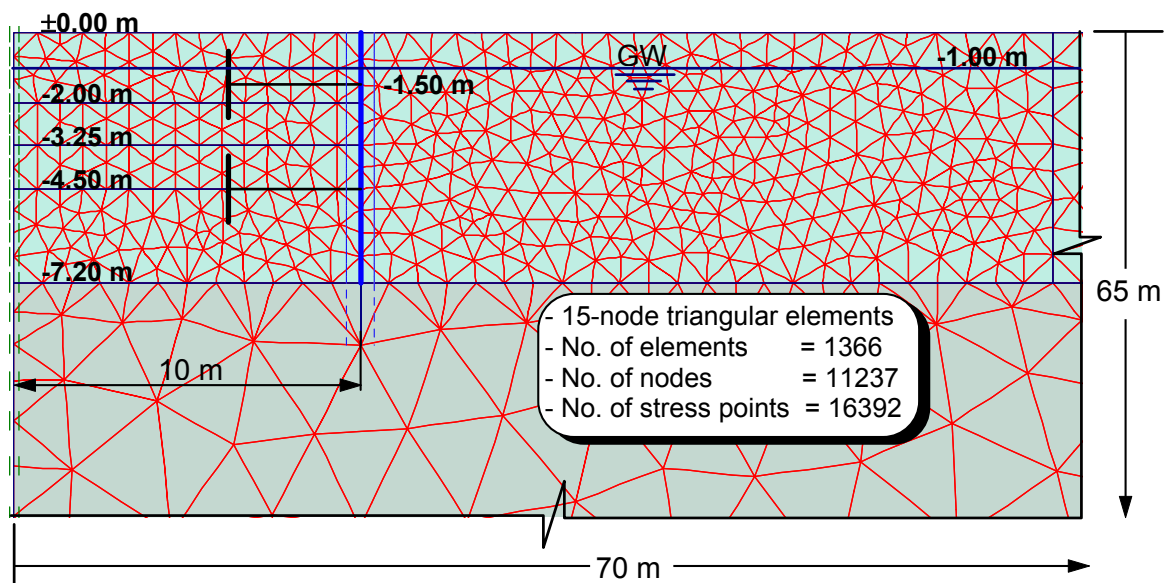
Figure 9.11:   A typical finite element model and its mesh

9.3.2.5   The influence of the interface property

The *EAB (1994)* recommends a wall friction angle of zero for the case of excavations in soft ground. On the other hand a value of zero wall friction in numerical analysis (in this case PLAXIS) would result in unrealistic and excessive deformation of the soil and the wall. This excessive deformation may in turn affect the section forces and the earth pressure distributions. In order to study the effect of the interface property on the performance of the excavation, three variations of the interface reduction factor R_{inter} = 0.1, 0.2 and 0.5 was considered in the numerical analysis of the variant-2 with groundwater condition. Figure 9.12 shows the result of the FE-computations for the selected variant. It appears from the figure that the effect of the interface property on the earth pressure on the active side and the reaction forces is negligible. On the

other hand, there is an increase of the maximum passive resistance by 10.9 kN/m² (around 20 % difference) for an increase of the R_{inter} from 0.1 to 0.5. This increase in the passive resistance had the consequence of reducing the bending moment of the wall. For example, about 10% and 49% of reduction of the span moment for the part of the wall above and below the bottom of excavation respectively can be observed from the Figure 9.12 - middle. The most remarkable influence of the interface property is on the displacement of the wall (Figure 9.12 - right). A slight increase of R_{inter} from 0.1 to 0.2 led to a remarkable reduction of the displacement of the wall at the top. This effect may be due to the fact that the reduction factor does not only reduce the shear strength, but also the stiffness of the of the contact surface even by $(R_{inter})^2$ (PLAXIS manual (2000/2002). For these reasons, the comparison of the analytical and numerical analysis results was restricted to the case of $R_{inter} = 0.5$.
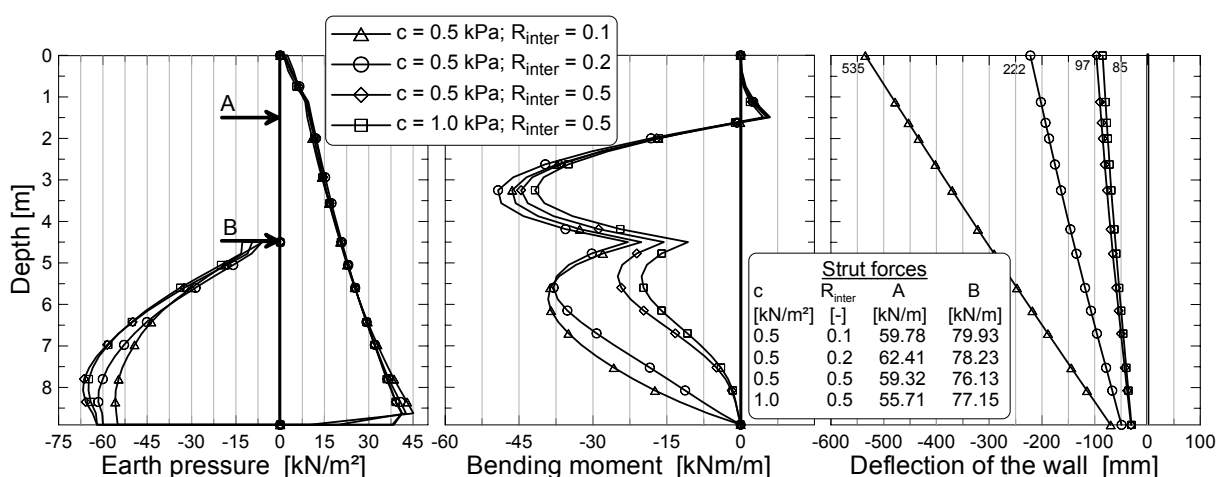
Figure 9.12: The influence of the interface parameter R_{inter}

9.3.2.6 Comparative presentation of the analytical and numerical results

The comparative presentation of the analytical and numerical analyses results for the case of the variant-2 with ground water is shown in Figure 9.13 and 9.14. The results of the rest of the other cases are documented in Appendix-C3. The results of the variant-2 at the end of the 2nd excavation and the varaint-1 at the end of the 2nd and final excavation show a fair match of the earth pressure distributions and the bending moments of the analytical and FE-computations. Sometimes a bit higher pressure on the active and passive side can be observed from the FE-results, but this effect compensate each other to give a comparable bending moment and reaction force results.

Figure 9.14 shows a lower earth pressure distribution on the active side and a higher resistance on the passive side than the assumed loading and resistance systems in the analytical analysis for the

end of excavation case. These two effects summed up to give a higher support moment at the bottom of excavation and a higher reaction forces at A and B. It can be conclude from this discussion that there still needs a further modification of the analytical loading and earth reaction systems.
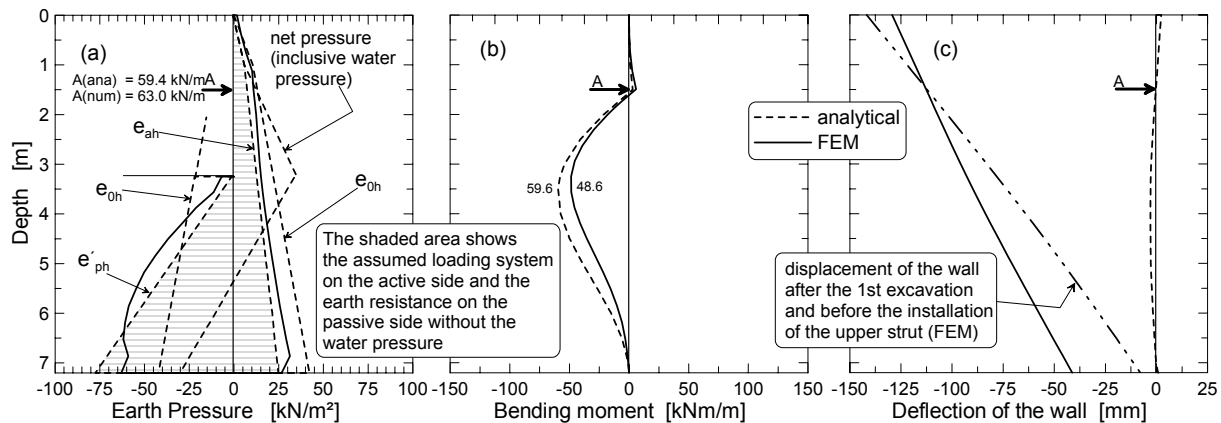

Figure 9.13: A comparative presentation of the analytical and numerical analyses results of the varaint-2 with the groundwater (2nd excavation)

For an obvious reasons, the results of the analytical and FE-computations of the displacement of the wall cannot be comparable. First, the analytical analysis is based on the elastic property of the wall only and does not consider a translation of the wall due to soil movements. Second, the numerical displacement results are the sum of the displacements right from the start of the 1st excavation. In fact, a higher proportion of the wall displacement at the top of the wall had already occurred during the 1st excavation and before the installation of the upper strut. A plot of the displacement of the wall during the first excavation is included in Figure 9.14 - right for the purpose of comparison. This again shows clearly the importance of placing the first strut as much as possible near the top of the wall.
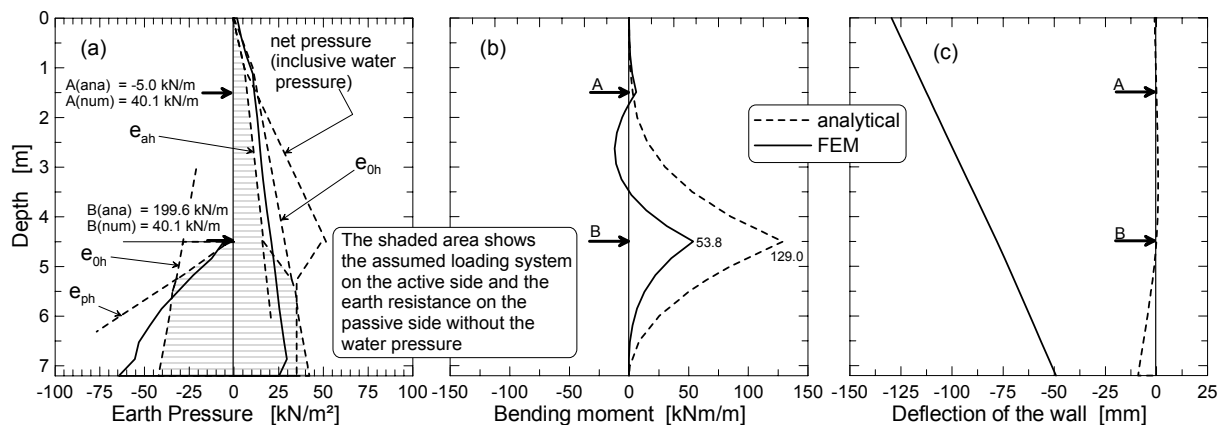

Figure 9.14: A comparative presentation of the analytical and numerical analyses results of the varaint-2 with the groundwater (Final excavation)

9.3.3 The third round of analytical and numerical studies

9.3.3.1 General

In order to secure the results of the previous studies, a further investigations were carried out on two excavation cases (Figure 9.15), which include two depths of excavations (4.0 m and 6.0 m) and considers the worst situation with building and traffic loads. Moreover, there was also a modification of the soil parameters. The numerical and analytical study of each case include further three variants. These include the case without the groundwater and the building load, with ground water but without the building load and with the groundwater and the building load. These variants are also shown in Figure 9.15.

Soil properties:
γ = 19 kN/m²; φ_s' = 25°;
δ = (1/3)·φ_s'; R_f= 0.90; m = 0.80
K_0 = 1 - sin φ_s' ν' = 0,37;
E = 5,2 MN/m²; p_{ref} = 100 kN/m²
E_{50} = 2,6 MN/m²,
E_{ur} = 15,6 MN/m², E_{oed} = 4 MN/m²

Sheet pile wall:
Hoesch 134, St 37

Strut:
IPB 360, St 37, L = 16 m at a spacing of 2,0 m centre to centre, no tension force

Variants:

- Case-Ia and case-IIa: without groundwater and building load

- Case-Ib and case-IIb: with groundwater but without building load

- Case-Ic and case-IIc: with groundwater and building load

Figure 9.15:   Idealized excavation problem, material properties and analysis variations

9.3.3.2   The penetration depth of the wall

In both cases the installation of the bottom support was assumed to take place before the 3rd excavation and before the installation of the second strut in case-II. Similar to the previous study, the depth of the penetration was determined at the end of the 2nd excavation phase (No. 3) in both cases but before the installation of the second strut in case-II according to the classical free earth support method.

9.3.3.3   The load and earth reaction system for the analytical analysis

The load and earth reaction systems case remain the same as in the previous study (Section 9.3.2.3). That is, for the final excavation phase, the passive resistance line follows the passive earth pressure line at limit state till it joins the earth pressure at rest line. The load on the active side follows the active earth pressure line above the bottom of excavation and below this level it starts to diverge toward the earth pressure at rest line and joins this line till the wall toe. The point of intersection of the line joining the active pressure line and the earth pressure at rest line was taken the same as the point of intersection of the passive pressure at limit state and the earth pressure at rest with its origin at the top of the wall. The pressure due to the traffic load, building load and water load follows parallel to the active load line (see for example Figure 9.18). For the case of the end of the 2nd excavation phase, the load and the earth reaction systems follow the classical active earth and passive earth pressure distribution with due consideration of the global safety factor $\eta_p = 2.0$ for the passive resistance.

9.3.3.4   The material properties

One can observe from the Table 9.6 that there is a modification of the soil parameters as compare to the previous studies and are partially based on the test results (Chapter 6). After long discussion, and based on the results of the laboratory tests on wall friction (Section 6.6), the EAB discloses to consider a wall friction angle $\delta = \pm\varphi'/3$ in the calculation of the active and passive earth pressures in the new draft recommendation. This is equivalent to $R_{inter} = 0.333$ in the FE-analysis, however, a separate material set was defined for the contact surface (Table 9.7) based on the MCM. The shear strength parameters had been adopted from the soil parameters after reduction by a factor of 1/3, but the stiffness parameter was assumed to remain the same as the surrounding soil, namely $E_{ref} = E_{50}^{ref}$.

Table 9.6: The soil parameters for the HSM under drained condition

$\gamma_{sat}/\gamma_{unsat}$	φ'	c'	E_{50}^{ref}	E_{oed}^{ref}	E_{ur}^{ref}	p^{ref}	m	R_f	K_0^{nc}	ν_{ur}	R_{inter}
[kN/m³]	[°]	[kN/m²]	[kN/m²]	[kN/m²]	[kN/m²]	[kN/m²]	[-]	[-]	[-]	[-]	[-]
19.0/19.0	25.0	0.10	2600	4000	15600	100	0.8	0.90	0.577	0.2	1.0

Table 9.7: The interface parameters for the MCM under drained condition

$\gamma_{sat}/\gamma_{unsat}$	φ'	c'	E^{ref}	ν	R_{inter}
[kN/m³]	[°]	[kN/m²]	[kN/m²]	[-]	[-]
19.0/19.0	8.3	0.10	2600	0.34	1.0

9.3.3.5 Comparative presentation of the analytical and numerical analyses results

Figure 9.16 shows the results of the analytical and numerical analyses of the worst case-IIc (with ground water and building load) at the end of the 2nd excavation phase (left) and final excavation stage (right). The results of the other variants can be found in Appendix-C4. The deformation of the wall at the end of the 2nd excavation was added to the deflection at the final excavation stage in order to directly compare it with the numerical results, since the numerical deformation results at the end of the final excavation are the sum of the deformations of the previous excavation stages.

9.3.3.6 Discussion and analysis of the results

The discussion and the analysis of the analytical and the numerical results follows in two section:

a) Results after the 2nd excavation stage

The following observation may be made from the analytical and numerical results at the end of the 2nd excavation phase:

- A higher pressure on the active side and more mobilised resistance on the passive side can be seen from the FE-computation results of the cases Ia, Ib, IIa and IIb. However, the effect of a higher load on one side and more mobilised resistance on the other side compensate each other to give a fairly comparable bending moment results.
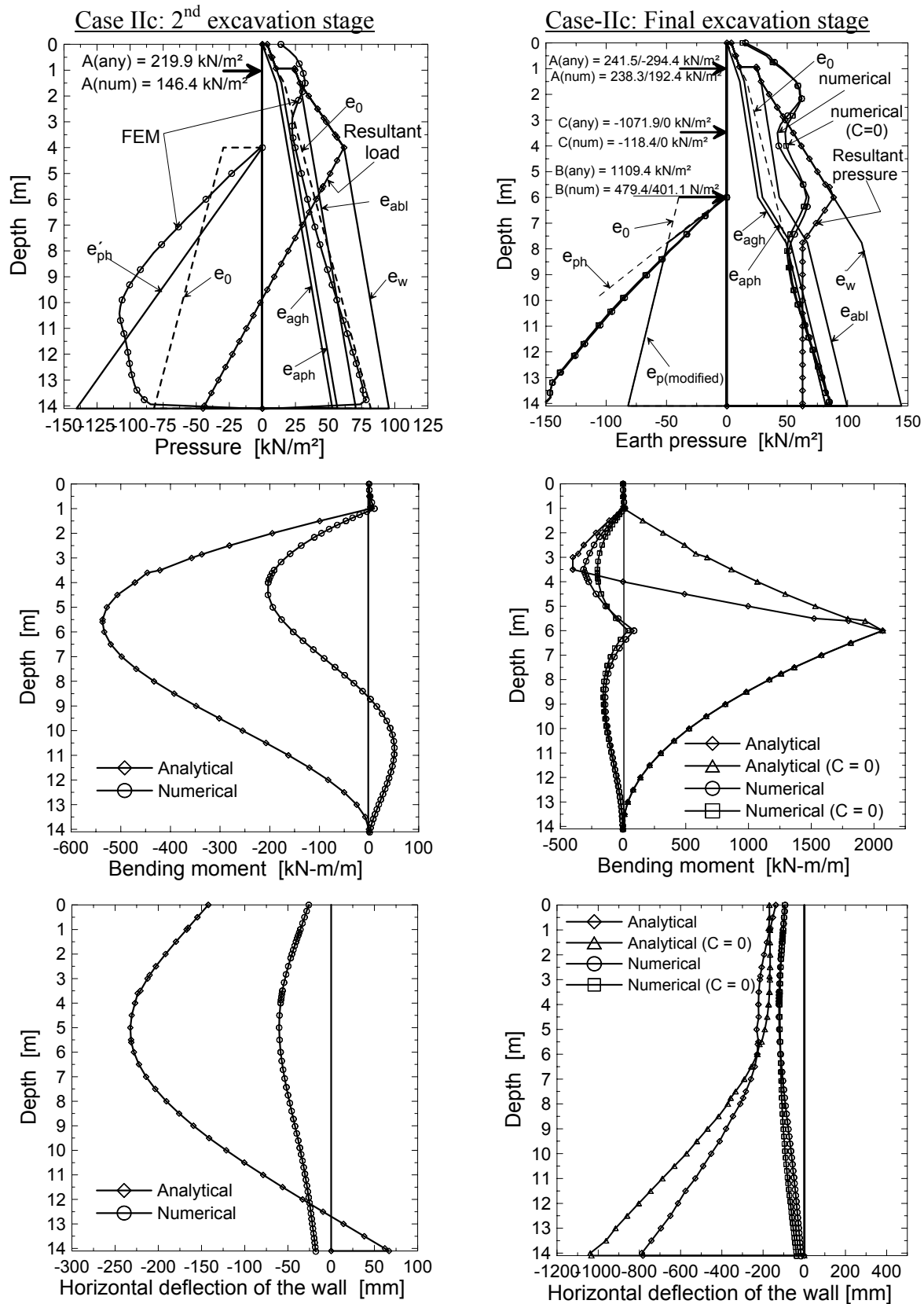
Figure 9.16: Comparative presentation of the analytical and numerical analyses results of
case-IIc (with groundwater and building load)

- For the cases Ic and IIc, however, a higher differences in the bending moment were observed, which is a result of relatively lower pressure load on the active side and comparatively the same resistance force on the passive side.

- For the known reason the displacements of the wall from the analytical and numerical analyses are not comparable, but the shape of the wall deflections are more or less the same

a) Results after the final excavation stage

The following observation may be drawn from the analytical and numerical results at the end of the final excavation phase:

- Both the pressure and the bending moment diagrams from the analytical and FE-computation of all the variants do not match each other. The difference is more remarkable in the cass of Ic and IIc.

- Though a direct comparison of the displacement of the wall is not possible, the exaggerated and unrealistic deflection of the wall below the excavation bottom in the analytical analysis is unacceptable.

The above two observations show the need of an additional support to the wall by means of a subgrade reaction in the analytical analysis in order to bring the displacement of the wall below the excavation bottom to a reasonable value and to close the big gab between the bending moment results. The topic of the additional subgrade reaction is presented in the following section.

9.3.4   The use of the modulus of subgrade reaction

For the reason discussed in all the previous comparative studies and in particular in Section 9.3.3.6, it was agreed to introduce an earth support to the wall by means of a subgrade reaction (Figure 9.17) in addition to the modified assumed earth reaction system. The subgrade reaction extends from the point of intersection of the e_{ph} and e_{oh} lines toward the toe of the wall. The modulus of the subgrade reaction may be approximated from:

$$k_s = \frac{E_{oed}}{t_B}$$
(9.8)

Based on the subgrade reaction approach shown in Figure 9.17, an analytical analysis had been carried out once more on all cases of the 3rd round of the comparative studies (Figure 9.15) with the exception of the cases Ia and IIa. In this additional analysis a full active earth pressure was assumed behind the wall instead of using the pressure diagram that diverges towards the earth pressure at rest below the bottom of excavation. Again two variants of the subgrade reaction was considered assuming two variations of the constrained modulus, namely E_{oed} = 1 and 4 MN/m².
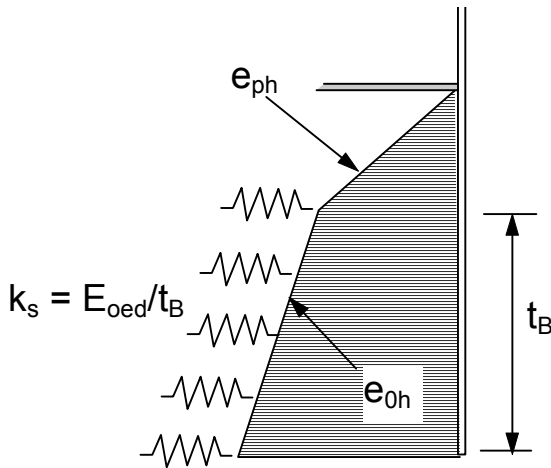
Figure 9.17:
Subgrade reaction to provide additional earth reaction to the wall below the excavation level

The results of the additional analytical analysis of the case IIc at the end of the excavation are plotted in Figure 9.18 against the already available numerical analysis results. The results of the rest cases can be found in Appendix-C5. It can be seen from the bending moment and deformation plot in Figure 9.17 and the rest of the figures in Appendix-C5, that a very good agreement of the analytical and the numerical results can be achieved by a providing a subgrade reaction to the wall with a subgrade reaction modulus of $k_s = 631$ kN/m³ that is derived based on the assumption $E_{oed} = 4$ MN/m².
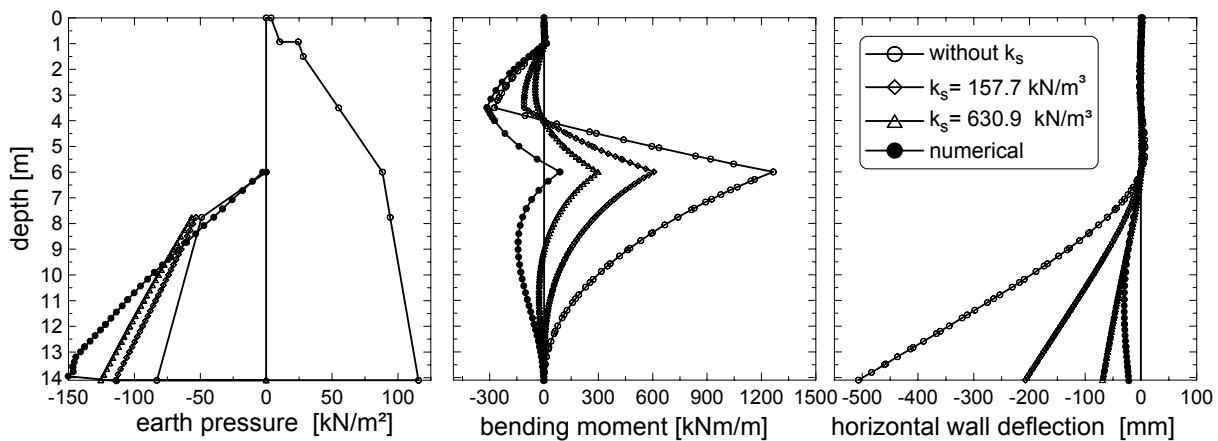

Figure 9.18:   The effect of the subgrade reaction for the case IIc at the end of the excavation

For a purpose of comparison, a further numerical and analytical analyses had been conducted on selected cases, namely the cases Ib and IIc assuming a diaphragm wall in order to show the effect of the stiffness of the wall on the application of the subgrade reaction. The results of this additional analysis of the case-IIc at the end of the final excavation are shown in Figure 9.19 and that of case-Ib can be found in Appendix- C5. It appears that the effect of the subgrade reaction is not as remarkable as the case of a flexible wall.
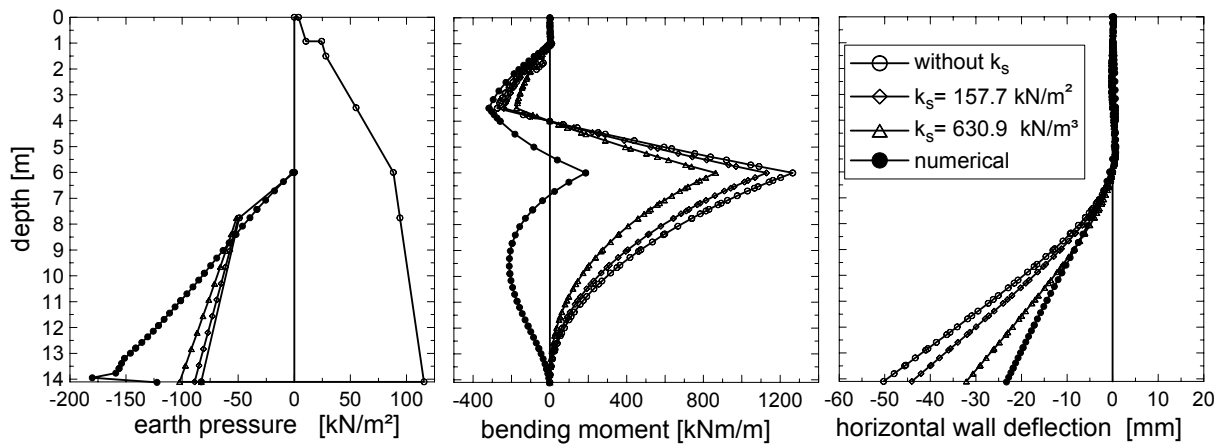
Figure 9.19: The effect of the subgrade reaction (case IIc, final excavation) in the case of a rigid wall (diaphragm wall)

9.3.5   Some comments on the previous sections

The goal of this chapter is partly to document the different stages, the draft recommendation has pass through and it should have been seen independent from the previous chapters in this work. An attempt was made to present the comparative studies starting from the early stage of the draft recommendation. However, that does not mean that the parameters in the preliminary analysis are still actual. The parameters are changed and modified each time. For example, the R_{int} (wall friction) was taken as 0.0 to 0.5 at the initial stage, because at this stage it was not clear which value to apply. On one hand, the old version of the EAB suggests a wall friction value of 0, and on the other hand, this value results in unrealistic deformations in numerical computations. However, later supported by laboratory tests, it was decided to fix the wall friction as 1/3 φ'. On the meantime the PLAXIS program has also offers the possibility of entering the interface properties separately, instead of adopting the parameters from soil clusters. Hence, one may avoid excessive deformations by keeping the stiffness of the interface the same as the soil, but reducing the shear strength by a factor of 0.33. This is the actual stand and it is not in conflict with some suggestion in the previous chapters.

9.3.6   A brief presentation of the final draft recommendation EB95 and EB96

9.3.6.1   General

Based on the analytical and numerical comparative parameter studies and the huge practical experiences of the members of the working group "Excavation" (EAB), the group recommends the

following approaches to calculate the earth pressure behind the wall and the earth reaction on the passive side.

9.3.6.2   The acting load on the active side of the wall

a) The earth pressure at rest

The earth pressure at rest for a homogeneous soil layer may be calculated from the Equation 9.9 below.

$$e_{og} = \gamma(\text{or }\gamma') \cdot K_0 \cdot z_a \tag{9.9}$$

The following conditions should be fulfilled before applying the earth pressure at rest as a governing load on the active side of the wall.

- When a minimum or no wall movements at the top of the wall or at the level of the bottom of excavation toward the excavation is expected, an earth pressure at rest can be applied above the bottom of the excavation. This can be the case, for example, when rigid walls are used, or when a bottom support can already be placed before the excavation starts by means of a jet pile column or soilcrete, or when the first support can be installed and pre-stressed before any major excavation starts (Figure 9.22b).

- When a minimum or no wall movements at the wall toe or at the level of the bottom of excavation toward the excavation is expected, an earth pressure at rest can be applied below the bottom of the excavation. This can be the case, for example, when rigid walls are used, or when a bottom support can already be placed before the excavation starts by means of a jet pile column or soilcrete (Figure 9.22b).

- When the earth pressure at rest would be applied in the case of rigid walls for the above mentioned reasons, for the same situation but relatively flexible, an increased active earth pressure (Figure 9.23a) according to the EB 22 (*EAB, 1994*) can be applied below and above the bottom of the excavation. Moreover, when the rotation of the wall top toward the soil and the wall toe toward the excavation due to the sum effect of the pre-stressing of the upper strut and a higher load from the building and water pressure is expected, an earth pressure at rest above and an active earth pressure below the bottom of excavation can be applied (Figure 9.23b).

b) The active earth pressure

Equation 9.10 may be used to determine the active earth pressure,

$$e_{agh} = \gamma(\text{or }\gamma') \cdot K_{agh} \cdot z_a \tag{9.10}$$

The coefficient of the active earth pressure K_a shall be determined with the assumption of a wall friction $\delta_a = \varphi'/3$.

In order to apply the active earth pressure as a governing load on the wall, the following conditions should be fulfilled:

- When the wall movements at the top of the wall or at the level of the bottom of excavation toward the excavation is expected. This may be the case, for example, when the first strut is located relatively deep, or when full mobilisation of the passive pressure can be expected, or when the bottom support is installed stepwise in slices.

- If on one hand a pre-stressing of the upper strut is required, and on the other hand, a full support of the wall toe may be claimed, the active earth pressure above the bottom of the excavation level may be redistributed to a trapezoidal or rectangular diagram (Figure 9.20b).

9.3.6.3 The earth reaction on the passive side of the wall

Dependant on the expected the amount and the art of the displacement of the wall, the earth resistance may take the value between the active and the passive earth pressure at limit state as described below.

In the case of an excavation supported by a strut at the top but without a bottom support (Figure 9.20), the classical reduced passive pressure can be assumed as earth reaction. The passive earth pressure at limit state can be obtained from

$$e_{pgh} = \gamma(\text{or } \gamma') \cdot K_{pgh} \cdot z_p \tag{9.11}$$

where K_{pgh} is the coefficient of the passive earth pressure based on wall friction angle $\delta_p = -\varphi'/3$.

In the case of an excavation with bottom slab installed stepwise in slices (Figure 9.21), the equilibrium condition of the forces is ensured primarily by the reaction from the bottom slab.

- If the bottom slab is in place before remarkable displacement of the wall below the excavation had occurred, one can assume the soil to retain the earth pressure at rest that exist before the excavation had started as follows

$$e_{og} = \gamma(\text{or } \gamma') \cdot K_0 \cdot (H + z_p) \tag{9.11}$$

Just below the bottom slab, the passive pressure at limit state (e_{pgh}) with $\delta_p = 0$ dominates the reaction diagram due to the rotation of the principal stresses in this region. The Equation (9.11) together with this assumption provides a basic modified reaction system.
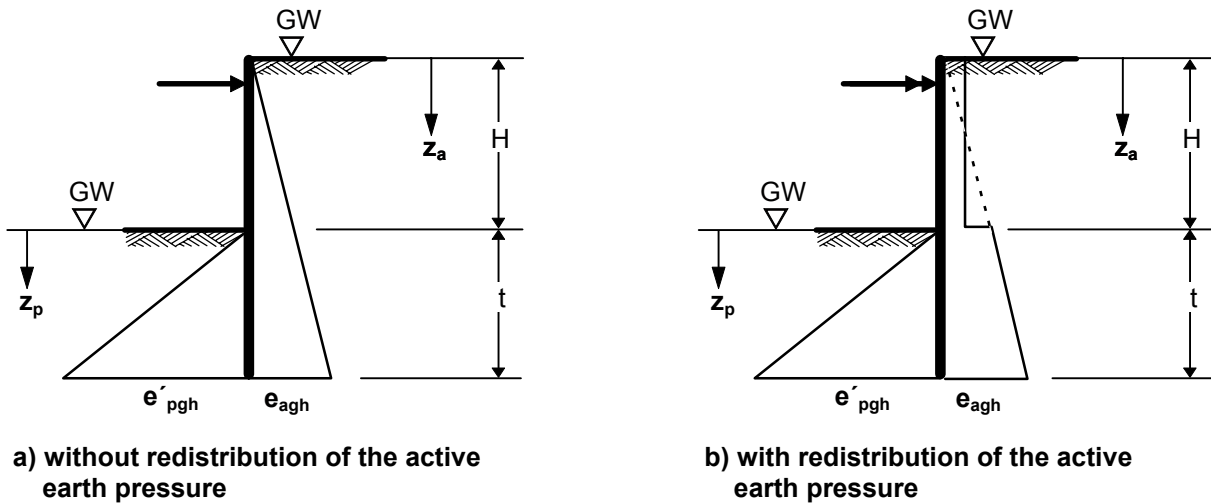
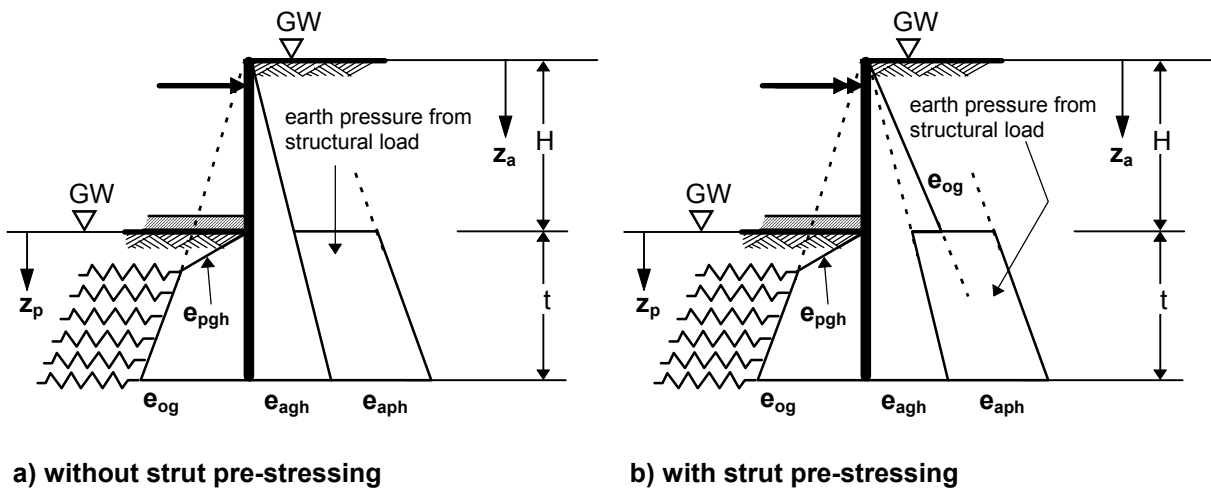*Figure 9.20:* Possible load diagram for a wall supported at the top only

Figure 9.21: Possible load diagram for a wall supported by a strut at the top and by stepwise installed bottom slab

- If an active earth pressure due soil weight only governs the loading system on the active side, the basic modified earth reaction should be reduced to a level equal to the available active pressure on the other side.

- If on the other hand, the sum of the acting pressures below the bottom of excavation is larger than the basic modified earth resistance due to earth pressure from structural loads or water pressures, a subgrade reaction $K_{s,h}$ can be introduced below the intersection point of the e_{og} and e_{pgh} lines to provide an additional earth reaction to the wall. The modulus of the

subgrade reaction may be determined from Equation (9.8). The earth reaction mobilised by the subgrade reaction, however, must not be higher than the following value

$$R_{ph} = \frac{(E_{pgh} - E_{og})}{\eta_p}$$
(9.12)

Where $\eta_p = 1.5$.

In the case of an excavation with bottom slab installed by means of column jet pile or soilcrete, the equilibrium condition of the forces is also ensured primarily by the bottom slab.

- If the wall is displaced in the direction of the active soil during the installation of the bottom slab, an active earth pressure with due consideration of the weight of the slab can be assumed as earth reaction on the passive side (Figure 9.22 and Figure 9.23a).

- If a flexible wall is used, the struts or anchors are heavily pre-stressed and the sum of the acting forces on the active side due to structural loads and water pressure is too large so that the wall below the bottom of the excavation level can deflect toward the excavation, the modified earth reaction system with or without the subgrade reaction (Figure 9.23b) can be used similar to the case with the stepwise installed bottom slab.
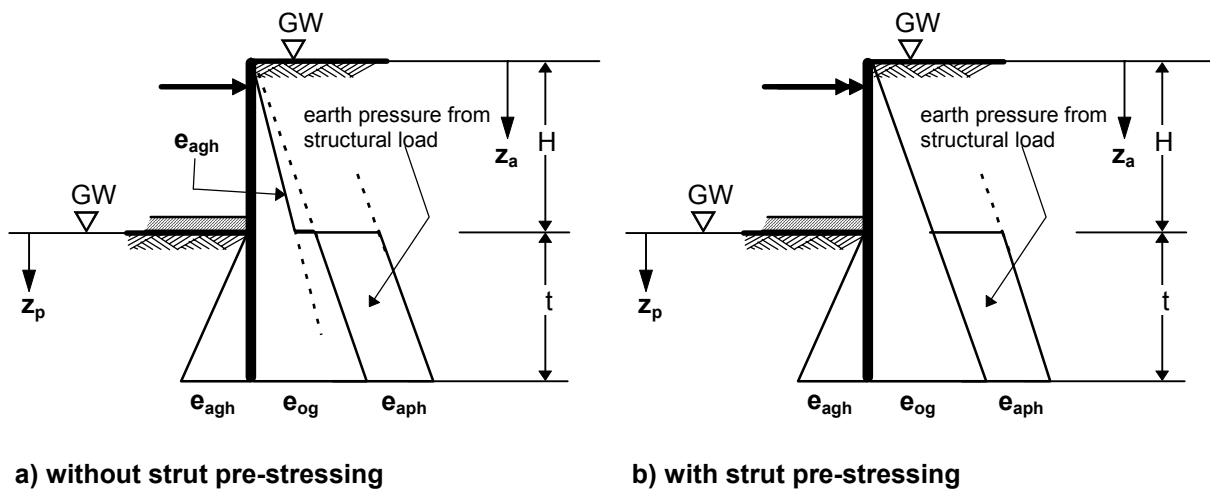

a) without strut pre-stressing   b) with strut pre-stressing

Figure 9.22: Possible load diagram for a rigid wall supported by a strut at the top and by a bottom slab installed by means of jet pile column or soilcrete

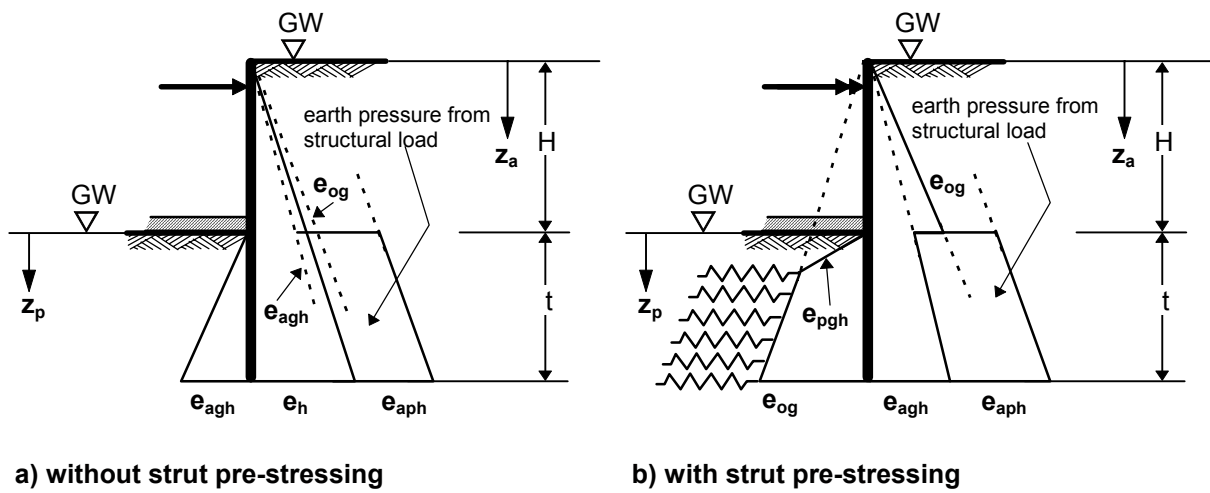**a) without strut pre-stressing**   **b) with strut pre-stressing**

Figure 9.23: Possible load diagram for a flexible wall supported by a strut at the top and by a bottom slab installed by means of jet pile column or soilcrete

10   Summary

10.1   Summary in English

This research work was directed towards a study of the behaviour of supported excavations in soft grounds. The increasing demand for construction of major buildings and transport facilities in urban areas is making excavations very common. The design and execution of such temporary supported excavations require a knowledge of the expected movements in and around the excavation site caused by the relief of stresses due to excavation. Total prevention of ground movements might not be possible, however, it should be possible to predict the extent and distribution of these movements in order to assess the damage potential and to evaluate the need for any preventive measures or changes in design necessary to minimise the movements. Because of the low strength and stiffness, excavations in soft soils are more prone to soil movements than other types of soils. In Germany, a normally consolidated lacustrine soft soils are distributed around Lake Constance (Bodensee) and South Bavarian Lakes. They are young and post glacial deposits. The thickness of the soft soil is estimated to be more than 20 m. Experiences in southern Germany, in the city of Constance show that building foundations are prone to excessive settlements, and excavations are associated with remarkable soil movements causing light and heavy damages to nearby structures. This was the main motive of this research work to focus on the study of the performance of an excavation in such soft soils.

To achieve the goal of the thesis, three methods have been employed. These are experimental, analytical and numerical methods. In the experimental part focus has been made on the determination of soil parameters relevant to excavation in soft soils and that describe the constitute soil models which were used in the numerical analysis. The analytical methods have served to evaluate the type of analyses, to develop some relationships between the effective and total stress parameters, and to examine the earth pressure, the earth resistance and section forces in comparison with numerical results. The numerical method, namely, the finite element method (FEM) was employed to study the influence of the various soil parameters on the performance of an excavation and behaviour of a soil specimen under triaxial and one-dimensional state of stress based on a parameter study, and to analyse practical projects.

The first task of the work was to document the "state of the art" of the construction and design principles of excavations in soft soils. This was done in Chapter 2. The causes of soil movements in and around an excavation are outlined and discussed. The relationships between the settlement of the surface behind the wall and the wall deflection on one side and the height of the excavation on the other side are presented. Settlement envelopes are given based on various measurements in the literature. The review of the soil movements show that a remarkable soil movement might occur prior to the start of excavation due to the installation of walls and in some cases wall extracting of sheet piles. This shows that soil movements may not be totally prevented. Further-

more, the development and the different way of application of the safety factor in the design of retaining structures in different regions are compared and analysed. Finally, the various factors that influence the performance of an excavations based on finite element parameter studies in the literature are briefly reviewed. It was found that the stiffness of the soil plays a major role in the performance of the excavation as it would be expected.

The material behaviour of soft soils in general are reviewed in chapter 3. Beside describing and outlying the strength and deformation characteristics of soft soils, it was possible to build up from the literature a data bank of empirical relationships of the compression, strength and deformation parameters with simple index properties tests. The application of these empirical relationships to the lacustrine soft soil in southern Germany has been proven and compared.

The discussion of the drained and undrained analysis is not new in soil mechanics. The most unfavourable situation for excavations in soft ground is believed to be the drained case, because the negative excess pore pressure due to excavation might contribute to the stability of the excavation in short term. However, for temporal supported excavations, the time of the construction might not be long enough to define the excavation as drained or short enough to define it as undrained. The actual state of an excavation in soft ground lies between these two extreme cases. This situation can only be described with the help of the consolidation analysis, but such analytical approach for restraining structures are not yet available. If one assumes the undrained condition to prevail, the determination of the depth of penetration of the wall based on undrained strength might lead to unrealistic results (*see Hettler et al. (2002)*). There is, however, a general understanding that the effective stress governs the behaviour of the soils even in the undrained condition. A relationship was developed in chapter 4 to calculate the active and passive earth pressures in short term based on the effective angle of the overall strength φ_s' and the *Skempton/Bishop* coefficient of pore water pressure at failure A_f. In practice, there is more confidence in the undrained shear strength of the soil c_u, because it can readily be determined at the spot with the field measurements. To make use of the huge experiences and data bank in the undrained strength c_u for estimating the effective shear parameter φ_s', equations were derived based on stress paths in undrained triaxial tests and again with the knowledge of the coefficient of pore water pressure at failure A_f. Based on these relationships and the assumption that the effective strength in extension and compression is the same, a further equations were derived to estimate the A_f value for the common stress paths from the value of $A_{f,s}$ from standard triaxial undrained compression test. The information on the later is available in the literature and it can also be readily determined in laboratory.

The basics of the constitutive models in soil mechanics are briefly reviewed and the merits and demerits are discussed in chapter 5. The finite element code PLAXIS, which was used in the numerical parametric study and back analysis of practical projects, was briefly introduced in this

section. The basic features of the material models in this code, the failure criterion assumed in the models, the definition of the yield surface, the state of stresses, the hardening and flow rule, their range of application and the material parameters needed to define the models are presented in tabular form. The hardening soil model (HSM) was chosen as a basic material model to simulate the behaviour of the soft soil in this study, because this model best satisfies the basic requirements of a constitutive model for an excavation.

One of the major requirements for predicting the performance of an excavation is an estimation of the relevant soil parameters. Besides the data obtained from geotechnical reports of various projects and the literature, samples were collected from three sites in the city of Constance in southern Germany, and a number of laboratory tests were carried out with in the frame work of this research work. These include standard isotropically ($\sigma'_h/\sigma'_v = K_0 = 1$) consolidated triaxial tests, anisotropically ($\sigma'_h/\sigma'_v = K_0 = 0.80$) consolidated triaxial tests, stress path triaxial tests (above the K_0-line or the isotropic line), one dimensional and isotropic compression tests. Moreover, a test was conducted to examine the contact behaviour between the soil and the wall using a large shear box (365×550 mm), a medium direct shear box (100×100 mm) and a small direct shear box (63×63 mm). Though the analysis and interpretation of the test results have a general nature, they were directed towards obtaining the relevant soil parameters for numerical analysis of an excavations with the application of the constitutive models in PLAXIS FE-program. A data bank of the main out put of the investigations is documented in chapter 6, and it is briefly summarised below:

- There exist a single and unique effective stress path above the isotropic line or the *K_0 - line* independent from the type of the test and type of the stress path and sample orientation. The value of the cohesion measured ranges between 10 - 22 kPa, which is much higher than usually expected.

- Contrary to the expectation, horizontally oriented specimens were found to be stiffer than the vertically oriented specimens, however, further investigation is recommended.

- The stiffness of the soil in *CAD* and *CAU* tests was higher than the corresponding *CID* and *CIU* tests with an average factor of 4.4 in drained and 1.5 in undrained condition.

- The following average ratios between the stiffness parameters were determined: *$E_i/E_{50} = 2.08$, $E_{ur}/E_i = 3.2$, $E_{ur}/E_{50} = 6.3$, $E_{oed,ur}/E_{oed} = 3.1$.* All values are at reference pressure of 100 kN/m² and does not include the values from site3, where higher values were observed.

- As expected, a higher stiffness was measured in undrained tests than in drained tests with an average factor of 1.08 and 1.29 at site1 and site2 respectively and they lie within the range of values according to the theory of elasticity.

- The undisturbed soil specimen under the postulated stress path B seems stiffer than under stress path C in *CAU* test, whereas no remarkable difference in the stiffness on reconstituted specimens under the stress paths A, B and C in *CIU* test was observed. The number of tests conducted are however not enough to give a general analysis of the results.

- Most of the test results show a divergence from a linear relationship in the transformed stress-strain curves at lower axial strains (up to 5%). Some data, particularly at low confining pressures, showed complete divergence from the linear relationship indicating that the stress - strain curves are not exactly hyperbolic. The problem at a lower strain may be solved with piece wise approach with the assumption of two hyperbola with two different lines of stiffness as suggested by *Amann et al. (1975)*.

- The wall friction is rather far from smooth as it would usually assumed. A value of $\delta = 0.460 \cdot \varphi'$ and a stiffness value as high as the stiffness of the soil for both soil to concrete and soil to steel sheet contact was measured in large shear box. Taking into account the effect of the ground water at field, the new draft recommendation of *EAB (2002)* that $\delta = \varphi'/3$ seems reasonable.

In the first part of the chapter 7, the soil parameters relevant to the excavations in soft soils were calibrated based on the hardening soil model (HSM). By means of the sensitivity studies of the strength and stiffness parameters of the HSM, their influence on the stress - strain, volume change, excess pore pressure characteristic of a triaxial and oedometer specimens have been studied. The important findings of the parameter studies are summarised below.

- The drained tests can fairly be simulated with the FEM with a slight modification of parameters. As would expected, the E_{50}^{ref} is the main parameter that determines the stress-strain behaviour of a soil specimen in a triaxial primary loading condition, and it has negligible influence on one - dimensional loading condition. Similarly, the E_{oed}^{ref} has insignificant effect on the triaxial loading condition, but plays the main role in one-dimensional loading. The E_{ur}^{ref} is the single parameter that influences the un/reloading condition both in triaxial and one dimensional state of stress. Contrary to the expectation, the v_{ur} has only an effect on the one-dimensional un/reloading condition. It seems that the K_0^{nc} as a model parameter will have no significant influence on the un/reloading state of stress in both loading systems.

- The use of the angle of the overall shear strength in numerical method should be taken with care, since it is dependant on the stress level. A constant value for the whole depth might lead to overestimation or underestimation of the strength of the soil.

- The E_{oed}^{ref} and K_0^{nc} values appear to play the leading role in determining the volume change characteristic of the specimen in a triaxial compression, although all the other parameters with the exception of the R_f contribute their part. This and the above discussion show the

separate function of the E_{oed}^{ref} as a cap parameter that controls the compression hardening and the E_{50}^{ref} as a parameter that controls the shear hardening.

- The undrained triaxial stress - strain behaviour in primary loading condition seems to be affected by various parameters. Beside the E_{50}^{ref}, the E_{ur}^{ref} and K_0^{nc} have a significant effect on its behaviour. The other parameters have also their part, but in a small scale. The simulation of the undrained test did not give the expected match of the computed and the measured results. This is partly due to the difficulty of simulation of the drop of the excess pore pressure on one hand and the increase of the deviatoric stress on the other hand. All the parameters appear to affect the development of an excess pore pressure, but the effect of the K_0^{nc} is very remarkable.

- The effective cohesion of soils might affect the value of K_0 according to *Janbu (1977)*. This effect has been studied by varying c' and φ' in the FE - calculation of a one-dimensional test model. A general tendency of increasing K_0 value was observed for all values of φ' considered, and an empirical equation was developed to estimate the influence of the c'.

- The state of stress at failure is entirely determined by the effective shear strength parameters in the case of drained analysis. The effect of the other parameters is to enhance or retard the axial strain at which the failure might occur. Beside the shear parameters, the volumetric behaviour may also govern the state of stress at failure in the case of undrained analysis.

- The effective stress paths for all total stress paths in compression zone (Stress paths A, B and C) on one side, and in the extension zone (Stress paths D, E and F) on the other side are unique. This is an approval of the test results in chapter 6. This also leads to a unique deviatoric stress at failure. The only thing that make a difference is the development of the excess pore pressures, which are quite different for different stress paths. The deviatoric stresses at failure in compression and extension are also different. This leads to different undrained shear strength c_u and the angle of the overall shear strength φ_s in compression and in extension. The ratios of the respective values are 1.38 and 0.90 for isotopic and 1.31 and 0.89 for K_0 - consolidation condition respectively. Comparing the isotropic with K_0 - consolidation, the later reacts stronger than the earlier one. The deviatoric stress at failure in the case of K_0 - consolidation is higher by a factor of 1.4 than the case of isotropic.

In the second part of chapter 7, a parameter studies of the geometry of the FE-model and the soil parameters for HSM were conducted based on an idealized excavation problem, in order to study the influence of these parameters on the performance of an excavation. The summery of the parameter studies are given as follows:

- Horizontal wall deflection and displacements do not be significantly affected by the size of the model, however, the deflection increases with the increase of the width of excavation. The main factor that influence the heave at the bottom of the excavation and settlement at the surface is the height of the model rather than the width of the model. The heave at excavation bottom increases with the increase of the width of excavation, where as the settlement at the surface tends to decrease with increasing width of excavation.

- The E_{50} seems to lead the role of the influence of the wall displacement, the active and passive earth pressure, the bending moments and the settlement behind the wall. Due to the non-linearity, however, increasing its value does not necessarily produce the same effect as the other way round. The influence of the E_{50} on bottom heave is limited to the heave near the wall only and its influence ceases at the middle of the excavation. The E_{ur} plays a dominant role in the heave of the excavation and the displacement of the wall toe, but it has insignificant influence on the bending moment. The v_{ur} has only an effect on the bottom heave and settlement at the surface. The R_f has a negligible effect on all the cases.

- The HSM treats K_0^{nc} and K_0 separately. While K_0^{nc} is a model parameter which is closely related to the stiffness parameters E_{50}, E_{ur}, E_{oed} and v_{ur}, the K_0 is purely used to define the initial state of the stresses. For normally consolidated soils, however, these values are more or less the same. The value of K_0^{nc} can not be varied indefinitely, for example, for the given reference parameters, the minimum and maximum possible values of K_0^{nc} are 0.437 and 0.71 respectively. In the parameter study the K_0 is assumed to vary with the K_0^{nc}. The K_0^{nc} value may affect the deformations, bending moment and the earth pressure, although the magnitude of its influence is moderate as compare to the triaxial state of stresses discussed in the first part of chapter 7. The K_0 value towards the lowest limit is more sensitive than varying its value towards the upper limit, although the difference between the reference value and the extreme values is almost the same.

- Contrary to expectation, a reduction of the reference value of the E_{oed} by 50% has caused a reduction of the wall and soil movements, the active earth pressure and the bending moment by about 17 to 30% instead of an increase in these values. A reduced wall movement would have resulted in an increased active pressure and reduced passive pressure. Increasing the reference value by same amount (50%) show no significant influence. In all cases the E_{oed} is more sensible to a change of value below than above the reference value. The ratio of the E_{50} /E_{oed} maybe is more important than the absolute value of the E_{oed}. For the reference case this ratio becomes 1.1. If the E_{oed} is increased or decreased by 50%, the ratio becomes 0.73 and 2.20 respectively. The ratio in the case of increasing the E_{oed} is more closer to the reference ratio than the other way round. This might be the reason why the change of the E_{oed} is more sensible to a value below than above the reference value.

- All the above observations are for the case of a drained condition, but the general tendency is almost the same under undrained condition with the exception of the following. K_0^{nc} seems to be more sensible to higher value. It appears that the E_{ur} plays the dominant role, for example, the settlement at the surface was primarily affected by E_{50} in the case of a drained condition, but the opposite is true under undrained condition. Unlike the drained condition, the v_{ur} has a negligible effect on the bottom heave and settlement at the surface. The contradictory observation and its explanation of the influence of the E_{oed} remain the same as the drained case.

- Similar to the triaxial state of stress, the excess pore water pressure in an excavation is more sensible to the variation of the K_0^{nc} value and the parameter E_{ur}. The influence of this two parameters on the excess pore water pressure is abundantly clear at point just below the wall toe.

- Some of the total stress paths are reasonably comparable with the idealised stress paths shown and discussed in chapter 3, 4 and 6. Some of them, however, follows different directions during the construction stages, and it is difficult to sort them with one particular stress path.

- By leaving about 50% of the soil mass intact to serve as a berm support to the excavation, where the excavation proceeds from the middle of the excavation towards the wall, 20 - 50% reduction of the associated deformations at different locations may be achieved. If the excavation proceeds in the opposite direction, however, the efficiency drops to 10 - 40%.

- The effect of the bottom support on deflection of the wall at the top is mainly limited to prevent the wall deflection towards the soil and has a negligible effect on the bottom heave irrespective of the time point of bottom slab installation. However, an efficiency of about 37 - 97%, 37 - 92% and 24 - 36% may be achieved on the reduction of settlement at the surface and wall displacement at the toe and excavation bottom level for the given case, if the wall would be installed before the 1st , 2nd and 3rd excavation phases respectively. It appears that the installation of the bottom support before the 1st excavation have no significance influence, i.e., a comparable efficiency may be achieved by installing the bottom support after the 1st excavation but before the 2nd excavation.

- The assumption drained = undrained + consolidation seems to work only in the case of heave at the bottom of the excavation. For displacement of the wall toe, the consolidation phase seems to play a negligible role. At other locations, such as the displacement of the wall at the top or at the excavation level and the settlement at the surface, the undrained + consolidation analysis seems to cause more deformation than the drained analysis. However, since the stress paths followed during the drained and the undrained + consolidation analyses are quite different, the assumption drained = undrained + consolidation may not necessarily always holds true.

At the end of the chapter 7, a study of the mobilisation of the passive resistance dependent on the stiffness of the soil, the type of the wall movement and the wall displacement was carried out using the FEM, and analytical approach was developed to approximate the passive resistance based on the hyperbolic function. Furthermore, an equation was derived for estimation of the total safety factor for the passive resistance, that depends on the stiffness of the soil and wall displacement and the type of wall movement.

Two well-instrumented case histories of supported excavations in soft soil from the Constance area in southern Germany were analysed in chapter 8 with the finite element method in order to calibrate further the soil parameters for HSM. In both cases the actual construction sequence and day to day out put were simulated as much as possible. Both drained and consolidation analyses were performed. The consolidation analysis give the possibility of modelling the consolidation process right from the beginning of the excavation at day one.

After the first preliminary analysis of the project-I has shown no match of the computed and measured results, a number of parameter studies were conducted on a simplified model of this project along the section IV. A total of 20 different analyses were carried out. Based on the result of the parameter study and the final analysis of the project-I the following conclusions may be drawn:

- The interface behaviour has definitely an influence on the FE- analysis result of an excavation, but even value of R_{inter} as high as 1 did not help to reduce the deformations to the measured level. Moreover, the efficiency in reducing deformation in general is very minimum for values of $R_{inter} > 0.5$. On the other hand, defining a separate material set with the stiffness properties adopted one to one from the corresponding soil layer and reducing the shear parameters by a factor 1/3 may lead to a reasonable results. In certain cases a shear strength reduction factor between 0.333 and 0.5 may be used for numerical analysis of excavations in soft soils.

- Obviously, the groundwater situation will have a remarkable impact on the computation results. Hence a maximum effort and care should be taken in locating the groundwater table. The different water tables for different soil layers should also be considered in the analysis. The next important thing is the investigation of the pore pressure situation in the relatively impermeable lacustrine soil layer. Usually, the water table in the impermeable layer is interpolated between the water table of the layer beneath and above it. The author presumes that the actual water pressure in the impermeable layer might be less than that obtained from interpolation, because no free water was usually observed in such layers during excavation. A further investigation of the water pressure in such layers is highly recommended.

- Although the effect of the stiffness of the soil on the deformation behaviour of the excavation is obvious, the author believes that the shear and stiffness parameters of the soft soil layer obtained from laboratory in combination with due consideration of the other effects and construction details may lead to a reasonable prediction of the upper bound of the deformations. Hence, the importance of performing triaxial, oedometer and permeability tests in laboratory for the soft soil layers should be underlined. In the absence of laboratory test results, however, the soil parameters of the relatively bearing layer may be estimated from the field penetration results after adjusting them to fit to the selective soil model.

- The bottom concrete slab should be modelled by means of plates, not by a fixed end support, since the later might lead to a rigid system in contrary to the reality.

- As far as this particular excavation project is concerned, the plasticity property of the sheet pile wall may have no impact on the deformation behaviour of the excavation.

- It was proved that the displacement of the top of the wall and the surface settlement behind the wall suffers most from the 3D-effect. The 3D-effect is here defined as the effect of the excavation and placement of the bottom concrete slab in slices of 2.5 m width. As shown in Figure 8.5, the bottom concrete slab in the first slice had already provided support to the wall during the next slice excavation. Such effect can only be modelled using a 3D-FE-programm, however, a simplified assumption has to be made to consider this effect in the 2D-FE-computations. For example, the bottom slab may be assumed to be effective after 50% of the soil mass above it had been removed. This however, is purely a rough assumption but not unreal, hence an investigation of the 3D-effect using the 3D-FE-program would be worthwhile before this factor is going to be applied for practical projects.

- The constructional stages and procedures will have definitely an influence on the computational result of the excavation. Hence, it is highly recommended that the one who analyse the project with the FE-computer program should have a first hand information on the details of the excavation execution processes in order to reasonably predict the deformation behaviour of the excavation.

- A consolidation analysis is the best way of evaluating the performance of an excavation at any time t after begin of the construction works. It provides the advantage of considering the yet not fully dissipated negative pore pressure in the excavation. This is also proved by the foregoing computations, where a better match of the numerical results and the measured values has been observed.

The back analysis of the project-II also shows that the performance of the excavation can fairly be estimated by means of the finite element method and using the advanced constitutive soil models such as the Hardening Soil Model (HSM) without any major modification of the material

properties from laboratory and field penetration and sounding tests. It also shows that a better match with measured data may be achieved by performing a consolidation analysis.

The last chapter of this work deals with the examination of the draft recommendation for excavations in soft soils of the working group "Excavations" (EAB) of the German Society of the Geotechnical Engineers. Based on various numerical and analytical study, the author has accompanied the draft of the new recommendations (*EB90 - EB101, Weissenbach (2002)*) with close corporation with the members of the group. The result of the analysis, the development and back ground of the different load and reaction diagrams are presented and evaluated in chapter 9.

10.2   Zusammenfassung in deutscher Sprache

In der vorliegenden Arbeit werden die Ergebnisse der Untersuchungen zum Verhalten der Baugruben in weichen bindigen Böden beschrieben. Auf Grund des zunehmenden Bedarfs an neuen Hochhäusern, Parkplätzen und Verkehrswegen in den städtischen Bereichen, werden Baugruben häufig benötigt. Die Planung und Durchführung solcher temporärer, gestützter Baugruben erfordert die Kenntnis der zu erwartenden Verformungen und Bodenbewegungen in der Baugrube, die durch Aushubentlastung und Bebauung verursacht werden. Die gänzliche Vermeidung der Verformungen wird kaum möglich sein, jedoch sollte es möglich sein, die Größenordnung und die Verteilung der Verformungen zu prognostizieren, um das Schadenspotenzial einzuschätzen sowie notwendige und mögliche Maßnahmen zu treffen oder die Planung anzupassen, so dass die Verformungen begrenzt werden. Wegen der geringen Festigkeit und Steifigkeit normalkonsolidierter, weicher bindiger Böden sind Baugruben in diesen Bodenarten bewegungsempfindlicher, als in anderen Bodenarten. In Deutschland sind die geologisch jungen, nicht vorbelasteten weichen bindigen Böden vor allem an der Nordseeküste (Klei) und an den süddeutschen Binnengewässern (See- und Beckenton), z.B. am Bodensee, anzutreffen. So ist die oberflächennahe geologische Situation im Bereich der Stadt Konstanz durch das Würmglazial und durch nacheiszeitliche Sedimentation geprägt. Die Mächtigkeit der weichen Schichten beträgt teilweise über 20 m. Erfahrungen in Konstanz zeigen, dass Gründungen durch große Setzungen gefährdet sind, und die Herstellung von Baugruben beträchtliche Verformungen in der Umgebung hervorrufen können. Aus diesem Grund lag das Hauptmotiv dieser Arbeit, auf der Untersuchung des Verformungsverhalten von Baugruben in weichen bindigen Böden.

Um das Ziel der Arbeit zu erreichen, wurden drei Methoden angewandt - experimentelle, analytische und numerische Untersuchungen. Der Mittelpunkt des experimentellen Teils der Arbeit besteht aus der Ermittlung der Bodenkenngrößen, die zur Berechnung von Baugruben in weichen Böden relevant sind und die in der numerischen Analyse angewendete Stoffgesetze beschreiben. Analytische Methoden wurden eingesetzt, um die Berechnungsarten (dräniert bzw. undräniert)

von Baugruben zu evaluieren und den Zusammenhang zwischen effektiven und totalen Scherparametern zu erarbeiten, die Erddruck, Erdwiderstand, und Schnittgrößen im Zusammenhang mit numerischen Resultaten beschreiben. Als numerische Methode wurde die Finite-Elemente-Methode (FEM) verwendet, um den Einfluss der verschiedenen Bodenkenngrößen auf das Verhalten einer Baugrube und eine Bodenprobe unter dem triaxialen und eindimensionalen Spannungszustand anhand von Parameterstudien zu untersuchen. Weiterhin wurde die FEM zur numerischen Analyse und Rückrechnung von Bauprojekten eingesetzt.

In einem ersten Schritt der Arbeit wird ein "State of the Art" über die Planungs - und Konstruktionsregeln bei der Durchführung von Baugruben in weichen Böden dokumentiert und in Abschnitt 2 ausführlich zusammengestellt. Die Ursachen von Verformungen in einer Baugrube und ihrer Umgebung wurden zusammenfassend dargestellt und diskutiert. Die Verhältnisse zwischen den Setzungen an der Geländeoberkante (GOK) hinter der Wand und den Horizontalverformungen der Wand einerseits und der Aushubtiefe andererseits wurden dargestellt. Basierend auf Setzungsmessungen in der Literatur wurden Setzungsmulden festgestellt. Die Auswertung der Verformungen aus der Literatur zeigt, dass beachtenswerte Verformungen vor dem Beginn des Aushubs bereits während der Herstellung der Baugrubenwand und ebenfalls während des Rückbaus der Wand auftreten. Daraus kann geschlossen werden, dass Bodenverformungen möglicherweise nicht völlig verhindert werden können. Weiterhin wurde die Entwicklung des Sicherheitsfaktors in Baugrubenberechnungen und die unterschiedliche Weise der Anwendung in unterschiedlichen Länder verglichen und analysiert. Schließlich wurden die verschiedenen Faktoren, die das Verhalten von Baugruben beeinflussen (können) anhand von FEM-Parameterstudien aus der Literatur zusammengefasst. Es wurde festgestellt, dass erwartungsgemäß die Steifigkeit des Bodens der Schlüsselfaktor im Verformungsverhalten der Baugrube ist.

Mit einer umfangreichen Literaturstudie wurde in Abschnitt 3 der Kenntnisstand und die wesentlichen Einflussgrößen zum Stoffverhalten von weichen, bindigen Böden dargestellt. Neben der Beschreibung von Festigkeits- und Steifigkeitseigenschaften der weichen Böden, war es möglich, aus der Literatur eine Datenbank der empirischen Ansätze zur Abschätzung der Kompressions-, Festigkeits- und Steifigkeitskenngrößen aus den einfachen Charakterisierungsversuchen aufzubauen. Die Anwendung dieser empirischen Gleichungen zum Seeton/Beckenton in Süddeutschland wurden überprüft und verglichen.

Die Diskussion über dränierte und undränierte Analyse ist nicht neu in den Bodenmechanik. Der ungünstigste Fall für Baugruben in weichen Böden ist scheinbar der dränierte Fall, da der Aushub (Entlastung) Porenwasserunterdruck erzeugt, der zur Stabilität der Baugrube beiträgt. Bei temporär gestützten Baugruben ist jedoch zu beachten, dass die Zeit der Herstellung ggfs. nicht lang genug ist, um die Baugruben als dränierten Zustand oder nicht kurz genug, um sie als undränierte Zustand zu definieren. Der tatsächliche Zustand einer Baugrube in weichen Böden liegt zwischen

diesen beiden Extremfällen. Die wirkliche Situation kann nur mit Hilfe der Konsolidationstheorie beschrieben werden, aber nach Auffassung des Autors sind derzeit noch keine zutreffenden analytische Berechnungsansätze für Baugruben vorhanden, in denen dies berücksichtige wird. Unter der Annahme von undränierten Bedingungen, kann die Bestimmung der Einbindetiefe der Wand mit der c_u-Methode zu großen Interpretationsschwierigkeiten führen, siehe *Hettler et al. (2002).* Es gibt jedoch ein allgemeines Verständnis, dass effektive Spannungen das Verhalten des Bodens auch unter undränierten Bedingungen bestimmen. Auf dieser Grundlage wurden analytische Berechnungsansätze zur Bestimmung der aktiven und passiven Erddrücke im Anfangszustand anhand des effektiven Winkels der Gesamtscherfestigkeit φ_s' und des Porenwasserüberdruckbeiwerts A_f entwickelt. Das Vertrauen der Baupraxis zur Scherfestigkeit des undränierten Bodens beruht auf Erfahrungen und der Möglichkeit sie in-situ mittels Flügelsondierung zu ermitteln oder aus Korrelationen mit Druck- und Rammsondierung herzuleiten. Um sowohl die langjährigen und umfangreichen Erfahrungen der Praxis als auch die vorhandene Datenbank der undränierten Scherparameter c_u zu nutzen, wurden Gleichungen zur Abschätzung des Winkels der Gesamtscherfestigkeit φ_s' aus c_u mit Hilfe des Spannungspfads von undränierten Triaxialversuchen und der Kenntnis des Porenwasserüberdruckkoeffizienten beim Bruch A_f abgeleitet. Weiterhin wurden Gleichungen basierend auf diesen Zusammenhängen unter der Annahme, dass die effektive Scherfestigkeit in Kompression und Extension gleich bleibt, entwickelt, um die A_f-Werte für andere beliebige Spannungspfade aus dem $A_{f,s}$-Wert von undränierten Standardtriaxialversuchen abzuschätzen. Informationen über den $A_{f,s}$-Wert finden sich mehrfach in der Literatur und er kann im Labor aus Standardtriaxialversuchen ermittelt werden.

Verschiedene Stoffgesetze, ihre Vor- und Nachteile, wurden in Abschnitt 5 zusammenfassend dargestellt. Es erfolgt eine kurze Einführung in das Finite-Elemente-Programm „PLAXIS", das für die numerischen Parameterstudien und in der Analyse der praktischen Projekte verwendet wurde. Die grundlegenden Eigenschaften der Materialmodelle in diesem Programmcode, das Bruchkriterium, das den Modellen zugrunde liegt, die Definition der Fließfläche, der Spannungszustand, die Verfestigungs - und Fließregel, ihre Anwendungsmöglichkeiten und Grenzen, und die Stoffparameter, die zur Definition der Modelle benötigt werden, wurden tabellarisch dargestellt. Das Hardening Soil Model (HSM) wurde in dieser Arbeit als Grundstoffgesetz für die Simulation des Verhaltens von Baugruben in weichen Böden ausgewählt, weil dieses am besten den Grundvoraussetzung eines konstitutiven Modells zur Untersuchung vom Baugrubenverhalten gerecht wird.

Eine der Hauptanforderungen für die Verformungsprognose einer Baugrube ist eine Abschätzung der relevanten Bodenkenngrößen, die für die numerische Berechnungen benötigt werden. Außer den Daten, die aus den geotechnischen Gutachten der verschiedenen Projekte und der Literatur hervorgehen, wurden ungestörte und gestörte Seetonproben an drei Stellen in Konstanz (Bodensee) entnommen. Ein umfangreiches Laborversuchsprogramm wurde im Rahmen dieser

Forschungsarbeit durchgeführt. Dieses beinhaltete klassische isotrop konsolidierte ($\sigma'_h/\sigma'_v = K_0 = 1$) Triaxialversuche, anisotrop konsolidierte ($\sigma'_h/\sigma'_v = K_0 = 0,80$) Triaxialversuche, spannungsabhängige Triaxialversuche (oberhalb der K_0-Linie oder der isotropen Linie), und eindimensionale, isotrope und anisotrope Kompressionsversuche. Außerdem wurde das Kontaktverhalten zwischen Boden und Wand mit einem großen (365 x 550 mm), einem mittleren (100 x 100 mm) und einem kleinen (63 x 63 mm) Rahmenscherversuch untersucht. Obwohl die Auswertung und Analyse der Versuchsergebnisse allgemeingültig sind, wurden sie zielgerichtet zur Ermittlung der relevanten Stoffparameter für eine numerische Analyse von Baugruben mittels der Stoffmodelle, die in PLAXIS vorhanden sind, durchgeführt. Die Untersuchungsergebnisse fließen in Abschnitt 6 in eine Datenbank ein und werden nachfolgend kurz zusammengefasst:

- Oberhalb der isotropen Linie oder der K_0 - Linie existiert nur ein einzelner und einzigartiger effektiver Spannungspfad, unabhängig von der Art des Versuchs, der Richtung des totalen Spannungspfads und der Orientierung der Proben.

- Entgegen der Erwartungen sind die horizontal orientierten Proben steifer als die vertikal orientierten Proben. Weitere Untersuchungen sind zwingend notwendig.

- Die Steifigkeit des Bodens unter CAD und CAU Versuchsbedingungen ist durchschnittlich um einen Faktor von 4,4 bzw. 1,5 höher als die entsprechenden CID und CIU.

- Folgende durchschnittliche Verhältnisse zwischen den Steifigkeitsparametern wurden festgestellt: $E_i/E_{50} = 2,08$, $E_{ur}/E_i = 3,2$, $E_{ur}/E_{50} = 6,3$, $E_{oed,\ ur}/E_{oed} = 3,1$. Alle Werte sind auf eine Spannung von 100 kN/m² bezogen und schließen nicht die Werte von Probenentnahmestelle 3 ein, in dem sehr viel höhere Werte beobachtet wurden.

- Wie erwartet, wurde eine höhere Steifigkeit unter undränierten Bedingungen gemessen als unter dränierten Bedingungen. Dabei wurde durchschnittlich ein Faktor von 1,08 und 1,29 an Probenentnahmestelle 1 bzw. 2 festgestellt. Diese Faktoren liegen innerhalb der Werte aus der Elastizitätstheorie.

- Die ungestörten Proben unter dem geforderten Spannungspfad B scheinen steifer als unter dem Spannungspfad C in den CAU-Versuchen, wohingegen kein bemerkenswerter Unterschied bezüglich der Steifigkeit der aufbereiteten Proben unter den Spannungspfaden A, B und C in den CIU-Versuchen beobachtet wurde. Jedoch ist die Anzahl der durchgeführten Versuche nicht ausreichend, um eine allgemeine Beurteilung der Ergebnisse zu ermöglichen.

- Die meisten Versuchsergebnisse zeigen eine Abweichung vom linearen Verlauf der transformierten Auftragung der Spannungs - Dehnungslinien vor allem im Bereich kleiner axialer Stauchungen (ca. bis 5%). Einige Versuchsergebnisse weichen sogar komplett vom linearen Verlauf ab, was darauf hinweist, dass das Spannungs - Dehnungsdiagramm vor allem bei klei-

nen Konsolidierungsspannungen nicht genau hyperbolisch ist. Das Problem im Bereich kleiner Dehnungen kann mit der Unterteilung der Spannungs - Dehnungslinien in zwei Hyperbeln mit unterschiedlicher Steifigkeit gelöst werden, wie von *Amann et al. (1975)* vorgeschlagen wurde. Vor allem kann damit die im Anfangsbereich beobachtete größere Steifigkeit erfasst werden.

- Der Wandreibungswinkel ist eher weit entfernt von Null, als er normalerweise angenommen wird. Ein Wert von $\delta = 0{,}460 \cdot \varphi$ und eine Steifigkeit so groß wie die Bodensteifigkeit wurde für Boden/Beton- und Boden/Stahlplattenkontakt im großen Rahmenscherversuch gemessen. Wenn der Einfluss des Grundwassers im Feld berücksichtigt wird, erscheint die neue Empfehlung von EAB, EB 95(2002) $\delta = \varphi/3$ angemessen.

Im ersten Teil des Abschnitts 7 wurden die Bodenkenngrößen, die für Baugruben im weichen Boden relevant sind, mittels der FEM-Berechnungen und auf der Basis des Hardening Soil Models (HSM) kalibriert. Durch Sensitivitätsstudien wurde der Einfluss der Steifigkeits- und Festigkeitsparameter des HSM auf das Spannungs-Dehnungs-, das Volumenänderungs- und das Porenwasserüberdruckverhalten unter Triaxial- und Oedometerversuchsbedingungen untersucht. Die wichtigsten Ergebnissen der Parameterstudien sind unten zusammengefasst.

- Der dränierte Versuch kann durch die FEM mit einer geringfügigen Verbesserung der Parameter ziemlich genau simuliert werden. Wie erwartet, ist E_{50}^{ref} der Hauptparameter, der das Spannungs - Dehnungsverhalten einer Bodenprobe unter triaxialer Primärbelastung bestimmt, er hat aber einen unwesentlichen Einfluss auf den eindimensionalen Belastungszustand. Ebenso hat E_{oed}^{ref} keinen bedeutenden Einfluss auf triaxiale Primärbelastung, spielt aber die Hauptrolle im eindimensionalen Belastungszustand. E_{ur}^{ref} ist der einzige Parameter, der den Ent- und Wiederbelastungszustand unter triaxialer und oedometrischer Belastung beeinflusst. Entgegen der Erwartung hat ν_{ur} nur einen Effekt auf den eindimensionalen Ent- und Wiederbelastungszustand. Es scheint, dass K_0^{nc} als Modellparameter keinen bedeutenden Einfluss auf den Ent- und Wiederbelastungszustand in beiden Belastungssystemen hat.

- Die Verwendung des Winkels der Gesamtscherfestigkeit $\varphi_s^{'}$ in der FEM-Berechnung sollte mit Vorsicht verwendet werden, da er vom Spannungsniveau abhängig ist. Ein konstanter Wert für eine gesamte Schicht kann zu Über- bzw. Unterschätzung der Bodenfestigkeit führen.

- E_{oed}^{ref} und K_0^{nc} Werte sind die Haupteinflussfaktoren zur Festlegung des Volumenänderungsverhaltens einer Bodenprobe unter triaxialer Belastung, alle anderen Parameter mit Ausnahme R_f sind von untergeordneter Bedeutung. Dieses und das o.g. Brechnungsergebnis bestätigen die unterschiedliche Funktion von E_{oed}^{ref} und E_{50}^{ref}. E_{oed}^{ref} ist ein Kappenparameter, der die Kompressionsverfestigung (Kappe) zur Erfassung irreversibler Zusammendrückung unter Erstbelastung steuert, und E_{50}^{ref} ist ein Parameter zur Beschreibung der Reibungsverfestigung.

- Es scheint, dass das triaxiale undränierte Spannungs - Dehnungsverhalten unter der Primärbelastung durch verschiedene Parameter beeinflusst werden kann. Neben E_{50}^{ref} haben die Parameter E_{ur}^{ref} und K_0^{nc} einen bedeutenden Einfluss auf das Spannungs - Dehnungsverhalten. Die anderen Parameter, wie z.B. E_{oed}^{ref}, ν_{ur} und R_f, leisten auch ihren Beitrag, aber in geringerem Ausmaß. Die Simulation von undränierten Triaxialversuchen mit der FEM ergab keine gute Übereinstimmung mit den Laborversuchsergebnissen. Ursachen liegen in der Schwierigkeit der Simulation des abfallenden Porenwasserüberdrucks einerseits und der Zunahme der Deviatorspannung andererseits. Alle Parameter beeinflussen die Entwicklung des Porenwasserüberdrucks, der Effekt von K_0^{nc} ist besonderes bemerkenswert.

- Nach *Janbu (1977)* beeinflusst die effektive Kohäsion den K_0^{nc} - Wert. Dieser Effekt wurde mittels einer FEM-Parameterstudie eines eindimensionalen Testmodells untersucht, indem c' und φ' abwechselnd variiert wurden. Aus den FEM-Berechnungen ergibt sich die allgemeine Tendenz eines zunehmenden K_0^{nc} - Wertes mit zunehmender Kohäsion c´ für alle Werte von φ'. Demzufolge wurde eine empirische Gleichung zur Abschätzung des Einflusses der Kohäsion c´ entwickelt.

- Der Spannungszustand beim Bruch in triaxialen dränierten FE-Berchnungen wird vollständig durch die effektiven Scherparameter beschrieben. Durch die anderen Parameter wurde nur die axiale Bruchdehnung erhöht oder verzögert. Im Fall von undränieten Analysen kann neben den Scherparametern das Volumenänderungsverhalten des Bodens die deviatorische Spannung beim Versagen beeinflussen.

- Es gibt einen eindeutigen effektiven Spannungspfad für alle totalen Spannungspfade in der Kompressions- (Pfade A, B und C) bzw. in Extensionszone (Pfade D, E und F). Dadurch werden die Versuchsergebnisse in Abschnitt 6 bestätigt. Wiederum ergibt sich bei Kompression und in Extension eine eindeutige deviatorische Spannung im Bruch. Das unterschiedliche Verhalten ist nur auf die Entwicklung des Porenwasserdrucks zurückzuführen, der sich für unterschiedliche Spannungspfade erheblich unterscheidet. Die deviatorischen Spannungen beim Versagen bei Kompression bzw. Extension unterscheiden sich ebenfalls, was verschiedene undränierte Scherfestigkeiten c_u und Winkel der Gesamtscherfestigkeit φ_s zur Folge hat. Die Verhältniswerte sind 1,38 und 0,90 für den isotropen bzw. 1,31 und 0,89 für K_0-konsolidierten Anfangszustand. Ein Vergleich der beiden Anfangszustände zeigt, dass die K_0-konsolidierten Proben stärker reagieren als die isotropen konsolidierten Proben. Die deviatorische Bruchspannung ist bei K_0-Konsolidation um einen Faktor von ca. 1,4 höher als bei isotroper Konsolidation.

Im zweiten Teil des Abschnitts 7 wurden Parameterstudien zur Geometrie des FE-Berechnungsabschnittes und zu den Bodenparametern des HSM mittels einer idealisierten Bau-

grube durchgeführt, um den Einfluss dieser Parameter auf das Verhalten von Baugruben zu untersuchen. Die Ergebnisse der Parameterstudien sind wie folgt zusammengefasst.

- Die Größe des Berechnungsabschnittes hat keinen wesentlichen Einfluss auf die horizontalen Wandverformungen, jedoch nimmt die Wandverformung mit der Breite der Baugrube zu. Der Hauptfaktor, der die Hebung an der Baugrubensohle (BGS) und die Setzung an der GOK hinter der Wand beeinflussen kann, ist die Höhe des Berechnungsabschnittes, nicht die Breite. Die Hebung an der BGS nimmt mit der Breite der Baugrube zu, wohingegen die Setzung an der GOK abnimmt.

- Der E_{50}-Wert scheint die Wandverformung, die aktiven und passiven Erddrücke, die Schnittgrößen und die Setzung hinter der Wand am stärksten zu beeinflussen. Wegen der Nichtlinearität bringt jedoch die Erhöhung von E_{50} nicht unbedingt den gleichen Effekt wie die Abminderung des Wertes. Der Einfluss von E_{50} auf die Hebung der BGS wird auf den Bereich direkt neben der Wand begrenzt; in Baugrubenmitte ist er unwesentlich. E_{ur} dominiert die Hebung an der BGS und die Wandverschiebung am Fuß, hat aber nur einen geringfügigen Einfluss auf der Schnittgrößen. Die v_{ur} hat nur einen Effekt auf die Hebung der BGS und die Setzung an der GOK hinter der Wand. R_f hat einen unwesentlichen Effekt in allen Fällen.

- Das Stoffgesetz HSM unterscheidet zwischen K_0^{nc} und K_0. Während K_0^{nc} ein Stoffparameter ist, der nicht beliebig verändert werden soll und der eng mit den Steifigkeitsparametern E_{50}, E_{ur}, E_{oed} und v_{ur} zusammenhängt, wird K_0 lediglich verwendet, um den Ausgangsspannungszustand zu definieren. Für normalkonsolidierte bindigen Böden sind jedoch diese Parameter mehr oder weniger dieselben. Für den gegebenen Fall liegen der minimale und der maximale mögliche K_0^{nc}-Wert zwischen 0,437 und 0,71. Der K_0^{nc}-Wert kann die Verformungen, die Schnittgrößen und die Erddrücke beeinflussen, jedoch ist sein Einfluss hier im Vergleich mit seinem Einfluss auf den triaxialen Spannungszustand (Abschnitt 7, Teil I) gemäßigt. Wenn K_0^{nc} in Richtung zur unteren Grenze variiert werden soll, ist er empfindlicher, als zur oberen Grenze, obgleich der Unterschied zwischen dem Referenzwert und den extremen Werten fast derselbe ist.

- Entgegen der Erwartungen verursacht eine Abminderung des Bezugswertes E_{oed} um 50% eine Abnahme der Wand- und Bodenverformungen, der aktiven und passiven Erddrücke und der Schnittgrößen um ca. 17 bis 30% anstatt einer Zunahme dieser Werte. Eine verringerte Wandverschiebung würde einen erhöhten aktiven Erddruck und einen verringerten passiven Erddruck ergeben. Erhöhung des Bezugswertes um den gleichen Betrag (50%) zeigt keinen bedeutenden Einfluss. In allen Fällen ist E_{oed} sensibler gegenüber Änderung des Referenzwertes nach unten als nach oben. Möglicherweise ist das Verhältnis E_{50} / E_{oed} einflussreicher als der Absolutwert von E_{oed}. Für den gegebenen Fall ist dieses Verhältnis 1,1. Wenn E_{oed} um 50% erhöht bzw. verringert wird, ändert sich das Verhältnis auf 0,73 bzw. 2,20. Das Verhältnis im

Falle einer Erhöhung von E_{oed} ist näher am Bezugsverhältnis als bei einer Verringerung. Dies könnte der Grund sein, warum die Änderung von E_{oed} nach unten bezogen auf den Refernzwert sensibler ist als eine Änderung nach unten.

- Alle o. g. Beobachtungen gelten für den dränierten Fall, wobei für den undränierten Fall eine ähnliche Tendenz gegeben ist mit Ausnahme von K_0. K_0 ist sensibler gegenüber einer Änderung des Referenzwerts nach unten als nach oben. Es scheint, dass E_{ur} die dominierende Rolle spielt. Z.B. ist die Setzung an der GOK im Fall des dränierten Zustandes hauptsächlich von E_{50} beeinflusst. E_{ur} ist demgegenüber der maßgebliche Parameter im undränierten Fall. Im Gegensatz zum dränierten Fall zeigt der Parameter ν_{ur} nur einen unwesentlichen Effekt auf die Hebung an der BGS und Setzung an der GOK. Die widersprüchliche Beobachtung und die Erklärung des Einflusses von E_{oed} bleibt die Gleiche wie im dränierten Fall.

- Ähnlich zum triaxialen Spannungszustand reagiert der Porenwasserdruck bei Baugruben sensibel auf die Änderung von K_0 und E_{ur}. Der Einfluss dieser zwei Parameter auf den Porenwasserdruck ist direkt unter dem Wandfuß deutlich bemerkbar.

- Einige der totalen Spannungspfade aus den Parameterstudien sind mit den idealisierten Spannungspfaden, die im Abschnitt 3, 4 und 6 dargestellt und diskutiert wurden vergleichbar. Einige von ihnen folgen jedoch unterschiedlichen Richtungen während des Aushubs und es ist schwierig, sie einem bestimmten idealisierten Spannungspfad zuzuordnen.

- Wenn ca. 50% des Bodenkörpers intakt als Bermenunterstützung der Baugrubenwand belassen wird und der Aushub von der Mitte in Richtung zur Wand fortfährt, kann ca. 20 bis 50% Reduktion der entsprechenden Verformungen und Verschiebungen an den unterschiedlichen Positionen erzielt werden. Wenn der Aushub jedoch in die entgegengesetzte Richtung fortfährt, wird eine Reduktion der Wandverformung von 10 bis 40% erreicht.

- Die Sohlaussteifung hat den Effekt, die Wandkopfverschiebung in Richtung zum Boden zu verhindern und sie hat einen unwesentlichen Effekt auf die Hebung der BGS, unabhängig vom Zeitpunkt der Sohlplatteninstallation. Jedoch wurde eine Reduktion von ca. 37 bis 97%, 37 bis 92% bzw. 24 bis 36% der Setzung an GOK, der Wandverschiebung am Fuß und an der BGS für den gegebenen Fall erzielt, wenn die Sohlaussteifung vor der 1., 2. bzw. 3. Aushubphase angebracht wurde. Es scheint, dass die Installation der Sohlaussteiffung vor der 1. Aushubphase keinen wesentlichen Einfluss bewirkt, d.h. eine vergleichbare Effizienz könnte erzielt werden, indem die Sohlaussteifung nach der 1. aber vor der 2. Aushubphase angebracht wird.

- Die Annahme dränierte Analyse = undränierte Analyse + Konsolidation scheint nur im Fall der Hebung an der BGS zulässig. Für die Wandfußverschiebung scheint die Konsolidationsphase von untergeordnetem Einfluss. An anderen Positionen, wie z.B. Wandverschiebung

am Kopf und an der BGS sowie die Setzung an der GOK ergibt die undränierte Analyse + Konsolidation größere Deformationen als die dränierte Analyse. Da die Spannungspfade während der dränierten Analyse und der undränierten Analyse + Konsolidation sich von den theoretischen Spannungspfaden wesentlich unterscheiden, ist die Annahme dränierte Analyse = undränierte Analyse + Konsolidation in der Regel nicht zutreffend.

Am Ende des Abschnitts 7 wurde eine Parameterstudie zur Mobilisierung des Erdwiderstandes in Abhängigkeit von der Steifigkeit des Bodens, der Wandbewegungsart und der Wandverschiebung mittels der FEM durchgeführt. Es wurde eine analytische Funktion zur Abschätzung des Erdwiderstands auf der Grundlage von Hyperbelfunktionen entwickelt. Ergänzend wurde eine Gleichung für die Abschätzung des Globalsicherheitsfaktors für den Erdwiderstand abgeleitet.

Im Abschnitt 8 wurden zwei praktische Projekte von gestützten Baugruben in weichen bindigen Böden aus dem Raum Konstanz (Bodensee) mittels der FEM und auf der Grundlage aller bisher durchgeführten Untersuchungen analysiert, um die Stoffparameter des HSM weiter zu kalibrieren. Die tatsächlichen Konstruktionsphasen auf der Grundlage von Tagesleistungen wurden möglichst genau abgebildet. In den numerischen Berechnungen wurden dränierte Berechnungen und Konsolidationsberechnungen angewendet. Die Konsolidationsberechnung gibt die Möglichkeit, den Aufbau und den Abbau des Porenwasserüber- und unterdruckes von Anfang des Aushubs am ersten Tag zu simulieren.

Nachdem die erste Vorberechnung des Projektes-I keine Übereinstimmung zwischen den berechneten und gemessenen Werten gezeigt hatte, wurden Parameterstudien eines vereinfachten Berechnungsausschnitts des Projektes-I entlang des Abschnitts IV ausgeführt. Insgesamt wurden 20 unterschiedliche Berechnungen und Variationen durchgeführt. Basierend auf den Ergebnissen der Parameterstudie und der abschließenden Analyse des Projektes-I können die folgenden Zusammenfassungen abgeleitet werden:

- Das Kontaktverhalten zwischen der Wand und dem Boden hat definitiv einen Einfluss auf das Berechnungsergebnis einer Baugrube. $R_{inter} = 1$ ist in diesem Fall keine zutreffende Annahme, um die Deformationen auf das gemessene Niveau zu bringen. Außerdem ist der Effekt des Parameters $R_{inter} > 0,5$ auf die Deformationen im allgemeinen minimal. Ein separater Materialsatz für das Kontaktelement mit der Steifigkeit gleich die Steifigkeit der entsprechenden Bodenschicht, aber mit reduzierten Festigkeitsparametern um den Faktor 1/3, führt zu zutreffenderen Ergebnissen. In bestimmten Fällen kann ein Festigkeitsfaktor zwischen 0,333 und 0,5 und ein Steifigkeitsfaktor von 1 für numerische Berechnungen einer Baugrube im weichen bindigen Boden verwendet werden.

- Offensichtlich hat der Grundwasserstand eine merkbare Auswirkung auf die numerischen Berechnungsergebnisse. Deshalb soll die Festlegung des Grundwasserspiegels wirklichkeitsnah

gewählt werden. Außerdem soll die unterschiedliche Grundwassersituation für unterschiedliche Bodenschichten in der Berechnung betrachtet werden. Wichtig ist die Untersuchung der Porenwasserdrucksituation in relativ undurchlässigen Seeton/Beckentonschichten. Normalerweise wird der Porenwasserdruck in der undurchlässigen Schicht zwischen dem Grundwasserspiegel unterhalb und oberhalb der Schicht interpoliert. Es ist zu vermuten, dass der tatsächliche Porenwasserdruck in der undurchlässigen Schicht kleiner ist als der durch die Interpolation erreichte, da während des Aushubs normalerweise kein freies Wasser in solchen Schichten beobachtet wurde. Es wird empfohlen, die Grundwassersituation in solchen Schichten genauer zu untersuchen.

- Obwohl der Effekt der Steifigkeit des Bodens auf das Verformungsverhalten der Baugrube offensichtlich ist, glaubt der Autor, dass die im Labor ermittelten Scher- und Steifigkeitsparameter der weichen Bodenschicht, in Verbindung mit Faktoren wie z.B. Herstellungsdetails, zu einer zutreffenden Prognose des oberen Grenzwertes der Verformungen führt. Deshalb wird die Wichtigkeit einer sorgfältigen Durchführung von Triaxial-, Oedometer- und Durchlässigkeitsversuchen im Labor für die weichen Bodenschichten unterstrichen. Sind keine Laborergebnisse verfügbar, können die Bodenparameter der tragfähigen Schicht aus den Felduntersuchungsergebnissen abgeschätzt werden, sollten aber erst dem entsprechenden Stoffgesetz angepasst werden.

- Die Sohlplatte sollte als Balkenelement anstatt einer festgelegten Steife modelliert werden, da die feste Steife ein zu steifes System im Gegensatz zur Wirklichkeit darstellen kann.

- Bezogen auf dieses bestimmte Baugrubenprojekt hat die plastische Eigenschaft der Spundwand keine Auswirkung auf das Verformungsverhalten der Baugrube.

- Es wurde nachgewiesen, dass die Wandverformung am Kopf und die Setzung an der GOK hinter der Wand am meisten unter dem 3D-Effekt leidet. Der 3D-Effekt wird hier als der Effekt des Aushubs in Lamellen von 2,5 m Breite und die gleichzeitige Installation der Sohlplatte definiert. Wie in Abbildung 8.5 zu sehen ist, leistet die Betonplatte in der ersten Lamelle bereits Unterstützung der Wand während des Aushubs der nächsten Lamellen. Ein solcher Effekt kann nur mit einem 3D-FE-Programm erfasst werden, jedoch muss eine vereinfachte Annahme getroffen werden, um diesen Effekt in 2D-FE-Berechnungen zu berücksichtigen. Zum Beispiel kann angenommen werden, dass die Wirkung der Betonplatte bereits eintritt, nachdem 50% der Bodenmasse über ihr ausgehoben wird. Dieses ist jedoch lediglich eine grobe aber realistische Annahme. Deshalb lohnt es sich, eine Untersuchung des 3D-Effektes mittels eines 3D-FE-Programmes durchzuführen, bevor dieser Faktor zur Berechnung praktischer Projekte verwendet wird.

- Die Abfolge der Bauphasen und die Bauverfahren haben definitiv einen erheblichen Einfluss auf das Berechnungsergebnis einer Baugrube. Deshalb wird empfohlen, dass vor der Projektanalyse mittels FEM detaillierte Informationen über den Aushubverlauf vorliegen, um das Verformungsverhalten einer Baugrube zutreffend zu prognostizieren.

- Eine Konsolidationsberechnung mit der FEM ist die beste Methode zur Untersuchung des Verformungsverhaltens von Baugruben zu beliebigen Zeiten t nach Beginn der Aushubarbeiten. Es bietet den Vorteil, dass der vorhandene Porenwasserüber- oder unterdruck nach der Aushubzeit t in die Berechnung einfließt. Dieses wurde durch die FE-Berechnung des praktischen Projekts-I nachgewiesen, wobei eine bessere Übereinstimmung zwischen den gerechneten und gemessenen Werten erzielt wurde als bei den dränierten Berechnungen.

Die Berechnungsergebnisse des Projektes-II zeigen auch, dass das Verformungsverhalten von Baugruben mittels der FEM unter Verwendung eines höher entwickelten Stoffgesetzes, z.B. des Hardening Soil Models (HSM) ohne wesentliche Korrektur der Materialeigenschaften aus Labor- und Felduntersuchungen zutreffend abgeschätzt werden kann. Es ist hier auch zu sehen, dass die Konsolidationsberechnungen zu einer besseren Übereinstimmung mit den gemessen Daten führt, sofern die Informationen über den Bauablauf zur Verfügung stehen.

Parallel zur Bearbeitung des Themas dieser Arbeit wurde vom Arbeitskreis „Baugruben" (EAB) der Deutschen Gesellschaft für Geotechnik (DGGT) die bekannten Empfehlungen *EAB (1994)* für Baugruben in weichen Böden erweitert. Die dabei erarbeiteten Entwürfe der Empfehlungen (*EB 90 bis EB 101, Weissenbach (2002)*) wurden vom Verfasser in enger Zusammenarbeit mit Mitgliedern des EAB-Ausschusses inhaltlich durch umfangreiche Parameterstudien und Vergleichsberechnungen für die in den Entwürfen der EAB erarbeiteten analytischen Berechnungsempfehlungen begleitet und überprüft. Die Berechnungsergebnisse, die Entwicklung und der Hintergrund der unterschiedlichen Belastungs- und Reaktionsdiagramme sind im Abschnitt 9 zusammengestellt und ausgewertet.

11 References

Alphan, I. (1967): The empirical evaluation of the coefficient K_0 and K_{0r}. Soils and foundations; 7: 31-40.

Amann, P / Breth, H. / Stroh, D. (1975): Verformungsverhalten des Baugrundes beim Baugrubenaushub und anschließendem Hochhausbau am Beispiel des Frankfurter Tons; Technische Hochschule Darmstadt, Heft 15.

Ari, K. / Jinki, R. (1990): A Lower - Bound approach to active and passive earth pressure problems; Soils and Foundations, 30, 4, 25 - 41 (quoted from Pradel (1994)).

Atkinson, J.H. / Bransby, P.L. (1978): The mechanics of soils - an introduction to critical state soil mechanics; McGraw - Hill, London. AVL

Atkinson, J.H. / Richardson, D. / Robinson, P.J. (1987): Compression and extension of K_0 normally consolidated kaolin clay; ASCE, Journal of Geotechnical Engineering Division, Vol. 113 No. 12, pp. 1468 - 1482.

Bang, S. (1985): Active earth pressure behind retaining wall; ASCE, Journal of Geotechnical Engineering Division, pp. 407 - 412 (quoted from Pradel (1994)).

Bell, F.G. (1993): Engineering treatment of soils; Spon, London.

Berner, U. (1997): Ausführung einer Spundwandbaugrube im Konstanzer Beckenton; 3. Stuttgarter Geotechnik-Symposium, Baugruben in Locker- und Festgestein, pp. 227-239.

Besler, D. (1998): Wirklichkeitsnahe Erfassung der Fussauflagerung und des Verformungsverhaltens von geschützten Baugrubenwänden; Schriftenreihe des Lehrstuhls Baugrund-Grundbau der Universitaet Dortmund, Heft 22.

Bica, A.V.D. / Clayton, C.R.I. (1998): An experimental study of the behaviour of the embedded length of cantilever walls; Geotechnique 48; No. 6, 731 - 745.

Bjerrum, L. / Eide, O. (1956): Stability of strutted excavation in clay; Geotechnique, Vol. 6, No. 1, pp. 32 - 47.

Bjerrum, L. / Simons, N.E. (1960): Comparison of shear strength characteristics of normally consolidated clays; Proc. of ASCE Conference on Shear Strength of Cohesive Soils, Boulde, Co.

Bjerrum, L. (1961): The effective shear strength parameters of sensitive clays; Proc. V ICSMFE, Paris, Vol. 1, pp. 23 - 28.

Bjerrum, L. / Clausen, C.-J. F. /Duncan, J.M (1972): Earth pressures on flexible structures, A State-of-the-Art-Report; Proc. of the 5th European Conference. on Soil Mechanics and Foundations Engineering, Madrid, Vol 2, pp. 169 - 196.

Bjerrum, L. (1973): Problems of soil mechanics and construction on soft clay soils and structurally unstable soils (collapsible, expansive and others); Proceeding of the VII ICSMFE, Moscow, vol. 3, pp. 110 - 155.

Bishop, A.W. (1958): Test requirements for measuring the coefficient of earth pressure at rest; Brussels Earth Pressure Conference.

Bishop, A.W. / Henkel, D.J. (1962): The measurements of soil properties in the triaxial test; Edward Arnold, London, 2nd ed.

Bishop, A.W. (1966): Strength of soils as engineering materials; 6th Rankine Lecture, Geotechnique, Vol. 16, No. 2, pp. 89 - 130.

Bolten, M.D. / Powrie, W. / Symons, I.F. (1990a): The design of stiff in-situ walls retaining overconsolidated clay: Part I, Short term behaviour; Ground Engineering, 23, No. 1, pp. 34 - 40.

Bolten, M.D. / Powrie, W. / Symons, I.F. (1990b): The design of stiff in-situ walls retaining overconsolidated clay: Part I, long term behaviour; Ground Engineering, 23, No. 2, pp. 22 - 28.

Boone, J.S. (1996): Ground - Movement-Related Building Damage; Journal of Geotechnical Engineering, Vol. 122, No. 11, pp. 886 - 895.

Bowles, J.E. (1984); Physical and geotechnical properties of soils; McGraw Hill Co. Inc., New York.

Brinch Hansen, J. (1953): Earth pressure calculations; Danish Technical Press, Copenhagen (quoted from Pradel (1994)).

Brinkgreve R.B.J. / Vermeer P.A. (1992): On the use of cam-clay models; Proc. IV Int. Symposium on Numerical Models in Geomechanics (eds. G.N. Pande, S. Pietruszczak). Balkema, Rotterdam, vol.2, pp. 557 - 565.

Brinkgreve R.B.J. / Vermeer P.A. (1998): Hand book of the finite element code for soil and rock analysis "PLAXIS" Balkema Publisher.

Brinkgreve R.B.J. (2002): Hand book of the finite element code for soil and rock analysis "PLAXIS" Balkema Publisher, Rotterdam.

Britto, A:M / Gunn, M.J.(1987): Critical state soil mechanics via finite elements; John Wiley & Sons, New York, 1987.

Brooks, N.J. / Spence, J. (1993): Design and recorded performance of a secant retaining wall in Croydon; Retaining Structures, Thomas Telford, London, pp. 205 - 215.

Burland, J.B. (1967): Deformation of soft clay; Ph.D. Thesis, Cambridge University.

Burland, J.B. / Hancock, R.J.R. (1977): Underground car park at the house of commons, London: geotechnical aspects; The Structural Engineer, No. 2, Vol. 55, pp. 87 - 100.

Burland, J.B. / Simpson, B. / St John, H.D. (1979): Movements around excavations in London clay; Design Parameters in Geotechnical Engineering, BGS, London, Vol. 1.

Burland, J.B. / Potts, D.M. / Walsh, N.M. (1981): The overall stability of free and propped cantilever retaining wall; Ground Engineering, London, pp. 28 - 38.

Burland, J.B. (1990): On the compressibility and shear strength of natural clays; Geotechnique 40, No. 3, pp. 329 - 378.

Campanella, R.G. / Vaid, Y.P. (1973): Influence of stress path on the plane strain behaviour of sensitive clay; Proceeding of 8th ICSMFE; Moscow, Vol. 1.1, pp. 85 - 92.

Casagrande, (1932): Research on the Atterberg limits of soils; Public Roads.

Chen, W.F. (1975): Limit analysis and soil plasticity; Elasevier.

Chen, W.F. / MaCarron, W.O. (1986): Plasticity modelling and its application to geomechanics; Proceedings of the International Symposium on Recent Developments in Laboratory and Field Testing and Analysis of Geotechnical Problems - Bangkok, edited by Balasubramaniam et al., A.A. Balkema, pp 467 - 510.

Chen, W.F. / Mizuno, E. (1990): Non-linear Analysis in Soil Mechanics; Elsevier, Amesterdam.

CIRA (1974): A comparison of quay wall design methods; Report No. 54, Constructional Industry Research and Information Association, London.

Clayton, C:R:I / Milititsky, J. / Woods, R.I (1993): Earth pressure and earth retaining structures; 2nd ed., Chapman & Hall, London.

Clough, G.W. / Duncan, J.M. (1971): Finite element analysis of retaining wall behaviour; Journal of Soil Mechanics and Foundation Engineering., ASCE Vol. 97, SM12, pp. 657 - 673.

Clough, G.W. / Denby, G.M. (1977): Stabilising wall design for temporary walls in clay; ASCE, Journal of Geotechnical Engineering Division, Vol. 103, GT2, pp. 75 - 90.

Clough, G.W. / Duncan, J.M. (1991): Earth pressures; Foundation Engineering Handbook, edited by H.-Y. Fang, 2nd ed., Chapman & Hall, pp. 223 - 235.

Clough, G.W. / Tsui, Y (1974): Performance of tied - back walls in clay; Journal of Geotechnical Division, ASCE, Vol. 100 GT12, pp. 1259 - 1273.

Clough, G.W. / Mana, A.I. (1976): Lessens learned in F.E. analysis of temporary excavation in soft clay; Proceeding of the 2nd International Conference on Numerical Methods in Geomechanics, Blacksburg, Va., pp. 496 - 510.

Clough, R.W. / Woodward, R.J. (1967): Analysis of embankment stresses and deformations; Journal of the Soil Mechanics and Foundation Division, ASCE, Vol. 93, SM4, pp 529 - 549.

Clough, G.W. / Schmidt, B. (1977): Design and performance of excavations and tunnels in soft clays; a State-of the-Art Report, International Symposium on Soft Clay, Bankok, Thialand.

Clough, G.W. / Smith, E.M. / Sweeney, B.P. (1989): Movement control of excavation support by system by iterative design; Foundation engineering - Current Principles and Practices, ed. Kulhawy, F.H., ASCE, New York, Vol. 2, pp. 869 - 884.

Clough, G.W. / O'Rourke, T.D. (1990): Construction induced movements of in-situ walls; Design and Performance of Earth Retaining Structures, Geotechnical special publication 25, ASCE, New York, pp. 439 - 470.

Coulomb, C.A. (1773): Essai sur une Application des Regles de Maximis et Minimis á quelques Problémes de Statique relatifs á l'Architecture; Memoires de Math. Et Physique; Imprimerie Royale, Paris, Vol. 7, pp. 343 - 482.

Das, B.M. (1987): Theoretical Foundation Engineering; Elsevier, The Netherlands.

Day, P.W. (1994): Factors influencing the movement of retaining structures; Proc. of the XIII ICSMFE, New Delhi, India, Vol. 5, pp. 109 - 114.

DeLory, F.A. / Lai, H.W. (1971): Variation in undrained shearing strength by semiconfined tests; Canadian Geotechnical Journal, 8, pp. 538 - 545.

DIN 1054 (2003): Sicherheitsnachweise im Erd- und Grundbau.

DIN 18 137 (1990): Bestimmung der Scherfestigkeit.

Drucker, D.C. / Gibson, E.E. / Henkel, D.J. (1957): Soil mechanics and work hardening theories of plasticity; Trans., ASCE, 122, pp. 338 - 346.

Drucker, D.C. (1964): Concepts of path independence and material stability for soils; Brown University , May 1964.

Dubrovsky, M.P. / Poizner, M.B. / Yakovlev, P.I. / Taran, V.M. / Omelchenko, Yu.M. / Bibichkov, A.G. / Shtoda, A.N. (1997): Determination of soil lateral pressure loads on retaining wall taking into consideration its displacements and deformation; Proc. Of 14th ICSMFE, Hamburg, pp. 795 - 798.

Duncan, J.M. / Seed, H.B. (1966): Anisotropy and stress reorientation in clay; Journal of Soil Mechanics and Foundation Division, ASCE, Vol. 92, No. SM5, pp. 21 - 50.

Duncan, J.M. / Chang, C.Y. (1970): Non-linear analysis of stress and strain in soils; Journal of the Soil Mechanics and Foundation Division, ASCE, Vol. 96, SM5, pp. 1629 - 1653.

Duncan, J.M. / Bentler, D.J. (1998): Evolution of deep excavation technology; International Conference on Soil-Structure Interaction in Urban Civil Engineering, Darmstadt Geotechnics, Darmstadt, pp. 139 - 150.

EAB (1994): Empfehlungen des Arbeitskreis „Baugruben" der Deutschen Gesellschaft für Geotechnik; 3. Auflage, Ernst & Sohn, Berlin.

Eden, W.J. / Law, K.T. (1980): Comparison of undrained shear strength results obtained by different test methods in soft clays; Canadian Geotechnical Journal, 17, pp. 369 - 381.

Evigin / Eisenstein (1985): Performance of an elstoplalstic model; Canadian Geotechnucal Journal, 22, pp. 177 - 185.

Fang, H.-Y. (1991): Foundation Engineering Handbook; 2nd ed., Chapman & Hall, New York.

Freiseder, M.G. (1998): Ein Beitrag zur numerischen Berechnungen von tiefen Baugruben in weichen Böden, Gruppe Geotechnik Graz, Institute für Bodenmechanik und Grundbau, Heft 3.

Fujita, K. (1994): Soft ground tunnelling and buried structures; Proc. of the XIII ICSMFE, New Delhi, India, pp. 89 - 107.

GCO (1982): Guide to retaining wall design; Geoguide 1, Geotechnical control Office, Engineering Development Department, Hong Kong.

Gourvenec, S.M. / Powrie, W. (1999): Three - dimensional finite element analysis of diaphragm wall installation; Geotechnique 49, No. 6, pp. 801 - 823.

Graham, J. / Noonan, M.L. / Lew, K.V. (1983): Yield states and stress strain relationships in natural plastic clay; Canadian Geotechnical Journal, 20, pp. 502 - 516.

Gudehus, G. / Meißner, H. / Orth, W. / Schwarz, W. (1987): Geotechnische Probleme bei der Gründung des Postamtes Konstanz; Geotechnik, 3, pp. 105 - 122.

Gudehus, G. (1981): Bodenmechanik; Ferdinand Enke Verlag, Stuttgart.

Gudehus, G. (1985): Requirement to constitutive relations for soils; Mechanics of Geomaterials, edited by Z. Bazant, John Wiley & Sons Ltd., pp 47 - 64.

Gunn, M.J. / A. / Clayton, C.R.I. (1992): Installation effects and their importance in the design of earth-retaining structures; Geotechnique 42, No. 1, pp. 137 - 141.

Gunn, M.J. / Satkunananthan, A. / Clayton, C.R.I. (1993): Finite element modelling of installation effects; Retaining Structures, Thomas Telford, London, pp. 46 - 55.

Hansbo, S. (1957): A new approach to the determination of the shear strength of clay by the fall - cone test; Royal Swedish Geotechnical Institute, Proceeding No. 4.

Hayashi, S. / Yamanouchi, T. (1986): Plasticity modelling and its application to geomechanics; Proceedings of the International Symposium on Recent Developments in Laboratory and Field Testing and Analysis of Geotechnical Problems - Bangkok, edited by Balasubramaniam et al., A.A. Balkema, pp 435 - 450.

Head, K.H. (1986): Manual of Soil Laboratory Testing; ELE International Limited, Pentech Press, London.

Heil, H.M. / Huder, J. / Amann, P. (1997): Determination of shear strength of soft lacustrine clays; Proc. of the XIV ICSMFE, Vol. 1, pp. 507 - 510.

Henkel, D.J. (1971): The relevance of laboratory measured parameters in field studies; Proceedindgs of Rosco Memorial Symposium, Foulis, pp. 669 - 675.

Herrero, O. (1983): Universal compression index equation; ASCE, Journal of Geotechnical Division, Vol. 109, GT 10, pp 1349.

Hettler, A. / Leibnitz, S. / Biehel, F. (2002): Zur Kurzzeitstandsicherheit bei Baugrubenverbau-konstruktionen in weichen Böden; Bautechnik, Heft 9, pp. 612 - 619.

Hough, B.K. (1957): Basic Soil Engineering; Ronald Press Company, New York, pp. 112 - 115.

Hu, Y.F. (2000): Zum Verformungsverhalten von wassergesättigten bindigen Böden unter zyklischer Belastung; Schriftenreihe Geotechnik, Universität Gh Kassel, Heft 8.

Jaki, J. (1944): The coefficient of earth pressure at rest; Journal of Society of Hungarian Architects and Engineers, Budapest, Hungary, pp. 355 - 358.

James, R.G. / Brandsby, P.L. (1971): A velocity field for some passive earth pressure problems; Geotechnique, Vol. 21, No. 1, 61 - 83 (quoted from Pradel (1994)).

Jamiolkowski, M. / Ladd, C.C. / Germaine, J.T. / Lancellotta, R. (1985): New developments in field and laboratory testing of soils; Proc. XI ICSMFE, San Franscisco, Vol. 1, pp. 57 - 153.

Janbu, N. (1957): Earth pressure and bearing capacity calculations by generalised procedure of slices; Proc. of IV ICSMFE, 2, 207 - 212 (quoted from Pradel (1994)).

Janbu, N. (1977): Slopes and excavations in normally and lightly overconsolidated clays; Proc. of the IX ICSMFE, Tokyo, Vol. 2, pp. 549 - 566.

Jörß, O. (1998): Erfahrungen bei der Ermittlung von c_u- Werten mit der Hilfe von Drucksondierungen in bindigen Böden; Geotechnik 21, Nr. 1, pp. 26 - 27.

Kempfert + Partner (1991-1993): Geotechnische Berichten und Aktenvermerk für das Bauvorhaben Wohnanlage Markgrafenstrasse in Konstanz; nicht veröffentlicht.

Kempfert + Partner (1994-1998): Geotechnische Berichten und Meßprotokollen für das Wohn- und Geschäftshaus Sigismundstrasse 9 in Konstanz; nicht veröffentlicht.

Kempfert, H.-G. / Stadel, M. (1994): Verfahren zur Berechnung und messtechnischen Überwachung von Baugruben in normalkonsolidierten weichen tonigen Böden; Bericht zum F + E- Projekt, nicht veröffentlicht.

Kempfert, H.-G. / Stadel, M. (1997): Berechnungsgrundlagen für Baugruben in normalkonsolidierten weichen bindigen Böden; Bauingenieur 72, Springer-VDI Verlag, pp. 207 - 214.

Kempfert, H.-G. (1997): Berechnung und Ausführung von Baugruben im Seeton; 3. Stuttgarter Geotechnik-Symposium, Baugruben in Locker- und Festgestein, pp. 209 - 225.

Kempfert, H.-G. / Gebreselassie, B. (1999): Effect of anchor installation on settlement of nearby structures in soft soils; Proc. Intl. Symposium on Geotechnical Aspects of Underground Construction in Soft Ground - IS-Tokyo'99, Tokyo, pp. 665 - 670.

Kempfert, H.-G. / Gebreselassie, B. (2000): Ergebnisse einer numerischen Vergleichs-berechnungen von Mitgliedern des DGGT - Arbeitskreises „Baugruben" an einer zweifach ausgesteiften Baugrube; Verformungsprognose für tiefe Baugruben, AK 1.6 „Numerik in der Geotechnik", ed. by H.F. Schweiger, pp. 68 - 84.

Kempfert, H.-G. / Gebreselassie, B. (2002): Zur Diskussion von dränierten oder undränierten Randbedingungen bei Baugruben in weichen Böden, Bautechnik, Heft 9, pp. 603 - 611.

Kempfert, H.-G. /Böhm, F. /Soumaya, B. / Hardt, Th. (2001): Verformungsanalysen von Flachgründungen in normalkonsolidierten bindigen Böden und Wirksamkeit von Stabilisierungsmaßnahmen mit schwimmenden Verpresspfählen auf der Grundlage von vorliegenden Setzungsmessungen; Zwischenbericht zur DFG, nicht veröffentlicht.

Kempfert, H.-G. / Gebreselassie, B. (2002): Zur Diskussion von dränierten oder undränierten Randbedingungen bei Baugruben in weichen Böden, Bautechnik, Heft 9, pp. 603 - 611.

Kirkgard, M.N. / Lade, P.V. (1993): Anisotropic three - dimensional behavior of a normally consolidated clay; Canadian Geotechnical Journal, 30, pp 848 - 858.

Klobe, B. (1992): Eindimensional compression und Konsolidation und darauf basierende Verfahren zur Setzungsprognose; Institut für Bodenmechanik und Felsmechanik der Universität Fridericiana in Karlsruhe, Heft 128.

Kondner, R.L. (1963); Hyperbolic stress - strain response: cohesive soils; Journal of Soil Mechanics and Foundation Division, ASCE, 89(SM1), pp 115 - 143.

Koppula, S.D. (1981); Stastical estimation of compression index; ASTM, Geotechnical Testing Journal 4, No. 2, pp. 68 - 73.

Kulhawy, F.H. / Mayne, P.H. (1990): Manuel on estimating soil properties for foundation design; Electric Power Research Institute, EPRI.

Ladd, C.C. (1964): Stress - strain modulus of clay in undrained shear; JSMFD, ASCE, Vol. 90, SM5, pp. 103 - 132.

Ladd, C.C. / Bovee, R.B. / Edgers, L. / Rixner, J.J. (1971): Consolidated - Undrained plane strain shear tests on Boston blue clay; Research Report R71 - 13, No. 273, No. 284, Department of Civil Engineering, Massachusetts Institute of Technology, Cambridge, pp. 243.

Ladd, C.C. / Foott, R. / Ishihara, K. / Schlosser, F. / Poulos, H.G. (1977): Stress - deformation and strength characteristics; Proc. IX ICSMFE, Tokyo, pp. 421 - 494.

Ladd, P.V. / Duncan, J-M (1976): Stress - path dependant behaviour of cohesionless soil; Journal of Geotechnical Engineering Division, ASCE, Vol. 102, GT1, pp. 51 - 68.

Ladd, P.V. (1977): Elasto-plastic stress - strain theory for cohesionless soil with curved yield surfaces; International Journal of Solids and structures 13, 1977, pp 1019-1035

Lafleur, J. / Silvestri, V. / Asselin, R. / Soulie, M. (1988): Behaviour of test excavation in soft champlain sea clay; Canadian Geotechnical Journal, 25, pp. 705 - 715.

Lambe, T.W. (1967): Stress - path method; ASCE, Journal of Soil Mechanics and Foundation Engineering Division, Vol. 93, pp. 309 - 331.

Lambe, T.W. / Whitman, R.V. (1969): Soil Mechanics; John Wiley & Sons, New York.

Lambe, T.W. (1979): Braced excavations; Proc. of the 1970 Speciality Conference on Lateral Stresses, ASCE, Cornel University, pp 149 - 218.

Lambe, T.W. / Mass, W.A. (1979): Stress - path method; 2nd ed., ASCE, Journal of Geotechnical Engineering Division, Vol. 105, pp. 727 - 738.

Larsson, R. (1977): Basic behaviour of Scandinavian soft clays; Swedish Geotechnical Institute, Linköping, Report No. 4.

Larsson, R. (1980): Undrained shear strength in stability calculation of embankments on soft clays; Canadian Geotechnical Journal, 17, pp. 591 - 602.

Lee, Y.N. / Jin, B.I. (1979): Measurement and prediction of K_0: Journal of Korean Society of Civil Engineering, pp. 226 - 233.

Lehr, H. / Mattle, B. / Jaeger, J. (1993): Nichtlineare Setzungsanalyse einer tiefen Baugruben mit anstehendem Grundwasser im Salzburger Seeton; Technische Universität Graz, Heft 10, pp. 78 - 93.

Leroueil, S. / Tavenas, F. / Le Bihan, J.P. (1983): Propprietes caracteristiques des argiles de l'est du Canada. Canadian Geotechnical Journal 20, pp. 681 - 705.

Leroueil, S. / Tavenas, F. / Locat, J. (1985): Discussion: Correlation between index tests and the properties of remolded clays; ed. by *W.D. Carrier III and J.F. Beckman*, Geotechnique 35, No. 2, 223 - 226.

Lim, K. / Hosoi, T. / Ishii, T. (1989): Behaviour of diaphragm walls and settlements in marine clay; Proc. 9th Asian regional Conference on Soil Mechanics and Foundation Engineering, Bangkok, vol. 1: pp. 331 - 334.

Lo, K.Y. (1965): Stability of slopes in anisotropic soils; Journal of Soil Mechanics and Foundation Division, ASCE, 91, No. SM4.

Lo, K.Y. / Milligan, V. (1967): Shear strength properties of two stratified clays; Journal of Soil Mechanics and Foundation Division, ASCE, 93, SM1, pp. 1 - 15.

Lo, K.Y. / Morin, J.P. (1972): Strength anisotropy and time effects of two sensitive clays; Canadian Geotechnical Journal, 9, pp. 261 - 277.

Lord, J.A. (1967): Stresses and strains in an earth pressure problem; Ph.D. Thesis Cambridge University.

Lunne, T / Robertson, P.K. / Powell, J.J.M. (1997): Cone Penetration Testing; Blackie Academic & Professional, London.

Mana, A.I. (1978): Finite element analysis of deep excavation behaviour; Thesis, presented in partial fulfilment of the Ph.D. Degree, Stanford University, Stanford, California.

McCarron, W.O. / Chen, W.F. (1987): A capped plasticity model applied to Boston blue clay; Canadian Geotechnical Journal., 24(4), pp. 630 - 644.

McRostii, G.C. / Burn, K.N. / Mitchell, R.J. (1972): The performance of tied - back sheet piling in clay; Canadian Geotechnical Journal, 9, pp. 206 - 218.

Meißner, H. (2002): Baugruben: Empfehlungen des Arbeitskreises 1.6 "Numerik in der Geotechnik"; Abschnitt 3, Geotechnik 25, pp. 44 - 56.

Mesri, G. (1975): Discussion on new design procedure for stability of soft clays; ASCE, Journal fo the geotechnical Eingineering Division, 101, GT4, pp. 409 - 412.

Mesri, G. / Godlewski, P.M. (1977): Time- and stress- compressibility interrelationship; ASCE, Journal of Geotechnical Engineering, Vol. 103, No. GT 5, pp 417 - 430.

Mesri, G. / Shahien, M. / Feng, T.W. (1995): Compressibility parameters during primary consolidations; Proc. of the intl. Symposium on Compression and Consolidation of Clayey Soils, -IS-Hiroshima, ed. by *Yoshikuni, H. / Kusakabe, O.* Vol 2, pp. 1021 - 1037. AVL (bibliothek)

Meyerhof, G.G. (1970): Safety factors in soil mechanics; Canadian Geotechnical Journal, 7, pp. 349 - 355.

Meyerhof, G.G. (1982): Limit states design in geotechnical engineering; Structural Safety, 1, pp. 67 - 71.

Meyerhof, G.G. (1984): Safety factors and limit states analysis in geotechnical engineering; Canadian Geotechnical Journal, 21, pp. 1 - 7.

Mitchell, J.K. (1993): Fundamentals of Soil Behaviour; 2nd ed., John Wiley & Sons, Inc.

Mizuno, E. / Chen, W.F. (1986): Plasticity modelling and its application to geomechanics; Proceedings of the International Symposium on Recent Developments in Laboratory and Field Testing and Analysis of Geotechnical Problems - Bangkok, edited by Balasubramaniam et al., A.A. Balkema, pp 391 - 426.

Moormann, C. / Katzenbach, R. / Arslan, U. (2000): Numerische Untersuchungen zum räumlichen Trag- und Verformungsverhalten von tiefen Baugruben; Verformungsprognose für tiefe Baugruben, AK 1.6 „Numerik in der Geotechnik", ed. by H.F. Schweiger, pp. 89 - 109.

Nagaraj, T.S. (1983): Prediction of soil behaviour; Recent development in laboratory and field tests and analysis of geotechnical problems, ed. by *Balasubramaniam, A.S. / Chandra, s. / Bergado, D.T.*, Bangkok, pp. 337 - 360.

*Naylor, D.J. / Pande, G.N. (1981):*Finite Elements in Geotechnical Engineering; Pineridge Press, Swansea.

Newson, T.A. (1997): Modelling the yielding behaviour of natural soft clay; Proc. Of the 14th int. Conf. Soil Mechanics and Foundation Engineering, Hamburg, pp. 381 - 386.

NG, R.M.C. / Lo, K.Y. (1985): The measurements of soil parameters relevant to tunneling in clays; Canadian Geotechnical Journal, 22, pp. 375 - 391.

Ng, C.W.W. / Yan, R.W.W. (1999): Three - dimensional modelling of a diaphragm wall construction sequence; Geotechnique 49, No. 6, pp. 825 - 834.

Ng, C.W.W. / Rigby, D.B. / NG, W.L. (1999): Observed performance of a short diaphragm wall panel; Geotechnique 49, No. 5, pp. 681 - 694.

Nishida, Y. (1956); A brief note on compression index of soil; ASCE; Journal of Soil Mechanics and Foundation Engineering Division, 82, No. SM 3, pp. 1027-1 to 1027-14.

Norman, L.E. J. (1958): A comparison of values of liquid limit determined with apparatus having basis of different hardness: Geotechnique, 8, pp.79 - 83.

Ohde, J. (1939): Zur Theory der Druckverteilung im Baugrund; Der Bauingenieur 20.

Olson, R.E. (1974): Shearing strength of kaolinite, illite, and montmorillonite; ASCE, Journal of Soil Mechanics and Foundation Engineering, Vol. 100, No. GT 11, pp. 1215 - 1229.

Omine, K. / Ohno, S. (1997): Deformation analysis of composite ground by homogenisation method; Proc. Of ICSMFE, Hamburg, pp. 719 - 722.

Palmer, J.H.L. / Kenny, T.C. (1972): Analytical study of a braced excavation in week clay; Canadian Geotechnical Journal, Vol. 9, pp. 145 - 164.

Parry, R.H.G. (1956): Strength and deformation of clay; Ph.D Thesis , London University.

Parry, R.H.G. (1960): Triaxial compression and extension tests on remoulded saturated clay; Geotechnique, Vol. 10, No. 4, pp. 166 - 180.

Parry, / Nadarajah (1974a): Observations on laboratory prepared lightly overconsolidated kaoli; Geotechnique, 24, pp. 345 - 357.

Parry / Nadarajah (1975b): Anisotropy in a natural soft clayey silt; Engineering Geology, 8(3), pp. 287 - 309.

Parry, R.H.G. (1995): Mohr Circles, Stress Paths and Geotechnics; E & FN Spon, London.

Parry, R.H.G. / Wroth (1981): Shear properties of soft clay; Soft clay engineering, edited by E.W. Brand and R.P. Brenner), Elsevier, Amsterdam, 311 - 364.

Peck, R.B. / Hansen, W.E. /Thorburn, T.H. (1974): Foundation Engineering; 2nd ed., John Wiley and Sons, New York.

Peck, R.B. (1969): Deep excavations and tunnelling in soft ground; State-of-the-Art Report, Proc. of 7th ICSMFE, Mexico, pp. 225 - 290.

Poh, T.Y. / Wong, I.H. (1998): Effects of construction of diaphragm wall panels on adjacent ground: Field trial; ASCE, Journal of Geotechnical and Geoenvironmental Engineering, Vol. 124, No. 8, pp. 749 - 756.

Potyondy, J.G. (1961): Skin friction between various soils and construction materials; Geotechnique, London, Vol. 11, pp. 339 - 352.

Potts, D.M. / Fourie, A.B. (1985): The effect of wall stiffness on the behaviour of a propped retaining wall; Geotechnique 35, No. 3, pp. 347 - 352.

Potts, D.M. / Addenbrooke, T.I. / Day, R.A. (1993): The use of soil berms for temporary support of retaining walls; Retaining Structures, Thomas Telford, London, pp. 440 - 447.

Potts, D.M. / Bond, A.J. (1994): Calculation of structural forces for propped retaining walls; XIII ICSMFE, New Delhi, India, pp. 823 - 826.

Powrie, W. (1997): Soil Mechanics: Concept and Applications; E & FN Spon, London.

Powrie, W. / Pantelidou, H. / Stallebrass, S.E. (1998): Soil stiffness in stress paths relevant to diaphragm walls in clay; Geotechnique 48, No. 4, pp. 483 - 494.

Pradel, D. (1994): Active earth pressure distribution in cohesive soils; Proc. of the XIII ICSMFE, New Delhi, India, Vol. 2, pp. 795 - 798.

Rankine, W.J.M. (1857): On the stability of loose earth; Trans. Royal Society, London (quoted from Pradel (1994)).

Richards, D.J. / Powrie, W. / Page, J.R.T. (1998): Investigation of retaining wall installation and performance using centrifuge modelling techniques; Proceeding of Institutee of Civil Engineers, Geotechnical Engineering, 131, pp. 163 - 170.

Richards, D.J. / Powrie, W. (1998): Centrifuge model test on doubly propped embedded retaining walls in overconsolidated kaolin clay; Geotechnique 48, No. 6, pp. 833 - 846.

Rosco, K.H. / Burland, J.B. (1968): On the generalized stress - strain behavior of 'wet clay'; In Engineering Plasticity, edited by Heyman/Leckie, Cambridge University Press, Cambridge, England, pp. 535 - 609.

Rowe, P.W. (1952): Anchored sheet pile walls; Proc. of ICE 1 (1), pp. 27 - 70.

Rowe, P.W. (1957): Sheet pile walls in clay; Proc. of ICE 7, pp. 629 - 654.

Ruppert, F.-R. (1980): Bodenmechanische Eigenschaften der Lauenberger Serie - Ein Beispiel für Statistik in der Bodenmechanik; Mitteilung des Lehrstuhls für Grundbau und Bodenmechanik, TU - Braunschweig, Nr. 80 - 4.

Russel, E.R. / Mickle, J.L. (1970): Liquid limit values of soil moisture tension; Journal of the Soil Mechanics and Foundation Division, ASCE, Vol. 96, pp. 967 - 987.

Scherzinger, T. (1991): Materialverhalten von Seetonen - Ergebnisse von Laboruntersuchungen und Ihre Bedeutung für das Bauen in weichem Baugrund; Institut für Bodenmechanik und Felsmechanik der Universität Fridericiana in Karlsruhe, Heft 122.

Schmertmann, J.S. (1975): Measurement of in-situ shear strength; State-of-the-Art Report, Proc. ASCE speciality on in-situ measurement of soil properties, Raleigh, Vol. II, pp. 57 - 138.

Schmidt, B. (1966): Discussion of "Earth pressure at rest related to stress history"; Canadian Geotechnical Journal, Vol. 3, No. 4, pp. 239 - 242.

Schofield, A.N. / Wroth, C.P. (1968): Critical State Soil Mechanics; McGraw-Hill, New York, NY.

Schweiger, H.F. / Breymann, H. (1994): Baugrubenverformung zufolge Wasserhaltung: Messung und rechnerische Betrachtung; Beiträge zum 9. Christian Veder Killoquim, Technische Universität Graz, Institut für Bodenmechanik und Grundbau, Heft 11, pp. 158 - 176.

Schweiger, H.F. / Freisder, M / Breymann, H. (1997): Deep excavation in soft ground in-situ measurements and numerical predictions; Proc. Of 14th ICSMFE, Hamburg, pp. 589 - 594

Schweiger, H.F. (2000): Ergebnisse des Berechnungsbeispieles Nr. 3 "3 - fach verankerte Baugrube", Gegenüberstellung der eingesandten Berechnungsergebnisse; Verformungsprognose für tiefe Baugruben, AK 1.6 "Numerik in der Geotechnik", ed. by H.F. Schweiger, pp. 7 - 67.

Schweiger, H.F. (2002): Some remarks on pore pressure parameters A and B in undrained analyses with the hardening soil model; PLAXIS Bulletin No. 12, pp. 6 - 9.

Sheng, D. / Westerberg, B. / Mattsson, H. / Axelsson, K. (1997): Numerical analysis of stress-strain inhomogeninities in a triaxial test specimen; Proc. of 14th ICSMFE, Hamburg, pp. 403 - 407.

Sherif, M.A. / Koch, D.E. (1970): Coeffient of earth pressure at rest as related to soil recompression ratio and and liquid limit: Highway Research Record, Washington, No. 323, pp. 39 - 48.

Simpson, B. (1992a): Retaining structures: Displacement and Design; Geotechnique 42, No. 4, pp. 541 - 576.

Simpson, B. (1992b): Partial safety factors for design of retaining structures; Geotechnique 42, No. 1, pp. 131 - 136.

Skempton, A.W. (1944): Notes on the compressibility of clays; Quarterly Journal of Geotechnical Society, London, pp. 119 - 135.

Skempton, A.W. (1953): Earth pressure, retaining walls, tunnels and strutted excavations; Proc. of the III ICSMFE, Vol. 2, pp. 353 - 361.

Skempton, A.W. / Northey, R.D. (1953): The sensitivity of clays; Geotechnique, 3, pp. 30 - 53.

Skempton, A.W. (1954): Discussion of the structure of inorganic soil; ASCE, Proc., 80, separate No. 478, pp. 19 - 22.

Skempton, A.W. / Bishop, A.W. (1954): Soils in "Building Materials; their elasticity and inelsaticity," *M.Reiner* ed., North Holland Publishing Co., Amsterdam, pp. 417 - 482 (see *Bowles (1984)*).

Skempton, A.W. (1957): Discussion on the planning and design of the new Hong Kong airport; Proc. the Institute of Civil Engineers, 7, pp.305 - 307.

Skopek, J. / TerStephanian, G. (1975): Comparison of liquid limit values determined according to Casagrande and Vasilev; Geotechnique, 25(1), pp. 135 - 136.

Smith (1968): Determining the settlement of soft clay; Highways and Public Works, London.

Smoltczyk, U. (1996): Grundbau - Taschenbuch; Teil I und II, 5th ed., Ernst & Sohn, Berlin.

Sokolovski, V.V. (1960): Statics of soil media; Butterworth, London (quoted from Pradel (1994)).

Steinmann, B. (1985): Zum Verhalten bindiger Böden bei monotoner einaxialer Beanspruchung; Baugrund Institut Stuttgart, Mitteilung 26.

Stroh, D. (1974): Berechnung verankerter Baugruben nach der Finite - Element - Methode; Mitteilungen der Versuchsanstalt für Bodenmechanik und Grundbau der TH Darmstadt, Heft 13.

Tait, R.E. / Taylor, H.T. (1974): Design, construction, and performance of rigid and flexible bracing systems for deep excavation in San Francisco bay mud; Paper Presented at ASCE National Meeting, Los Angeles.

Teng, W.C. (1962): Foundation Design; Prentice-Hall, New Jersey.

Terzaghi, K. (1943): Theoretical Soil Mechanics; John Wiley and Sons, New York.

Terzaghi, K. / Peck, R.B. (1948/67): Soil Mechanics in Engineering Practice; 2nd ed., John Wiley and Sons, New York.

Tschebotarioff, G.P. (1973): Foundations, Retaining and Earth Structures; McGraw-Hill, New York.

Tsukada, Y. / Yasuhara, K. (1995): Scale effects in one-dimensional consolidation of clay; Proc. of the International Symposium on Compression and Consolidation of Clayey Soils, ed. by *Yoshikuni, H. / Kusakabe, O.*, Hiroshima, Vol. 1, pp. 211 - 216

Valsangkar, A.J. / Schriver, A.B. (1991): Partial and total factors in anchored sheet pile design; Canadian Geotechnical Journal, 28, pp. 812 - 817.

Vaid / Campanella (1974):

Vaziri, H.H / Troughton, V.M. (1992): An efficient three - dimensional soil - structure interaction model for analysis of earth retaining structures; Canadian Geotechnical Journal 29, pp. 529 - 538.

Vermeer P.A. / Brinkgreve R.B.J. (1995): Hand book of the finite element code for soil and rock analysis "PLAXIS" Balkema Publisher.

Vermeer, P.A. / Meier, C.-P. (1998): Stability and deformations in deep excavations in cohesive soils; International Conference on Soil-Structure Interaction in Urban Civil Engineering, Darmstadt Geotechnics, No. 4, Vol. 1, pp. 177 - 192.

Vermeer, P.A. / Meier, C.-P. (1998): Standsicherheit und Verformungen bei tiefen Baugruben in bindigen Böden; Baugrundtagung, Stuttgart, pp. 133 - 148.

Vermeer, P.A. (1998): Column Vermeer; PLAXIS Bulletin, No. 5, pp. 2 - 3.

Yong, R.N. / Townsend, F.C. (1982): Application of plasticity and generalised stress - strain in geotechnical engineering; ASCE.

Youssef, M.S. / El - Ramle, A.H. / El-Demery, M. (1965): Relationship between shear strength, consolidation, liquid limit and plastic limit for remoulded clays; Proc. of ICSMFE, Vol. 1, pp. 126 - 129.

Walker, A.F. (1965): Stress-strain relationships for clay; Ph.D. Thesis, Cambridge University.

Weißenbach, A. (1985): Baugruben; Teil I, II und III, Ernst & Sohn, Berlin.

Weißenbach, A. / Kempfert, H.-G. (1995): German national report on braced excavation in soft ground; Proc. International Symposium on Underground Construction in Soft Ground, New Delhi (eds. Fujita, K. / Kusakabe, O.), A. A. Balkema, pp. 33 - 36.

Weßenbach, A. (2002): Empfehlungen des Arbeitskreises „Baugruben" der DGGT zu Baugruben in weichen Böden; Bautechnik, Heft 9, pp. 569 - 588.

Whyte, I.L. (1982): Soil plasticity and strength: a new approach using extrusion; Ground Engineering, 15(1), pp. 16 - 24.

Windisch, É.J. / Yong, R.N. (1990): A statistical evaluation of some engineering properties of eastern Canadian clays; Canadian Geotechnical Journal, pp. 373 - 386.

Wong, I.H. (1971): Analysis of braced excavations; Thesis Presented to the Massachusetts Institute of Technology in 1971, in Partial Fulfilment of the Requirements for the Degree of Doctor of Science.

Wong, P.K.K. / Mitchell, R.J. (1975): Yielding and plastic flow of sensitive cemented clay; Geotechnique, 25, pp. 763 - 782.

Wong, S. / Broms, B. (1994): Analysis of retaining walls using the hyperbolic model; Soil Structure Interaction: Numerical Analysis and Modelling (ed. By John W. Bull), E & FN SPON, pp. 605 - 645.

Wroth, C.P. / Wood, D.M. (1978): The correlation of index properties with some basic engineering properties of soils; Canadian Geotechnical Journal, 15, pp. 137 - 145.

Wood, D.M. (1983): Index properties and critical state soil mechanics; Recent development in laboratory and field tests and analysis of geotechnical problems, ed. by *Balasubramaniam, A.S. / Chandra, s. / Bergado, D.T.*, Bangkok, pp. 309 - 331.

Wroth, C.P. / Wood, D.M. (1978): The correlation of index properties with some basic engineering properties of soils; Canadian Geotechnical Journal, Vol. 15, No. 2, pp. 137 - 145).

Wroth, C.P. / Houldby, G.T. (1985): Soil mechanics - Property and analysis procedures; Proc. XI ICSMFE, San Francisco, Vol. 1, pp. 1 - 55.

Zdravkovic, L /Potts, D.M. (1999): Advances in modelling soil anisotropy; Constituive modelling of granular materials, ed. by Kolymbas, Springer, Berlin, pp. 491 - 521.

Zeng, G.X. / Pan, Q.Y. / Hu, Y.F. (1986): Behaviour of excavation with sheet piling in soft clay; The international conference of deep excavation, Bejing, 3.1 - 3.6.

Zhu, B. / Liu, G. (1994): Elasto - Plastic Analysis of deep excavation in soft clay; XIII ICSMFE, New Delhi, India, Vol. 2, pp. 905 - 908.

Appendix

A Measurement of soil parameters relevant to an excavation

A.1 The triaxial apparatus

A.2 One - dimensional compression

Site1 (Damcon1)

C_C = 0.1498, λ = 0.0651, λ^* = 0.0392
C_S = 0.0524, $\kappa \approx 0.0454$, $\kappa^* \approx 0.0153$

Site1 (Damcon2)

C_C = 0.2001, λ = 0.0870, λ^* = 0.0462
C_S = 0.0406, $\kappa \approx 0.0171$, $\kappa^* \approx 0.0093$ (1st un/reloading)
C_S = 0.0568, $\kappa \approx 0.0244$, $\kappa^* \approx 0.0130$ (2nd un/reloading)

Site2 (Maxcon1)

C_C = 0.2210, λ = 0.0961, λ^* = 0.0529
C_S = 0.0406, $\kappa \approx 0.0187$, $\kappa^* \approx 0.0113$

Site2 (Maxcon2)

C_C = 0.1592, λ = 0.0692, λ = 0.0403
C_S = 0.0306, $\kappa \approx 0.0133$, $\kappa^* \approx 0.0083$ (1st un/reloading)
C_S = 0.0570, $\kappa \approx 0.0248$, $\kappa^* \approx 0.0097$ (2nd un/reloading)

A.3 The variation of the constrained modulus with consolidation pressure

Site1 (Damcon1)

E_s^{ref} = 3590 kPa, m = 0.82
$E_{s(ur)}^{ref}$ = 6223 kPa, m = 0.87

Site1 (Damcon2)

E_s^{ref} = 3268 kPa, m = 0.85
$E_{s(ur)1}^{ref}$ = 8411 kPa, m = 0.73
$E_{s(ur)2}^{ref}$ = 6700 kPa, m = 1.42

Site1 (Damcon3)

E_s^{ref} = 2633 kPa,   m = 0.82
$E_{s(ur)1}^{ref}$ = 10092 kPa, m = 0.76
$E_{s(ur)2}^{ref}$ = 8541 kPa,   m = 1.20

Site2 (Maxcon1)

E_s^{ref} = 2512 kPa,   m = 0.84
$E_{s(ur)}^{ref}$ = 14146 kPa, m = 0.69

Continued: A.3 The variation of the constrained modulus with consolidation pressure
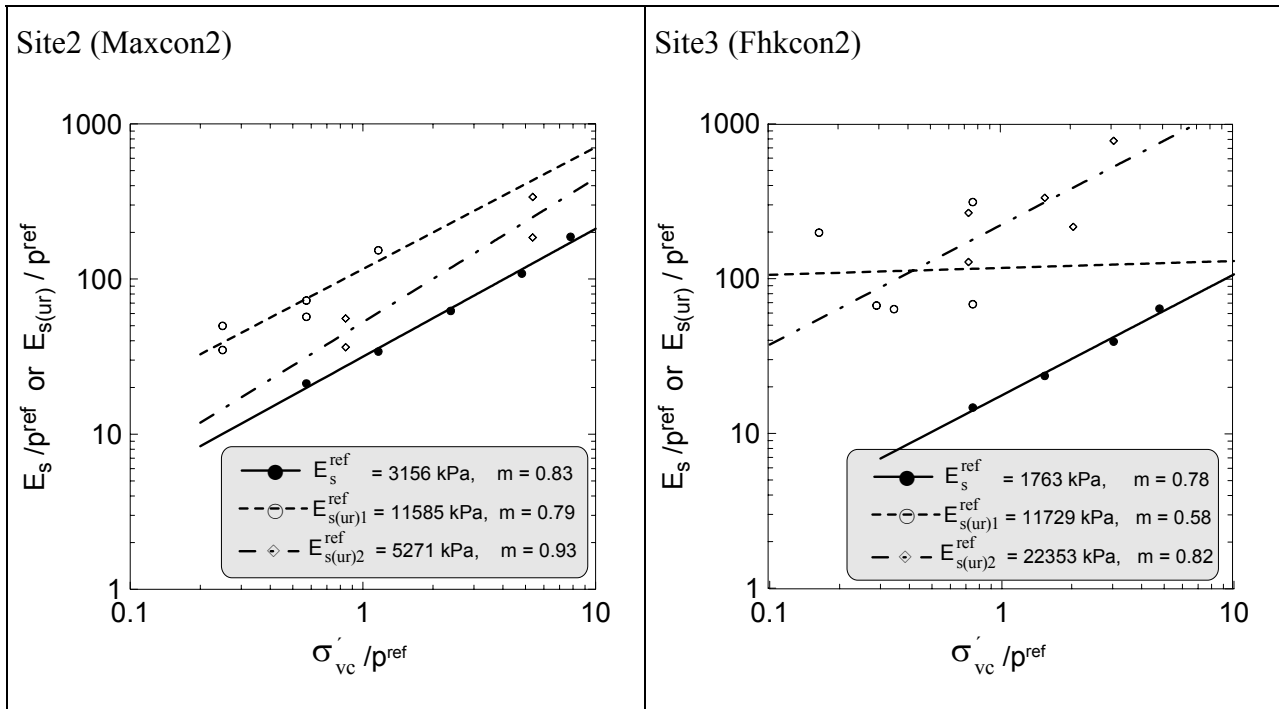
A.4 Isotropically consolidated undrained triaxial test at site1

A.4.1 Damciu4/Damciu30
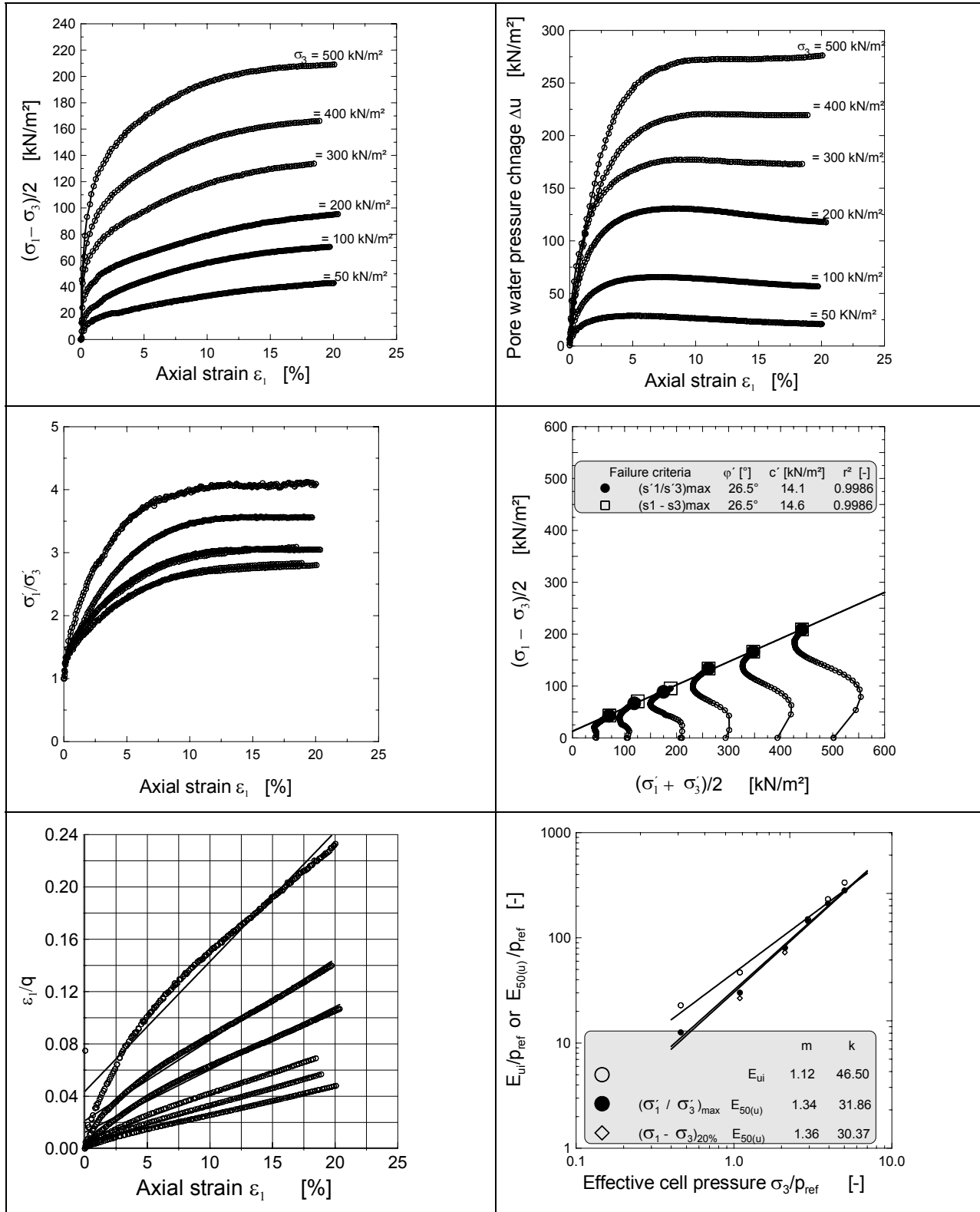
A.4.2 Damciu6
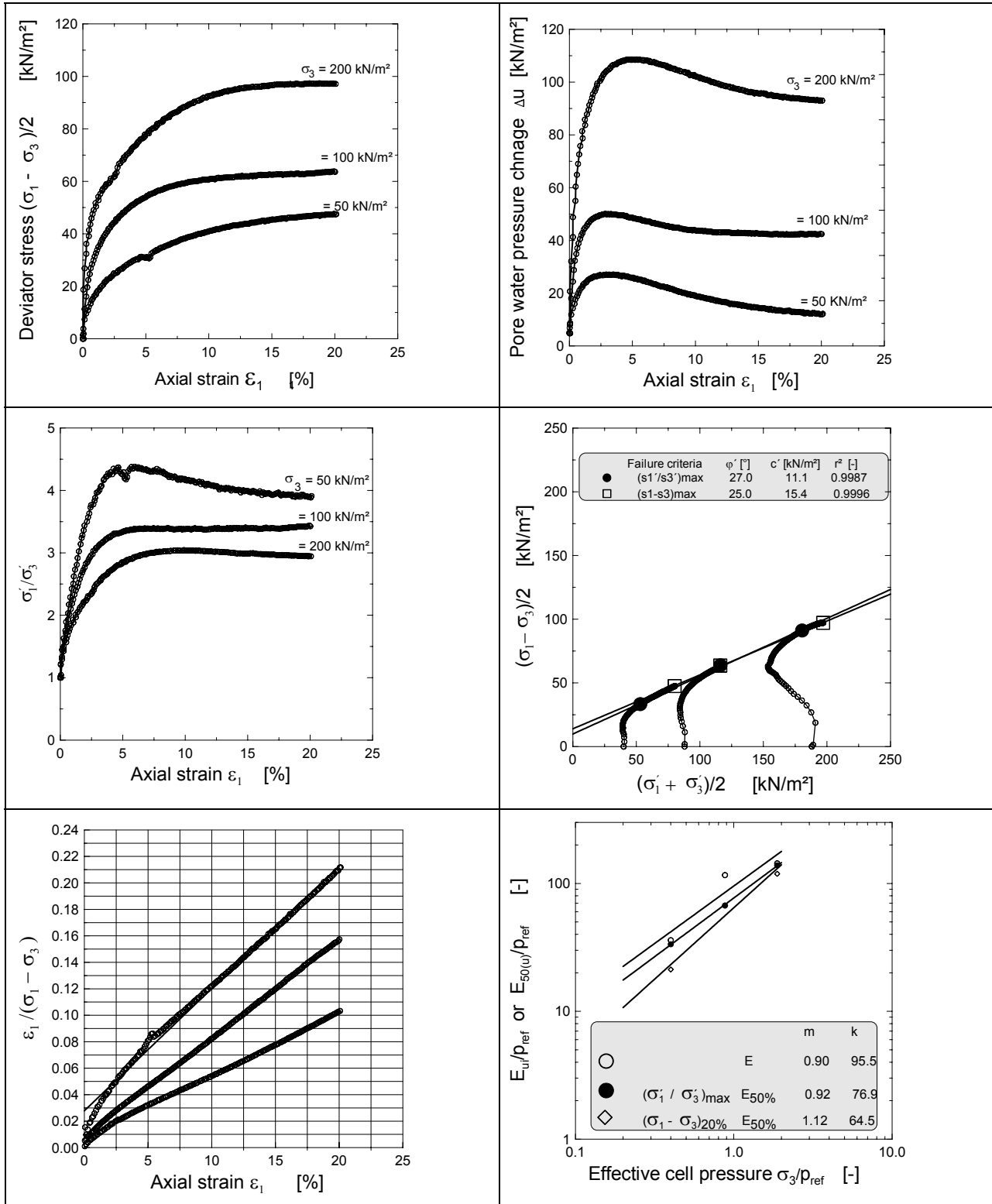
A.4.3 Damciu10
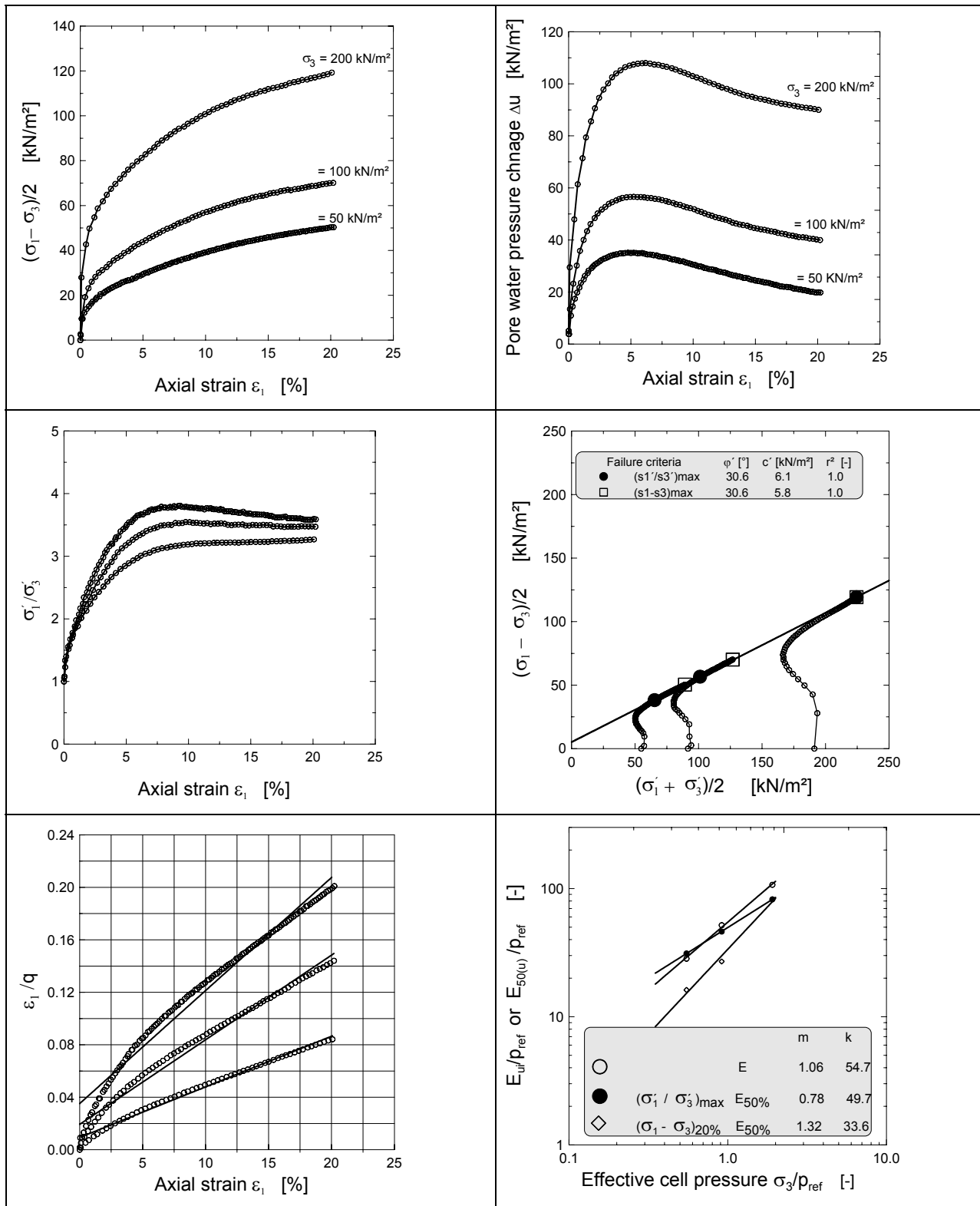
A.5 Isotropically consolidated undrained triaxial test at site2

A.5.1 Maxciu (remolded)
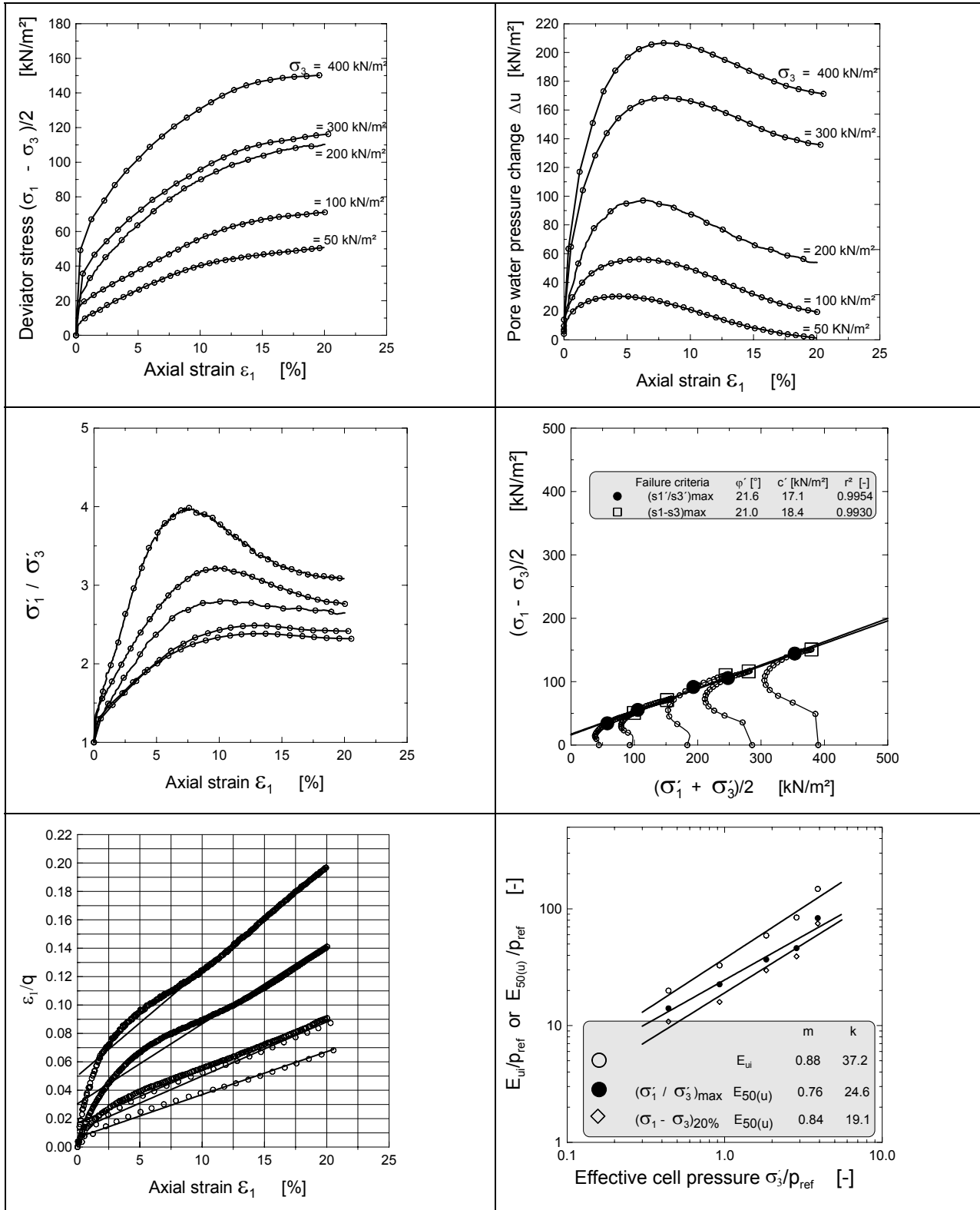
A.5.2 Maxciu3 (Horizontally oriented samples)
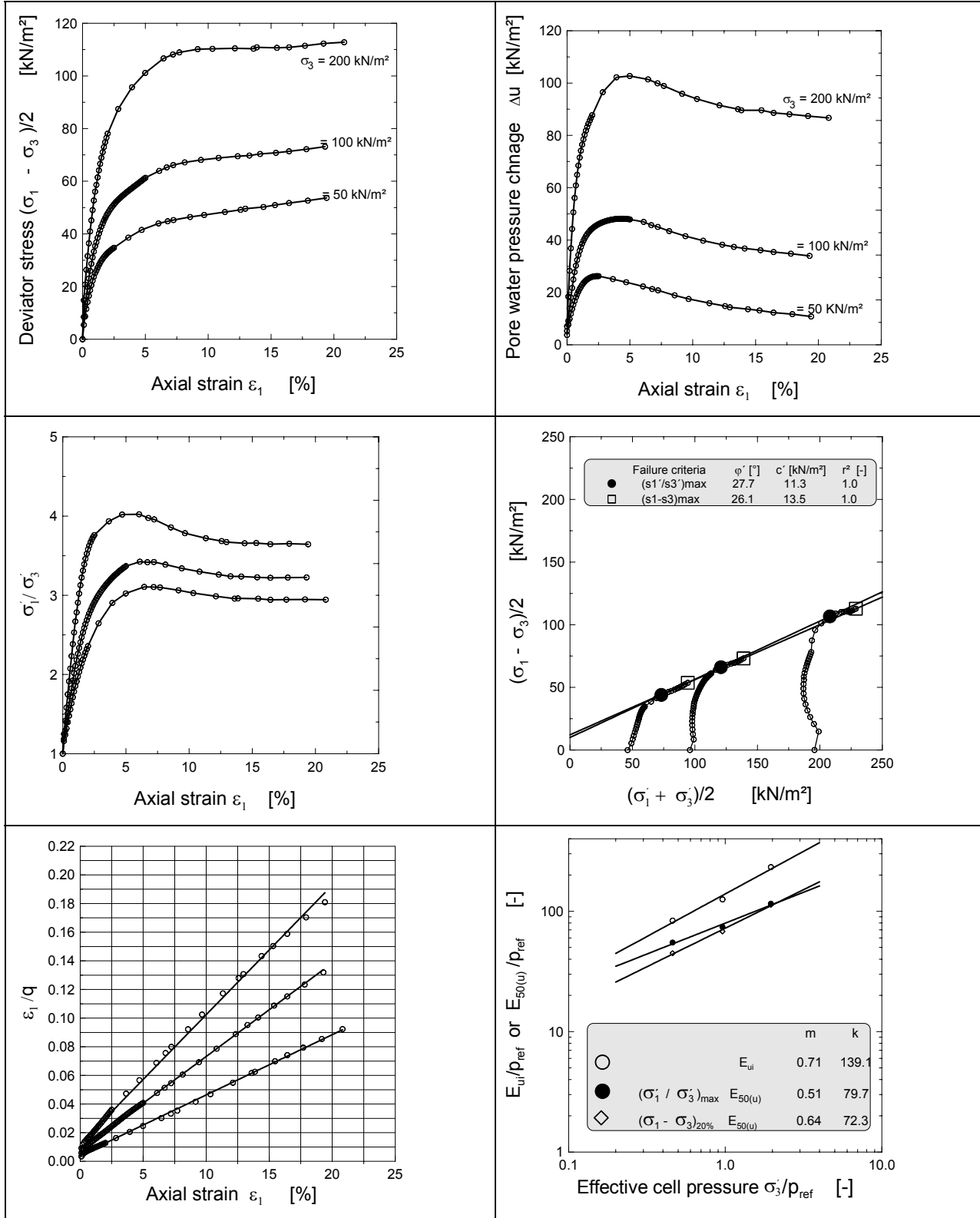
A.6 Isotropically consolidated drained triaxial test at site1

A.6.1 Damcid05
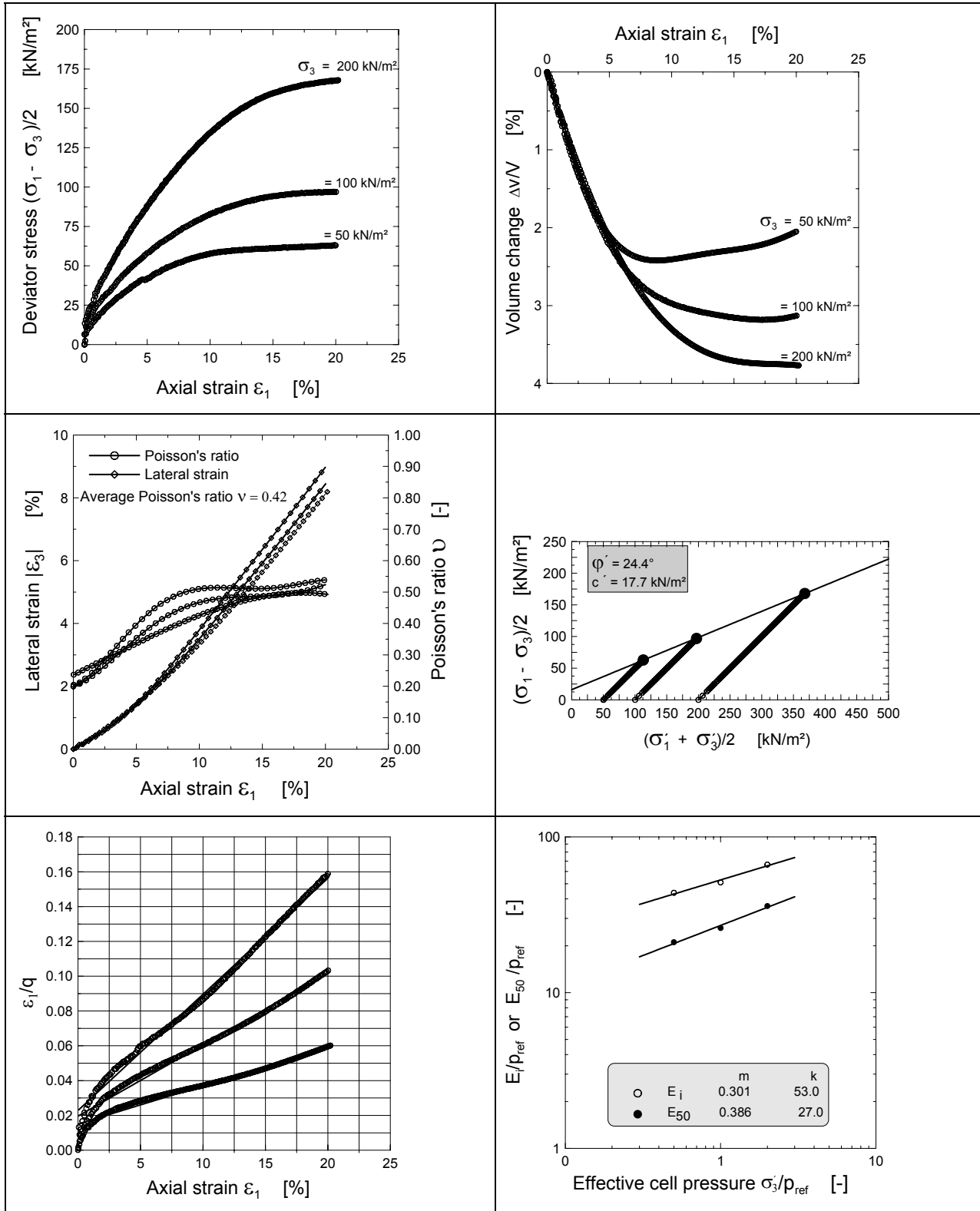
A.6.2 Damcid07
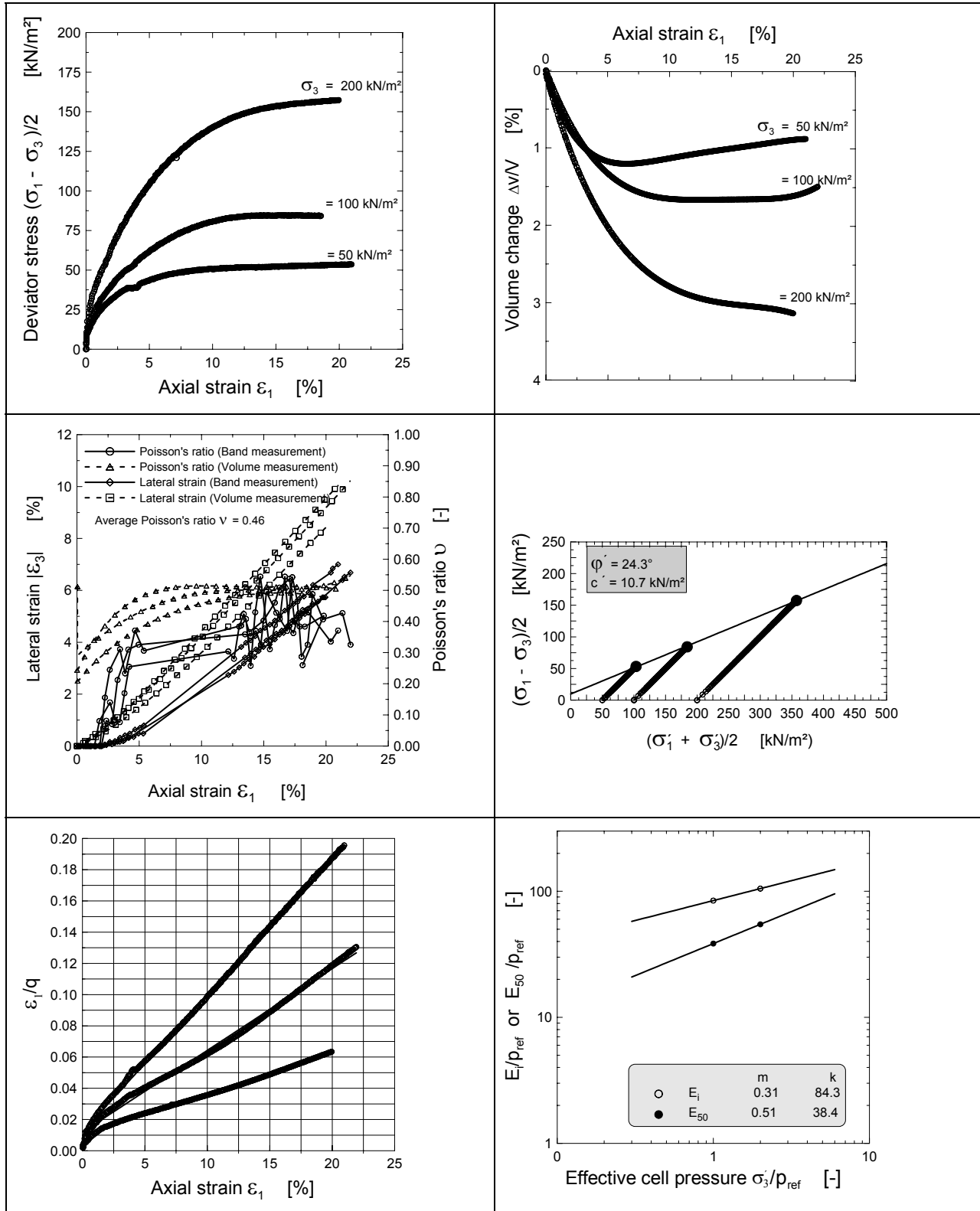
A.7 Isotropically consolidated drained triaxial test at site2

A.7.1 Maxcid01
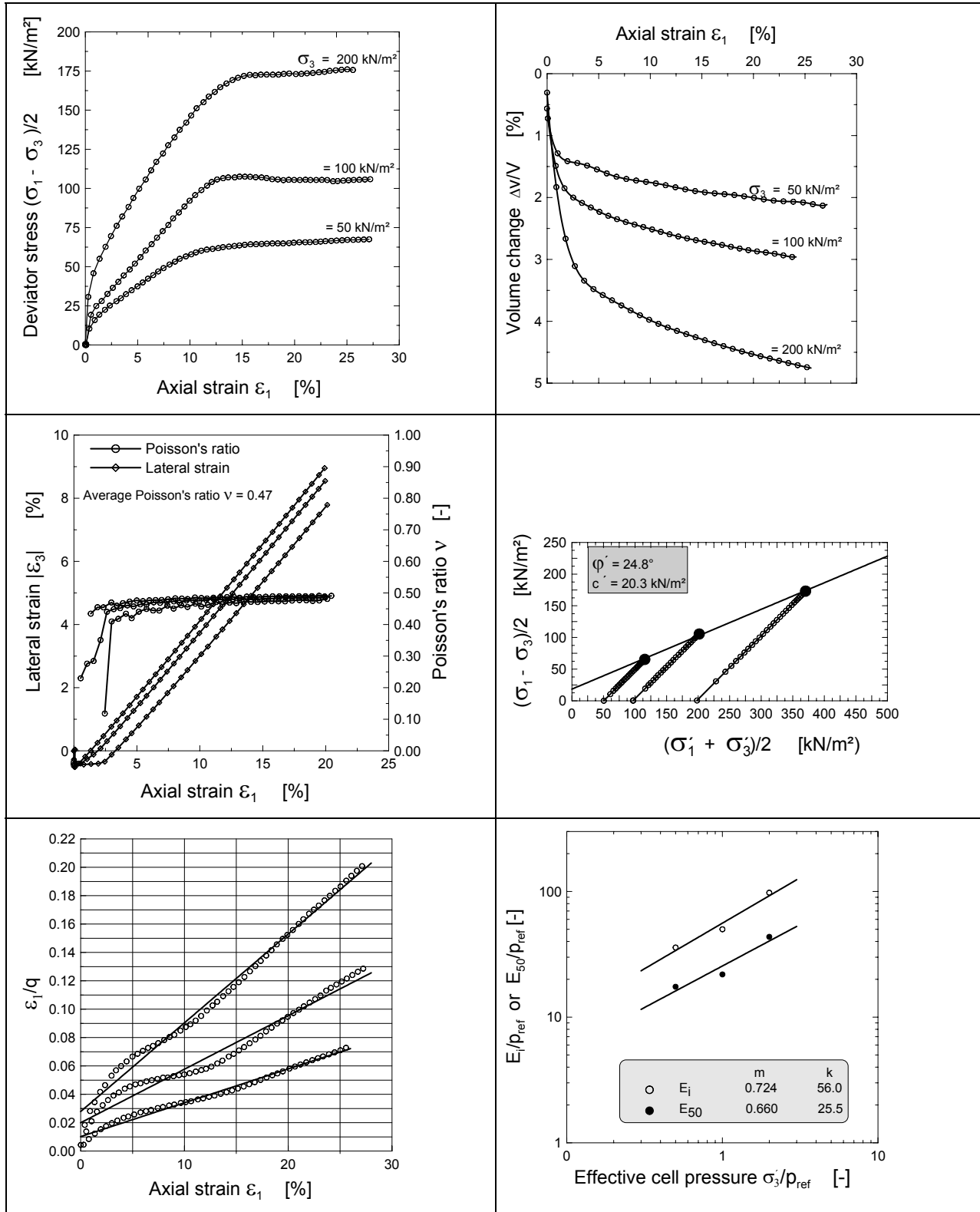
A.7.2 Maxcid05
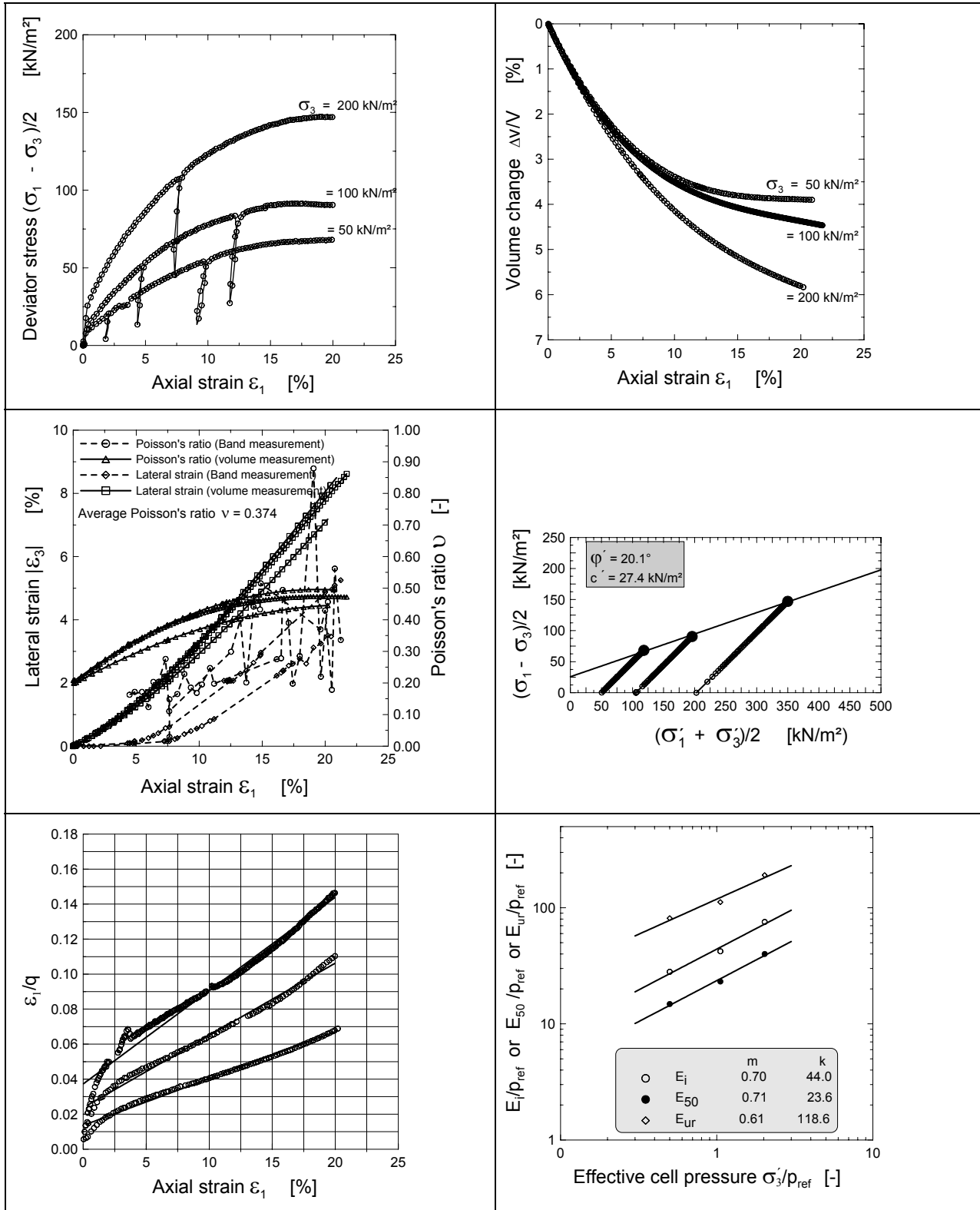
A.7.3 Maxcid (at 97% proctor , at the wet side reconstituted samples)
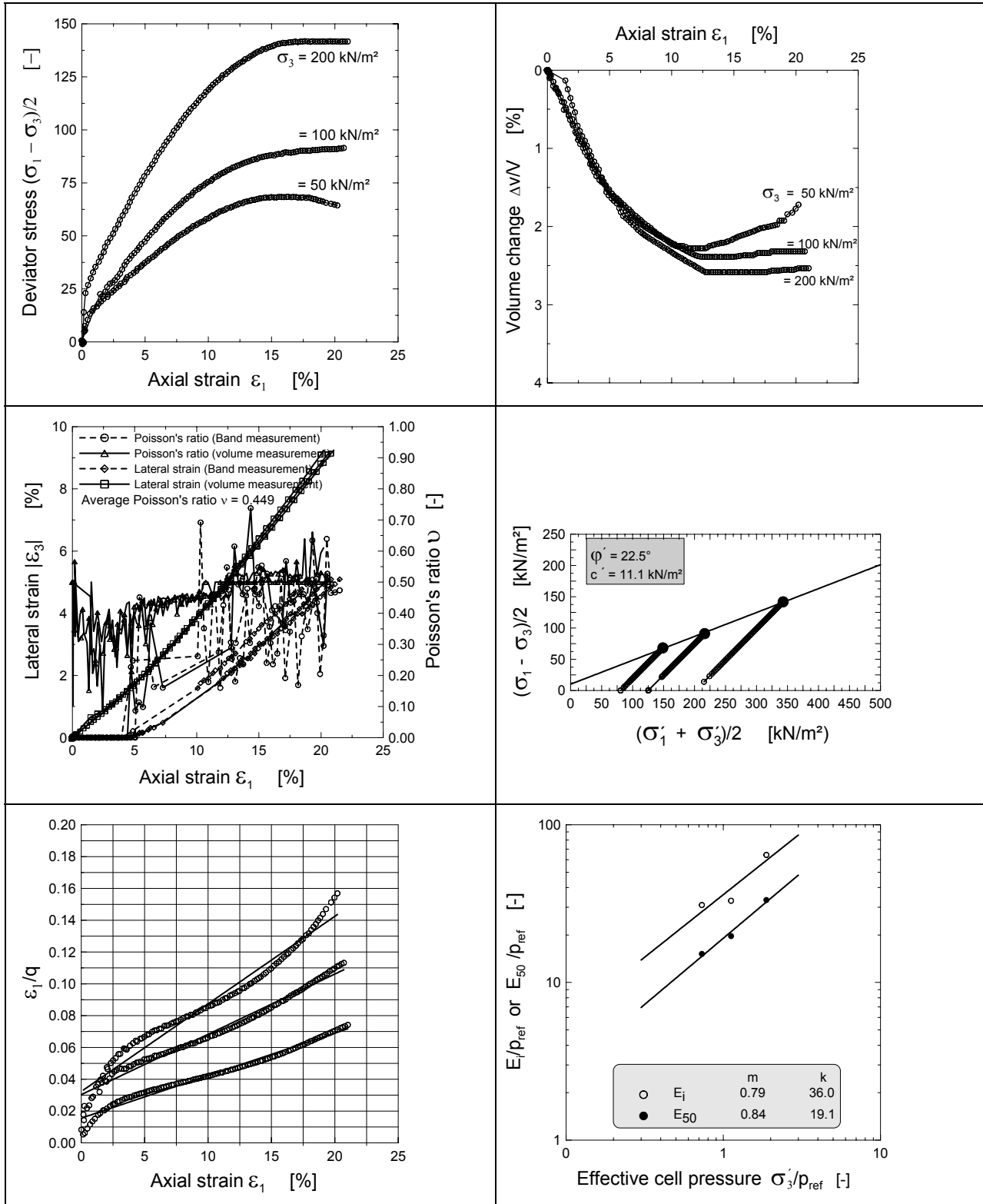
A.7.4 Maxcid13 (Horizontally oriented samples)
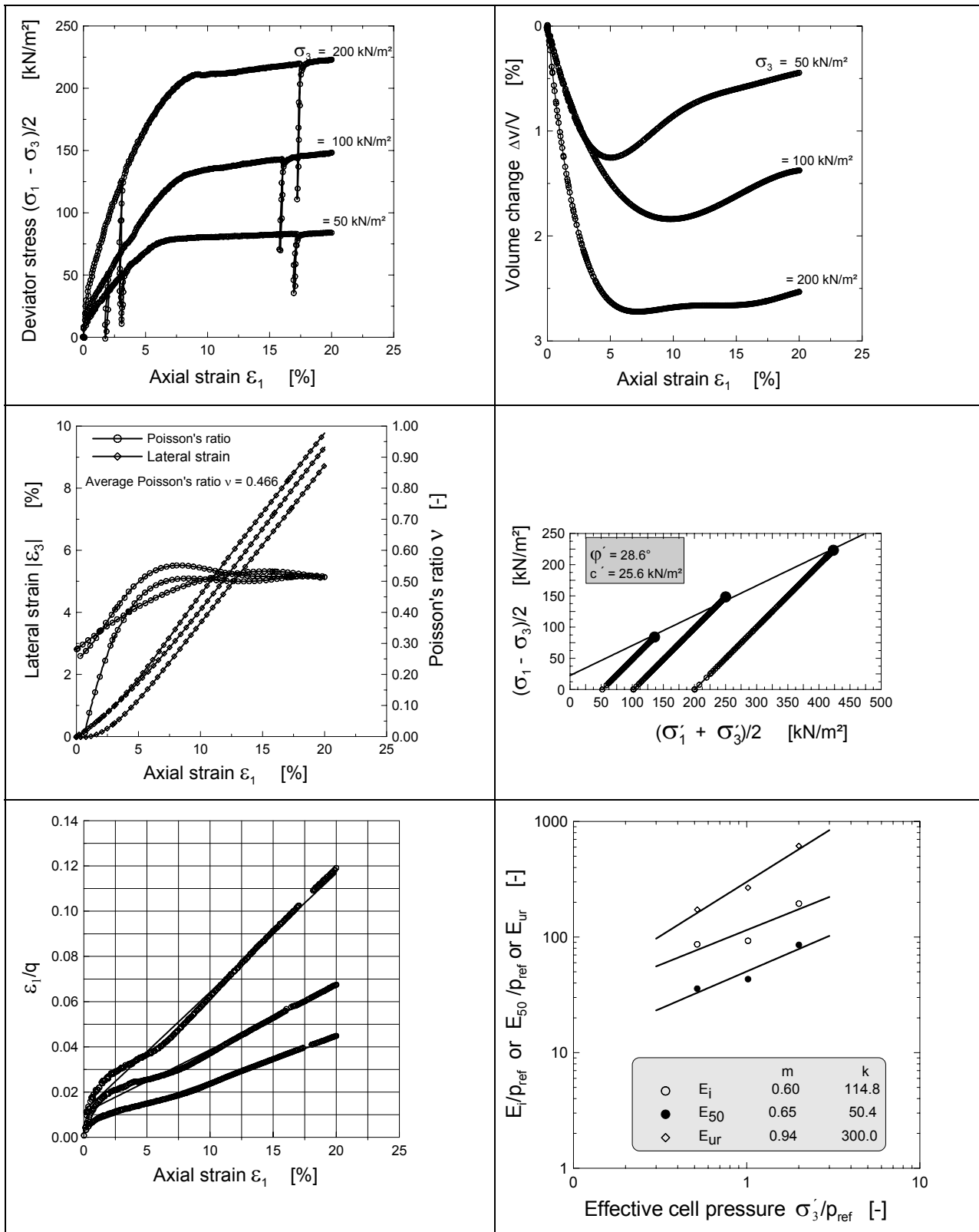
A.8 Isotropically consolidated drained triaxial test at site3

A.8.1 Fhkcid34
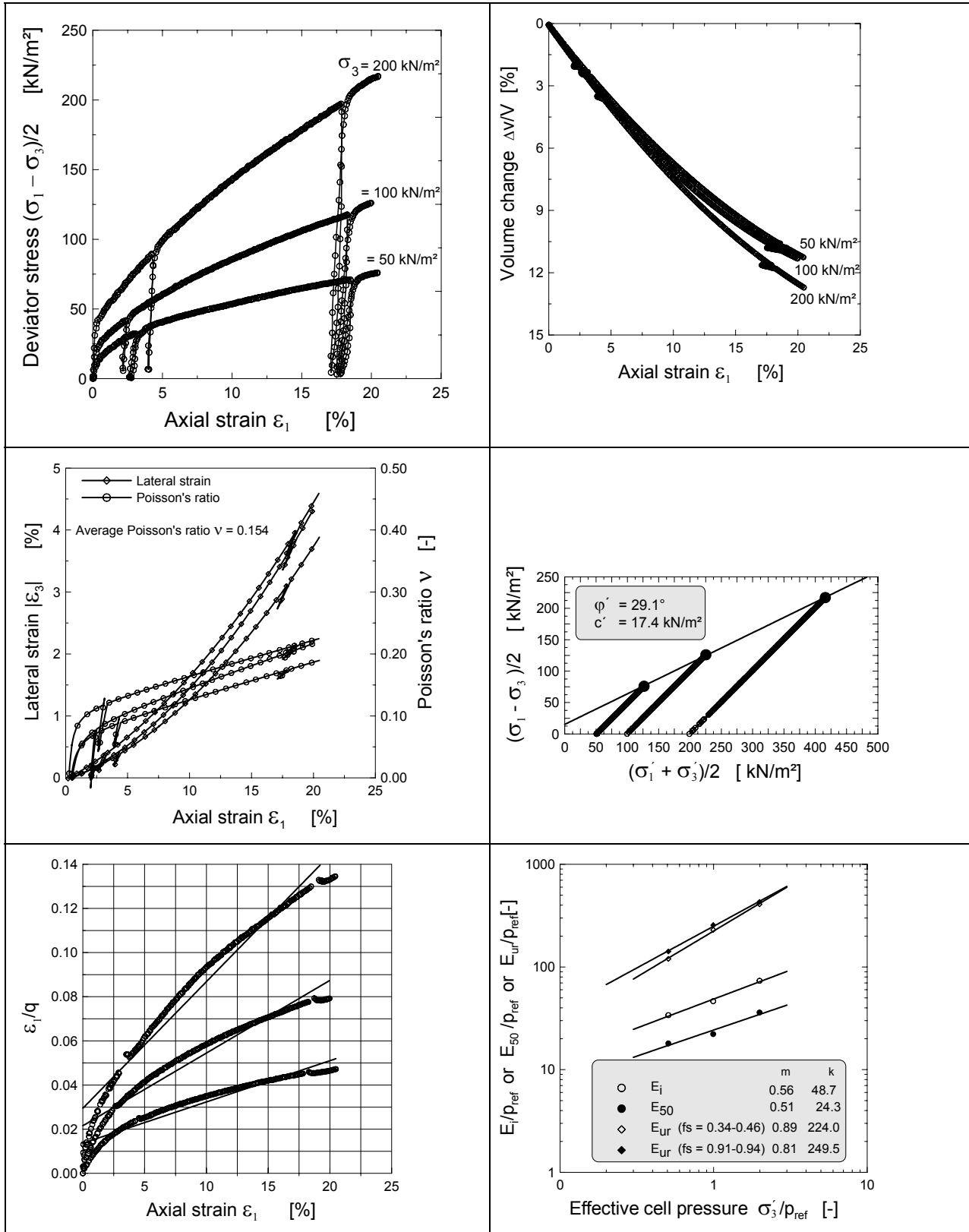
A.8.2 Fhkcid389 (Horizontally oriented samples)
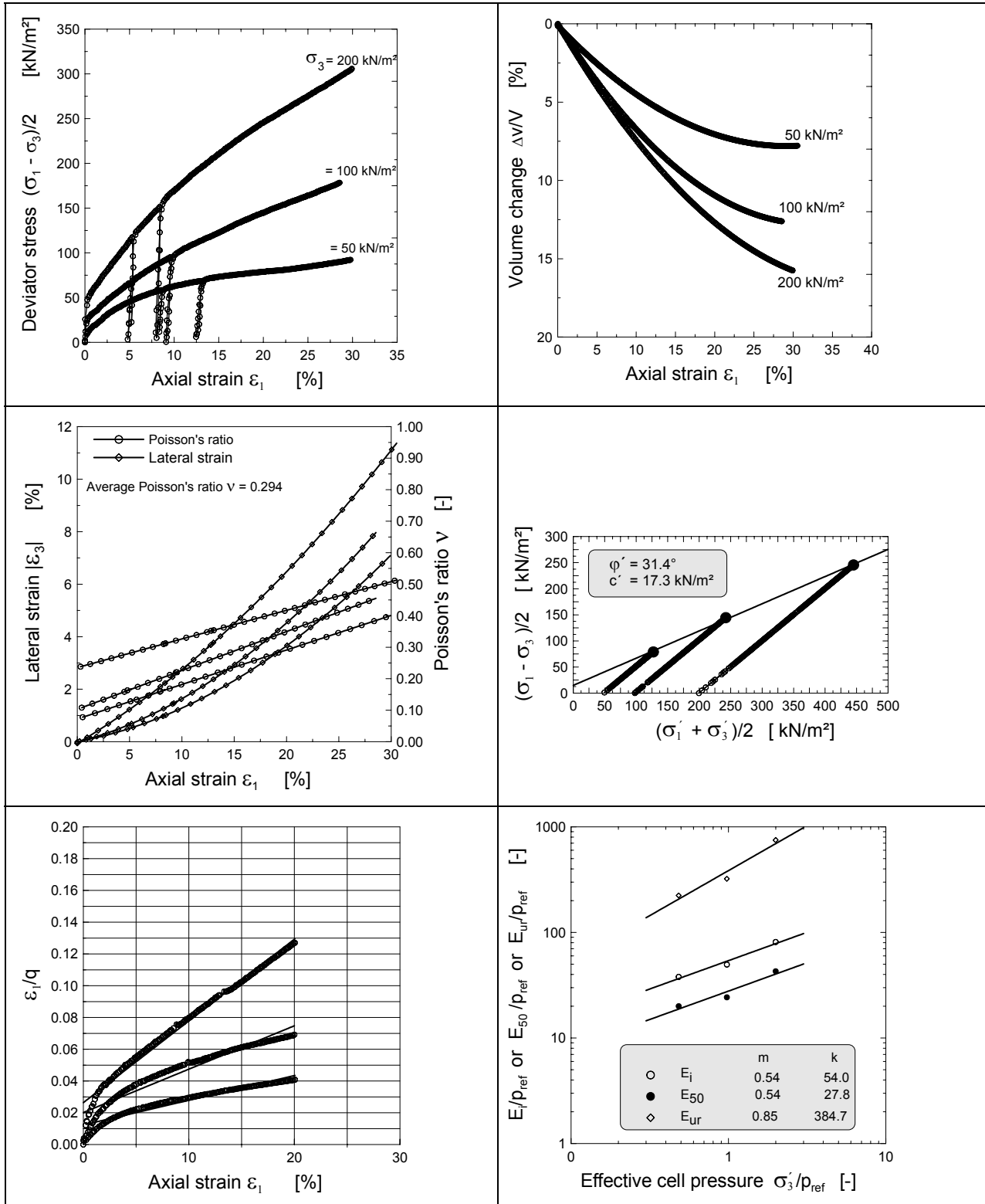
A.9 Isotropically consolidated undrained controlled stress path

A.9.1 Postulated stress path A
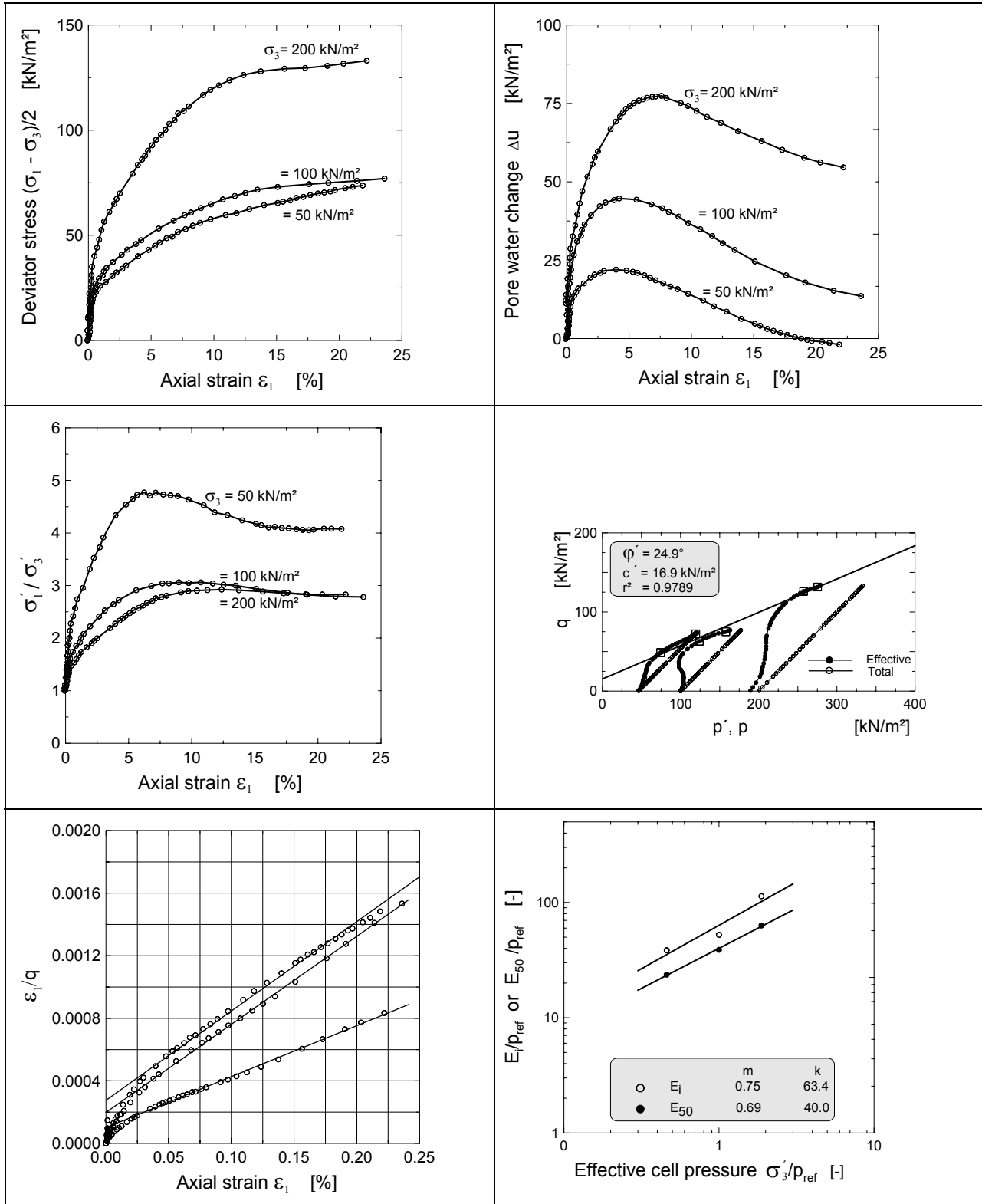
A.9.2 Postulated stress path B
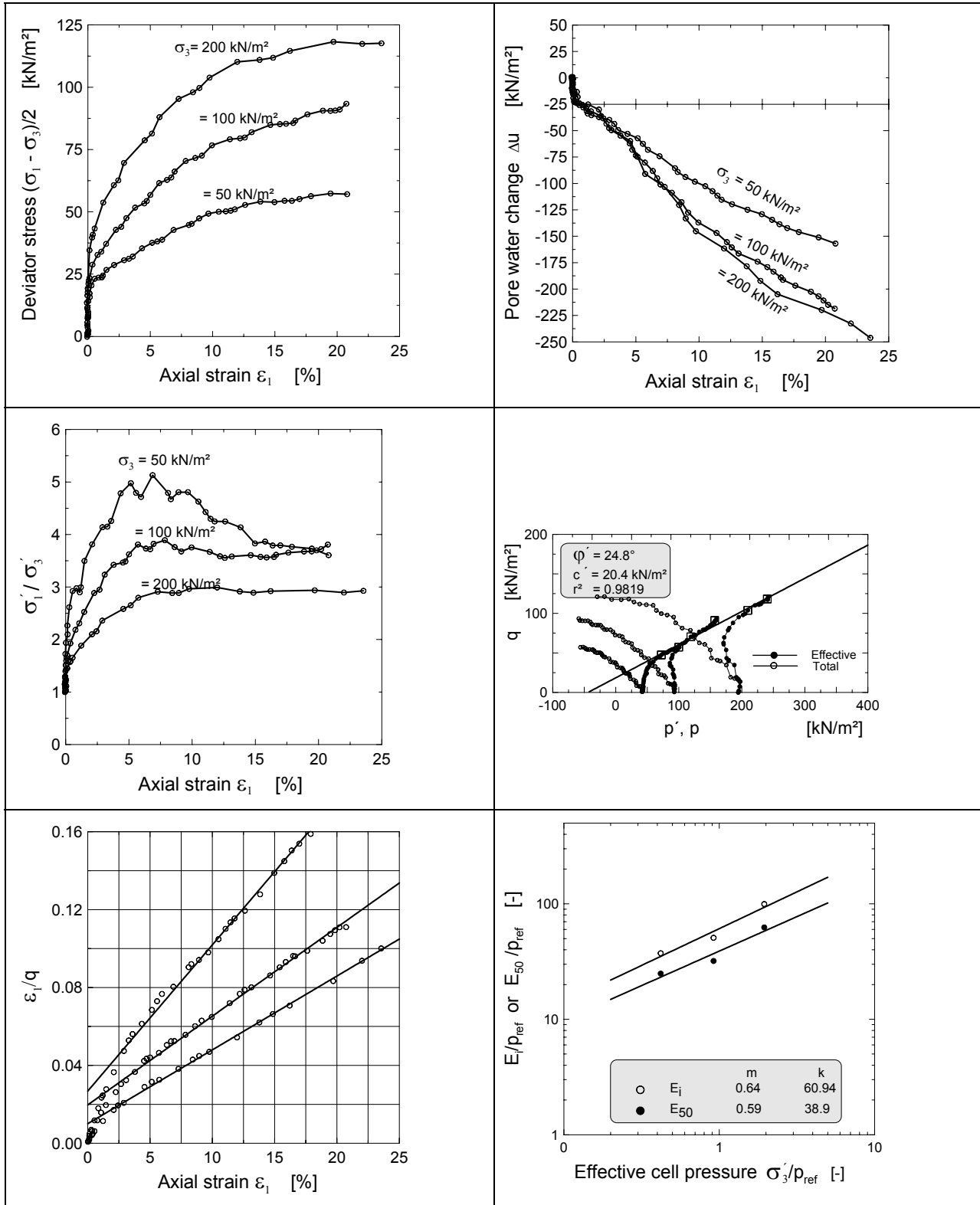
A.9.3 Postulated stress path C

A.10 Deformation parameters from CID tests

Test		Loading						Un/ re-loading			
		Tangent modulus			Secant modulus			Un/re-loading modulus			
	σ_3	E	m	k	E_{50}	m	k	E_{ur}	m	k	R_f
	[kN/m²]	[kN/m²]	[-]	[kN/m²]	[kN/m²]	[-]	[kN/m²]	[kN/m²]	[-]	[kN/m²]	[-]
Site1											
damcid05	50	4379			2180						0.84
	100	5104	0.30	53.0	2600	0.39	27.0				0.79
	200	6648			3600						0.79
damcid07	50	8307			3753						0.84
	100	8430	0.31	84.3	3844	0.51	38.3				0.88
	200	10495			5465						0.93
damcid15	50	4564			2409			11155			0.84
	100	5288	0.42	59.9	2838	0.45	32.3	17500	0.74	191.7	0.80
	230	9035			4984			36834			0.77
Site2											
maxcid01	50	3583			1745						0.82
	100	5003	0.72	56	2189	0.66	25.5				0.80
	200	9778			4357						0.83
maxcid05	50	2808			1482			8156			0.74
	100	4219	0.70	44.0	2316	0.71	23.6	11198	0.61	118.6	0.86
	200	7551			4000			19077			0.79
maxcid16/	50	4083			1620			12000/13400			0.86
maxcid15	100	6261			2581			12467/19133			0.87
	200	11866	0.52	64.0	4928	0.66	26.6	32167/40000	0.67/	167.1/	0.87
	300	11679			5424			34400/34750	0..67	206.9	0.82
	400	12385			6833			40556/50000			0.77
	500	13182			7000			50417/68333			0.76
maxcid	50	3098			1517						0.75
(remolded	100	3297	0.79	36.0	1967	0.84	19.1				0.69
samples)	200	6438			3331						0.76
maxcid13	50	8651			3576			17278			0.88
(horz.)	100	9275	0.60	114.8	4327	0.65	50.4	26704	0.94	300	0.83
	200	19485			8555			61419			0.87

Continued: A.10 Deformation parameters from CID test

Site3											
34fhk	50	3395			1800			12000/14154			0.87
	100	4640	0.56	48.7	2222	0.51	24.3	23000/25550	0.89/	224.0/	0.83
	200	7334			3600			40800/43000	0.81	249.5	0.81
36fhk	25	2823			1584						0.87
	50	3485	0.42	46.8	1867	0.38	24.8	22165/19667	0.79/	365.0/	0.86
	100	3893			2047			32000/26000	0.53	278.8	0.78
	200	7073			3674			68000/42000			0.76
389fhk	50	3791			2000			22400			0.81
(horz)	100	4961	0.54	54.0	2429	0.54	27.8	32200	0.85	384.7	0.79
	200	8120			4286			75000			0.76

The un/re-loading parameters in the shaded box are for stress level 0.58 - 0.71 and 0.79 - 1.00 respectively.

A.11 Deformation parameters from CIU tests

Test					$(\sigma'_1/\sigma'_3)_{max}$				$(\sigma_1 - \sigma_3)_{20\%}$			
	σ_3	E	m	k	E_{50}	R_f	m	k	E_{50}	R_f	m	k
	[kN/m²]	[kN/m²]	[-]	[kN/m²]	[kN/m²]	[kN/m²]	[-]	[kN/m²]	[kN/m²]	[kN/m²]	[-]	[kN/m²]
Site1												
damciu04	50	2285			1263	0.85			1263	0.85		
	100	4687	0.83	43.6	3013	0.82	1.21	30.6	2667	0.87	1.14	28.5
	200	8053			8000	0.85			7267	0.92		
damciu06	50	3594			3345	0.62			2120	0.88		
	100	11620	0.90	95.5	6720	0.94	0.92	76.9	6720	0.94	1.12	64.5
	200	14366			13867	0.86			11900	0.92		
damciu10	50	2840			3120	0.66			1619	0.87		
	100	5177	1.06	54.7	4622	0.73	0.78	49.7	2700	0.90	1.32	33.6
	200	10702			8244	0.92			4200	0.92		
damciu14	50	8304			6133	0.83			4800	0.95		
	100	10335	1.48	106	6133	0.91	1.58	72.3	5475	0.96	1.43	58.8
	200	28909			22000	0.85			15733	0.97		
damciu30	300	15023			14461	0.93			14461	0.93		
	400	23319	1.50	29.9	21184	0.94	1.25	37.8	21184	0.94	1.25	37.8
	500	33487			28194	0.94			28194	0.94		

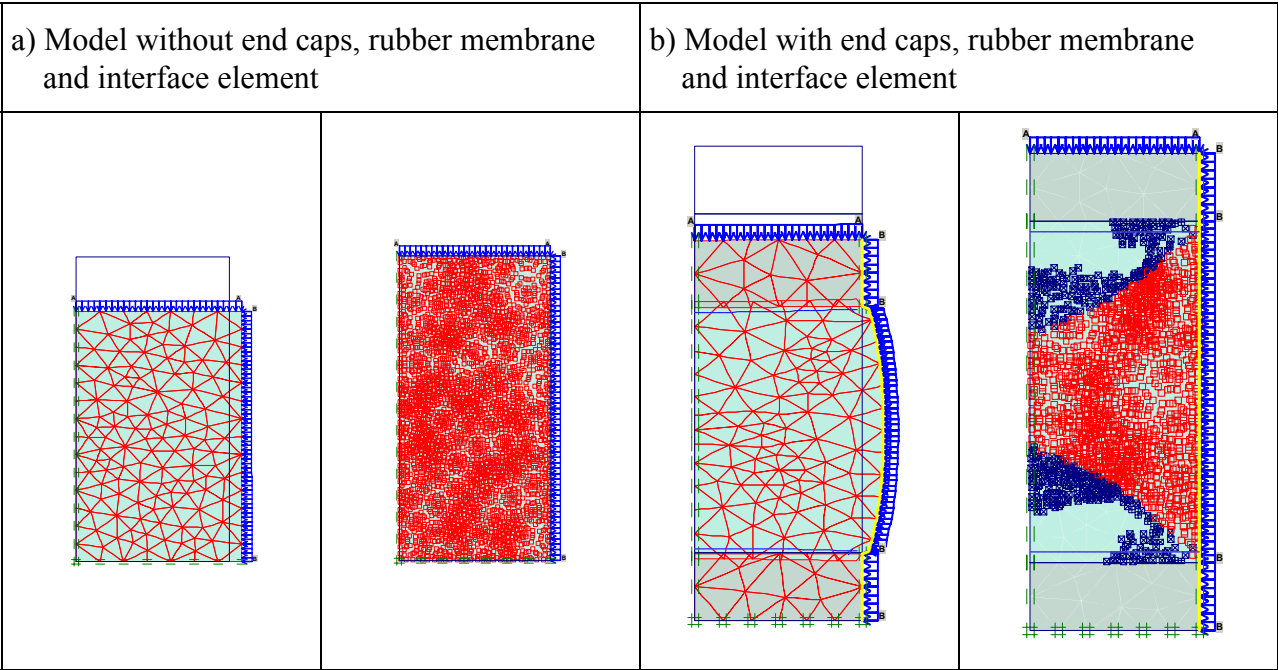*Continued: A.11 Deformation parameters from CIU test*

Site2												
maxciu02	50	2286			1778	0.58			1222	0.83		
	100	6061	0.99	67.1	4000	0.79	0.91	46.4	3445	0.90	1.11	40.4
	200	12268			8421	0.85			8222	0.85		
maxciu	50	1993			1405	0.51			1083	0.76		
	100	3278			2257	0.62			1592	0.80		
	200	5905	0.88	37.2	3682	0.68	0.76	24.6	2977	0.83	0.84	19.07
	300	8428			4607	0.81			3931	0.87		
	400	14804			8333	0.87			7478	0.91		
maxciu03 (horz.)	50	8364			5600	0.80			4483	0.97		
	100	12547	0.71	139.3	7400	0.86	0.51	79.7	6800	0.95	0.64	72.3
	200	23273			11557	0.92			11317	0.97		
Site3												
fhkciu35	50	13058			7364				7364	0.98		
	100	94648	1.73	515.6	14800		1.48	170.5	14800	0.99	1.48	170.5
	200	122751			49600				49600	1.00		
Others												
Jaegerk.	88	6068			6000	0.60						
	206	13313	0.86	68.6	14320	0.70	0.92	68.9				
	302	17161			18244	0.79						
Schwand	100	14213			10037	0.58			9400	0.91		
	196	17367	0.78	129.3	14044	0.71	0.57	98.7	13547	0.92	0.62	92.2
	295	34576			18627	0.86			18530	0.95		
Stromey.	100	5431			3342	0.72						
	200	11454	0.87	56.1	8634	0.77	0.98	35.7				
	300	13678			18963	0.81						

B Calibration of the hardening soil model parameters

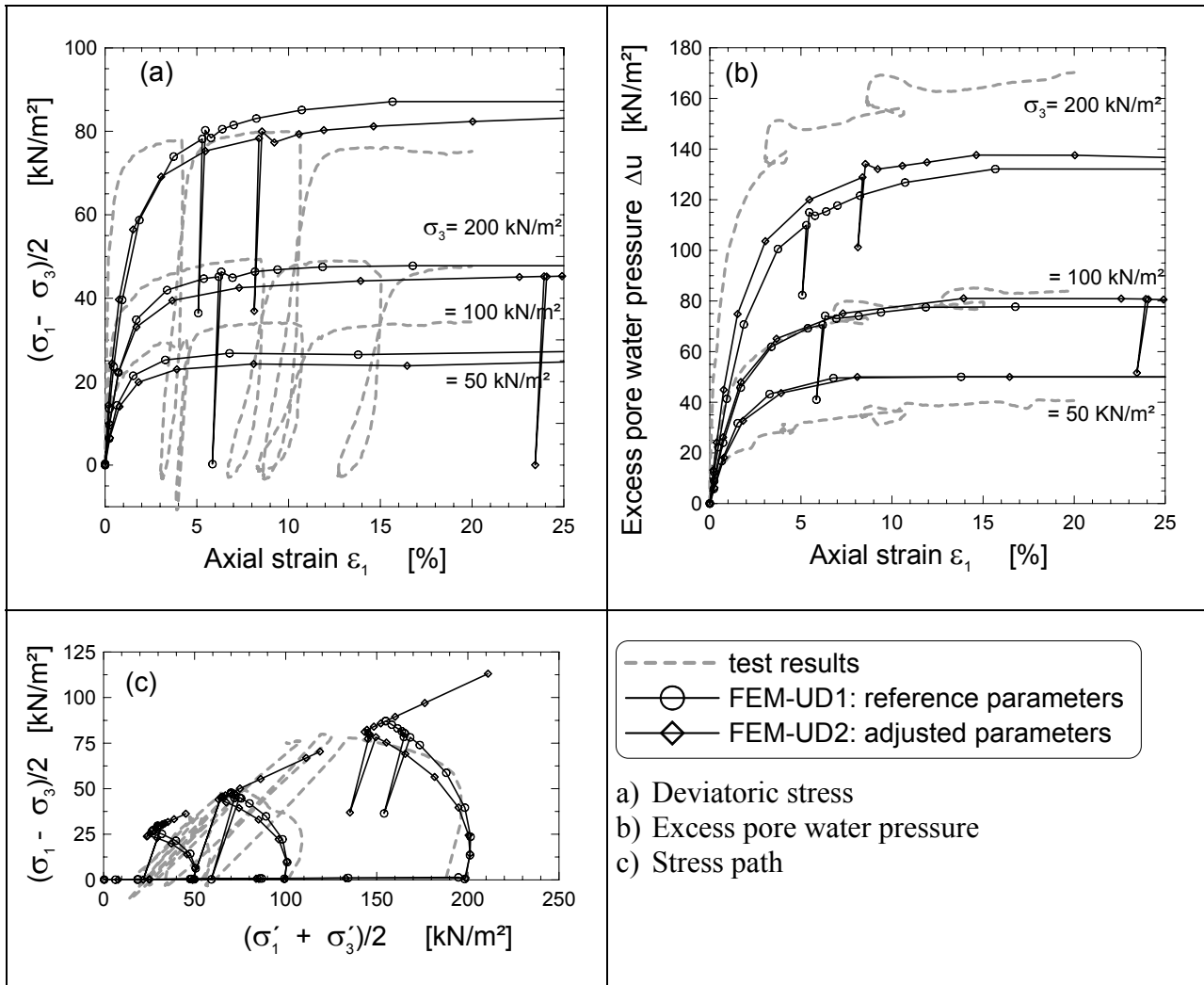## B.1 Geometry and the boundary conditions for a triaxial test FE-model

a) Model Geometry without end caps, rubber membrane and interface element	b) Model Geometry with end caps, rubber membrane and interface element
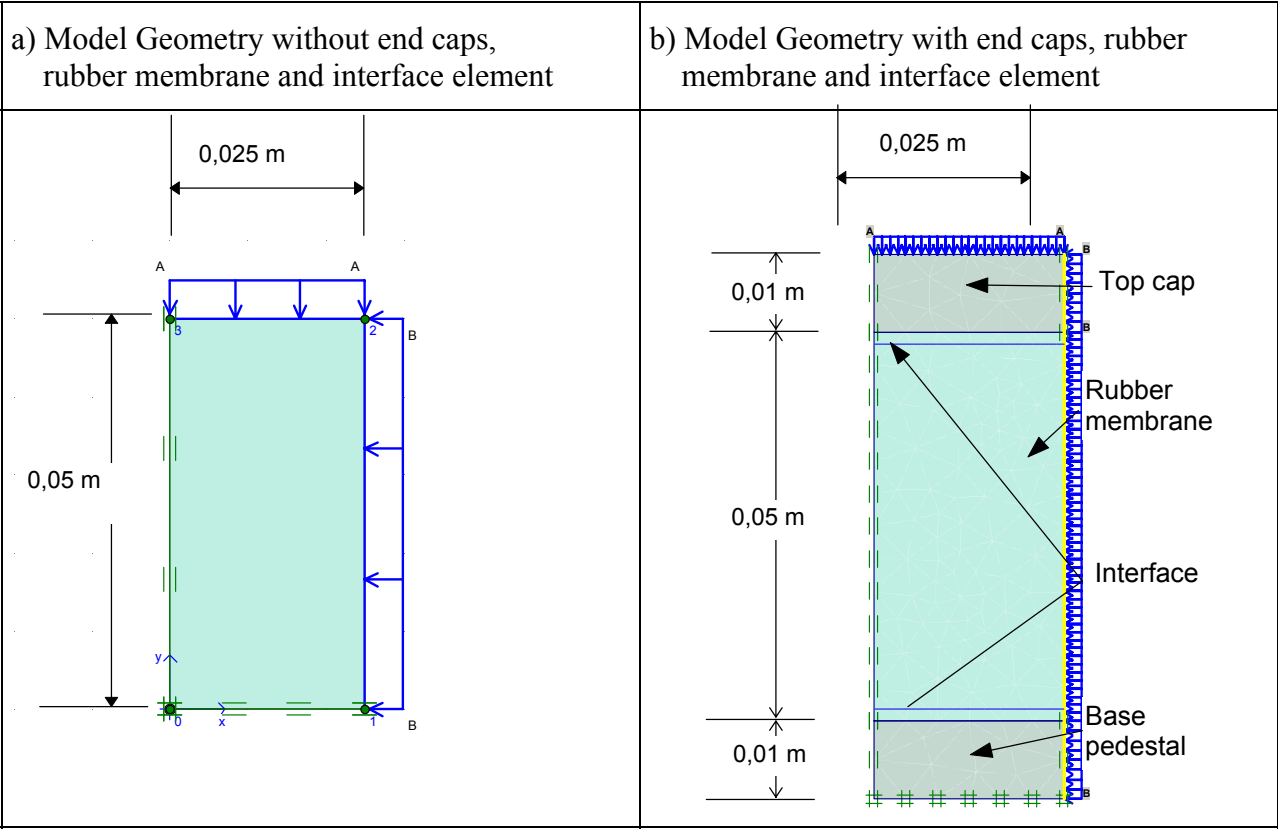
B.2 Deformed mesh and plastic points

a) Model without end caps, rubber membrane and interface element	b) Model with end caps, rubber membrane and interface element

B.3   Drained test at site 2

Calibration of parameters for a hard soil model at site 2 under drained condition

Case	γ	φ'	ψ'	c'	E_{50}^{ref}	E_{oed}^{ref}	E_{ur}^{ref}	p^{ref}	m	R_f	K_0^{nc}	ν_{ur}
	[kN/m³]	[°]	[°]	[kN/m²]	[kN/m²]	[kN/m²]	[kN/m²]	[kN/m²]	[-]	[-]	[-]	[-]
FEM-1	19.5	23.2	0	20.1	2523	3054	14285	100	0.95	0.82	0.606	0.20
FEM-2	same as FEM-1, but $E_{50}^{ref}=3785\ kN/m^2$, $E_{oed}^{ref}=2901\ kN/m^2$, $K_o^{nc}=0.629$, $m=0.90$, $\nu_{ur}=0.05$											

B.4 Drained test at site 3

a) Deviatoric stress versus axial strain in triaxial test

b) Stress -strain diagram in oedometer test

c) Volume change behaviour in triaxial test

Legend:
- - - - Test results
- ○ FEM-1: reference parameters
- △ FEM-2: adjusted parameters
- ◇ FEM-3: adjusted parameters

Calibration of parameters for a hard soil model at site 3 under drained condition

Case	γ	φ'	ψ'	c'	E_{50}^{ref}	E_{oed}^{ref}	E_{ur}^{ref}	p^{ref}	m	R_f	K_0^{nc}	ν_{ur}
	[kN/m³]	[°]	[°]	[kN/m²]	[kN/m²]	[kN/m²]	[kN/m²]	[kN/m²]	[-]	[-]	[-]	[-]
FEM-1	15.3	27.6	0	17.3	2455	1763	29450	100	0.62	0.83	0.537	0.20
FEM-2	same as FEM-1, but, $m=1.0$, $K_o^{nc}=0.574$, $R_f=0.70$, and $\nu_{ur}=0.05$											
FEM-3	same as FEM-2, but with two step of loading: $E_{50}^{ref}=2*2455=4910\ kN/m^2$ up to an axial strain of 0.5% and thereafter with $E_{50}^{ref}=2455\ kN/m^2$ till failure											

B.5   Undrained test at site 2

Calibration of parameters for a hard soil model at site 2 under undrained condition

Case	γ	φ'	ψ'	c'	E_{50}^{ref}	E_{oed}^{ref}	E_{ur}^{ref}	p^{ref}	m	R_f	K_0^{nc}	ν_{ur}
	[kN/m³]	[°]	[°]	[kN/m²]	[kN/m²]	[kN/m²]	[kN/m²]	[kN/m²]	[-]	[-]	[-]	[-]
FEM-UD1	reference parameters: the same as FEM-1 in Appendix B3 (drained condition)											
FEM-UD2	adjusted parameters: the same as FEM-2 in Appendix B3 (drained condition)											

B.6 Undrained test at site 3

Calibration of parameters for a hard soil model at site 3 under undrained condition

Case	γ	φ'	ψ'	c'	E_{50}^{ref}	E_{oed}^{ref}	E_{ur}^{ref}	p^{ref}	m	R_f	K_0^{nc}	ν_{ur}
	[kN/m³]	[°]	[°]	[kN/m²]	[kN/m²]	[kN/m²]	[kN/m²]	[kN/m²]	[-]	[-]	[-]	[-]
FEM-UD1	reference parameters: the same as FEM-1 in Appendix B4 (drained condition)											
FEM-UD2	adjusted parameters: the same as FEM-2 in Appendix B4 (drained condition)											

B.7   Controlled stress path B

Calibration of parameters for a hard soil model at site 2 under a controlled stress path B (undrained)

Case	γ	φ'	ψ'	c'	E_{50}^{ref}	E_{oed}^{ref}	E_{ur}^{ref}	p^{ref}	m	R_f	K_0^{nc}	v_{ur}
	[kN/m³]	[°]	[°]	[kN/m²]	[kN/m²]	[kN/m²]	[kN/m²]	[kN/m²]	[-]	[-]	[-]	[-]
FEM-SP-B1	reference parameters: the same as FEM-1 in Appendix B3 (drained condition)											
FEM-SP-B2	adjusted parameters: the same as FEM-2 in Appendix B3 (drained condition)											

C   Comparative analytical and numerical analysis of the draft recommendation for excavations in soft soils "EAB"

C.1   Results of preliminary analytical analysis (end of excavation)

case 1a to 2b: without ground water but drained (Table 9.2)
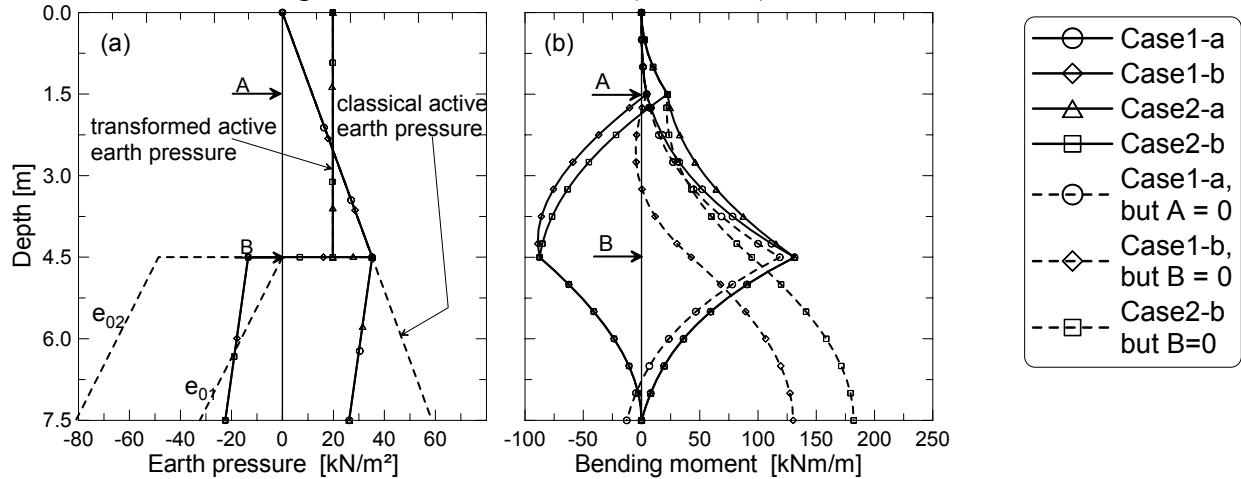
case 3a-1 to 3b-2, case 4a and case 4b: without groundwater and undrained (Table 9.2)
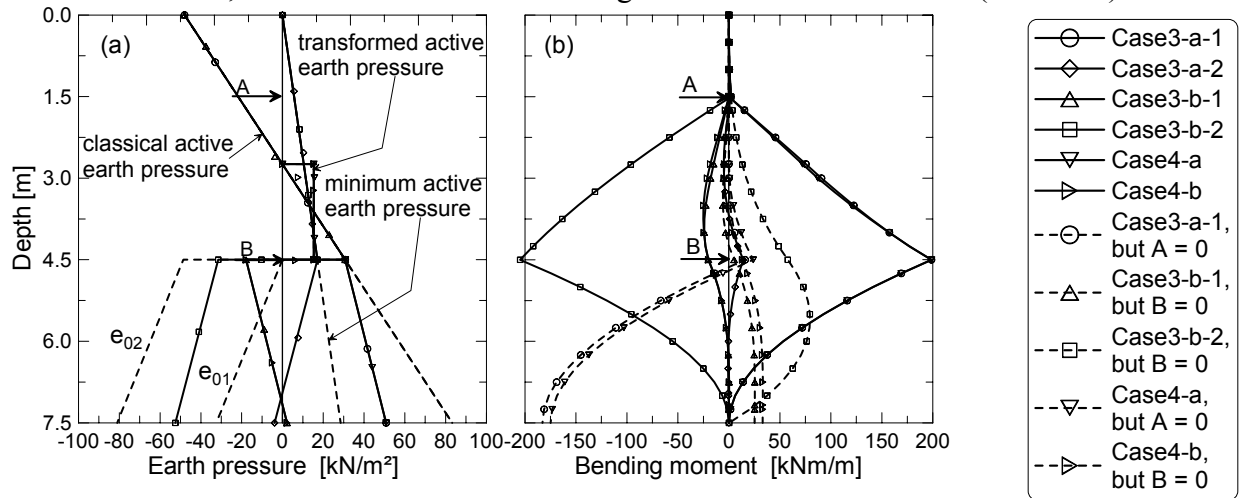
case 3-1a-1 to 3-1b-2, case 4-1a and case 4-1b: with groundwater and undrained (Table 9.2)
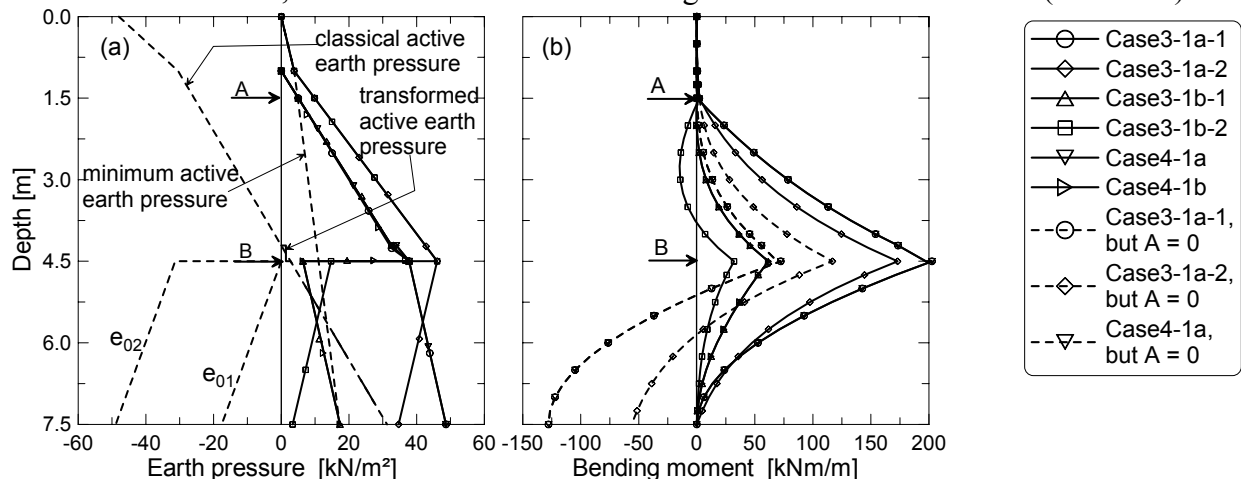
C.2 Results of the preliminary numerical analysis (end of excavation)

Variant-1ad to 4ad: without groundwater, without pre-stress, drained
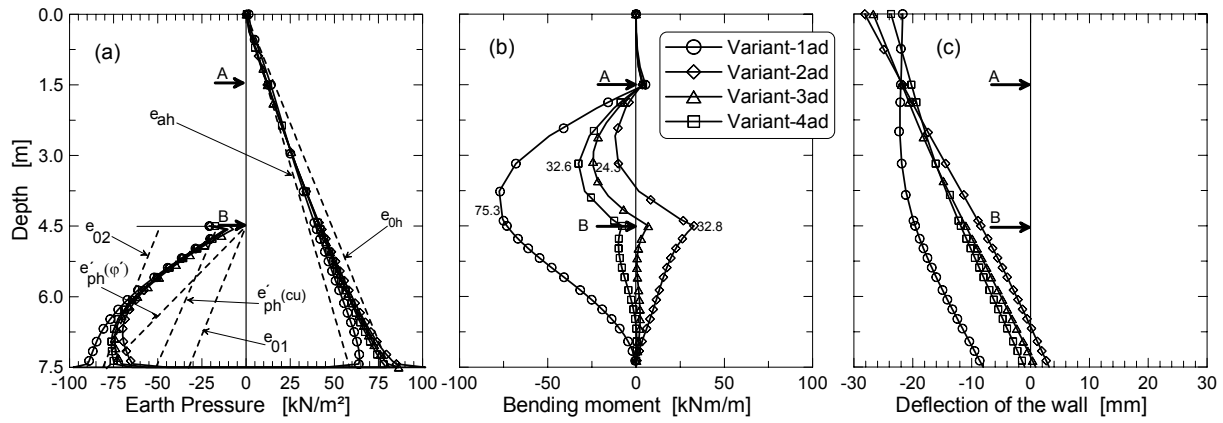
Variant-1bd to 4bd: without groundwater, with pre-stress, drained
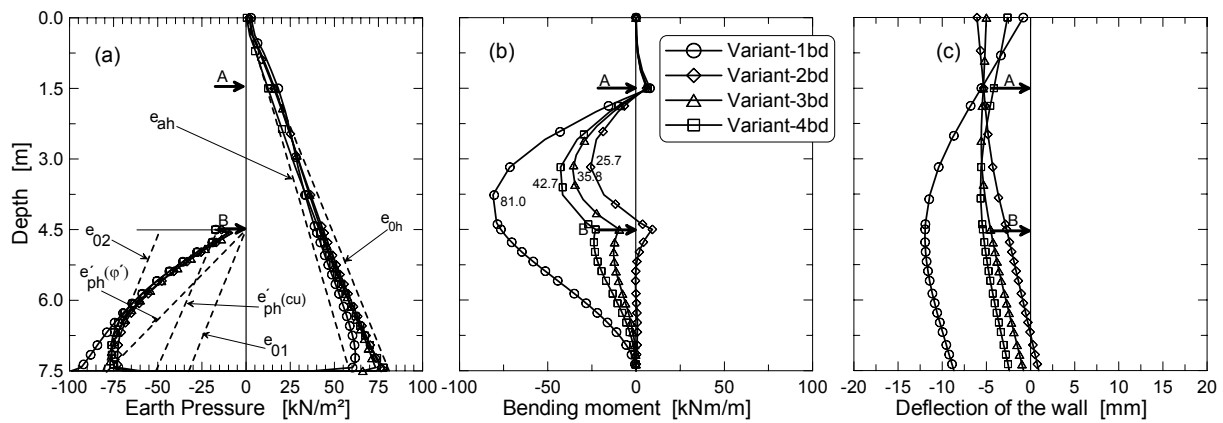
Variant-1au to 4au: without groundwater, without pre-stress, undrained
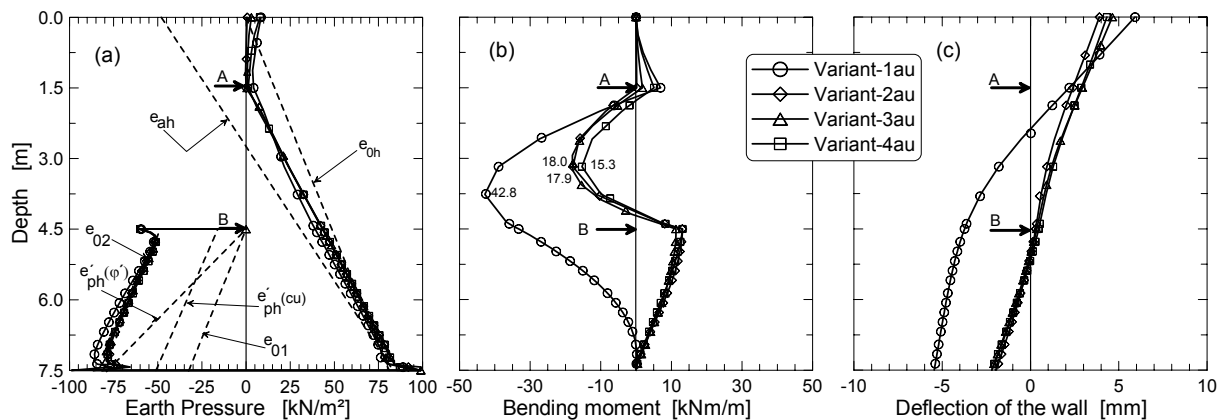
Variant-1bu to 4bu: without groundwater, with pre-stress, undrained
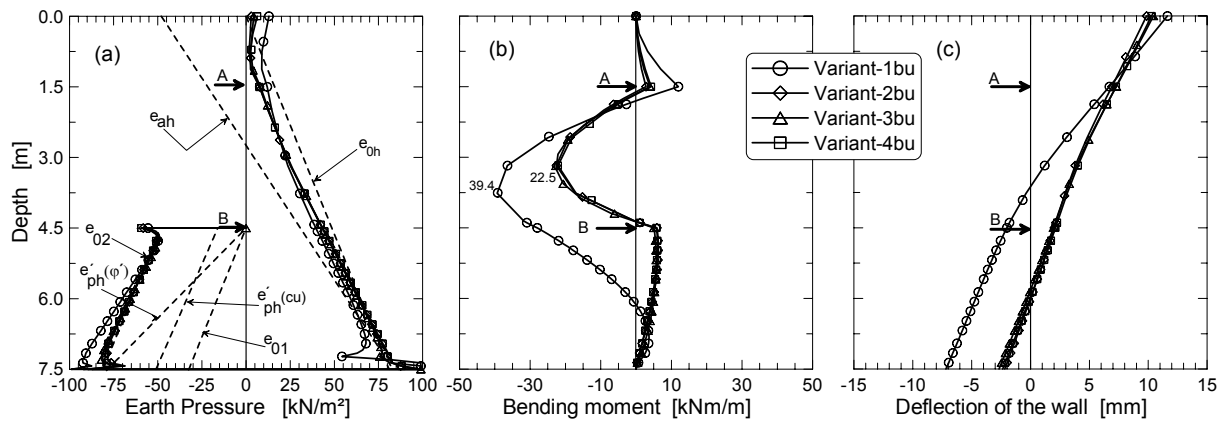
Variant-1awu to 4awu: with groundwater, without pre-stress, undrained
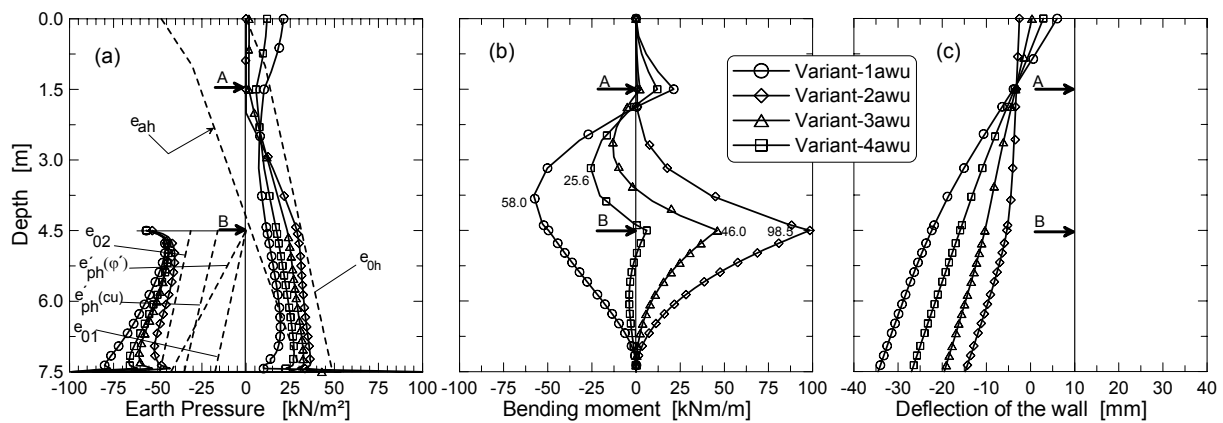
Variant-1bwu to 4bwu: with groundwater, with pre-stress, undrained
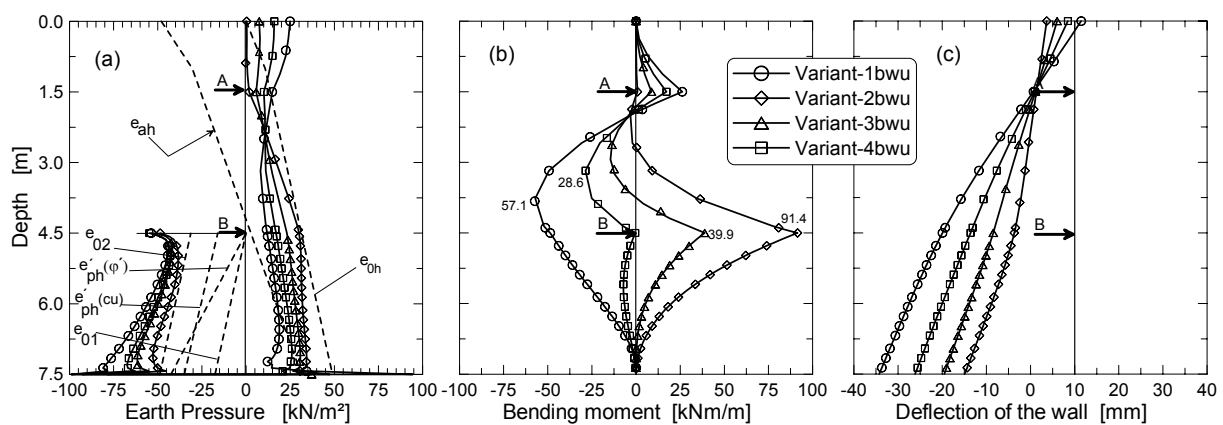
C.3 Results of the second round of the analytical and numerical analysis

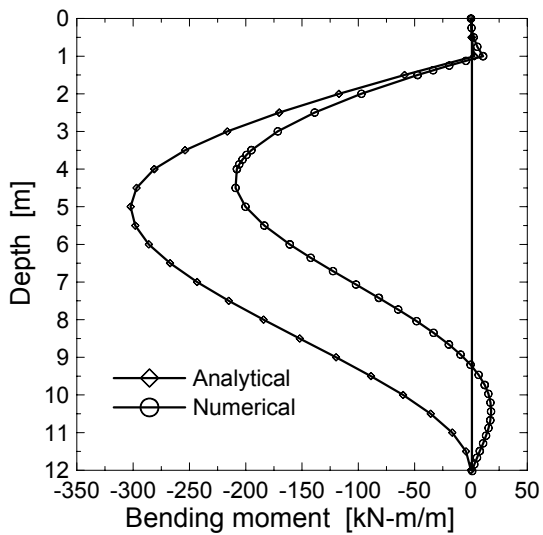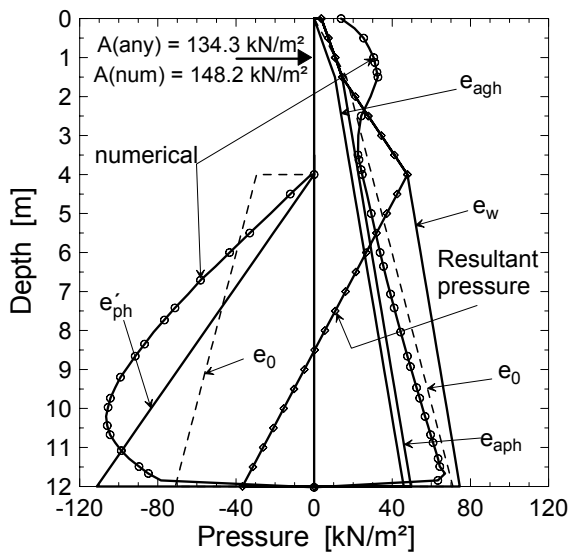| Case 2: without groundwater, 2nd excavation stage, R_{inter} = 0.5	Case 2: without groundwater, final excavation stage, R_{inter} = 0.5

Case 2: without groundwater, 2nd excavation stage, R_{inter} = 0.5

A(ana) = 25.7 kN/m
A(num) = 30.0 kN/m

Earth pressure (analy.)
Net earth pressure (analy.)
Earth pressure at rest
Earth pressure (num.)

Case 2: without groundwater, final excavation stage, R_{inter} = 0.5

A(ana) = 30.1 kN/m
A(num) = 40.92 kN/m

B(ana) = 33.9 kN/m
B(num) = 50.4 kN/m

Earth pressure (analy.)
Net earth pressure (analy.)
Earth pressure at rest
Earth pressure (num.)

Case 1: with groundwater, final excavation stage, $R_{inter} = 0.5$	Case 1: without groundwater, final excavation stage, $R_{inter} = 0.5$

Case 1: with groundwater, final excavation stage, $R_{inter} = 0.5$

A(ana) = 119.6 kN/m
A(num) = 132.4 kN/m

Earth pressure (analy.)
Net earth pressure (analy.)
Earth pressure at rest
Earth pressure (num.)

222.6
198.2

Analytical
Numerical

94.3
25.7

Case 1: without groundwater, final excavation stage, $R_{inter} = 0.5$

A(ana) = 44.5 kN/m
A(num) = 62.6 kN/m

Earth pressure (analy.)
Net earth pressure (analy.)
Earth pressure at rest
Earth pressure (num.)

63.2
48.5

Analytical
Numerical

C.4   Results of the 3rd round of the analytical and numerical analysis

Case Ia: 2nd excavation	Case-Ia: final excavation

Case Ib: 2nd excavation	Case-Ib: final excavation
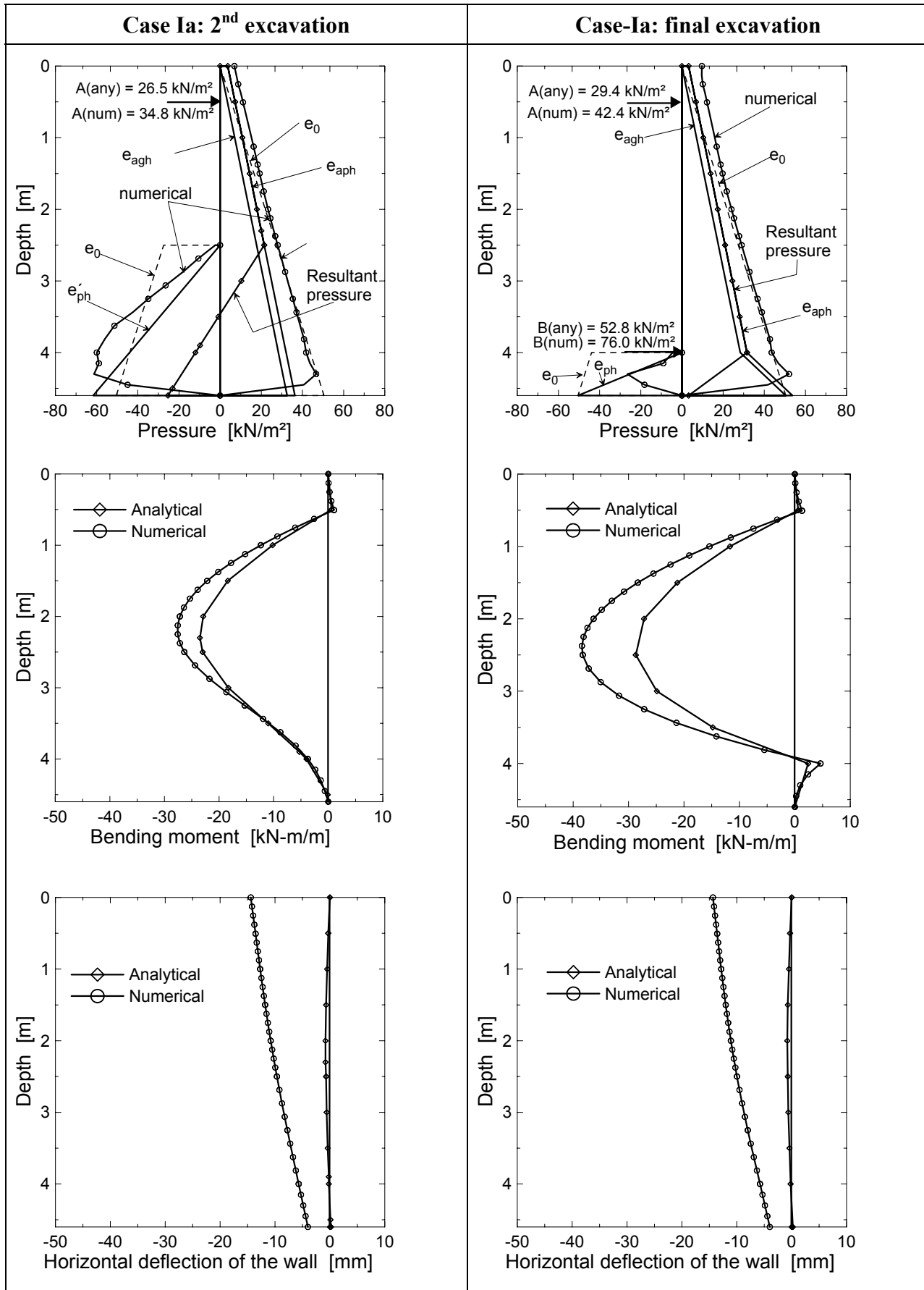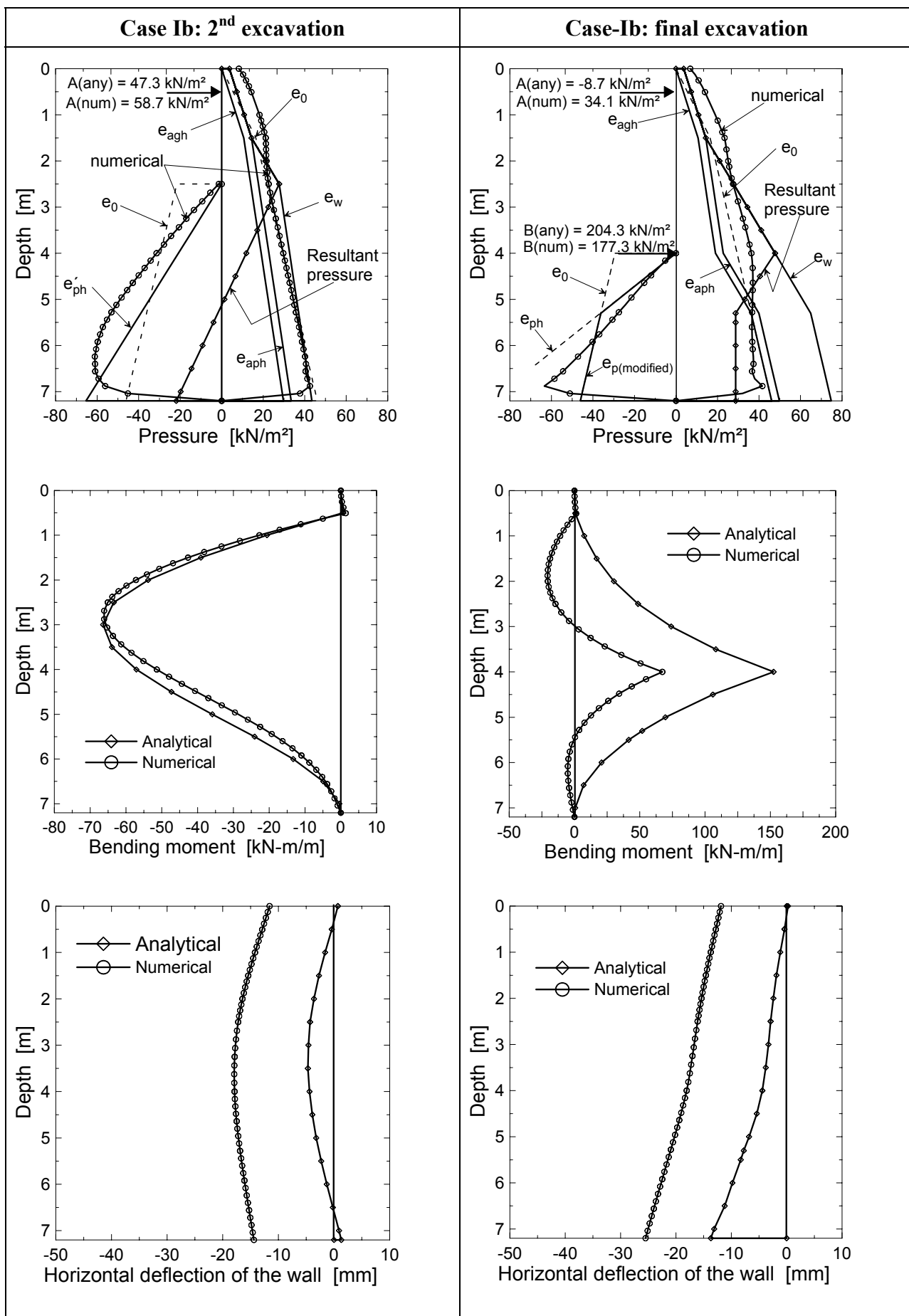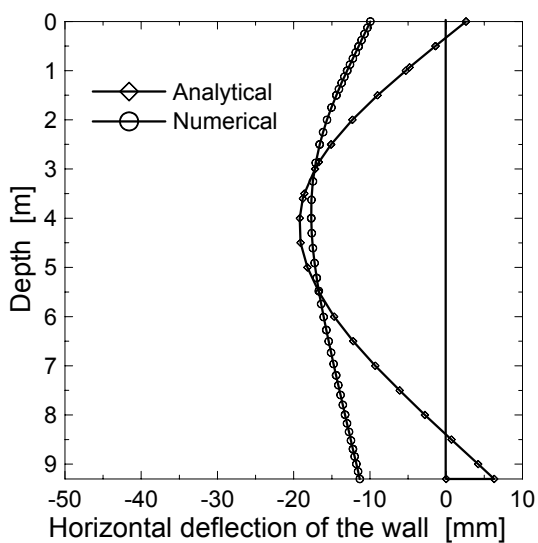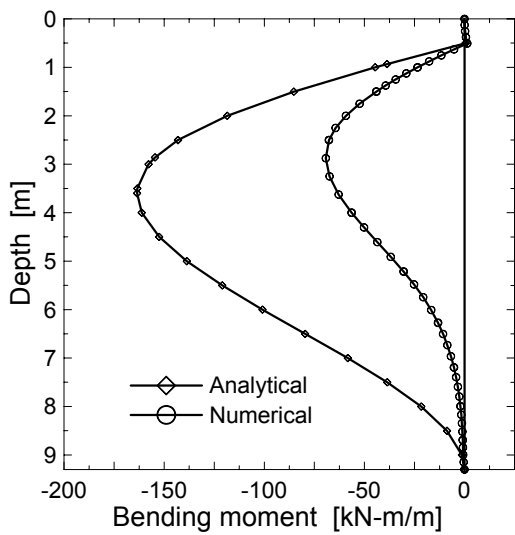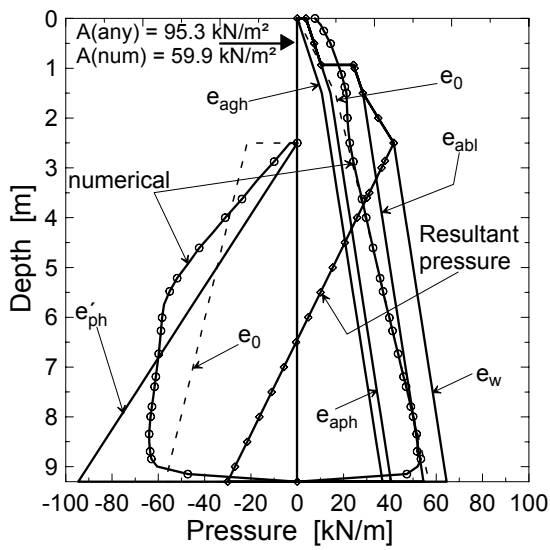
Case Ic: 2nd excavation	Case-Ic: final excavation
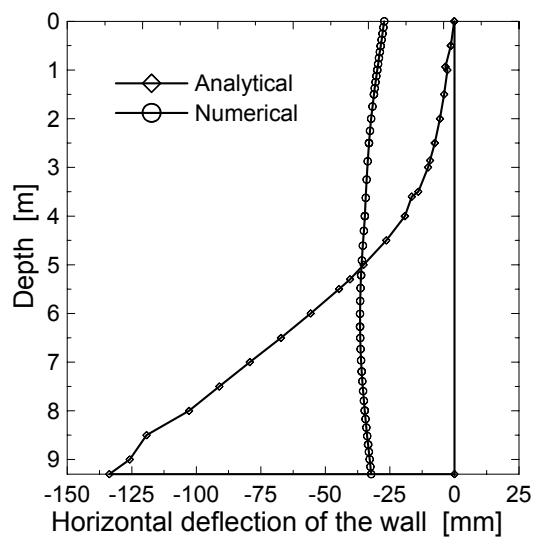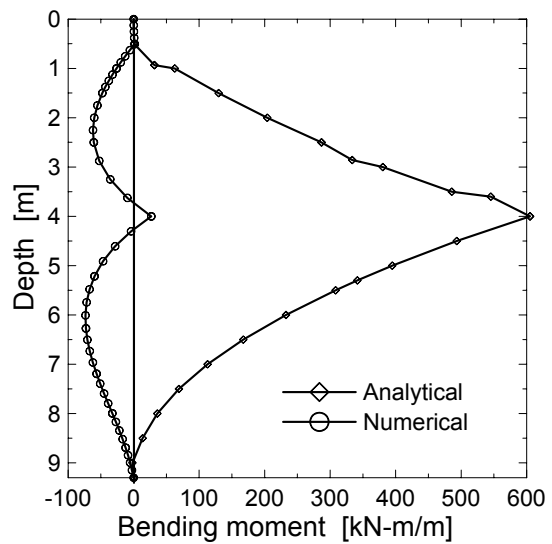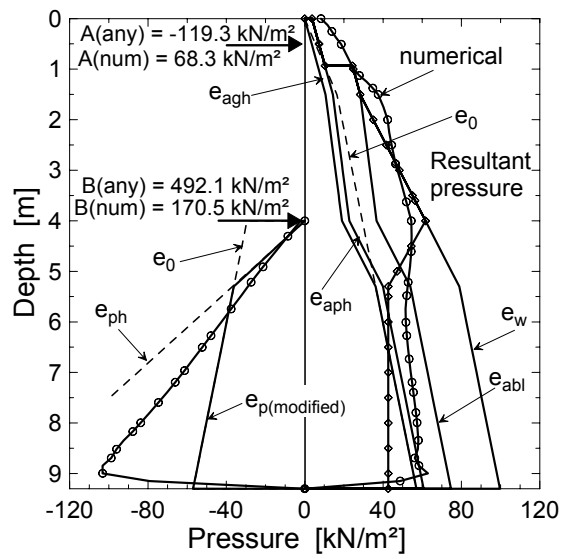
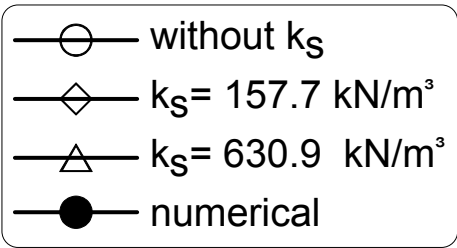| Case IIa: 2nd excavation	Case-IIa: final excavation
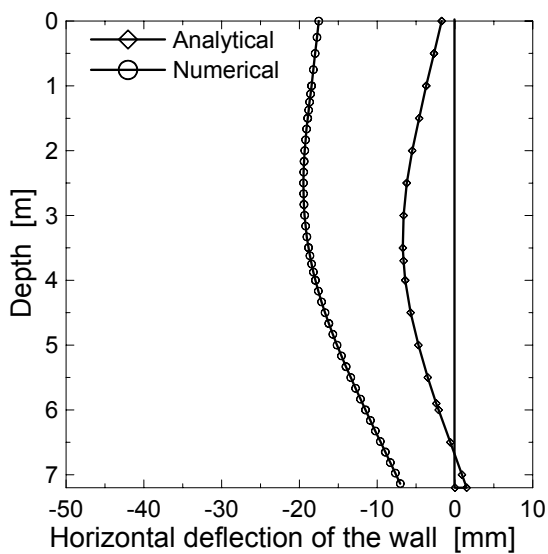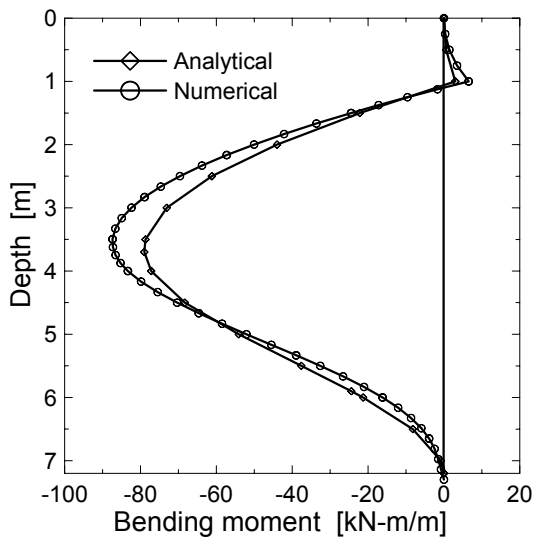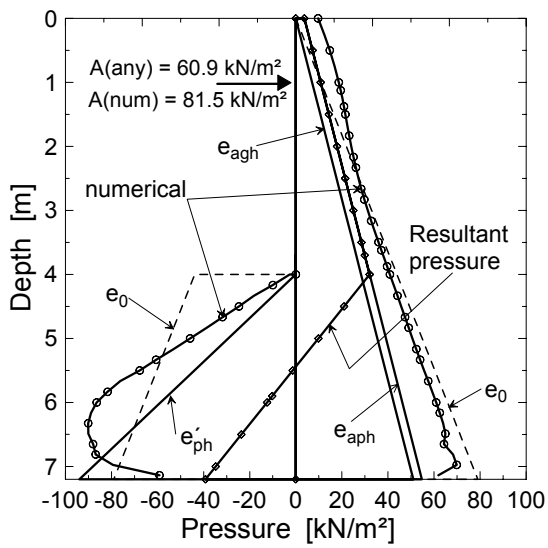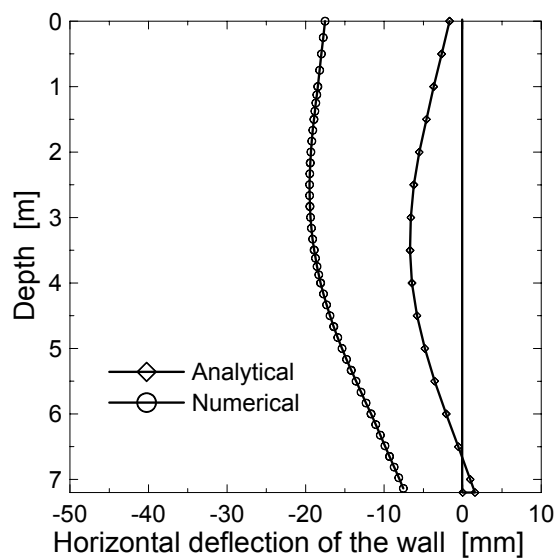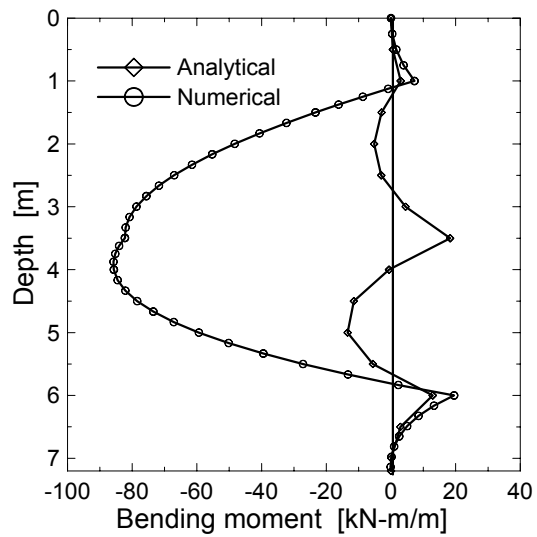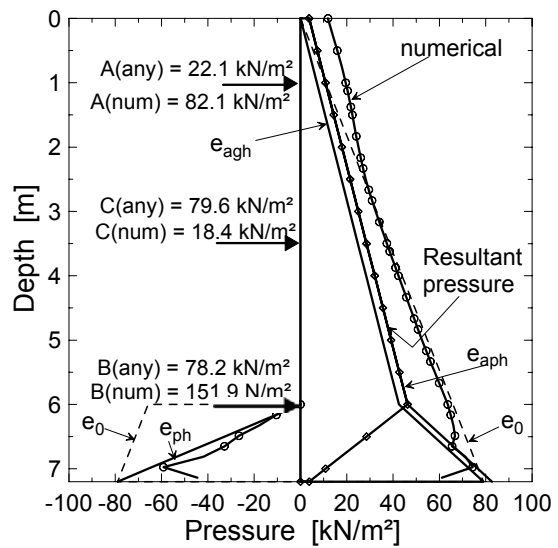
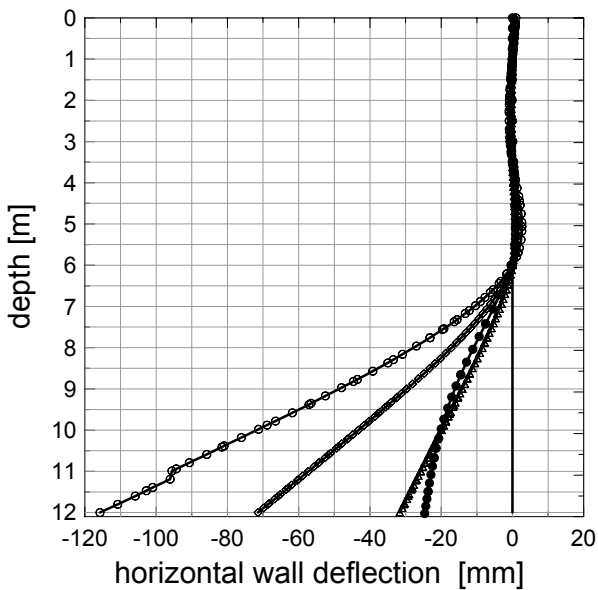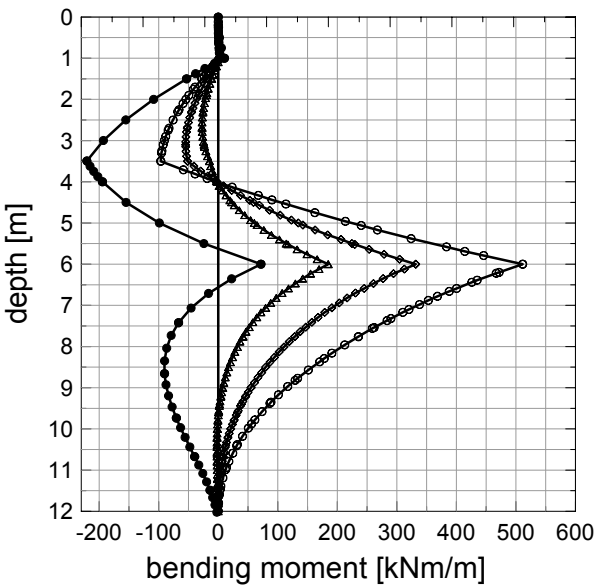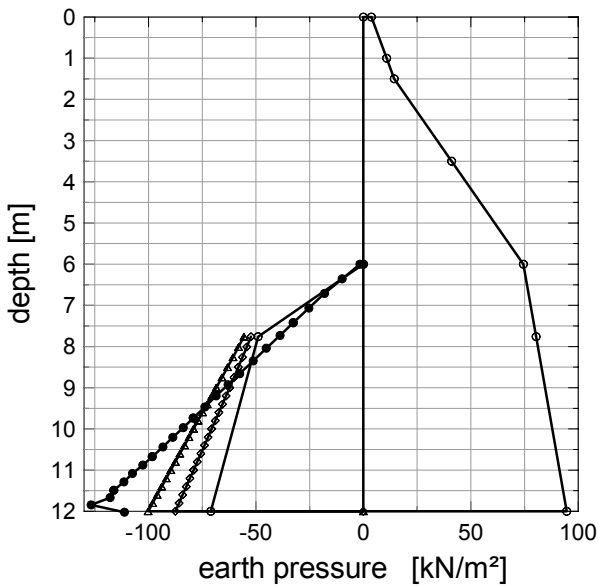| Case IIb: 2nd excavation	Case-IIb: final excavation
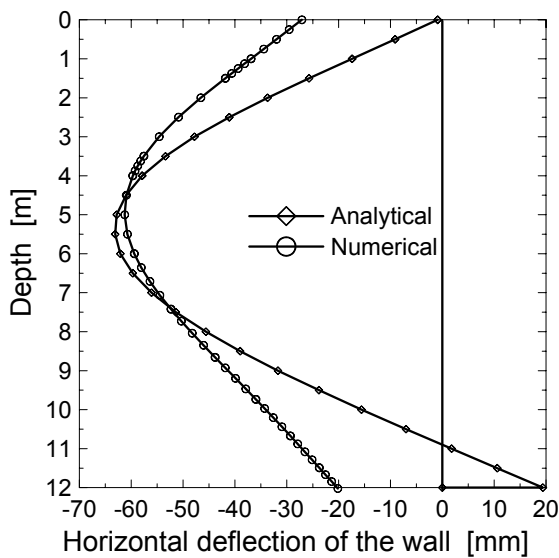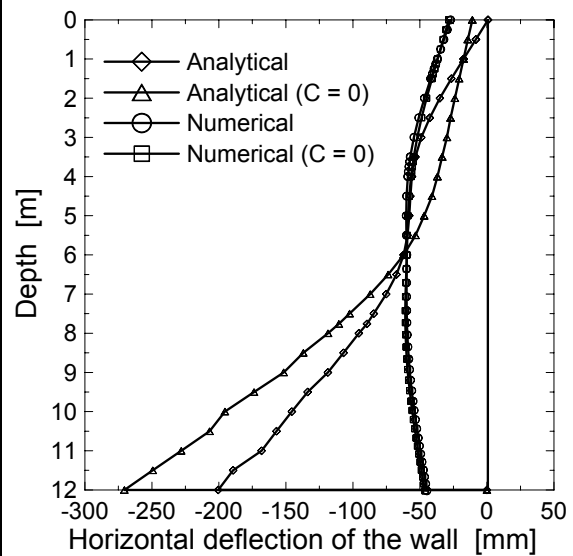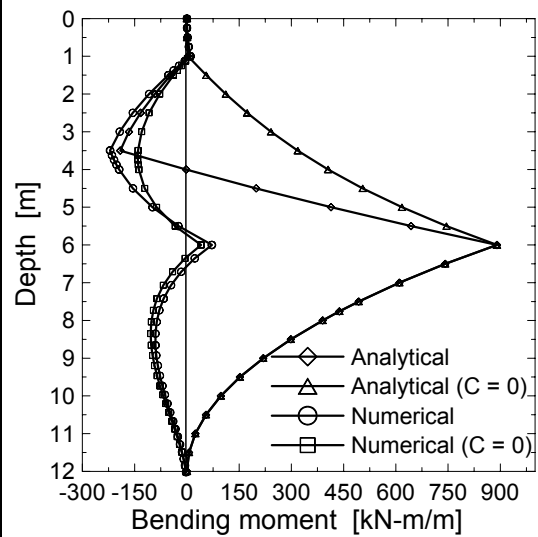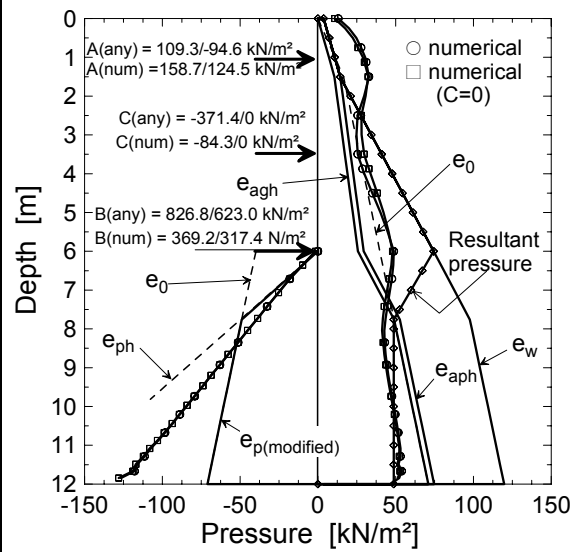
C.5   The use of the modulus of the subgrade reaction
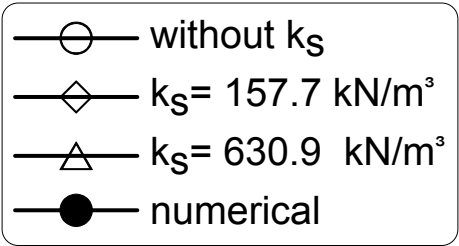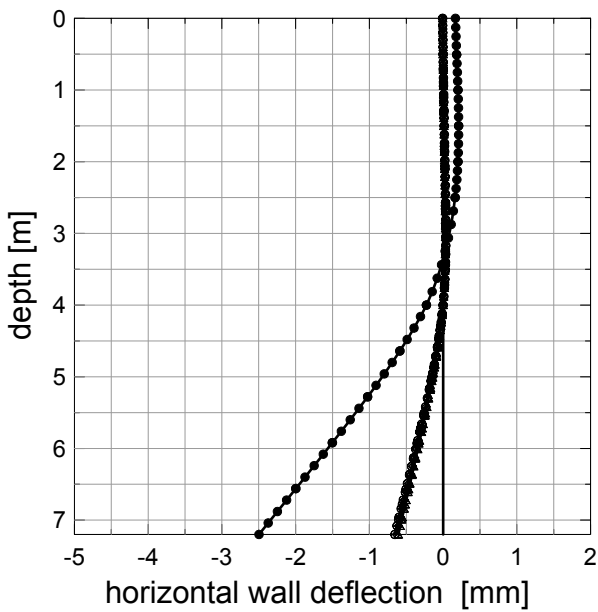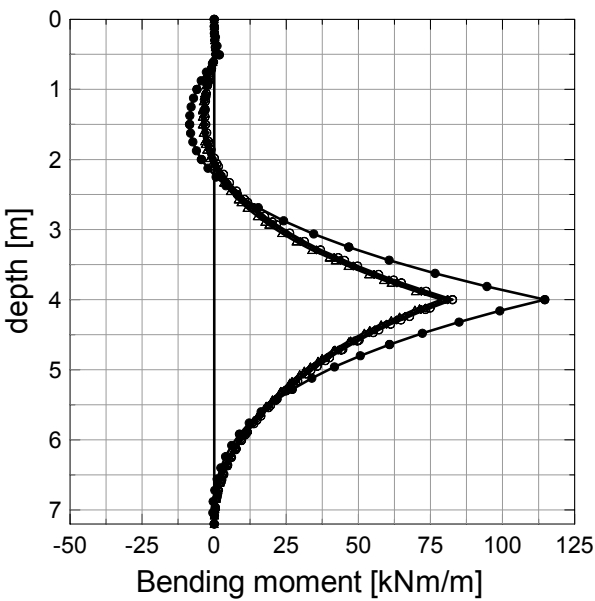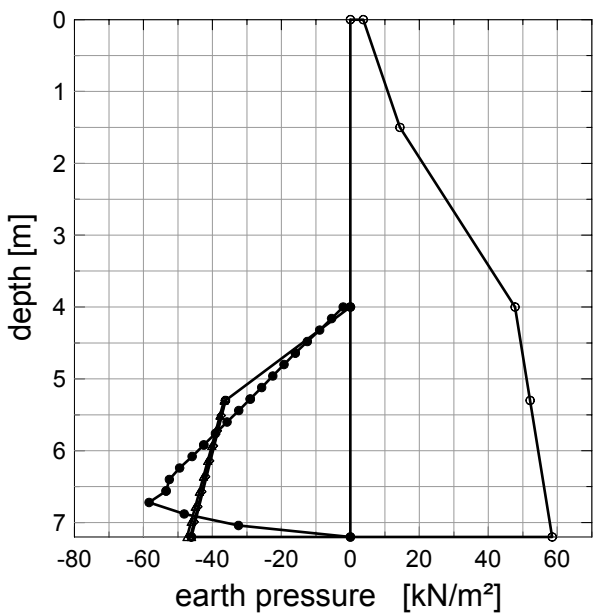
Case-Ib: Final excavation
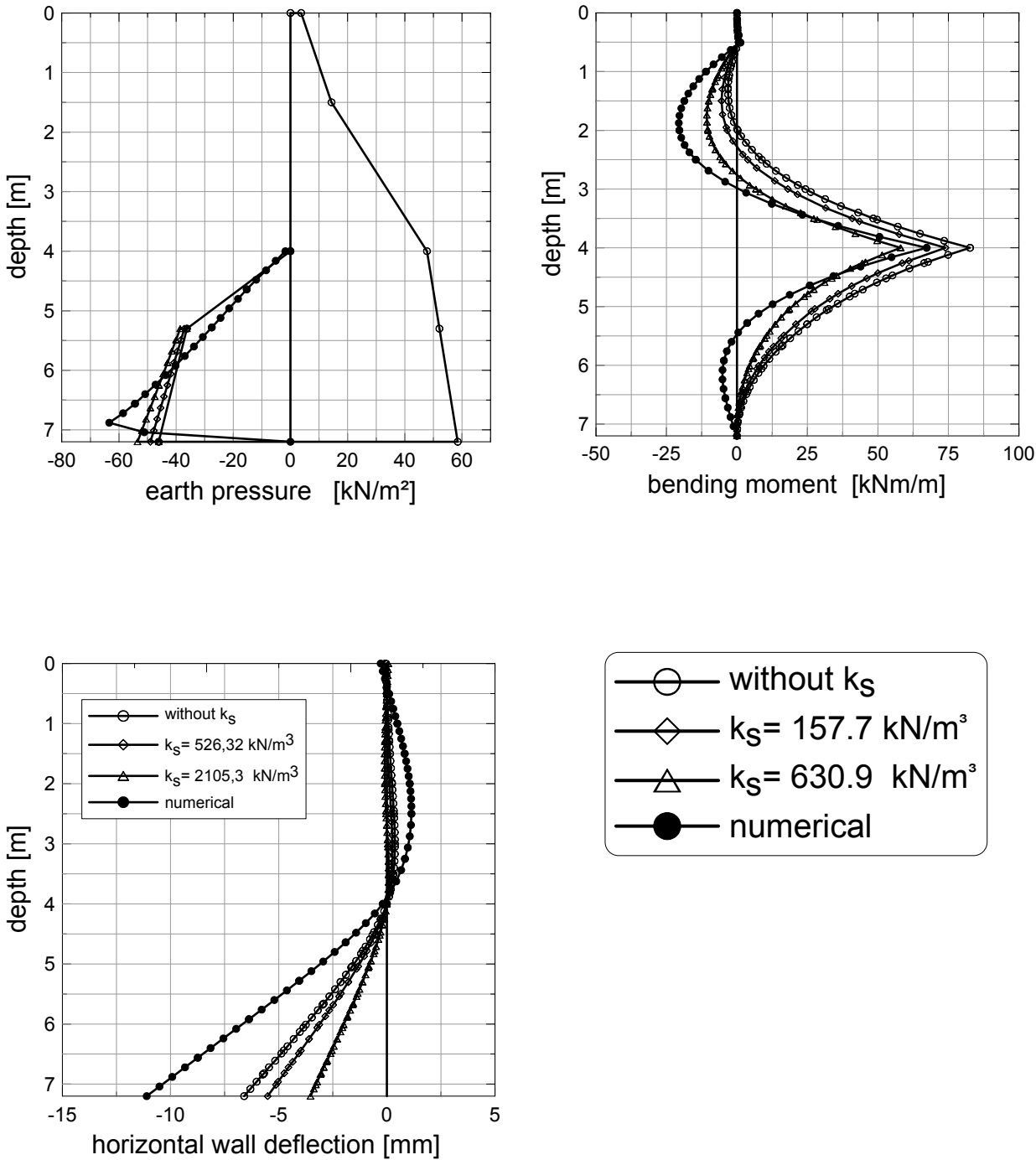
Case-Ic: Final excavation
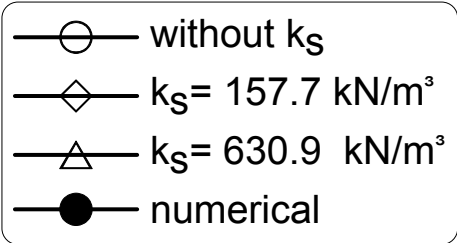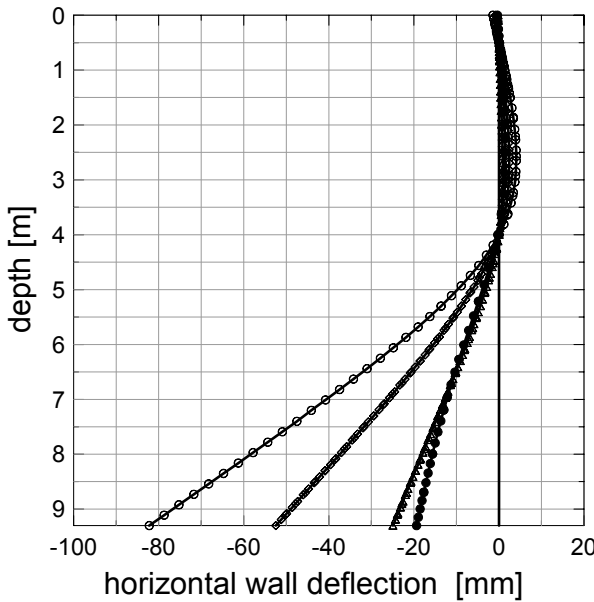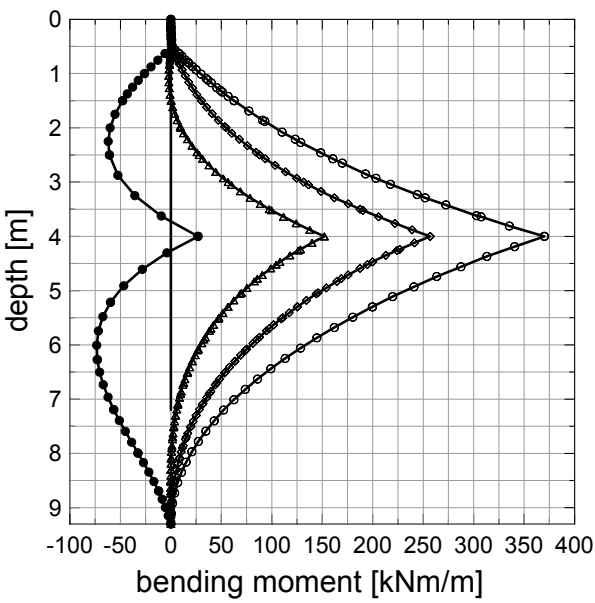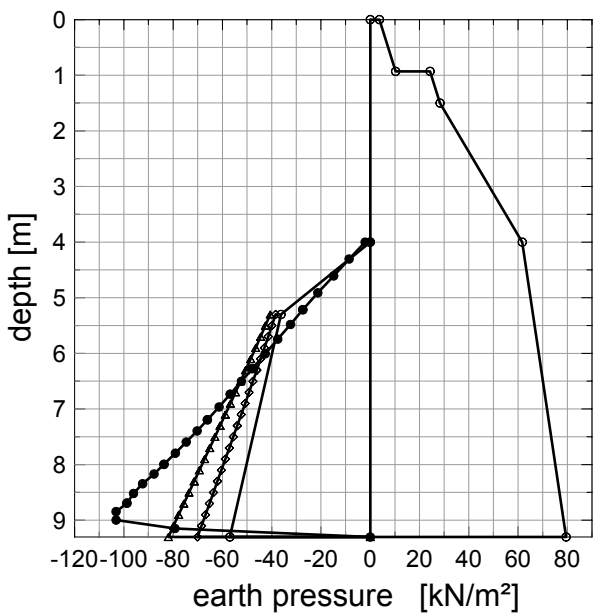
Case-IIb: Final excavation

Case-IIb: Final excavation (Diaphragm wall)

D Frequently used symbols and expressions

Here are the most frequently used symbols, abbreviations and expressions. Actually, most of the symbols are already locally defined in the text. Some symbols may also have one or more definitions.

D.1 Geometrical symbols and abbreviations

Symbol	Unit	Description
z	[m]	depth from the ground surface
z_c	[m]	depth to the tension crack from the surface
z_p	[m]	depth from bottom of excavation
h	[m]	depth of excavation, height of soil specimen
H	[m]	height of the retaining wall
d	[m]	distance from behind the wall
b	[m]	width of an excavation
h_E	[m]	depth to the active force from the surface
h_B	[m]	depth to the passive force from the bottom of excavation
D	[m]	drainage path

D.2 Material parameters

Symbol	Unit	Description
K_0	[-]	coefficient of earth pressure at rest
$K_{0(NC)}, K_{0(OC)}$	[-]	coefficient of earth pressure at rest for normally consolidated and overconsolidated soils respectively
OCR	[-]	overconsolidation ratio
K_a	[-]	coefficient of active earth pressure
K_a^T	[-]	ratio of the total horizontal and vertical stresses in active state

K_p	[-]	coefficient of passive earth pressure
K_p^T	[-]	ratio of the total horizontal and vertical stresses in passive state
κ	[m/s]	coefficient of the permeability of soil
c_v	[m²/y]	coefficient of compressibility
δ	[°]	wall friction
φ	[°]	angel of internal friction
φ_s'	[°]	total angel of internal friction (inclusive cohesion)
M	[°]	slope of the critical state line in p - q diagramm
φ_c', φ_t'	[°]	the effective angel of internal friction in compression and in tension respectively
φ_{cu}	[°]	undrained angel of internal friction
c	[kN/m²]	cohesion
c_a	[kN/m²]	adhesion
c_u	[kN/m²]	undrained shear strength
c_{uc}, c_{ut}	[kN/m²]	undrained shear strength in compression and in tension respectively
c_{uv}, c_{uh}	[kN/m²]	undrained shear strength in vertical and in horizontal directions respectively
τ_f	[kN/m²]	field vane shear strength
τ_{uv}, τ_{uh}	[kN/m²]	vane shear strength in vertical and in horizontal directions respectively
γ_w	[kN/m³]	unit weight of water
γ	[kN/m³]	unit weight of soil
γ_r	[kN/m³]	saturated unit weight of soil
γ'	[kN/m³]	buoyant unit weight of soil
γ_d	[kN/m³]	dry unit weight of soil
λ_{cu}	[-]	normalised undrained shear strength
c_u	[kN/m²]	undrained shear strength
E_u	[kN/m²]	undrained modulus of elasticity
$E_{u,i}$	[kN/m²]	initial undrained modulus of elasticity
E	[kN/m²]	drained modulus of elasticity

E_{ur}	[kN/m²]	modulus of elasticity for un/reloading
E_t	[kN/m²]	tangent modulus of elasticity
E_{sec}	[kN/m²]	secant modulus of elasticity
E_{50}	[kN/m²]	secant modulus of elasticity at 50% the deviator stress at failure
E_{oed}	[kN/m²]	constrained modulus of elasticity
$E_{oed,ur}$	[kN/m²]	constrained modulus of elasticity for un/reloading
E_h, E_v	[kN/m²]	modulus of elasticity in horizontal and vertical directions respectively
K	[kN/m²]	bulk modulus of elasticity
G	[kN/m²]	shear modulus
k	[-]	dimensionless modulus number
m	[-]	stiffness exponent
w	[%]	water content of the soil
I_p	[%]	plasticity index
w_L	[%]	liquid limit
I_c	[-]	consistency index
I_L	[-]	liquidity index
ν	[-]	Poisson's ratio
ν_{ur}	[-]	Poisson's ratio for un/reloading
υ	[-]	specific volume
e	[-]	void ratio
e_0	[-]	initial void ratio
e_L	[-]	void ratio at the liquid limit
λ	[-]	slope of the normal consolidation line
κ	[-]	slope of the un/reloading line
C_c	[-]	compression index
C_s	[-]	swelling index
G_s	[-]	specific gravity of a soil
C_α	[-]	coefficient of secondary compression

A, B	[-]	coefficient of pore pressure
A_f, B_f	[-]	coefficient of pore pressure at failure
$\underline{D}^e$	[-]	elastic material stiffness matrix
$\underline{D}^{ep}$	[-]	elasto - plastic stiffness matrix
$\underline{K}^{ep}$	[-]	elasto - plastic material stiffness in the finite element formulation
ψ	[°]	angle of dilatancy

D.3 Deformations, forces and stresses

Symbol	Unit	Description
e_h	[kN/m²]	Earth pressure
e_{0h}	[kN/m²]	Earth pressure at rest
e_{ah}	[kN/m²]	Active earth pressure
e_{ph}	[kN/m²]	Passive earth pressure
p	[kN/m²]	surcharge load
σ'_{vc}	[kN/m²]	effective consolidation stress
σ_{v0}, σ'_{v0}	[kN/m²]	total and effective overburden pressures respectively
σ'_z, σ'_v	[kN/m²]	effective vertical stress
σ'_h	[kN/m²]	effective horizontal stress
σ'_1	[kN/m²]	effective major principal stress
σ'_3	[kN/m²]	effective minor principal stress
$(\sigma'_1 - \sigma'_3)_f$	[kN/m²]	deviator stress at failure in triaxial test
σ'_e	[kN/m²]	Hvorslev's equivalent stress
u	[kN/m²]	pore water pressure
u_0	[kN/m²]	pore water pressure at steady state (hydrostatic)
Δu	[kN/m²]	excess pore water pressure
Δu_f	[kN/m²]	excess pore water pressure at failure

q_c	[kN/m²]	cone resistance
σ'_{vm}	[kN/m²]	previous maximum vertical effective stress in which the soil was subjected
p'_m	[kN/m²]	previous maximum mean effective stress in which the soil was subjected
τ	[kN/m²]	shear strength of soil
p, p'	[kN/m²]	total and effective mean principal stresses respectively
p_f, p'_f	[kN/m²]	total and effective mean principal stresses at failure respectively
q	[kN/m²]	deviatoric stress
ε	[-] or [%]	strain
ε_f	[%]	strain at failure
$\dot{\varepsilon}$	[mm/min]	rate of strain of the load application
ε_v	[-] or [%]	volumetric strain
δ_v, δ_v	[mm]	horizontal and vertical deflection of the wall
p_{ref}	[kN/m²]	reference pressure (atmospheric pressure = 100 kN/m²)
$\underline{\sigma}$	[-]	stress tensor
$d\underline{\sigma}$	[-]	incremental stress tensor
$d\underline{\varepsilon}^e$	[-]	incremental elastic strain tensor
$d\underline{\varepsilon}^p$	[-]	incremental plastic strain tensor
$d\varepsilon_v$	[-]	incremental volumetric strain
$d\varepsilon_q$	[-]	incremental shear strain
$d\underline{\varepsilon}^{vp}$	[-]	incremental visco - plastic strain tensor
W	[-]	strain energy density function
dp	[kN/m²]	incremental mean principal stress
dq	[kN/m²]	incremental shear stress
$F(\underline{\sigma})$	[-]	yield function
Q	[-]	potential function
$h(d\underline{\varepsilon}^p)$	[-]	hardening function
λ	[-]	positive scalar of proportionality dependant on the state of stress and load history

I_1	[kN/m²]	$= \sigma_1 + \sigma_2 + \sigma_3 =$ the first invariant of the stress tensor
J_2	[kN/m²]	$= \dfrac{1}{6} \cdot \left[(\sigma_1 - \sigma_2)^2 + (\sigma_2 - \sigma_3)^2 + (\sigma_3 - \sigma_1)^2 \right]^2$
		= the second invariant of the deviatoric stress tensor
J_3	[kN/m²]	$= \left[(\sigma_1 - \sigma_2) \cdot (\sigma_2 - \sigma_3) \cdot (\sigma_3 - \sigma_1) \right]$
		= the third invariant of the deviatoric stress tensor
$\underline{B}$	[-]	strain matrix
μ	[-]	fluidity parameter
R	[-]	aspect ratio of the cap

D.4   Miscellaneous

Symbol	Unit	Description
F.S	[-]	factor of safety against basal heave
η_p	[-]	global safety factor on passive pressure
F_φ, F_c, F_{cu}	[-]	partial safety factors on friction φ, cohesion c and undrained strength c_{cu} respectively
F_{np}	[-]	factor of safety on the moment of the net active forces
F_{sp}	[-]	factor of safety on the soil parameters before the passive earth pressure coefficients are calculated
F_d	[-]	factor of safety on the depth of penetration
F_r	[-]	factor of safety on the moment of activating forces
η_F, η_R	[-]	safety factors on action forces and resisting forces respectively
f_q, f_{wa}	[-]	safety factors on action forces and water pressure on the active side respectively
f_r, f_{wp}	[-]	safety factors on passive forces and water pressure on the passive side respectively
N, N_b, N_c	[-]	Stability number
μ_1, μ_2	[-]	the effect of the width of excavation
μ_A	[-]	correction factor to the undrained strength from vane field test to account the effect of anisotropic

μ_R	[-]	correction factor to the undrained strength from field vane test to account the effect of anisotropic and the rate of shearing
ξ	[-]	E_u/c_u
C_r	[-]	shape factor
$\lambda_t, \lambda_b, \lambda_c$	[-]	bearing capacity coefficients
k	[-]	principal stress ratio
CIU		isotropically consolidated undrained
CID		isotropically consolidated drained
CAU		anisotropically consolidated undrained
CAD		anisotropically consolidated drained
UU		unconsolidated undrained
TC		triaxial compression
TE		triaxial extension
DSS		direct simple shear
N_k	[-]	empirical cone factor
ξ	[-]	factor of anisotriophy
β	[-]	reciprocal of the gradient of the stress path
t_f	[min]	time to failure
r^2	[-]	coefficient of correlation
R_f	[-]	failure stress ratio
R_{int}	[-]	interface element parameter (parameter reduction factor to account the wall friction and adhesion)

Mitteilungen des Fachgebietes Grundbau, Boden- und Felsmechanik der Universität Kassel
Herausgeber: Prof. Dr.-Ing. H. Sommer

Heft 1   **Buczek, H., 1991:**
Beitrag zur Berechnuung der horizontalen Belastung auf steife Elemente zur Stabilisierung von Rutschungen in Tonhängen.

Heft 2   **Böckmann, F.-J., 1991:**
Modellversuche zur Grenzlastermittlung von Pfahlgruppen, Vertikalpfähle unter Vertikallast in symmetrischer Anordnung.

Heft 3   **Meyer-Kraul, N., 1991:**
Geomechanische Eigenschaften von Röttonsteinen, Scherfestigkeit bei schichtenparalleler Beanspruchung.

Heft 4   **Müllner, B., 1991:**
Beitrag zur Untersuchung der Erosionssicherheit bindiger Mischböden bei vertikaler Durchströmung.

Schriftenreihe Geotechnik der Universität Kassel
Herausgeber: Prof. Dr.-Ing. H.-G. Kempfert

Heft 5   **Voß, T., 1996:**
Beitrag zur Festigkeitsentwicklung von Klärschlämmen in Monodeponien

Heft 6   **Raithel, M., 1999:**
Zum Trag- und Verformungsverhalten von geokunststoffummantelten Sandsäulen

Heft 7   **Jaup, A., 1999:**
Anwendung von 1g Modellversuchen auf das Setzungsverhalten im Hinterfüllungsbereich von Brückenwiderlagern

Heft 8   **Hu, Y., 2000:**
Zum Verformungsverhalten von wassergesättigten bindigen Böden unter zyklischer Belastung

Heft 9   **Sammelveröffentlichung, 2001:**
Beiträge aus der Umweltgeotechnik

Heft 10   **Zaeske, D., 2001:**
Zur Wirkungsweise von unbewehrten und bewehrten mineralischen Tragschichten über pfahlartigen Gründungselementen

Heft 11   **Ott, E., 2001:**
Zum bodenmechanischen Verhalten von Abfallrostaschen

Heft 12   **Gotschol, A., 2002:**
Veränderlich elastisches und plastisches Verhalten nichtbindiger Böden und Schotter unter zyklisch-dynamischer Beanspruchung

Heft 13   **Stöcker, T., 2002:**
Zur Modellierung von granularen Materialien bei nichtruhenden Lasteinwirkungen

Heft 14   **Berhane Gebreselassie, 2003:**
Experimental, analytical and numerical investigations of excavations in normally consolidated soft soils